STRUCTURAL BEHAVIOUR OF HISTORIC MASONRY CROSS VAULTS

Dimitrios Theodossopoulos, Dipl.Civ.Eng, Spec.Cons

A thesis submitted for the Degree of Doctor of Philosophy

School of Civil and Enviromental Engineering
The University of Edinburgh

September 2001

DECLARATION

This thesis is the result of research work for the degree of Doctor of Philosophy undertaken in the School of Civil and Environmental Engineering, University of Edinburgh.

I declare that the work in this thesis has been, unless otherwise stated, carried out by myself under the supervision of Prof. B. P. Sinha, Dr. A. S. Usmani and Dr. A. J. Macdonald.

Edinburgh, September 2001

D. Theodossopoulos

ACKNOWLEDGEMENTS

This project aimed to give a multidisciplinary approach to the assessment of the structural behaviour and safety of historic masonry cross vaults and it would not have been possible without the coordination, advice and direction of Prof. B. P. Sinha, my principal supervisor. Thanks are also due to my other supervisors, Dr. A. S. Usmani and, from the Department of Architecture, Dr. A. J. Macdonald for their guidance.

Essential technical assistance was provided during the construction of the model cross vault by Mr. A. Jones, manager of the workshop at the Department of Architecture, the technical staff at the School of Civil Engineering, especially Mr K. Broughton, and technicians from Historic Scotland, especially Mr D. Peet. Valuable suggestions on Gothic architecture, vaulting techniques and the history of Holyrood Abbey were given by Dr. R. Fawcett, Principal Inspector of Ancient Monuments with Historic Scotland, and Mr. B. Heath, architect. The useful comments and help of Mr. P. Beckmann, Dr. P. B. Lourenço, Dr. A. Viskovic, Prof. C. A. Syrmakezis, Prof. D. Beskos, Dr. R. F. Pedreschi, Prof. M. C. Forde, Dr. R. Capozucca, Prof. W. Jäger, Dr. S. Huerta and Prof. R. Barthel are also kindly acknowledged. Thanks are also due to the support staff at the School of Civil Engineering for their help throughout.

Finally I should thank my family and my fiancée, Cristina González-Longo, architect, for their love and support during this important period. Cristina's contribution to the construction of the model vault and the presentation of the thesis has been invaluable.

ABSTRACT OF THESIS

The preservation of the architectural heritage presents one of the greatest technical challenges due to the complexity of the geometry of the structures, the variability of the material used or the loading history of the buildings. The knowledge of their pathology and collapse modes become therefore essential for the planning of structurally compatible and economic conservation programmes. In the case of gothic cathedrals, masonry cross vaults play a fundamental role in the roofing scheme and they are very sensitive to deformations imposed by failure of the system that contains their lateral thrusts.

An experimental and theoretical study for the assessment of the safety of cross vaults is presented in this thesis. The case study is based on an aisle vault from the partially collapsed Abbey Church of Holyrood, Edinburgh. A replica in 1/4-scale was built reproducing this ribbed vault, which has straight vertices and was made of rubble masonry.

Initially, dead weight was applied to study the elastic response of the structure under service conditions. The effect of some parameters that are the source of uncertainty in the behaviour of historic buildings (load distribution, stiffness of the groins, support conditions, height of the spandrel fill) upon the deflections and strain distribution of the structure has been investigated. Finally, the abutments were allowed to move and the behaviour of the vault was assessed by correlating the deflections and strains recorded with the crack pattern that developed. Failure was reached when a sufficient number of fracture lines was formed, transforming the structure into a mechanism.

Finite Element (FE) models were developed to simulate the behaviour of the vault. The material properties required (stress/strain relationship and flexural strength) were established by wallette tests under four-line loading. The response to dead weight was studied in the linear elastic range and the influence of the groin geometry and the support conditions, among other features, were also investigated.

In the course of the movement of the abutments, the formation of the fracture lines was simulated with a smeared-crack approach. The initial continuous FE model was further modified to concentrate failure at the weaker mortar joints. The sensitivity of the solution to some of the parameters examined earlier was investigated. The degree of safety of the structure was also evaluated with a limit state analysis.

The analytical study of historic constructions is highly influenced by complicated interactions of a variety of factors and suggestions for further research are given based on the findings of this project.

TABLE OF CONTENTS

CHAPTER 3

THE MODEL OF A VAULT FROM THE CHURCH OF HOLYROOD ABBEY

CHAPTER 4

MATERIAL PROPERTIES AND EXPERIMENTAL SET-UP

CHAPTER 6

INVESTIGATION OF THE BEHAVIOUR OF THE VAULT DUE TO MOVEMENT OF ABUTMENTS

Chapter 1

INTRODUCTION

1.1 INTRODUCTION

Masonry cross vaults were an essential part of the structural scheme of many historic buildings like cathedrals and abbeys at least until the early Renaissance. They were employed to roof compartments of a wide variety of spans and proportions, making an optimal and cost-effective use of the materials available (Fig. 1.1). Cross vaults can be defined as an intersection at right angles of two barrel vaults. The predominance of the pointed profile in the Gothic period suggests the evolution from the earlier semicircular form, which improved their bearing capacity and allowed to cover large spans. Important examples of cross vaults can be found as early as in the Roman times, but the benefits of the form were best exploited at the cathedrals of the High Gothic period (13th century).

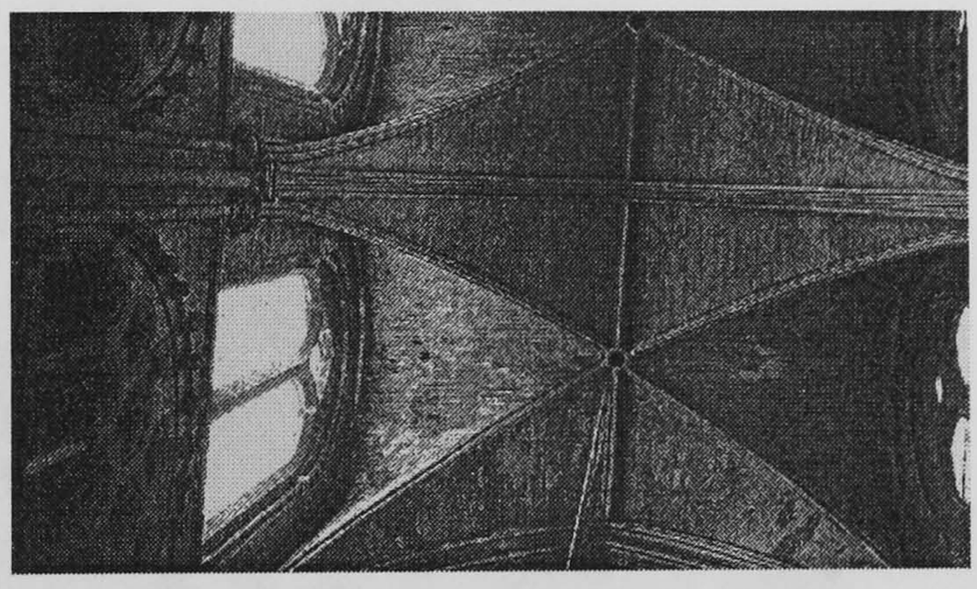

(a) High (nave) vaults

(b) Aisle vaults

FIGURE 1.1 Typical quadripartite cross-vaults (from Burgos Cathedral)

An important characteristic of these cathedrals was the necessity to admit sufficient amounts of natural light into the building. As a consequence, the central nave had to be raised, so its vaults required a different form and support conditions (Fig. 1.1a) than those at the aisles (Fig. 1.1.b), resulting eventually in a quite distinct structural behaviour. A better understanding of the behaviour and pathology of cross vaults in this scheme is essential for the preservation of many ancient and medieval monuments as it can enable minimal, low-cost conservation interventions, avoiding structural incompatibilities.

It is important, therefore, to classify the variety of the existing types of vaults according to their technical features and structural role within the building and for each type to establish a scheme of structural behaviour. Essential steps in this process are the definition of loadings and partial safety factors and the assessment of material properties. The response of the structure to the basic types of stress (axial forces, bending moment, shear, torsion) should be evaluated and, in compliance with modern practice, serviceability limit states of deflection and cracking must be determined.

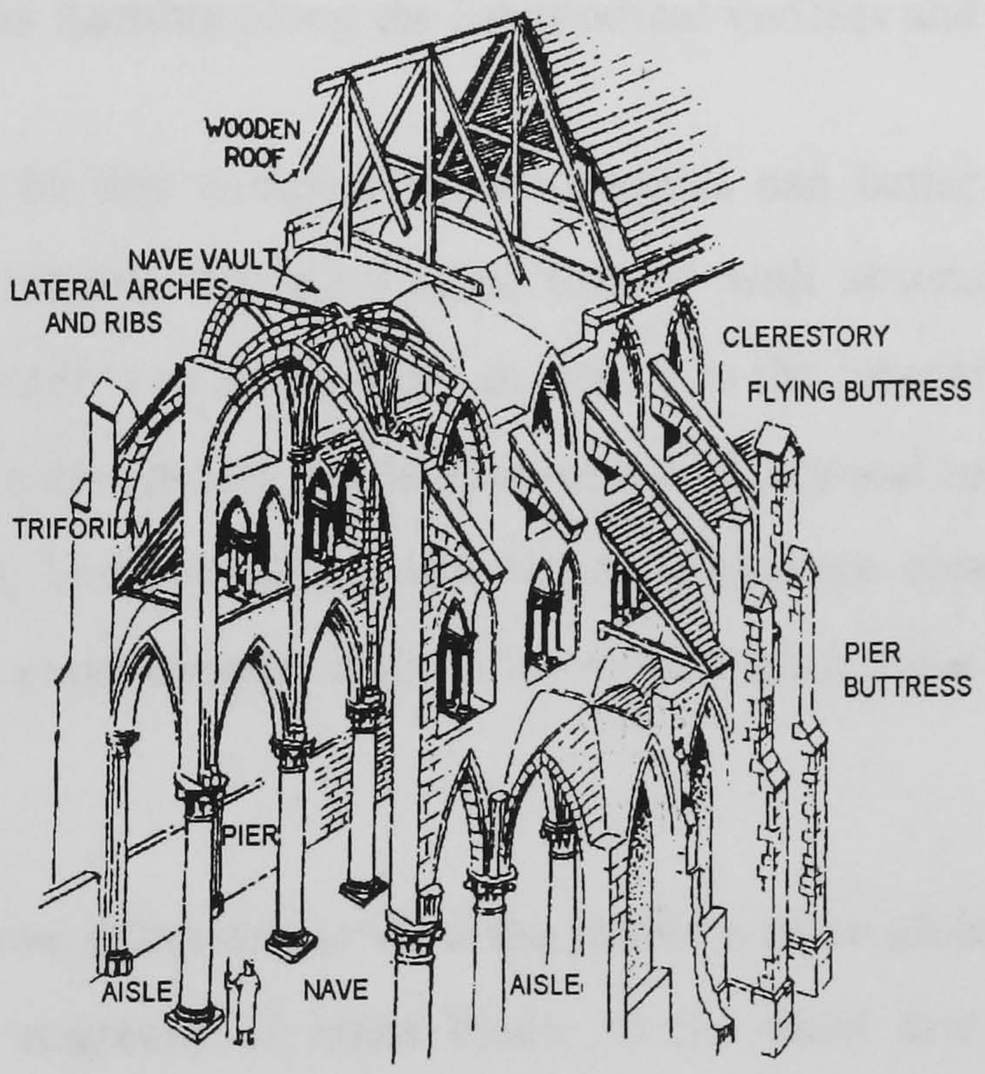

FIGURE 1.2 Basic structure of a Gothic church (after Acland 1972)

The general layout of the structure of a Gothic cathedral is illustrated in Fig. 1.2. During the development of this structural configuration, its full potential was exploited by concentrating the vertical supports of the vaults to their four corners. In this manner, the lateral walls became structurally less important and large windows could be opened,

creating well-lit public-assembly spaces. Balancing the lateral thrusts was therefore an essential condition and external buttresses or diaphragm walls were usually employed. A successful application of this scheme can reduce bending (and therefore tension) in both the vault and the lateral walls, allowing most of the load to be carried mainly with membrane compressive forces. When ribs were introduced later at the groins, the integrity and the stiffness of the intersection were enhanced and a better co-action between the joining webs was guaranteed.

Any action that could compromise the ability of the structure to retain the lateral thrust was more likely to cause the collapse of the vault than a large amount of dead load. Movement of the buttressing system or wide changes of the vaults' geometry (usually due to unexpected loadings or degradation of the fabric) are the most common reasons. To summarise the associated pathology, the unrestrained thrust would cause the lateral walls to move out-of-plumb and the weight of the upper structure to be transmitted with an offset to the base of the aisle vault, imposing a rotation that the local cross-section could not resist. The abutments would subsequently transform into hinges and the vaults would deform rapidly, with cracks forming along the longitudinal vertices and edges, leading to failure.

The nature of this complex failure process can better be understood through the critical study of reliable historical data, backed with structural surveys and monitoring programs and through tests carried out in situ or in the laboratory. Most of the research so far in this field has focused on the development of analytical models, which, in the majority of the cases, have been validated with rather qualitative observations upon specific case studies. Only few experimental projects have been carried out to deal with specific aspects of the problem.

It is, therefore, necessary to view the problem more globally by establishing the basic principles of the response of cross vaults to the most dominant loadings. The project presented here deals with the safety level of rib vaults of a configuration that prevailed in Europe between the 11th and the 13th century and this typology is representative of a wide variety of cross vaults. As a case study, a vault was chosen from the aisle of the Church of the Abbey of Holyrood in Edinburgh, which had partially collapsed. As the vault spans over a square plan and is quadripartite, it can be treated as a quite typical example. A scale model was built and tested initially at service loads, namely dead load. Subsequently, collapse of

the vault due to imposed deformations caused by the failure of the upper structure was assessed, by simulating the action as a horizontal movement of the front abutments. A prediction of the experimental data in both tests was carried out with Finite Element (FE) models analysed with the program Abaqus, which were further used afterwards to interpret other aspects of the behaviour of the structure.

This introduction presents the problems linked with the evaluation of the safety of cross vaults and their structural context is defined in §1.2. The original structural configuration was constantly being developed by the Master Masons in order to address effectively technical and geometric needs and the major types that were devised in response to the specific conditions of every period are discussed in §1.3. Defects would arise when this scheme was not sufficiently understood or adequately performed and an examination of some indicative cases of failure illustrates aspects of vault pathology (§1.4). Finally, the outline of the thesis is presented in §1.5.

1.2 RIB CROSS VAULTS

1.2.1 Rib cross vaults

Rib cross vaults dominated the structures of medieval buildings like cathedrals and abbeys etc. after the 11th century. They were usually generated by the intersection at right angles of two pointed barrels and their common joint (the groin) was further stiffened by ribs (Fig. 1.3). The function of the vault depended on its location within the church and it can be distinguished between that of the nave or high vault (symmetrically supported - Fig. 1.1a) and that of an aisle or lateral vault (spanning mainly between the wall and the arcade - Fig. 1.1b). The vaults at the aisles are the object of this project, but, inevitably, when dealing with matters of form and function, references will be made to the nave vaults also.

Aisle vaults were usually employed over square compartments and any deviations can usually be associated with the re-use of pre-existing foundations, faults during the construction that have forced structural changes, or the adoption of a particular system of proportions. Until recently, the role of the ribs in reinforcing, both visually and structurally, the lines of intersection (groins) has been the subject of controversy between researchers considering them as either an auxiliary decorative element or an important load-bearing

member (see §1.2.3 for a more detailed discussion). It has to be stressed, however, that the changes in the use of the ribs during the 11th century were a critical factor for the development of Gothic Architecture. The edge of the vault along the nave arcade (Fig. 1.1b) is marked by an arch which has a substantial cross section (*arc-formeret*), whose width depends on the size of the elevation wall it supports.

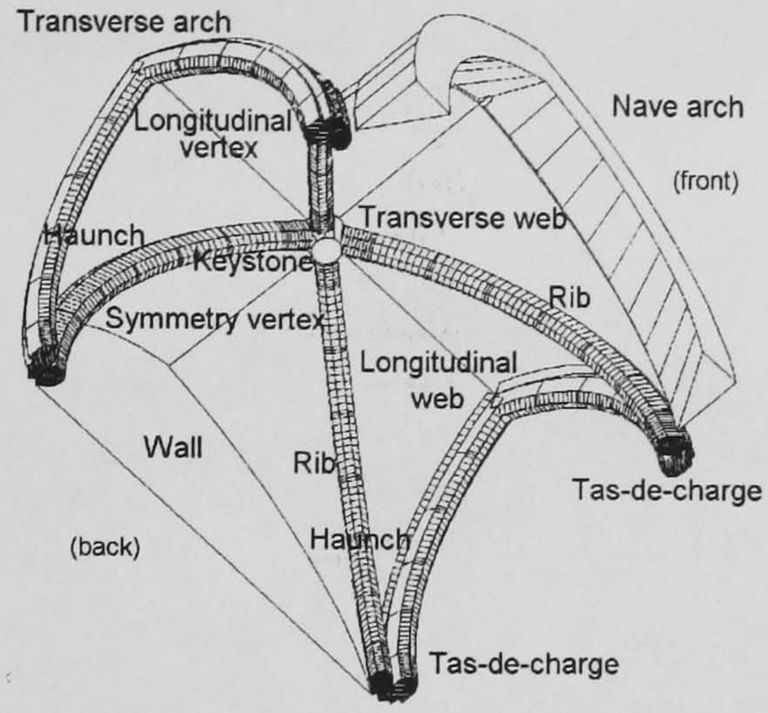

FIGURE 1.3 Geometry of a quadripartite aisle cross vault and definitions

A wide variety of masonry types was employed for the webs, ranging from rubble, (irregular blocks laid in a rich mix of lime mortar or concrete) to ashlar (where precisely cut blocks permitted a greater degree of prefabrication and control during building). Usually, the conoid pockets created over the haunches would be filled up to almost half of the vault's height with a coarse mix of stones and mortar. A thick coat of mortar usually covered the extrados of the vault under the roof, mainly for insulation purposes, and, so far as the intrados was concerned, many vaults were plastered and then frescoed, unless their masonry was of an exceptional quality.

1.2.2 The structural scheme

Cross vaults were an integral part of buildings characterised by these parameters: the provision of the right amount of light for the services (ranging from abundant in c. Europe to moderate in south Europe); the optimum use of material and human resources; and the creation of a water- and fire-proof structure. The quite distinctive character of Gothic structures is due to the innovative use by the designers (the master masons) of already existing elements (like the rib or the pointed vault) (Acland 1972).

In a classic plan configuration, a wide nave is flanked with one or two narrower aisles along the sides (Fig. 1.4). East of the crossing, the choir of the church ends at the semicircular apse. The massive structure of the façade closes the west end, usually further strengthened, both visually and structurally, by two towers, while the crossing is usually emphasised with another tower, supported on four solid piers. Between these focal areas, the nave is regularly divided into bays along the axis, following in elevation, from the ground to the top, the sequence of arcade, triforium and clerestory windows (Fig. 1.5).

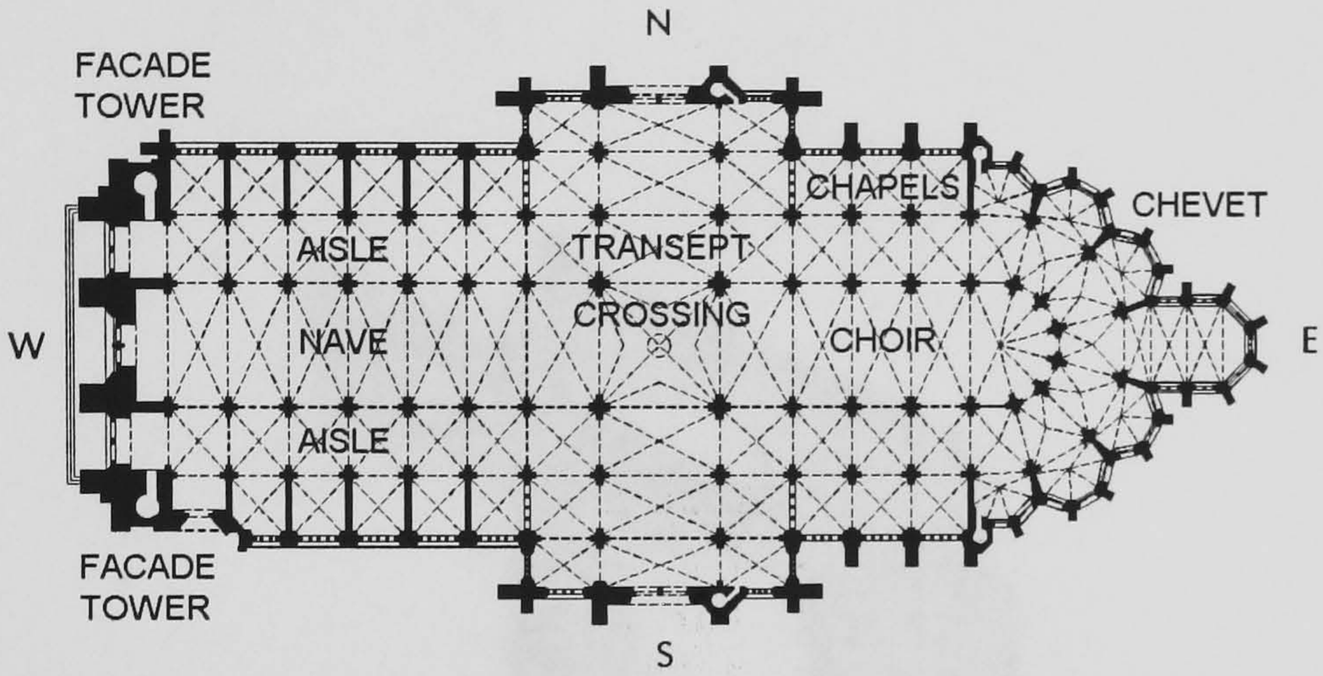

FIGURE 1.4 Plan of a classic High Gothic cathedral (Amiens Cathedral)

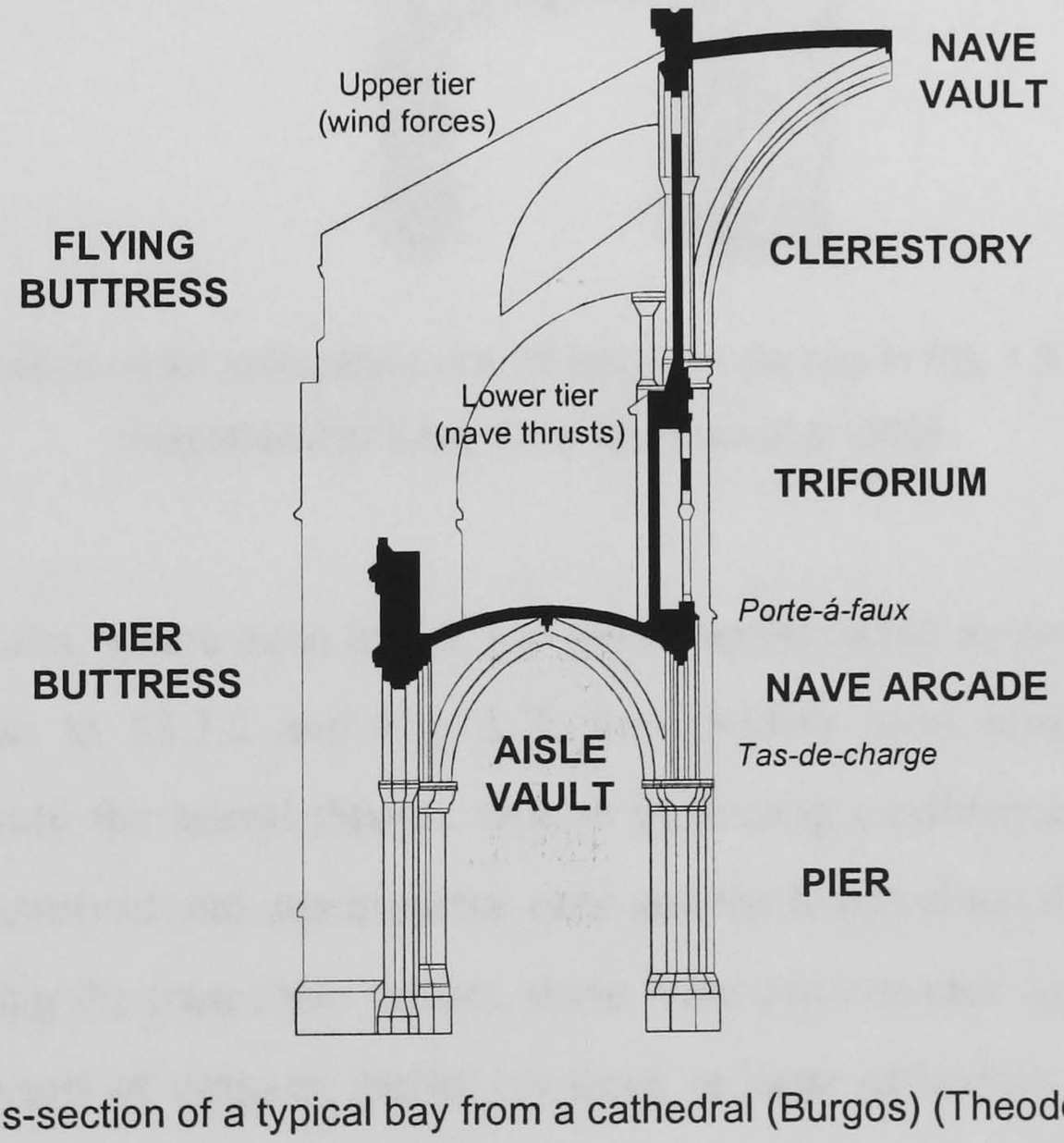

FIGURE 1.5 Cross-section of a typical bay from a cathedral (Burgos) (Theodossopoulos 1995)

The role of the apse and the façade is to provide the necessary diaphragms at the extremes of the long barrel of the nave and allow the bays to abut efficiently each other

along the longitudinal axis. This feature becomes very significant during construction, which usually proceeded with the bays being built successively along the longitudinal axis and not erected simultaneously from a pre-established plan. A further benefit of this feature today is that the structural behaviour of the complete building can be significantly simplified through the study of a single bay. The examination of the FE model of a bay from the nave of Burgos Cathedral deformed under its own weight (Fig. 1.6) makes evident the contribution of the most important members of the structure to the overall response (Theodossopoulos 1995).

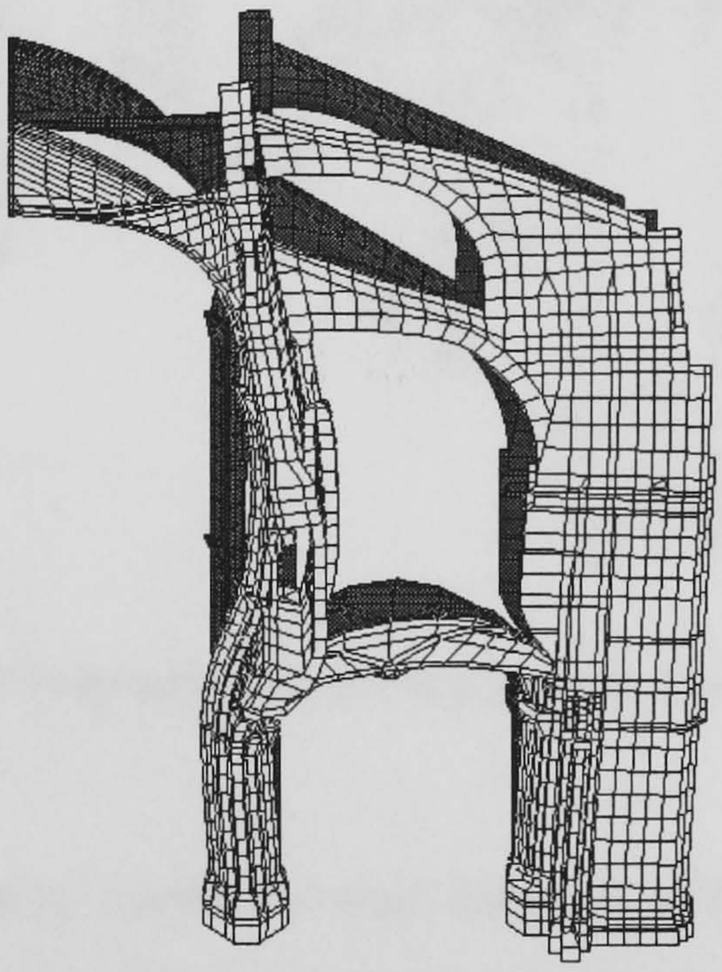

FIGURE 1.6 Deformation under self-weight of a FE model of the bay in Fig. 1.5 (Burgos Cathedral) magnified 200 times (Theodossopoulos 1995)

Sexpartite vaults, where each bay of the nave corresponded to two bays of the aisles (see later discussion in §3.3.2 and Fig. 3.7) were widely used initially as they could distribute conveniently the lateral thrusts. Due to increasing confidence among the master builders, the vaults evolved into quadripartite ones and the longitudinal thrusts were reduced (Fig. 1.7). Concerning the transverse thrusts, these were counteracted by a system of flying buttresses with two sets of rampant arches (or three in large cathedrals such as Beauvais). The function of the lower set was to stabilise the action of the gravity loads, while the higher set, located almost at the same height as the vertex, was expected to act as a cross-bracing against the wind pressure, as was confirmed in recent studies (Bork 1997).

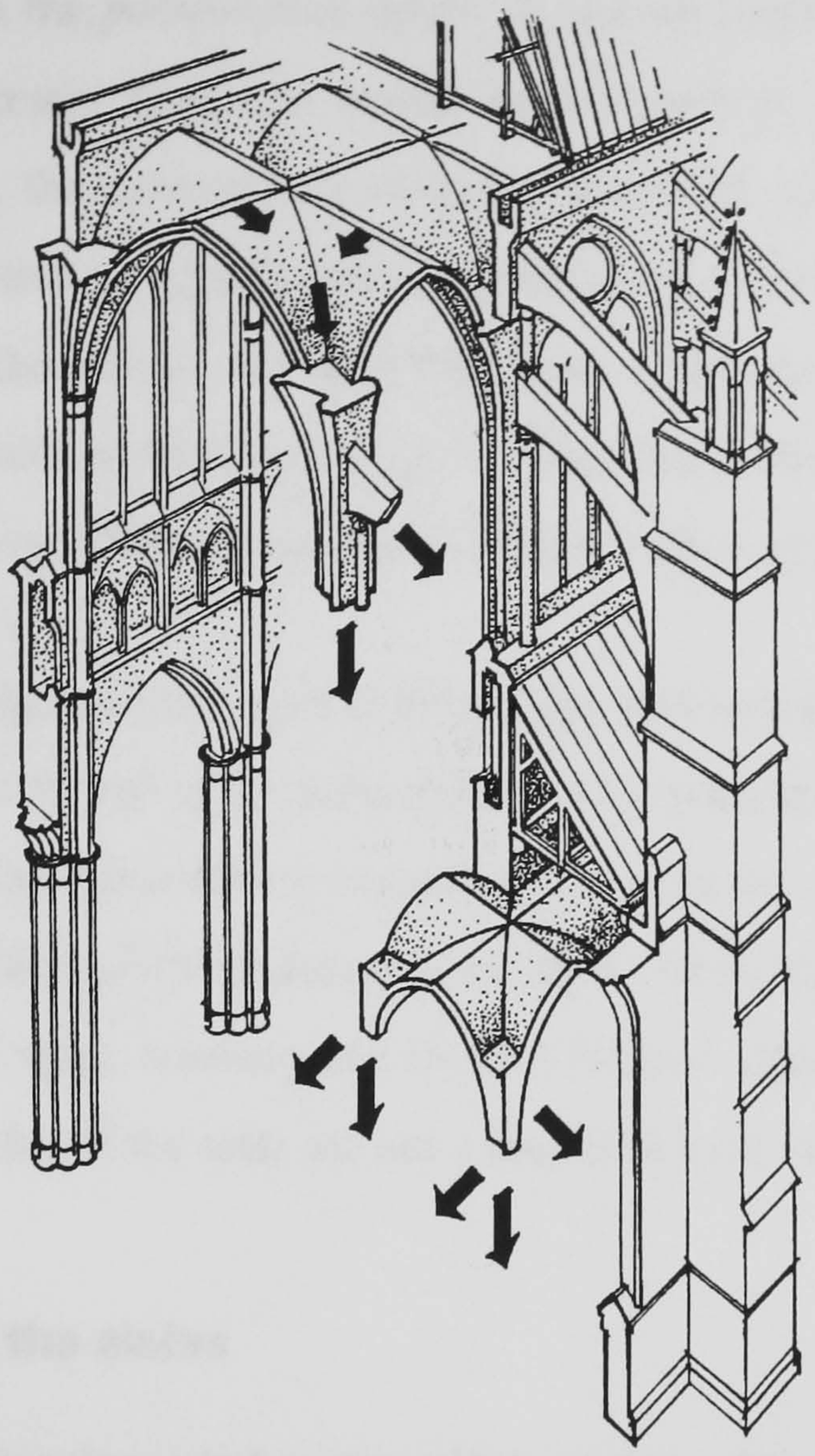

FIGURE 1.7 Free body diagram of a cathedral (Acland 1972)

The zone of the clerestory marks the main function of the wall and a significant part of the evolution of Gothic structures design has been focused on it, as it can be traced at the contrast between the solidity of Durham Cathedral (1093-1133) and the transparency of the Sainte Chapelle in Paris (1240) (§1.3). Further below, the triforium passage introduces an area of structural weakness and makes necessary an enlargement of the wall section (Fig. 1.5). Enclosed with a series of light columns towards the nave, its functional importance for the services kept reducing, in favour of an increase of the surface of the clerestory windows. As the wall approaches its support upon the arcade and the piers, its cross-section progressively reduces to fit within the haunches of the vault in order to avoid resting directly upon the webs. As a result, the wall is carried with an offset over the pier, projecting partially over a void (Fig. 1.5), a feature called *porte-á-faux* (Fitchen 1961).

If the flying buttresses effectively counter the lateral thrust of the nave, the walls remain vertical and bending stresses are avoided. However, a second source of bending

stresses can be found in the *porte-á-faux* detail. If, during construction, the wall were not properly braced transversely (and this would happen usually when the buttresses were erected at a later stage), the nave-vault's weight was carried with an offset from the axis. This area may then function as a hinge and the lateral wall would burst outwards at the top and inwards just above the capital. An early indication of this development can be detected in the response of the vault to dead load (Fig. 1.6) and the procedure is examined again in detail during the discussion of the collapse of Holyrood Abbey (§3.3.4.3).

When its horizontal component was effectively minimised, the weight of the upper structure could be safely carried to the ground, since the total normal stresses transmitted to the piers are usually below the crushing strength of the masonry. Typical values of stresses at the base are about 1 N/mm^2 (Theodossopoulos 1995) while the minimum values for the compressive strength of stone masonry are about 3 N/mm^2 (Hendry 1976). This way, the lower stresses acting on top of the aisle are not a source of local failure of the material.

1.2.3 Cross vaults at the aisles

The aisle vaults develop a behaviour which is quite distinct from that of the nave vaults. Since they span over a square compartment whose area is usually half of the corresponding nave bay, none of their two main axes is expected to prevail in the distribution of the stresses. In addition, the vaults are not supported symmetrically, as the boundary conditions are provided by a different system. Like in the nave, the vaults of neighbouring bays abut each other in the longitudinal direction (Fig. 1.7). The weight of the upper structure serves further to deviate the thrust of the aisle vaults in the other sense towards the vertical (Fig. 1.7), while the opposite side is retained safely by the external wall. Moreover, this weight allows the pier to be loaded mainly axially. Due to the relatively high stiffness of the nave arch and the solid wall, the transverse direction (Fig. 1.2) becomes dominant for the distribution of the loads in this vault. This in turn causes the transverse arches to play a secondary role, even when they are reinforced with ribs (*arcs-doubleau*).

Since the master masons had realised the weakness of masonry in tension, the vaults were designed to allow only compressive forces to develop (or a membrane state of stress under the concept of the theory of shells). A necessary condition, however, is the presence of diaphragms at the end arches of each web and stiffeners along their edges (Flügge 1973).

These conditions are fulfilled mainly at the transverse direction of the bays (Figs 1.7): where the diaphragms are provided by the external wall and the rigid system of nave arch/lateral wall, while the edges are stiffened against bending by the change of curvature along the junction, further strengthened by the ribs.

Concerning the longitudinal direction, the solutions were much more limited, since any attempt to strengthen the boundaries between the bays would cause an interruption of the visual continuity. The ultimate solution was to employ straight vertices and provide light ribs along the transverse ends, whose role was principally to reinforce the symmetry boundary, as it used to happen in plain barrel vaults, and to improve the continuity between the successive phases of construction.

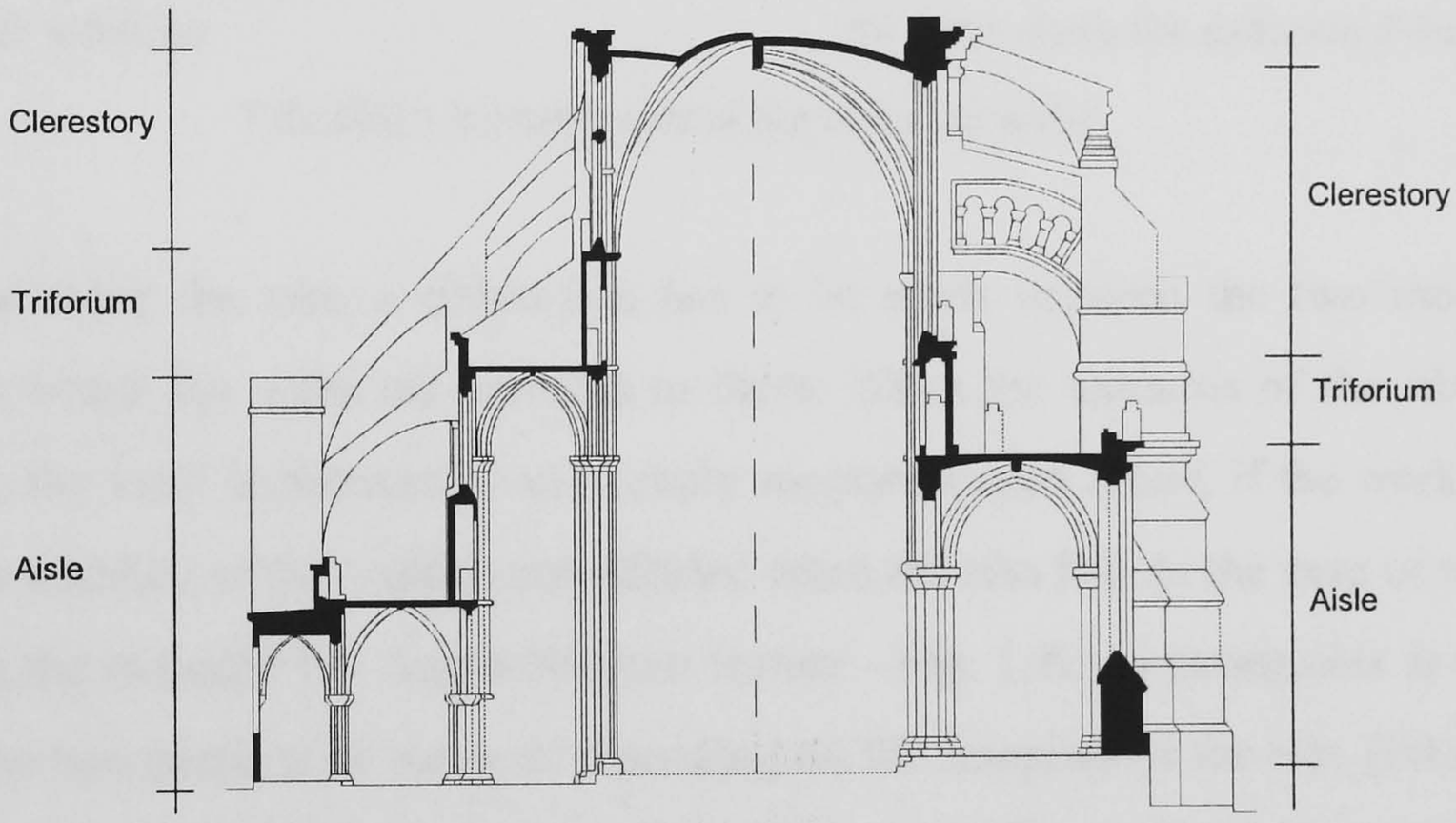

(a) Bourges (b) Chartres

FIGURE 1.8 Comparison between the two major structural configurations of Gothic cathedrals (after Mark 1990)

In common with the nave, if properly braced, the aisle behaves like a long barrel vault. Each bay can be considered then as a cross-section of this barrel and the behaviour of the vaults in the aisle can be investigated by modelling a single bay. The effect of the inward thrust acting just above the capital of the aisle vaults, affecting the stability of the pier, can be further reduced if the difference of height between nave and aisles is more moderate, as in the case of the buildings following the tradition of Bourges Cathedral (hall churches – Fig. 1.8a). Despite this more balanced solution, technical convenience (especially at the early stages of building) and a certain conservatism led to the domination

of the type of Chartres Cathedral (Fig. 1.8b). The evenly graded heights of the Bourges school found success in the Mediterranean areas or the hall-churches of south or central Europe (Acland 1972).

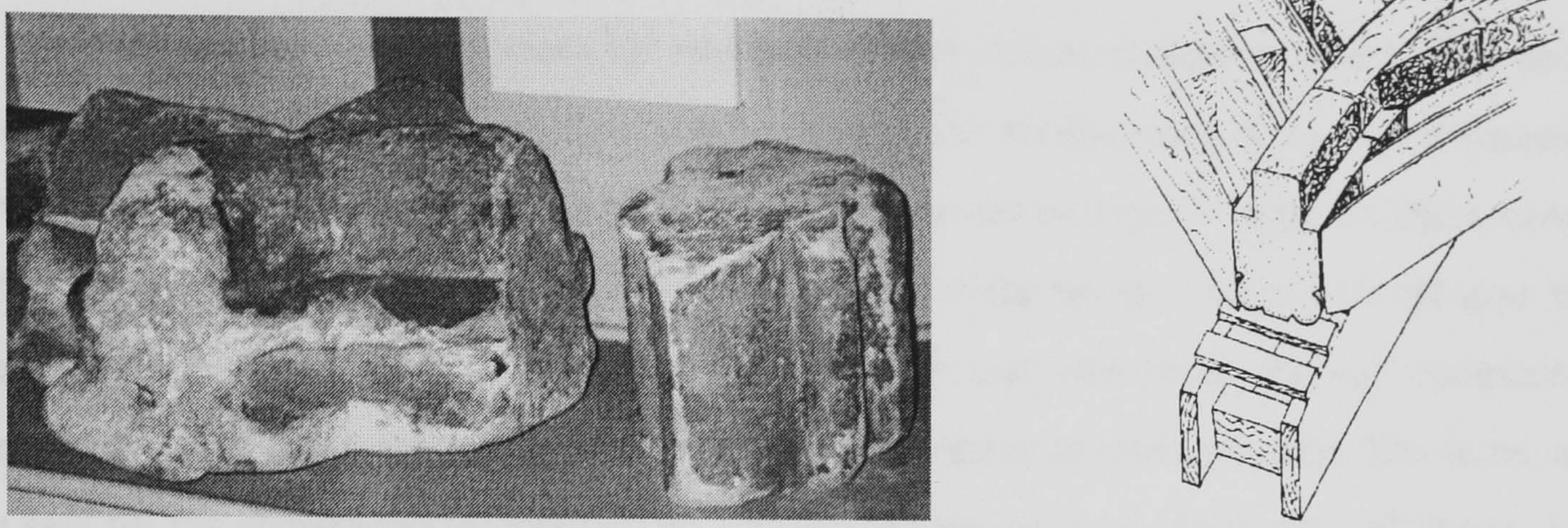

(a) Smooth extrados

(b) Stem along the extrados (Fitchen 1961)

FIGURE 1.9 Attachment of the rib to the webs

Concerning the ribs, a distinction has to be made between the two most frequent systems in which the webs are attached to them. When the extrados of the rib is smooth (Fig. 1.9a), the vault is continuous and simply supported upon it and, if the work is of good quality, the stability of the vault is not affected when the ribs fail. In the case of a projecting stem along the extrados (an Anglo-Norman feature - Fig. 1.9b), a strong link is established between the two parts, with the web depending on the integrity of the ribs (Fitchen 1961). This distinction can explain the variety of failure patterns for vaults, especially after heavy shelling during the First World War (see for example Soissons Cathedral): whether the webs stayed intact (as shell structures they can have an independent structural entity) or the ribs, depended exactly on this degree of rigid support (Gilman 1920).

During the High Gothic period (1130-1284), the rib along the groin would enhance the composite action between the joining webs of the vault by improving the quality of the difficult construction detail of the junction of the webs over its extrados. Concerning the transverse arches, they have kept the function they had in the barrel vaults as stiffening rings, when the aisles (or naves) are considered in this scheme. Eventually, the whole system of arches would serve to emphasise and define the roles and hierarchy of the main vaulting components (Stalley 1999), to improve and stiffen complicated construction details

and to further concentrate the loads into more reliable paths to the ground, permitting large openings instead of massive lateral walls.

1.3 THE DEVELOPMENT OF THE FORM AND FUNCTION

This research project places an emphasis on the technical aspects of masonry cross vaults. It would not be accurate, however, to present the development of form and function on the basis of structural solutions only or in a strictly chronological order. In many cases, an aesthetic breakthrough (like the "re-introduction" of the rib in Durham) would give the masons the confidence to explore its structural benefits and, vice-versa, the well established behaviour of an element would permit safe experimentation in other variants. The same can be said for the chronological criteria, since there were periods when both state-of-the-art and obsolete structural motifs would be used even in areas geographically close to each other, as it happened with the contemporary employment of very light and very solid vaults in south-western Europe.

1.3.1 Groin vaults

The Romans were the first in Europe to consistently employ cross vaults. The variety of forms they managed to experiment with was a direct result of their ability to mobilise effectively workers and powerful machinery and of the innovative use of construction materials like concrete. Voussoir barrel vaults were already common in the Greek (Boyd 1978) and Etruscan civilisations and the Romans adopted initially the form in their aqueducts and bridges. When, however, internal spaces had to be roofed, it became clear that using barrel vaults would require a continuous support over a very thick wall along the whole of their longitudinal edge, limiting both access and lighting from the sides.

By intersecting two barrel vaults, the supports could be virtually reduced to piers at the base of the four junctions, the groins (*ducti*), and even when lateral walls were needed across the sides, these could be of a much reduced thickness or they would allow the opening of lunette windows on their top. The benefits of using concrete instead of ashlar masonry became evident soon and cross vaults would be usually cast in mass monolithic Roman concrete caps, in horizontal layers. A layer of bricks was used as a permanent

formwork, upon which the concrete was poured and tiles could be used to reinforce the structure in some points (Giovannoni 1972, Giuliani 1990, Adam 1999).

Domical vaults were used initially, as it can be seen in the Tabularium in Rome. Conceived as a hybrid between a dome and a vault, their groins are semicircular and therefore the keystone is higher than the crown of the sides. Visual unification of the space, however, became important, so horizontal vertices would be preferred afterwards

The first known example of a groin vault within this tradition can be found in Nero's Domus Aurea (68 AD). It is a rather depressed vault, with groins not clearly defined, and made of tufa rubble concrete, spanning over a bay of 4.50x3.70m. The Colosseum (completed 80 AD) was probably the first example of a wide experimentation on vault techniques. The main barrel vaults used at the corridors display transverse bands of ribs that were used as a kind of permanent centering, while groin vaults appear in the less representative areas of the upper floors. For almost the whole of the 1st century AD, cross vaults would be used tentatively, but eventually their typology took profit from contemporary developments of the supports for barrel vaults, like the extensive use of incorporated ribs or the springing from projecting pillars from the wall.

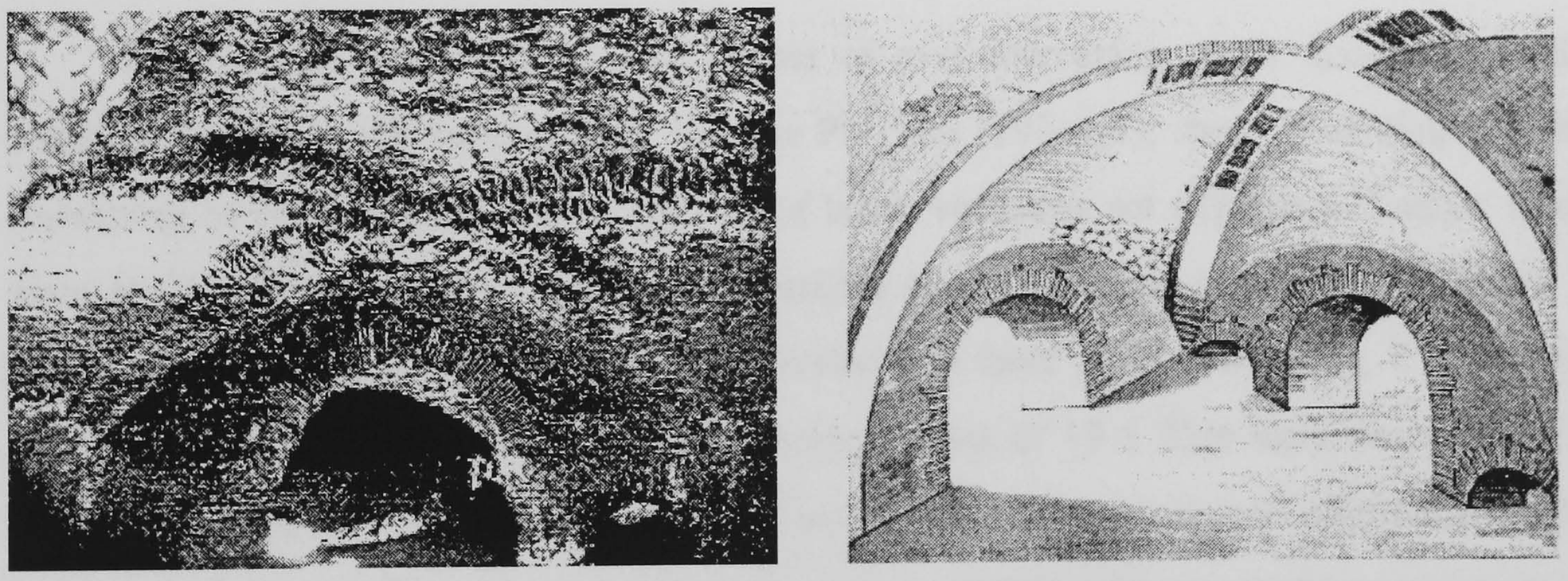

FIGURE 1.10 Ribbed cross vault from the *Villa di Sette Bassi* (Rivoira 1925).

After the building diversity of the times of Hadrian (117-138) and a preference for more Eastern forms (see the domes and vaults of audacious plasticity in the Small Baths of his Villa Tiburtina), cross vaults become widely spread, successfully incorporating all the existing vaulting techniques. The first, probably, visible ribs appear at the *Villa di Sette Bassi* in Rome (123-134), at a vault in the ground floor (Fig. 1.10) spanning over 7.60m.

The groins are reinforced by arches 650mm wide, composed of two outer lines of bricks (Rivoira 1925), but they form an organic whole, as they are not conceived as an independent centering. This detail is not found in rooms of shorter spans and the reason would be that ribs would help the vault support a reservoir on the above floor.

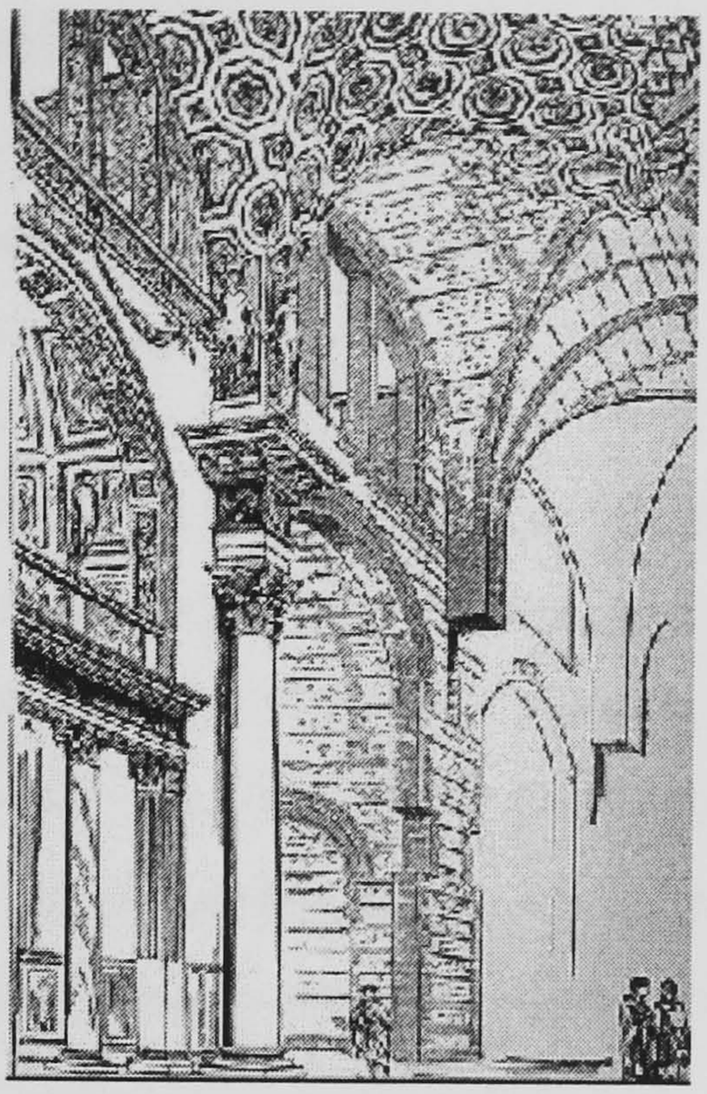

FIGURE 1.11 The central hall of the Thermae of Caracalla in Rome

Cross vaults were used to roof spaces of ever increasing spans. Examples at the Imperial Palace on the Palatine Hill, like the Pulvinar (193-211), show stout diagonal ribs consisting of three parallel chains formed of brick voussoirs set edgeways. Longer spans were reached in later stages. The central basilica of the Thermae of Caracalla (started in 212) measured 58 x 24m in plan and was divided into three groin vaults (Fig. 1.11). In the case of the Thermae of Diocletian (305) compartments of 19 x 23m were covered in the central hall. The weak semi-elliptical groins would not reduce the thrusts efficiently, so the masons had to develop a set of raking buttresses, lightened by a communication-arch, creating in this manner for the first time a dynamic equilibrium of thrusts and counter-thrusts that would be found again later in the Gothic period. Even larger spans would be covered in the later *Basilica Nova* of Maxentius (312) but the decay and collapse of the Roman Empire shortly afterwards in the West would interrupt further applications of these achievements.

In the greater Roman Empire, vaults were not attempted on the same scale as in Rome and brick was used mostly instead of concrete. These brick vaults were much more uniform in thickness, with weighting added around the foot at a later stage of construction. The massive character of the classic Roman vault and the construction process by horizontal layers reduces consistently the effect of shell action and guarantees the line of thrust is always contained within the thickness. This, from the other hand, would increase the thrust exerted, but the Roman architects resolved the problem by adding either massive buttresses or an articulated system of semi domes that introduced counter-thrusts (like in the so-called Temple of Minerva Medica in Rome).

The typology survived at the Eastern Roman Empire (Byzantium) in Christian buildings that were usually of a much smaller scale and the tradition of concrete groin vaulting is still in use in Greece and SE Europe. In Western Europe, however, only when social order was restored after 800 AD, through the establishment of new political (Milan, Aachen) and religious centres (shrines, abbeys), did the need and technical capacity for such kinds of roofing over buildings of monumental scale come back to surface.

1.3.2 Rib vaults

Roman vaulting techniques were taken up to a great degree in the eleventh century when many vaults, made of bricks, were constructed in Lombardy (Porter 1911). The earlier disadvantage of the more flat diagonal junctions, however, became more evident and the masons used again the form of domical vaults. Arch rings of rectangular section had already been employed to transversally brace Romanesque banded barrel vaults and now they were used as ribs to further reinforce the groins, as the nave of S. Ambrogio in Milan shows.

FIGURE 1.12 The joint between the webs along the groin (Melrose Abbey)

This typology did not have a great diffusion in Europe but it was certainly an exercise in the use of elements like the rib that would bring real progress later on. The masons had to make the best use of the restricted labour force and material resources, so vaults could not be designed on the scale of the Roman ruins they tried to copy. The diagonal junction proved to be an area of weakness (Fig. 1.12), both during construction and under load, so an immediate solution was to lay the vaults over oblong and not square bays (Fitchen 1961).

The difference in span between the diagonal and the long side was now reduced but in this manner the groin was twisted and was not contained any more into a vertical plane, as happened in the Madeleine, at Vézelay. Moreover, a difference in height was caused between the groins and the sides that would obstruct the visual continuity of the nave. Pointed transverse arches were the solution as their height could be fixed according to needs and they were introduced for the first time at the nave of Durham Cathedral (1093-1133). In this manner, it was possible to avoid the complexities of previous solutions to the problem like stilting or skewed panels.

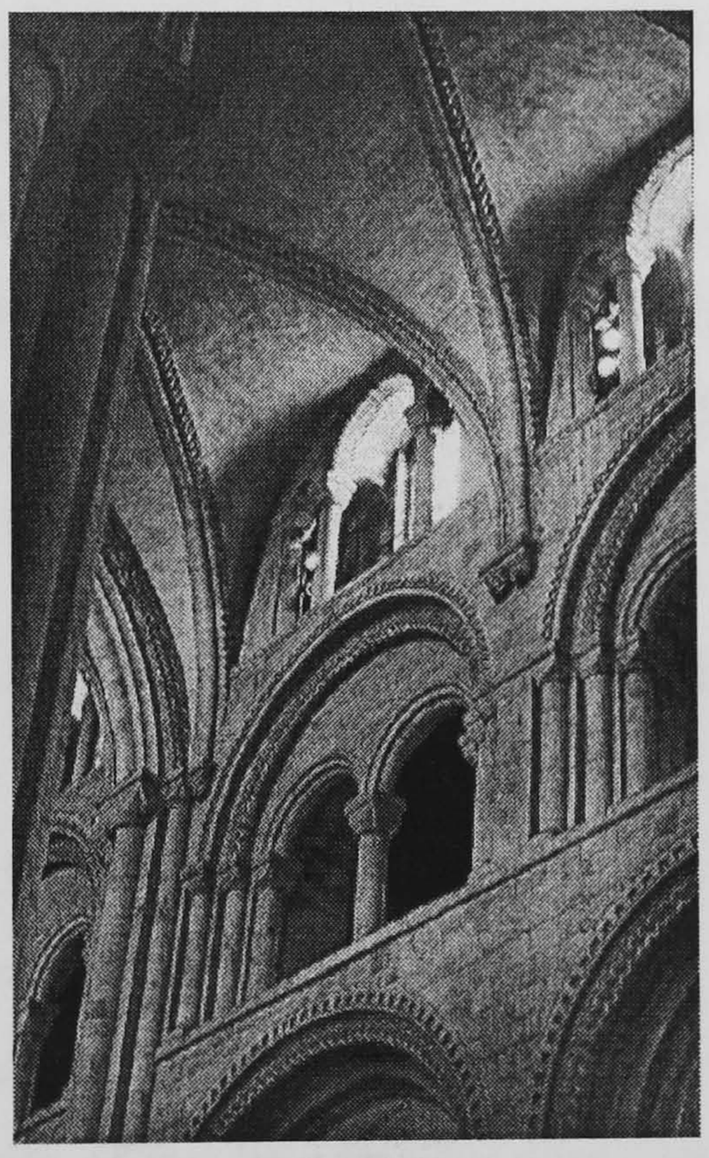

FIGURE 1.13 The form by which the groins were emphasised at the rib vaults of Durham Cathedral

Durham Cathedral displays also for the first time ribs in the form that would be used in later stages (Fig. 1.13). Although they would be useful in correcting irregularities along the groins, as those at Vézelay, their role was initially aesthetic. Being the product of a

linear emphasis in design, they were necessary to highlight and decorate the angles of the structure, acting as an extension of the engaged shafts of the piers and recent studies (James 1991) showed that they were not conceived as a separate permanent centering.

Between 1130 and 1180, the main elements of the Gothic vocabulary (ribs, webs, engaged piers, lateral elevation etc.) were developed in North France as parts of the new unified approach to roofing and division of interior space that characterises Gothic (Grodecki 1986). In their essence, Gothic structures were conceived as frameworks of arches organised into coherent systems, reducing the structural functions of walls to a minimum. In St Denis Abbey (1130-1144), the decisive step was taken in this direction to open two large windows in each of the radiating chapels of the apse and underline therefore the importance of natural light in the overall design. Ribs were used throughout the whole ambulatory, creating a unified and structurally articulated space, whose lightness was further underlined by the supporting slender columns.

The windows, however, under the vaults of the higher Notre-Dame in Paris (1163-1182) were relatively smaller. Although the walls were already thinner, the masons were not completely certain about their stability, further securing the nave with one of the first sets of flying buttresses. The whole building, and the aisle vaults specifically, were made of ashlar masonry of good quality, with noticeable joints and oblong blocks, probably in response to the difficult junction at the groins. These vaults are supported upon heavy cylindrical piers 6.5m high, covering a square compartment of 6.5m, and their profile is clearly pointed.

The scale of cathedrals was constantly increasing so the interest in vault construction was focused on the reduction and containment of their thrusts. In the Cathedral of Chartres (1194-1220) the beginning of the classic High Gothic is marked, as the merger of all the structural elements under a single context is complete (Fig. 1.8b). The masonry is solid, with carefully squared blocks, and in conjunction with the linearity of the interior configuration, the spatial limits of the structure become clear, giving the impression of a skeletal frame (Grodecki 1986). As a result, the ribs were extended to the engaged shafts of the pies and, since this resembles a centering system, it is an indication that the masons were more aware of the benefit of using the ribs as such in a permanent manner.

The increasing scale of the buildings would cause higher thrusts, so massive flying buttresses were an immediate solution (Fig. 1.8b) and continuous experimentation would lead to extreme refinements. The quest for better-lit spaces resulted in further enlargement of the windows, with the pier extension being constantly thinned down. The ideal of the scheme was attained in the complete transparency of the Sainte Chapelle in Paris (1240), while structural and stylistic balance between all the elements was achieved at Soissons and, even better, at the nave of Amiens Cathedral in the 1230s (Murray 1996). Here the masses are correctly distributed, with the weaker lateral wall thickened and longitudinally braced at the rear of the triforium with embedded arches. Responds and engaged shafts adequately reinforce the piers that support the aisle vaults at a height of 14.6m, while the latter span over a compartment of 8.80 x 7.44m. A typical bay of the nave has a plan of 14.66 x 7.44m, reaching a height of 42.3m (Fig. 1.4). The effectiveness of the supports (buttresses and piers) and the slightly domed profile of their vertices allow a minimal thickness of the vaults at 20 cm.

Exceeding these limits, however, would have disastrous consequences, as the collapse of Beauvais in 1284 demonstrated. Extreme spans were reached at the bays of the nave (15.30x9.05 m) and the aisles (7.90x7.90 m) that would enhance the effect of any error, like the misplaced flying buttress upright at the middle of the south side of the choir (Murray 1989). The precarious state of the unfinished cathedral (Taupin 1993) may have favoured the exploration of the alternative and more balanced disposition of volumes and windows of the Bourges Cathedral (c. 1190-1275): the height decreases gradually between the nave and the two aisles (Fig. 1.8a), so the piers are better braced and less prone to buckling. More pointed aisle vaults and a complete set of thin flying buttresses contribute further to the stability. Although many of the classic Gothic churches adopted the pattern of Chartres (Fig. 1.8b), the tendencies after Beauvais were towards hall churches, where nave and aisles have a similar height and they mutually eliminate their lateral thrusts with the help of moderate buttresses, following the principle established in the Bourges model.

Similar developments occurred at a different pace in Britain. Political links with Normandy and Brittany favoured initially the diffusion of technical features from those areas, like domical vaults (§1.3.1). Elements like the rib vaults in Durham (1093) were highly innovative (Fig. 1.13) but the rest of the structure was not purposely designed to contain the reduced thrusts and remained heavy. Genuine Gothic design concept appeared

for the first time in Britain at the rebuilding of the east end of Canterbury Cathedral (1175-1185). A sexpartite vaulting system, inspired by Notre Dame in Paris, was used over long spans in the nave, allowing for more concentrated supports and more light.

FIGURE 1.14 The nave of Lincoln Minster (Clifton 1986)

An important example of Early English Gothic is found in Lincoln Minster: building started in 1192 and the nave vaults are quadripartite, characterised by a rib running along the whole longitudinal axis (ridge-rib), while the webs are further subdivided by the earliest found tierceron ribs, a pattern due probably to the origin of many master masons from carpenters (Fig. 1.14). The aisle vaults were plain quadripartite and lime-washed in the early stages, but they received also tiercerons later, as for example in the Angel Choir (1256-80). Despite the added ribs, the structure remains in essence a quadripartite vault and it is built with well-shaped ashlars, which become thinner closer to the vertex. In Chapter 3 it will be seen how Lincoln has influenced Holyrood Abbey.

During the same period, much simpler quadripartite vaults were created in Salisbury Cathedral (1220-84). The richly moulded nave arches are clearly pointed and carry effectively the elevation wall upon the cylindrical piers. The arrangement emphasises the prevalence of the longitudinal axis in the structural behaviour of the building, something that can also be verified at the modest system of flying buttresses arresting the nave thrusts

(as in Lincoln). Tierceron-ribbed vaults dominated by that time the important ecclesiastical buildings, like Westminster Abbey (1245-69), that were built. A wider use of the bar tracery in the windows and a more complete system of flying buttresses permitted lighter supporting walls and piers. However, it was the pattern of the vaults in Lincoln that would prevail in this phase until, later in the Decorated style, fan vaults would adopt a completely new structural scheme.

1.3.3 Later developments

As seen earlier, many of the elements considered to characterise Gothic (like ribs, pointed arches etc.) were already known before the establishment of the style. Their integration to the new structural vocabulary of Gothic, however, was the result of the change in attitude towards a mainly visual unity of the building (Grodecki 1986, Stalley 1999). On the other hand, in the initial Gothic period the design of the building did not explicitly develop around the technical advantages from the use of these elements. A possible explanation was that the manner in which this new vocabulary was applied had its origins in the wooden constructions and high-skilled joinery practised by the Normans, to whom one of the major trends in Romanesque and Gothic architecture is attributed (Acland 1972). Matters of safe construction and structural performance would be then implicitly linked with the proportions and visual aspects of the building. This may explain why even later any theory that would be formulated by the masons and codified in the few existing treatises (Sanabria 1982, Benvenuto 1990) would focus mainly on the form.

After the structural scheme had settled in Europe by the beginning of the 14th century (due to political as well as technical reasons), the development would focus on specific elements. The importance of the rib in the visual integration and construction sequence of the vault would be enhanced and eventually, during the Flamboyant period (after 1375), Gothic moved beyond the balance between structure and form achieved earlier. The thin vaults, which characterised High Gothic, were transformed to a skin over an elaborate network of ribs (as happened in Germany) or assumed other non-conventional forms (like fan vaults). Alongside this alteration of the concept and the later invasion of Renaissance types like domes and lunetted vaults, many of the specific techniques developed for the successful construction of cross vaults were lost (although to a lesser degree in Britain). A side effect of this was that maintenance became difficult and the delicate equilibrium of the

thrusts would be severely disturbed in many cases, making evident the weaknesses of the system. The associated pathology is outlined in the next section.

1.4 FREQUENT DEFECTS AND THEIR CAUSES

1.4.1 The effect of various loadings

An attempt is made here to comment on the loadings that usually act upon Gothic buildings (in particular the static actions) and to understand how they are transmitted to the vaults. Moreover, the effect of some types of dynamic loads could be simplified with a quasi-static approach and provide useful insight on the damage due to the instability of the structures.

1.4.1.1 Dead and imposed loads

The weight of the structure as it was applied gradually during construction was the main loading for the master masons. The density of the stone can be considered as the unit value of this weight and this is 20-26 kN/m^3 for sandstone, 21 kN/m^3 for limestone and 11-23 kN/m^3 for tufa. Marble (weight 27 kN/m^3) is much less available in central Europe and Britain and, due to its cost, it was used mainly for decorative elements or cladding (cf. the use of Purbeck stone in Lincoln).

Wind, snow and ice are the most important imposed loads on these structures. The roofing system has been usually inaccessible to the public, so no crowd loads were considered. Loose debris (of low density) left over from past interventions can accumulate over the vaults, but in static conditions does not represent a danger. Where snow loads are significant, pitched roofs of a very high rise were built on top of the vaults (a feature quite common in northern France), but when this was not very usual, the vaults could even be left exposed, as in Seville Cathedral (Acland 1972). If the roof is properly braced, the snow load is transferred into the lateral walls as a purely vertical force and subsequently follows the usual path to the ground.

Wind can have quite serious effects. High-rise pitched roofs and the exposed surface of the walls can be subjected to very high and asymmetric pressures. The lateral walls may

be forced out of plumb if bracing is insufficient, causing the weight of the nave to be transmitted eccentrically over the piers. Moreover, resonance due to vortex shedding around the complex geometry of the buttressing system (Fig. 1.2) can yield very complicated dynamic loads.

1.4.1.2 Other loadings

Central Europe and Britain are zones of low seismic risk. In southern Europe, where earthquakes are more frequent, the religious buildings have quite solid elements and closely-spanned piers or, where larger volumes were required, they follow the "hall church" pattern, where aisles and naves of similar height abut each other (cf. the pattern of Bourges in Fig. 1.8a). The seismic action between the vaults and the ground can be amplified up to three times (Croci 1998c) and, despite the inherent flexibility of the vaults, high deformations resulting from such accelerations may oppose to the recovery of their form, causing change of curvature and eventually collapse. Other dynamic loads however, like traffic vibrations, are more likely, especially in modern cities.

As an elementary modelling, the seismic action can be resolved to horizontal loads in two orthogonal directions. The facade and the apse brace the structure effectively along the axis (§1.2.2), so it is the transverse resultant that causes the most serious distortions. Consequently, this dynamic lateral force can have an effect similar to that of thrusts insufficiently contained by the buttressing system, which in this project were simulated as a movement of the lower supports.

Stresses can also be generated due to the difference in temperature between the exterior of the building and its warmer interior, causing a differential thermal expansion between the two faces of the wall (Martínez 2000). Low external temperatures can in addition lead to the crystallisation of salts within the pores of the stone, with their subsequent volume increase resulting to micro-fissures. The way the whole structure reacts however to these actions is very specific for each building and their effect is not fully studied from the point of view of overall stress regime (Scherer 1999).

Other sources of failure include accidental loadings like shelling during warfare (Soissons and Noyon cathedrals), sharp changes in the water table (York Minster) etc. Shell

fire damages on the upper structure can have an immediate effect to the rest of the structure as a sudden loss of equilibrium of the lateral wall (Allemands 1919, Gilman 1920).

As a conclusion, the study of the structural behaviour of the cross vault under self weight and movement of the abutments, which constitutes the main topic of this thesis, covers a wide area of the normally expected loads during the life of these buildings. Moreover, the results from these cases can provide useful suggestions for the rest of the actions mentioned above, when it is possible to resolve them into sets of more simple forces.

1.4.2 The most frequent types of pathology

Cross vaults can in theory resist quite high values of dead loads. This is, however, subject to a properly designed system of support, a good state of the fabric and absence of unpredictable incidents, like inappropriate interventions. Holyrood Abbey Church collapsed due to the side effects of a very high load placed over the inadequately braced high vaults (NAS E310/1/2) (see §3.3.4.3). St. Francis in Assisi was damaged by the irrecoverable displacement of the excessive spandrel fill (Croci 1998a, b). Many mediaeval Abbeys in Britain (Melrose, Fountains) degraded very quickly when the roof was removed and the natural elements eroded the fabric.

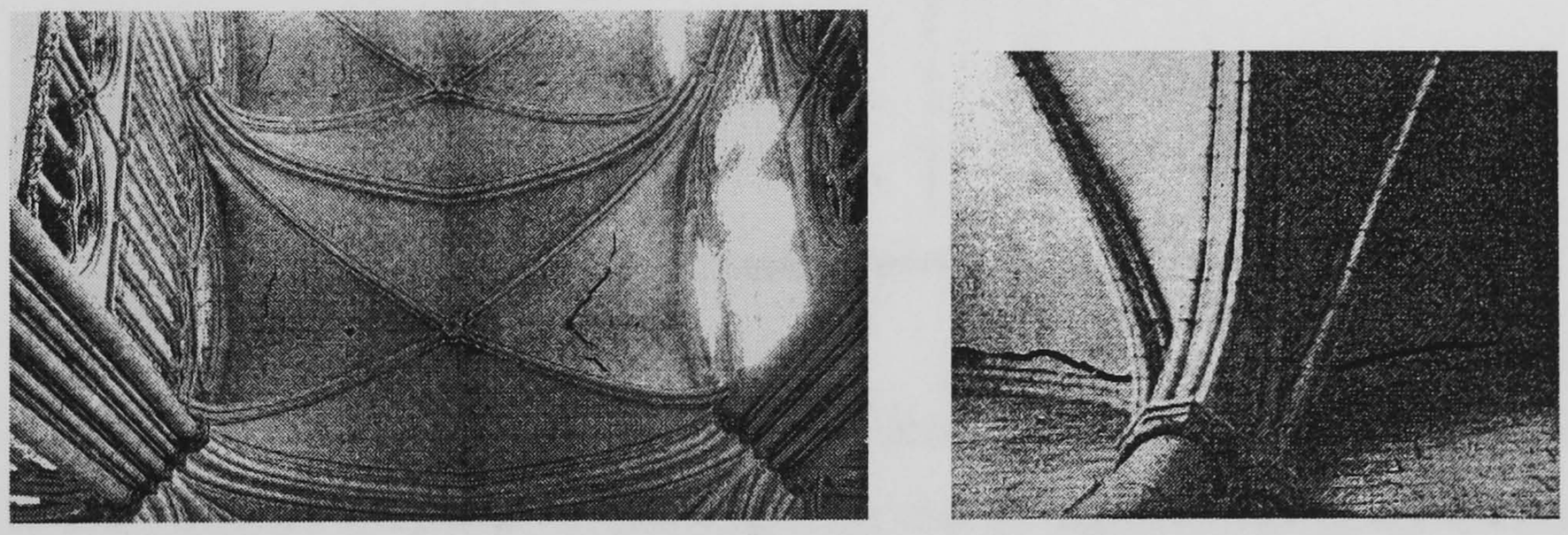

(a) Amiens Cathedral - Nave (Murray 1996) (b) Vitoria Cathedral (Croci 1995)

FIGURE 1.15 Typical crack patterns

Equally crucial is the effect of ground movement or weak foundations, causing differential settlement of the supports, as it happened in York Minster (Beckmann 1994) for example. Inadequate design can also compromise the ability of the masonry to accommodate large deformations: in the case of the choir in Amiens (Fig. 1.15a), the high

vaults have suffered cracks parallel to the walls as a result of the insufficient open-work flying buttresses erected in later stages (Murray 1996).

The aisle vaults are structurally less demanding but they are usually subjected to secondary effects from the deformations of the piers, therefore the containment of the trusts of the nave is crucial here too. Distorted piers, especially around the haunches, are quite frequent in Gothic structures. Flying buttresses were not widely employed at the early stages (Fitchen 1961) and in many cases they were added later, once the piers had bowed extensively, "freezing" the distortions, as it happened in Vitoria Cathedral in Spain (Croci 1995).

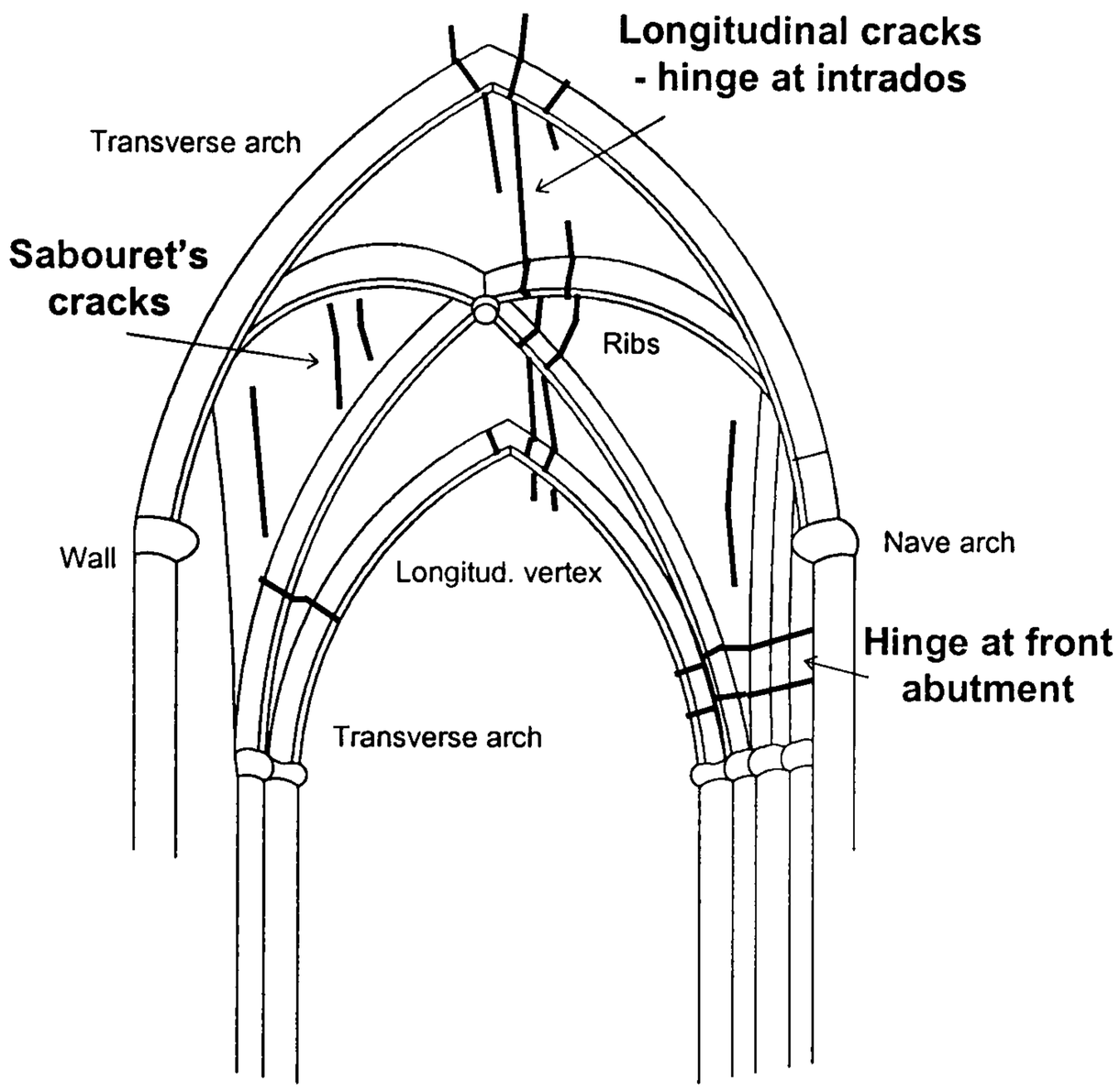

FIGURE 1.16 Summary of crack patterns in an aisle cross vault

In theory, an aisle vault is adequately contained between two strong areas: the nave arch, stabilised by the weight of the pier extension and the upper structure, and the external wall. The groins' role, especially when reinforced with ribs, is important in reducing the deflections. If the nave arch becomes distorted, the maximum deflection would shift in the direction of the nave for an amount dependent on this arch's stiffness. Fig. 1.16 shows a typical damage pattern for pointed aisle vaults with straight vertices. The development of a one-way behaviour in the transverse direction becomes evident from the manner in which the cracks spread parallel to the two stronger supports (the wall and the nave arch). The most important cracks appear close to the longitudinal vertex at the intrados (associated

with the maximum deflections), sometimes on both its sides. They are caused by bending stresses and they are expected to generate high compressive forces at the extrados that may lead to crushing of the stone and transformation of the area into a (plastic) hinge line. The geometry and quality of work of the vertex and the condition of the materials influence the extent to which these hinges may propagate over larger areas.

The next crucial area for the safety of the vault are the extrados of the wall and the nave arch, where a complete detachment of the fabric can occur (the faults at the nave arch are also known as Sabouret's cracks (Abraham 1934)). These cracks can further spread towards the haunches, separating the stiffer area of the *tas-de-charge* from the rest (cf. Fig. 1.5). Once a section of shell had cracked normally or parallel to the bed joints, it is isolated and virtually transformed into an arch with a thickness probably insufficient to contain its own line of thrust. This has lead many researchers to formulate the limit state of the vault by segmenting the barrels into a series of finite arches (see later discussion in §6.4).

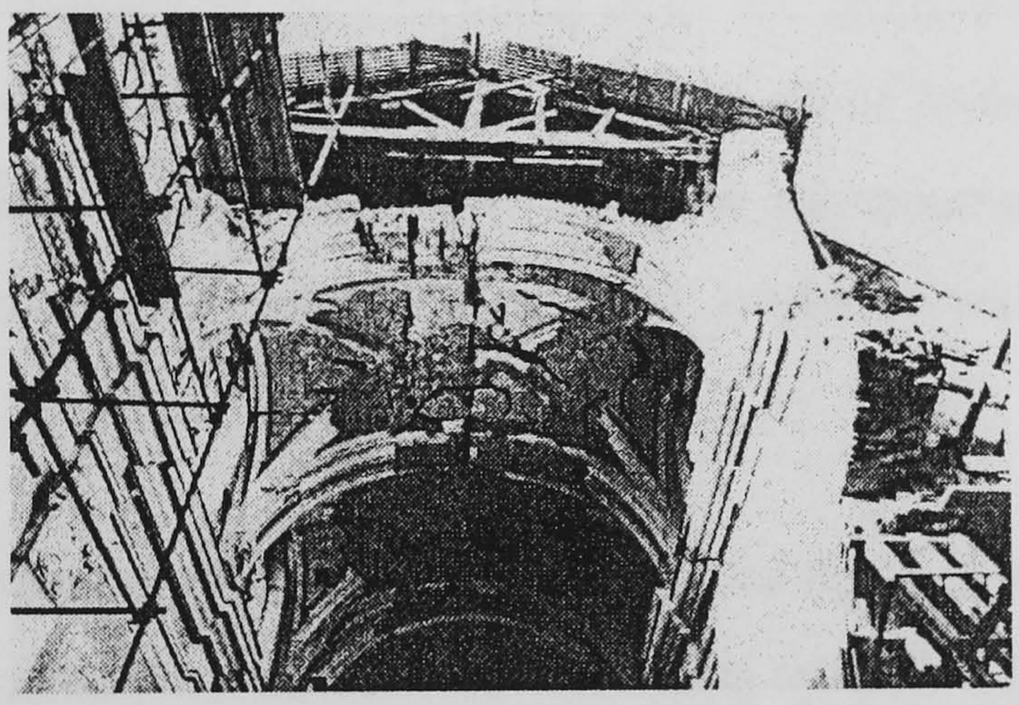

FIGURE 1.17 Crack pattern at the nave of Sant'Angelo dei Lombardi Cathedral (Giuffré 1988)

These cracks can be seen at the high vaults of Amiens (Fig. 1.15a) and along the lateral wall of Vitoria Cathedral (Fig. 1.15b), the former being probably the result of insufficient buttressing, despite a generally good state of conservation. In addition to these examples, the collapse of the Cathedral of Sant'Angelo dei Lombardi after the 1980 earthquake of Irpinia (Fig. 1.17) illustrates the similarity of the damage pattern caused by the transverse component of the seismic action to that of the imposed deformations studied here (Giuffré 1988).

A greater confidence in construction as the Gothic style progressed made possible a continuous reduction of the thickness of the vaults, while the spans kept increasing, but this

meant the line of thrust could more easily burst out of the safe middle third (Heyman 1995). From 40 cm in St Denis, it went down to 25 cm in Noyon, to 20 cm in Amiens and even to 11 cm at the fan vaults of King's College Chapel in Cambridge (Fitchen 1961). It became essential therefore to pay particular attention to the supporting conditions, so buttresses went through a great degree of experimentation and their maintenance was later a constant matter of preoccupation (Mark 1982). By reducing, strengthening or even suppressing the weaker triforium, the pier extension became even more stable and, eventually, accidents, warfare and insufficient maintenance would be left as the main reasons of failure.

1.5 SUMMARY AND CONCLUSIONS

The examination of the evolution of cross vaults showed a tendency for constant improvement from the Roman until the late Gothic period, when increasing spans in buildings like churches had to be roofed efficiently, safely and at a low cost. The design of cross vaults had been successful and resulted from an understanding of the structural behaviour of the form, cross-experimentation with a variety of building techniques and the necessity to optimise the available resources. With the improvements in this process, the thickness of the vaults was refined and a stylistic emphasis was placed on the linear elements of the system, like ribs.

A fundamental aspect of the structural behaviour of this scheme was the containment of their lateral thrusts, usually by means of a buttressing system. Although cross vaults can carry high amounts of dead load and they require a minimum maintenance programme, their performance is very sensitive to any imposed geometric alterations. Failure of the buttresses or even small displacements of their supports can initiate the widely observed crack pattern of longitudinal cracks at the intrados of the vertex and the extrados of the lateral edges. As a consequence, dead load and movement of the abutments are the most important actions upon these vaults and a variety of structural loadings can be studied as a combination of these actions. In the next chapter, an overview of the actual scientific research in the field is presented, alongside with a discussion on some assumptions regarding design problems faced by the original masons.

1.6 OUTLINE OF THE THESIS

The structure of this thesis is organised as follows:

In Chapter 2, a survey of the existing literature is presented and the actual state of research concerning the structural behaviour of cross vaults is reported in more detail.

In Chapter 3, the preparation of an experimental model vault that represents one of the remaining vaults at the collapsed church of the Holyrood Abbey in Edinburgh is dealt with. Also, an account is given on the collapse of the prototype structure and the construction of the model vault.

In Chapter 4, the set-up of the experimental programme is presented. Wallette tests were performed to assess the properties of the materials used and the placement of the instrumentation was assisted by a preliminary Finite Element (FE) analysis of the model vault under dead load. The failure criterion that was adopted and its implementation to the FE program are also discussed.

In Chapter 5, the series of tests that were performed under dead load and their results are presented and discussed. The behaviour of the model vault was assessed with a FE model, which was further refined with a more detailed simulation of some important geometric and experimental features of the test.

In Chapter 6, the testing of the structure until failure due to the movement of abutments is presented and the behaviour of the vault is discussed. The experimental results were further interpreted with the FE model following a smeared crack approach. A theoretical investigation of the ultimate limit state of the structure was also carried out.

In Chapter 7, a summary of the present project and the main findings are presented. Practical suggestions for further research are also discussed.

Chapter 2

LITERATURE SURVEY

2.1 INTRODUCTION

Up to the present, there has been very limited experimental research carried out into the behaviour of masonry cross and barrel vaults in general. However, the wider range of tests on arch bridges can give a useful insight to some of the experimental and analytical problems associated with vaults. This review discusses all the published studies on cross vaults.

In addition to these experimental works, several existing buildings have been monitored and their behaviour was subsequently evaluated analytically, as is discussed in §2.3. Moreover, some of the design rules employed by the original masons have been used today to evaluate the strength of some monuments and they are briefly presented in §2.4.

2.2 PREVIOUS EXPERIMENTAL WORK

2.2.1 Work of R. Mark and J. F. Abel

In an attempt to investigate the structural function of ribs in cross vaults, Mark and Abel tested in 1973 a photoelastic model in 1/50-scale representing two bays of the quadripartite choir vaults at Cologne Cathedral (Mark et al. 1973). As the geometry of the vault shows (Fig. 2.1), the proportions in plan are 1:2, the intersecting barrels are pointed, with curved vertices and a constant thickness throughout, and no ribs stiffen the groins. The haunches were filled with "rubble" up to 2/3 of the height and, in order to simulate the effect of the buttressing system, the abutments were considered as fixed.

The model was constructed from stress-free, cast epoxy plastic. After it was loaded, it was observed in a polariscope to determine first the overall stress pattern and then, after slices were taken, the distribution of loads in the cross sections, using scaling theory to

transfer the results to the prototype. The test showed that highly localised compressive stress (corresponding to 2.8 N/mm^2 in the prototype) developed only close to the springings and they could be probably reduced if ribs were employed. Bending moments were low, causing negligible tensile stresses, and the compressive stresses followed trajectories directed towards the supports and not the groins.

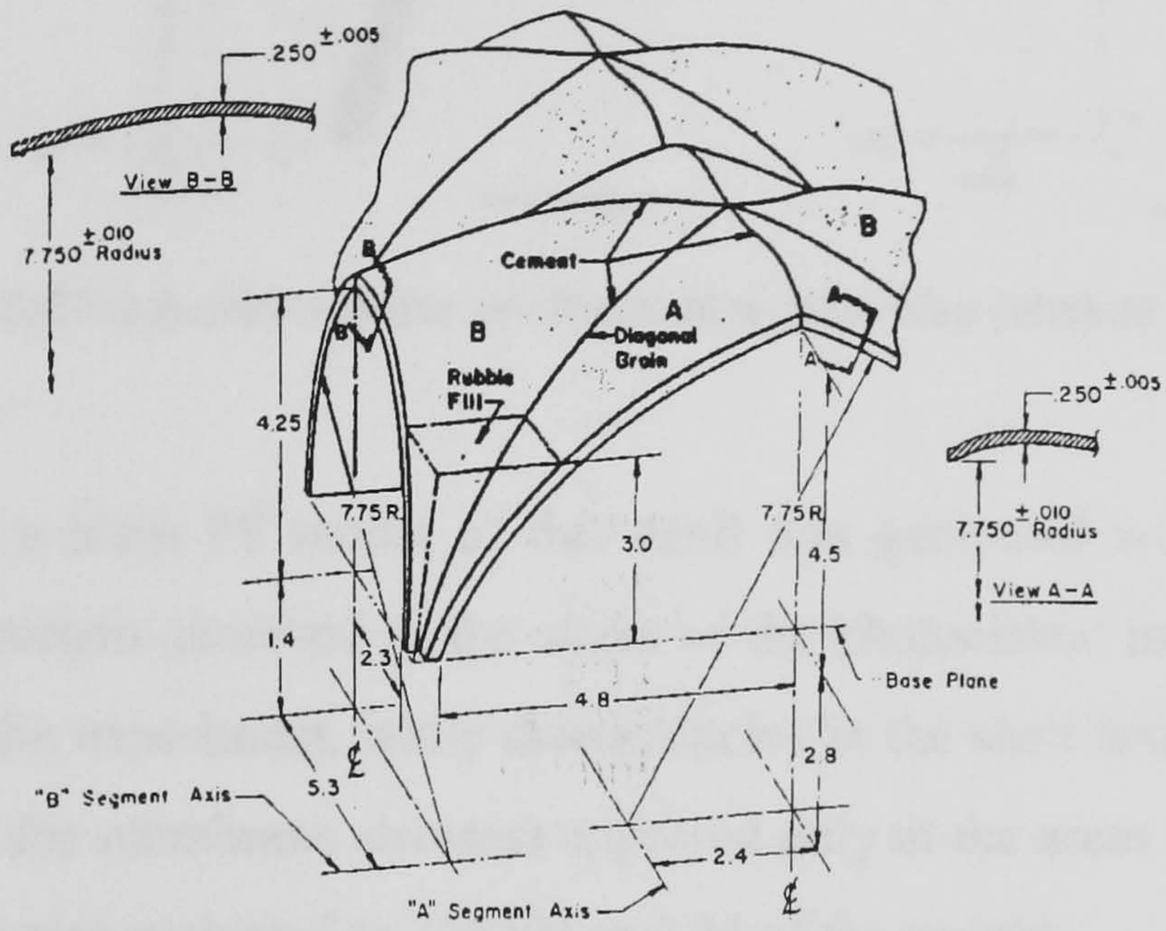

FIGURE 2.1 Model geometry of the vault in the experiments by R. Mark (units in inches) (Mark et al 1973)

In order to evaluate the thrust exerted upon the lateral supports, the base plates were moved horizontally by 0.25 in. (6.4 mm or 1/19 of the span) and deflections were measured with dial gauges at various critical points. The maximum value of 0.106in. (2.69 mm) was recorded close to the keystone. Using the Müller-Breslau principle (Hetenyi 1950), that correlates the horizontal reaction to horizontal and vertical displacements, the thrust of the prototype was found to be 240 kN.

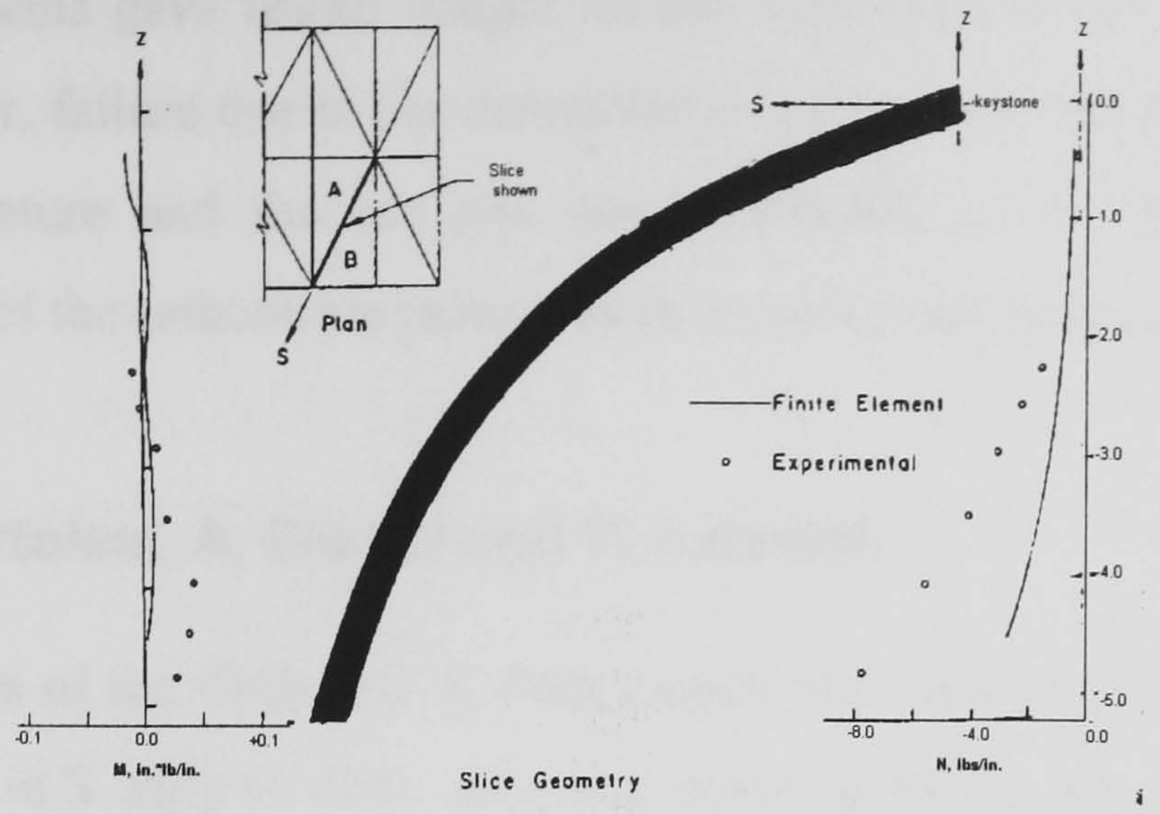

FIGURE 2.2 Vault model stress resultants at a groin slice (Mark et al 1973)

Subsequently, a plain FE model of this vault was generated and the stresses were compared with the pattern observed in the slices of the photoelastic model. Overall, these results agreed with the experiment, while discrepancies in the shell bending moments (and to a lesser degree in the membrane stresses) appeared only at the areas near the boundaries (Fig. 2.2). The thrust was evaluated to 250 kN or 0.34 of the weight.

Using this pattern as the base, further plain FE models were formed to study the effects from the presence of ribs and variations in geometry (Mark 1982). For all the possible combinations, the vault was almost everywhere under low compression, of the order of 10 lb/in^2 (0.07 N/mm^2). In the area of the springings (*tas-de-charge*) however, the compressive stress increased sharply to 250 lb/in^2 (1.75 N/mm^2) but, in the places were ribs were added, these stresses were reduced to 70 lb/in^2 (0.5 N/mm^2). Tensile stress developed in few areas in the ribs but it was only about 0.05 N/mm^2.

Overall, the level of compressive stress was below the strength of stone masonry and within the values expected. Small changes in vault geometry did not alter significantly this pattern and the same result was observed even when the double curvature of the shell was changed to single. As a result, the authors concluded that a simple singly-curved quadripartite model could provide valid information for a wide range of cases, while attention had to be paid on the numerical problems close to the bases. An interesting remark was that these vaults behave clearly as three-dimensional structures and the widespread assumption until then that they could be assimilated as a series of parallel arches was misleading.

These experiments gave useful insight on the behaviour of the geometric form of cross vaults. However, failure due to the movement of abutments was not studied until the collapse of the structure and the analysis was conducted in the linear elastic range. Moreover, the effect of the orthotropic properties of masonry was not examined.

2.2.2 Work of F. Ortolani, A. Giuffré and V. Ceradini

The nave vaults of the Cathedral of Sant'Angelo dei Lombardi collapsed during the earthquake of Irpinia in S. Italy in 1980. As it was shown in §1.4.2, the rapid changes of the geometry caused by the seismic action provoked three sets of longitudinal fracture lines, which can be identified in the remaining vaults close to the supports and along the axis of the nave (Fig. 1.17). The original lunetted cross vaults had intersecting barrels with a circular profile (Fig. 2.3), their groins were unribbed and the courses of the brick masonry followed a pattern that allowed them to be perpendicular to the end arches and the area of the intersection.

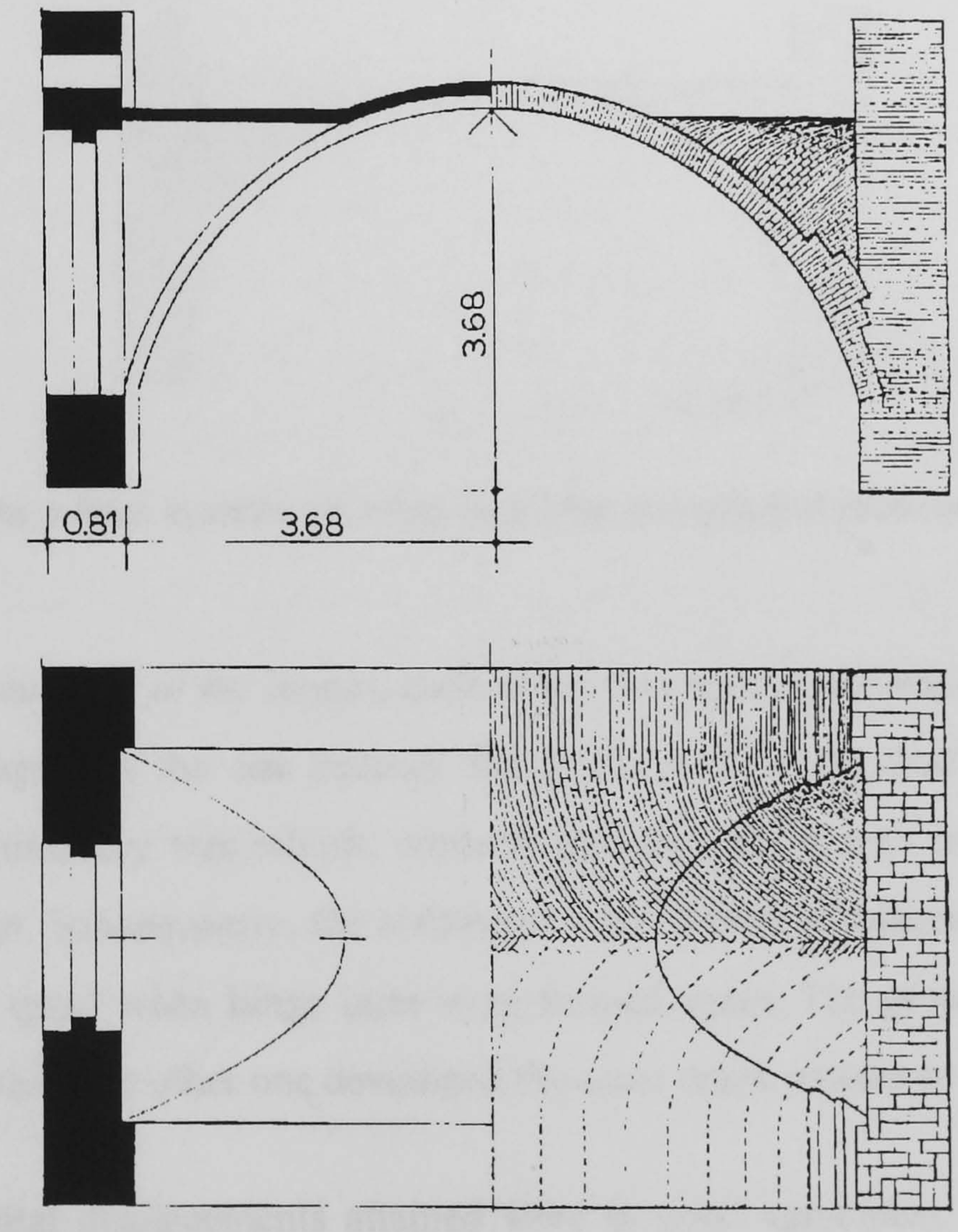

FIGURE 2.3 Vault model geometry (Ortolani 1988)

A model was constructed in full scale and it was tested to failure by progressive movement of the abutments, in order to simulate the seismic effect. The masonry pattern had to be slightly changed in order to improve the bond between the two barrels (Fig. 2.3) and it was preliminary defined by means of a small model in gypsum, which was used also to train the technicians involved in the project. In the first phase of the test, the supports were shifted outwards using hydraulic jacks until 180 mm (1/40 of the transverse span), when three hinge lines were created, one at the intrados along the longitudinal axis and two at the haunches at the extrados (Fig. 2.4).

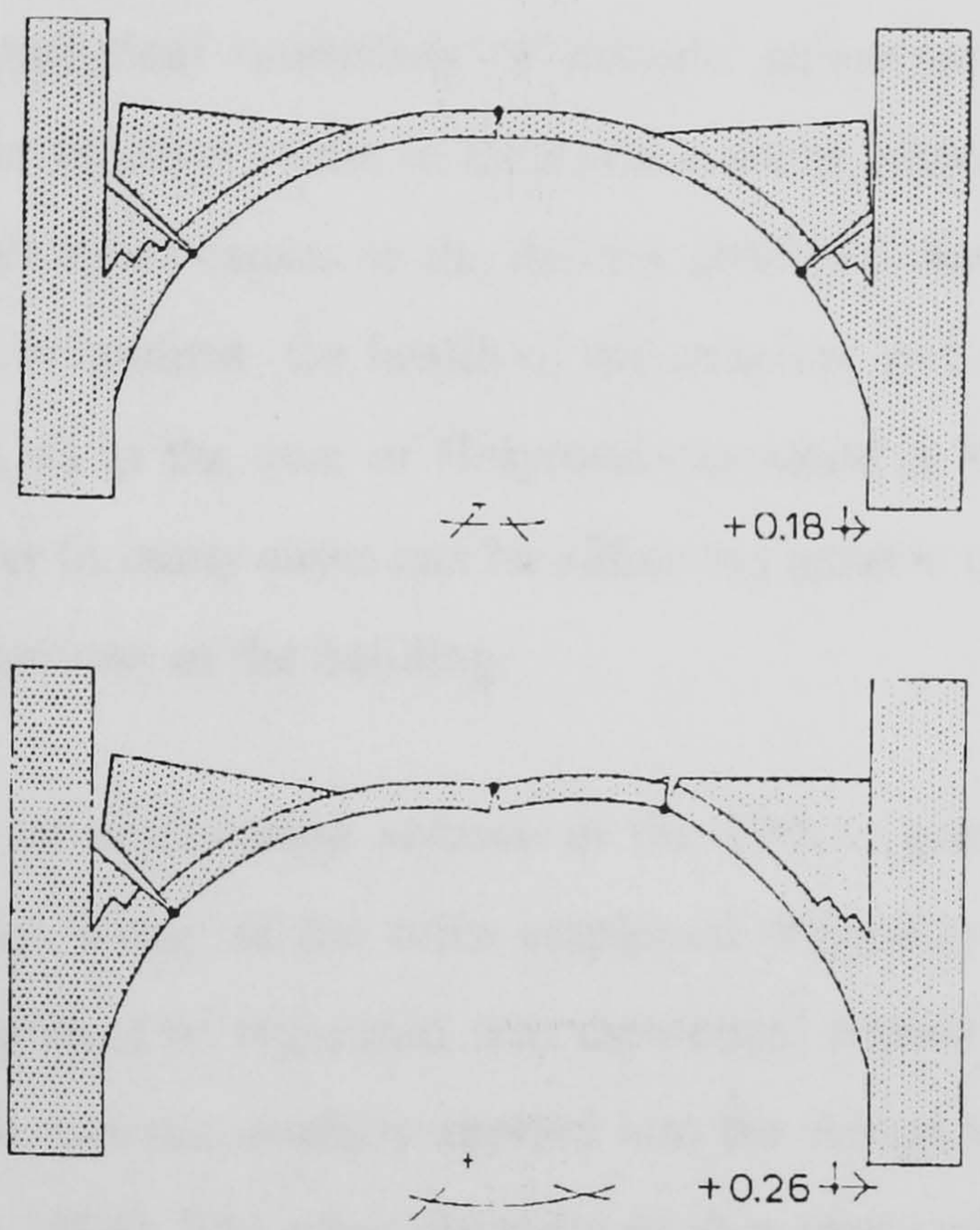

FIGURE 2.4 Crack pattern in brickwork cross vault after movement of abutments (Ortolani 1988)

After the formation of the hinges, each of the two parts of the vault was repaired with a different technique. In the one section, the bricks around the crack were completely removed and the masonry was rebuilt, while in the other the cracks were repaired with a high strength grout. Subsequently, the abutments were further displaced to reach a total of 260 mm (1/28 of span) when hinge lines were formed again. The grouted portion became rapidly unstable while the other one developed the same crack pattern as before.

The horizontal displacements attained were in good agreement with the long term defects usually encountered in churches whose geometry is already stabilised under their

own weight, as it was reported from the survey on Amiens Cathedral (Bilson 1906). Unfortunately these experimental results are very limited, as the authors did not record the development of strain or deflections in some critical points. Following the successful performance of this model, however, it was possible to reconstruct with confidence the vaults of the Cathedral. The range of abutments movement that was observed in this experiment is further discussed in §6.4.1.

2.3 CROSS VAULTS IN HISTORIC STRUCTURES

Monitoring and analytical modelling of historic structures has provided a useful insight into the behaviour of cross vaults in their real context, although it is not possible in all the cases to assign the exact causes to the defects observed. Surveys of the fabric have always been carried out to monitor the health of the structure and research in archives can be an invaluable source, as in the case of Holyrood examined in this project (see §3.3.4). This information however in many cases can be either too generic or not properly linked to the overall structural behaviour of the building.

The development of engineering science in the 19th c. promoted the definition of global structural schemes. Many of the rules employed originally by the Gothic builders were then either re-discovered or organised into theoretical frames like the Line of Thrust (see next section), which was successfully applied into the design of masonry arch bridges (Benvenuto 1990, Coste 1998). The great diversity of damaged vaults in France during the First World War (Gilman 1920) caused a debate over whether the rib had a functional or purely decorative role, since many vaults lost their ribs without collapsing completely. The reconstructions of several buildings however (Soissons) and later detailed studies (Fitchen 1961, Mark 1982) have re-instated the importance of the ribs in the resolution of the difficult intersection along the groin.

2.3.1 Work of J. Heyman and Ultimate Limit State analysis

A renewed interest for the structural analysis of historic vaults and monuments in general initiated in the 1960's when some new analytical techniques for modern structures started to emerge. The principles of plastic design, developed originally for steel frames, were applied by Heyman in 1966, considering the Gothic structure to be reduced into a

skeleton of stone. Assuming stone has no tensile strength and infinite compressive strength, and that sliding between blocks is not possible, failure in an arch is assumed to occur with the formation of hinges as stated by Coulomb. Developing the application by Kooharian of limit theorems to masonry arches (Kooharian 1953), the stability of the shell itself was investigated by considering each of the webs "sliced" into a series of parallel rings. The shell would be considered safe if a line of thrust could be found to be in equilibrium with the external loads and lying completely within the masonry.

Heyman then proceeded to calculate the thickness sufficient for a safe solution and the shell thrust, for semicircular and pointed profiles. These values were quite conservative, as it was assumed there was no interaction between adjacent rings and therefore no beneficiary effects from a shell action. If, however, the thrust was considered as reduced close to the crown, due to a shorter length of the rings, the resultant of the thrust at the base of the diagonal rib would have acted at a lower point, reducing the dimensions of the buttressing system (Heyman 1977).

These lines of investigation that disregard the shear resistance of the vaults along the longitudinal axis were followed by many other researchers. Stagnitto and Cauvin prepared a programme that verifies the stability of arches and sliced vault rings, translating the lines of thrust using vectorial algebra (Cauvin 1995). Lenza analysed masonry barrel and lunetted vaults with both the above method of arch models and membrane theory in order to establish the limits of variation of their behaviour (Lenza 1991). Studying separately each of the two intersecting barrels, a state of membrane compression was produced and the necessary boundary conditions were defined in such a manner that the stress resultants normal to the groin were composed into a force acting inside the groin's plane.

Despite these formulations being practical and conservative, using them out of context may result to underestimation of the bearing capacity of the ribs and excessive interventions. Moreover, they do not provide any information on the stress distribution or the deflection pattern before failure and, where the shell action is guaranteed, biaxial behaviour and material orthotropy are ignored.

2.3.2 Work of R. Mark

Concrete shell roofs were quite common during the 1960's and some of the tools used for their analysis were applied by R. Mark to historic structures (Mark 1982). The photoelastic experiments on cross vaults (§2.2.1) were correlated with FE models that showed good agreement at the vertices area and in a lesser degree close to the springings, a common problem in deep shells. Computational limitations of the period did not allow for a three-dimensional analysis of the shells in their structural context or a wider variation of crucial parameters (like thickness or orthotropic properties). As a result, transverse sections of the naves of some important cathedrals (Amiens, Beauvais, Palma) were tested with photoelastic models and then analysed as plane structures mainly under lateral wind loading. The modular method of gothic construction lends itself to this approach.

2.3.3 Work of G. Croci et al

Later developments in FE techniques allowed better simulations of the geometry and the material properties to be made. G. Croci has studied three-dimensional models for both entire buildings (Vitoria (Croci 1995), S. Francis in Assisi (Croci 1998b, c)) and single representative modules (Burgos (Theodossopoulos 1995), Vitoria (Sabbadini 1993, Croci 1995)). Under static conditions, the effect of applied structural load, the later addition of flying buttresses and different construction sequence was examined. This made it possible to understand the origin of the horizontal displacements at the springings of some vaults and the factors that may cause instability in the system.

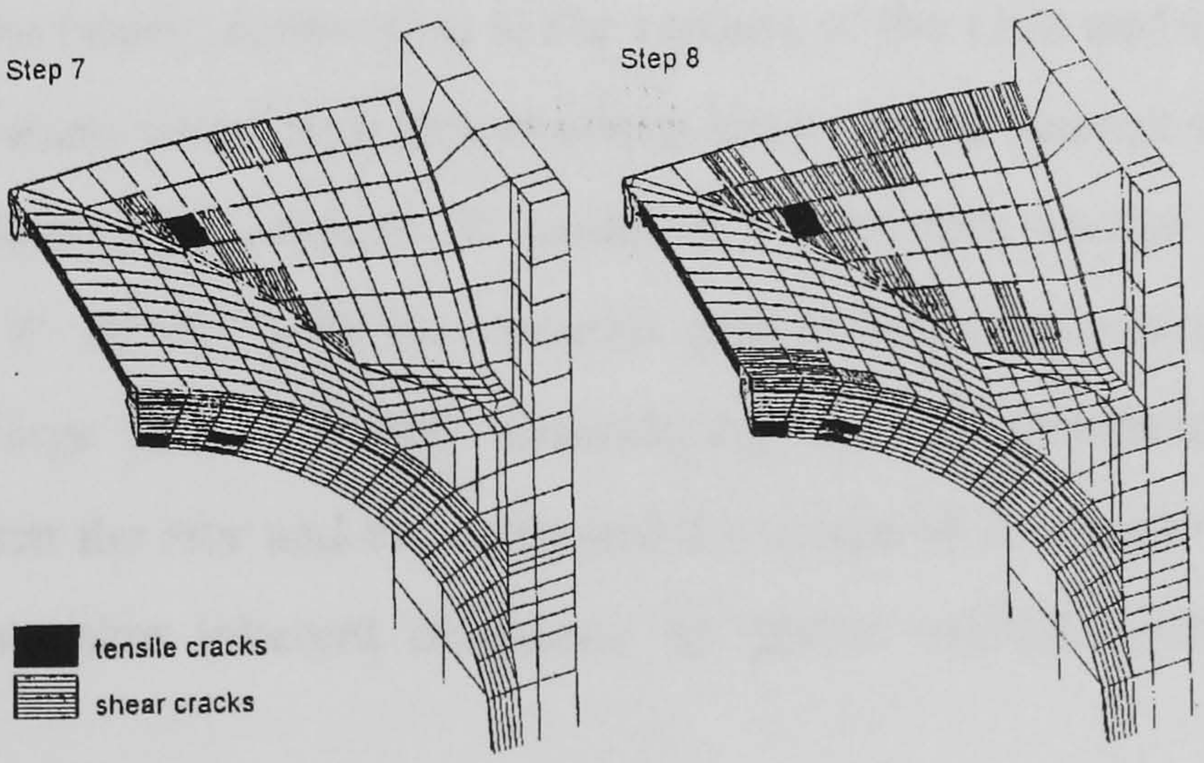

FIGURE 2.5 Development of cracks in a FE model during abutments movement (Croci 1995)

In this context, the nave vaults from Vitoria Cathedral were singled out (plan dimensions 9.2x5.5 m) and analysed under dead weight and a progressive amplification of imposed support movements, using a stress-resistant domain in the space of the three principal stresses (Croci 1995). In the first load case, the good collaboration between webs and ribs produced overall moderate stresses, with tensile stress only normal to the wall (0.05 N/mm^2). The shear strength of the rib-web joint, however, was reached very rapidly when the supports started to spread and the webs started to separate. Moreover, tensile cracks appeared at the crown of the transverse arches, which later developed along the vertex, normal to the movement, until instability was reached after several centimetres (Fig. 2.5).

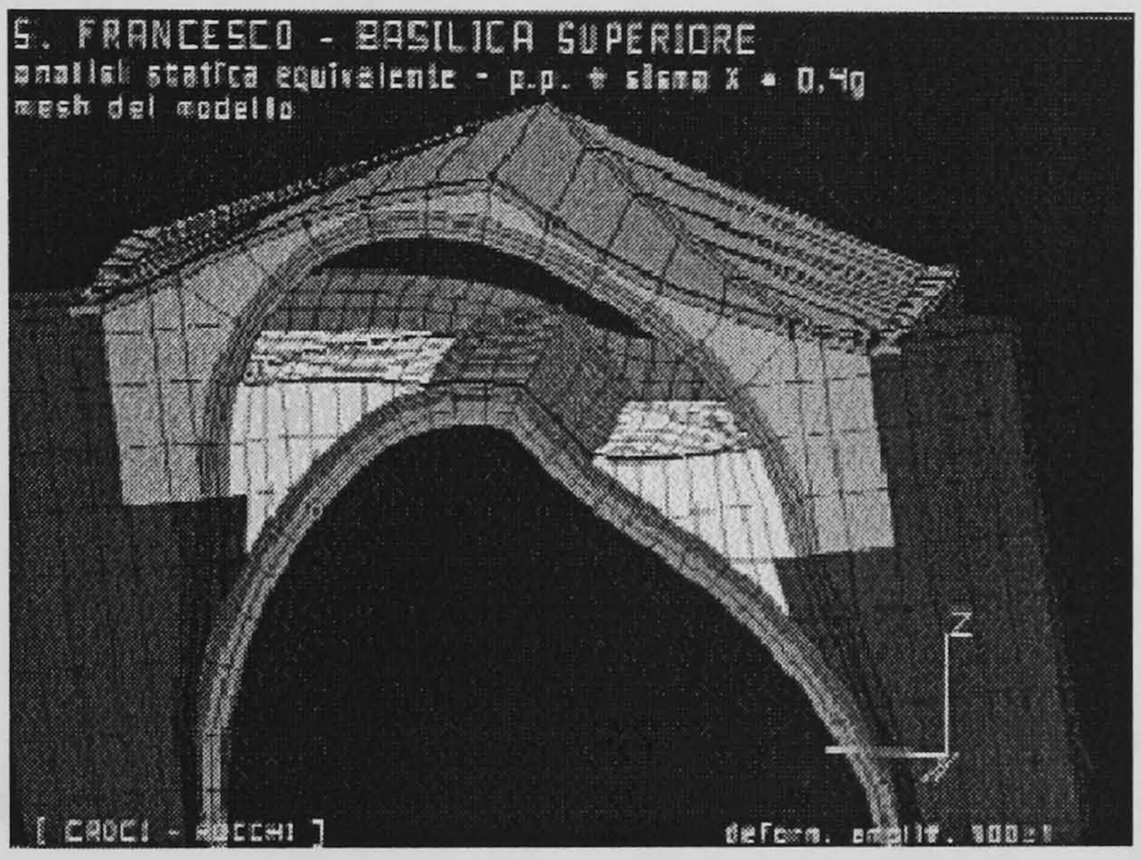

FIGURE 2.6 High deformation of a vault from St. Francis Basilica under seismic action (Croci 1998b)

A similar 3D FE model was used for the interpretation of the collapse of St. Francis in Assisi (Croci 1998a, 1998b). The study confirmed that excessive volumes of the spandrel fill could increase the tensile stress close to the vertices of the vault and cause unrecoverable changes of the curvature when high deformations occur due to seismic action (Fig. 2.6). A limit kinematic analysis of a simpler 2D model of a transverse section of the same vaults was carried out by P. Ronca, with the material split between voussoirs and mortar joints modelled with springs (Ronca 2000). Considering various structural schemes for the collaboration between the ribs and the webs and the action of the spandrel fill, the collapse was attributed to a rather inherent incapacity by gothic vaulted structures to withstand seismic forces.

2.3.4 Work of P. Roca and C. Molins

Roca and Molins have used Generalised Matrix Formulation (GMF) to study the non-linear behaviour of various cross vaults (Roca 1998, Molins 1998). In this method, the vault can be effectively modelled as an equivalent frame composed by the arches only, while the webs are treated as a set of stiff links connecting the ribs and restraining their movement. Consistent with the principles of matrix methods, the stiffness formulation is based exclusively on the equilibrium between external and internal forces at any point of the arch, so that no additional hypotheses over the displacement or stress field are required. Since the movements are fully free, arbitrarily high curvatures associated with damage can be reproduced and perfectly brittle materials, as the masonry in this case, can be employed (using a smeared crack approach).

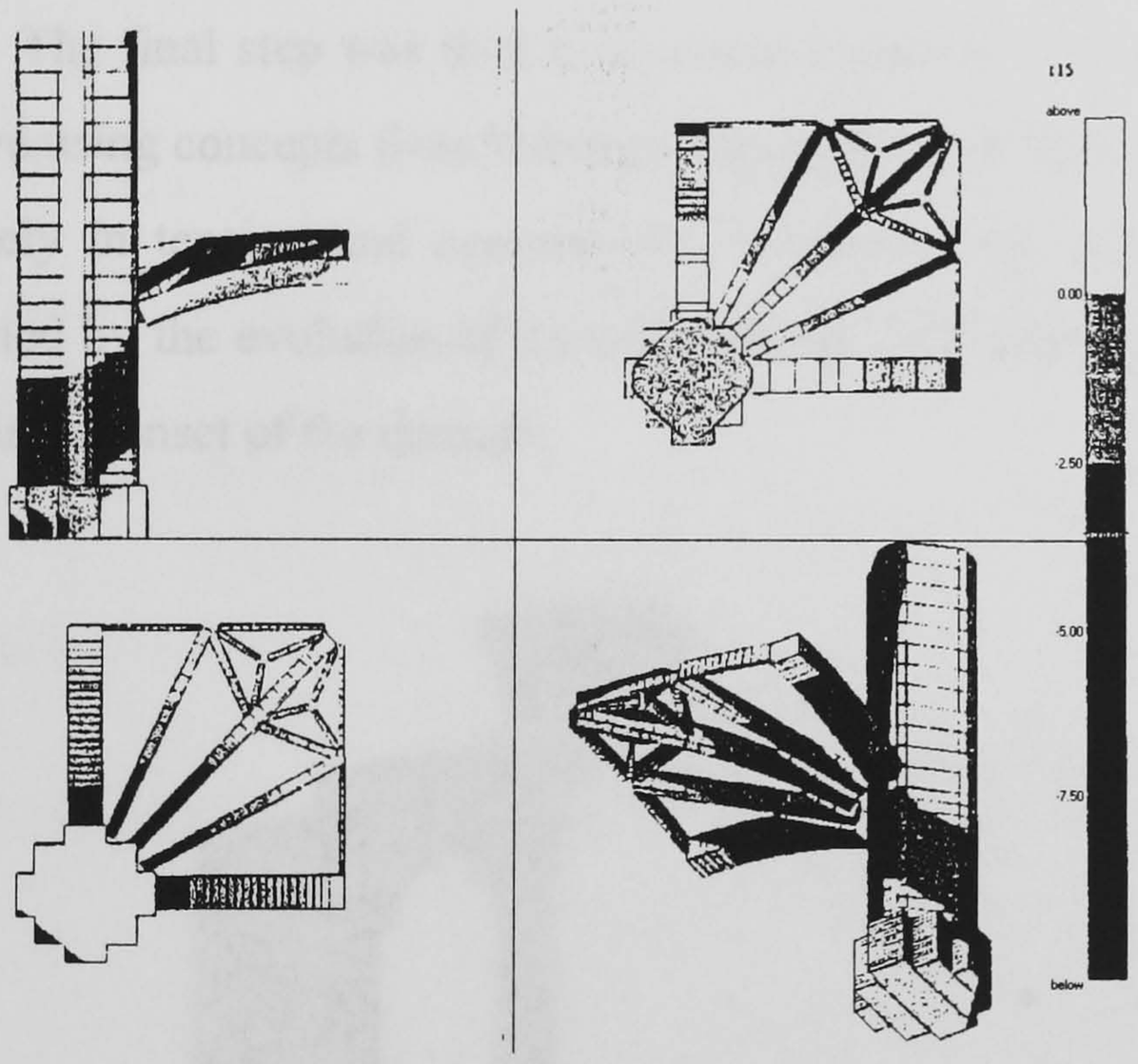

FIGURE 2.7 Stress state of a lierne vault from Morella Church at failure - cracked areas in white (Molins 1998)

Non-linear material and geometric analysis (NLMA and NLGA) was performed first for the case of a lierne vault built within an existing Gothic church in Morella, Spain (Molins 1998). The webs were further supported by a system of intermediate ribs that created a star pattern around the crown, therefore modelling like a frame of curved beams with GMF was quite suitable. Considering dead load of 4 kN/m^2 and same live load, an ultimate stress of 12.4 kN/m^2 was attained for NLMA, with deep cracks at the springings of

all arches, at the crowns of the lateral arches and at the bases of the four supporting piers (Fig. 2.7).

When the plain quadripartite nave vaults of Barcelona Cathedral were modelled with the same method (Roca 1998), NLMA, however, predicted failure for a uniformly applied load smaller than the actual dead load of the structure. This underestimation showed that it was the shell action of the webs that carried the most significant part of the load, with the ribs being subordinated elements in this scheme, and that the use of a 3D FE model would be more adequate.

This modelling resulted in a predicted ultimate capacity unrealistically higher than what was expected (over three times the total dead load), as the construction details of the supports on the pier extension were not integrated into the model and the bases were considered as fixed. The final step was then to simulate a quarter of a complete transverse section from the nave using concepts from Damage Theory to model the non-linear response of masonry separately in tension and compression. Cracking was interpreted as a local damage effect, defined by the evolution of known material parameters and by an adequate function that controls the onset of the damage.

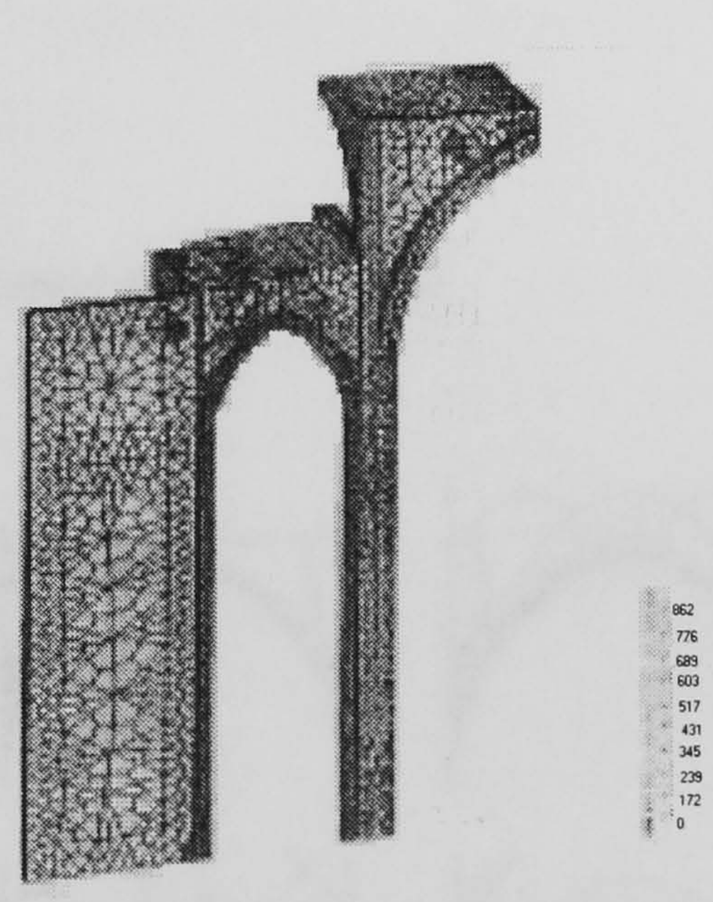

FIGURE 2.8 Distribution of damage at Barcelona Cathedral - loading corresponding to a dead-load factor 2.0 (Roca et al 1998)

After cracks have appeared at the crown of the transverse arches at the nave, they spread further to the aisle vault around the keystone, the haunches of the transverse arches and finally to the bases of the piers (Fig. 2.8). The collapse mechanism was similar to that

produced by the GMF model and occurred at a load of double the dead load, but the FE model predicted correctly the area of maximum damage at the section close to the haunches. Therefore, failure of the global structural scheme was induced in the aisle vaults due to the movement of their abutments.

2.3.5 Work of R. Barthel and M. Jagfeld

As part of the research projects of the German Special Research Committee on the Preservation of Historic Buildings (SFB 315), Barthel compared the capacity of the most commonly used analytical methods (mainly lines of thrust and FEM) to evaluate the structural safety of the most important types of cross vaults (Barthel 1994). Four main types of vaults spanning over a square compartment were considered according to their geometry and failure mode (Fig. 2.9):

a) Semi-circular profile with straight genetrices and crowns of equal height;

b) Pointed profile with straight genetrices and crowns of equal height; semicircular ribs;

c) Pointed profile with curved vertices;

d) Domical cross vaults.

The first two cases are of interest for this project.

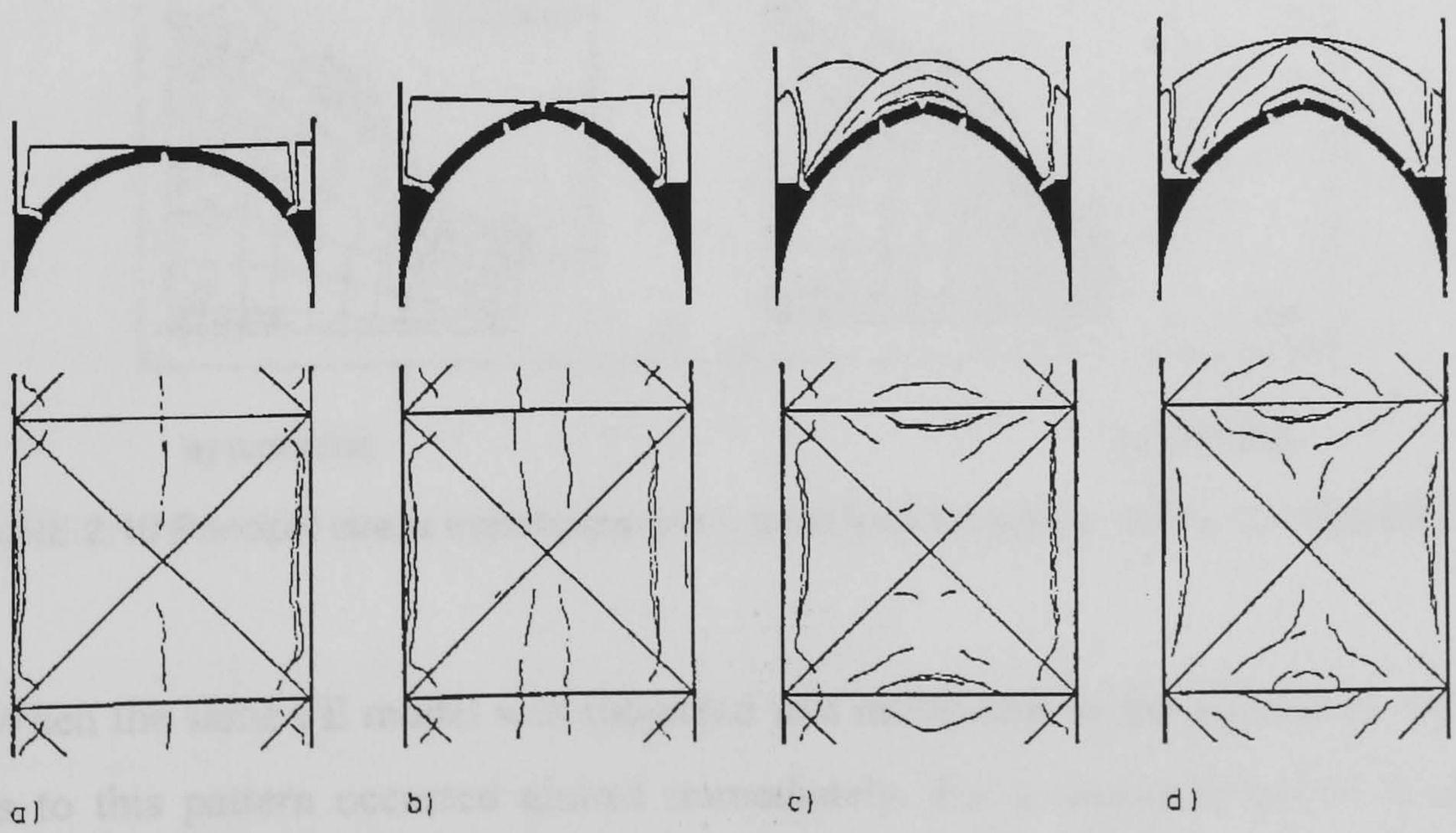

FIGURE 2.9 Four main types of cross vaults and their failure pattern (Barthel 1994)

At first, Barthel evaluated the thrusts with graphic methods by segmenting (slicing) each of the joining barrel vaults into a series of parallel rings. The thrusts from each one of these rings was a function of the cut-off angle (Heyman 1995) and when these were added, the total value H could be found. This was applied to a semi-circular vault (case **a**) with radius R equal to 5 m and thickness d equal to 0.25 m (R/d=20), cut-off above an angle of 55^{o} to simulate the constraints induced by the spandrel fill. A thrust of $0.79wR^2$ resulted, applied at a height of 0.35R, where *w* is the self-weight as a surface load. Alternatively, when the whole vault was examined, the hinge lines were assumed to form where the thrust line was tangent to the surface of the shell, i.e. at the crown and at a height defined by an (unknown) angle φ. From equilibrium, the resulting thrust was reduced to $0.67wR^2$, while the hinge was formed at $\varphi = 58.2^{o}$.

The same vaults were studied with a 3D FE model, solved with the package ADINA. 3D brick elements were used and the in-built constitutive law for concrete was assumed for the material, with a non-linear stress-strain curve in compression and zero tensile strength. The lateral arches were supported upon diaphragms. As R. Mark had observed (Mark 1982), the stress trajectories for the case of self-weight flew directly towards the supports and not the groins (Fig. 2.10a). Small tensile stresses were recorded only in limited areas at the vertices and the compressive stresses had a maximum of 0.6 N/mm^2, a value well below the assumed strength of the material.

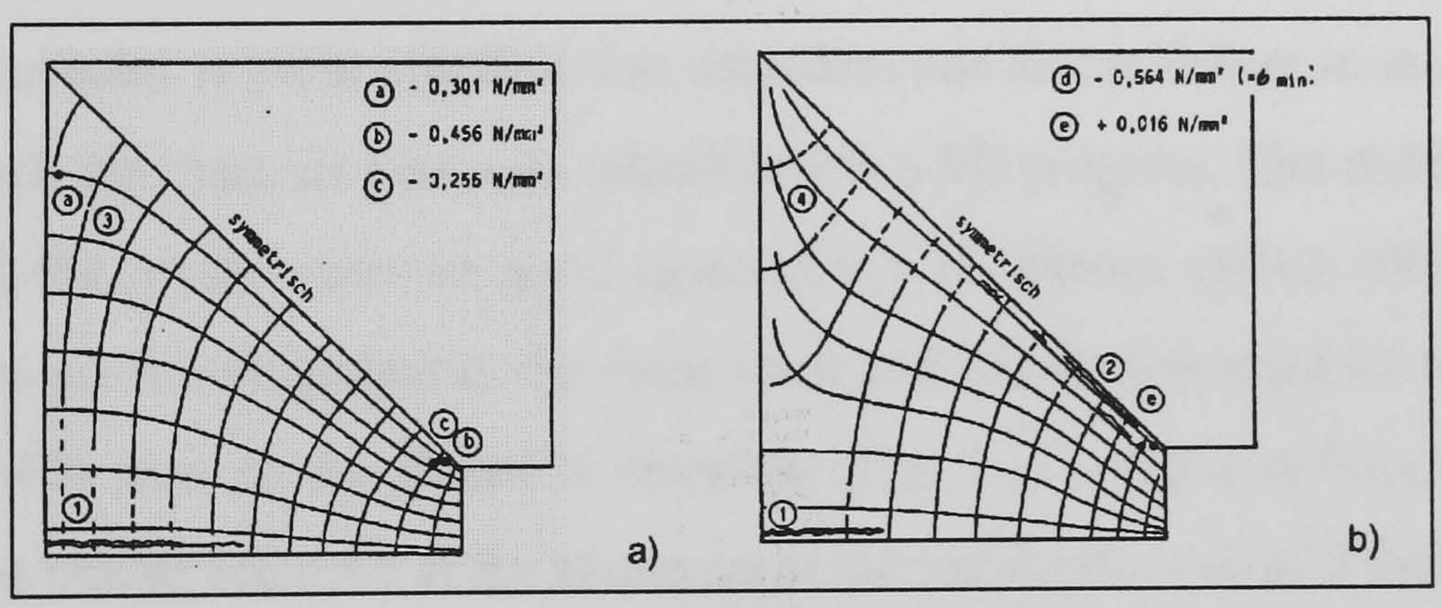

a) extrados b) intrados

FIGURE 2.10 Principal stress trajectories under dead load for type *a* in Fig. 2.9 (Barthel 1994)

When the same FE model was subjected to a movement of the abutments, substantial changes to this pattern occurred almost immediately. For a displacement of 1 mm (Fig. 2.10b), horizontal membrane tensile stress developed that caused cracks parallel to the nave

arch (normal to the movement). The cracks that existed already close to the crown of the transverse arch due to dead weight did not propagate any further. Cracks at the intrados of the longitudinal vertex completed the crack pattern and failure of the model occurred shortly afterwards due to numerical instability. The lateral thrust was 133 kN ($1.06wR^2$) for the dead weight case and, after a reduction during the first stages of the abutment movement, it stabilised at 77kN ($0.62wR^2$). As hinges were already considered along the vertices, this thrust was almost equal to the value obtained by the graphic method.

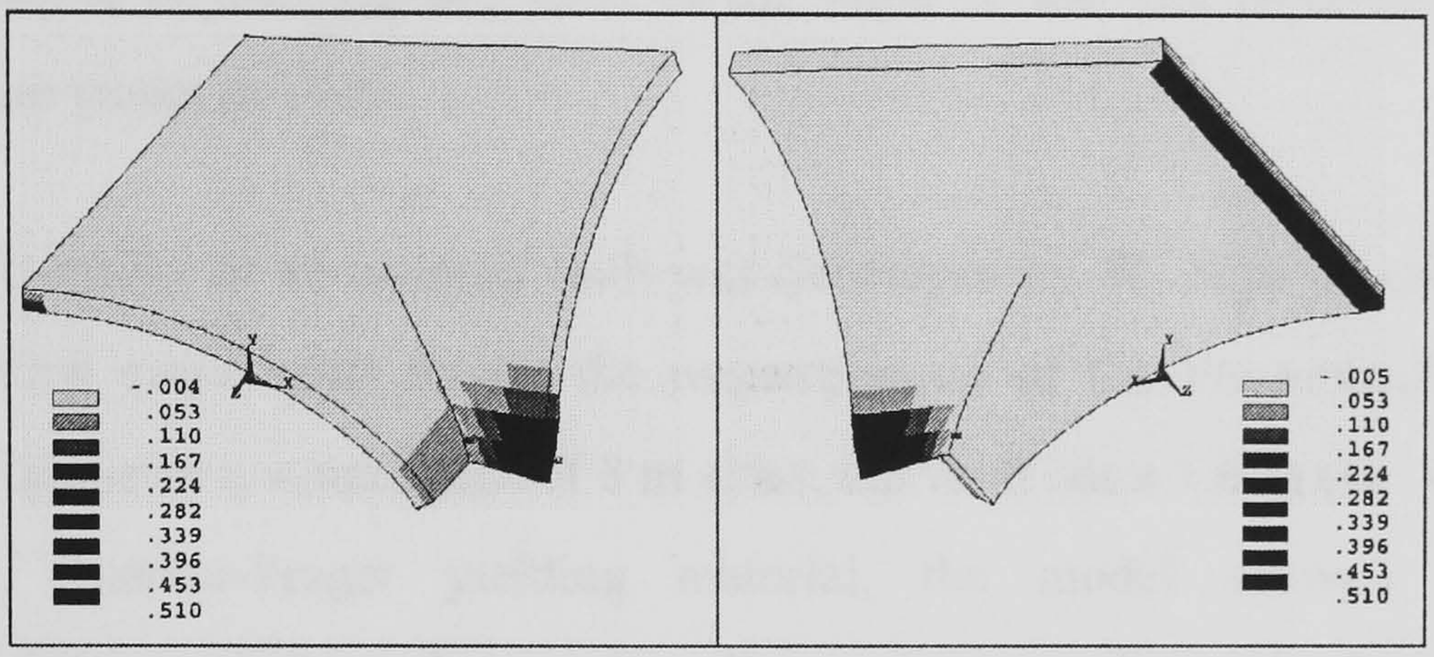

a) extrados b) intrados

FIGURE 2.11 Plastic strain in the hoop direction at an abutment movement of 404 mm in Z direction (Jagfeld 2000)

This FE model was further improved by Jagfeld (2000), focusing on the orthotropic material properties of the masonry and the high geometric non-linearity caused by the appearance of cracks. A yield criterion that considers non-linear failure in compression and tension, for both the material axes was introduced in a FE program. The method was tested on arches and the results were in good agreement with known earlier solutions (Harvey 1988). Afterwards, it was applied to the cross vault and failure was reached at an abutments movement of 404 mm, in the global X direction (Fig. 2.11). The resulting smeared crack pattern showed failure occurred at the abutment of the transverse web and the intrados of the longitudinal vertex, which was in agreement with a part of the pattern that Jagfeld had observed earlier in some Gothic churches.

No provision was made however for the function of the ribs and the discontinuity expected at the intersection of the webs along the groin, while the arches at the lateral edges were replaced with diaphragms. The study, however, improved the understanding of the behaviour of the vault barrel under the most important structural actions.

2.3.6 Other analytical models

In another attempt to understand faults detected in real structures, Martínez et al. used a simplified FE model of the nave cross vaults at León Cathedral to calculate the thrusts exerted against the counteraction tower behind the transepts (cf. Fig. 1.4) and to establish upper and lower bound limits (Martínez 2000). The model could then be used to design a monitoring system and the data from the measurements could subsequently calibrate the numerical models. The collapse of a single vault spanning 7.5 m was evaluated to occur at 100 mm movement of the supports, close to the value of 150 mm reported for the partial collapse of those vaults in 1743.

A 3D FE model of an isolated vault was developed by W. Jäger in order to verify a new-built shallow cross vault during the reconstruction of the Frauenkirche in Dresden (Jäger 1997). Laid over a square plan of 8 m sides, the vault has a 1.6 m rise. Introducing an ideally-plastic Drucker-Prager yielding material, the model showed an improved performance of the vault from the previous linear elastic analysis: the bending moments decreased and the eccentricity of the thrust line stayed within the middle third of the thickness of the shell. Applying the same procedure to an existing cross vault with a span of 9.1 m and a rise of 4.5 m, the model showed that only few cracks close to the edges could be expected. The drawback of the method, however, was that the computational load was huge, limiting the practical use of applications in cases with more complex material or geometric properties.

P. Lourenço applied a non-linear material and geometric analysis to the vaults of the Church of Christ in Outeiro, Portugal, to assess the origin of their damages (Lourenço 1999). The dynamic loads were simulated as equivalent, quasi-static horizontal loads, added to the permanent dead load of the structure. Assuming a simplified linear elastic law for the material, the vault was modelled with shell elements for the webs and beams for the ribs and arches. The analysis made evident the inadequate design of the vaults, as the thrusts from either the vertical or the horizontal loads could not be sustained by the columns and the insufficient joint between the shell and the web. Moreover, the stiffness of the nave arch proved to be inappropriate. Although the FE model underestimated the magnitude of deformations recorded in the survey of the building, the strain patterns and the magnitudes yielded by the model were sufficient to explain the origin of the failure.

Cross vaults from the cathedrals of Burgos and Seville were modelled with 3D solid elements by Cassinello (1997). An elastic analysis performed under dead weight made evident how the passage from the semi-circular lateral webs of Burgos to the pointed webs of Seville brought the vaults almost completely under compression. Bending developed mainly around the vertices, while purely membrane compression forces acted at the haunches.

Lilley performed a similar analysis for the nave vaults of Durham Cathedral, using data from a photogrammetric survey to generate a homogeneous isotropic FE model with smooth changes in curvature and without ribs (Lilley 1993, 1995). The transverse sides were restrained between the tower at the crossing and the adjacent vaults. As a result, the maximum deflections of 0.64 mm for self-weight were recorded at the tower side while the tensile stresses around the vertices were 0.1 N/mm^2, with maximum stresses in general at the extrados surface. Next, the haunches were considered to be filled with slate debris material and this increased the deflections to 1.5 mm. Finally, springs were introduced to the supports in order to simulate the effect of the thrust upon the lateral wall and their stiffness was chosen so that the maximum horizontal displacement under self-weight would be 1.5 mm. The maximum deflections at the same positions increased to 6 mm and the tensile stresses to 3.5 N/mm^2.

For all these cases, however, unexpectedly high tensile stresses were observed at the springings due probably to inaccurate modelling of the curvature changes at the haunches area. A more critical approach to the results of the photogrammetry is probably required, together with a closer investigation of the material properties and the effect of important construction details. No mention was made, for instance, of the role of the ribs, used very innovatively in this Cathedral.

Quintas and De la Torre assumed that membrane state prevails in the behaviour of masonry cross vaults and, similarly to Lenza (§2.3.1), they developed closed expressions that can be applied to vaults of either semi-circular or pointed profile, spanning over a square compartment (Quintas 1993). With this method, the distribution of the strains and the thrusts can be evaluated. For some important cathedrals (Amiens, Beauvais), this study showed that higher thrusts would occur at the area of the crown of the lateral arches,

justifying the tendencies in the later stages of construction to place the point of application of the flying buttresses higher.

2.4 THE EMPLOYMENT OF ORIGINAL DESIGN RULES

2.4.1 Design rules by Gothic masons

Based on the available evidence from archive material, it is most probable that the original masons during the High Gothic period had not established an independent set of structural design tools, but that they had intuitively developed some rules of dimensioning individual members incorporating them into spatial proportioning methods. Even when Mignot, for example, asserted during the debates on the design of the new Milan Cathedral in 1400 that "*Ars sine scientia nihil est*" (There can be no technique without science), he was referring to a "geometric science", expressed in a predetermined geometric grid for the whole building (Mainstone 1968). These proportioning methods would then be transmitted either orally through the corporations of the masons or more effectively by using the building itself as a *compendium* of solutions to specific structural problems.

The few sketchbooks that exist from that period (like the pattern book of Villard de Honnecourt or the Reims palimpsest) contain mainly construction or proportioning details and do not have any intention of use as a manual. Attempts were made however in later stages to codify the building experience into a separate set of design rules, like those proposed by Rodrigo Gil de Hontañón in the 16th century (Kubler 1944, Sanabria 1982). As a Late Gothic architect, he had to compromise between the declining Gothic style, where the construction problems were more evident, and the revival of Classicism that promoted purely aesthetic criteria.

In his attempt to produce a complete theory for the design of a whole church, seven formulae can be distinguished that evaluate the necessary depth of a buttress to support rib vaults or arches. These are divided into arithmetic or structural rules, where close expressions are given, and geometric formulae, that derived from geometric constructions. The very interesting Third Structural Rule assesses the depth of an outer wall buttress for a hall church as double the width W which is:

$$W = \frac{1}{3} \cdot \sqrt{H + \frac{2}{3} \cdot \sum R} \qquad (2.1)$$

where H is the height of the buttress to the springing and ΣR is the sum of the perimeters of all the ribs converging to the buttress, measured from the springing to their keystones, usually a quadrant.

Clearly, the units are handled inconsistently and this is a result of their purely empirical nature. The second set of rules however establishes also the height of the (spandrel) wall of an arch or barrel vault, apart from the buttress depth. The First and Second Geometric Formulae give a height of 2.081R and 2.894R respectively, where R is the radius of the arch profile. Sanabria regards the two methods as if two experiments were conducted in which two arches of a given span and slightly different buttress depth were loaded until they failed (Sanabria 1982). Although the concept of dimensioning individual structural members was just emerging at that period, it is very possible that Rodrigo Gil had the chance to identify and test some samples, as he was the architect and director of several construction sites.

2.4.2 Later developments in design methods

Structural mechanics would soon develop as a science independent from geometric proportions with the works of Leonardo da Vinci and Galileo. It is not completely clear whether Chr. Wren performed a mathematical dimensioning of his vault for St. Paul's in London (1675-1709) with the aid of R. Hooke. However, the first asserted application of mathematical rules occurred in 1742 when three French mathematicians were invited to give their opinion about the apparent structural instability of the dome of St. Peter's in Rome. Although this study was challenged later by the report of G. Poleni (Poleni 1748), it constitutes the first structural analysis recorded. Couplet (1730) and Coulomb (1776) established the 4-bar chain collapse mode for arches and Méry and Moseley formulated the theory of Lines of Thrust between 1830-40.

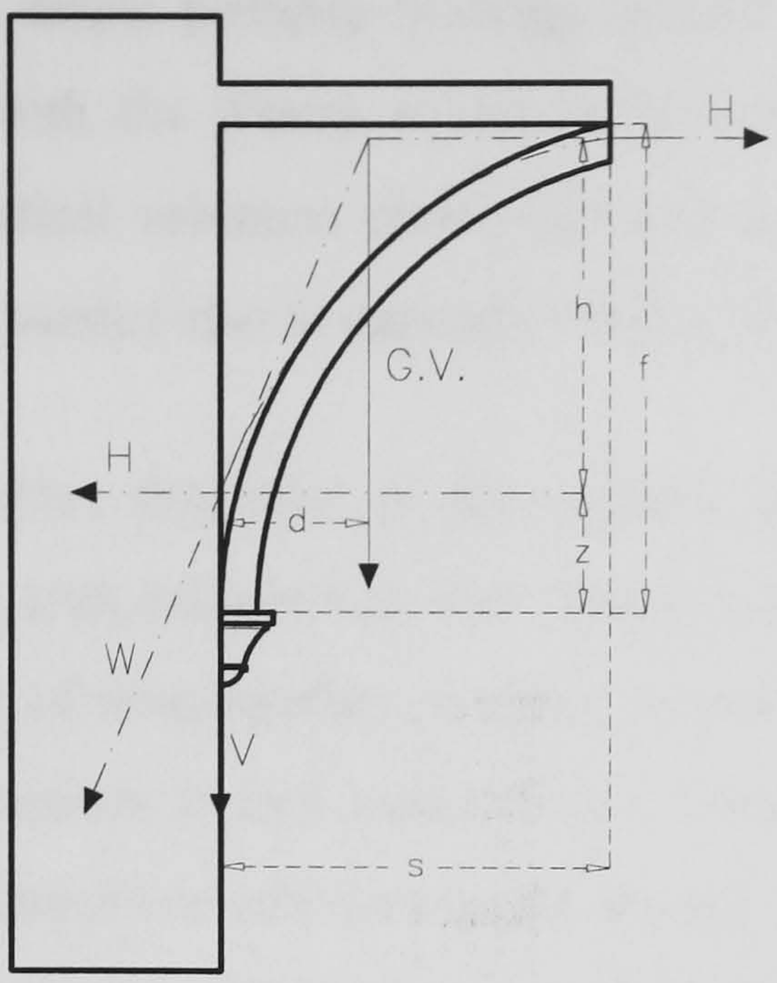

FIGURE 2.12 Definitions of dimensions and forces used in Table 2.1 (Ungewitter 1890)

TABLE 2.1 Thrusts and weights for quadripartite vaults for a unit plan area (kN/m^2) (Ungewitter 1890)

Height/span (f/s)	1:3		1:2		2:3		5:6 to 1:1		
	V_o	H_o	V_o	H_o	V_o	H_o	V_o	H_o	d
½ lightweight brick	2.3	1.6-1.8	2.6	1.1-1.2	2.9	0.9-1.0	3.4	0.8-0.9	1.6
½ strong brick	3.1	2.2-2.4	3.5	1.4-1.6	3.8	1.1-1.3	4.5	1.0-1.1	2.3
¾ strong brick	4.2	3.0-3.3	4.8	1.9-2.2	5.3	1.6-1.8	6.5	1.5-1.6	3.1
200 mm sandstone	5.7	4.2-4.5	7.0	2.8-3.2	7.5	2.2-2.5	9.0	2.1-2.3	4.0
300 mm rubble	10.0	7.1-7.5	12.0	4.8-5.5	13.0	4.0-4.3	15.0	3.5-3.7	7.2
lever arm h/f	0.85-0.75		0.8-0.7		0.8-0.72		0.8-0.75		

Rondelet conducted experiments on arches and vaults and published the first set of practical dimensioning rules in 1810. This work remained in wide use until Ungewitter & Mohrmann (Ungewitter 1890) and Kröner published new and more accurate tables in 1890 on the calculation of the weight V_o and thrust H_o based on the assessment of the line of thrust (Fig. 2.11). These values and the unit weight applied as a surface load *d* can be found in Table 2.1, reproduced by Heyman (Heyman 1977), for various unit materials and height to span (*f/s*) ratios. The forces were calculated for a unit plan area and they included allowances for the ribs. Their validity will be discussed in later chapters against FE results.

Graphic Statics and the funicular polygon as developed by Méry were further enhanced by Fuller in a method that provides information about the grade of safety of a

structure and permits to define possible loadings to improve it. Ultimately, this proved method was combined with the theory of Limit Analysis by Kooharian and Heyman (Heyman 1995) into practical solutions mainly for masonry arches, which, under certain safe conditions, can be expanded also to masonry vaults (§2.3.1).

It is evident, however, that most of the original design rules for spatial masonry structures focused on the arch bridges that were being built in that period, as can be also confirmed by the number of investigations actually carried out on their safety assessment. Most of the pre-elastic theories treated masonry as a system composed of rigid voussoirs subjected to unilateral constraints and developed around the "static" theory of Coulomb (1776) and the "kinetic" theory of Mascheroni (1785) (Benvenuto 1990, Sinopoli 1997). The equilibrium conditions were sought on the determination of a range of admissible thrusts or the identification of a collapse mechanism without evaluating the reactions, respectively. These theories can extend to masonry vaults of an accurate stereotomy, whose webs consist of regular and uniform blocks with very fine mortar joints. Again the limit design principles apply and solutions for a geometric safety factor can be provided.

To conclude with this examination of the historic design rules, it is interesting to study the inverse process, i.e. the effect the same Gothic structures have had in the formulation of these rules. New construction materials were introduced after the Industrial Revolution and in France the new class of engineers turned to Gothic Architecture in search of a new structural vocabulary for the solutions of portal frames they were applying (Coste 1998). The notion of balance and the systematic methods of composition employed by the gothic masons would be combined with a renewed need for economy and many important structures of the period, like St. Geneviève in Paris, would be "calculated" for the first time. As a result, models for the understanding and analysis of Gothic structures inhabit in many of those design theories.

2.5 SCOPE OF THE PRESENT WORK

The structural behaviour and pathology of High-Gothic structures have been established during their long useful life mainly through experience. It has been possible to assess the individual performance of many of their elements, first arches and later vaults, but full application of the analytical tools of Structural Mechanics occurred only in the last

100 years. Several researchers have developed FE models for particular case studies (Mark, Croci, Roca, Barthel), in which specific aspects have been examined separately. Vaults were examined among others in the linear elastic field, in their global structural context within the entire building or in some specific configurations, as a "net" of tierceron ribs. On the other hand, when the orthotropic properties of the masonry are taken into consideration, too much emphasis is placed on the non-linear plastic behaviour of the vault in compression. The resulting sophisticated models have then to treat some geometric characteristics of vault as less important in order to reduce the computational load.

Only few experiments carried so far have correctly addressed the issue of failure due to the movement of abutments. Some of the earlier case studies however were quite particular and the available data are not sufficient. Moreover, data from surveys of vaults in their real context are either not enough or not suitable to correlate with the analytical results.

Increasingly, a different approach to the collection of data either by improved survey campaigns or by simulating the response of vaults to selected loadings in the controlled conditions of a laboratory is required for economic and structurally sustainable interventions. An experimental programme is presented which aims to provide more data to improve the calibration of the FE models and some of the other analytical methods mentioned earlier

A case study of the collapsed church of Holyrood Abbey in Edinburgh was chosen. The geometry and failure mode is representative of a wide variety of Gothic buildings. The vaults failed in 1768 due to an excessive movement of their abutments and failure of the buttressing system. Quadripartite cross vaults of quite typical proportions roof the aisles and one of these is reproduced as a scale model.

The mechanical properties of the masonry are going to be assessed with flexural tests on wallettes. The evaluated strength will be later used in the definition of a failure criterion in biaxial bending which is required for the non-linear FE analysis.

The behaviour of vaults under service loading conditions will be studied by testing the model vault under dead load. The effects that will be examined in this series are:

1) The elastic range of the response of the vault.

2) The effect of the geometry of the groins.

3) The height of the spandrel fill.

The preliminary FE model will be used to analyse these tests and further refinement must be done to take into account the geometry or material properties for better interpretation of the behaviour of the model vault.

The vault will be tested to failure by moving the abutments, the action that precipitated the collapse of the church of Holyrood, in order to develop a method for the safety assessment of such structures. A refined FE model incorporating non-linear material and geometric properties will be used for the analysis. A parametric study will be performed to examine the effect of factors like material properties or the geometric configuration on the safety of the vault. The result will also be compared with empirical methods.

Chapter 3

THE MODEL OF A VAULT FROM THE CHURCH OF HOLYROOD ABBEY

3.1 INTRODUCTION

The case study for the safety assessment of cross vaults should deal not only with the major geometric typologies, but also the range of loading effects that can lead to collapse, such as movement of the abutments, as discussed in Chapter 1. The aisle vaults, that constitute the object of this study, are usually encountered in a quadripartite configuration (resulting from the intersection of two barrel vaults), spanning over a square compartment and their major forms are presented in §3.2. Subsequently, the church of Holyrood Abbey in Edinburgh was chosen for the case study and its behaviour is discussed within the structural scheme of the building in §3.3. The construction of the model cross vault and its response to the movement of its abutments is finally reported and discussed in §3.4.

3.2 MAJOR GEOMETRIC TYPES

In the previous chapters, the structural and geometric features of the churches of the Gothic period were analysed. During the discussion of their pathology, the importance of equilibrium of the structural actions in the transverse direction appeared to be critical. In this project, the effects from any disturbance in this equilibrium have been focused on the lateral (aisle) vaults. These vaults are usually laid over a square bay and are quadripartite, even in the case of early tierceron vaults composed of multiple ribs, as the latter were usually decorative attachments. Four major types of geometric configuration for cross-vaults can be considered, distinguished by the proportions of their intersecting webs. These are:

1) Pointed diagonal rib: arched profiles with equal radii and heights (Fig. 3.1a);

2) Semicircular diagonal rib: equal arch radius but different arch heights (Fig. 3.1b);

3) Pointed diagonal rib: equal arch radius but different arch heights (Fig. 3.1c);

4) Semicircular diagonal rib: different arch radius but equal arch heights (Fig. 3.1d).

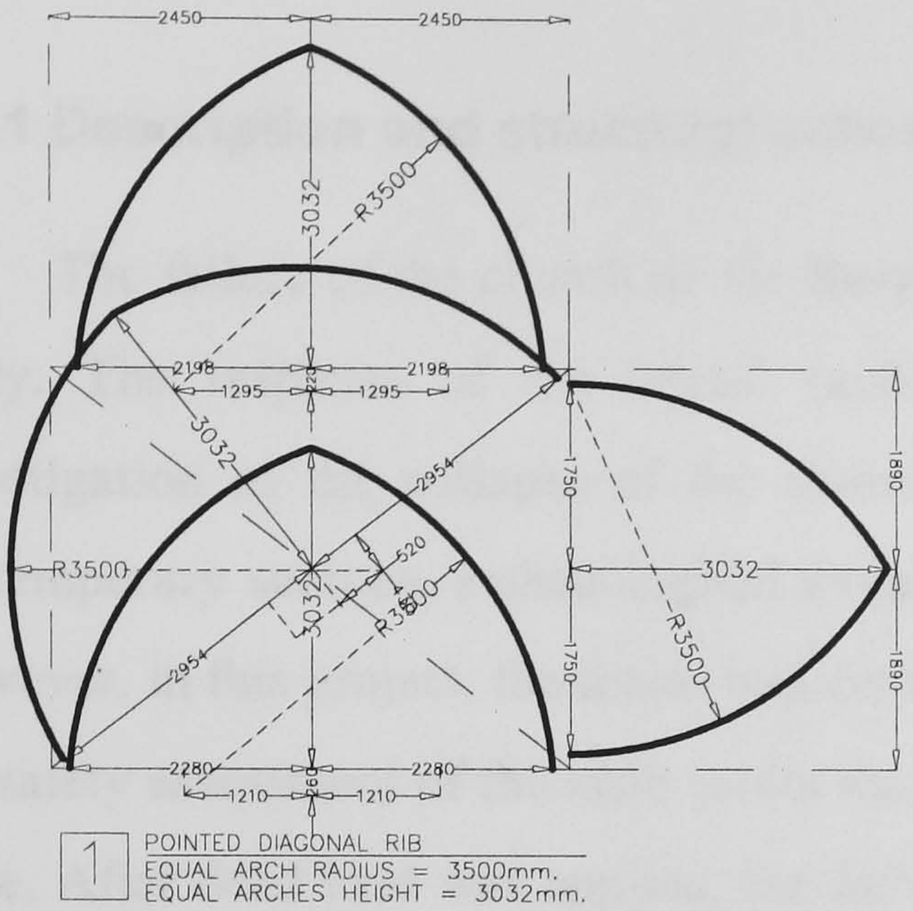

(a) Type a

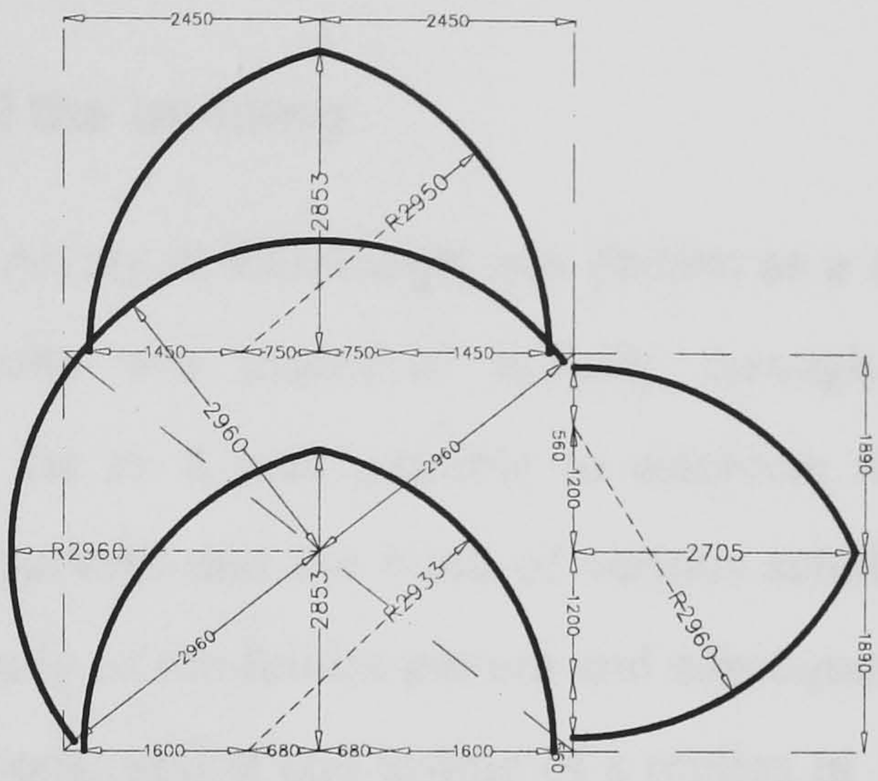

(b) Type b

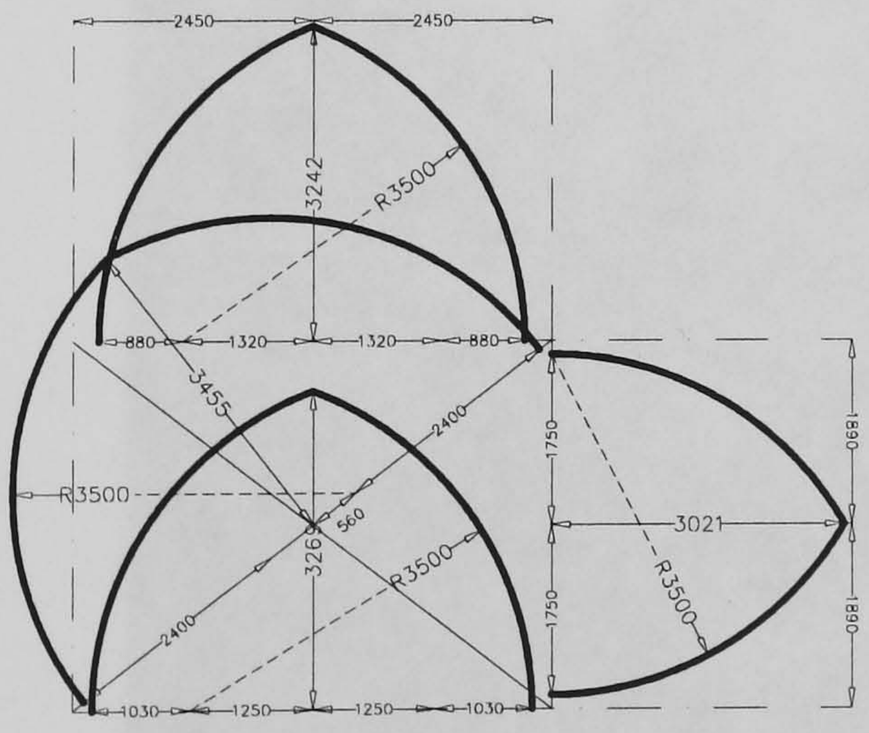

(c) Type c

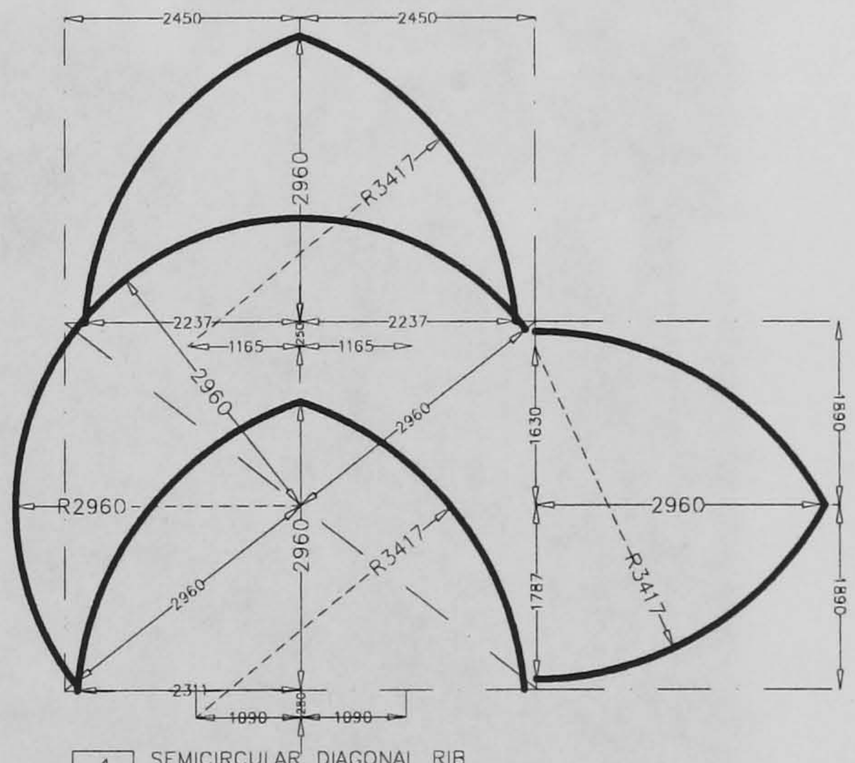

(d) Type d

FIGURE 3.1 Major types of geometric configuration for quadripartite cross vaults as they can be applied to the case study of the Holyrood Abbey church

The geometry for the original vault at the Abbey of Holyrood corresponds to type 1 (Fig. 3.1a) and it is examined in detail in §3.3.3.

3.3 THE PROTOTYPE VAULT FROM THE CHURCH OF THE HOLYROOD ABBEY

3.3.1 Description and structural scheme of the building

The failure of the church of the Holyrood Abbey in Edinburgh was chosen as a case study. The response of the lateral (aisle) vaults was examined initially through an investigation of the collapse of the church, as far as it was possible to establish from contemporary sources, archaeological evidence, surveys and the work of various scholars. However, in this project, the major tool for the study of the failure pattern and subsequently the safety assessment of the aisle vaults was the construction and testing of a replica in 1/4-scale. After dead load was applied, the failure was reproduced as a movement of the front abutments. In this section, the collapse procedure and the geometry of the vault under examination are presented and discussed, preceding the construction and set-up of the model and application of the loading.

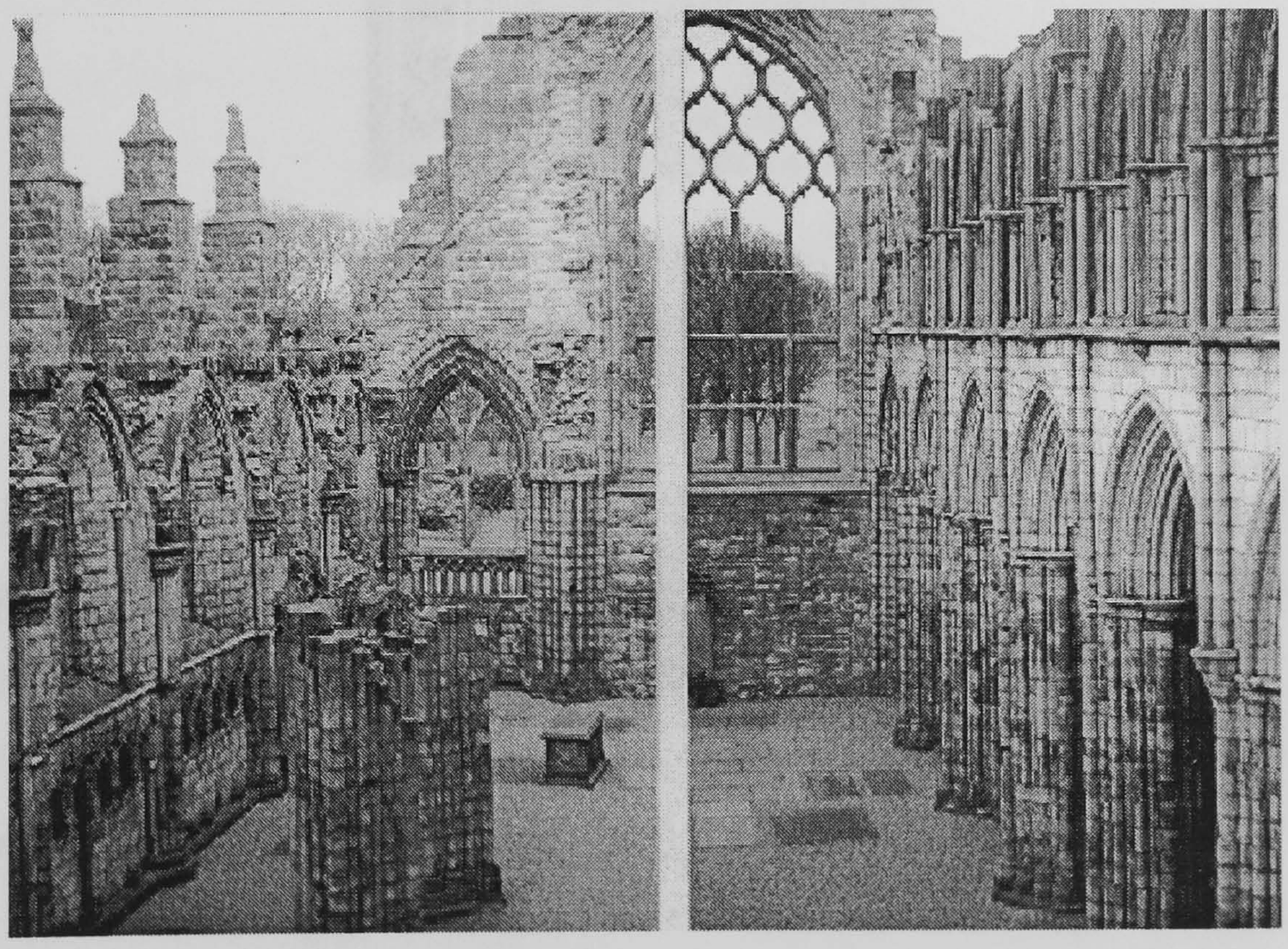

(a) Present state of the nave. View from the façade

FIGURE 3.2 The Abbey Church of Holyrood

(b) The east end seen from the garden of the Palace

(c) A hypothetical view of the nave (NMR EDD/3/143/P)

FIGURE 3.2 The Abbey Church of Holyrood

The church is situated at the NE side of the Palace of Holyroodhouse, at the east end of the Royal Mile in Edinburgh. Sole survivor from the original Abbey of Holyrood, it is found today in a ruinous state after a devastating collapse in 1768 (Fig. 3.2). The whole compound is built upon a blue clay subsoil and the existing marshlands were drained before the foundation of the Abbey (RCAHMS 1951). Originally, the church was cruciform in plan, until it was reduced to the nave in 1570, and its extent was asserted by archaeological excavations (Oldrieve 1911). The nave has eight bays and was separated by a two-bays wide transept from the shorter choir of six bays (Fig. 3.3). Remains of a cloister are visible to the

south side of the building, while the east quarter of the palace surrounds the SW corner. The exterior is characterised by the remains of the west façade, whose north tower is truncated, while the other is incorporated in the north wing of the Palace (Fig. 3.3). The church ends at the east gable with a window in tracery, built between the remaining west piers of the crossing.

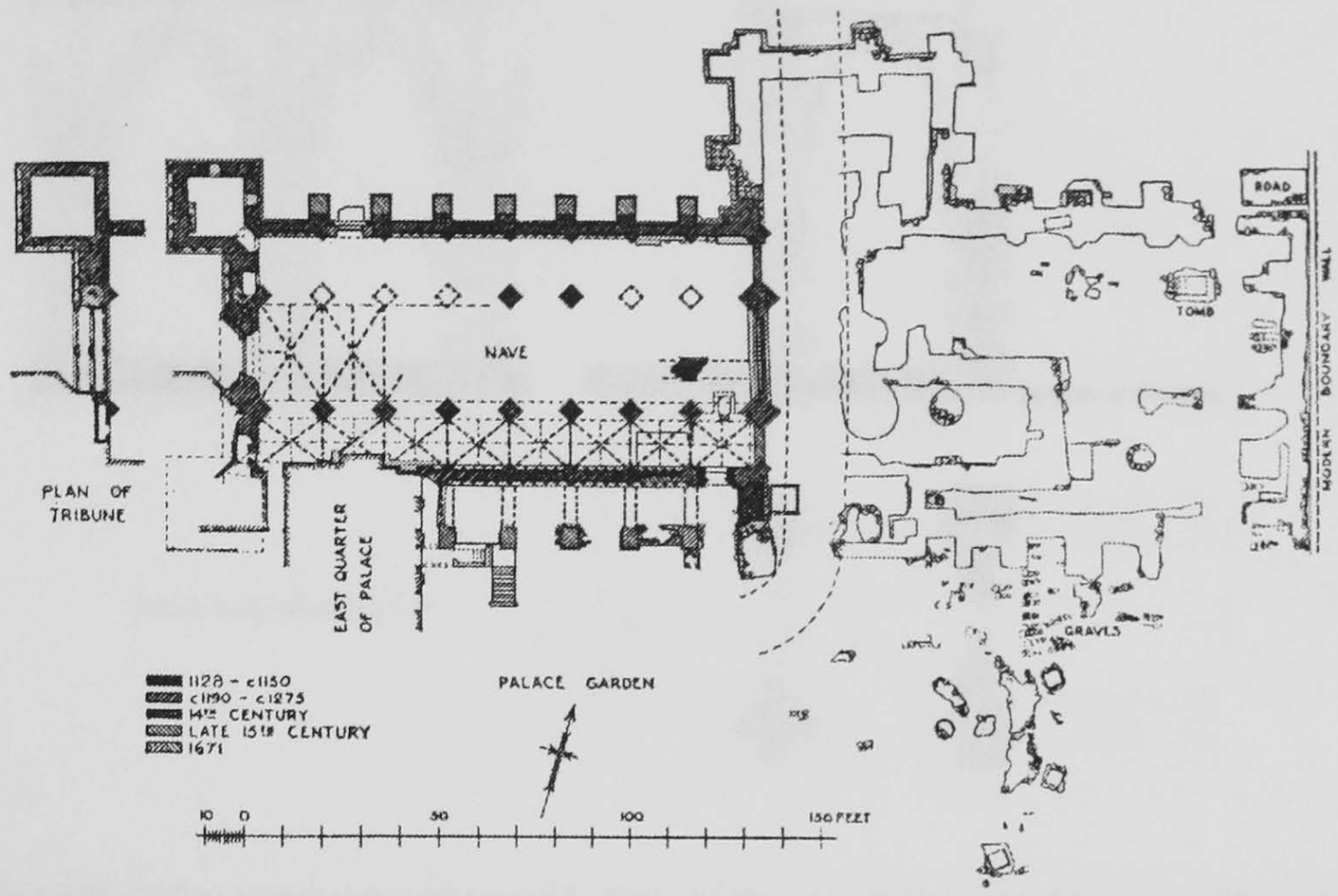

FIGURE 3.3 Plan of the Abbey Church of Holyrood. Major building campaigns and actual state (Oldrieve 1911)

The collapse in 1768 destroyed the whole of the north aisle, the nave, the top portion of the façade and the clerestory of the south aisle (Fig. 3.2a). At present, the east gable and the south aisle until the triforium level remain intact, after consolidation work in 1909 (Baldwin). On the north aisle, the outer wall stands until the level of the crown of the wall ribs of the vaults and only few of the north piers of the nave are still of a considerable height.

From archaeological evidence (Oldrieve 1911) and stylistic affinities with Lincoln Minster (Eeles 1915, Gifford et al 1984), the central nave was assumed to be roofed with sexpartite vaults (Fig. 3.4). A reconstruction of the original cross-section of the nave is proposed in Fig. 3.5, based on these references but further reviewed following considerations on the proportions and design procedures for Gothic churches (Fitchen 1961). Contrary to the typical configuration of the scheme, the nave vaults were oblong and they corresponded to only one bay at the aisles (Fig. 3.4), similarly to the assumed prototype at the transepts of Lincoln (Fig. 3.6) (Gifford et al 1984, BAA 1986).

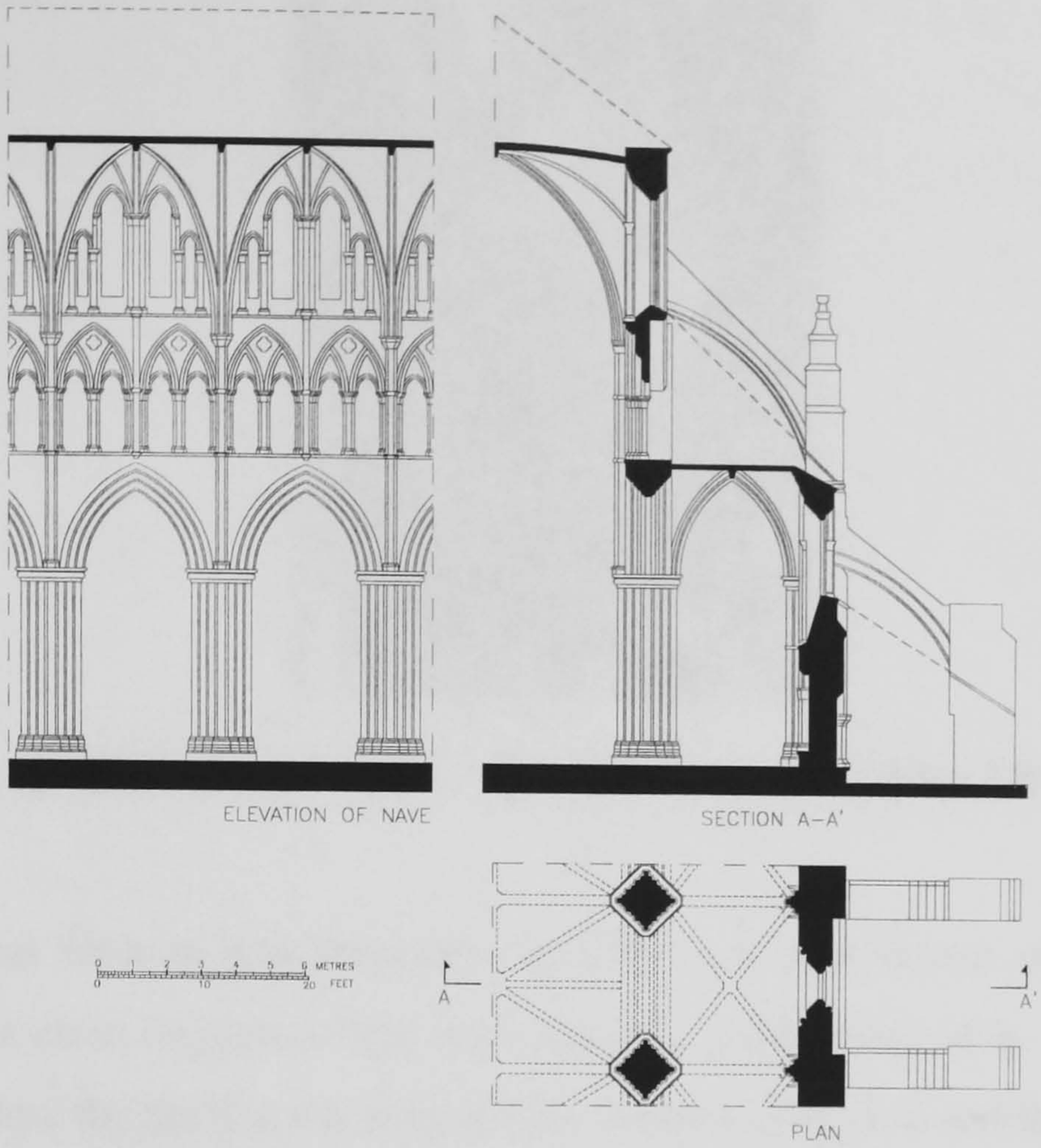

FIGURE 3.4 Hypothetical reconstruction of a bay of the church in its final configuration before the collapse

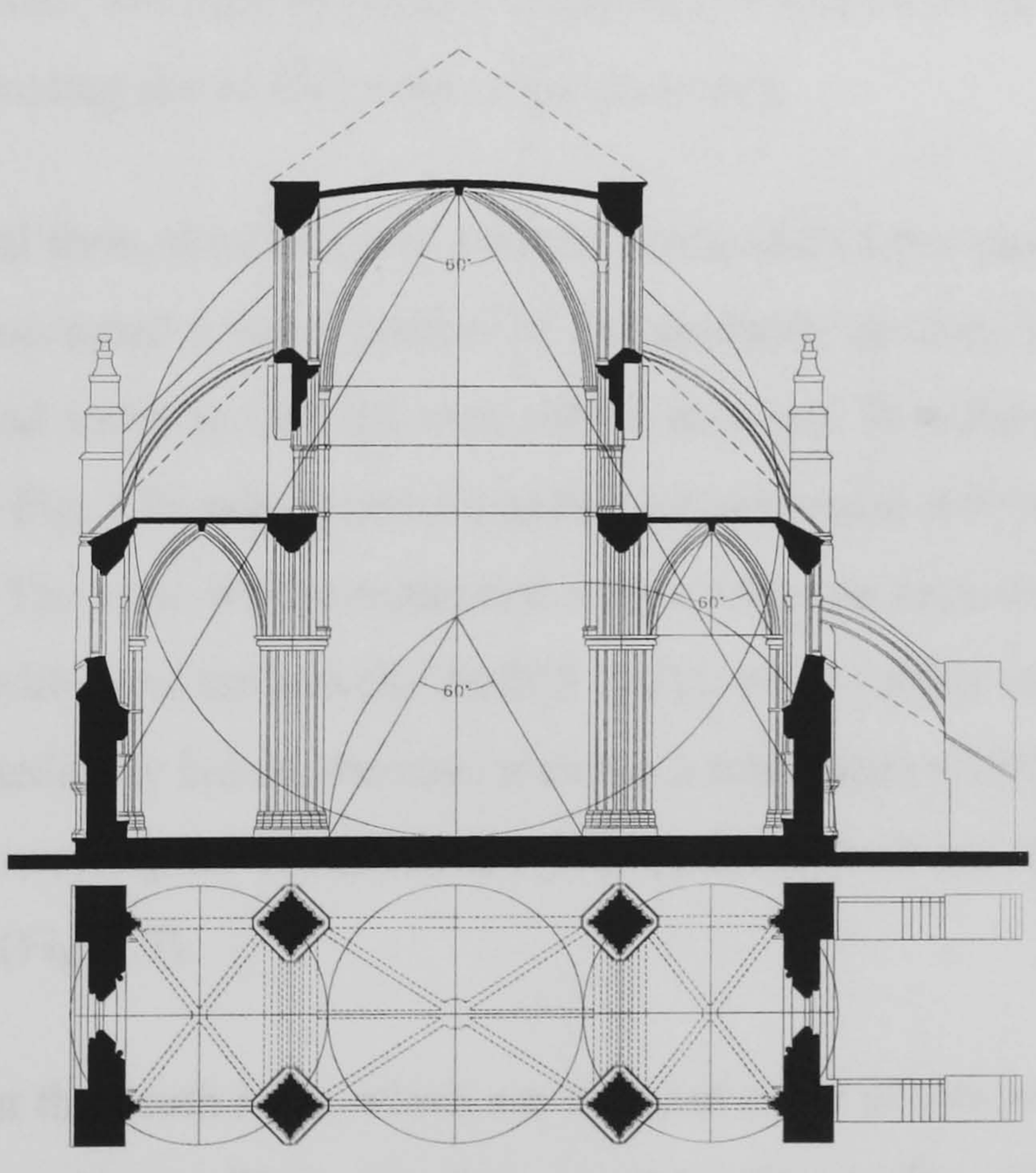

FIGURE 3.5 Geometric proportions in the cross section of the church. Hypothetical reconstruction of the final configuration before collapse

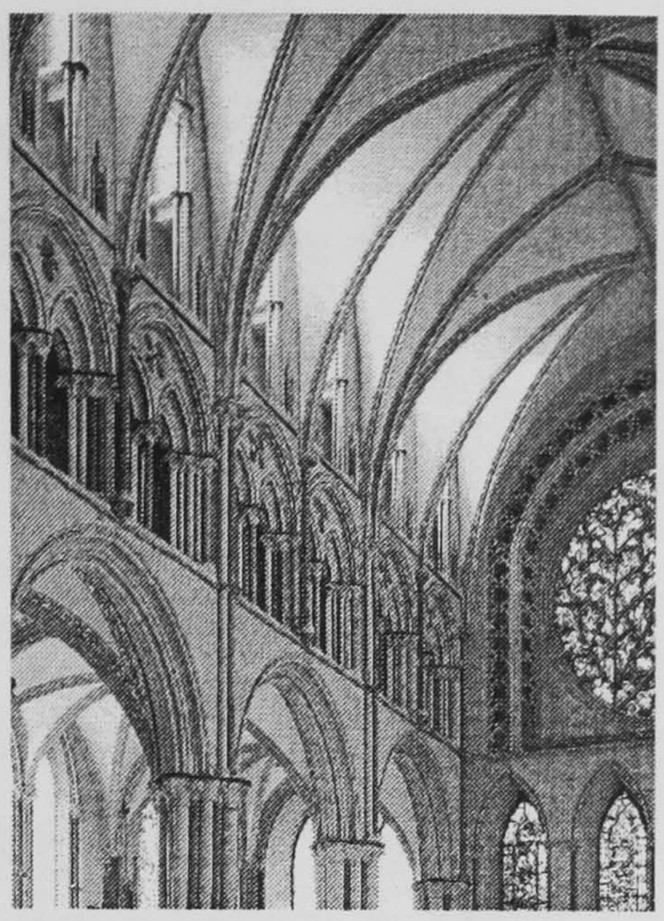

FIGURE 3.6 The north transept of Lincoln Minster (Clifton 1986)

The typical division into clerestory, triforium and nave arcade was observed at the lateral wall. The main imposts of the vault are still visible today (Fig. 3.2a). They spring immediately below the lintel at the base of the clerestory (Fig. 3.4) and they are carried by a wall shaft, which continues to the nave piers, clearly marking the division into bays. Regarding the impost of the secondary, transverse tierceron rib (Fig. 3.4), it probably sprung from a quite higher level, in order to reduce the visual obtrusion of the transverse vaults. A much leaner wall shaft was used to visually integrate this support to the structural scheme of the building, terminating above the crown of the nave arch.

In its original form, the clerestory probably consisted of two pairs of lancet windows (Fig. 3.4), which occupied a small portion of the available surface. The triforium zone is preserved entire and today is blocked with rubble masonry. It is formed by two recessed pointed arches (cf. Fig. 1.2), which create a quite narrow passage with access to the extrados of the aisle vault. The zone was strengthened with a relieving arch on the outer side, with which it was tied with bond timbers (RCAHMS 1951), while further protected originally by the aisle roof. Immediately below, the nave arch has a substantial width, providing sufficient space for a rather more regular transition between the lateral wall and the pier than the usual *porte-á-faux* form (Fig. 1.5).

The vaults at the south aisle, which are the case study of this research, span over an almost square compartment. They are plain, quadripartite vaults, with diagonal ribs and straight vertices at mid-height of the nave (Fig. 3.5). At their outer edge, they are supported

upon the wall and responds attached to it. The edge of the vault along the nave rests upon the main arcade, which has obtusely pointed arches with three orders of mouldings that continue to the compound piers (Fig. 3.4). Transverse pointed arches mark the edge between the neighbouring bays. The nave piers and the wall responds are carried upon octagonal bases. Remains of the original pavement can be found in only few areas

So far as the buttressing system is concerned, a system of flying buttresses abutted the nave vault above the springings of the main transverse arches only, on both sides (Fig. 3.5). Their flyers were spanning above the aisles and only their lower imposts attached to pier buttresses remain today, immediately above the aisle vaults (Fig. 3.2a). The buttresses are capped with the necessary stabilising pinnacles, most of which are still in place. In addition, a group of rampant arches abuts the outer south wall only, spanning above the north side of the cloister (Fig. 3.3).

3.3.2 Structural scheme

As in the majority of buildings with a basilical plan, the end structures (façade and apse or east gable) can be considered to act as diaphragms, containing the longitudinal thrust of the naves. So far as the transverse thrusts of the central vault are regarded, it has to be noted that sexpartite vaults in general (as those assumed here) do not exert thrust to their supports equally (Fig. 3.7). This form of vaulting was employed in Europe mainly during the transition from Romanesque to early Gothic period, when uninterrupted transversally vaults had to be built at the nave over closely spaced ranges of piers (Acland 1972). This partition to skewed compartments resulted to a lower magnitude of thrust, with higher values exerted to the main piers than to the intermediate ones.

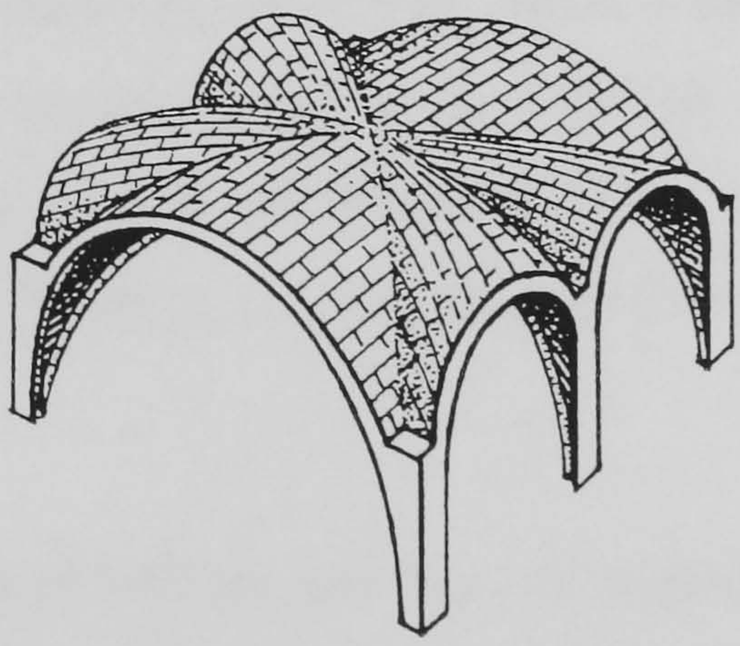

FIGURE 3.7 Geometry of a sexpartite vault (Acland 1972)

The choice of this relatively archaic vaulting system and the narrow windows at the clerestory were probably adapted by the original architects as safe solutions to treat uncertainties in the performance of the upper structure. This design preference for lofty constructions can be also seen in the dimensions of the piers or the outer walls (Fig. 3.5). However, as it will be seen later, the upper structure was completely remodelled in the early 16th century, probably with more plain quadripartite vaults strengthened with tierceron ribs.

During that phase, signs of geometric instability prompted the application of flying buttresses, which had not been present previously. No trace of a second tier of flyers above can be found today on the existing pier buttresses, which would have braced the structure against wind action. Based on the existing evidence and measured surveys at the building, the flying buttresses abutted the vault above the springings, at about 0.3 of its total height. The approximate tables developed by Ungewitter and Mohrmann (Heyman 1995) yield for this hypothetical reconstruction a lever arm for the position of the propping action of 0.2-0.3 of total height, from the springings (Table 2.1). The sensitivity of the area will be discussed again during the study of the collapse of the church.

With the thrusts of the nave vaults stabilised by the flying buttresses, in normal, service conditions and when its integrity had not been compromised, the lateral wall of the nave would be expected to carry only the weight of the upper structure to the columns (§1.2.2). Despite the comparatively solid lower structure (Fig. 3.5), the zone of the triforium could still represent an area of weakness, which may function as a hinge in the case of instability of the upper structure (Fig. 1.5).

Regarding the aisle vaults, the thrusts they exert in their longitudinal direction are mutually cancelled by those of the immediately adjacent vaults of the aisle. Thrusts in the transverse direction are retained by the outer wall, which is further strengthened in the south side only by a lower tier of rampant arches (Fig. 3.5). The relatively stiff nave piers and spandrel walls can retain the vault in the other end of the transverse direction, while the weight of the upper structure would reduce the resultant force from the weight and thrust of the aisle (Fig. 1.7).

Part of the foundations of both the existing and original church were exposed during the consolidation works in 1911 (Fig. 3.3). Their dimensions appear to be sufficient for their

function and no differential settlement of the arcade has been recorded or historically observed.

3.3.3 The cross-vaults of the aisles

A more detailed examination of the vaults at the south aisle follows, which consist the case study of this project (Fig. 3.8). The east archway of the aisle is filled with the screen wall built at the east end of the church. The first three bays from the west façade are blind as they are blocked by the Palace building, while the last two bays at the east end are partially occupied by burial vaults (Fig. 3.3). The remaining bays have a relatively narrow lancet window. This edge of the vaults is further supported upon the responds that project from the wall. The *formeret* (longitudinal-nave) arches that support the edge of the vault towards the nave have a substantial cross-section, with a recessing roll-and-hollow moulding pattern.

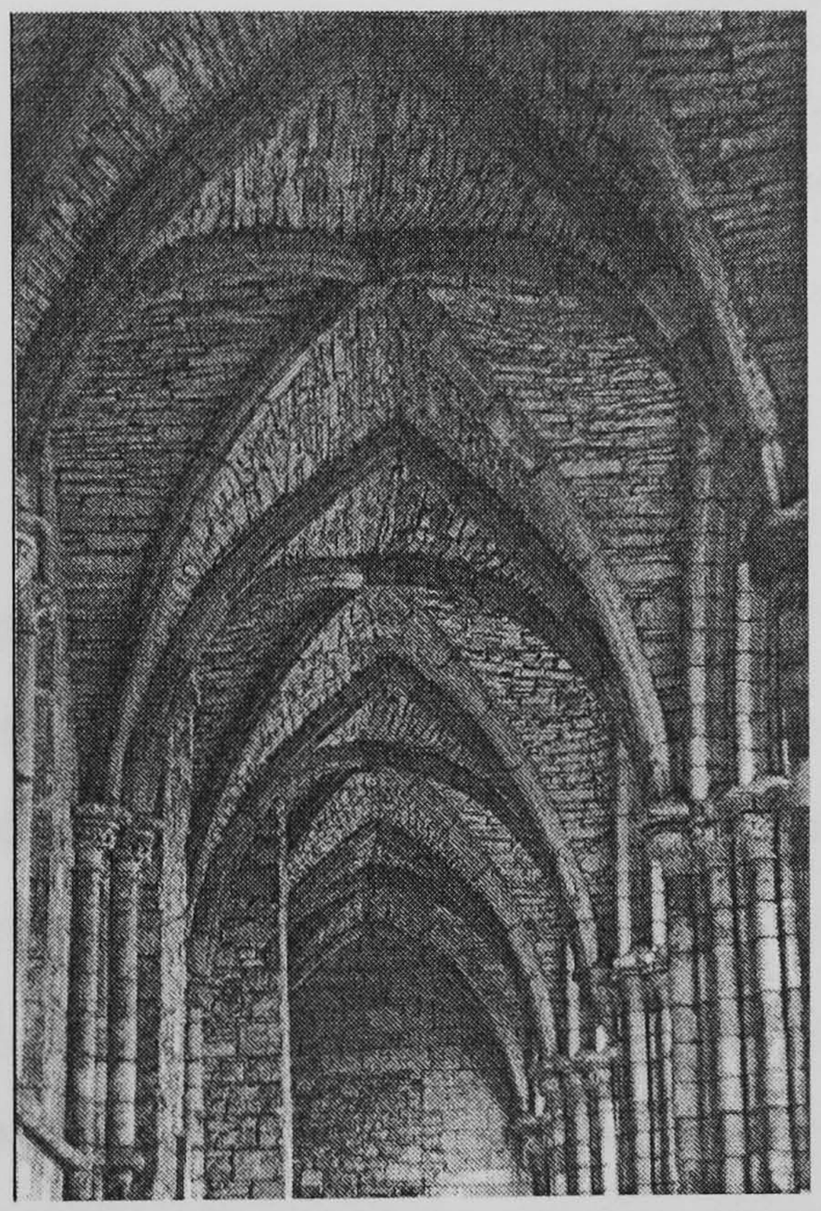

(a) Longitudinal aspect

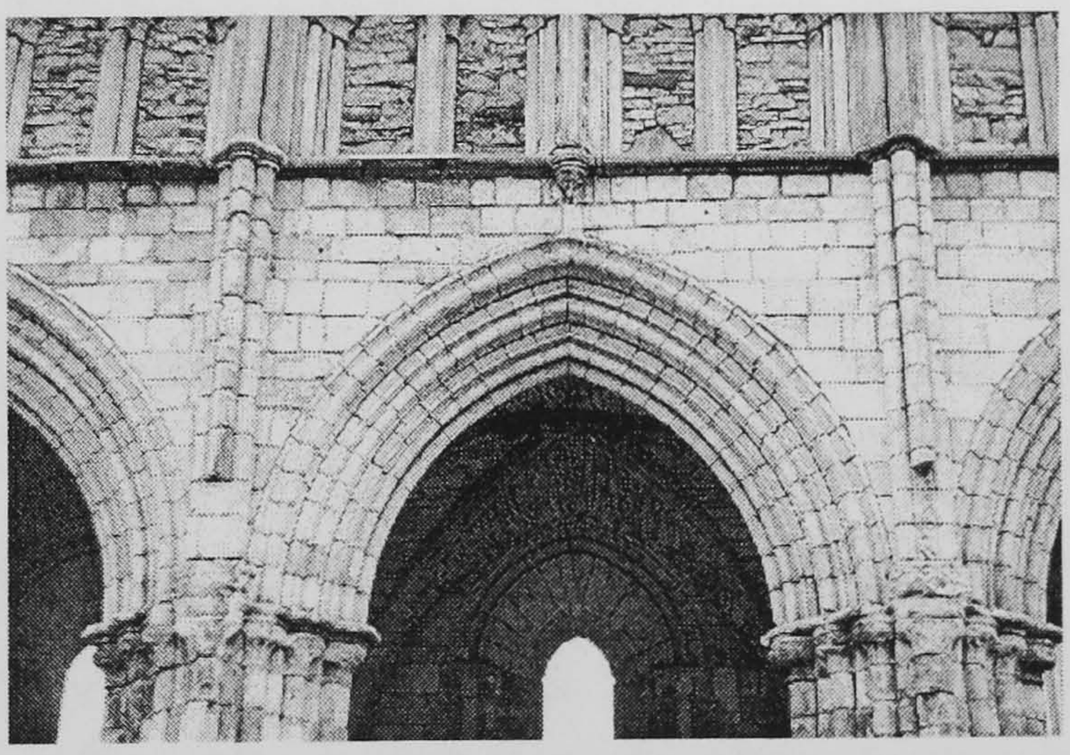

(b) Nave arcade

FIGURE 3.8 View of the south aisle

The masonry of the wall is faced throughout with ashlar leaves of hard yellow sandstone, filled with a rubble core of large stones laid on their beds and thoroughly grouted (Fig. 3.9) (RCAHMS 1951). During the repairs of 1909 (Baldwin), it was found that the stone in the building varies significantly in both aspect and hardness, affecting the removal

of the accumulated encrustation around the mouldings. From a visual inspection, it appears that the Hawkhill type of stone was used, which according to data for the building stones of Edinburgh (Bunyan et al 1987) has a unit weight of 23.7 kN/m^3, elasticity modulus 27.1 kN/mm^2 and compressive strength 42.8 N/mm^2.

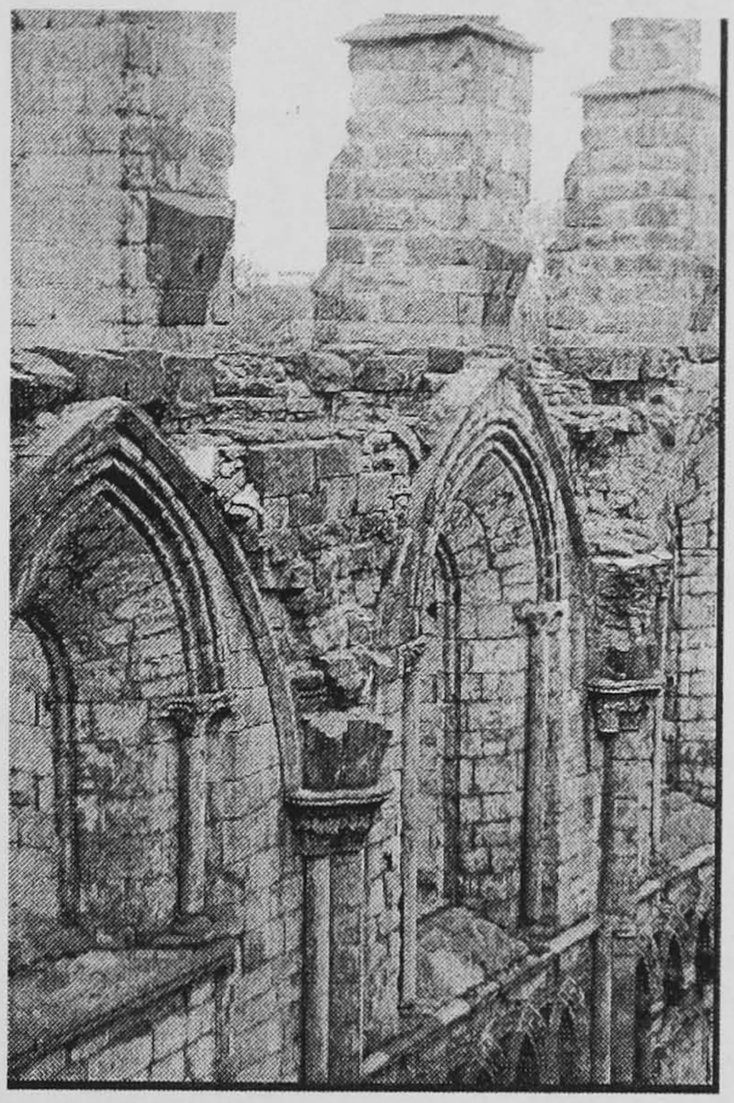

FIGURE 3.9 Detail of the composition of the outer wall in the north aisle

Both the ribs and the transverse (*doubleaux*) arches have a plain cross section and they spring from a *tas-de-charge* of single voussoir, while the conoid pockets created between the abutments of the vault and the spandrel wall are filled probably up to the third of height (Fig. 3.9). The web is constructed of rubble masonry, made of long thin slabs of irregular thickness (Fig. 3.10) but probably not as large as those employed at the nearby St. Anthony's Chapel, attributed to the same Austin Canons of Holyrood (Coles 1896), as it can be confirmed in the abutments of the collapsed north aisle (Fig. 3.9). The webs were probably plastered for reasons of durability and aesthetics and the last remains of this coat were probably removed as degraded in the restorations of 1909 (Baldwin) (Fig. 3.11). The vault is protected today by a wooden roof of single pitch, probably lower than the original one, as the remains on the outer pier buttresses show (Fig. 3.5).

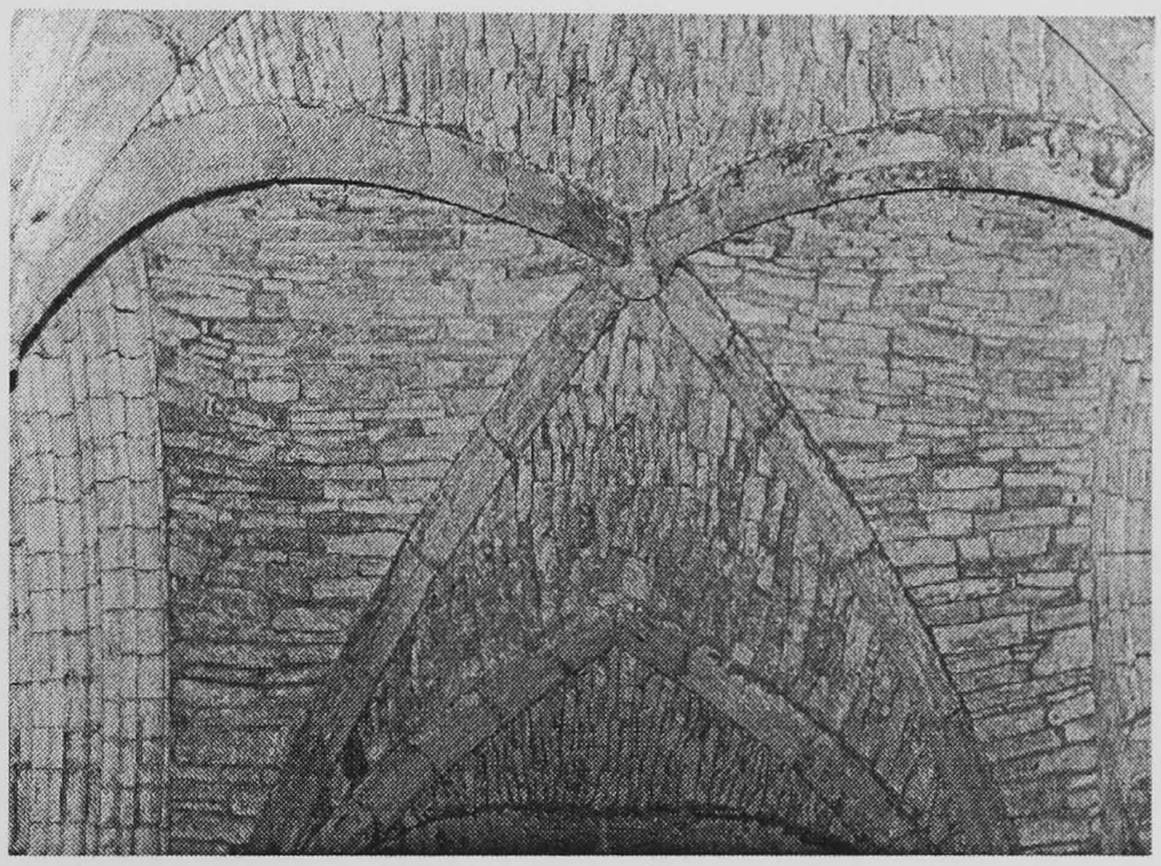

FIGURE 3.10 Aspects of the aisle vaults

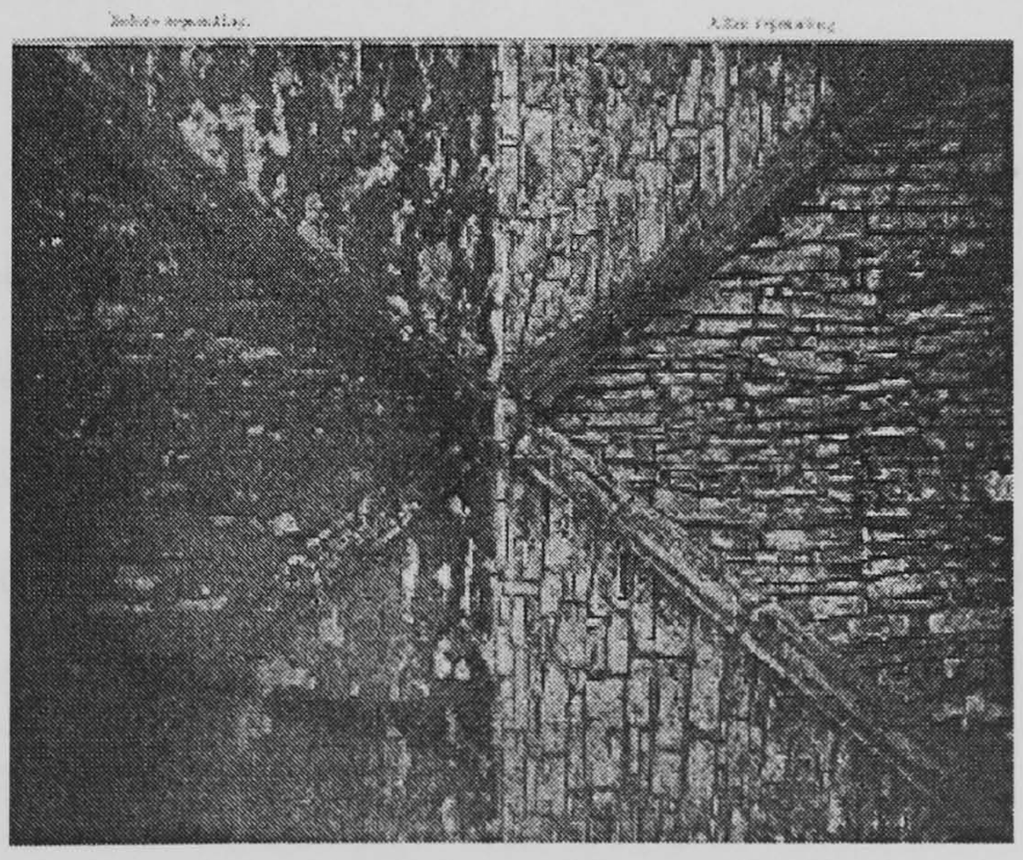

(a) Before (b) After

FIGURE 3.11 Consolidation works of 1909 (Baldwin)

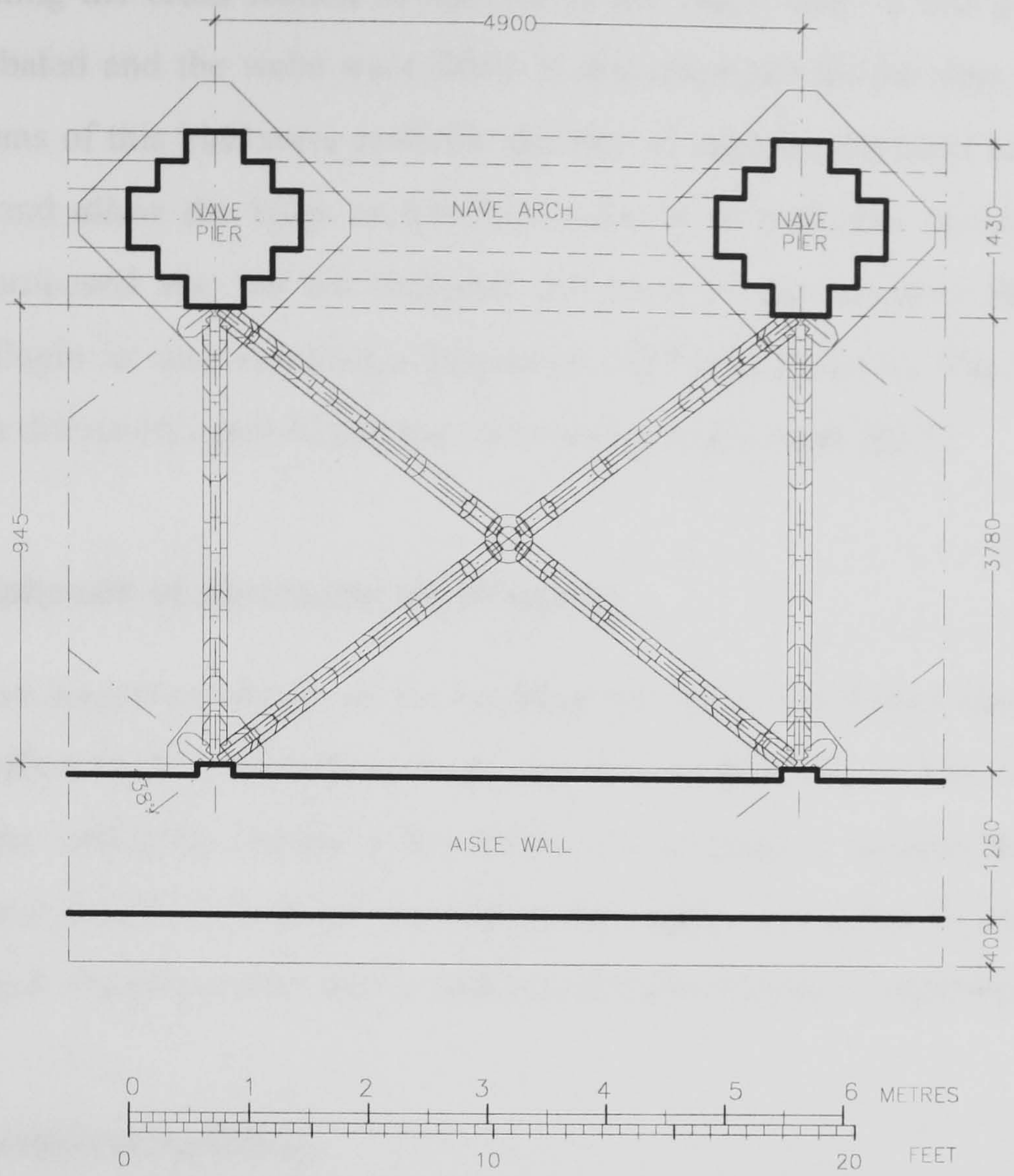

FIGURE 3.12 Measured survey of the vault in the fourth bay of the south aisle - ground plan (dimensions in mm)

A measured survey of the ground plan was performed for all the accessible bays and a typical plan arrangement can be illustrated by the fourth bay (Fig. 3.12). A critical study of this plan according to design rules frequently observed by the Gothic masons (Rovira 1899, Fitchen 1961, Benedetto 1991, Fletcher 1996) together with existing measured surveys (NMR EDD/E/7 and 8) help to establish the proportions of the intersecting barrels. As an essential criterion, it was considered that the ribs and profile of the vaults were generated by the same radius. With reference to the four types of cross vaults over a square bay (Fig. 3.1), the first type was found to apply better in this case (straight vertices and pointed diagonal rib: arched profiles with equal radii and heights (Fig. 3.1a)). The radius was taken as equal to the span of the transverse archway, so an equilateral triangle could be inscribed within the transverse arch. The centres of the ribs and longitudinal (nave) arch were determined accordingly.

Concerning the cross section of the ribs of the cross vault, it was assumed that the extrados is rebated and the webs were fitted in the space left by the stem at the extrados (Fig. 1.9). Stems of this kind were probably devised to improve the bond between the shell and the ribs and allow the latter to function properly as stiffeners (Fitchen 1961). This feature was proposed also for the diagonal and most of the tierceron ribs by Gillespie Graham and Pugin in their restoration project of 1837 (see §3.3.4.4). The function of this feature will be discussed again during the construction of the vault (§3.5).

3.3.4 Major phases of structural significance

The most important phases in the building history of the Abbey church which may have had an effect on the structural performance of the south aisle will be outlined. After it was built as the collegiate church of the Abbey of Holyrood, it became the Chapel Royal when the Palace was developed and the Abbey was suppressed. After its partial collapse in 1768, the church was abandoned and no restoration project has been approved since.

3.3.4.1 The original building

The Abbey of Holyrood was founded by David I in 1128 and was manned with Austin Canons. As established after the excavations in the beginning of the 20th c. (Oldrieve 1911 and 1912), this first church was of a modest scale (Fig. 3.3) and today only a wall of this building is incorporated in the south aisle wall.

A new and bigger church was initiated by 1195. As it was the practice of the time, the previous building was not demolished until the new structure was almost complete. As a result, construction started from the choir and the transept, while later the nave was surrounding the older church starting from the north aisle and the new façade. By 1220 the outer north wall had reached its actual height (Fig. 3.9), the south wall and west front were progressing and the bases of the piers were set up (RCAHMS 1951). By 1260, the pier arcade was completed and all the walls had reached their maximum level, while probably the original church had been demolished. Consequently, the high vaults were constructed, as their abutments at the triforium level were also ready, and the aisles were probably vaulted afterwards, as the ribs of the north aisle are of later cross-section than those of the nave. By the end of these works, however, the transept and choir had to be remodelled as the

foundations indicate (Fig. 3.3). During the warfare against Edward II in 1322 the works were interrupted. By the middle of the 14th c., the church was complete lengthwise.

3.3.4.2 Significant structural alterations

Until that time however, no provisions for lateral support to the nave and the aisles had been made and some preparations started at the south aisle. It is assumed that in the time of Abbot Crawford (1487-1503) a more global solution to the problem was undertaken by remodelling completely the upper structure. It is considered that the 13th century sexpartite vaults were replaced by tierceron rib vaults (probably quadripartite, according to Fig. 3.2b) and a system of flying buttresses was added to the nave. According to the architect Thomas Ross (EAA 1910), these works were carried out with great knowledge of the function of the vaulting. The north outer wall and clerestory were probably already leaning outwards. As a consequence, the pier buttresses had to be lighter than in the south aisle to avoid adding load and increasing the thrusts, and they were added as an almost independent structure. This, however, resulted to longer rampant arches than in the south aisle, although their section was wider (9 in - 0.23 m). Moreover, the east end was remodelled and, although the church was complete, a low screen wall was erected separating the west crossing from the nave. The wooden roof was later protected with lead.

The NE corner of the Palace incorporates today a portion at the SW of the church. Between 1501-5, the first significant form of this structure was probably built, followed by additional phases until 1536, although Holyrood was already considered as a royal residence from the 15th c. (Gifford 1984). Later, the fires caused by Hertford's invasion in 1544 and 1547 seem they did not cause any critical damage to the fabric, as only some annex buildings were burnt (Laing 1892, Mylne 1893). However, the lead of the roof was removed, leaving the vaults almost open to the weather, and during the warfare gun shots were fired at the Palace, leaving visible traces at the unprotected north aisle of the church.

Neglect and probable side effects from riots and looting during the Reformation resulted to a dangerous state of the choir and transepts. As a consequence, the Commendator Adam Bothwell pulled these parts down in 1570 and closed the church with a wall at the west crossing. With the profit made by the sale of the stonework, repairs were carried out to the nave and lofts were added to increase the seating space.

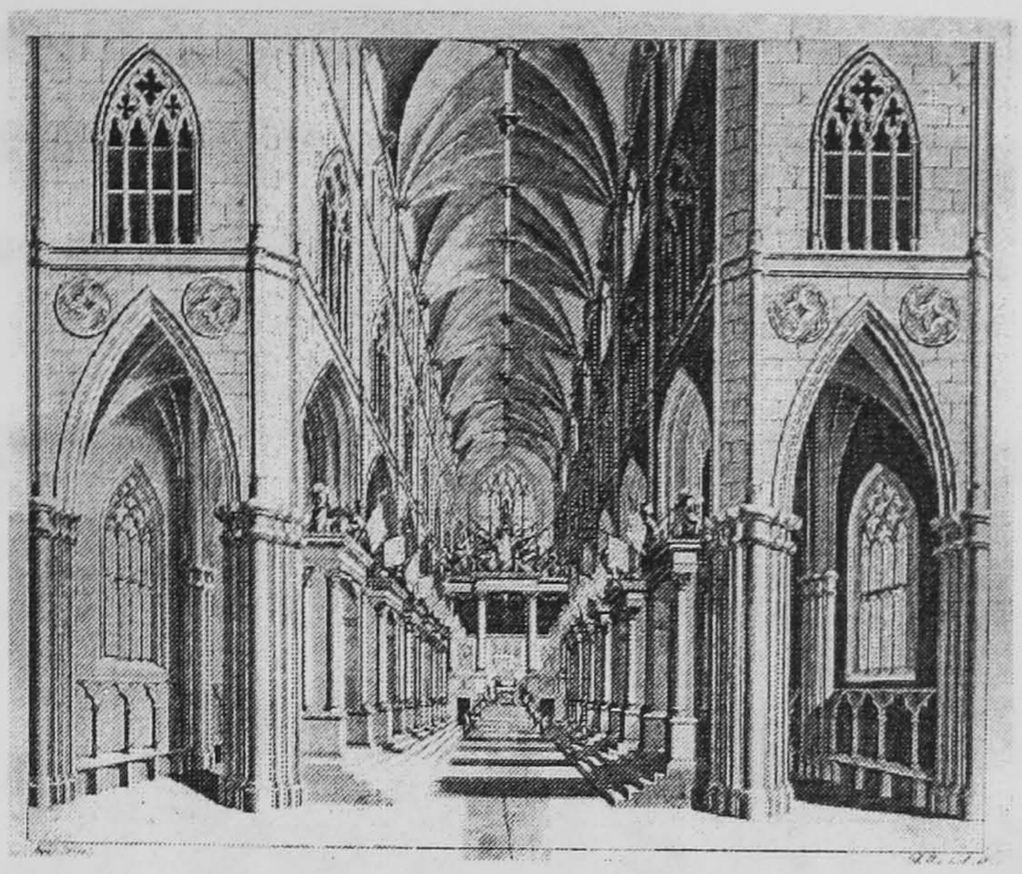

FIGURE 3.13 Alterations to the Abbey Church for the coronation of Charles I in 1633 (NMR EDD/3/14/P)

In 1633, Charles I decided to hold his coronation in Edinburgh, so the Abbey church underwent a general remodelling, remains of which can be seen today only at the west façade and the tracery window added to the east gable. At the interior, the lofts were removed and the rest of the interventions regarded mainly the decoration (Fig. 3.13). Later, in 1650, the palace was damaged by a fire when Cromwellian troops were stationed at the building, but no faults were reported at the church (Harrison 1919). After the Restoration in 1660, the actual Palace of Holyroodhouse was built between 1671-9 by W. Bruce and R. Mylne (NMR EDD/4/105). On the occasion, the last remains of the walls and columns of the transept and choir were cleared (Maitland 1757) and a part of the west front was blocked. Later in 1687 the church was officially declared as Chapel Royal and in the next year refurbishments were performed hastily, which most probably weakened further the fabric. During the religious riots that broke in December of the same year, however, the fittings were destroyed but no major structural damages were reported.

3.3.4.3 The collapse of 1768

The looting of the church was followed by a further period of neglect during which the unprotected rafters of the roof were decaying and the state of the abandoned church became very dangerous. In 1754 the Duke of Hamilton (hereditary keeper of the Palace) reported the situation to the Barons of Exchequer (responsible for crown property in Scotland), asking funds for repairs (NAS Exchequer Records E306/2). The major problem concerned the ruinous state of the roof, with the timbers in need of urgent repairs (Fig.

3.14). The Barons approved his petition and in 1758 they awarded the project to John Douglas, Architect, and James McPherson, Mason in Dean, allocating a sum based on their estimate (NAS Exchequer Records E306/3).

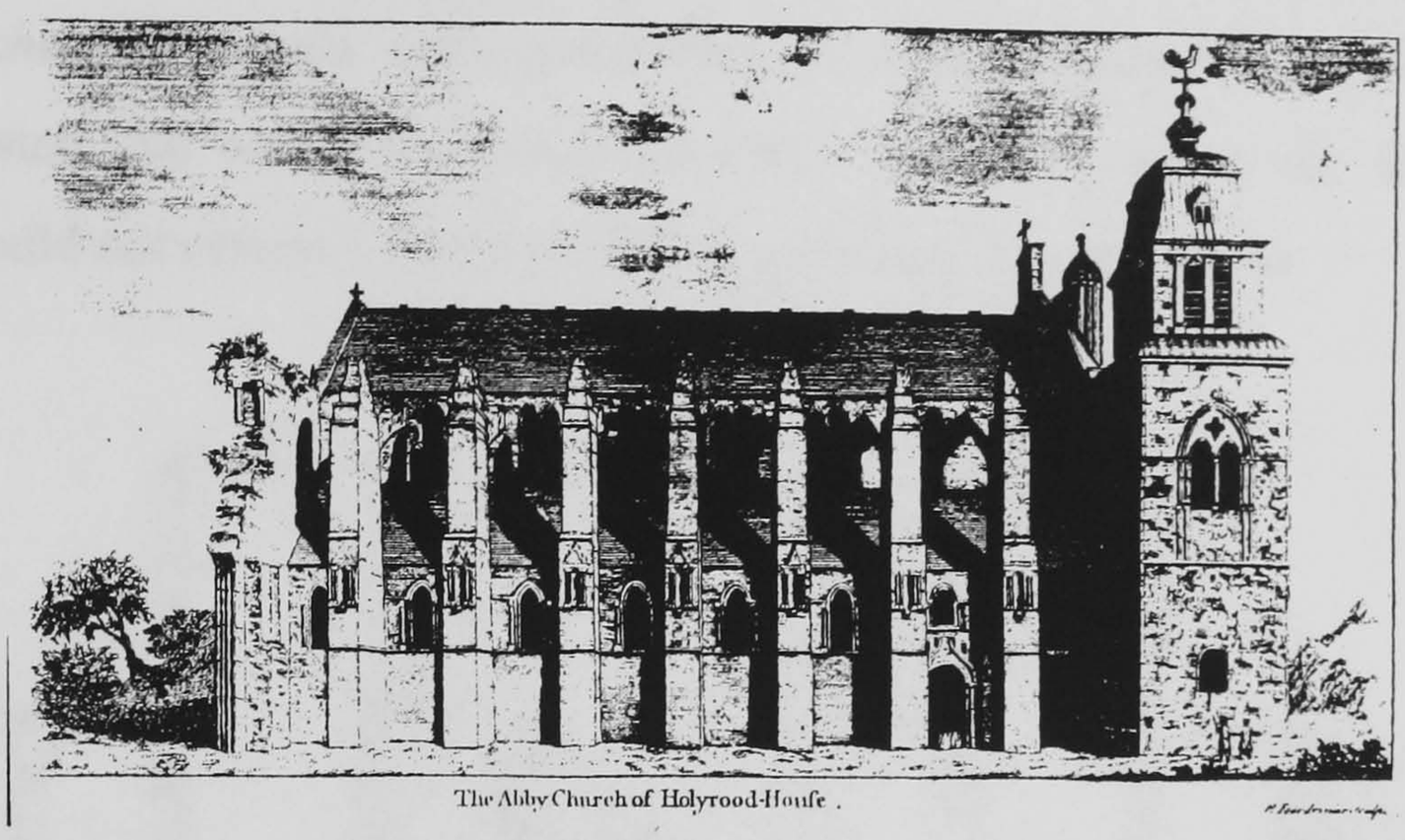

FIGURE 3.14 The state of the Abbey Church in 1753 prior to the interventions of 1758 (Maitland 1757) - the springing height of the flying buttresses is probably incorrect (cf. Fig. 3.9)

Their proposal in 1757 was to replace the existing wooden roof with transverse diaphragm walls 1 ft 4 in (40 cm) thick, spaced at 2 ft (61 cm), over the extrados of the vaults "so as to raise and frame the reverse of the arch" (NLS MS 5371 f. 196). In this manner it was thought that the pends of the roof could be safely covered by "hewn stone" or thick stone flags. From the final estimate they submitted (NLS MS 5371 f. 198) it is not sure whether it was planned to roof the aisles with the same system, but probably the south aisle needed less repairs as it was not exposed to the weather as the north aisle (Fig. 3.3). There is also a possible reference to the triforium zone ("the windows where the Stone Roof of the Isles is to join to the side walls of the Main body of the Church"), which was filled or strengthened with rubble masonry. The Barons accepted their project and contracts were signed on 28/6/1758. The works were concluded exactly two years later.

In 1766, however, the building had entered into an even more dangerous condition, so the Barons asked the architect William Mylne (d. 1792) to survey the fabric. On 10/12/1766 he reported that many of the walls and pillars inclined to the north 2 to 3 in out of perpendicular at some feet height. The east gable inclined 3 to 4 in to the east at 10 ft height, so he supposed that "*the walls & pillars will incline seven or eight inches from the perpendicular that is at the greatest height*" (NAS Exchequer Records E310/1/2). He also

observed that "*there is one of the Coins* (voussoirs) *of the Arches fallen down, another just ready to drop away, several of the small columns on the Pillars come away, others fast following; the walls much bent in several places and the whole building approaching ruin at swift pace*". As a reason for the failure he considered "*the great load of building later laid above the Arches; a load the walls and pillars were never intended to carry*". W. Mylne further suggested that unless the heavy roof was taken off and so the damaging effect arrested, he could not estimate the extent of the necessary remedy works.

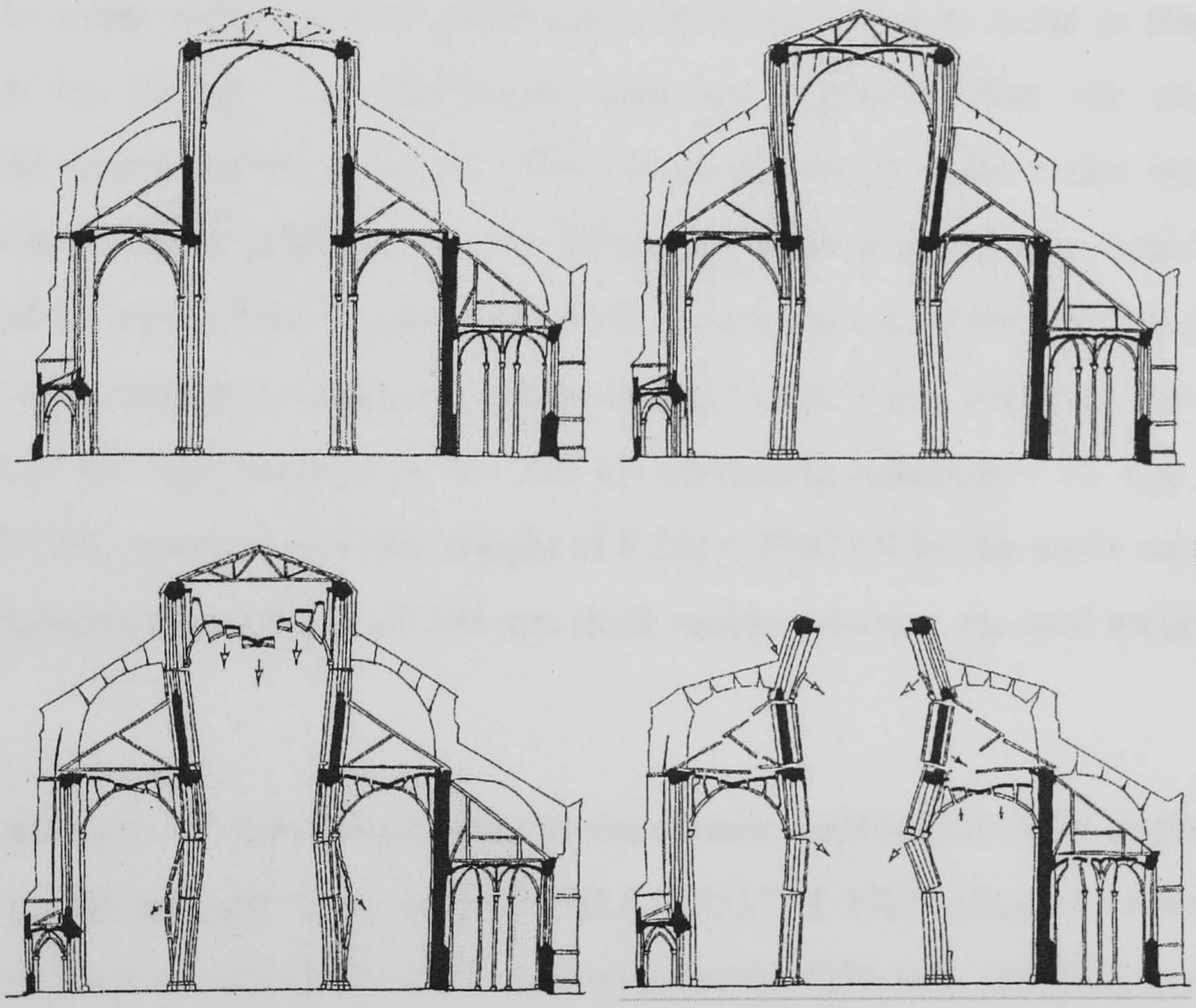

FIGURE 3.15 A hypothesis for the failure of the Abbey Church following the interventions of 1758 (Pieper 1983)

After this report, probably no action was taken towards repairs. The situation apparently deteriorated and the roof and walls collapsed on 2/12/1768, followed probably at a later stage during the same day by the aisles ("Holyroodhouse" 1768). According to a new report by William Mylne to the Barons, part of the roof was still standing, while the damage had extended to the top of the NW tower and the stairs it contained (NAS Exchequer Records E305/7). As these reports show, a quite typical process of failure developed within these eight years, which can be summarised in Fig. 3.15. According to the actual ruinous state and a study by T. Ross (EAA 1910), the collapse initiated from the north side of the church. The neglected rampant arches were more severely weathered and weakened than in

the south aisle and the failure of one flying buttress would be sufficient to destabilise the transverse equilibrium, releasing disproportionally the thrust of the south side. Consequently, the weight of the falling clerestory would crash the remaining tiers, which in turn would destabilise the rest of the upper structure in a similar manner, destroying finally the north aisle.

After the collapse, W. Mylne demolished the most dangerous parts and blocked several windows and the remaining stairs for safety reasons (NAS Exchequer Records E305/7). As stone vaults of these dimensions were quite rare to build at that time, the intervention by Douglas and McPherson probably originated from the contemporary technique of supporting the joists of a floor upon shallow masonry vaults with masonry footings (Cigni 1987). Although in the following claim disputes they argued that the execution of the repairs was of good quality (NAS Exchequer Records E342/9), it is evident the project was completely unsuitable for the ageing vaults. Using Table 2.1, an estimate of the weight of the high vault gives V= 250 kN (assuming sandstone - cf. Fig. 3.8) and a thrust of 107 kN, resulting to a total weight of 8·250 = 2000 kN for the entire nave. Even for the more conservative estimate of 300 mm thick rubble masonry, the total weight becomes 3420 kN.

According to the dimensions given by the masons, approximately 40 diaphragm walls were built above the vault. Their estimate (NLS MS5371 f. 198) indicated a total surface of "54 Rood 18 yards of Rubble Building" was intended (or 1381 m^2), resulting in a volume of $0.41m \cdot 1381m^2 = 566m^3$. Considering a unit weight for masonry of 20 kN/m^3, this yields a total weight of 11330 kN, a number compatible with the available volume under the roof. Even if the weight of the stone flags is not added, it becomes apparent the four-times increase of the weight of the structure and subsequently the thrust was impossible to be contained by the insufficiently maintained buttressing system and lateral walls, although some strengthening was provided for the latter.

3.3.4.4 The present state

After the collapse, there had not been any immediate proposal for restoration (Fig. 3.16). Robert Reid supervised general repairs and cleanings, within the campaign of restorations at the Palace between 1824 and 1834. In 1837, a restoration project of the

Abbey Church as a Hall to the General Assembly of the Church of Scotland, by J. Gillespie Graham and A. W. N. Pugin was dismissed as too expensive. However, this project can give some insight on the perception of the structural configuration of the vaulting system from two important architects of the Neogothic movement (Fig. 3.17). Both the high and the aisle vaults are treated as quadripartite and are visually and probably structurally strengthened with tierceron ribs. This eclectic choice to stress the linear bearing elements is followed also in the rest of the building.

FIGURE 3.16 The state of the Abbey church in 1788 (ECL pYDA 2065(753) - 599)

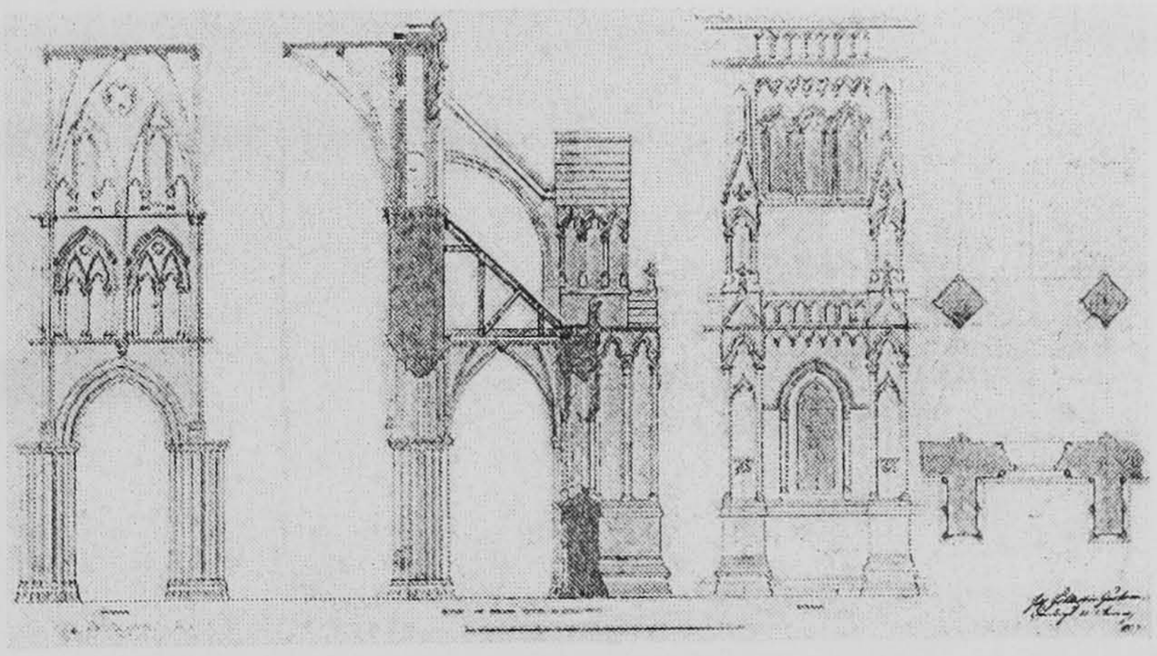

FIGURE 3.17 Scheme for the restoration of the Abbey church as proposed by J. Gillespie-Graham and A. W. N. Pugin in 1837 (NMR EDD/3/232)

New plans for the restoration of the church were advanced again in 1906. On request from the Earl of Leven and Melville in his Will, the church was the first option for the location of the Thistle Chapel (before its actual placement at St Giles'). W. Lethaby was appointed to survey the fabric and assess the viability of the project. In his report he gave a negative opinion on the grounds that the fabric was in such a ruinous state that too much

new material may have to be added, altering drastically the integrity of the building both structurally and aesthetically (EAA 1910). He detected extensive decay of the stone material and relatively large deformations. In particular, "*the south wall of the nave, containing the triforium, leans inward from the third pillar to the fifth (counting from east) from 14 in over the former to 11 in over the latter... The external wall of the north aisle leans out 4 in at the middle, the south aisle wall also leans outwards. And the east gable leans out 5 in*".

T. Ross objected to this report, observing that these deviations were either ancient and stable or relatively meaningless (EAA 1910) and that the structure was solid enough to support the weight of a vault, as long as the thrusts could be better contained than in the original structure. However, Lethaby's report was finally adopted and the project was abandoned. Since then, no other proposal for a complete restoration has come forward.

At the same period, interventions were carried out to the existing fabric, but mainly of conservation and maintenance character. The intrados of the lateral vaults was cleaned and consolidated (Fig. 3.11), removing probably the last remains of the original plastering (Baldwin 1909). A quite comprehensive archaeological campaign was also directed by the then Office of Works (Oldrieve 1911, 1912), which revealed the extent of the church and the evolution of the structure. Since then, blocks from the columns or the nave walls have been consolidated or substituted, during regular maintenance in various phases. No further faults have been reported on the fabric of the vault.

3.4 VAULT TEST MODEL

3.4.1 General

In order to study in detail the response of the aisle vaults to the deformations imposed by the failure of the upper structure (Fig. 3.15), a model in 1/4 scale of one of the bays of the south aisle was built and tested to failure. The action was simulated as an inward movement of the supports, in the transverse direction. In this section, the process of construction of the vault test model is presented and discussed, while the preparation of the test is explained in Chapter 4.

Various textbooks on vaulting construction were consulted, some dating from the 19th c., when the interest for Gothic design had revived in churches that were being built

according to the Neogothic style (Viollet-le-Duc 1868, Rovira 1899). More recently, J. Fitchen published a comprehensive and critical study on stone vaults (1961), followed by an examination on the evolution of the role of the vaults within the entire building by J. Acland (1972) and an exhaustive and detailed research on the construction process of a single cathedral (Chartres) by J. James (1979). These important texts have been constantly referred to during the construction of the vault.

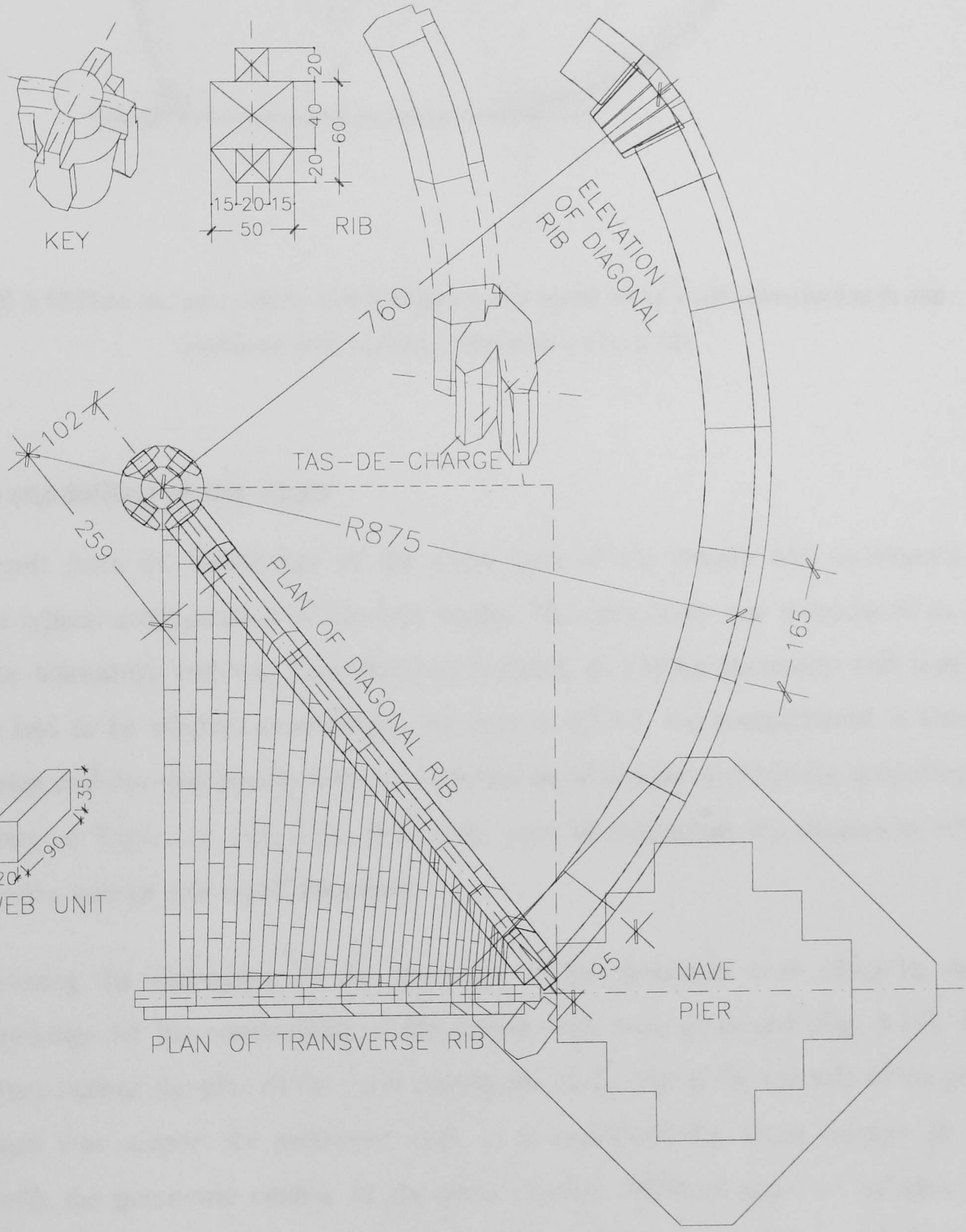

FIGURE 3.18 Overall construction drawings of the voussoirs and web units in the model cross vault (dimensions in mm)

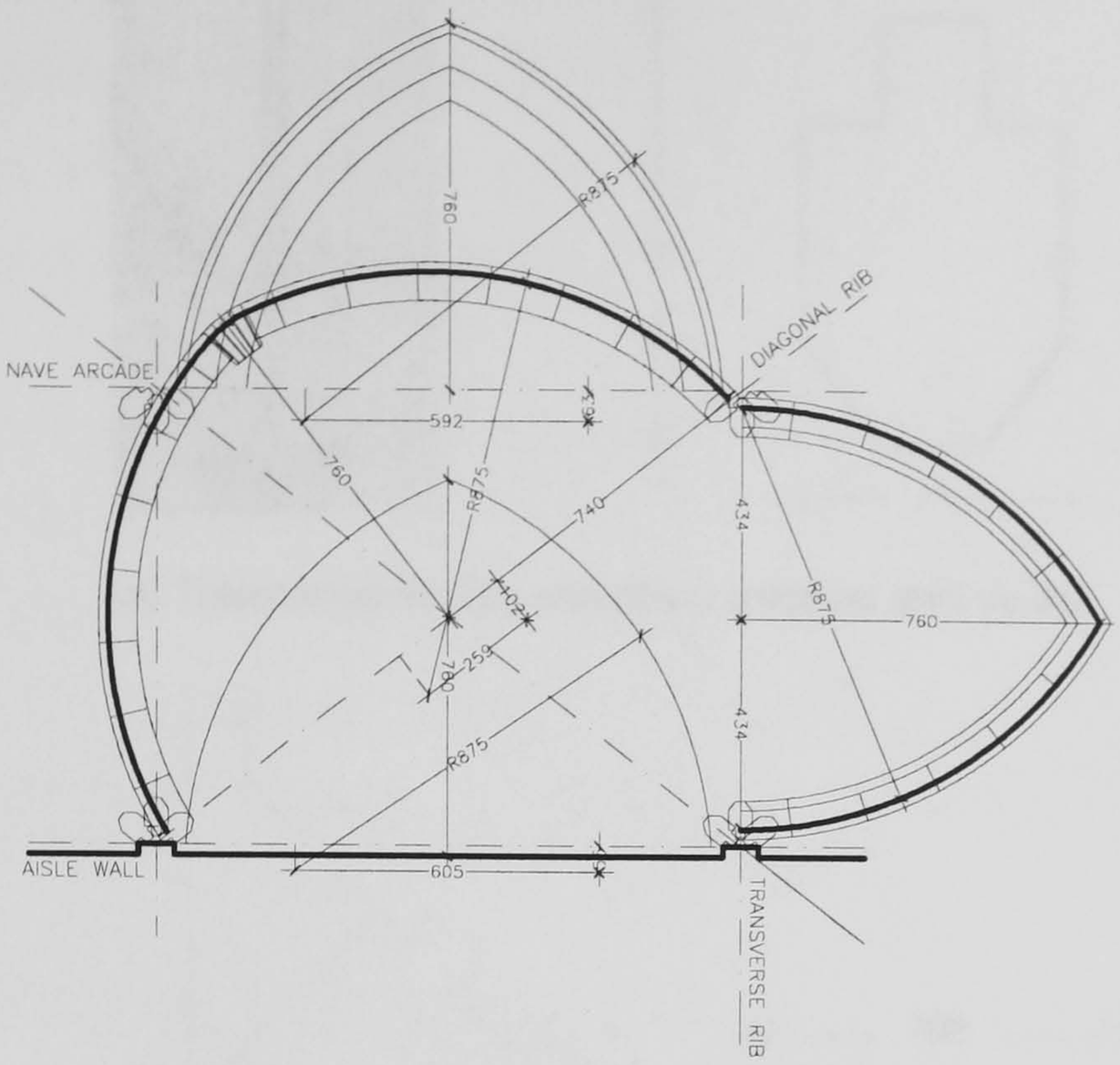

FIGURE 3.19 Plan and proportions of the arches in the model cross vault - dimensions in mm
(compare with prototype structure in Fig. 3.12)

3.4.2 The modelling of the vault

A vault from the fourth bay of the south aisle of the church was considered to represent a typical configuration of the aisle vaults. The case study was reproduced in 1/4 scale in the laboratory and was considered as isolated, so certain geometric and support conditions had to be adapted accordingly. As seen in §3.3.3, the compartment is almost square in plan and the vault results from the intersection of two pointed barrels, according to the geometry of Type 1 in Fig. 3.1a. Ribs were used to strengthen the diagonals, while arches played a similar role on all the edges.

Following the discussion on the geometry of the prototype vault (§3.3.3), more detailed drawings for the construction of the model vault were produced (Fig. 3.18). The corners which outline the plan of the vault correspond to the top of the capitals of the piers and responds that support the prototype vault. It is important that these corners do not coincide with the geometric centres of the piers (Rovira 1899) in order to enhance the stiffening role of the ribs. In this manner, the cross section of the lateral arches at the abutments of the vault is offset from the pier extension (cf. Fig. 1.5) and the line of thrust can be contained more safely within a wider section, while the span of the arch is reduced.

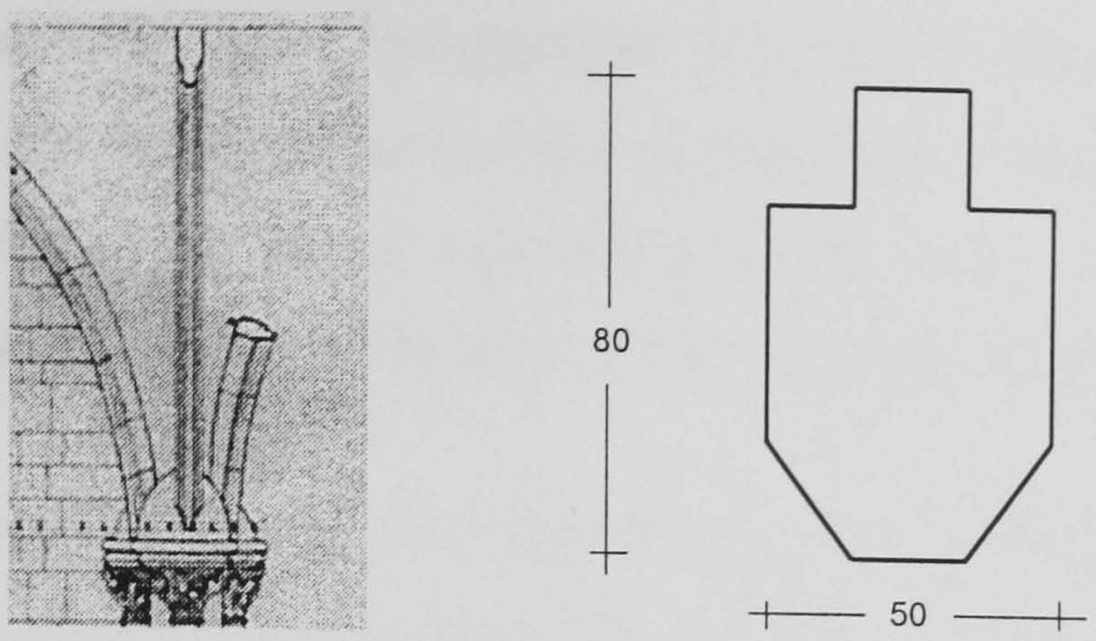

a) Transverse arches and ribs: prototype and model

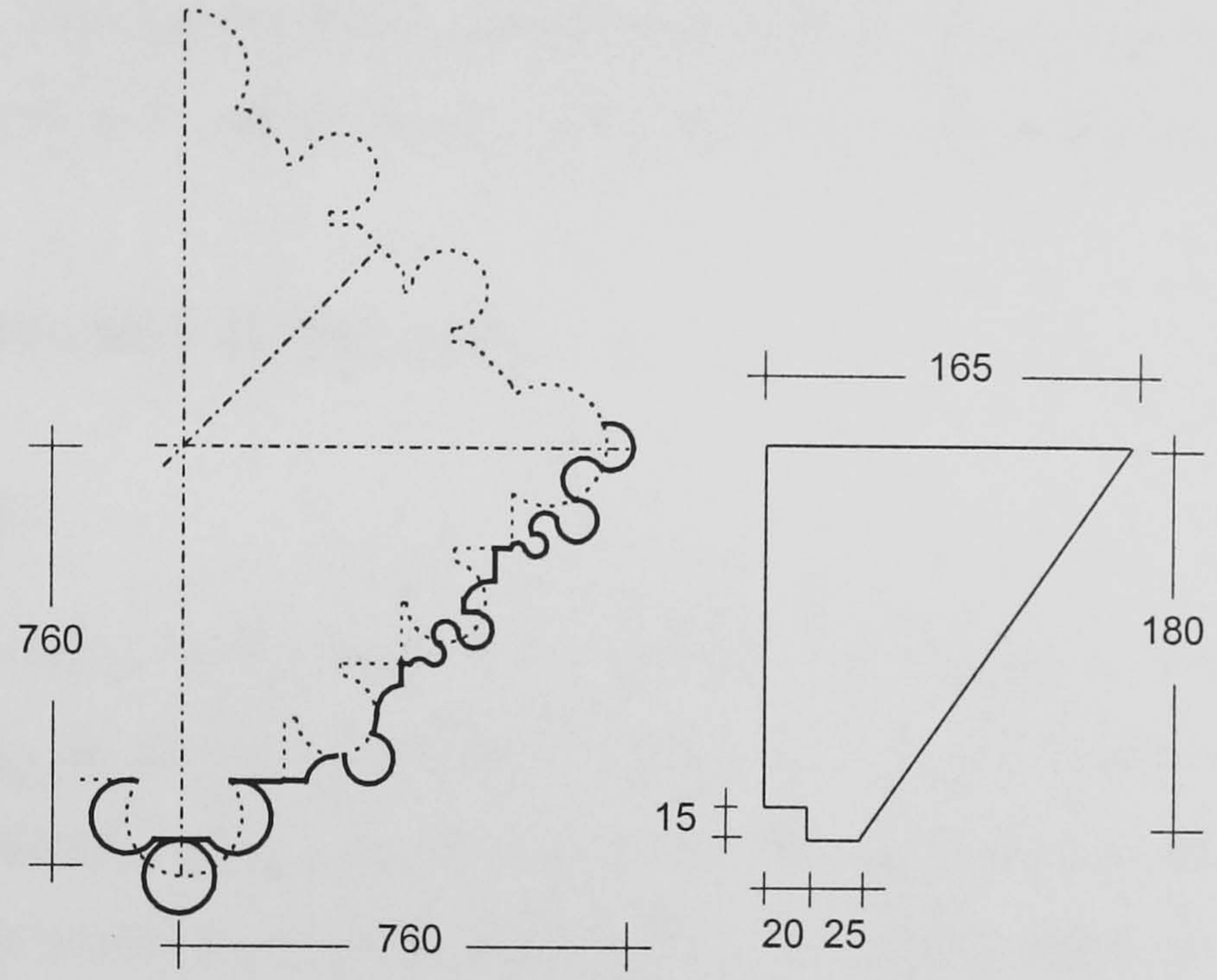

b) Nave arch: prototype and model

FIGURE 3.20 Modelling the voussoirs of the arches in the vault model - cross sections

As in the prototype, the same radius of curvature was used for both the intersecting webs of the vault model, following a practice of the period which facilitates the production of the centering for arches and falsework for the shell. Both the transverse (*doubleau*) arches and the ribs have the same cross section and form of voussoirs (Fig. 3.19). The nave arch (*formeret*) however has a more deeply moulded profile and only a quarter was considered here. Reproducing in detail the mouldings of these arches would require the skills of a specialised stone-mason. Most importantly, however, this would not affect significantly the structural performance of the model. As a result, a form geometrically similar to the original was chosen, which would yield the same second moment of inertia. In this manner, the cylindrical torus of the transverse and diagonal arches was modelled as a polygonal ending (Fig. 3.20a) and the recessing cross-section of the nave arch, with the roll-and-hollow mouldings, was reproduced as a trapezoid (Fig. 3.20b).

A similar assumption as in the prototype vault was made regarding the rebated voussoirs of the ribs and transverse arches (§3.3.3). The stem at the extrados provides the intersecting webs with a stiff lateral support along the groin, avoiding the associated geometric problems, and improves the balance of the webs over the groin (cf. Fig. 1.9b).

The continuity of the vault to the adjacent vaults was restored by means of lateral panels applied to the transverse arches. The whole of the model was supported on four solid concrete pillars and the device that would shift the front two abutments was attached on their outer edge. The edge of the prototype vault which is supported upon the outer south wall was considered in the model to rest upon a brick wall, adequately profiled.

3.4.3 The construction of the model

3.4.3.1 General

The construction of the model vault followed the criteria outlined in the previous section. Regarding the materials employed, wood was considered as the solution that would allow a fast production of the both the arches and the webs masonry. All the blocks of the model cross vault were carved using simple tools of carpentry and with the guidance of a specialised technician. The ease of working with a wood of medium hardness allowed a better approach to the general geometry and the resolution of details, especially concerning the web blocks, by means of trial and error. For the voussoirs, it was very useful to prepare templates, with which the geometry was transferred from the drawings to the unshaped pieces of wood. As for the more bulky blocks (nave arch, keystone), they were formed by separate parts which were bonded together with PVA glue.

3.4.3.2 Layout and *tas-de-charge*

Using templates for the cross-sections and sides, the voussoirs of the ribs and arches were shaped (Fig. 3.21a). The templates were traced with a compass used by stone-masons and then they were cut out of thin plastic sheets. A curved plane was used to shape the curvature of the voussoirs and the cross-sections were tapered to the desired angle (Fig. 3.21b). The blocks of the nave arch required a more complex treatment, as they had to be composed of four parts (Fig. 3.22). The final shape of all these voussoirs was determined

later, after each arch was assembled in dry, following the formation of their keystones (§3.4.3.3).

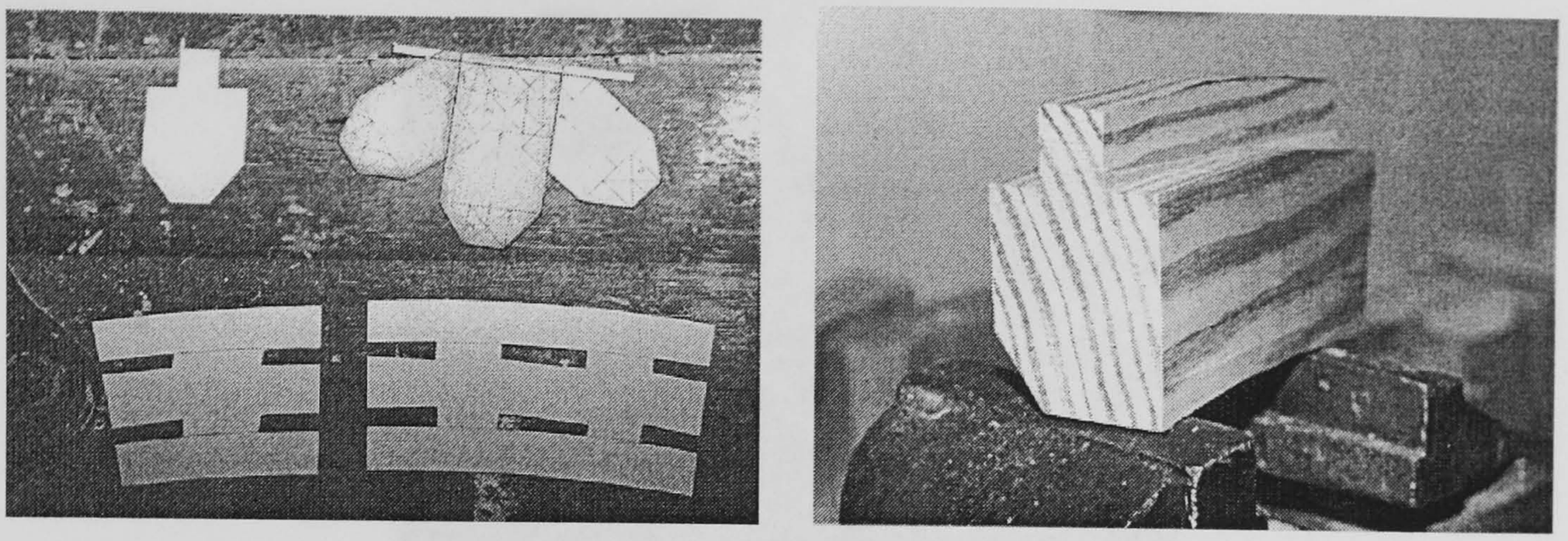

(a) Template of the cross-section and side (b) Preparation

FIGURE 3.21 Formation of the voussoirs of the transverse arches and the ribs

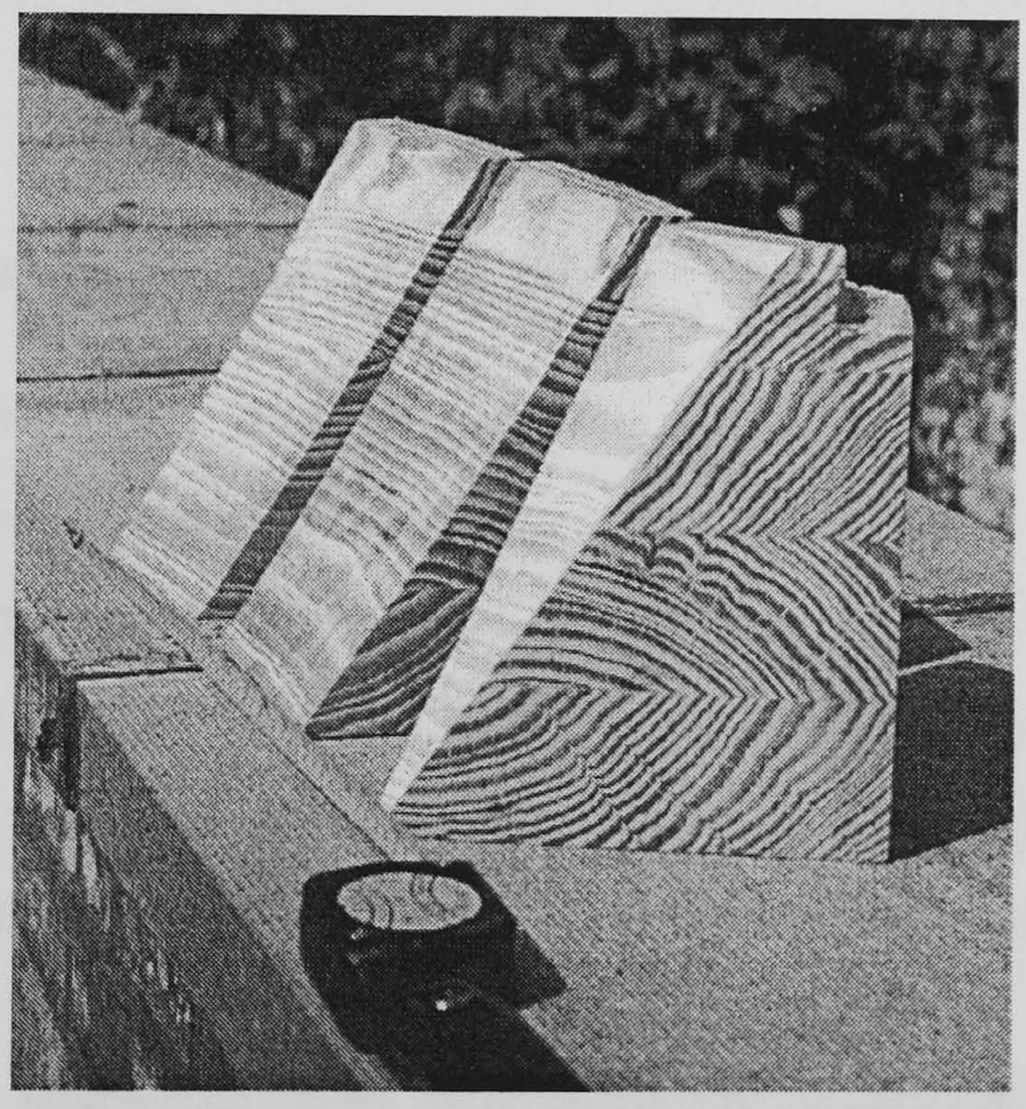

FIGURE 3.22 Voussoirs of the nave arch

After the supports of the model (wall, piers) were ready, the abutments were the first parts of the model vault to be built into place. Over each concrete pier, the arches converge to a single block, the *tas-de-charge*, which corresponds only to the first block. A template of the base of the block was used to control the process (Fig. 3.22): the axis of each converging member was drawn and then their cross-sections were overlapped, in order to bring the axes to a common centre (Fig. 3.18). The lower voussoirs of the ribs and transverse arches (Fig.

3.21a) were further carved to meet into the common block and, after the excessive portion of each block was marked and cut-off, the separate bases were bound together.

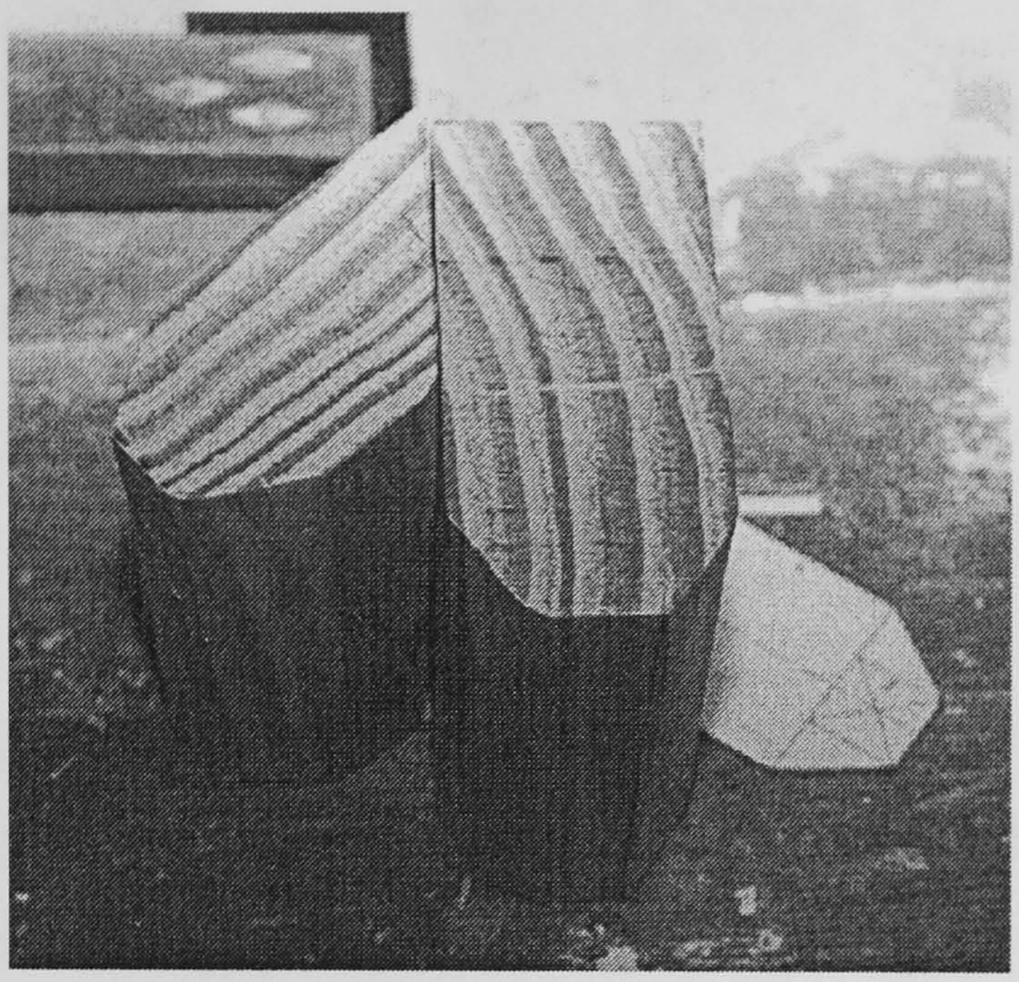

FIGURE 3.23 Construction of the *tas-de-charge* at the abutments. The finished block and template.

3.4.3.3 Set-out and construction of the ribs

Once the bases and voussoirs were ready, the arches were put up together. The crucial parts in this stage were the keystones, as their geometry and weight was expected to "lock" all the voussoirs together and allow the self weight to give the real configuration of every arch. So far as the transverse arches are concerned, the last two voussoirs were meeting below the vertex, leaving a wedged space at the top. The overlapping portions of these blocks were cut-off and a wedge-shaped block was inserted into the open vertex (Fig. 3.24).

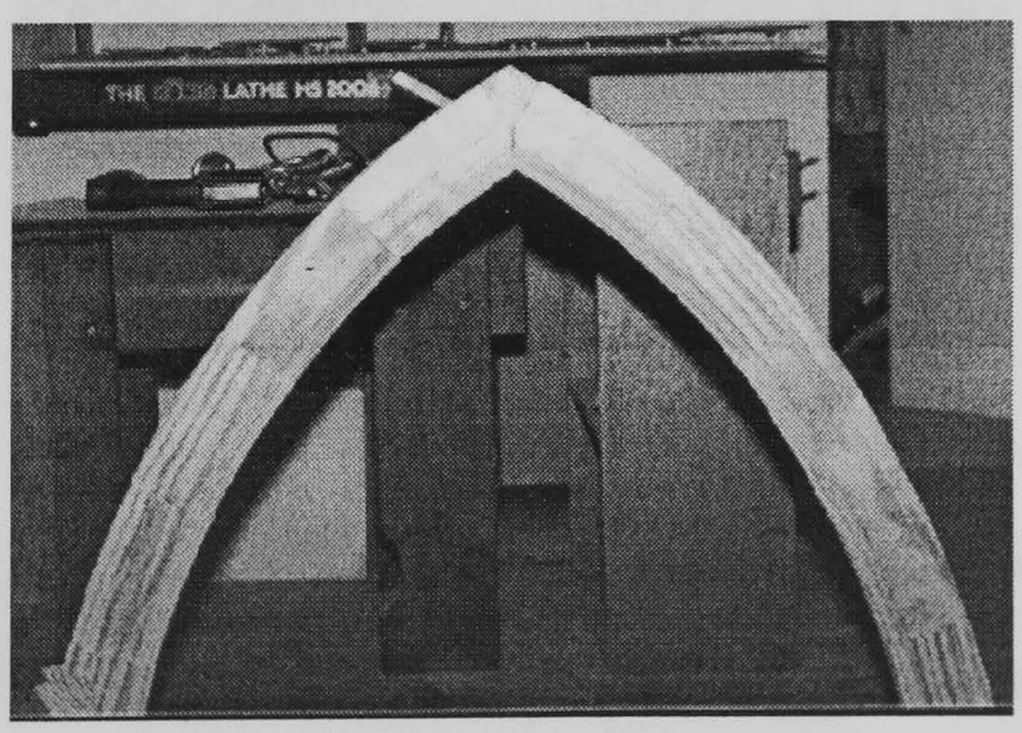

FIGURE 3.24 Crown of the transverse arches

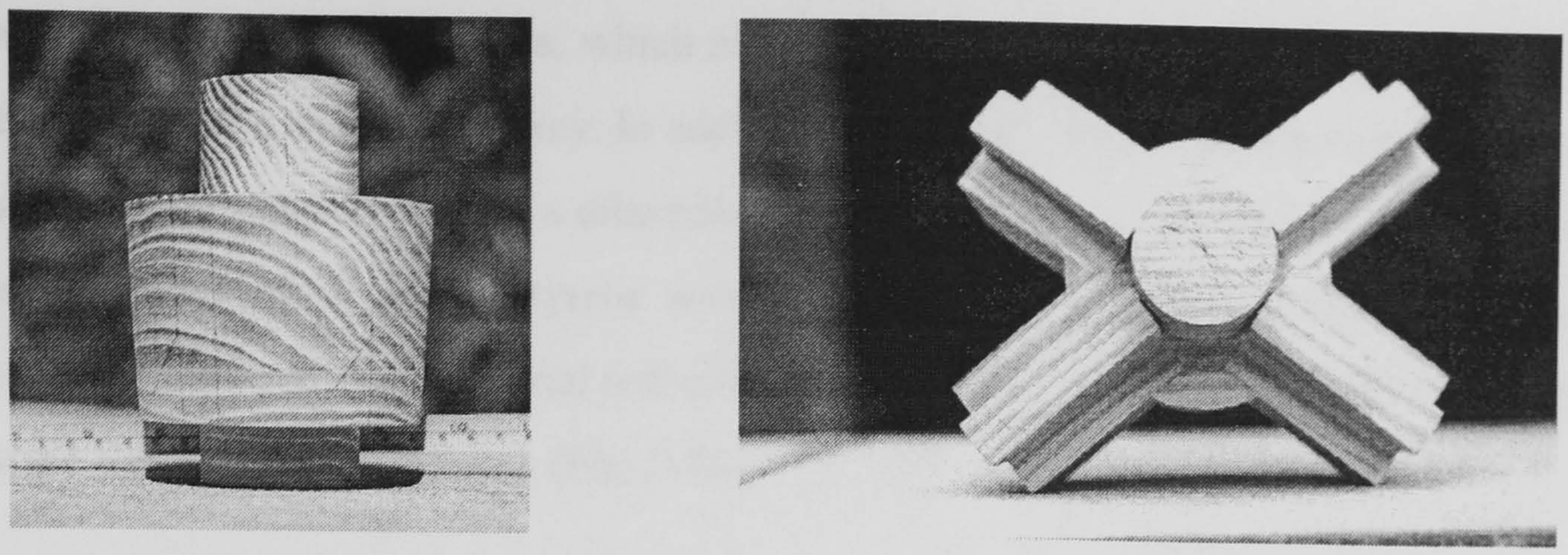

(a) Core

(b) The finished key block

FIGURE 3.25 The keystone of the ribs

The keystone of the ribs was based on a tapered cylinder, rebated at the top (Fig. 3.25a), to which the four last voussoirs of the joining arches were fixed (Fig. 3.25b), which were shorter than in the rest of the ribs. It was fundamental to ensure that these four antennas were attached at the correct angle, as the smallest deviation from the axes of the joining ribs could result in weak, wedged joints between the voussoirs and a geometric instability of the entire system. For this purpose, a template was used to control their orientation and transfer the geometry correctly from the drawings (Fig. 3.21a).

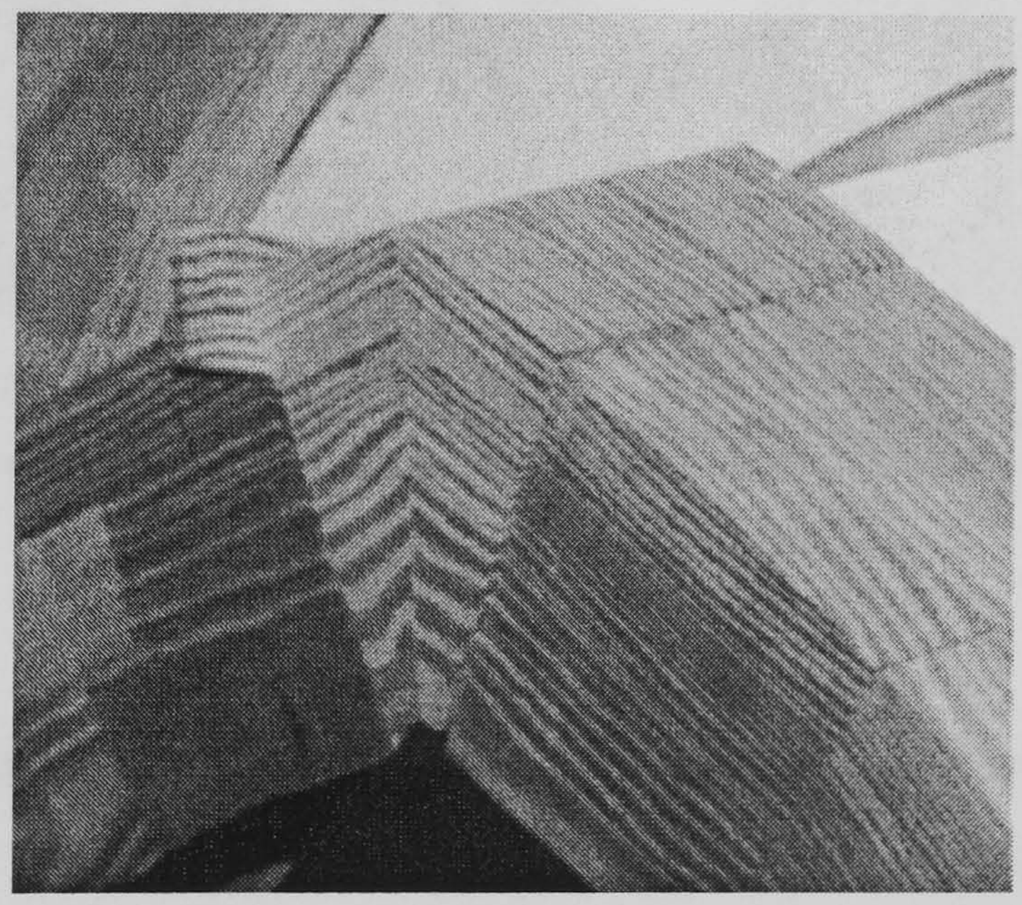

FIGURE 3. 26 The crown of the nave arch

As seen in Chapter 1, one of the main characteristics of Gothic architecture was the high dependence of the final outcome on the construction process, rather than the ability to establish and design in advance the form of the structures (Rebasa 1997). This became quite clear in the case of the keystone for the nave arch. The voussoirs were quite bulky in

comparison with the other arches, which made it more difficult to assemble the arch dry, in order to assess the shape of the key. In addition, this block, apart from the wedge shape, had lateral cross sections defined by a dihedral angle, with respect to the outer plane of the arch. As a solution, a block of polystyrene was prepared to the dimensions estimated at design and then dressed accurately by trial and error. Once the geometry was defined, it was copied to wood and adjusted to the arch (Fig. 3.26).

This purely constructive character of the Gothic architecture became further evident during the setting up of the arches. When the keystones were positioned in place, the arches changed configuration in order to accommodate the line of thrust and any small differences in the angles between the voussoirs would distort the transmission of the loads, resulting in hinges and twists. Minor discontinuities were expected to be compensated later during the mortaring of the joints. Consequently, the rib centering was devised more like a stable surface onto which the voussoirs would be laid before their final placement, rather than a formwork following exactly the profile of the arch.

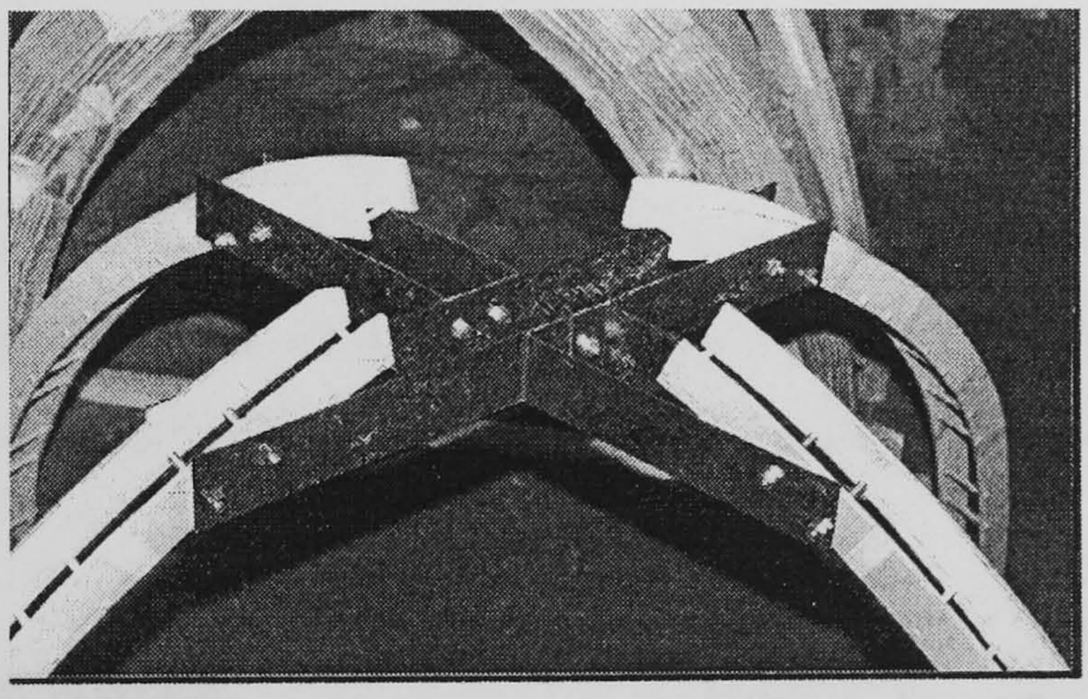

FIGURE 3.27 The centering of the ribs

Although the Gothic masons would usually devise a continuous system, using the ribs centering as a support for the shell formwork (Fig. 1.9b), the centerings were formed as independent from each other and it was considered more appropriate to design also the web formwork as completely separate. The main reason for this was that due to the reduced dimensions of the vault, decentering would become more crucial and any problems associated with the skeleton of the vault (ribs, arches) should not be allowed to affect the webs and vice-versa. The centering was composed of two limbs, connected together under their crown with brackets (Fig. 3.28). For the diagonal and transverse arches, these limbs were similar and they were made of plywood sheets connected with struts. Two sets were

used for the ribs that were linked with bolts at their top brackets. The centering left sufficient space around the crown of both ribs and arches for a safe decentering after the mortar had set.

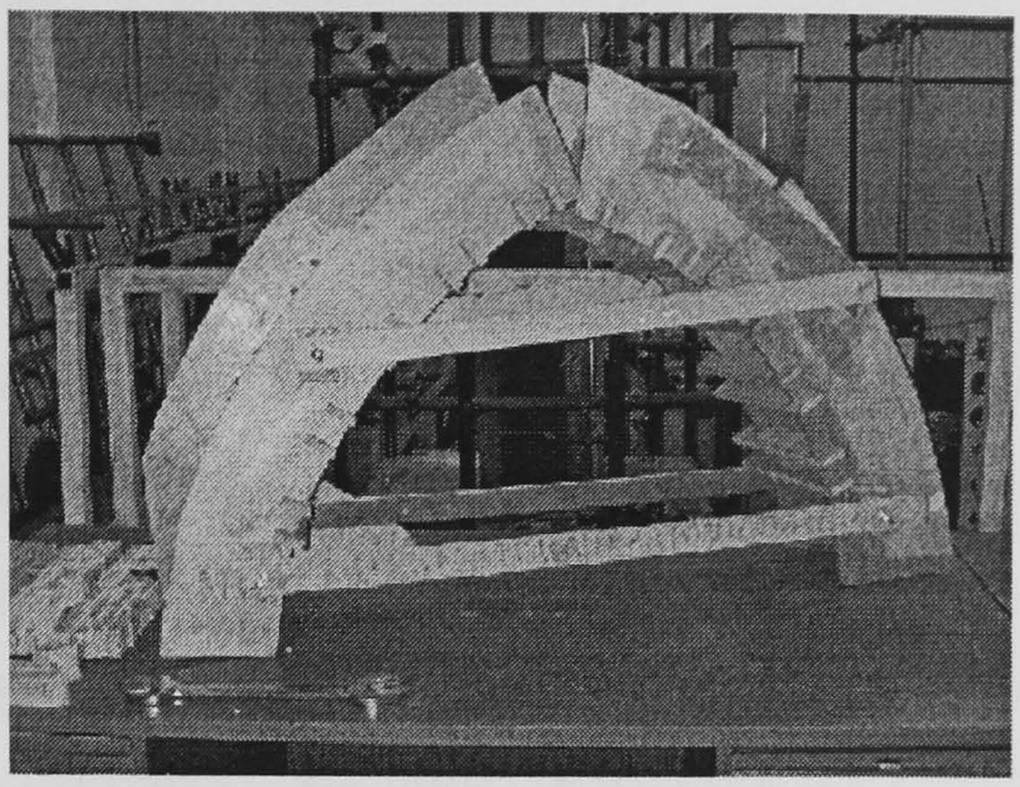

FIGURE 3.28 Centering for the nave arch

A quite different type of centering was used for the nave arch (Fig. 3.28). The voussoirs were not symmetrical about their axis, forming an acute angle on their outer side (Fig. 3.22). As their weight was quite substantial, the centering was required to fully support each voussoirs in at least two points. Stiffer, wooden panels were used in this case instead of struts (Fig. 3.27), which were then slotted into the centering, and the limbs had to be braced in more locations than before. Decentering was expected to be more complicated than in the previous case, so the top part of one limb was further split in two and joined with the rest with brackets.

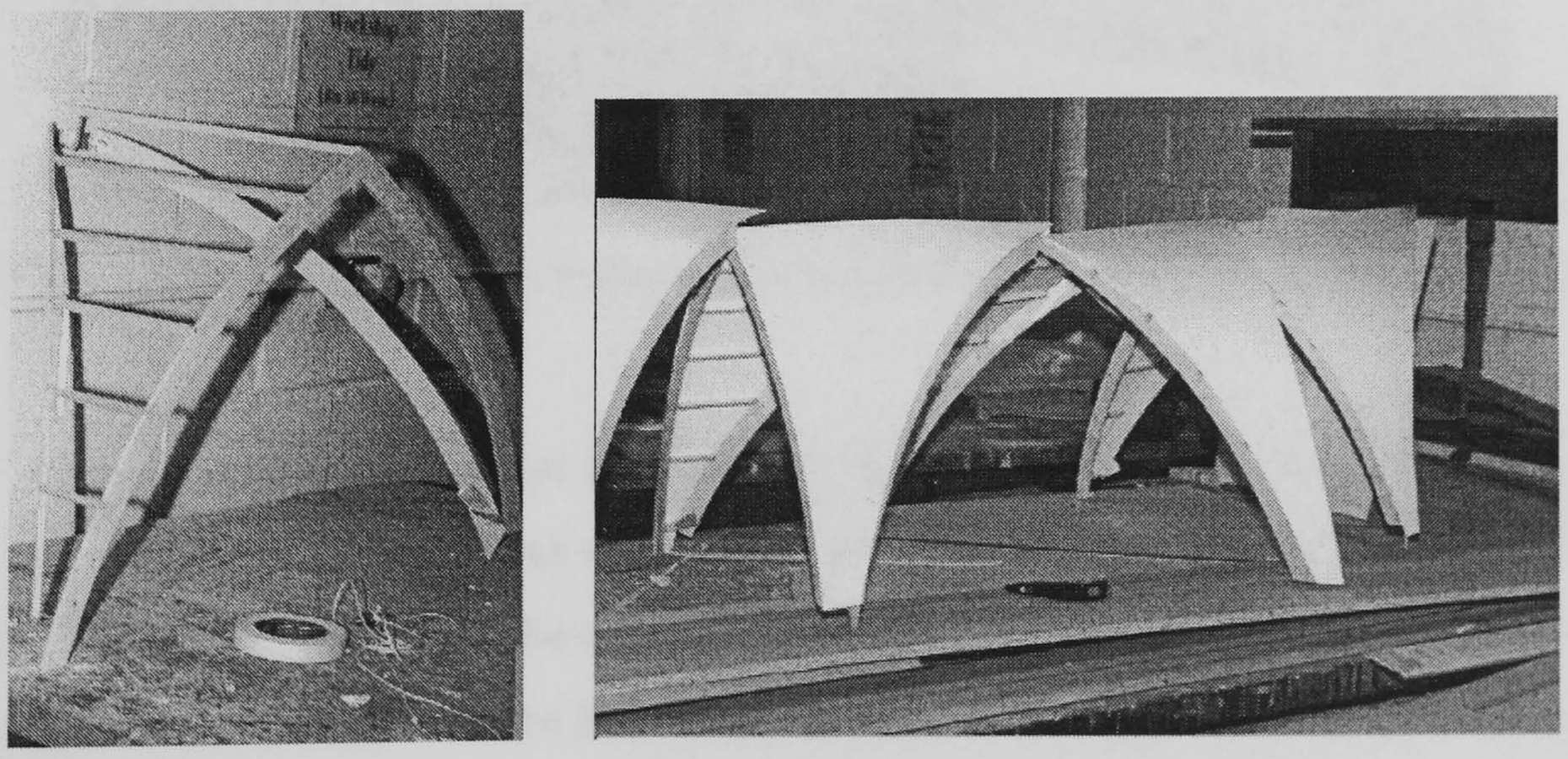

(a) The skeleton (b) Finished form

FIGURE 3.29 Falsework for the webs

As mentioned earlier, a separate system of falsework was devised for the webs (Fig. 3.29). In order to form each panel, a frame was designed, whose members followed the lines of the two confining ribs and transverse or longitudinal arch at the level of the rebate at their extrados. The right shape of the angles between the ribs and the arches was copied after trials using metal brackets, which were then fastened to the members and the whole frame was assembled together (Fig. 3.29a). The frame was stiffened with transverse struts and the curved surface of the vault was re-created with the use of thin plastic sheets (Fig. 3.29b). This falsework was supported on three points. Props were inserted under the keystone, which could slide during decentering without punching the webs, and devices mounted over the pillars, whose height could be regulated, were supporting the abutments. After the construction of the webs and the setting of the masonry, these supports would be easily released and lowered and the formworks could drop without interfering with the vault.

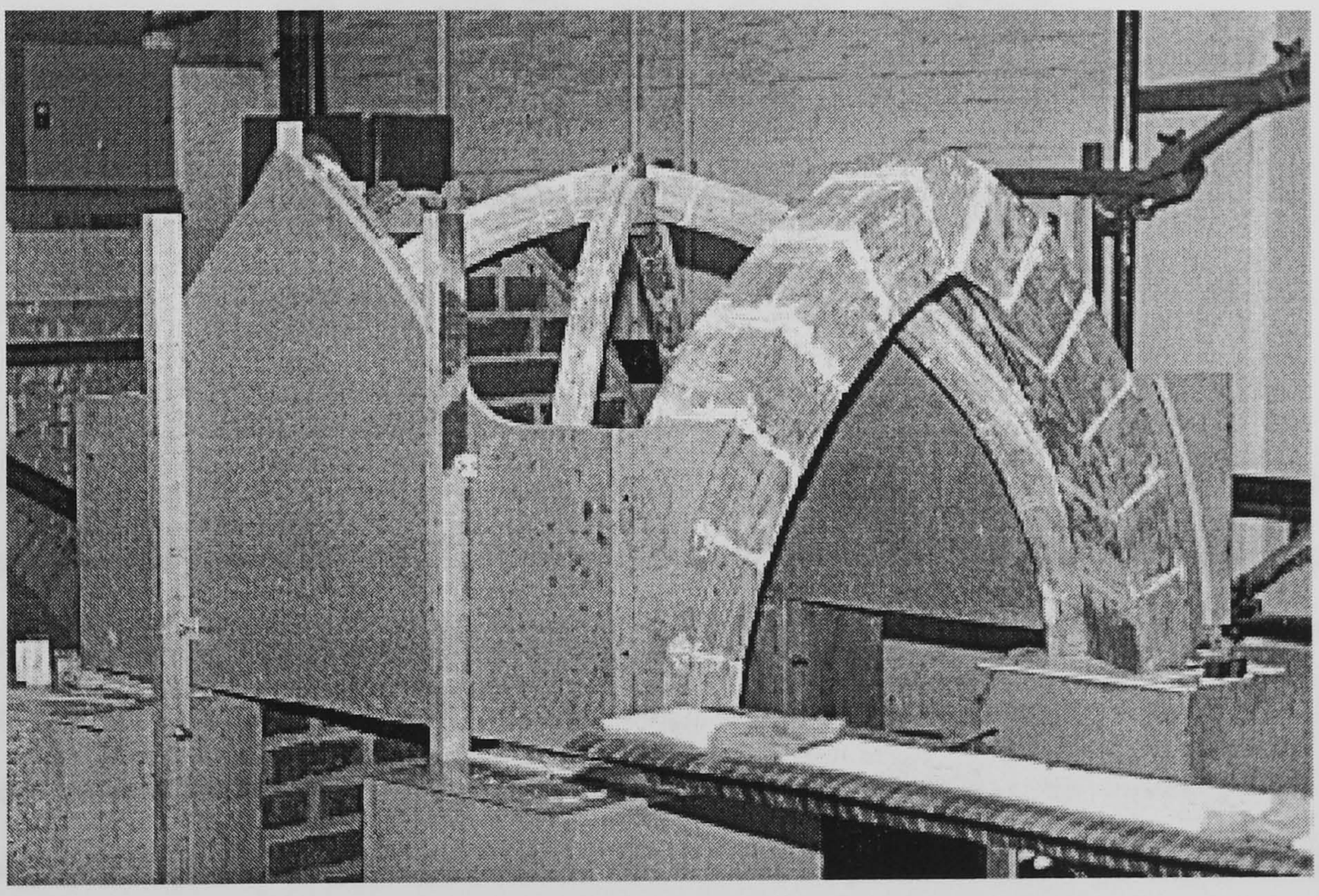

FIGURE 3.30 Lateral support for the transverse edges and conoid pockets for the spandrel fill

As seen earlier, the support conditions at the transverse arches due to the continuity with the neighbouring vaults was reproduced with panels mounted on posts fixed on the concrete pillars (Fig. 3.30). At the edges of the panel, a pocket was formed with the wall or the longitudinal arch, which were later filled up with gravel until approximately 1/3 of the total height of the vault. This represents the spandrel fill used in many similar buildings to stabilise this lower part.

One of the roles of the rib is to act like a permanent scaffolding for the webs, facilitating, at the same time, the formation of the groins area, which would otherwise present serious geometric difficulties concerning the stereotomy of the blocks. It is essential thus to erect the arches before the webs, which would then function as a skeleton. The mortar between the voussoirs was required to have characteristics similar to the prototype and to be compatible with the nature of the scale of the model and the materials used. A lime based mortar, without sand, provided the adequate strength and was easy to work with and to apply on the voussoirs. The assessment of the mechanical characteristics of the masonry produced this way are presented in Chapter 4.

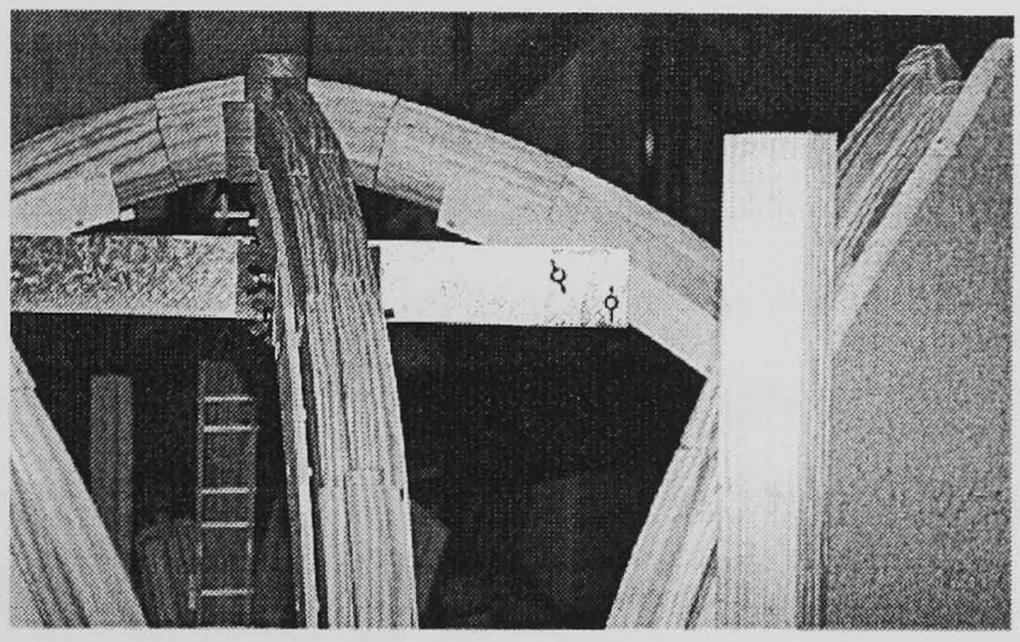

FIGURE 3.31 Stage from the construction of the ribs

The ribs were built first and their centering was removed almost immediately after minor rearrangements (Fig. 3.31). After the mortar had almost set, the nave arch was erected, but its centering was kept in place for longer, as any accidental movement of this arch could damage the ribs. Finally and after the mortar in the nave arch had set, the transverse arches were built. After all the centerings were removed, the lateral panel was put into place with great attention and at the closest possible to the transverse arch (Fig. 3.28). This way, the arch would not sway outside its vertical plane and the lateral boundary would take the right position before proceeding.

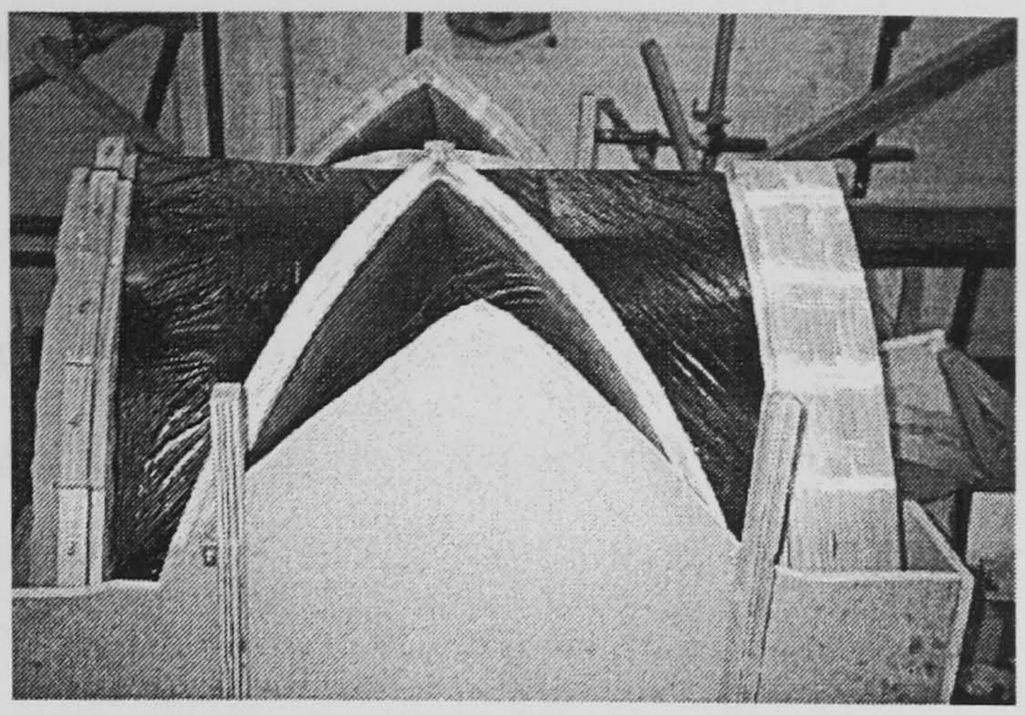

FIGURE 3.32 Placement of the web formwork after the completion of the skeleton of the vault

3.4.3.4 The filling of the webs

Once the formwork of the webs was inserted, the form of their units would be defined to create the web (Fig. 3.32). The webs of the prototype vault are made of rubble masonry consisting of non uniform longitudinal units, bonded with joints of hydraulic mortar of very irregular thickness. The whole material acts more like a "conglomerate", closer to the earlier Roman construction rather than the contemporary techniques that employed discrete rigid blocks as in France, Germany and Spain. The disposition and form of the units in the model vault reproduced this pattern in a rather regular way (Fig. 3.18), as they were designed with a constant width and thickness.

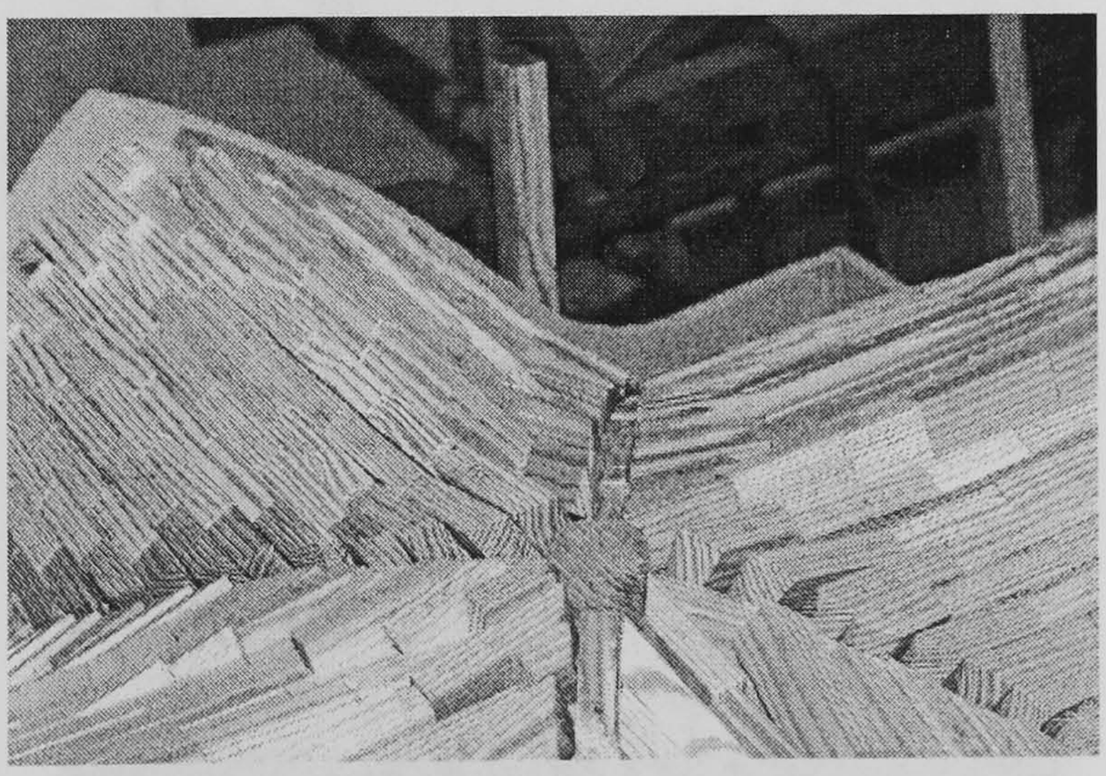

FIGURE 3.33 The form of the units of the web along the ribs

The most crucial detail was the cross section of the last unit in each course, on the side over the rebate of the ribs (Fig. 1.9b). This section was formed by two angles, as the unit was first slanted to follow the diagonal and then had to be adjusted to the space left by

the stem (Fig. 3.33). Due to the inclination of the diagonal voussoirs, the stem was not any more at right angles with the horizontal and, especially in the lower courses, its projection on the extrados of the rib exceeded the available space. Both the angles of the section kept changing due to the variation of the angle between the tangent to the lateral arches and the horizontal (Fig. 3.33). As a result, each web block at this position had to be shaped almost individually for every course.

During the construction of the webs, a standard size was used for most of the units. Since the joints in each course should not be aligned with those of the previous one, smaller units had to be carved. As a result, every course was unique and its units had to be appropriately labelled (Fig. 3.34). In addition, all the units and voussoirs had to be varnished in advance with a mat solution, to prevent the water of the mortar in the joints from soaking and damaging irreparably the blocks. Most importantly, however, the water would not be absorbed by the wood and the mortar could set properly, without rapid volume changes.

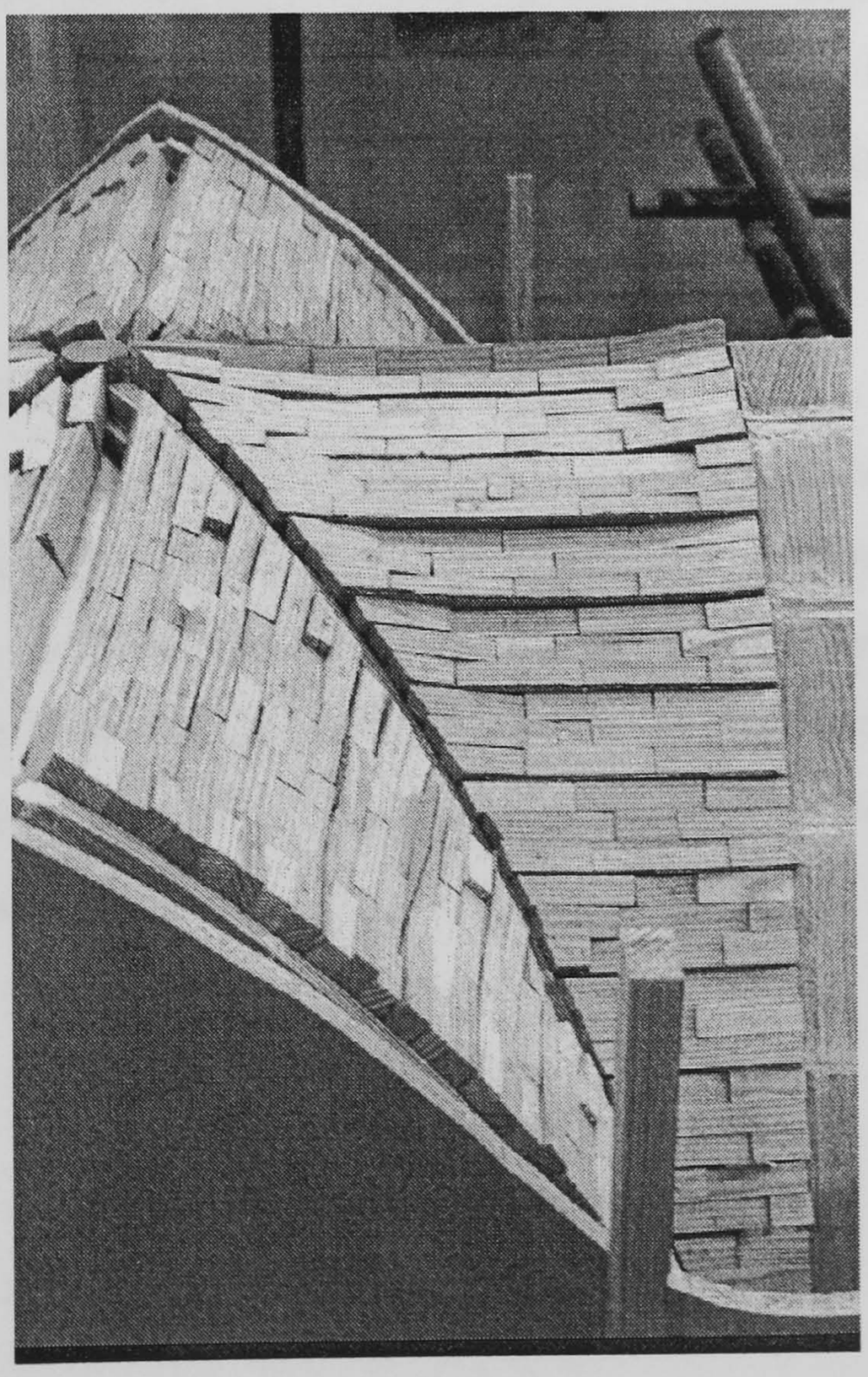

FIGURE 3.34 The units of the web before construction

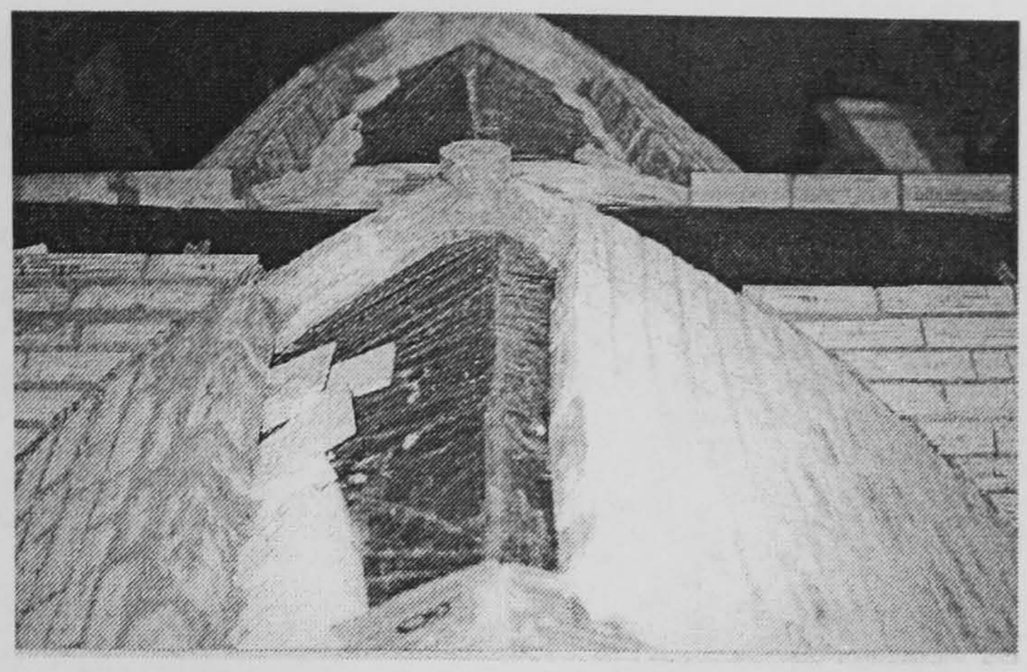

FIGURE 3.35 The construction of the webs

Building started from the abutments and the sequence should allow the increasing weight of the webs to be distributed evenly on the supporting arches. Courses were laid simultaneously on all the webs, adding the load symmetrically and letting the webs around each rib to pin each other (Fig. 3.35). The most of the lower courses consisted of up to two units and they did not need a centering. Every course had to be placed carefully on top of the previous, paying attention to keep it at right angles with the corresponding lateral arch. In the prototype vault, discrepancies from this line were covered by inserting wedges in the gaps left between the courses. Here, a stock of blocks in various lengths was used to restore this continuity and avoid mortar joints of an excessive thickness.

As a result, the final form of the vault was defined in stages, after the setting of the lower courses. When the final courses were laid and the vertices were mortared, the complete weight affected directly only those last areas, as the previous ones had already set. The decentering of the vault was done while the mortar was still "green", in order to allow the weight to form the final configuration. Due to the inherent elasticity of lime mortars resulting from their long time of setting, minor discrepancies were expected to "heal" slowly as the mortar was drying.

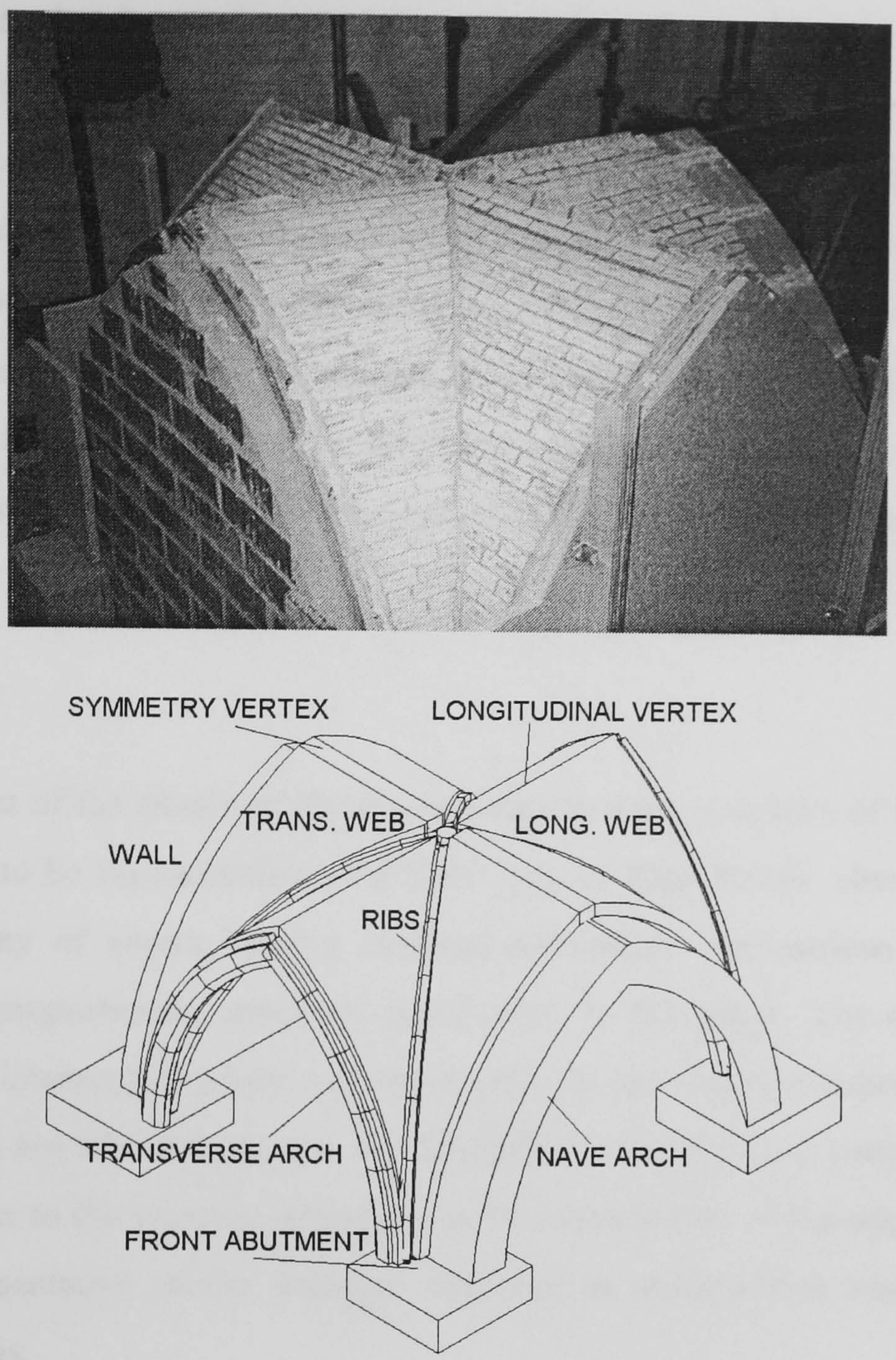

FIGURE 3.36 Aspects of the completed model cross vault

Finally, the web centering was removed three days after the completion of the construction (Fig. 3.36). Not properly compacted mortar or gaps at the intrados which was not possible to fill were repaired afterwards. The vault was left for two weeks to set, under the action of the total weight, and finally the spandrel pockets were filled with gravel.

3.4.4 Discussion

The construction of the vault was a unique opportunity to understand several problems the master masons could have faced during the erection of the prototype vault at Holyrood. Constant alignment of the courses as they were laid was of fundamental importance, because not only the correct geometry but ultimately the structural response

would be guaranteed. After the lateral supports (wall. nave arch, side panels) were secured, the role of the ribs became critical. Attention during the formation of its voussoirs and the use of a reliable and easy to handle centering (Fig. 3.28) resulted in a quality of execution sufficient for this task. As the system of the ribs was balanced by the keystone, they provided a safe boundary for the webs as they were being built-up so their increasing lateral thrusts could be efficiently mutually cancelled. The use of rebated ribs was instrumental for the performance of the groin during that critical phase, although this feature would not cause a significant difference in the case of the continuous masonry over the transverse arches.

3.5 SUMMARY

The lay-out of the church of Holyrood Abbey and the geometry of the existing aisle vaults appeared to be representative of a wide type of High Gothic churches. During its lifetime, a variety of events ranging between meticulous interventions and negligence accumulated disproportionate structural significance to the fabric. The collapse of 1768 resulted after an intervention which was not suitable for the structural scheme of the church and certainly did not take into account the detrimental effect of these events. The response of the aisle vaults to the imposed deformations from the failure of the upper structure was also quite representative of the damages observed in quadripartite vaults with similar support conditions.

The vault model that would be tested to failure reproduced the irregular rubble masonry of the prototype with uniform units, while an effort was made to keep the same average proportions. Classic stone vaulting techniques were employed, appropriately adapted for the dimensions of the test structure and during construction, the critical role of the ribs became evident. The boundary conditions along the four edges were suitably represented and the action of the imposed geometric changes would be subsequently simulated as a movement of the abutments of the vault.

Chapter 4

MATERIAL PROPERTIES AND EXPERIMENTAL SET-UP

4.1 INTRODUCTION

After the construction, the model vault was prepared for the experiment and the locations of the monitoring instrumentation were defined. A preliminary prediction of the behaviour of the vault with a FE model (§4.5.1) helped in selecting the location of the instruments for the measurements. The necessary mechanical properties in the two orthogonal directions of the masonry (elastic modulus, strength) were determined by wallette tests (§4.2.2).

The anisotropic nature of the masonry became evident from these tests. This was further interpreted with an analytical micromodelling of the wallette tests (§4.2.4), using the properties of the constituent materials experimentally determined earlier (§4.2.3). The material strength in the two orthogonal directions was obtained from the wallette tests. These were used to define the failure criterion of masonry under biaxial stresses. The failure criterion was subsequently incorporated into the FE analysis (§4.3).

The magnitude and mode of application of the loadings (dead weight and movement of the abutments) were defined (§4.4) and subsequently a preliminary FE model was generated (§4.5.1). The response of the structure during the tests was monitored by recording deflections and strains in critical points (§4.5).

4.2 PROPERTIES OF MASONRY

4.2.1 General

As was seen in §3.4.3.1, the choice of wood as a material for the units gave several advantages during the formation of the geometry and the construction of the model vault. Regarding the mechanical properties of the masonry, although wood has a lower strength

than stone, no failure was expected to occur at the units. Cracks would develop along the joints and a geometric type of collapse of the vault is more probable. So far as the response in the elastic range is concerned (as in the case of dead load), the behaviour of the model vault can be compared with the prototype using factors evaluated from the method of dimensional analysis. These expressions require the modulus of elasticity of the masonry, which can be experimentally obtained. In addition, timber has a high degree of orthotropy that is quite similar to that of the sandstone used in the prototype (§3.3.3).

Disadvantages on the other hand due to the capacity of wood to absorb moisture, causing the mortar to dry too quickly, were prevented by varnishing the blocks. Moreover, the low heat conductivity of wood was expected to affect the data from the electric resistance strain gauges and this effect was minimised by using a low voltage.

It is generally believed that cross vaults were conceived to develop almost everywhere axial compression, limiting bending to a minimum. Results from other researchers in the field (Barthel 1994, Croci 1995, Roca 1998), however, have demonstrated that the upper part of the vault is subjected to bending, with axial forces limited mainly around the haunches (§2.3). As no membrane compressive or tensile failure of the material is considered likely, it is important to assess the strength and stiffness properties of masonry in bending. In addition, masonry exhibits orthotropy in the elastic modulus and strength. Both properties were evaluated with wallette tests in the material axes, parallel to and normal to the bed joints (X- and Y- directions respectively). Compressive tests could also be used for the assessment of the moduli, but earlier tests have shown that the values obtained are similar to those given by the flexural tests (Sinha 1978).

4.2.2 Experimental assessment of stress/strain relationship and flexural strength

4.2.2.1 Flexural strength

The wallettes were built in the same bond pattern as the webs of the vault to obtain the strengths in two orthogonal directions. In both cases, the shear-span / depth ratio was kept constant. Three specimens for each type were tested until failure under line loads placed at the third of the span. The specimens were tested spanning horizontally between the

supports (Sinha 1997) and were not placed vertically (BS 5628), in order to avoid any possible rotational restraint caused by their weight. The dimensions of the wallettes and the test arrangement can be seen in Fig. 4.1. The wallettes were considered as simply supported upon the bearings and the load was applied in constant increments. In each increment, the stress at the centre of the wallette was calculated and the stress / strain relationship was established. The stress/strain relationship was also determined from the load-deflection readings.

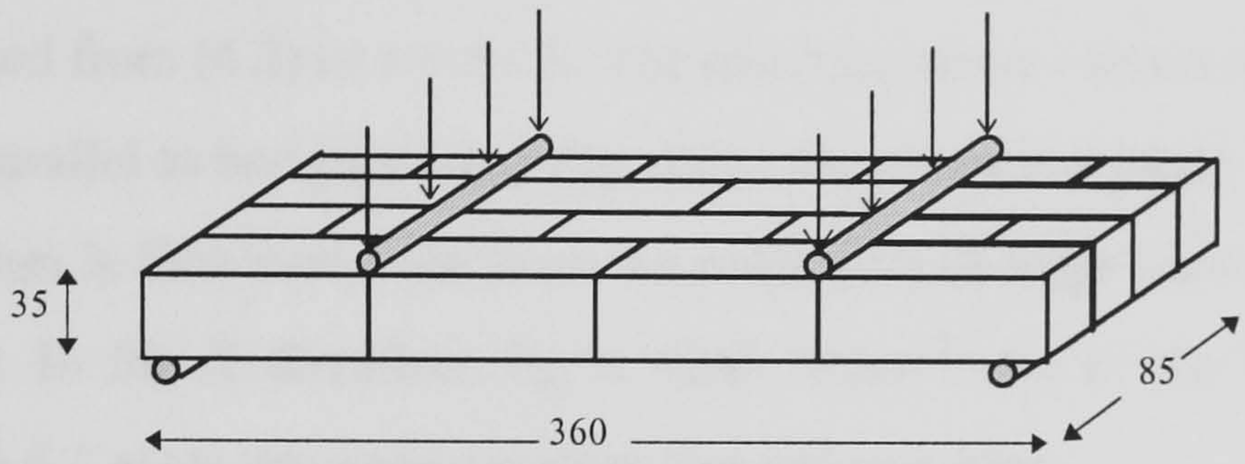

(a) Direction parallel to bed joints (X direction)

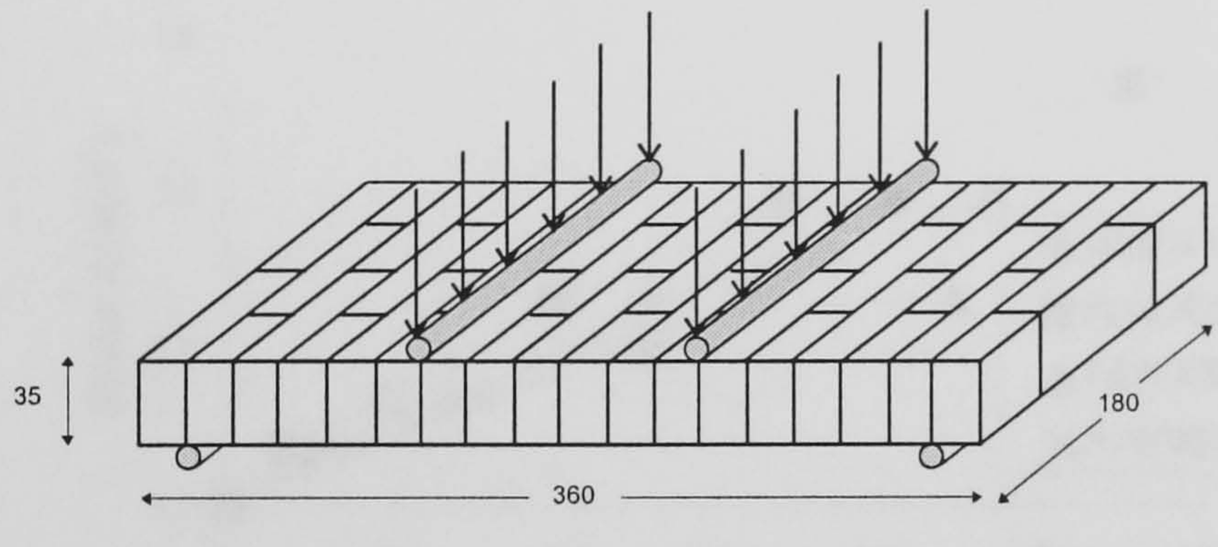

(b) Direction normal to bed joints (Y direction)

FIGURE 4.1 Set-up of the wallette tests

a) Load-deflection method

In this method, strain was evaluated indirectly, after the elastic modulus E was obtained from the deflection recorded at the centre. Dial gauges were used for the purpose and they were mounted above the centre and the supports of the specimen from a frame that was independent from the rig. Recording deflections at the ends of the wallette served to eliminate any local settlement from the evaluation of the net deflection at the centre δ_c.

The value of δ_c is given by the expression for a simply supported beam:

$$\delta_c = \frac{PL^3}{6EI}\left(\frac{3}{4}\cdot\frac{1}{3} - \frac{1}{3^3}\right) = \frac{23PL^3}{648EI} \qquad (4.1)$$

where I is the moment of inertia of the wallette. By rearranging (4.1), E is found to be:

$$E = \frac{23PL^3}{648I\delta_c} \qquad (4.2)$$

Stress in the middle of the wallette is known from the applied force P, while the strain can be evaluated from (4.2) as $\varepsilon = \sigma / E$. The resulting stress / strain relationships are plotted in Fig. 4.2a (parallel to bed joint) and Fig. 4.2b (normal to bed joint). The elastic modulus E in each direction is then evaluated from the respective average curve, which is also plotted in the figures. In the X direction, E_x is 4260 N/mm^2 and in the Y direction E_y is 670 N/mm^2. Table 4.1 gives the corresponding flexural strengths.

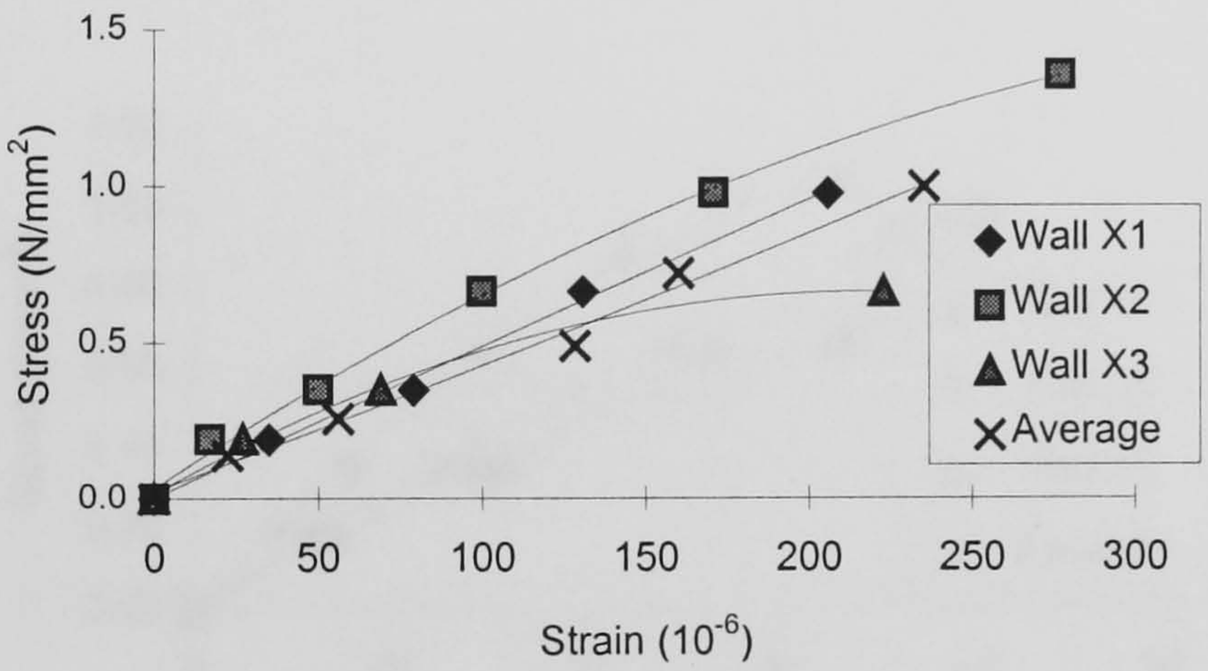

(a) X-direction

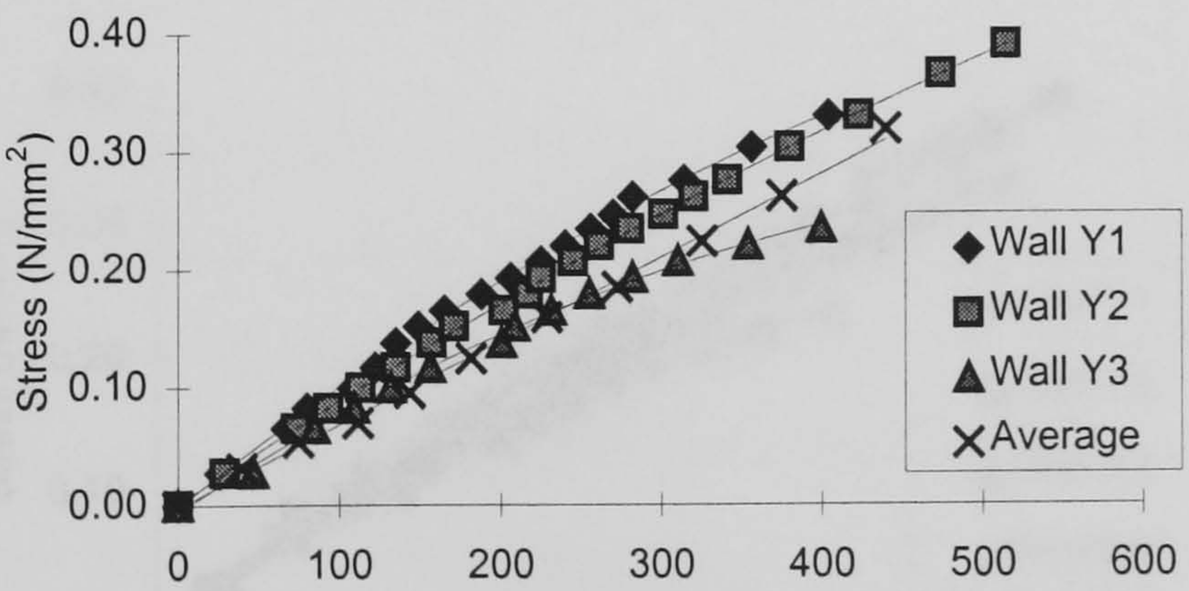

(b) Y-direction

FIGURE 4.2 Stress-strain relationship obtained from the load-deflection method

TABLE 4.1 Flexural strength in the two orthogonal directions (N/mm^2)

Wallette	Parallel to bed joint (X)	Normal to bed joint (Y)
1	1.34	0.33
2	0.96	0.39
3	0.64	0.23
Average	0.98	0.32

b) Stress-strain method

In the other method, electric resistance strain gauges were placed at the centre of the wallette, on both the compression and tension surfaces, so strain could be recorded directly. However, the gauges had to be mounted on the units only as the surface of the mortar joint was quite rough and irregular. A more detailed account on the set-up of the method will be given in §4.5.4 where the instrumentation of the vault is discussed.

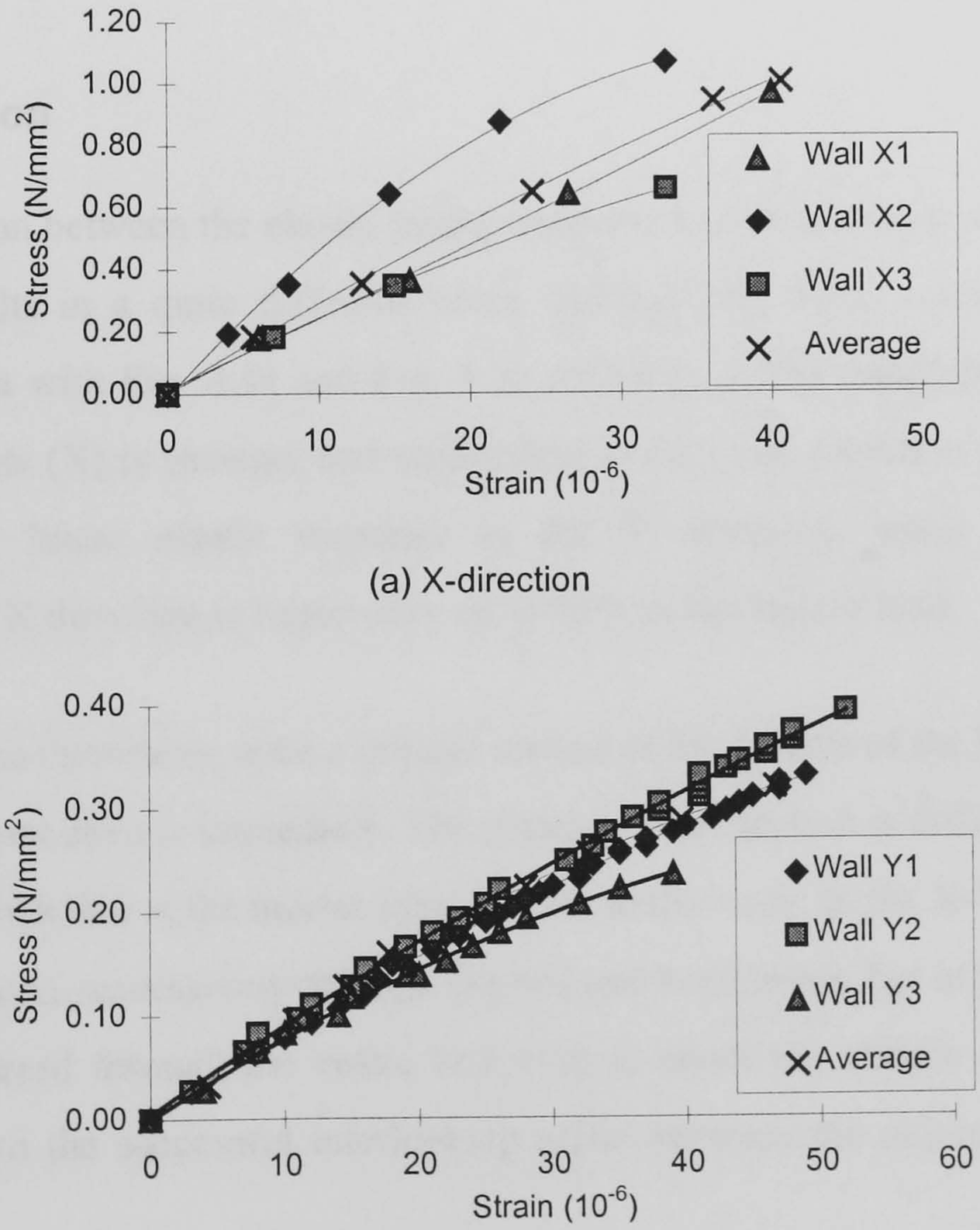

FIGURE 4.3 Stress-strain relationship obtained from the stress-strain method

The bending moment at the centre of a simply supported beam, M_c, under a four-point load is given by:

$$M_c = \frac{PL}{3} \tag{4.3}$$

and Hooke's Law yields the value for E as:

$$E = \frac{\sigma}{\varepsilon} = \frac{M_c y}{I\varepsilon} = \frac{PLy}{3I\varepsilon} = \frac{PL}{3Z\varepsilon} \tag{4.4}$$

where y is the maximum distance from the neutral axis and Z is the section modulus.

The resulting stress / strain relationships for this method are plotted in Fig. 4.3a (parallel to bed joint) and Fig. 4.3b (normal to bed joint), together with the respective average curve. From the latter, the elastic moduli were evaluated as 27100 N/mm^2 for the X direction and 8910 N/mm^2 for the Y.

4.2.2.2 Discussion

A comparison between the elastic moduli evaluated in the previous section shows that each method results in a quite different value, although the trend recorded is the same (compare Fig. 4.3a with Fig. 4.4a and Fig. 4.3b with Fig. 4.4.b). Masonry in the direction parallel to the joints (X) is stronger and stiffer than in the other direction (Y). The material exhibits a brittle linear elastic response in the Y direction, while the stress-strain relationship in the X direction is linear only up to 40% of the failure load.

In both of the directions, once a critical section at the middle of the beam is fractured, the failure of the specimen is immediate. The pattern of this section is different in each case, but all the wallettes failed at the mortar joint and not at the units. In the X-beams (Fig. 4.5a), the cracks propagated successively through the bed and head joints, but in the Y-beams (Fig. 4.5b) failure occurred through the entire bed joint at about the middle of the beam. The difference is due to the successful interlocking effect between the oblong units parallel to the bed joints.

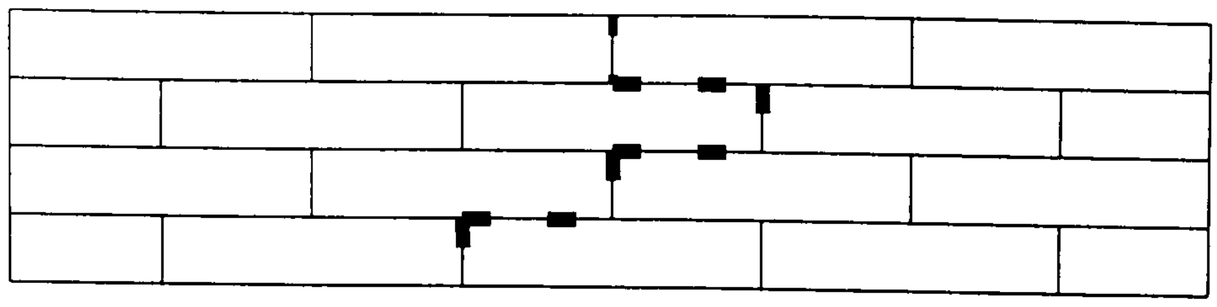

(a) X-direction: failure through the units and joints

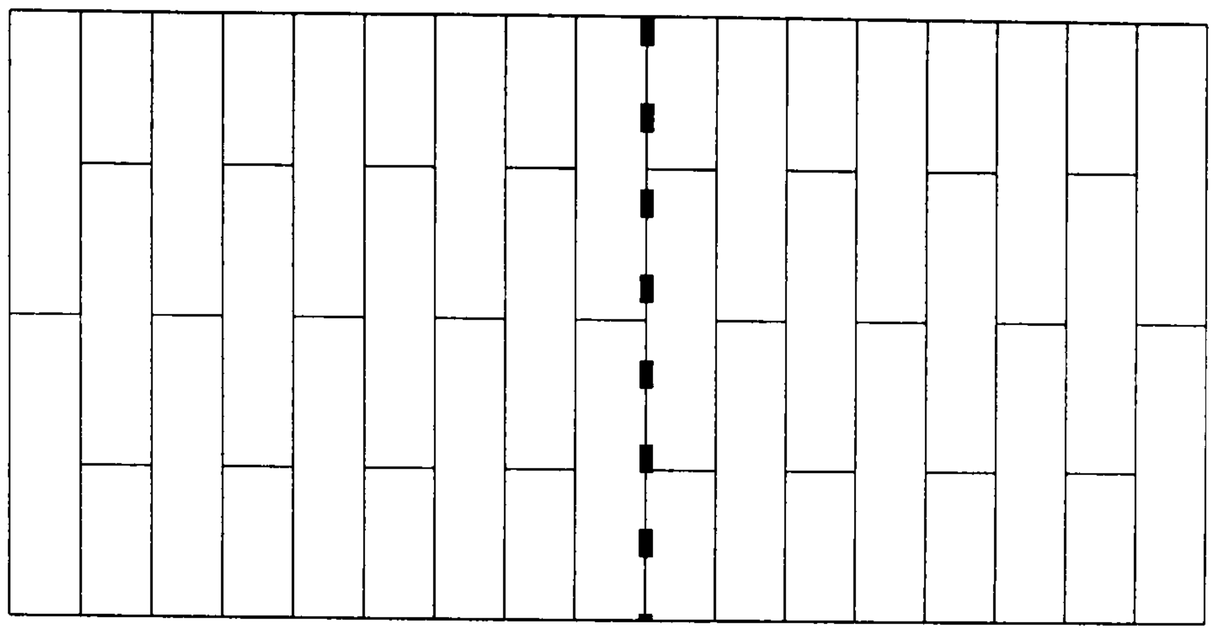

(b) Y-direction: failure along the bed-joints only

FIGURE 4.4 Failure pattern of the wallettes

So far as the elastic modulus is concerned, a closer examination of the instrumentation set-up can explain the discrepancy between the two methods. In the stress-strain method, the strain gauges were applied on the units, measuring therefore only the response of the wood to the load. The elastic modulus of this species of wood (Southern yellow pine) is 16400 N/mm^2 (Illston 1989) and it is higher than what is expected for a lime mortar (around 900 N/mm^2 (Baronio 1991)). Higher values of strain should be therefore concentrated in the weaker mortar joints and the response of the masonry at that point is the result of a combination of the individual responses of the constituent materials. On the other hand, the load-deflection method measures directly the combined behaviour of masonry in the area. The two methods can yield similar results only when the properties of the constituent materials do not differ significantly, as in the case of a masonry made of bricks and cement-based mortar (Ng 1996).

This phenomenon can be better understood if the wallette tests are simulated analytically with 3D FE models, where the material can be considered split between units and joints. It would be necessary in this case to obtain a more accurate knowledge of the properties of the constituent materials, so further tests had to be performed before the analytical study.

4.2.3 Properties of the constituent materials

4.2.3.1 Wood

A set of three beams was cut out of the wood in each of the two principal orthogonal directions, parallel to the grain (L) and tangential, in the radial direction (R). As in the case of the wallettes, the beams had the same shear-span / depth ratio and they were tested under four-point load, while the same loading arrangements were used to determine the elastic moduli. The flexural strength was not necessary to evaluate, as failure did not occur at the units during the wallette tests.

TABLE 4.2 Modulus of elasticity of the wood from flexural tests

	Parallel to the grain (L)	Radial direction (R)
Load-deflection test (N/mm^2)	21600	1730
Stress-strain test (N/mm^2)	23600	1900

The average values of the elastic modulus in each direction (Table 4.2) show that the difference between the two methods is quite small. As it was expected from the already available properties for Southern Yellow Pine, the modulus of elasticity in the radial direction is much lower than in the longitudinal. This is another reason that confirms the higher strains recorded in the Y-wallettes for the same amount of load as in the X-wallette.

4.2.3.2 Mortar

As discussed earlier in the section §3.4, the mortar used in the masonry was purposely chosen to be weak in order to reproduce similar mechanical characteristics with lime mortars found in historic buildings (very low modulus of elasticity and strength). On the other hand, the low strength of the test mortar would make any direct experimental evaluation of its properties quite unreliable. Any beam specimens would be very fragile to test and the small amount of load that would have been possible to apply would not compensate the effects of any uncertainties caused by minor misplacements of the load or the instrumentation.

As a result, the elastic modulus of the mortar can be evaluated as an approximation of

values from tests in historic lime mortars. Cubic specimens extracted from intact fragments of the collapsed Civic Tower of Pavia (Baronio 1991) had a modulus between 870 and 960 N/mm^2. Regarding the flexural strength, from laboratory tests on mortars fabricated following proportions used in historic techniques (Angotti 1991), the strength of a hydraulic lime mortar was evaluated as 0.54 N/mm^2.

It would be, therefore, safe to assume initially a value of 1000 N/mm^2 for the elastic modulus, which is still quite lower than that of the wood. At the analytical study in the next section, the sensitivity of the wallette to the mortar properties will be examined starting from this basis.

4.2.4 Discussion

The flexural tests on the wallettes were reproduced analytically with a 3D FE model of each type and solved with the program Abaqus. Both the units and the mortar joints were simulated with 3D brick elements and a constant thickness of 2 mm was considered for the joints. The values of the mechanical properties of the materials discussed in the last sections were assigned to the relevant elements. A material and geometric nonlinear analysis (NLMGA) was performed and smeared cracks were allowed to develop, but only at the mortar joints. The maximum stress failure criterion was used to initiate the cracks, after it was introduced into the FE program, allowing the matrix of the elements concerned to change accordingly. A more detailed account on the implementation will be given in §4.3.

The modulus of elasticity of each wallette was re-evaluated following the same procedure as in the tests. A four-line load was applied in constant increments and in each increment the modulus was separately calculated from the deflections and the strains recorded at the centre. However, for the initial value of 1000 N/mm^2 used for the elastic modulus of the mortar, no match was observed between the experimental and theoretical curves. The modulus was varied and the best approximation, for both orthogonal directions, occurred for a value of 500 N/mm^2. In Fig. 4.5, the analytical stress-strain relationships are compared with the experimental.

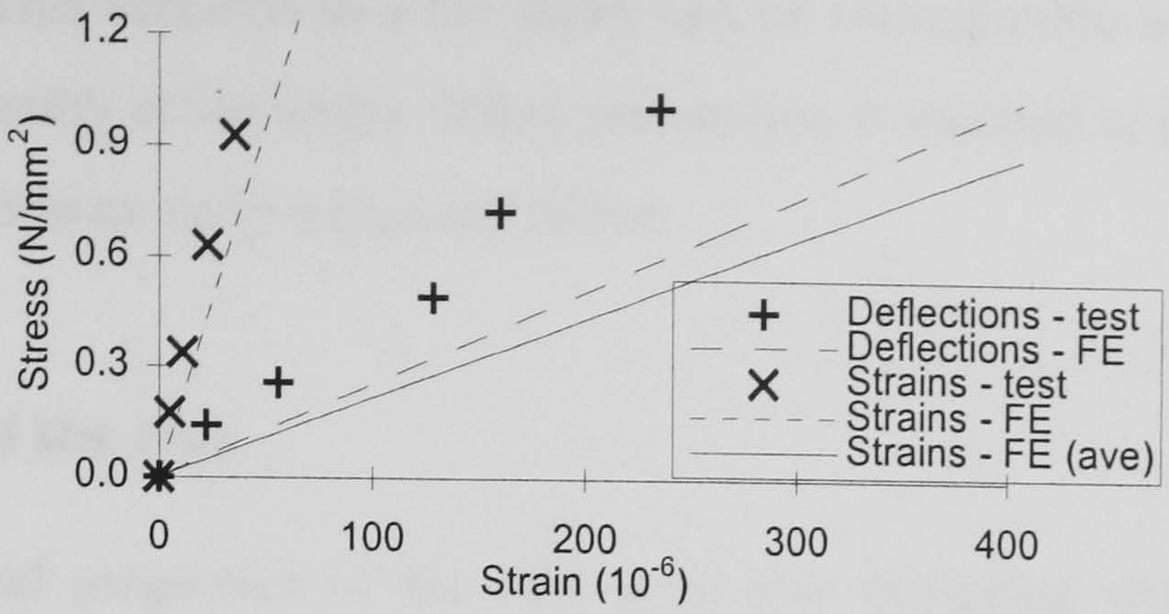

(a) Parallel to bed -joints - X direction

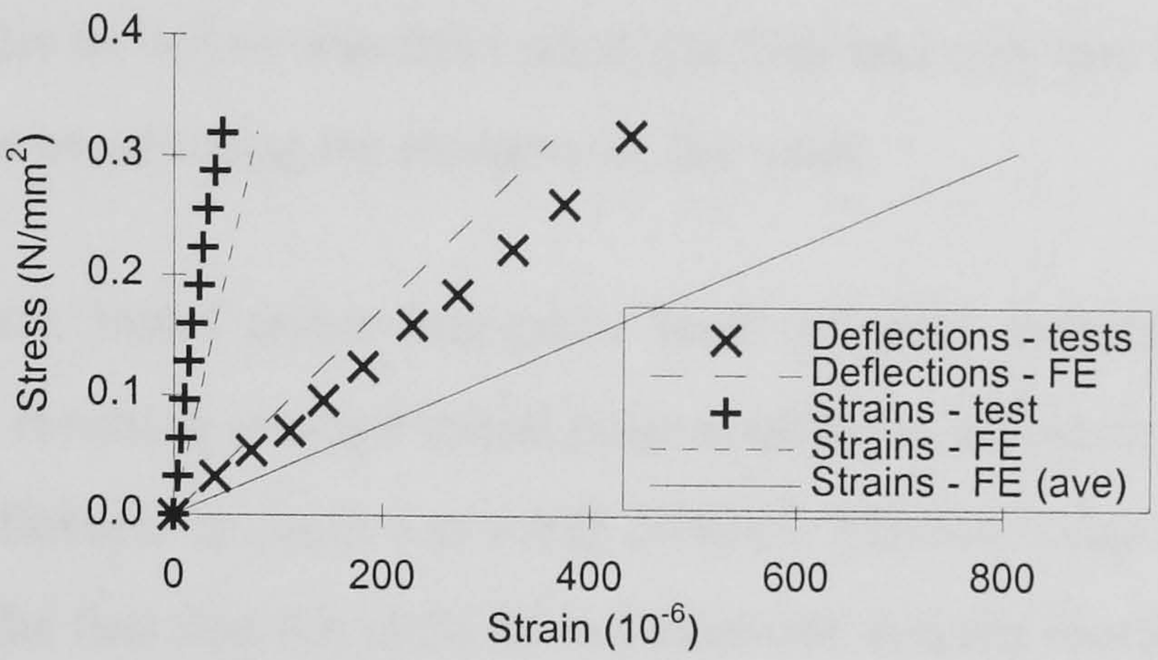

(b) Normal to bed joints - Y direction

FIGURE 4.5 Stress-strain relationship in two orthogonal directions

The difference observed between the analytical curves derived from each method is in agreement with the discrepancy observed during the tests and this study confirms that this difference originates in the strain recorded directly on the units, whose elastic modulus is quite high compared with the mortar. The sensitivity of the analysis to the value accepted for the elastic modulus of the mortar showed also that the stress-strain relationship retrieved from the load-deflection method is equally sensitive to variations of the modulus of both materials, while the stress-strain method is more influenced by the properties of the units.

Both methods can give the same results when the properties of the constituent materials do not differ much. As a final examination of the possibilities of the FE model, strain was examined at the nodes shared between the units and the joints. The stress-strain relationship produced by the average of strain is much closer to the curve obtained from the load-deflection method. The difference, especially in the case of Wall Y, shows the limitations of the FE method in these cases of highly variable elastic properties. The low strains at the units alternate with high strains at the joints, which are also concentrated in

very narrow bands. This variation in a FE model can be incompatible with the fundamental assumptions of continuity at the nodes. If this assumption is violated in more complex stress distributions it results to an early numerical failure.

4.2.5 Properties of the ribs

The mechanical properties of the ribs were also evaluated with flexural tests. A different kind of beams had to be prepared, as this member is composed of voussoirs connected with each other with lime mortar. Therefore, a set of three beams with the same shear-span / depth ratio as before was fabricated, but they had only one row of five units, of the same size as those constituting the masonry of the vault.

The beams were tested under four-point load and only deflections were recorded during the tests. The resulting average initial tangent modulus of elasticity was found to be 530 N/mm^2 and the flexural strength was 0.025 N/mm^2. The low values of these properties can be attributed to the fact that the units do not interlock and the mortar contains no sand, as it was essential for the joints between the voussoirs to be as thin as possible (§3.4.3.3).

4.2.6 Discussion

The theoretical interpretation confirmed the discrepancy observed during the tests and this information will be equally useful during the interpretation of the data from the later experimental phase of the movement of abutments. In addition, the limits of application of the values from each method can be defined. The moduli of elasticity derived from the load-deflection method is more suitable for the FE models that treat the material as homogeneous and these will be used initially. If, however, high strains are expected to develop during the tests, low strains will be recorded eventually at the units and a similar discrepancy will occur between these and the predicted values of the FE model. In that case, a simulation of the material as split between its constituents will allow to interpret better the magnitude of the results.

After the properties of all the materials were evaluated, it is important to incorporate the nonlinear effects observed to the FE model. In the next sections, an adequate failure criterion will be established and the way the program uses this criterion to simulate failure will be implemented.

4.3 FAILURE CRITERION

4.3.1 Choice of criterion

In the course of both the phases of the test (dead load and movement of the abutments) the vault is loaded normal to its plane. It is therefore necessary to estimate the ultimate strength of the structure in bending or that in combined bending and axial force. The theories developed to assess the strength of masonry under biaxial stresses (with the stress in the third principal direction equal to zero) concentrate mainly on the biaxial tension region and the compressive strength of masonry is considered infinite.

The most important failure theories for masonry concerning its biaxial flexural strength are illustrated in Fig. 4.6 in terms of the moment of resistance in the stronger (x) and weaker (y) directions, M_{ux} and M_{uy} respectively (Sinha 1997). These are the elliptical criterion proposed by Baker (4.5), the maximum principal stress theory (Rankine's Theory) and the biaxial failure criterion developed by Sinha (4.6) (Sinha 1997).

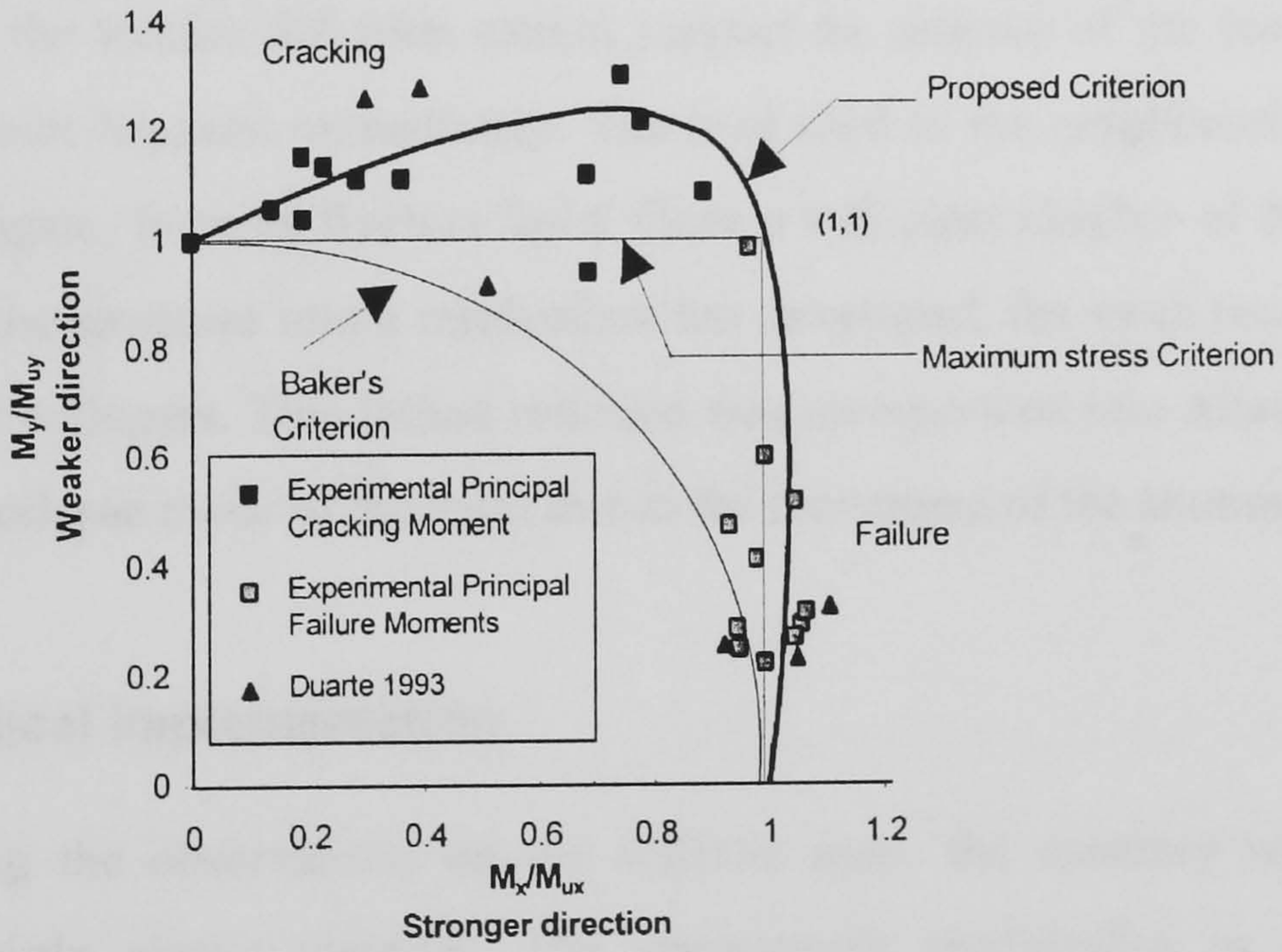

FIGURE 4.6 Strength of masonry under biaxial stresses (Sinha 1997)

$$\left(\frac{M_y}{M_{uy}}\right)^2 + \left(\frac{M_x}{M_{ux}}\right)^2 = 1.0 \qquad (4.5)$$

$$\left(\frac{M_y}{M_{uy}}\right)^2+\left(\frac{M_x}{M_{ux}}\right)^2-0.75\cdot\frac{M_x}{M_{ux}}\cdot\left(\frac{M_y}{M_{uy}}\right)^2-0.25\cdot\frac{M_x}{M_{ux}}\cdot\frac{M_y}{M_{uy}}=1.0 \qquad (4.6)$$

The last theory was established from the failure envelope of tests performed on brickwork specimens using a novel system of cross beams. The flexural tests on the wallettes showed that cracks are concentrated only at the joints, so the major directions of interest will be either parallel or perpendicular to the bed joints (X- and Y- directions respectively). In addition, the cross beam tests showed that the uniaxial ultimate moments obtained from the wallettes for each of the orthogonal directions, M_{ux} and M_{uy}, can be used safely in the criterion. The theory exploits sufficiently the reserves of strength of the masonry, in contrast with Baker's conservative criterion (Fig. 4.6).

According to this theory, cracking occurs when the moment reaches the value of the moment of resistance in that direction. For those points lying to the left of the intersection point (1,1) in Fig. 4.6, the weaker direction will crack first and the load would then shed to the stronger direction. If ultimate strength in that direction is subsequently exceeded, failure of the joint will occur. When, however, the stronger direction cracks first (points on the right of (1,0)), the weaker direction cannot support the amount of the load transferred, so failure of the joint happens immediately. The load shed to the neighbouring points causes failure to propagate, forming fracture lines. Once a sufficient number of fracture lines that can transform the structure into a mechanism has developed, the vault reaches an Ultimate Limit State and collapses. This failure criterion was incorporated into Abaqus and was used to predict the collapse mode of the vault due to the movement of the abutments.

4.3.2 Theoretical implementation

Following the observations on the wallette tests, the masonry was treated as an orthotropic, brittle elastic material. The stress-strain relationship in each orthogonal direction was considered to increase linearly, with the elastic moduli derived from the load-deflection tests, until strength was exceeded. At that stage an immediate rupture would occur, the stress would drop to zero and the load would be transferred to the other direction.

The FE model of the vault was generated with continuous shell elements and the loading was applied by constant increments. At the end of each increment, the solution at a

node was checked against the failure criterion. When the strength of the material had been exceeded, the cracks developed were modelled with the smeared crack analytical technique, which considers that, since the section cannot transmit any more stress in that direction, the corresponding elastic modulus should drop to a very low value. The stiffness matrix of the elements was modified accordingly and the cracks were represented as very large plastic strains. The program was stopped when excessive deformations occurred, resulting in numerical instability.

The rigidity matrix of a plane stress element, similar to the ones that were used at the vault, before cracking (in the linear elastic phase) was:

$$D = \frac{t^3}{12}\begin{bmatrix} \frac{E_x}{(1-\nu_{xy}\nu_{yx})} & \frac{\nu_{xy}E_y}{(1-\nu_{xy}\nu_{yx})} & 0 \\ \frac{\nu_{yx}E_x}{(1-\nu_{xy}\nu_{yx})} & \frac{E_y}{(1-\nu_{xy}\nu_{yx})} & 0 \\ 0 & 0 & G_{xy} \end{bmatrix} \tag{4.7}$$

After the element had cracked, the rigidity crack matrix D_{cr} had to be modified as:

$$D_{cr} = \frac{t^3}{12}\begin{bmatrix} \frac{E_x}{(1-\nu_{xy}\nu_{yx})} & \alpha\frac{\nu_{xy}E_y}{(1-\nu_{xy}\nu_{yx})} & 0 \\ \alpha\frac{\nu_{yx}E_x}{(1-\nu_{xy}\nu_{yx})} & \alpha\frac{E_y}{(1-\nu_{xy}\nu_{yx})} & 0 \\ 0 & 0 & \beta G_{xy} \end{bmatrix} \tag{4.8}$$

The value of the reduction factors α and β in (4.8) serve to simulate the stress discontinuity caused by the cracks (Chen and Shaleeb 1982). The factor α represents the incapacity of the section to carry any stress in the direction perpendicular to the crack and it is very small, but not zero, in order to avoid the formation of singular stiffness matrices. The factor β indicates the reserve in shear strength after the crack has formed, as a result of residual friction at the interface between brick and mortar. Here, the shear modulus was reduced to 9% (Sinha 1997).

In Abaqus, the above modification can be carried out upon the elastic rigidity matrix by introducing solution dependent properties. The matrix can be defined as a function of

field variables, which can be further dependent upon quantities at the integration points of the section, like stresses or strains, using the interface of the Fortran subroutine USDFLD provided by the program. In the case of the vault FE model, three cases were considered for the material: undisturbed; crack in the weaker direction (α=0, β=0.09); complete failure or crack in the stronger direction (α=0, β=0.09 and $E_x \cong 0$). A set of field variables is defined in each case and the rigidity matrix is modified accordingly.

As the cracks were the result of damaged elasticity, it is possible that the presence of compressive forces in a later stage at the section examined may have caused the high tensile plastic strains at the cracks to invert and disappear. State variables can be used therefore to prevent any further changes to the rigidity matrix at the element once the criterion is exceeded. The subroutine also makes provisions to assign the correct flexural strength in the transverse web of the vault model, where the orthogonal directions change the global axes they are parallel to (§4.4).

4.3.3 Verification of the FE program

The capability of the FE program to modify the rigidity matrix can be tested upon a simple structure where the load shedding to the stronger direction, after the weaker has cracked, can be easily detected. The same experiments that were carried out to study the application of the moment failure criterion were examined here as well (Ng 1996), (Sinha 1997). A series of brickwork panels were tested to failure under lateral load, studying the influence of the aspect ratio and the support conditions. Wall 1 was a square panel (1140 x 1140 mm, thickness 53 mm), simply supported on all the four edges. The elastic moduli were derived by wallette tests and they were found to be 15509 N/mm^2 parallel to the bed joints (E_x) and 10642 N/mm^2 normal (E_y), while the flexural strength in the respective directions were 1.79 N/mm^2 (F_x) and 0.70 N/mm^2 (F_y).

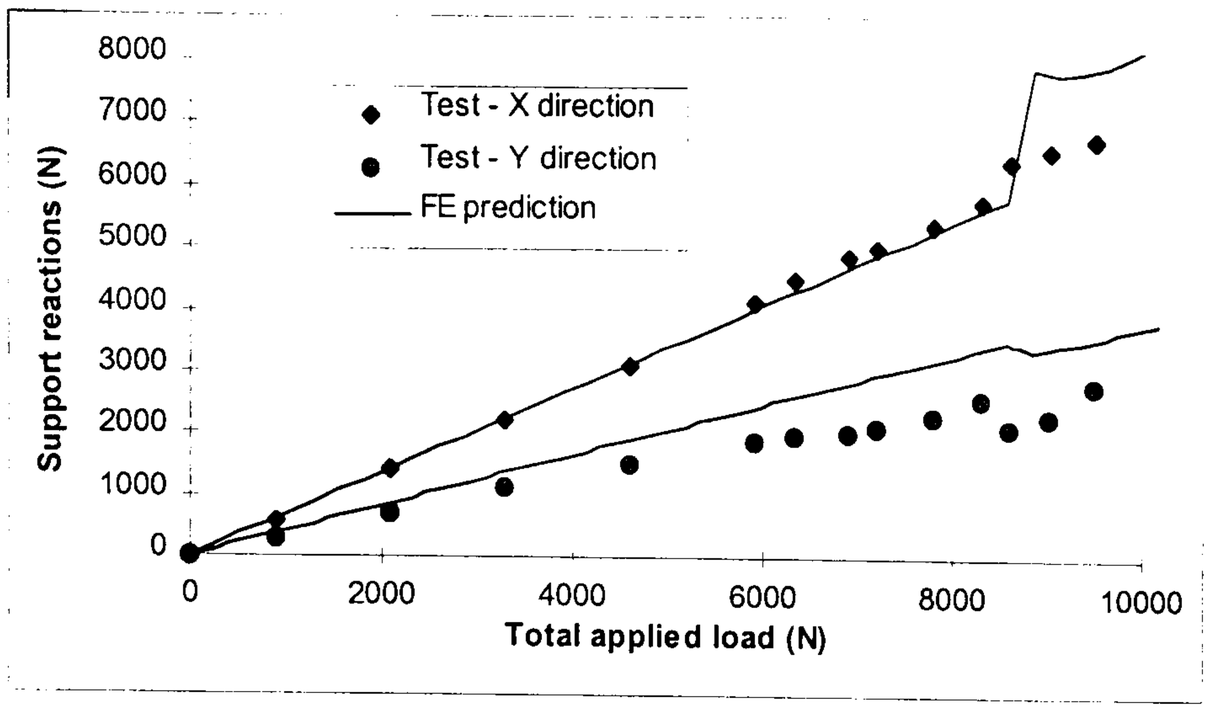

FIGURE 4.7 Distribution of the applied load in the X and Y directions in Wall 1 (after Ng 1996)

The panel was loaded uniformly and strains, deflections and reactions were monitored to assess the response of the structure. The recorded average reactions indicate the distribution of load in each direction and their development is plotted as a function of the total applied load in Fig. 4.7. At a pressure of 6.6 kN/m^2, corresponding to a total load of 8450 N, cracks in the weaker direction occurred at the centre and an amount of the load was transferred to the other direction. The FE model of the panel incorporated the routine using the biaxial failure criterion in (4.6) and was loaded in constant increments of 0.2 kN/m^2. When the central section cracked at 6.6 kN/m^2, the model predicted satisfactorily the load shedding to the stronger direction, which subsequently failed quite rapidly at a pressure of 7.6 kN/m^2 (total load 9880 N) very close to the experimental value of 7.46 kN/m^2.

A similar good agreement was detected when the maximum stress failure theory was used instead, as the panel is in a biaxial pure bending stress state. The routine can therefore successfully modify the rigidity matrix and it will be used with both the criteria to predict the strength of the vault under a forced movement of its abutments.

4.4 TESTING PROCEDURE

4.4.1 Test of vault under dead load

The experimental assessment of the structural efficiency of cross vaults focuses mainly on the failure due to imposed displacements at the abutments and the set-up of the test is developed accordingly (§4.4.2). Beforehand, however, dead load will be applied over the vault, in an attempt to reproduce the response of the original structure to a nominal value of service loads and to provide a benchmark test from a less complex structural behaviour with which to calibrate the FE model.

There is no available information on the actual dead and imposed loads on the Church of the Holyrood Abbey, despite several archaeological and restoration campaigns (Baldwin 1909, Oldrieve 1911). Therefore, an estimation of the original dead load was made from the weight of the constituent materials. Hard yellow sandstone (RCAHMS 1951) was used in the construction of the Abbey Church and the unit weight of this material is 22 kN/m^3 (Bunnyan 1987), so, as a conservative approximation, this value can be considered instead for the unit weight of the masonry.

The amount of load applied during the test had to be such that the stresses yielded both at the prototype and the model would be similar. Stresses are expressed in units of force over surface $[F/L^2]$, which can be equivalent to $[F \cdot L/L^3]$ or the units of the product {unit weight * length}. Since the geometric scale of the model is 1/4, the resulting self weight model should be 4 times that of the prototype, i.e. 88 kN/m^3. If, however, it is possible to apply only a lower weight, the results of the model can be made compatible to those of the prototype with a dimensional analysis, as long as the correct material properties are used.

Loading arrangements for shells depend on the geometry and amount of the applied load and they are usually very specific for each case. In the model vault, the load was distributed uniformly over the surface. From a survey after the structure was built, the area was evaluated as 2.15 m^2 so the volume was 2.15 $m^2 \cdot 0.035$ m = 0.075 m^3. This means that, according to the stress criterion, a total load of 88 $kN/m^3 \cdot 0.075$ m^3 = 6.64kN (or surface load of 3080 N/m^2) had to be applied to the structure. However, the instrumentation

(dial and strain gauges) would not allow the load to be distributed evenly over the extrados (by means of an airbag for example) and the delicate nature of the fabric would make impossible to fix hooks at the intrados from which to hang weights. A solution therefore was to split the load into blocks (lead weights).

So far as the amount of load was concerned, a preliminary FE analysis (see section §4.5.1 later) showed that the level of stresses expected would be below the strength of masonry in both directions. It was considered prudent however to tentatively apply lower amounts which would be subsequently increased until the theoretical amount could be attained safely. Furthermore, data from experimental research in similar structures were not available. So, in a first instance (Test DL1), the load of the vault was limited to a total of approx. 1kN, equivalent to a surface load of 420 N/m^2 (or unit weight of 13.3kN/m^3). The results from this phase showed a very low level of stresses, so a higher weight could be applied safely. The experimental response of the vault during this and the rest of the phases is presented and discussed in more detail in §5.2.

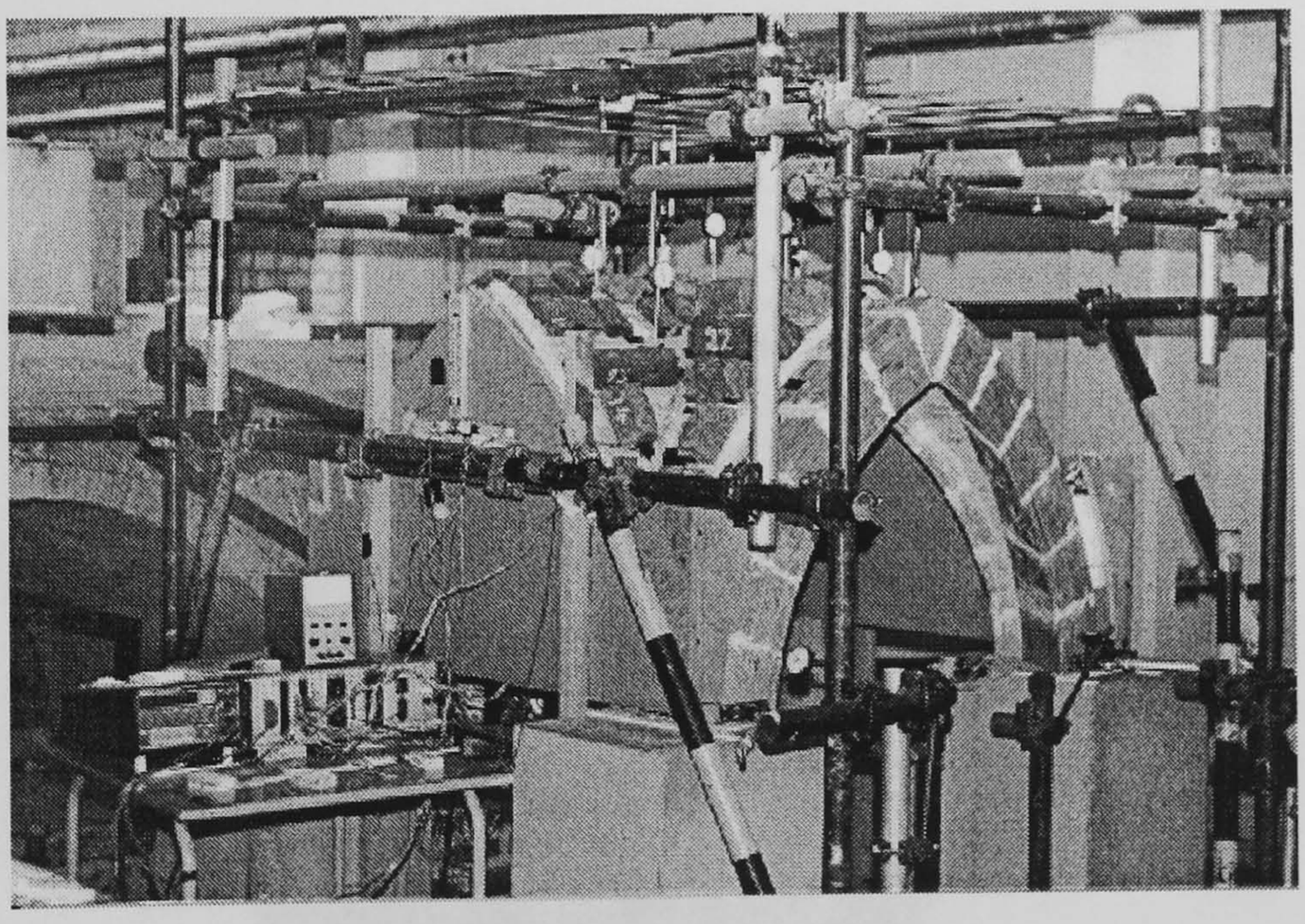

FIGURE 4.8 Loading arrangement for the dead load case (Test DL3)

In the next phase (Test DL2) the total weight rose to 1.5kN or pressure of 670 N/m^2 (unit weight 20kN/m^3). The maximum weight that was possible to attain (Test DL3) was 3.3kN or 1930 N/m^2 (54kN/m^3), less than the theoretical 88 kN/m^3 due to the above mentioned limitations (Fig. 4.8). In all the phases, the lead weights were secured on their

position with brackets, but below the middle of the height, the blocks had to be supported completely by these brackets, due to the curvature of the vault, and the tangent component of the load upon the web would be much higher than the normal. Any further increase became impossible, since the weights would start toppling or sliding and their placement on the vault would be more difficult to control.

In each test, the sequence of loading started with the area around the vertices, continued to the middle of the webs and finished at the haunches and spandrel fill. Strains and deflections were recorded in all the phases in order to monitor the response of the structure and the set-up of the instrumentation is described in detail in §4.5. Seven sets of loadings were performed for each test case and in the relevant sections where the results are presented (§5.2) the standard deviation (StDev) is also provided.

The vault was supported upon the wall at the end of the back transverse web, while the *tas-de-charge* blocks were mounted upon plates at the top of concrete pillars. The plates of the front supports made also part of the mechanism that produced the movement of the abutments (see next section). Regarding the continuity of the prototype vault with its neighbouring bays in the aisle of the Abbey church, this was restored in the model by means of two panels, fixed upon the concrete pillars, that did not allow the longitudinal web to deform out of the vertical plane that contained its end arches (Fig. 4.9) (see also §3.4.3.4).

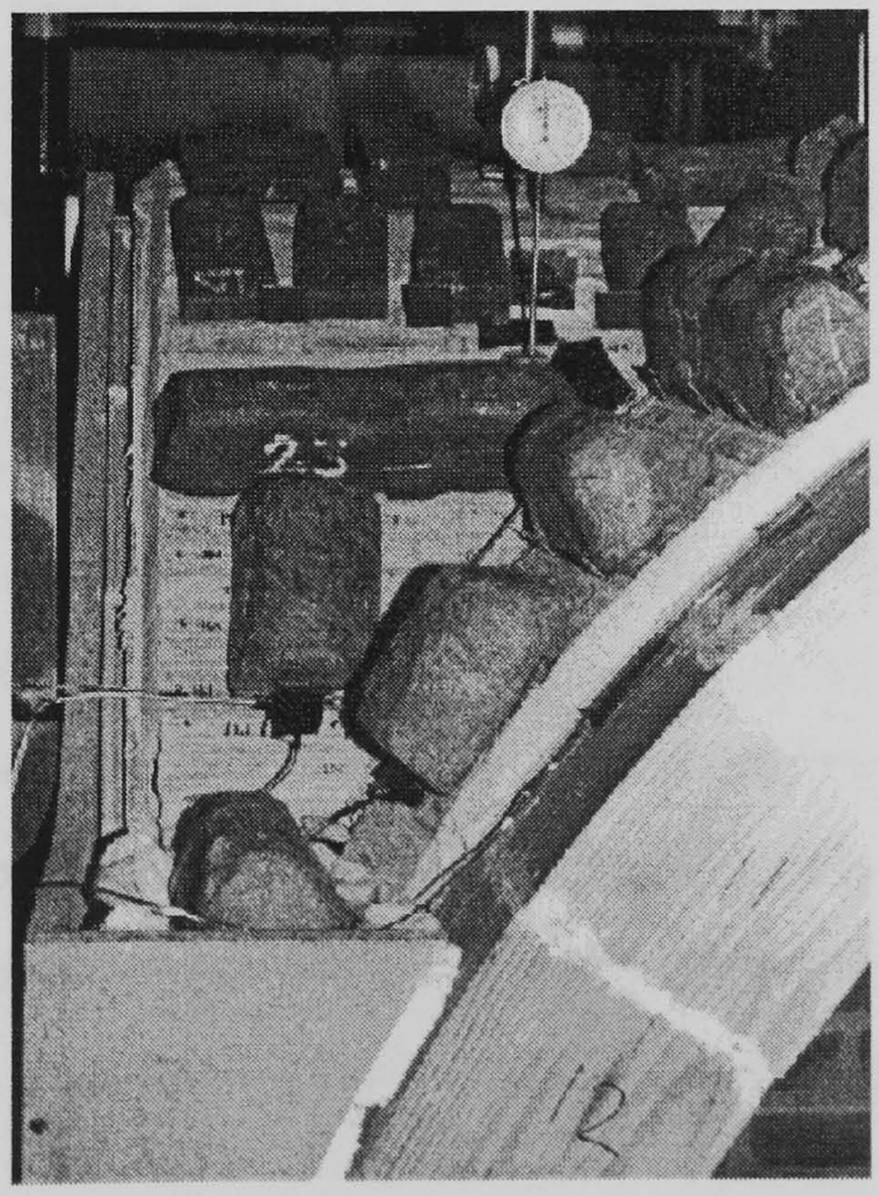

FIGURE 4.9 Spandrel wall and fill

So far as the fill over the haunches was concerned, the height was decided according to examples of other vaults where the correct practice of a fill until the middle of the total height of the vault was observed. The fill consisted of gravel carefully compacted and kept out of contact with the movement mechanism, while it was contained within the spandrel walls that were constructed as a continuation of the lateral panels (Fig. 4.9).

There are several parameters that can be the source of uncertainty in the behaviour of historic buildings, like the stiffness of the groins, the support conditions, the height of the spandrel fill. Their effect upon the deflections and strain distribution of the structure was investigated in this phase as well and the set-up of the respective tests is presented in the relevant sections of Chapter 5 together with the corresponding experimental results.

4.4.2 Dead load and movement of the abutments

The tests under dead load provided enough data to calibrate the FE model and evaluate the applicability of other analytical methods. The final stage of the experiment was the movement of the two front abutments until the structure failed, maintaining the weight of Test DL3. To achieve a controlled movement at the rate of millimetres, these supports were mounted upon plates that could slide between two guides as they were pulled by means of a turnbuckle whose other end was fixed to the test rig (Fig. 4.10). The displacement was monitored with dial gauges and this control was essential as the structure could have reached its elastic limit quite early and the cracks would then have propagated faster than expected due to abrupt changes of geometry.

The pathology of cross vaults for this kind of loading was discussed in §1.4 and it follows the crack pattern of Fig. 1.16. In the case of vaults with similar geometry, their stability is considered to reach a limit for displacements of their abutments in the range of 5 to 10 cm (which would be 5/3700 = 1:74 to 1:37 of the prototype's span here), although values up to 18 cm have been recorded, as in the case of Vitoria Cathedral in Spain (§1.4). Therefore, it was reasonable to expect the test vault would reach failure for a movement of the supports up to 30 mm. A more detailed account on the expected range of displacements is discussed in §6.4.1.

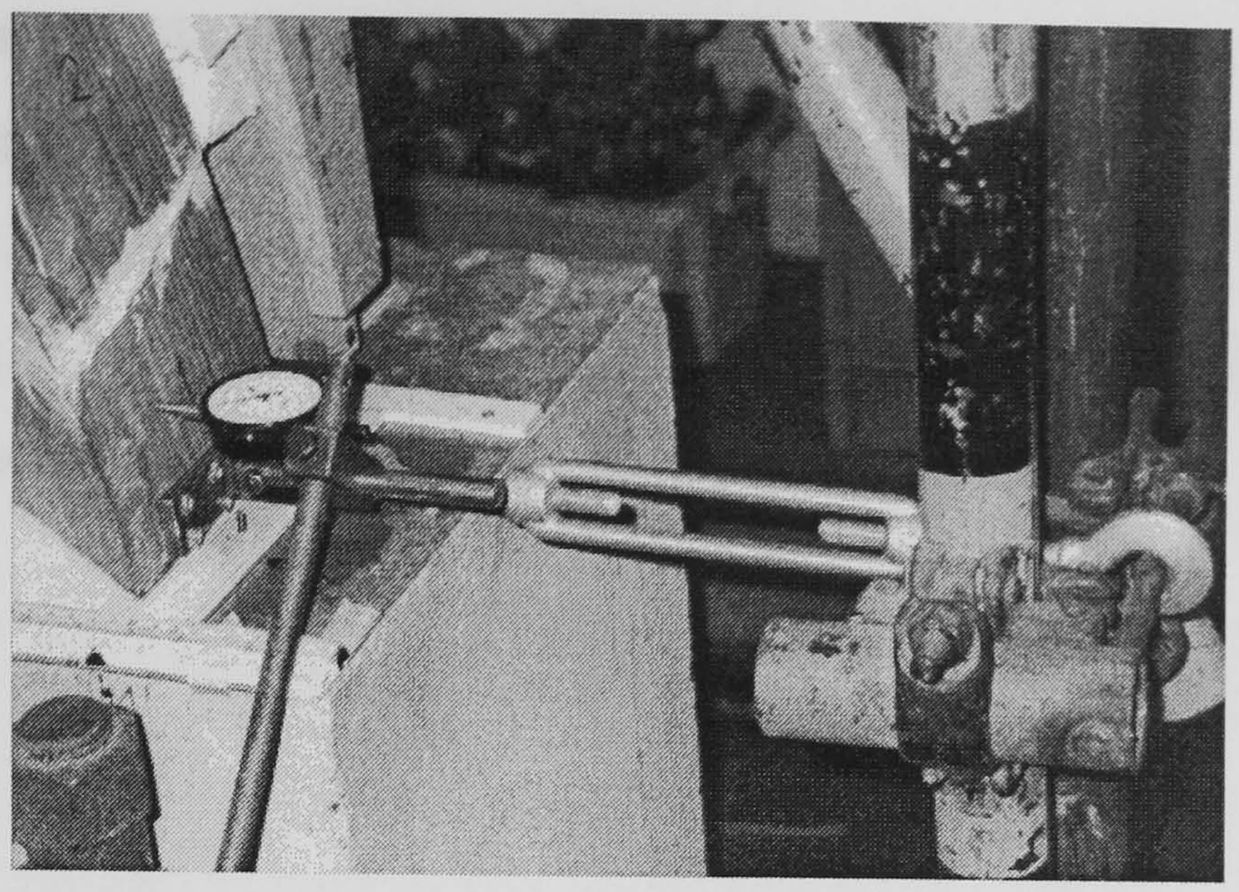

FIGURE 4.10 Mechanism for the movement of the front abutments

Provision was also made to limit the constraints along the direction of the movement induced by the presence of the spandrel fill and a margin between the spandrel and the fill of up to 5 cm was introduced. The behaviour of the vault was assessed by correlating the deflections and strains recorded with the crack pattern that developed.

4.5 INSTRUMENTATION DURING THE EXPERIMENTS

4.5.1 Preliminary assessment of the structural behaviour

In this section, the preparation of the experiment, after the construction of the test structure was completed, is described in detail. The quantities that were monitored were deflections and strains and the decision on the type and location of the instrumentation was highly dependent on their magnitude and distribution. Therefore, their range had to be determined beforehand and a FE model was considered suitable for the purpose, as it would later be the main analytical tool for the evaluation of the experimental results.

A FE pre-processor program written in Fortran was used for the generation of a FE mesh with shell elements for the program Abaqus and a more detailed account on this pre-processor and the use of shell elements is given in §5.3.1. As the transverse vertex defines also a plane of symmetry, only half of the structure was studied. The input data required to define the geometry were: transverse span 945 mm; longitudinal span 1225 mm; height 818 mm; thickness of shell 35 mm. The mechanical properties of the materials were evaluated

from the tests described in the previous sections and the values taken here were for the beams: modulus of elasticity E_b = 500 N/mm^2 and Poisson's ratio ν = 0.2. For the shell, the orthotropic elastic moduli were E_1 = 4200 N/mm^2 (stronger direction), E_2 = 670 N/mm^2 (weaker direction) and the Poisson's ratio ν_{12} = 0.3. The shear modulus G_{12} is linked to the other orthotropic mechanical properties as:

$$\frac{1}{G_{12}} = \frac{1}{E_1} + \frac{1}{E_2} + \frac{2 \cdot \nu_{12}}{E_2} \tag{4.9}$$

TABLE 4.3 Geometric properties of the cross sections of the arches

Arch	Area (cm^2)	Ixx (cm^4)	Iyy (cm^4)	Ixy (cm^4)	J (cm^4)
AF	186	2793	4245	170	5734
AD / AO	31	121	51	0	137

The skeleton of the vault consisted of the nave arch (AF), supporting the front side of the vault (Fig. 3.19), the ribs (AO) and the transverse arches (AD), while the section properties of the two latter groups are equal. The arches were modelled with quadratic spatial beam elements attached as stiffeners (ribs) on the shell, with the same node shared between the beam and the shell. Their section properties (Table 4.3) were evaluated with reference to the local beam section axes. Since the calculation of the Torsional Rigidity J is quite complicated for non-conventional forms, the trapezoidal arch sections were simplified to rectangular cross-sections with a similar area and second moments of inertia, so the corresponding torsional rigidity formula could be used then.

The 9-node doubly curved shell elements S9R5 were used in the analysis, with 9 integration points (see §5.3.1 for more details). For the arches, the 3-node quadratic beam elements B32 were chosen, that have 25 integration points as a default. The boundary conditions in that stage considered the bases as pinned, the side resting upon the wall as fixed, the other three (arched sides) free but supported on the respective ribs and a plane of symmetry normal to the X axis (XSYMM) along the transverse vertex. The load was acting over the whole vault as a uniformly distributed body force (BZ).

As was discussed during the set-up of the experiment (§4.4.1), the vault was planned to be uniformly loaded in subsequent sets with the amounts of surface load 0.42 kN/m^2, 0.67 kN/m^2 and 1.93 kN/m^2. In this manner the elastic response of the structure would be tested, so, assuming such a behaviour would occur at the final stage, the FE model was loaded with the corresponding weight, applied as a body force of a unit weight of 54 kN/m^3.

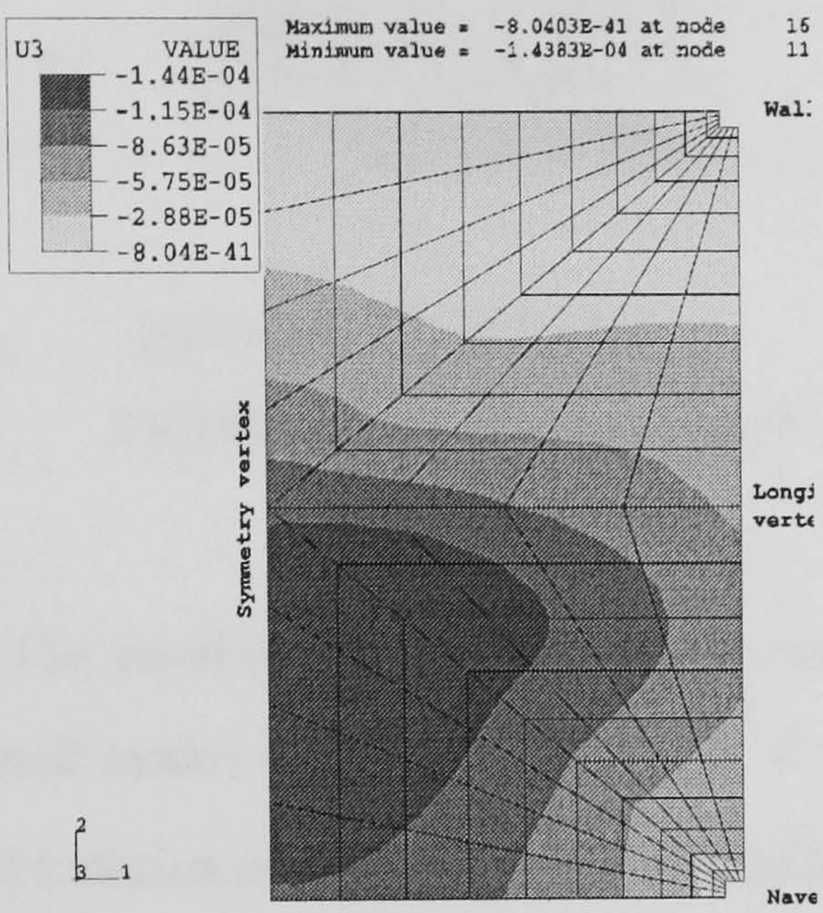

(a) Deflections (m)

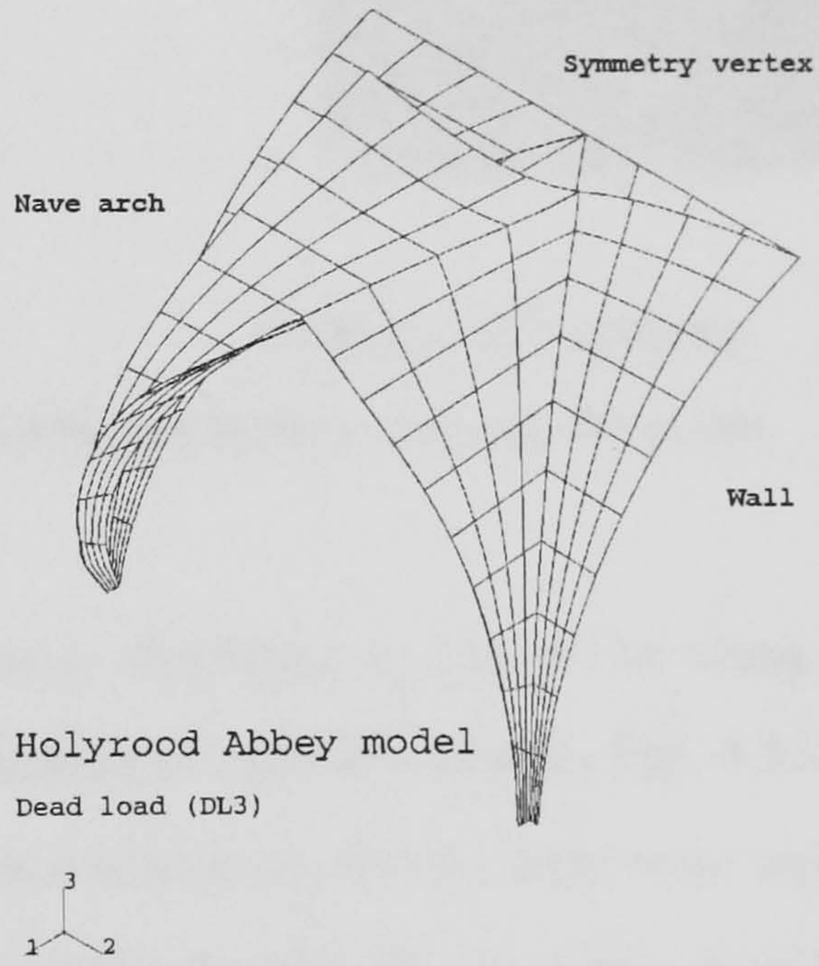

(b) Deformation of the vault

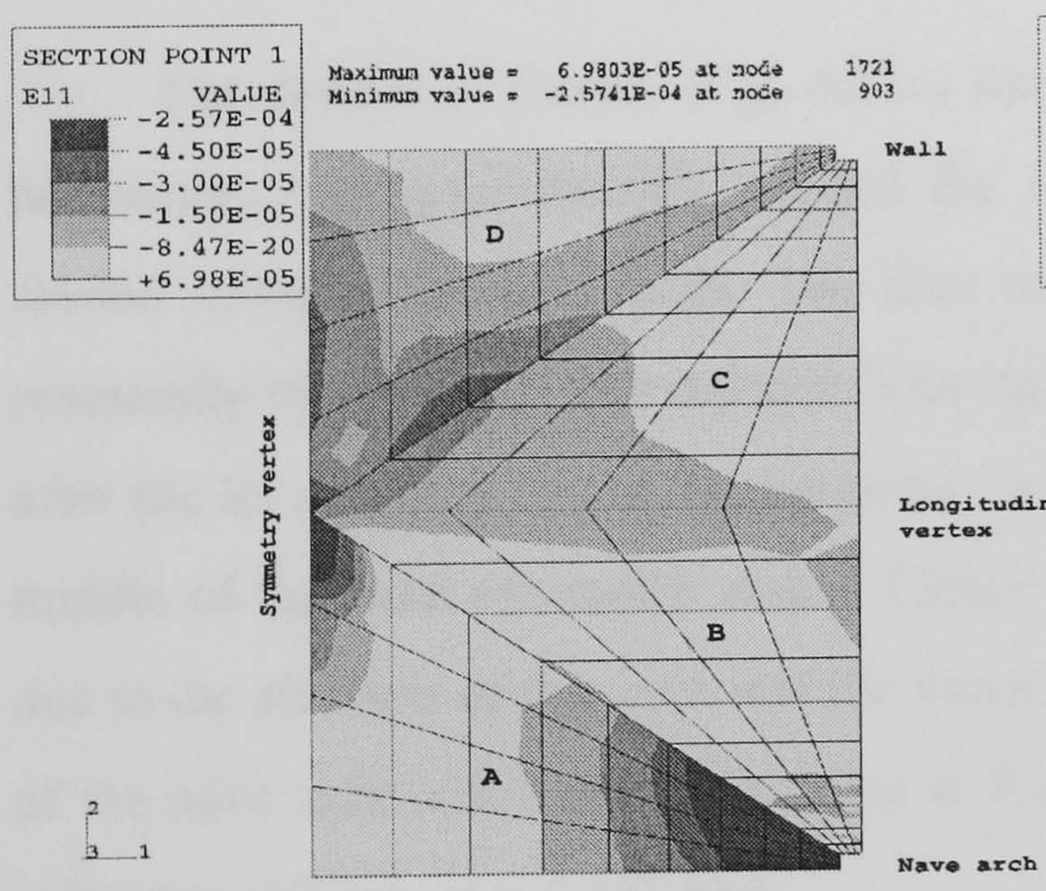

(c) Strains E11, intrados

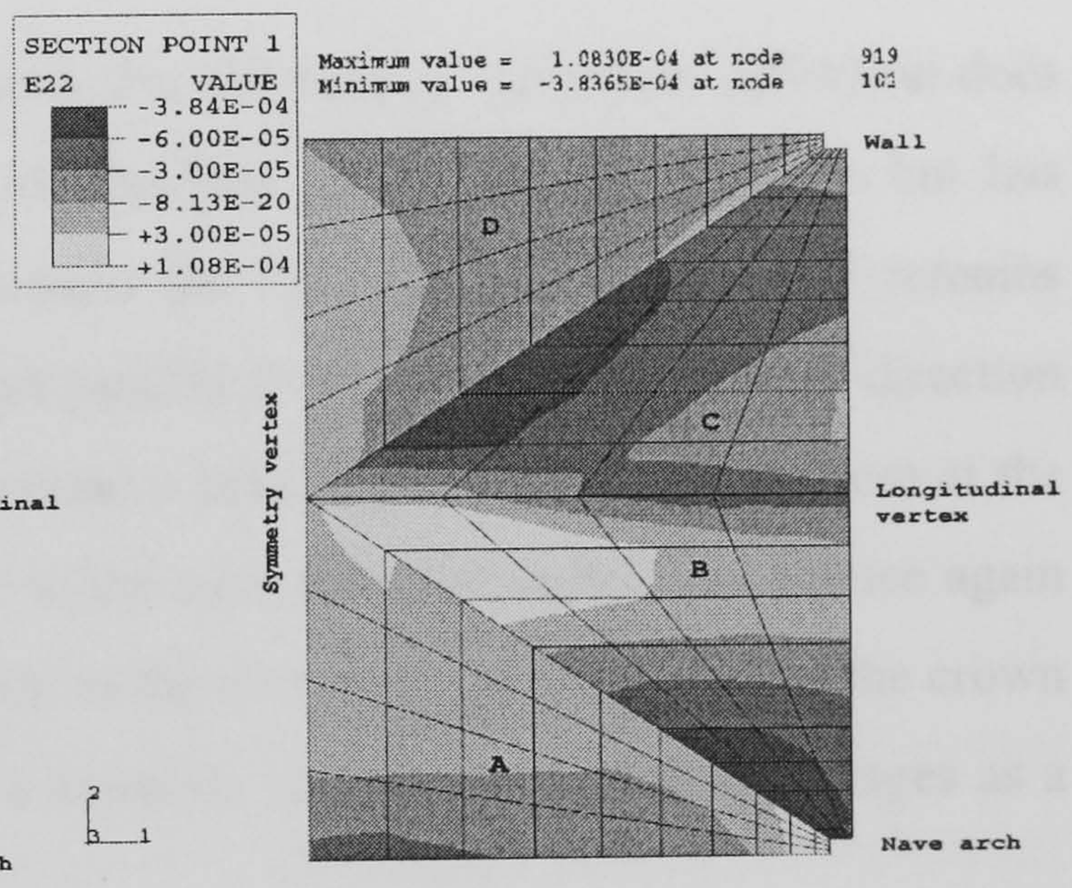

(d) Strains E22, intrados

FIGURE 4.11 Distribution of strain and deflection in the preliminary FE model

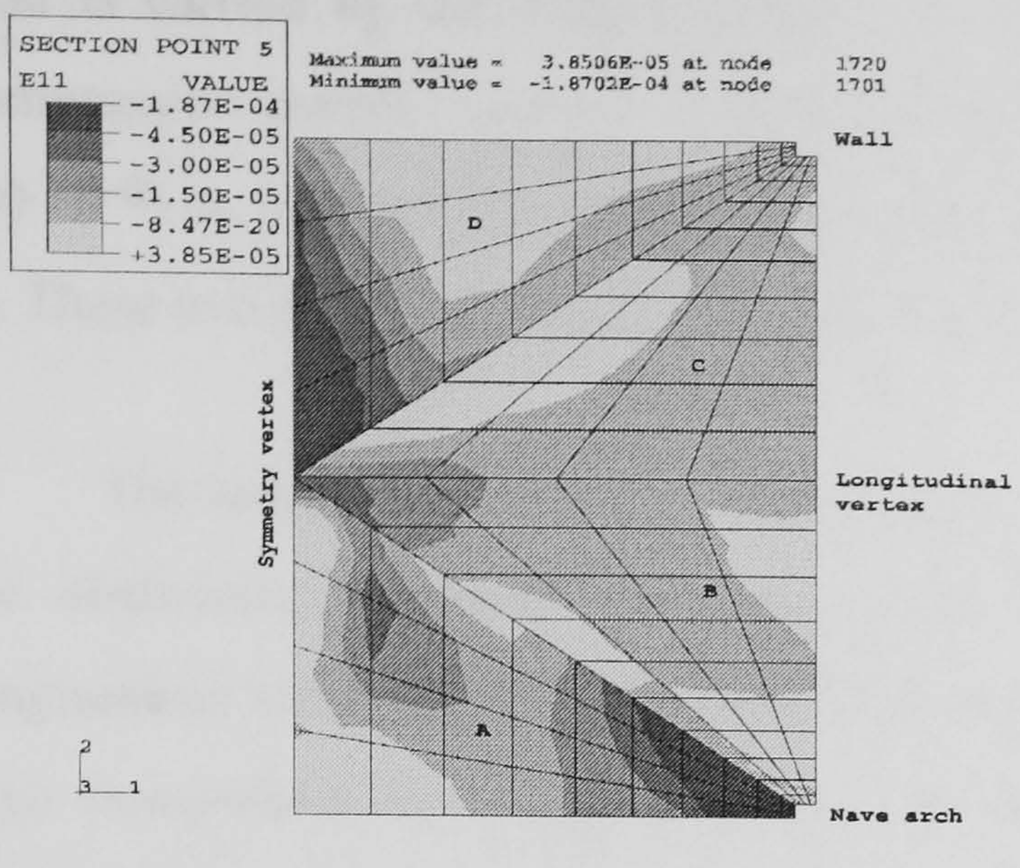

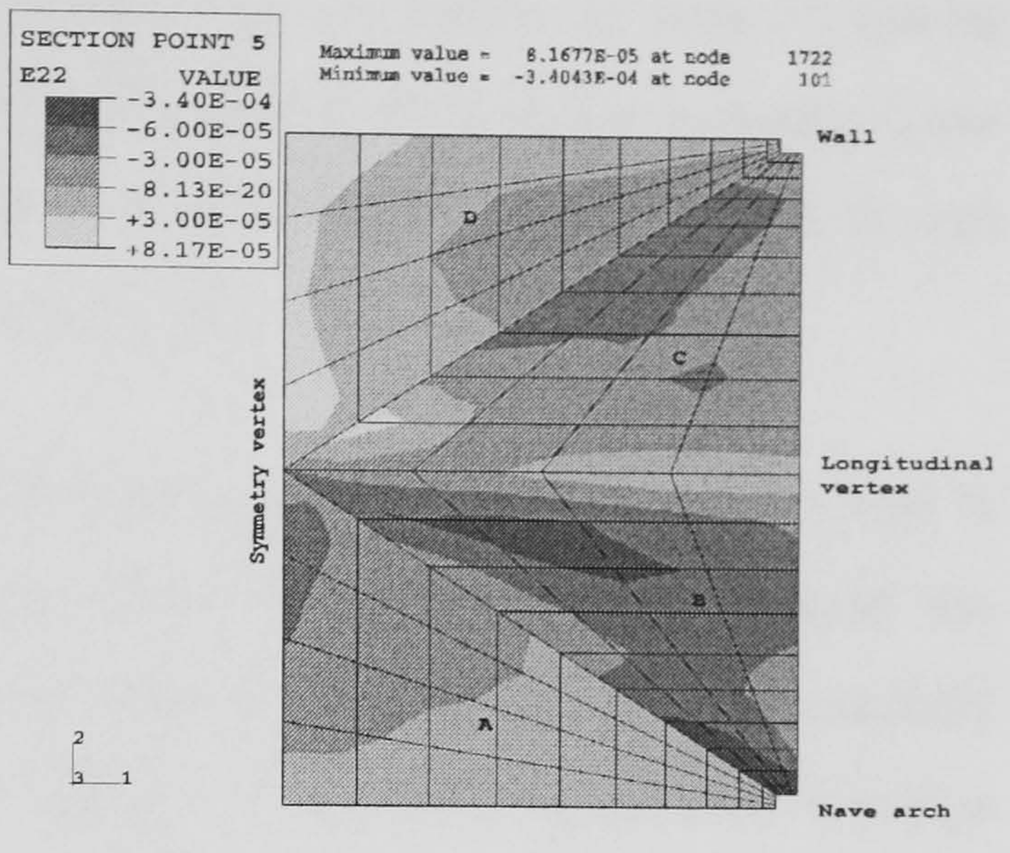

(e) Strains E11, extrados (f) Strains E22, extrados

FIGURE 4.11 Distribution of strain and deflection in the preliminary FE model

The resulting pattern for the deflections is displayed in Fig. 4.11a along with the deformed model in Fig. 4.11b and the distributions of strains follow in Fig. 4.11c, d, e, f. The E11 strains correspond to the circumferential strains (ε_γ) for the transverse webs (A, D) and to the longitudinal strains (ε_x) for the longitudinal webs (B, C), while the E22 strains are the opposite.

The deflection pattern (Fig. 4.11a) shows that the area of maximum deflection does not concentrate symmetrically around the longitudinal vertex and the keystone but has shifted towards the nave arch. The area around the rigid support of the wall remains practically undeformed. The contour lines start parallel to the wall but they change direction after the longitudinal vertex, concentrating around a peak displacement of 0.144 mm at the middle of the front symmetry vertex. Closer to the nave arch, the deflections reduce again due to the stiffness of that arch and the vicinity to the abutments, and the value at the crown of the nave arch is 0.1 mm. The value at the keystone can be used in the next stages as a reference and here it is 0.109 mm.

Regarding the associated development of strain, the pattern and range of values of the hoop strains ε_γ at the top of the transverse webs A and D (E11) is similar at both the intrados (Fig. 4.11c) and the extrados (Fig. 4.11e), indicating the presence of a membrane stress state. The web supported upon the wall, D, is under relatively high compression values at the vertex (over $-45 \cdot 10^{-6}$), which progressively reduce towards the springings, since all the

load is carried by the wall. At the front transverse web, A, below an area of similar compression around the crown, the compressive strains increase towards the springing (over $-60 \cdot 10^{-6}$) as, contrary to web D, the corresponding part of the load is carried directly by web A. These two areas are bridged with low tensile strains on both surfaces of the web.

The longitudinal webs (B, C) develop a different ε_y contour (Fig. 4.11d, f). Close to the abutments, the levels of compression are similar on both surfaces. Around the longitudinal vertex and close to the keystone, however, the extrados is under a relatively high compressive strain regime of over $-60 \cdot 10^{-6}$ (Fig. 4.11d), while the intrados develops tensile strains over $30 \cdot 10^{-6}$ (Fig. 4.11b), although below the experimental limit value ($440 \cdot 10^{-6}$). These maximum values are recorded at the front area of the vertex, as a result of the asymmetric concentration of higher deflections beyond the keystone. This zone of tension is where, from experience, the major cracks are expected to start (Fig. 1.16), so special attention is required during the monitoring. Outside these areas, the levels of compression recorded were similar on both the extrados and the intrados around the middle of the groin close to the wall, resulting in a membrane action.

So far as the longitudinal strains ε_x, are concerned, tension develops at the transverse webs A and D (E22) close to the areas where the corresponding degree of freedom (DOF) is effectively constrained, i.e. the support upon the wall and the nave arch (Fig. 4.11d, f). Tensile strain of over $30 \cdot 10^{-6}$ at the extrados (Fig. 4.11d) indicated a possible area of cracks similar to those observed by Sabouret (Fig. 1.16) (Abraham 1934). Close to the keystone the strains change to compressive at the extrados (Fig. 4.11f), following the sharp increase of deflections. Small values were generally observed at the longitudinal webs (E11 in B, C), which changed to slightly higher compression next to the key of the vault (Figs. 4.11c, e).

The overall behaviour of the analytical model suggested that during the dead-load test the vault is expected to deform mostly towards the nave arch, as this is relatively weaker than the wall standing opposite (Fig. 4.11b). The whole vault should sag principally in the direction along the symmetry vertex and the tensile strains that are expected mainly in the areas of the higher bending moments (longitudinal vertex and supports upon the wall and the nave arch) should confirm this pattern. The strains normal to the transverse arches were very low but those normal to the symmetry vertex were in high compression, especially around the keystone.

4.5.2 Measurement of deflections with dial gauges

Fourteen dial gauges were placed on the locations shown in Fig. 4.12a to record the deflections at the most significant positions, as these were identified from the preliminary FE analysis at the previous section. In general, the number of points for both strains and deflections was kept to a minimum possible in order to avoid interference with the applied loads. Since the sagging of the symmetry vertex is quite representative of the behaviour of the whole vault, care was taken to measure this faithfully, by using as many gauges as possible (dials SV1 to SV5). SV1 and SV2 were located at the back symmetry vertex (the latter was added later in order to refine the response of this area). SV3 represented the keystone, while SV4 was at the middle of the front part of the vertex and SV5 was close to the nave arch. The deflections along the transverse vertex were recorded with LV1 (at the outer third of the right portion), LV2 (middle of the right portion) and SV3.

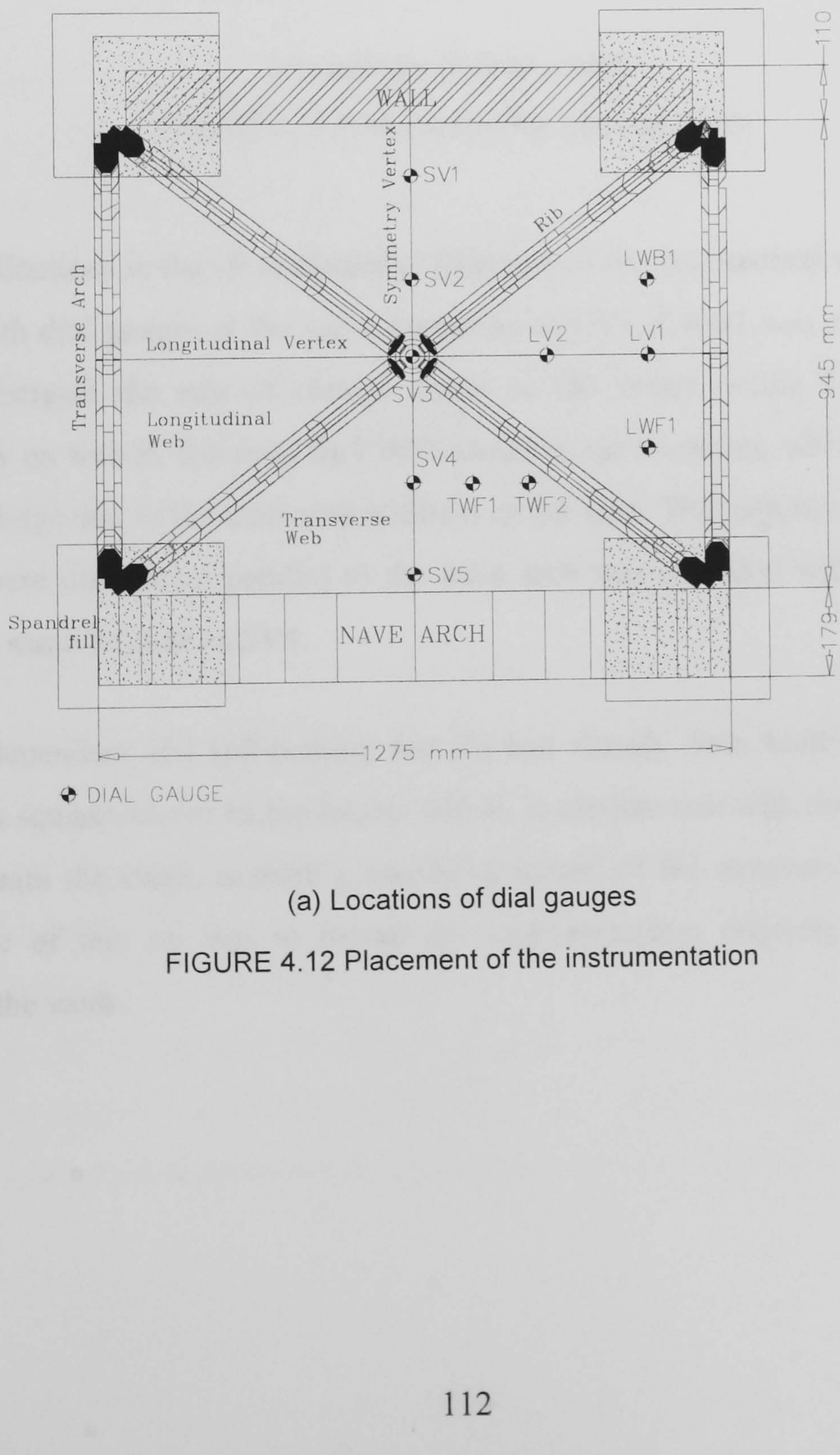

(a) Locations of dial gauges

FIGURE 4.12 Placement of the instrumentation

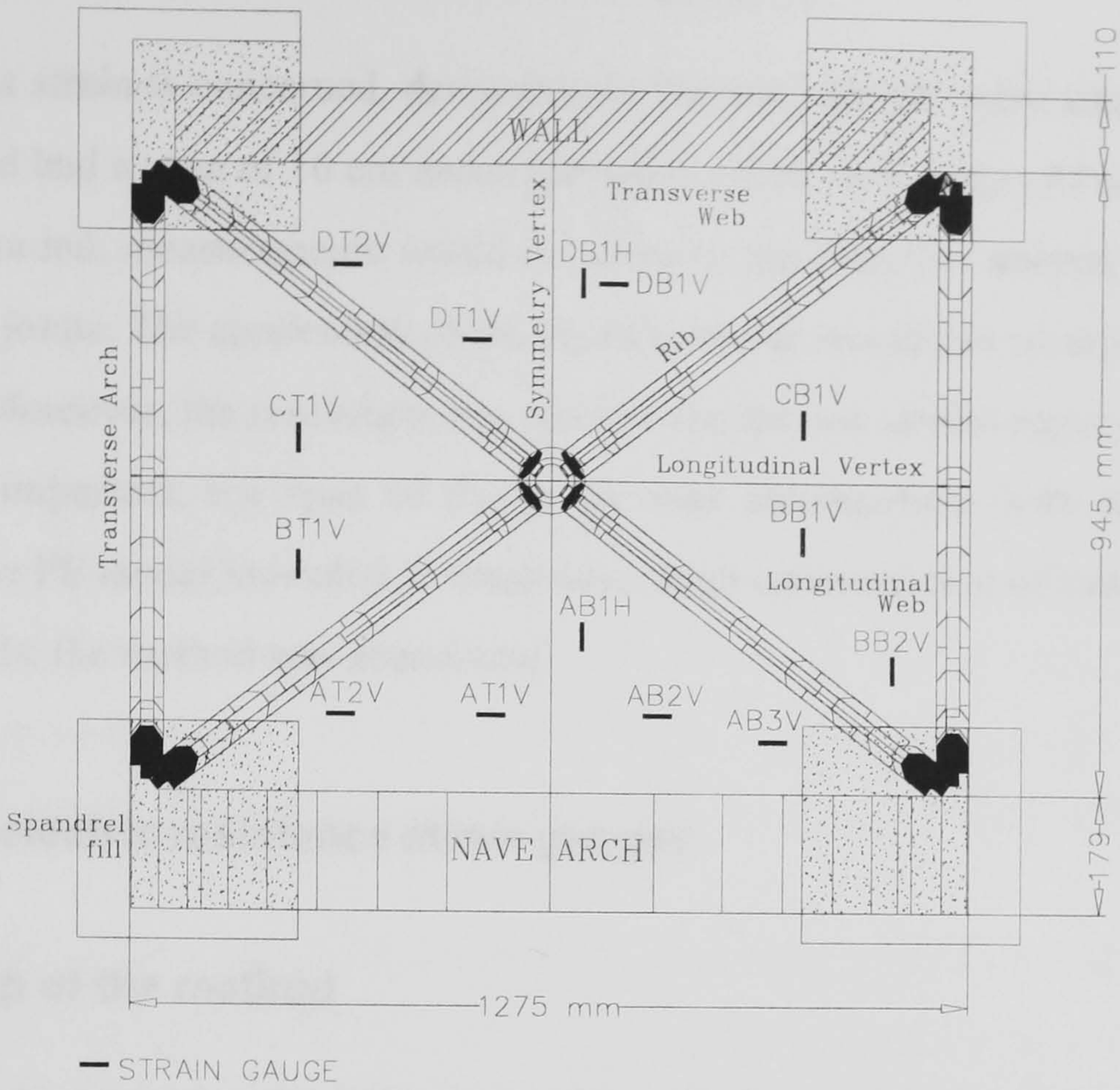

(b) Locations of strain gauges

FIGURE 4.12 Placement of the instrumentation

The deflections in the circumferential direction of the longitudinal webs B and C were monitored with dial gauges at the same longitude as LV1. LWB1 was placed in web C in order to investigate the rate of change closer to the vertex, while LWF1 was located symmetrically on web B, followed by LWF2 closer to the haunches, which was expected to give low readings due to the increased stiffness of the area. The pattern in which the higher deflections were distributed parallel to the nave arch was recorded with dials TWF1 and TWF2, at the same latitude as SV4.

An independent and self-bearing test rig had already been built to accommodate a grid of 20 cm squares above its top beams which, in conjunction with the grid drawn on the floor underneath the vault, enabled a measured survey of the structure to be carried. The main purpose of this rig was to mount the instrumentation properly over the selected positions on the vault.

4.5.3 Measurement of strain with "Demec" gauges

So far as strain is concerned, demountable "demec" gauges were employed initially. The gauge used had a span of 10 cm and a resolution of $16 \cdot 10^{-6}$ strain. At each point where strain was recorded, measurements would be taken in the direction normal, parallel and at 45° to the bed joints. The application of the loads however would not permit the readings at the extrados. Moreover, the resolution was too low for the low strains expected in the initial stages. More important, the span of the gauge was incompatible with the scale of the structure, as the FE model indicated in many areas high concentration of strains. As a result, after a few trials, the method was abandoned.

4.5.4 Use of electric resistance strain gauges

4.5.4.1 Set-up of the method

In order to overcome the limitations of the previous method and to provide a more effective collection and storage of the data, electric resistance strain gauges were applied on both the surfaces. Some of the disadvantages of the method had already become clear in the course of the wallette tests (§4.2), but the discussion that followed gave useful insight on how to interpret the results during the tests on the vault.

As in the case of the wallette tests, the gauges had a length of 5 mm. The usual practice requires they were mounted on the surface of the material after it was thoroughly cleaned and smoothened. A primer had to be added therefore to impregnate the area of application and make the porous surface of wood compatible with the prescriptions.

The change in resistance occurring when the gauge was strained was determined using a Wheatstone bridge. The circuit was arranged as a half bridge, where, alongside with the active gauge and the two fixed resistors, a dummy gauge was provided for temperature compensation. A Microlink logger was used to complete the circuit and record the data (Microlink 1994). The dummy gauge was mounted on a specimen from the masonry (in the form of wallettes) and it had to follow the same direction according to the grain of wood as the active. All the gauges and the immediate area of their support were protected with aluminium foil against any ambient temperature or humidity variations and the varnish applied on the units before construction helped minimise similar effects on the wood itself.

4.5.4.2 Placement of the gauges

The load arrangement conditioned also the placement of the gauges, which is shown in Fig. 4.12b. Fourteen strain gauges were mounted on the vault, with their respective dummy gauges on wallette specimens kept close to the model. The vault is considered to be composed of four webs, indicated in Fig. 4.12a as A (front transverse), B (front longitudinal), C (back longitudinal) and D (back transverse). The notation of the gauges begins with an upper-case letter 'A' to 'D' indicating the web they belong to. A letter represents the extrados (T) or intrados (B) surface, followed by the number of gauges within the same web (1~3) and the distinction between the hoop (V) and the longitudinal (H) direction of measurement. For example, 'AT1V' refers to a gauge mounted on web A, at the extrados (T), being the first (1) within the web and measuring hoop strain (V).

The gauges in the circumferential direction were installed at the extrados immediately below all the vertices (AT1V, BT1V, CT1V, DT1V), where high compressive stresses were expected, and at the intrados, below the longitudinal vertex (BB1V, CB1V), where significant tensile and compressive forces respectively should develop, and at the vertex of web D (DB1V) at the intrados. Other positions included the abutments of the transverse webs, A and D, at the extrados (AT2V, DT2V) and the intrados (AB3V), as also at the intrados of web B (BB2V), where the highest compressive strains were expected. Other important locations at the intrados included the middle of web A, along the circumferential direction (AB2V), and the middle of the vertices of webs A and D, in the longitudinal direction (AB1H, DB1H).

4.6 CONCLUSIONS

The evaluation of the mechanical properties of masonry with wallette tests under four-line loading showed clearly the elastic brittle nature of the material. The use of dial gauges and electric resistance strain gauges can give a quite different picture of the behaviour of the vault and an analytical modelling of the wallette tests attributed the reason to the differences between the properties of the constituent materials. In this manner, it was possible to use the results from the tests in order to assess the biaxial strength of masonry and provide the required input for the FE program.

The results from the latter were used to assess the locations of the instrumentation. According to the FE model, the vault deforms asymmetrically around the longitudinal vertex and closer to the nave arch, as a result of the reduced stiffness of this element with respect to the wall opposite. Moreover, the axis parallel to the symmetry vertex can be identified as the principal direction along which the structure is carrying the loads.

Chapter 5

INVESTIGATION OF THE BEHAVIOUR OF THE VAULT UNDER DEAD LOAD

5.1 INTRODUCTION

This chapter deals with the investigation of the response of the vault to dead load through experimental and analytical programmes. The previous chapter dealt with the properties of the test materials, the set up of the test and a preliminary appraisal of the behaviour of the vault with a FE analysis using the program Abaqus (§4.5.1). The convergence of the elements library was tested with a benchmark test on a barrel vault and is discussed here in §5.3.1. Dead load tests were performed to study the effect of the load distribution (Tests DL1 to DL3), geometry of the groins (DL4) and height of the spandrel fill (DL5) upon the deflections and strain distribution of the structure. The results of the tests are presented and discussed in §5.2.

The evaluation of the experimental data gave indications for further refinements of the FE model and aspects like the distribution of the load or the stiffness and geometry of the groins and the vertices were investigated (§5.3). The sensitivity of the vault to other parameters like the geometry of the groins, the material properties or geometric imperfections improved the understanding of the vault's behaviour. Based on the refined FE models, further aspects of the behaviour of the vault, such as the role of the support conditions in determining the deformation of the vault and the development of thrust were examined (§5.4).

5.2 EXPERIMENTAL RESULTS

5.2.1 General

Testing the vault under dead load was essential in order to assess its behaviour under service conditions and to establish a pattern of response under a plain loading. It also

enabled a comparison to be made between the experimental data from this stage and the work of other researchers. The elastic range of response of the structure was also evaluated, in anticipation of the non-linear phase which was expected to occur in the course of the displacement of the abutments.

Summarising the test set-up (§4.4), the load was applied uniformly over the vault and three sets of load tests were performed initially. The amount of load was increased between the sets in an attempt to reach the theoretical value that corresponds to the self weight of the vault (§4.4.1). Moreover, further tests were performed to assess the effect of other features like the groin geometry and the spandrels. The complete set of tests under dead load was as follows:

1) Test DL1: unit surface load 420 N/m^2

2) Test DL2: unit surface load 670 N/m^2

3) Test DL3: unit surface load 1930 N/m^2

4) Test DL4: same amount of load as DL3; groins strengthened with mortar

5) Test DL5: same arrangement as DL4; spandrel fill increased to 0.5 and 0.7 of total height

Problems related to the actual configuration of the vault meant that the amount of load in Test DL3 was the maximum possible load that could be applied (§4.4.1). The effect of these loads on the deflection of the vault and the distribution of the loads was monitored with dial gauges and electric resistance strain gauges respectively (§4.5). The examination of the first three tests in the next section gave some information on whether the response of the structure was still in the elastic range. The behaviour of the vault is discussed mainly for Test DL3 in §5.2.3, since the magnitude of the readings of the quantities considered was high enough to minimise any errors from the resolution of the instrumentation used.

5.2.2 Evaluation of the elastic response of the vault (Tests DL1 to DL3)

The deflected profile of the symmetry vertex was indicative of the overall behaviour of the vault and it is plotted in Fig. 5.1 against the predictions of the initial FE model

(§4.5.1). In the course of all the tests, the maximum values were recorded at the front part of the vertex and it was noted that the contrast with the back portion of the vertex increased with the amount of load. Moreover, the maximum value clearly shifted to the keystone in test DL3. The agreement with the FE results so far was mainly in terms of pattern and the reduction of deflections observed in the vicinity of the nave arch was regarded as an effect of its relatively low stiffness.

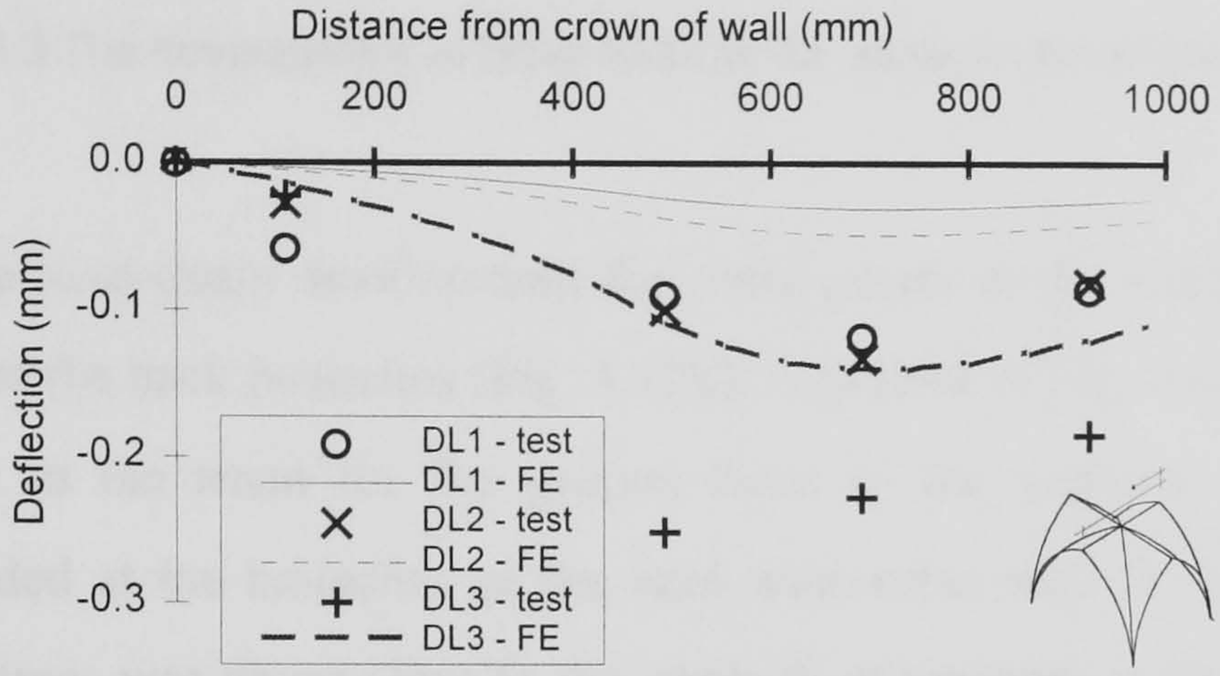

FIGURE 5.1 Deflection of the symmetry vertex for all the tests and corresponding FE results

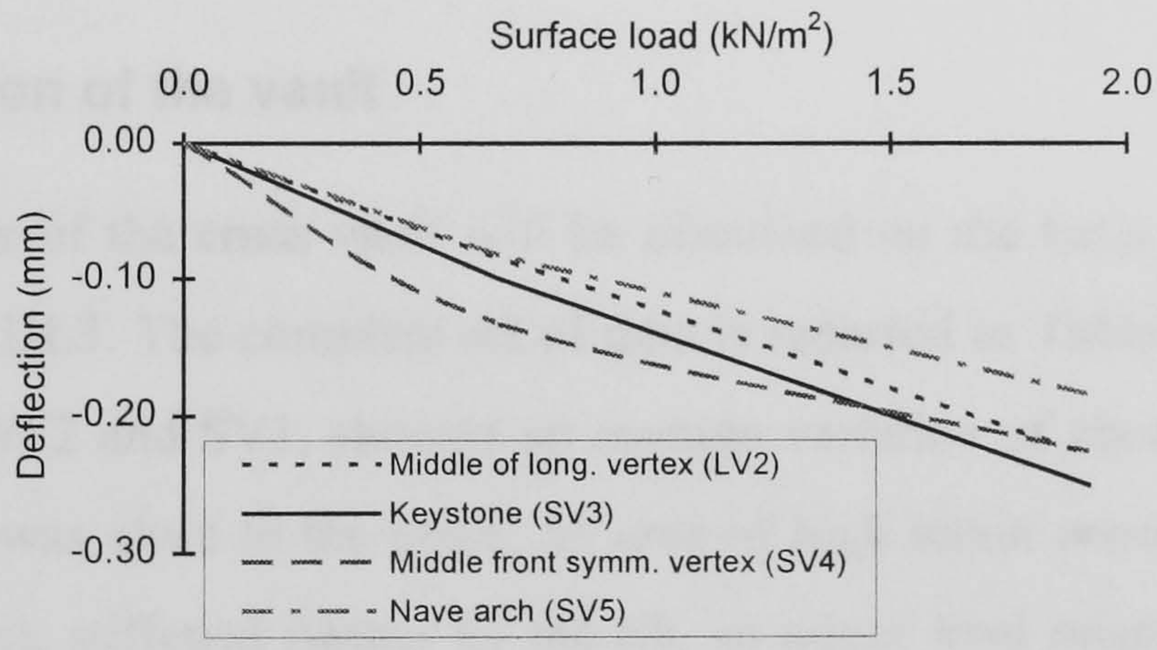

FIGURE 5.2 The development of deflection for the tests DL1 to DL3

The load-deflection relationship for some critical points at both the longitudinal and symmetry vertices is shown in Fig. 5.2 (see Fig. 4.12a for their locations on the vault). Most of these points follow a linear trend and the deviations at the initial stages can be associated with the low magnitude of the readings and the resolution of the instrumentation. The pattern recorded at the symmetry vertex (Fig. 5.1) represents a wider area at the centre of the vault parallel to this vertex, as the similar values at the keystone and the middle of the longitudinal vertex indicate.

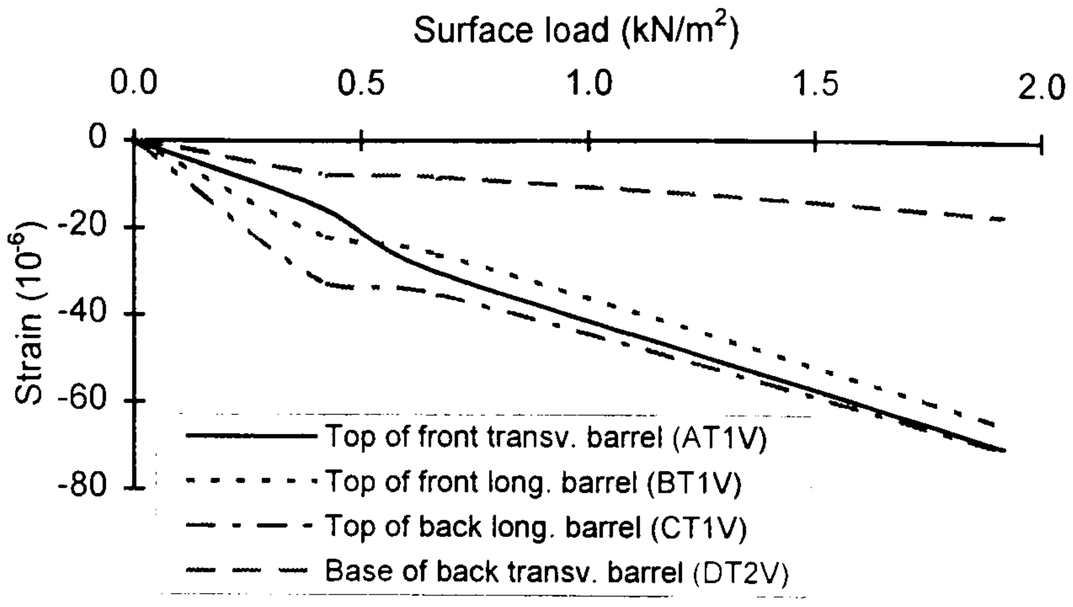

FIGURE 5.3 The development of hoop strain at the extrados for all the loadings

Similarly, the load-strain development for some points at the extrados, located close to the vertices and at the back haunches (Fig. 4.12b), is plotted in Fig. 5.3. It is interesting to note the similarity in the trend for the gauges close to the vertices, while a moderate increase was recorded at the haunches of the back transverse web D. The strain recorded indicated that the stress was never close to the strength of masonry in that direction, which shows that the vault remained in a linear elastic state of stress during the dead load tests, justifying the application of a linear FE analysis for this loading.

5.2.3 The deflection of the vault

The behaviour of the cross vault will be discussed on the basis of the experimental evidence from Test DL3. The complete set of data is reported in Table 5.1 and most of the dials, except for TWF2 and SV1, showed an average variation of about 33%. The reasons may be that TWF2 was close to the groin, an area of high strain concentration (especially around the haunches), stiffened further by the rib, so minor load misplacements may have had a significant and immediate effect there. SV1, on the other hand, recorded generally low values which can be easier affected by errors.

The deflections recorded at the symmetry vertex had a maximum at the keystone, SV3 (Fig. 5.1). The pattern is not symmetrical about the longitudinal axis as a result of the lower rigidity of the nave arch compared with the wall, so the thrusts exerted by the longitudinal webs are not contained by web A to the same degree as by web D. As a consequence, the whole vault shifts towards the front, sagging mostly at a zone spreading around the symmetry vertex of web A, as the high value in the immediate areas can confirm

(SV4, TWF1). The asymmetry of the pattern can be detected also at the area close to the transverse edge, where the gauge at the front transverse web LWF1 recorded a higher value than that at the back web, LWB1.

TABLE 5.1 Deflections for test DL3 (mm)

Dial	Test DL3		FEA
	Data	St Dev	Initial
LWB1	0.125	0.042	0.045
LV1	0.150	0.055	0.079
LWF1	0.165	0.053	0.104
LV2	0.210	0.073	0.101
TWF1	0.201	0.058	0.124
TWF2	0.072	0.043	0.099
SV1	0.022	0.026	0.017
SV2	N/A	N/A	
SV3	0.252	0.076	0.109
SV4	0.228	0.084	0.141
SV5	0.186	0.064	0.122

Overall, the FE model underpredicted the deflection of the vault, except from the case of TWF2 at the haunches. The pattern, however, developed in a similar manner as the test, asymmetrically about the longitudinal vertex, with maximum values around the front portion of the symmetry vertex (Fig. 4.11a and Fig. 5.1), although the maximum deflection in that area was recorded not at the keystone but at about the middle of this part.

The longitudinal vertex did not deflect uniformly together with the keystone as the gauges LV1, LV2 and SV3 indicate. This can be further confirmed by comparing the values between the vertex (SV3 and SV4) and those locations close to the transverse arch with similar distances from the longitudinal vertex (LV1 and LWF1). Probably the more pointed longitudinal webs B and C contributed to this reduction of deflection in the longitudinal axis, especially closer to the transverse end that is supported directly upon the abutments. The differences, however, from the corresponding points at the symmetry vertex are not very high and this indicates that the load is carried mainly to the transverse direction, from the wall to the nave arch, in a manner similar to one-way slabs. The pattern at the FE model confirms this behaviour, although it is more concentrated to the front webs and the deflections close to the transverse edge are more reduced than in the test.

So far as the displacements at the haunches are concerned, the low magnitude recorded at TWF2 demonstrates the effect of the ribs in this area and probably of the fill. Moreover, the slope of the vault was quite steep in the area and mainly membrane compressive stresses were expected which should yield comparatively lower vertical displacements. The FE model appears more flexible in that area and allows higher deflections to develop, probably as a result of the modelling with shell elements, which are not stiff enough to represent the area of the haunches.

5.2.4 Development of strain and neutral axis depth

From the study of the strain measured during the tests (Table 5.2), it appears that the most of the load was carried mainly by the three front webs A, B and C, as the higher values recorded there can indicate. The deflection pattern (Table 5.1) showed that the effect of the support upon the wall extended to a large part of the back transverse web D as it can be confirmed by the low strains recorded. At the extrados, the compressive hoop strains decreased towards the springings, at both the transverse webs (AT1V to AT2V and DT1V to DT2V). Similar strain pattern was recorded at the intrados in webs A and B and the strain on both faces of the vault at the front web A (AT2V, AB3V) demonstrated the loads were carried to the front abutments with membrane forces.

TABLE 5.2 Strains recorded in test DL3 (in 10^{-6})

Gauge	Test DL3		FEA
	Data	St. Dev.	Initial
AT1V	-70	19	-34
AT2V	-37	15	-46
BT1V	-65	17	-61
CT1V	-71	13	-28
DT1V	-29	9	-30
DT2V	-18	4	-11
AB1H	2	1	11
AB2V	-8	3	3
AB3V	-28	18	-50
BB1V	-3	13	32
BB2V	-32	12	-61
CB1V	-6	2	-39
DB1H	0	2	2
DB1V	0	5	-6

The pairs {BT1V, BB1V} and {CT1V, CB1V} are gauges located on both faces of the same point (Fig. 4.12b) and they indicated the presence of bending, with higher compression recorded at the extrados. However, the low level of tension agrees with the traditionally accepted concept that this form of vaults develops mainly membrane compressive forces. These membrane forces were more evident closer to the haunches, as the pair {AT2V, AB3V} can demonstrate. It is also interesting to note that bending was distributed almost symmetrically around the longitudinal vertex, as the afore mentioned pairs had similar values.

The longitudinal strains at the intrados of the vertices of webs A and D, AT1H and DT1H, were very small, although AB1H was located close to the area where the high deflections recorded were expected to be accompanied with tensile stresses. Observations similar to the tests on wallettes in the stronger X direction (§4.2.2) can be made: the strain gauge was mounted on the stiffer unit and a significant part of the strain was concentrated on the more flexible mortar joints.

The results from the FE analysis are also tabulated in Table 5.2. The agreement with the experiment is overall satisfactory, confirming that compression prevailed at the extrados. Contrary to the test however, the analytical values at the pair {CT1V, CB1V} showed axial compressive forces prevailed in the hoop direction, while the area of bending was concentrated into a narrow area at the front of the longitudinal vertex at web B (Fig. 4.11d, f). It appears that the sharp change of curvature over the vertex acted as a "barrier" that did not allow the stresses to spread over a wider area behind the vertex to the same degree as in the test. This can also be the cause of the overall low deflections in the FE model (Fig. 5.1) and the lower deformation at the front symmetry vertex (AT1V). A further consequence of this effect at the FE model was that a higher amount of the total dead load was carried by the front abutments, as shown by AT2V and DT2V.

The overall assessment from test DL3 is that the vault deflected asymmetrically towards the nave arch (Fig. 4.11b). As a consequence, the extrados was mostly compressed around the vertices, while the front haunches carried the loads to the abutments with membrane compressive forces. In general, the FE model underestimated at a constant ratio the deflections (about 60%) and the strains at the extrados. The improvements which were made to the analysis had to result in an increase of the deflections in the central area and the

effective redistribution of the deformation around the longitudinal vertex and they are presented and discussed in §5.3, focusing on the influence of features like the load distribution, the stiffness of ribs or the geometry of the vertices.

5.2.5 Influence of the stiffness of the groins (Test DL4)

Further experiments under dead load were carried out in order to investigate two important aspects of the design of vaults, the effect of the stiffness of the groin (Test DL4) and the height of the spandrel fill (Test DL5). Since many of the observations were based on the behaviour of the symmetry vertex, the monitoring was enhanced by adding the dial gauge SV2 at the back symmetry vertex, 200 mm from the keystone (Fig. 4.12a).

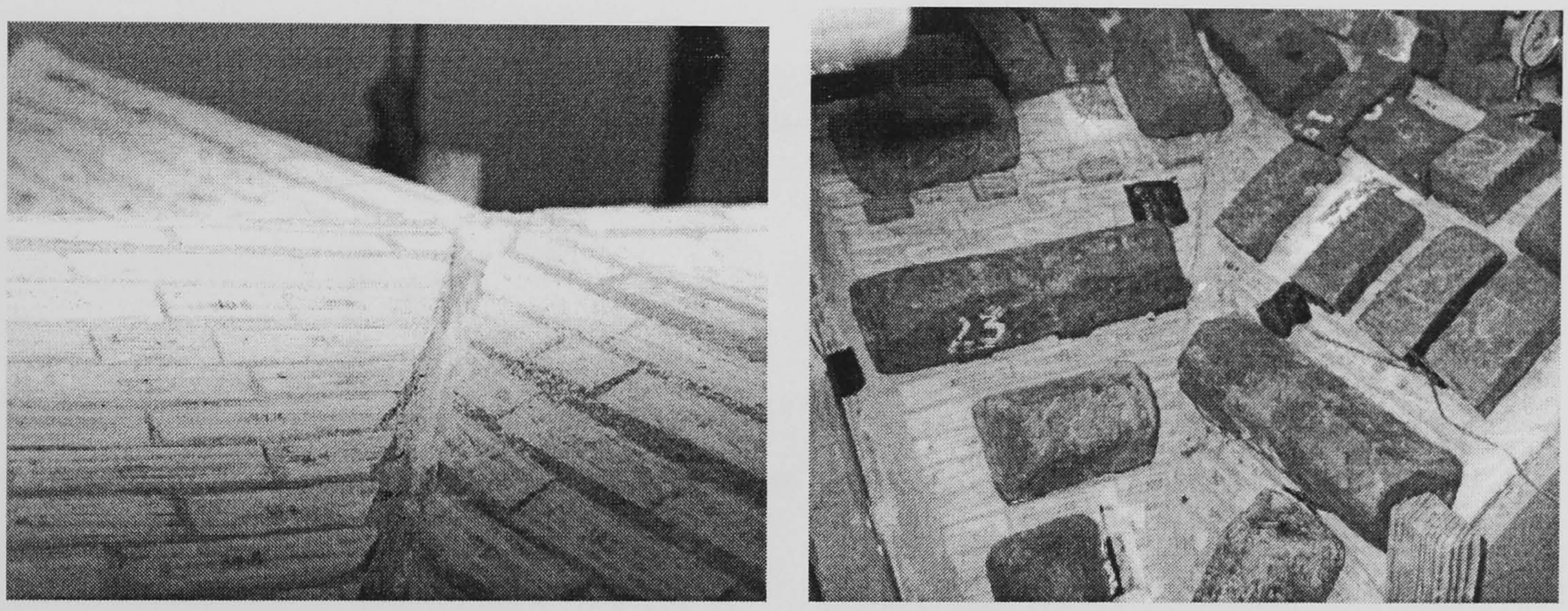

(a) Before the intervention (b) After the intervention

FIGURE 5.4 The strengthened groins in Test DL4

Along the groins, the webs were supported upon the rebate of the ribs, which resulted in a kind of a duct at the extrados of the rib (Fig. 5.4a). This may further reduce the capacity of the variable joint between the webs to withstand the higher stresses expected in the following stages due to imposed deformations, most probably contrary to what occurs in historic vaults. Therefore, after Test DL3, the extrados of the groins was filled with the same type of mortar as in the vault masonry, for the length between the keystone and the spandrel fill. The mortar was carefully compacted and the geometric continuity between the adjacent compartments was improved (Fig. 5.4b). A new series of tests, DL4, was performed applying the same amount and arrangement of dead load as in test DL3.

TABLE 5.3 Deflections for test DL4 (mm)

Dial	Experiment			FEA	
	Test DL3	Test DL4	St Dev	Initial	Stiff ribs
LWB1	0.125	0.157	0.016	0.045	0.041
LV1	0.150	0.103	0.021	0.079	0.069
LWF1	0.165	0.068	0.009	0.104	0.088
LV2	0.210	0.157	0.015	0.101	0.087
TWF1	0.201	0.110	0.022	0.124	0.109
TWF2	0.072	0.078	0.008	0.099	0.085
SV1	0.022	0.074	0.007	0.017	0.016
SV2	N/A	0.184	0.014	0.067	0.060
SV3	0.252	0.183	0.009	0.109	0.094
SV4	0.228	0.215	0.015	0.141	0.124
SV5	0.186	0.145	0.008	0.122	0.112

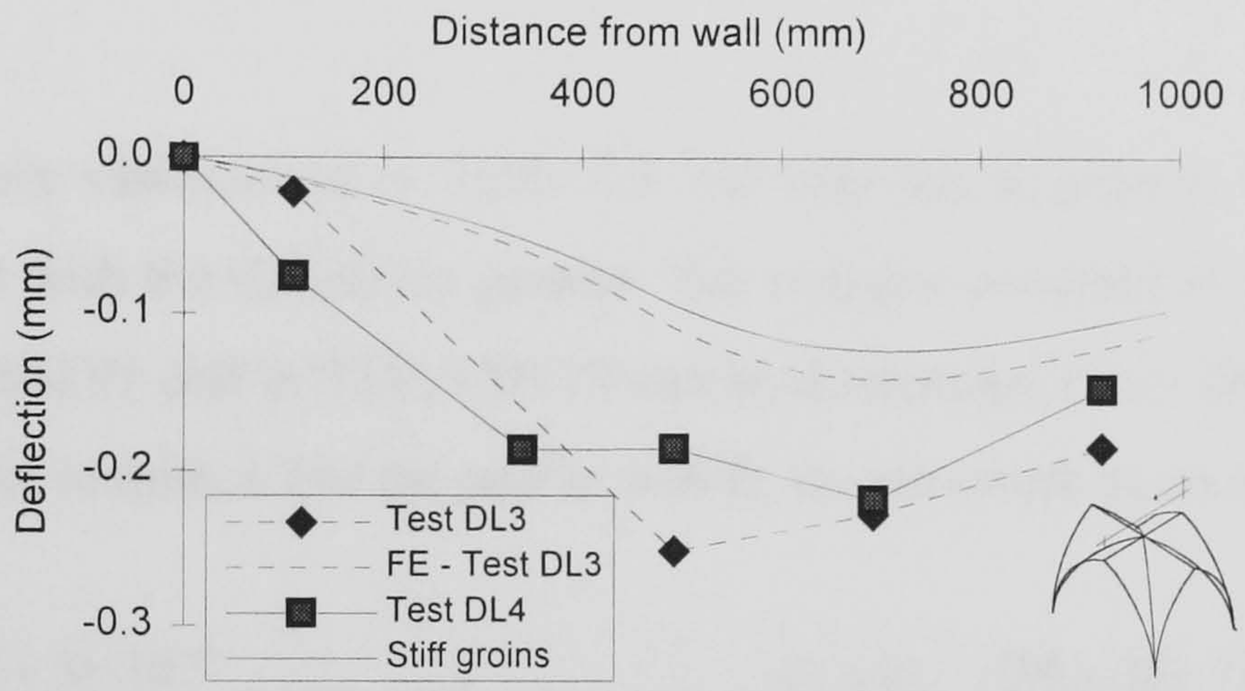

FIGURE 5.5 Deflection of symmetry vertex for vault with stiffened groins

With this intervention the structure was strengthened and the role of the ribs in the response of the vault enhanced. A general reduction of deformations was attained in the vault at the order of 30% (Table 5.3), most significantly around the keystone. The deformed profile of the symmetry vertex (Fig. 5.5) makes evident that the stronger ribs and keystone reduced effectively the deflection around the centre of the vault and resulted in a more uniform redistribution at the rest of the ridge, as the new dial gauge SV2 can also indicate.

This pattern was more pronounced at the section of the vault close to the transverse arch (LWB1, LV1, LWF1), where the maximum deflections spread at the back of the longitudinal vertex. The latter deflected in a similar pattern as before (LV1, LV2, SV3), decreasing closer to the transverse edge, although with lower values. A similar magnitude reduction was observed at the section of the vault parallel to the nave arch (TWF1, TWF2).

TABLE 5.4 Strains for test DL4 (in 10^{-6})

Gauge	Experiment			FEA	
	Test DL3	Test DL4	St Dev	Initial	Stiff ribs
AT1V	-70	-29	4	-34	-24
AT2V	-37	7	4	-46	-35
BT1V	-65	-30	5	-61	-54
CT1V	-71	-34	7	-28	-26
DT1V	-29	-11	5	-30	-29
DT2V	-18	2	5	-11	-9
AB1H	2	1	3	11	13
AB2V	-8	1	1	3	1
AB3V	-28	1	2	-50	-24
BB1V	-3	20	10	32	6
BB2V	-32	-18	4	-61	-26
CB1V	-6	-9	2	-39	-40
DB1H	0	-1	2	2	4
DB1V	0	3	3	-6	-6

Strain data are summarised in Table 5.4 and they are in general lower than in test DL3, in agreement with the deflection pattern. The changes occurred in the curvature φ at the pairs {BT1V, BB1V} and {CT1V, CB1V} can be determined by dividing the total strain with the depth of the section, *t*. For the pair in web B, the curvature decreased slightly:

$$\varphi_{B1} = \frac{\varepsilon_t + \varepsilon_b}{t} = \frac{(65-3)\cdot 10^{-6}}{35} = 1.77\cdot 10^{-6} \quad \text{to} \quad \varphi_{B2} = \frac{\varepsilon_t + \varepsilon_b}{t} = \frac{(30+20)\cdot 10^{-6}}{35} = 1.43\cdot 10^{-6}$$

while for the pair on web C the reduction was more pronounced:

$$\varphi_{C1} = \frac{\varepsilon_t + \varepsilon_b}{t} = \frac{(71-6)\cdot 10^{-6}}{35} = 1.86\cdot 10^{-6} \quad \text{to} \quad \varphi_{C2} = \frac{\varepsilon_t + \varepsilon_b}{t} = \frac{(34-9)\cdot 10^{-6}}{35} = 0.71\cdot 10^{-6}$$

The change at the front side of the vertex (web B) can be attributed to the presence of higher tensile forces, accompanied by an inversion of curvature on the other side, reflecting the wider spreading of the deformation of the vault to areas behind the longitudinal vertex and the keystone. Moreover, the appearance of tension in BB1V confirmed the empirical expectation of development of cracks at the intrados of the front area of the longitudinal vertex, which can be enhanced in higher loadings.

The strengthening of the structure caused also a similar reduction of hoop strain at the top portions of the transverse webs A and D. Very low hoop strains were observed however at the haunches (AT2V, AB3V, DT2V). This is an indication of the development of alternative load paths in the structure or changes in the support conditions, as the comparison with the strain at the haunch of the longitudinal web (BB2V) that was reduced similarly to the top regions can show. Concerning the longitudinal strain developing at the symmetry vertex (AB1H and DB1H), the actual lower deformation of the structure was not expected to cause any changes to the pattern and the conditions detected in the previous test.

Regarding the analytical assessment of the experimental data, the preliminary FE model was analysed within two limits established for the elastic modulus of the beam elements at the ribs. E_r was given a value of 500 N/mm^2 initially, which was then doubled (arbitrarily) to 1000 N/mm^2. This caused a uniform reduction of the deflections, but to a lower degree than the test (Table 5.3), while the symmetry vertex deformed mostly at the front, like before (Fig. 5.5). The problems associated with the capacity of the FE model to allow the deformation to spread behind the pointed longitudinal vertex that were detected in the previous test became therefore more evident here. Similar conclusions as before can be made and an overall underestimation was observed.

Strain also dropped in the FE model with stiffer ribs (Table 5.4) and the smaller magnitude of the data improved the agreement with the experiment. However, the high hoop compression at the back of the longitudinal vertex at the intrados (CB1V) showed that further modifications must be made to the FE model to increase the deflections and smoothen the "barrier" effect of this vertex (§5.3). No significant change was caused to the pattern of the hoop strain at the haunches, indicating that simply assigning a higher elastic modulus at the ribs of this model would not result in a major redistribution of the loads.

5.2.6 Influence of the height of the spandrel fill (Test DL5)

Until this stage, the haunches of the vault had been filled up to 40% of the total height H of the vault (0.33 m) with rubble material which was retained by a spandrel panel. In many cases of historic vaults, the conoid pockets formed in this manner are filled up to higher levels and, where maintenance is irregular, this level can reach the crown after debris from repairs in the roof has accumulated for long periods (Croci 1998b). However,

increasing permanently the fill of the test vault to such heights would hamper the mechanism of the abutments movement (§4.4), as the reaction from the fixed spandrels to the movement would apply an undesirable thrust against the haunches.

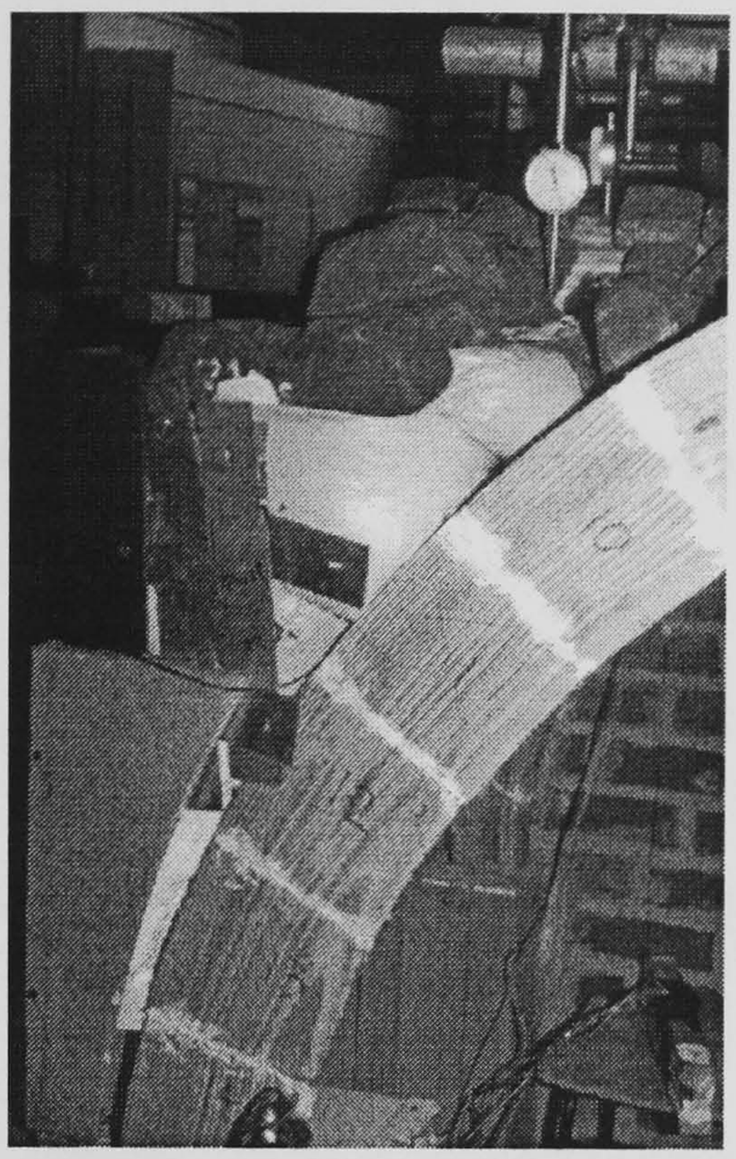

FIGURE 5.6 Test DL5b: spandrel fill at 0.7 of total height

It was considered useful however to assess the effect of the fill on the stress distribution for the dead load case, applying it to service conditions levels. The tests were performed on the strengthened structure of the previous phase. Two levels of fill were considered: 50% of the height H (0.41 m - Test DL5a) and 70% (0.57 m- Test DL5b). Plates were mounted temporarily on the existing pockets of the spandrels and the pockets were filled with light gravel. The weight corresponding to each level of the fill was reproduced during the loading of the vault with lead weights placed on top of the fill. The amount of load applied per haunch was 350N for Test DL5a and 620N for Test DL5b (Fig. 5.6).

The test resulted in a moderate increase of the deflections (Fig. 5.7 and Table 5.5) which, except from the relatively higher data recorded at the back half of the vault, was rather uniform. A probable reason is that the amount of the load applied over both cases of the fill was not higher than the load that had to be replaced in the corresponding area of the shell. Moreover, the reduction of the slope is significant only above the level of 0.7H and the stresses around the vertices, which result from the bending developing there, are affected mainly by local load pattern changes.

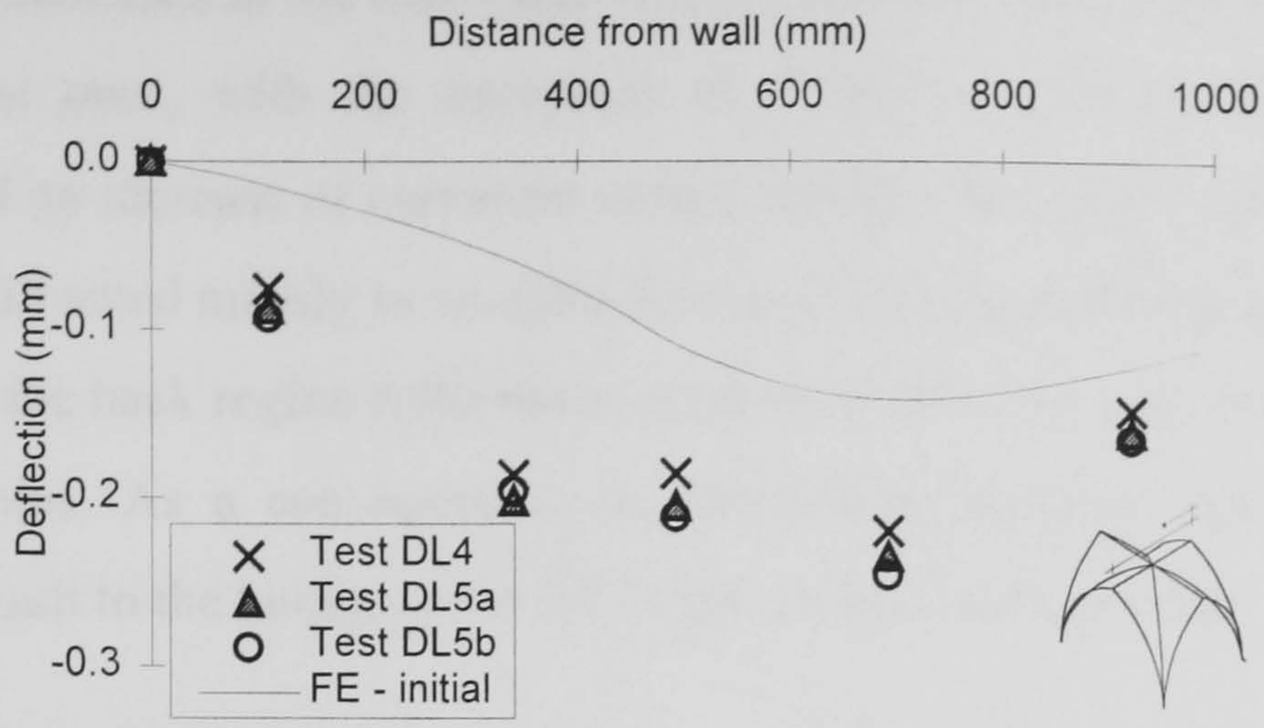

FIGURE 5.7 Deflection of the symmetry vertex considering increased spandrel fill (Test DL5)

TABLE 5.5 Deflections for test DL5 (mm)

Dial	Experiment					FEA
	Test DL4	Test DL5a	St. Dev.	Test DL5b	St. Dev.	Initial
LWB1	0.157	0.182	0.009	0.164	0.012	0.045
LV1	0.103	0.112	0.012	0.113	0.022	0.079
LWF1	0.068	0.076	0.009	0.034	0.012	0.104
LV2	0.157	0.165	0.005	0.179	0.027	0.101
TWF1	0.110	0.129	0.018	0.157	0.030	0.124
TWF2	0.078	0.077	0.007	0.097	0.016	0.099
SV1	0.074	0.088	0.000	0.093	0.032	0.017
SV2	0.184	0.200	0.003	0.196	0.091	0.067
SV3	0.183	0.197	0.011	0.211	0.029	0.109
SV4	0.215	0.236	0.003	0.245	0.014	0.141
SV5	0.145	0.148	0.019	0.165	0.016	0.122

TABLE 5.6 Strains for test DL5 (in 10^{-6})

Gauge	Experiment					FEA
	Test DL4	Test DL5a	St. Dev.	Test DL5b	St. Dev.	Initial
AT1V	-29	-43	1	-47	7	-34
AT2V	7	26	3	7	3	-46
BT1V	-30	-26	4	-19	5	-61
CT1V	-34	-46	0	-42	5	-28
DT1V	-11	-14	6	-20	2	-30
DT2V	2	8	4	5	1	-11
AB1H	1	1	1	-1	1	11
AB2V	1	-4	2	-2	1	3
AB3V	1	1	0	-4	2	-50
BB1V	20	11	10	15	4	32
BB2V	-18	-26	9	-22	4	-61
CB1V	-9	-6	1	-7	3	-39
DB1H	-1	-1	1	0	1	2
DB1V	3	5	0	4	2	-6

The strains increased at the transverse webs A and D (Table 5.6), while they dropped at the longitudinal ones, with the exception of CT1V, where the higher compression recorded indicated an increase of curvature at that section. The pattern that emerges shows that the spandrel fill acted mainly as an extra source of weight, affecting more the front part of the vault while the back region followed as a result of the enhanced co-action established by the stiffer groins. As a consequence, no significant variation was observed on the responses of the vault to the height of the fill in the present configuration.

The importance of the loading sequence to the behaviour of the structure was investigated during one of the loading sets in test DL5b and compared with a similar phase performed earlier in test DL4. In all the tests so far, the application of the load on the structure was carried out in three successive stages (§4.4): first around the vertices (a), then on the middle of the webs (b) and finally on the haunches and spandrel fill (c). The development of strains and deflections was recorded in each stage and not at the end of the loading as in the rest of the sets. The deflections recorded showed that:

a) when the vertices were loaded, corresponding to 45% of the total amount, all the dial gauges close to this area reached almost 70% of their final value, with those close to the haunches (TWF1, TWF2 and LWF1) at 50%;

b) when the central area was loaded (70% of load), all the gauges at the vertices area attained their final value and the rest were at about their 80%;

c) the final stage of the load application caused no alteration to the vertex, providing only final adjustments to the deflections of the haunches area.

After the structure was unloaded, it was interesting to observe that the data would return closer to the initial zero readings than in the previous cases with the lower spandrel fill. This gives credence to the opinions expressed previously regarding the beneficial action of the fill on the retention of the lateral thrusts and the stability of the vault.

The overall small changes did not cause any notable improvement on the agreement with the preliminary FE model (Fig. 5.7 and Tables 5.5 and 5.6). The degree to which the spandrel fill can act as a possible source of boundary constraints will be discussed in more

detail in section §5.3.5, where the FE model is modified to improve the assessment of the behaviour of the structure.

5.3 FINITE ELEMENT (FE) ANALYSIS

5.3.1 The use of FE analysis

The Finite Element method facilitated a very flexible approach to the assessment of the behaviour of the model vault. It allowed a model geometry quite close to the prototype to be generated, a variety of boundary conditions to be assigned, some particular construction details to be simulated and the load to be more accurately applied. The FE program ABAQUS, v. 5.8 (HKS 1998), has been the main tool through all the stages, when initially linear elastic and then non linear material and geometric analyses (NLMGA) had to be performed. The geometry of the preliminary FE model that has been used until now and the suitability of the method for this problem will be presented in the following sections.

5.3.1.1 FE modelling of the structure

In order to maximise the benefits of the FE analysis and minimise effectively the computational load, which can be affected by the 3D nature of the problem, doubly curved shell elements were used for the webs and curved beam elements for the arches. Using 3D brick elements instead would have made the geometry of the mesh more complicated and it would have increased the computational demands of NLMGA in the next phase. A regular mesh of quadrilateral elements was generated in all the phases of the problem (Fig. 5.8). A program written in Fortran was used as a pre-processor for Abaqus, which made the mesh generation more flexible and facilitated the assignment of certain boundary and load conditions.

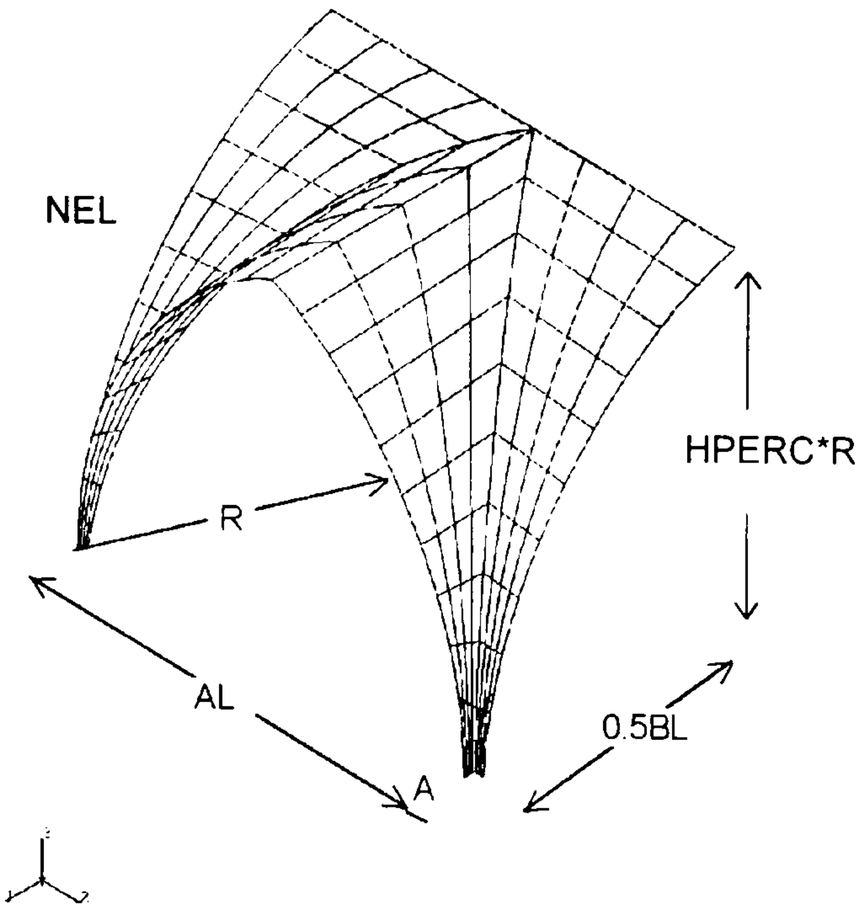

FIGURE 5.8 The FE mesh of the cross vault model and geometric variables for the Fortran pre-processor

The geometry for the original vault at the Abbey of Holyrood corresponds to Type 1, as it was defined in §3.1: pointed diagonal rib and arched profiles with equal radii and heights, with the common radius being equal to the transverse span (Fig. 3.1a). The essential variables for the generation of the mesh input (Fig. 5.8) were: the dimensions in plan (AL, BL); the height of the vault as a percentage of the radius R (HPERC); the offset at the springing of the arches (A) and the density of mesh along the arches (NEL). Other parameters included the dimensions of the cross sections of the ribs, transformed into equivalent rectangular sections, (AFA, AFB) and (ADA, ADB) for the nave and transverse arch respectively; the shell thickness (SHTH); the material properties of the ribs (HOOKE, POISSON) and the webs (moduli of elasticity in the two orthogonal directions E1 and E2; Poisson ratio V and shear moduli); and the movement of the abutments (MOVABUT).

The density of the FE mesh along the vertices was determined so that every quadrilateral element would have approximately equal sides. The mesh was regularly spaced in both directions but this could be biased towards any side according to a desired polynomial law. The lateral and diagonal arches were attached to the shell as spatial beam elements, assigning the necessary section properties (Table 4.3).

5.3.1.2 Benchmark tests

Before using the FE model, the accuracy and the rate of convergence of the method had to be examined by performing a benchmark test against the solution of a well-known shell problem. A shallow barrel vault of intermediate length was studied and the deflection at the middle of the free edge was compared with the results of FE models produced by various meshes and shell elements available in the Abaqus' library (Ashwell 1976). The analytical solution was based on the Theory of Shells developed by Gibson and Cooper (1958), which provides a bending solution and applies to thin shells supported along their end arches upon diaphragms and it is outlined as it follows.

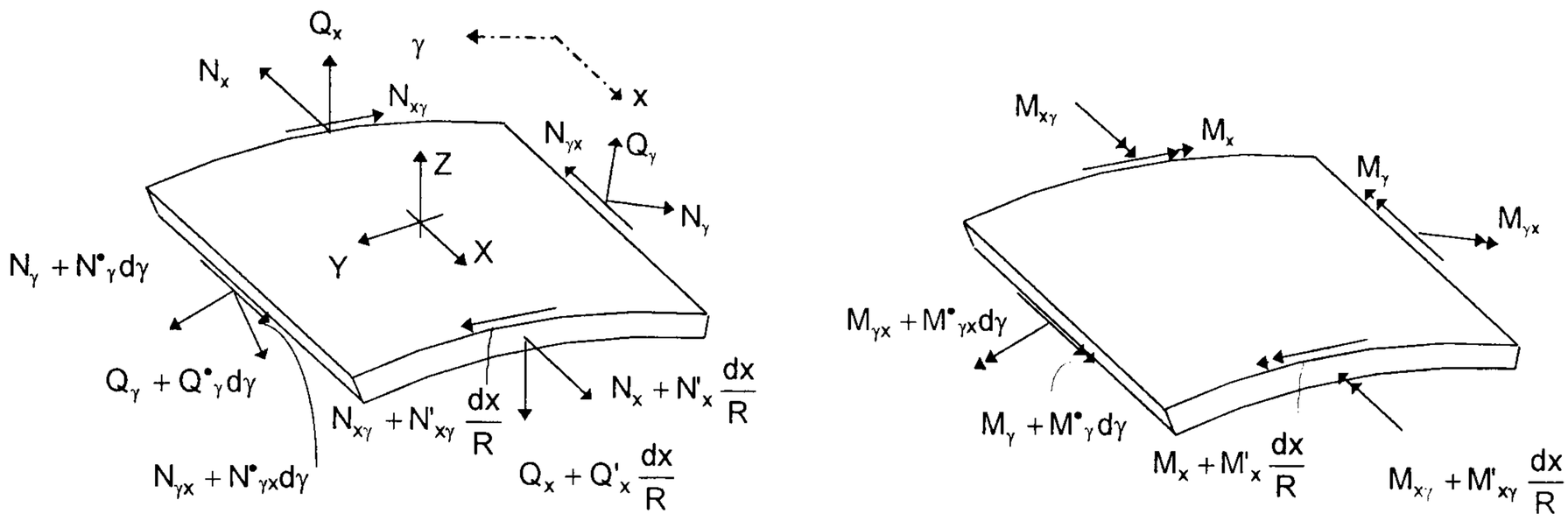

FIGURE 5.9 Internal and external forces, and moments acting on a shell element

The equilibrium of an element of the shell is considered (Fig. 5.9). At first all the external forces X, Y, Z, and then the section forces (N_x, N_γ, $N_{x\gamma}$, Q_x, Q_γ) and moments (M_x, M_γ, $M_{x\gamma}$) are applied at the element and six equations of equilibrium are formed. Then, three strain-displacement equations between the strains ε_x, ε_γ, $\varepsilon_{x\gamma}$ and the displacements $\boldsymbol{u}$, $\boldsymbol{v}$, $\boldsymbol{w}$, are produced. Next, the relations between these strains and the stresses σ_x, σ_γ, $\sigma_{\gamma x}$, give further three expressions. Finally, all these expressions are combined, resulting in a set of eleven equations for the eleven independent unknowns (five section forces, three moments and three displacements).

By successive elimination, it will be possible to derive one single differential equation of compatibility in terms of one convenient variable, the deflection normal to the shell plane $\boldsymbol{w}$. The solution consists of a complementary function and a particular solution and the former has an arbitrary constant which will take eight arbitrary values. These constants can be determined by eight boundary conditions, four at each side of the shell, that

involve combinations of the unknown forces and displacements. For a shell of single curvature, with geometry and loading arranged symmetrically about the centre line, the forces and displacements along each edge are the same, so the edge conditions are reduced into two identical sets of four. The solution for the complementary function for w becomes:

$$w = 2 \cdot \left[a \cdot \cos\beta_1\gamma \cdot \cosh\alpha_1\gamma - b \cdot \sin\beta_1\gamma \cdot \sinh a\alpha_1\gamma + c \cdot \cos\beta'_1 \cosh\alpha'_1\gamma - d \cdot \sin\beta'_1 \cdot \sinh\alpha'_1\gamma \right] \cdot \cosh x \qquad (5.1)$$

where *a, b, c, d* are the arbitrary real constants, γ the angle to any desired point on the shell cross-section and α_1, α_1', β_1, β_1' are the powers of the indicial roots.

Once w is determined, the expressions for N_x, N_γ, Q_x, M_x, M_γ and **u** can be found using functions derived from w by differentiating an even number of times and the expressions for $N_{x\gamma}$, Q_γ, Q'_γ, $M_{x\gamma}$, v and θ by differentiating w an odd number. The general form of these functions are tabulated in (Gibson and Cooper 1958). Using a Fortran program the final solution was produced for regularly spaced points along the genetrix and each corresponding hoop.

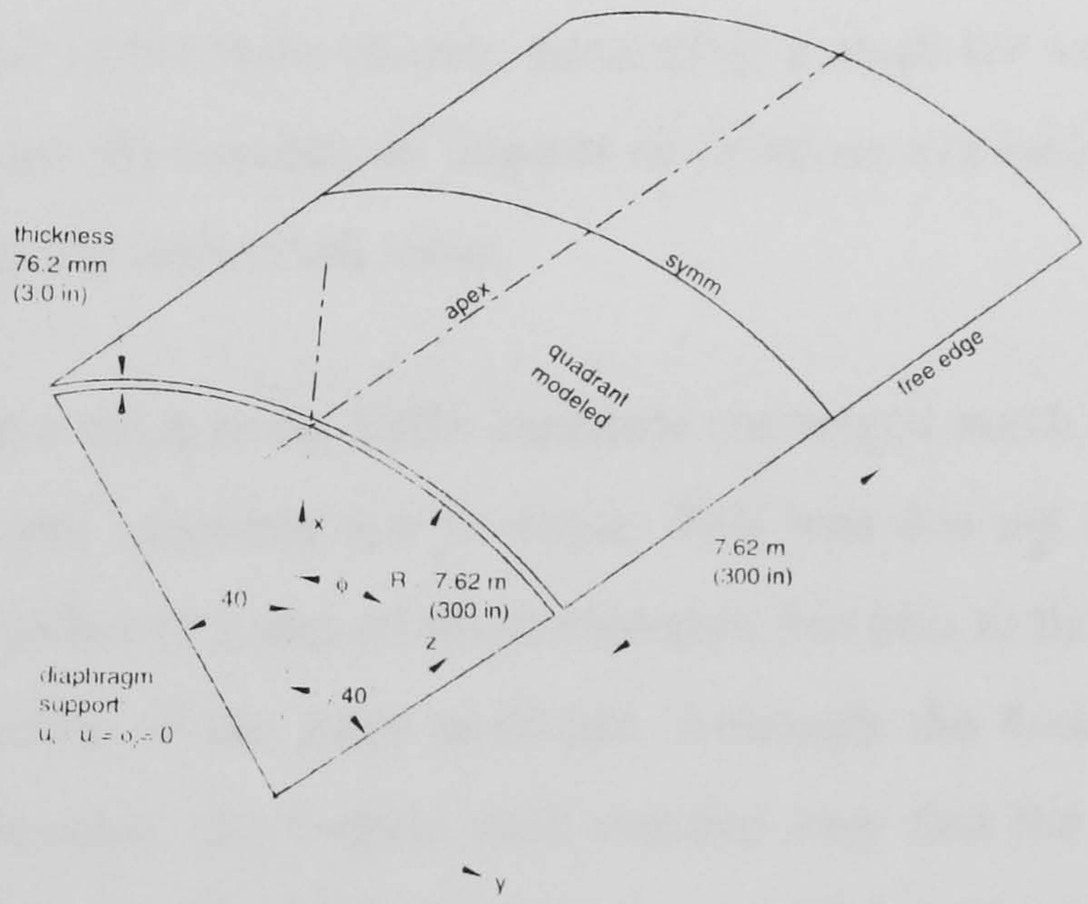

FIGURE 5.10 Geometry of barrel vault used at the benchmark test

The theory was applied to a barrel vault roof of length L = 120 ft, radius R = 30 ft, half angle $\gamma_n = 40^o$ and thickness $2h$ = 0.25 ft = 3 in. (Fig. 5.10). A uniformly distributed surface load of 50 lb/ft^2 was applied and the boundary conditions considered the edges free

($M_\gamma = N_\gamma = Q'_\gamma = N_{x\gamma} = 0$). The longitudinal co-ordinate x varied between +L/2 to -L/2, so the middle profile of the shell lies on x = 0.

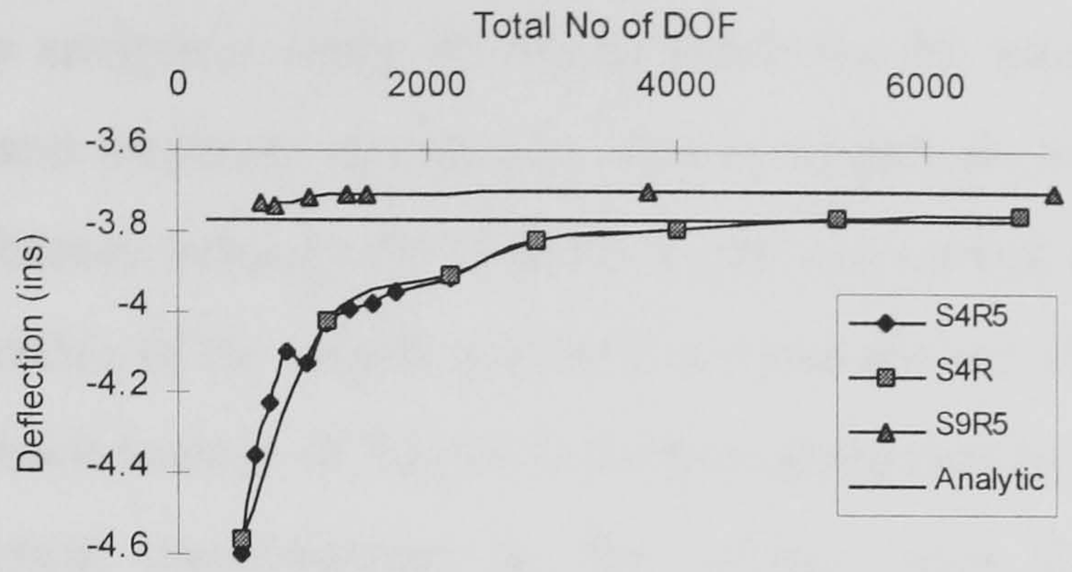

FIGURE 5.11 Benchmark test. Convergence for FE analysis of a barrel vault

The deflection at the middle of the free edge value was 3.7705 in. The same problem was then studied with a FE model. From the general shell elements library provided by Abaqus (HKS 1998), the elements S4R (4-node doubly-curved thin or thick shell, reduced integration, finite membrane strains), S4R5 (4-node doubly-curved thin shell, reduced integration, with 5 degrees of freedom per node) and S9R5 (9-node doubly-curved thin shell, with 5 DOF's per node) were chosen, generating a mesh for various densities. Their convergence rate against the number of degrees of freedom available (DOF) is plotted in Fig. 5.11, together with the theoretical value.

It is evident that a mesh using S9R5 elements converged much faster than the others, even when the mesh was relatively not so dense. This was due not only to the beneficial effect of the double number of nodes of these elements, but also to the higher flexibility the extra nodes at the middle of the sides provided. Although the 4-node elements gave an overall better approximation, the 9-node shell reached very fast the 98% of the expected value, remaining stable thereafter. Further comparisons of the rest of the deflections in this vault between this Theory of Shells and the FE model showed a very good agreement.

As a conclusion, Abaqus can be used safely for simple shell problems. Modelling the structure with 9-node elements allowed for a fast convergence, thus reducing the effect of mesh dependence problems, at least in the linear elastic range. The benefits of using a not very dense mesh will be more evident in the following chapter where material and geometrical non linearity (NLMGA) is introduced as the structure is tested until failure.

5.3.2 The initial plain cross vault (DL3)

5.3.2.1 General

Throughout the analytical study of all the tests, the FE model underestimated the deflections recorded and produced strains of a similar magnitude with the experiments. It appeared that the difference between the normals to the two curved surfaces meeting at the pointed longitudinal vertex of the model is quite sharp and did not allow the deformation to spread further to the back portion of the vault, further obstructed by the rigid support upon the wall. The analytical modifications in this section must therefore focus on the improvement of the continuity between either parts of the vault, that will allow the deformation to spread more evenly around the longitudinal vertex.

In this section, the analysis focuses on the original, plain geometry of Test DL3. Initially, the effects of the geometry of the groins and the arrangement of the load were examined. The sensitivity of the response of the FE model to parameters like the elastic moduli of the ribs or the masonry and the degree of geometric imperfections is discussed in §5.3.3. The results from all the analytical modifications are summarised in Table 5.7 (deflections), Table 5.8 (strains) and Fig. 5.12 (deflection of symmetry vertex) together with the data from the experiment and the preliminary FE model.

5.3.2.2 The assumption of hinge lines at the groins and vertices

It was difficult to determine directly the geometry of the joint between the web and the arches, and in particular the ribs (Fig. 3.33), as it was highly dependent on the constantly changing local curvature of these members (§3.4.3.3). Every effort was made, during construction, to fit the units around the rebate over the rib by suitably dressing them and carefully repointing their joints afterwards. However, the joint had a variable quality that was difficult to simulate in the FE model. A similar situation occurred during construction also at the pointed vertices, where a tapered joint was formed between the joining webs that had to be filled with mortar and a combination of wedges.

a) Introduction of hinge lines to the groins

If the groins and the vertices are carefully executed, then the fold line created marks a sharp change of curvature between the joining parts which can lead to a local stress concentration. A FE or other analytical model can be quite sensitive to the boundary conditions resulting in the area. The variable geometry of these sections however may result in a smoother transition between the webs. Starting with the groins, an initial and conservative simulation of this feature was to detach the webs from each other and assume they were linked directly to the rib only by means of a pin joint. The relevant option in Abaqus, MPC (Multiple Point Constraint) Type = Pin, enforces equal displacements between the linked nodes and permits a relative rotation about an axis parallel to the rib, which itself is able to rotate during the loading.

TABLE 5.7 Analytical modifications for Test DL3 - deflections (mm)

Dial	Test DL3	FEA			
	Data	Initial model	Hinges	Hinges and top load	Hinges at vertices
LWB1	0.125	0.045	0.052	0.050	0.046
LV1	0.150	0.079	0.088	0.089	0.087
LWF1	0.161	0.104	0.111	0.112	0.124
LV2	0.210	0.101	0.117	0.123	0.129
TWF1	0.201	0.124	0.133	0.140	0.165
TWF2	0.072	0.099	0.105	0.108	0.122
SV1	0.022	0.017	0.016	0.018	0.020
SV3	0.252	0.109	0.133	0.143	0.170
SV4	0.228	0.141	0.157	0.170	0.215
SV5	0.186	0.122	0.130	0.141	0.229

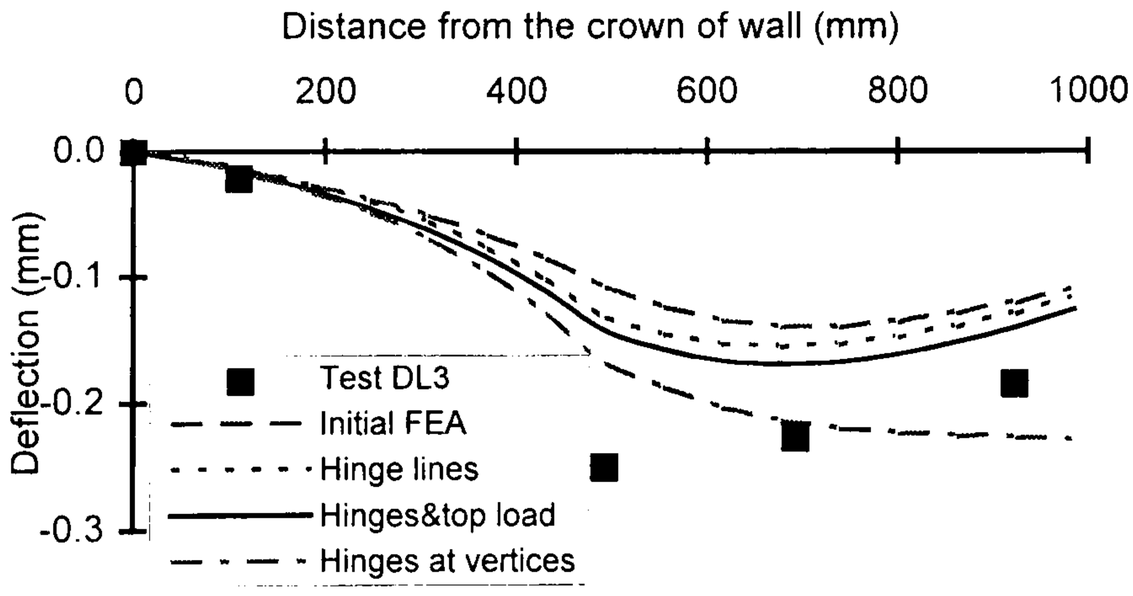

FIGURE 5.12 Analytical modifications for Test DL3 - deflection of the symmetry vertex

TABLE 5.8 Analytical modifications for Test DL3 - strains(in 10^{-6})

Gauge	Test DL3	FEA				
	Data	Initial model	Hinges	Hinges and top load	Hinges at vertices	Springs
AT1V	-70	-34	-35	-38	-40	-48
AT2V	-37	-46	-44	-51	-91	-24
BT1V	-65	-61	-63	-65	-67	-85
CT1V	-71	-28	-2	-3	-3	-85
DT1V	-29	-30	-28	-28	-28	-22
DT2V	-18	-11	-11	-11	-11	11
AB1H	2	11	10	13	13	8
AB2V	-8	3	3	2	-37	-5
AB3V	-28	-50	-50	-55	-98	-65
BB1V	-3	32	42	42	42	42
BB2V	-32	-61	-62	-65	-62	-101
CB1V	-6	-39	-61	-62	-62	37
DB1H	0	2	-2	-2	2	-8
DB1V	0	-6	-7	-7	-12	7

The results from this modelling show a small and uniform increase for almost all the deflections (Table 5.7). As before, maximum was recorded at the front part of the symmetry vertex, SV4, and not at the keystone, SV3, but the pattern of the symmetry vertex (Fig. 5.12) illustrates the small improvement in the area of maximum deflections, which spread further towards the centre of the vault. Regarding the strain pattern (Table 5.8), the introduction of hinges affected mainly the back portion of the vault, as the development of negative curvature at the pair {CT1V, CB1V} indicates. Bending prevailed on either side of the longitudinal vertex like before, but the actual configuration did not cause any further significant redistribution of the loads behind this vertex as it was desired.

b) Introduction of pin joints between the voussoirs

The next step was to investigate the effect of another feature of the ribs, the joints between their voussoirs. These joints were wider than those of the masonry of the webs and therefore less strong and more brittle, so cracks were more prone to develop here rather than in the webs. Pin joints were introduced this time at the nodes of the spatial beam elements of the ribs and, like in the previous case, the task was carried out by the MPC option in Abaqus.

The improvement was very small, for both deflections and strains, with the relatively most significant changes occurring at the area of the symmetry vertex close to the wall. As a result from the last two cases examined, it can be assumed that the area of the groins, as long as it is carefully detailed (and the ribs are an essential element of the process), can function as a plane of symmetry between the two joining barrel vaults. The thrusts from each barrel are almost mutually cancelled, limiting the ability of rotation about an axis tangent to the ribs. Moreover, any rotation of the joints between the voussoirs of the ribs are strongly restrained by the adjacent webs as in the present configuration the ribs are modelled as linear elements attached to the shell.

c) Introduction of hinges along the vertices

Further to the introduction of hinge lines along the groins, the effect of the geometry of another crucial area, the joint along the vertices, was investigated. As a lower limit, freedom of rotation was introduced at the nodes of the symmetry and longitudinal vertices by means of the MPC option of Abaqus, while keeping the rest of the boundary conditions. The resulting deflection of the front symmetry vertex was quite different (Fig. 5.12), as it increased towards the nave arch, but this pattern was confined within a narrow area around the vertex and did not spread to the rest of the model. A significant amount of the load was therefore transferred to the front web A and this can be also illustrated by the high hoop strains towards the front abutments (Table 5.8), while strains in the other three webs B, C and D remained essentially unchanged. The behaviour in this configuration was completely different than what the experiment had indicated and as a consequence the assumption of weak vertices is not a realistic one.

5.3.2.3 The distribution of the dead load

Possibilities of further improvement can be investigated first on the effect of the load arrangement. As seen in §4.4, the major difficulties during the application of the dead load arose at the haunches where the vault is quite steep and brackets were required to keep the lead weights into place. Moreover, the weight at that area had only a moderate influence on the deformation of the vault (§5.2.6), so the lower parts can be considered as unloaded. As a result, the load was applied mainly over the top half of the model and the exact distribution

was evaluated by considering it covered an area above a height ranging between 0.4 and 0.7 of the total height H.

The use of the Fortran pre-processor enabled many attempts between these two bounds and for 0.5 of the height a uniform improvement in the deflections of all the points was attained at the order of 10% (Table 5.7), with no significant change to the pattern (Fig. 5.12). The changes in the strains distribution were less significant, apart from the area of the haunches where the low bending moments increased slightly (Table 5.8), since the same amount of load as before was concentrated around the centre of the span.

5.3.2.4 Further on the joint between the webs and the ribs

Alternatively to the assumption of hinge lines, another conservative modelling of the joint of the webs across the ribs can be performed by introducing springs. The elements SPRINGA were used that function as an axial spring between two nodes and their line of action is in the direction joining the two nodes. The webs were split along the groin, each part was considered to be linked directly on the ribs and the two parts were linked again with the springs. Their length was assumed similar to the width of the joint (approximately 3 mm) and the Fortran program was modified in order to allow for a joint of constant width along the whole groin. The required stiffness of the springs was evaluated as equivalent to the elastic modulus of the webs in the weaker direction, 670 N/mm^2 ($1.1 \cdot 10^5$ kN/m).

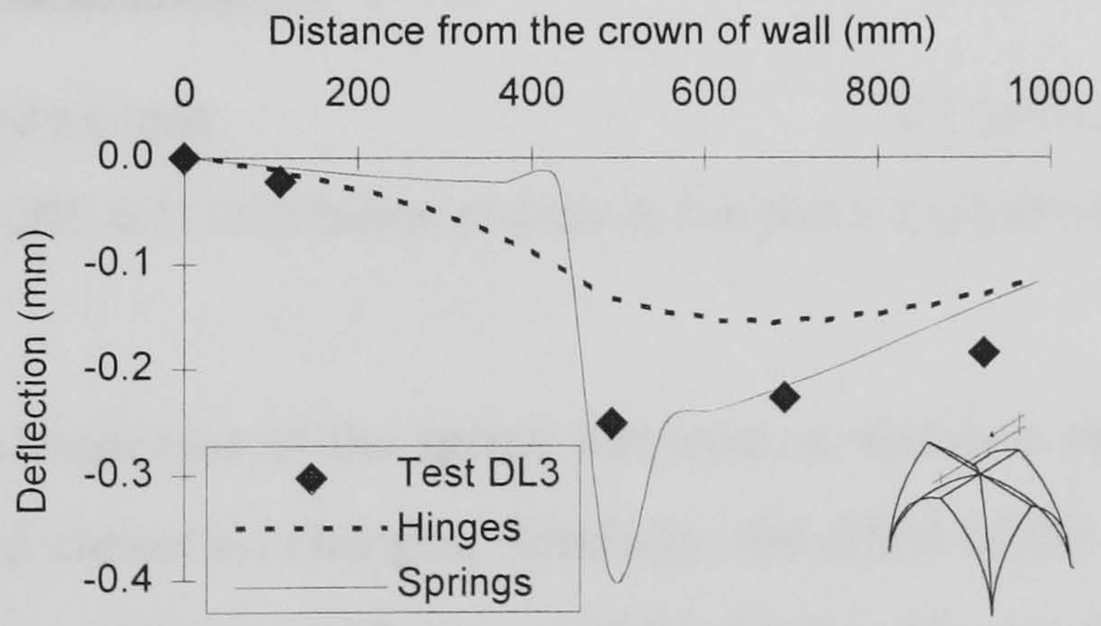

FIGURE 5.13 The effect on the deflection of the symmetry vertex due to the simulation of the joint between the webs and the groin with springs

Introducing this feature resulted in deflections of a magnitude similar to the experiment, which were concentrated mainly around the longitudinal vertex and the

keystone, as it can be seen in Fig. 5.13. The change of curvature at the back symmetry vertex became sharper close to the keystone, while the nave arch restrained the deformation of the vault at the front edge.

The modelling had a more significant effect on the behaviour of the longitudinal web, as the strain was distributed symmetrically about the vertex (Fig. 5.14), a major improvement from the response in Fig. 4.12. Similar to the experiment, the curvature on either side of this vertex had the same sign (Table 5.8) and the transition between the two parts of the web over the vertex became more smooth. This configuration reduced the interaction between the two barrels and the longitudinal one acted as a (pointed) barrel vault simply supported upon the ribs. This was also evident in the response of the back transverse web D, where the changes were much more limited.

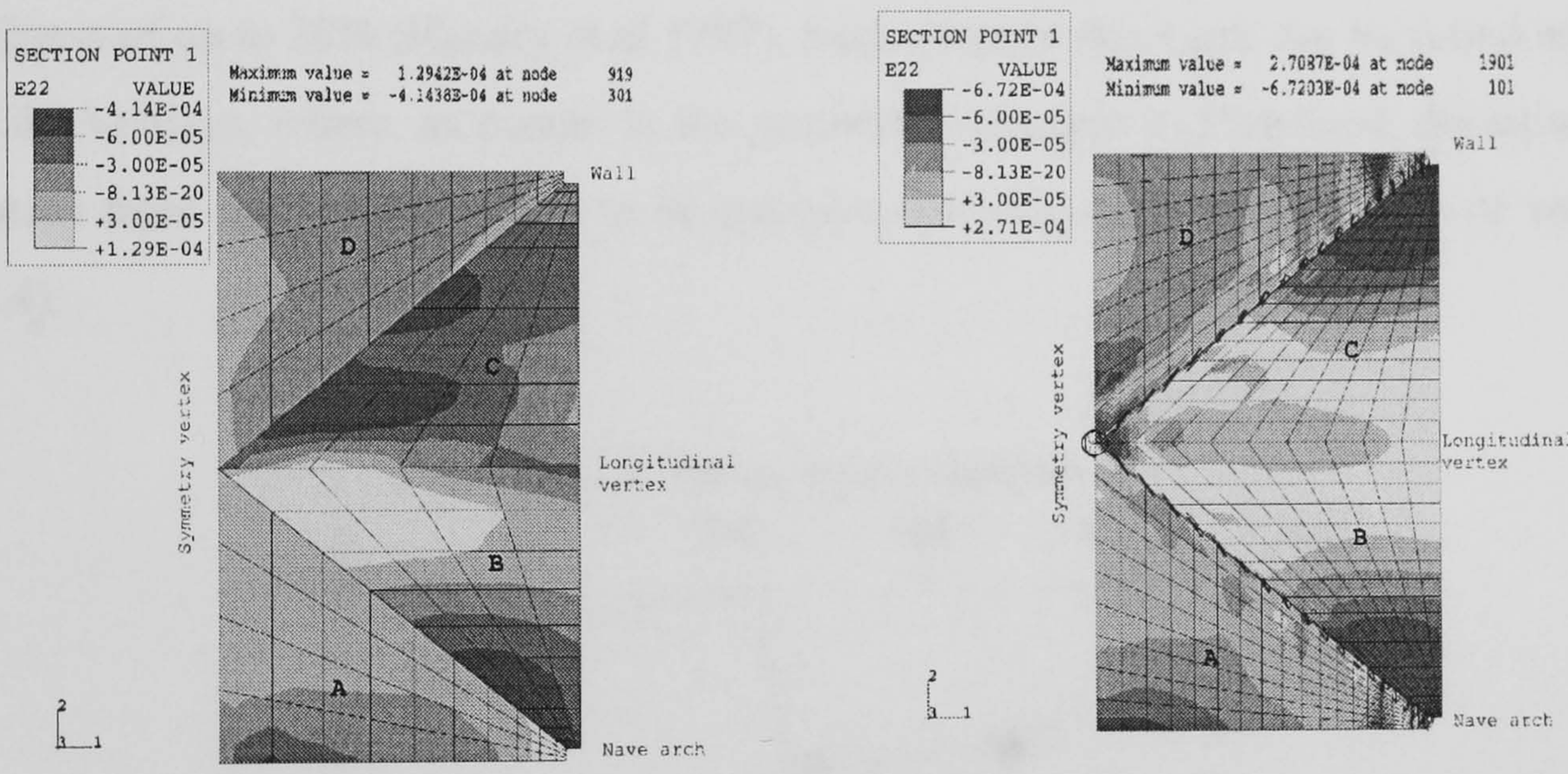

(a) Hinges and top load

(b) Springs along groin

FIGURE 5.14 Distribution of strain in the global Y (2) direction

Concerning the properties of the spring elements, a variation was performed in their stiffness, which caused almost no changes. Similarly, the effect of the length of the element was quite local, as even a length of 10 mm would increase only the deflections around the keystone by a relatively small amount. It is therefore useful to keep the length of the spring close to the width of the joint and investigate the effect of other parameters on the behaviour of the vault.

5.3.3 Parametric study

A study on the sensitivity of the FE solution under dead load to some parameters like the properties of the constituent materials and other aspects of the geometry of the structure could result in further improvement of the quality of the analytical predictions.

5.3.3.1 The modulus of elasticity in the two directions

Changes in the modulus of elasticity of masonry were expected to affect not only the magnitude of the deformation, but also the distribution of loads in the vault. The experimentally established values (§4.2) range between E_1 = 1530 N/mm^2 & E_2 = 360 N/mm^2 (E_1/E_2 = 4.17 - actual value 6.27) and E_1 = 6130 N/mm^2 & E_2 = 880 N/mm^2 (ratio 7.03). This variation accounts also for the effect of the joint thickness which is irregular in some areas, since excessive thickness of the bed joints can result in a reduction of strength and stiffness of up to 30% (Hendry et al 1997). Such areas in this vault can be found mainly around the vertices, where, as occurs in the prototype structure in Holyrood, deviations of the courses from the horizontal had to be straightened with thick mortar joints or wedges (§3.4.3.4).

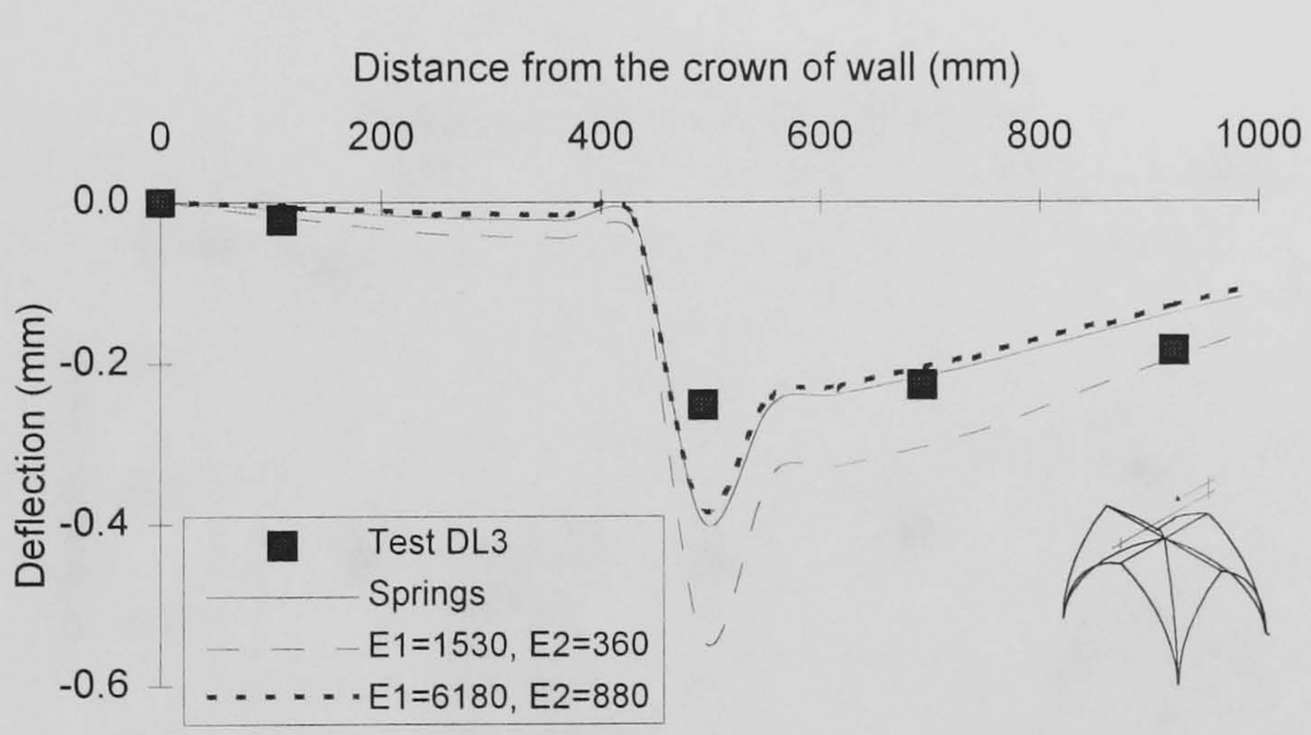

FIGURE 5.15 The effect of the variation of the modulus of elasticity on the deflection of the symmetry vertex

Employing the lower bound of the elastic moduli values, the deflection of the symmetry vertex increased almost uniformly (Fig. 5.15) and except from the area close to the nave arch, the experimental values were largely overpredicted. This value of the ratio made more evident the relatively sudden drop around the keystone, which in turn illustrates the independence, to a certain degree, of shell action of each of the joining webs.

Accordingly, no significant changes were recorded in the strain distribution as the hoop strains increased uniformly and higher longitudinal strain occurred close to the keystone, where maximum deflections developed.

Similarly, the application of the higher set of the values yielded a small and uniform reduction in both strains and deflections. As a conclusion, the deformation of the vault is affected mainly by the modulus of elasticity in the hoop direction and this concerns principally the magnitude of the quantities under examination.

5.3.3.2 The stiffness of the ribs and arches

In addition to the possibility of rotation between the voussoirs of the ribs and arches examined with the introduction of revolute joints, the overall higher flexibility of the area of the groins can be also represented as a drop in the stiffness of the beam elements that form the area in the present configuration. On the other hand, the tapered profile of the voussoirs and the high compressive axial forces that develop when the ribs function as arches may restrain significantly the action of bending moments, yielding lower deformations. This effect can be simulated as an increase in the modulus of elasticity of the beams.

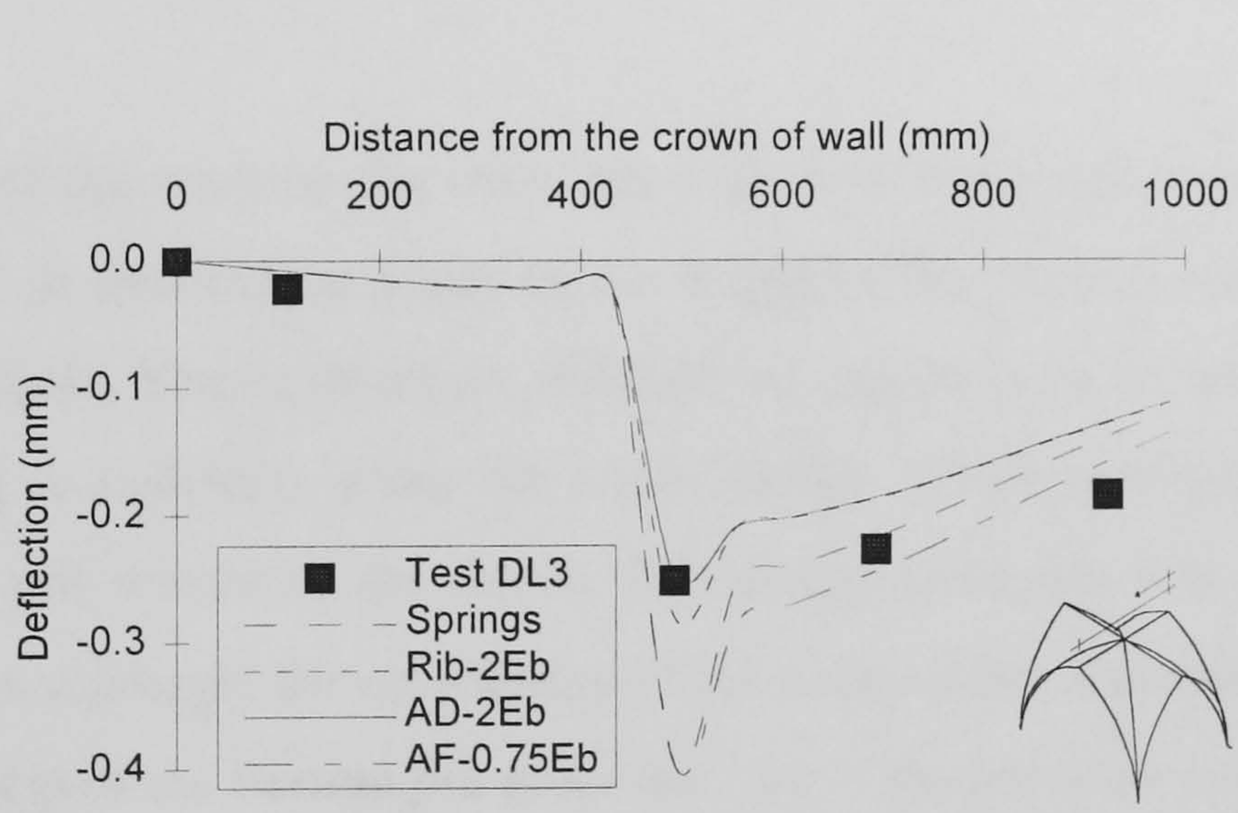

FIGURE 5.16 The effect on the deflection of the symmetry vertex due to the variation of the elastic moduli of the ribs and arches

Focusing on the stiffness of the ribs only, for a range between half and double the original value of 500 N/mm^2, the study of the deflection of the symmetry vertex showed that this feature affects mainly the magnitude of the deformation, yielding a relatively smoother deformation around the keystone (Fig. 5.16). When the modulus of elasticity of

the nave arch was reduced by 25% (AF), the change in the pattern was localised at the area of the front symmetry vertex.

5.3.3.3 Variations of the geometry

Variation of the thickness of the joints can be a source of deviation from the geometry of the original design. This does not mean necessarily low quality of the fabric, as these changes were necessary in order to achieve horizontal courses, both in the test structure and in real vaults (§3.4.3.4). The irregularity of this variation could be generally simulated by applying random imperfections to the FE mesh. The routine *RAN2* (Press 1992) is a portable random number generator that returns a uniform random deviate between 0.0 and 1.0. Since it is the Fortran pre-processor that generates the mesh, a random number within the range of a few millimetres produced with this routine was added to the coordinates of the nodes.

A first application in the range of ±10mm produced several highly warped elements and no solution was possible until a range of ±8mm. This range had a limited effect on the behaviour of the FE model and consequently the prediction of the experimental response. The moderate and uniform increase in the deflections and strains caused no redistribution of the loads.

The survey of the vault on the other hand (§3.4.4) indicated the profile of the ridge was smoother than in the original plans, as the height of the vertices was lower by 15mm (2% of the total height). These reductions of height are typical in cross vaults and they occur after the centering is removed, when the vault reaches a new configuration in order to accommodate the self weight of the fabric. This height reduction was applied to the FE model, modifying accordingly the coordinates of the nodes in the immediate area around the vertices with the help of the Fortran pre-processor. As in the previous case, this change had a moderate effect, which was concentrated mainly around the symmetry vertex.

5.3.3.4 The distribution of the load between the webs

In the FE models previously described, the applied load was distributed as a body force on each web according to the proportions established during the experiment. It was considered that it would be useful however to evaluate the sensitivity of the FE solution to this distribution and the degree to which the load of each web would affect the response of

the entire vault. At first, the load in the longitudinal web was reduced by 20%, while in the other web it was increased accordingly. The effect was concentrated mainly on the front transverse web A, causing a uniform increase to the deflections of the symmetry vertex for almost 1/3 of its length (Fig. 5.17), improving the agreement with the test at the area of the nave arch. As a consequence, the strains at the front web increased to a similar degree.

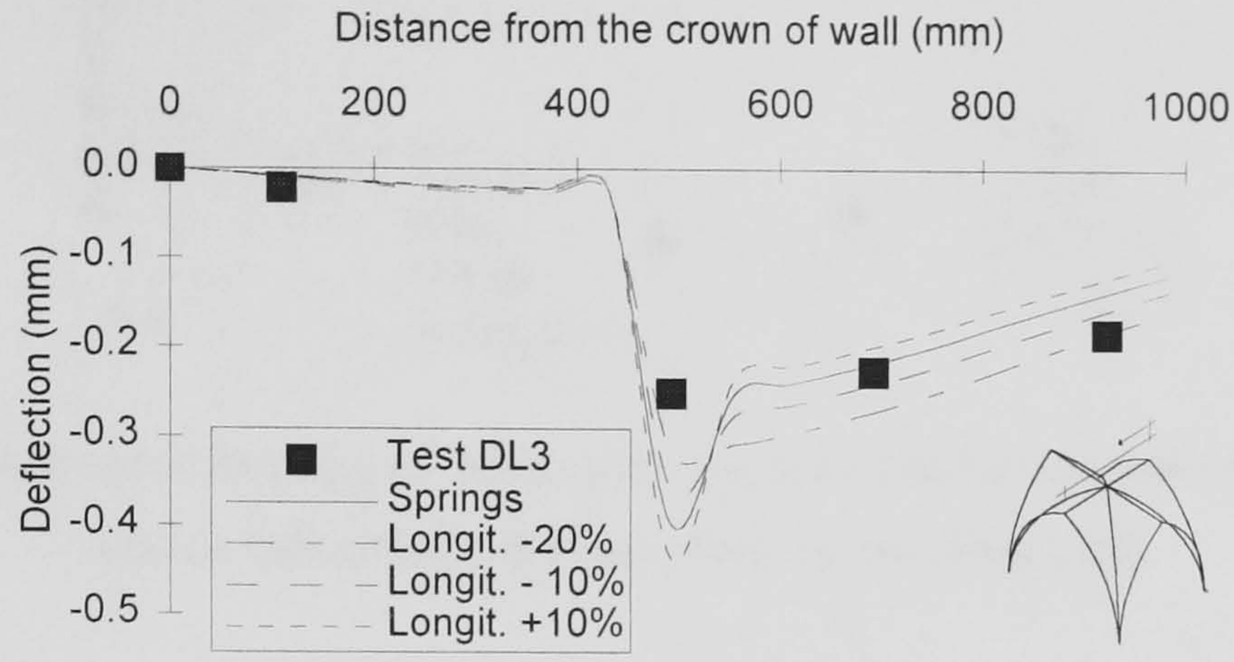

FIGURE 5.17 The effect of the distribution of the load between the webs on the deflection of the symmetry vertex

When on the other hand 20% more load was applied on the longitudinal web, the deflection of the symmetry vertex followed a pattern very similar to the test, while it affected a wider area around the keystone at the transverse web. The examination of those two cases confirmed further the relatively independent behaviour of the two webs, which is quite close to the behaviour of the structure in this test. This limited co-action indicates that each web carries directly the corresponding portion of the load and the role of the ribs becomes more important as they provide the main support for the longitudinal web.

5.3.3.5 The behaviour of the vault in Test DL3

Combinations of the modifications developed in the previous sections permit a better prediction of the experimental response within a reasonable range of the material and geometric properties. An excellent agreement with the experiment was achieved for E_1 = 5250N/mm^2, and E_2 = 840N/mm^2 (or 25% increase of the original values), a reduction of the elastic modulus of the nave arch by 15% and a redistribution of load by 15% to the transverse barrel vault, as the deflection of the keystone illustrates (Fig. 5.18). The overall

distribution of deflections and strains, as also the deformed vault under the dead load are shown in Fig. 5.19.

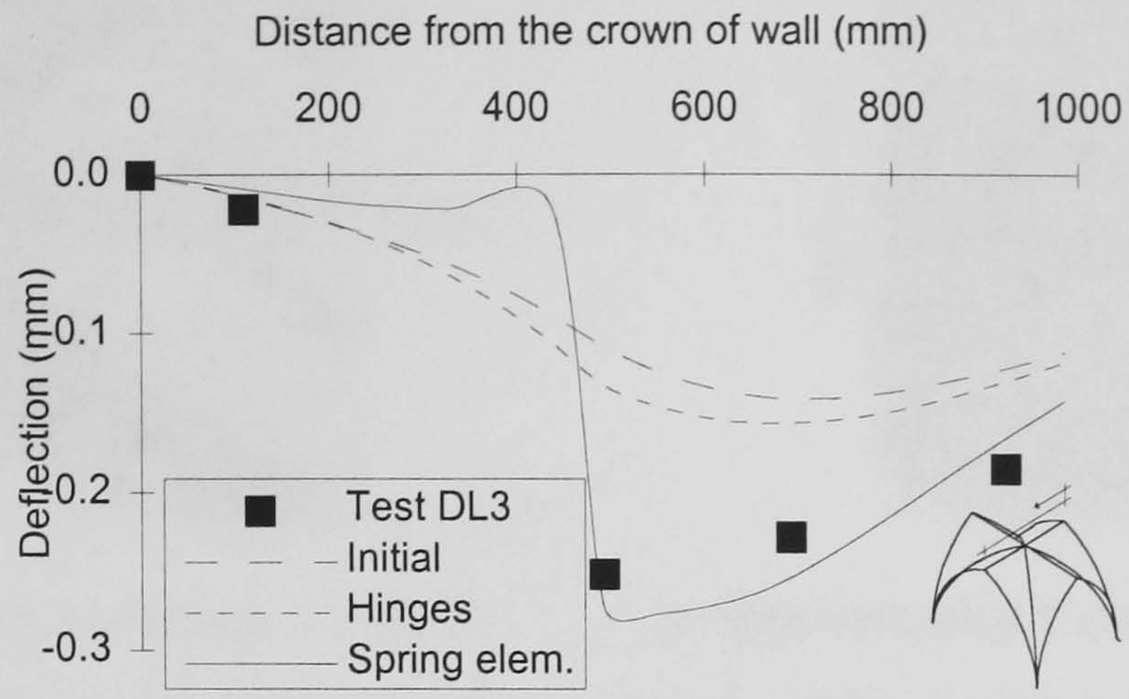

FIGURE 5.18 Effect of the combination of modifications in the material and geometric properties of the model: deflection of the symmetry vertex (Test DL3)

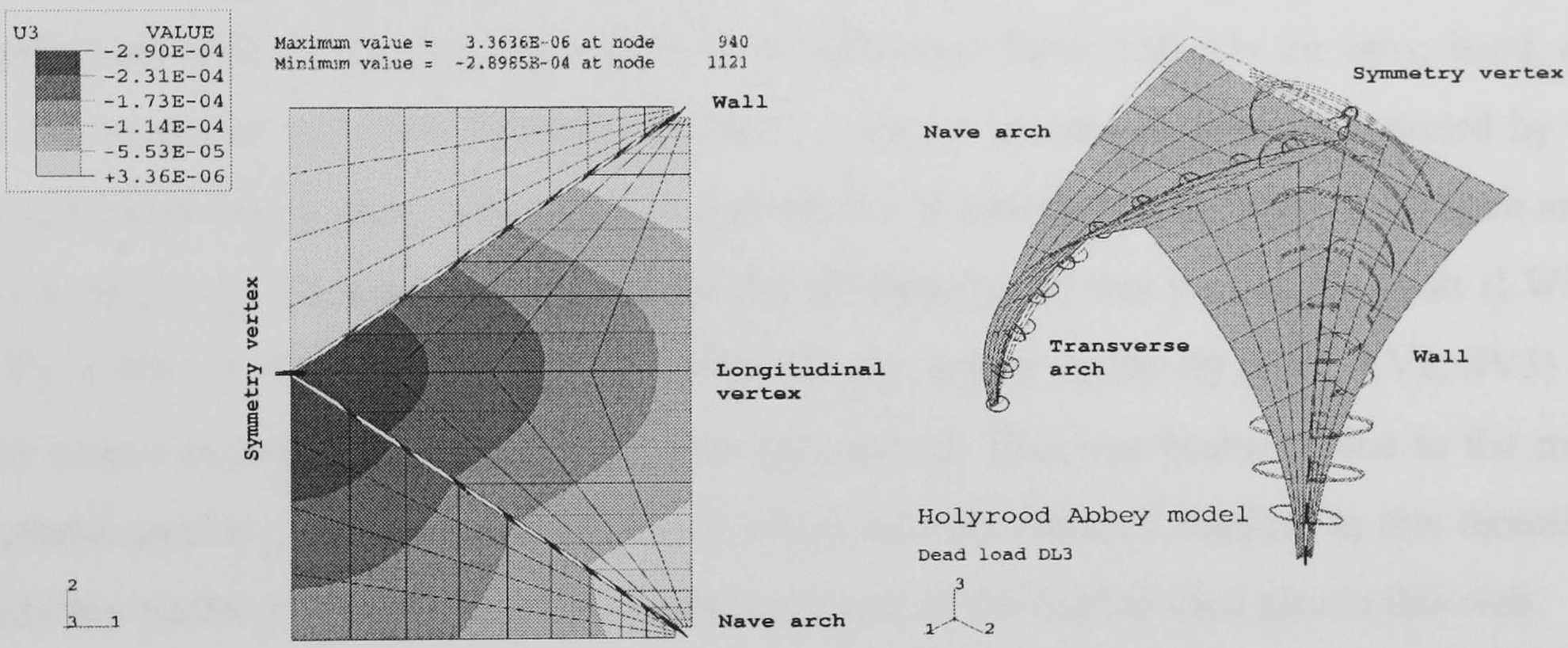

(a) Deflections (m)

(b) Deformation of the model

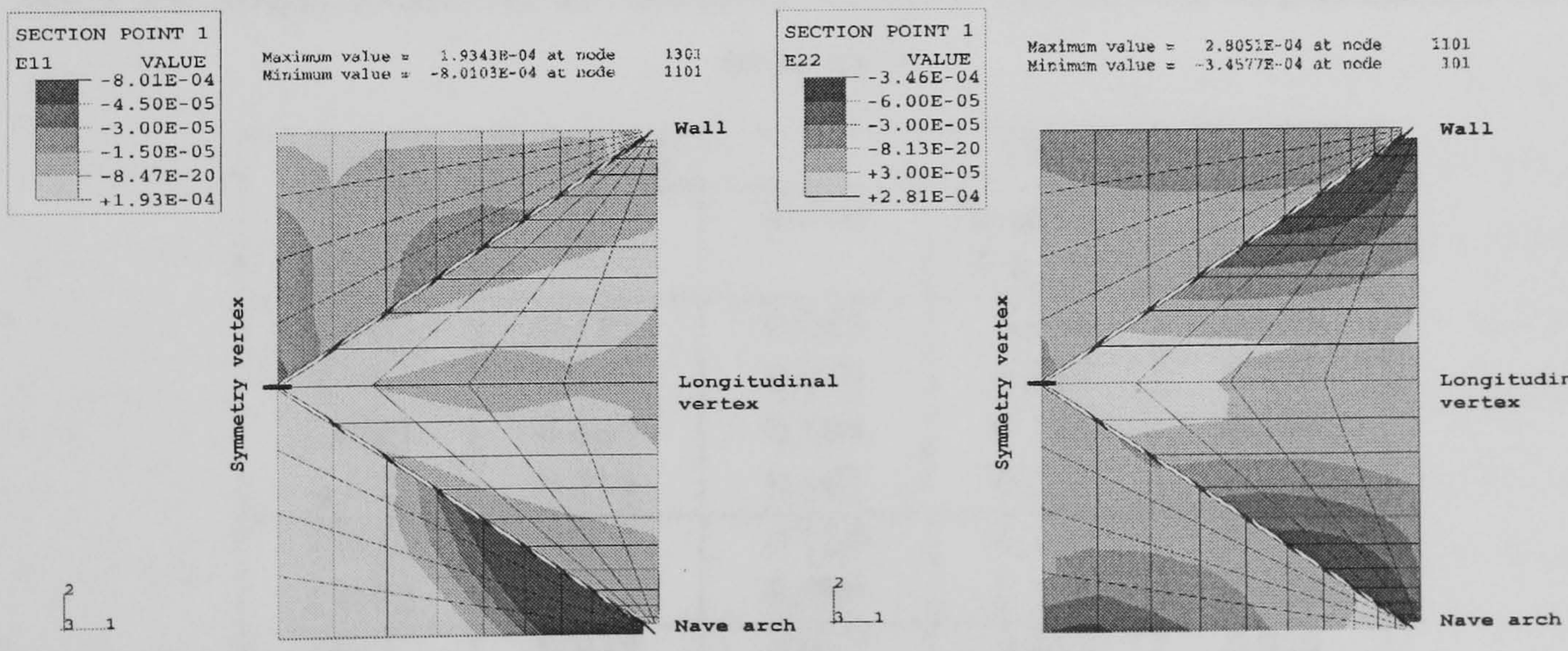

(c) Strain in global X direction - intrados

(d) Strain in global Y direction - intrados

FIGURE 5.19 Deflections and strains from the FE model for Test DL3

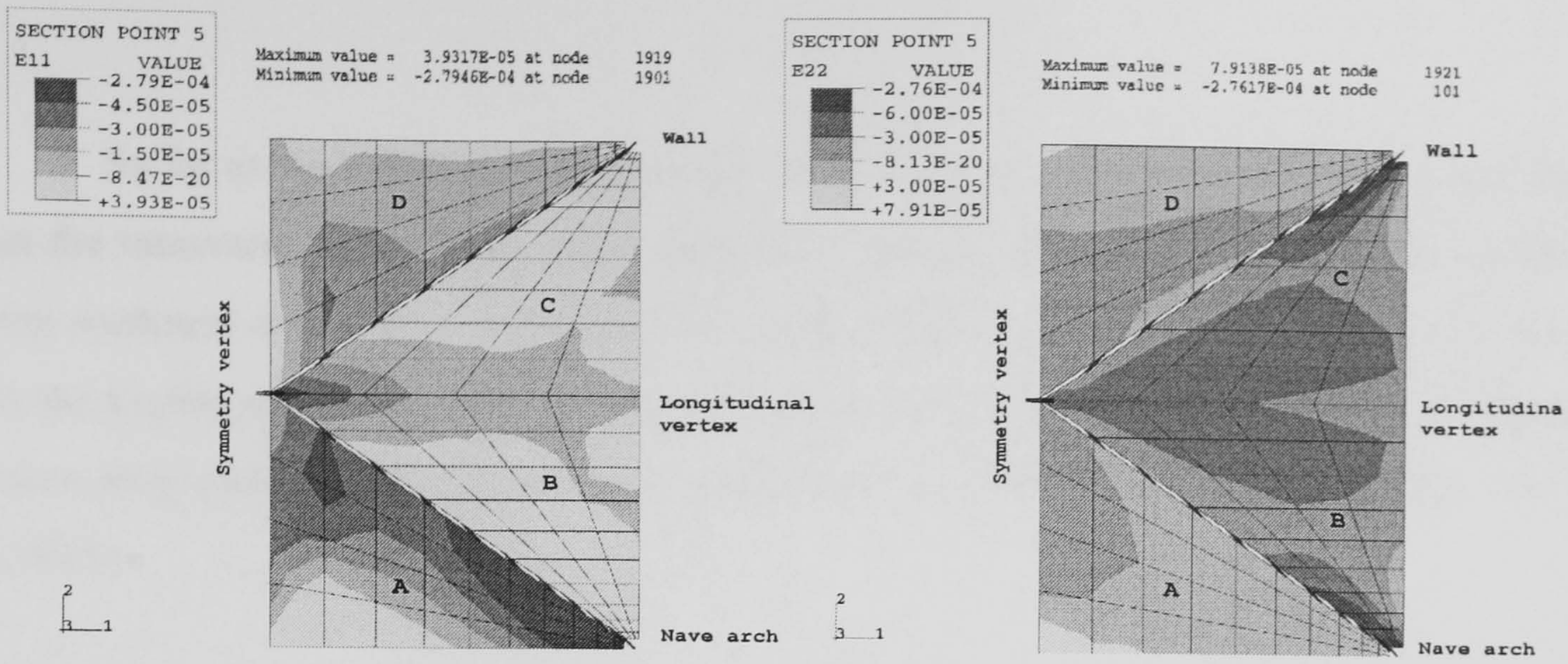

(e) Strain in global X direction - extrados (f) Strain in global Y direction - extrados

FIGURE 5.19 Deflections and strains from the FE model for Test DL3

A higher degree of symmetric deformation around the longitudinal vertex was dominant in this configuration of the FE model (Fig. 5.19a - cf. Fig. 4.12a) and the agreement with the experiment improved considerably (Table 5.9). On the other hand, due to the moderate co-action between the webs, a higher amount of load was carried by the longitudinal barrel vault independently and was not transferred to the wall or the nave arch. As a result, the FE model overpredicted the deformation of this part of the vault (LWB1, LV1, LWF1, LV2). The longitudinal vertex did not deflect uniformly (LV1, LV2, SV3) but the values increased as the keystone was approached. This was probably due to the more pointed profile of the longitudinal barrel which initially reduced bending in this direction, until the flatter area of the keystone permitted a part of the load to shed also in this web.

TABLE 5.9 Comparison between the deflections recorded in Test DL3 and the predictions of the FE model (mm)

Dial	Test DL3	FEA		
	Data	Initial	Hinges and top load	FE prediction
LWB1	0.125	0.045	0.050	0.194
LV1	0.150	0.079	0.089	0.223
LWF1	0.165	0.104	0.112	0.196
LV2	0.210	0.101	0.123	0.264
TWF1	0.201	0.124	0.140	0.180
TWF2	0.072	0.099	0.108	0.129
SV1	0.022	0.017	0.018	0.014
SV3	0.252	0.109	0.143	0.248
SV4	0.228	0.141	0.170	0.237
SV5	0.186	0.122	0.141	0.169

So far as the transverse barrel vault is concerned, its support conditions depend more on the transverse edges (wall, nave arch) rather than on the ribs. As a result, the effect of any weakness at the joints with the ribs (modelled here with springs) is more evident close to the keystone (the most distant area from those edges) and the high deflections recorded there drop more rapidly at the front transverse web towards the haunches (SV4, TWF1, TWF2).

TABLE 5.10 Comparison between the strains recorded in Test DL3 and the predictions of the FE model (10^{-6})

Gauge	Test DL3	FEA		
	Data	Initial	Hinges and top load	FE prediction
AT1V	-70	-34	-45	-38
AT2V	-37	-46	-53	-36
BT1V	-65	-61	-71	-51
CT1V	-71	-28	9	-57
DT1V	-29	-30	-18	-19
DT2V	-18	-11	-6	-16
AB1H	2	11	5	11
AB2V	-8	3	-6	0
AB3V	-28	-50	-61	-66
BB1V	-3	32	44	23
BB2V	-32	-61	-65	-66
CB1V	-6	-39	-55	28
DB1H	0	2	3	-6
DB1V	0	-6	-17	4

Similar conclusions can be made from the study of the strain distribution. The model predicted well the rather symmetrical distribution of deformation around the longitudinal vertex. Furthermore, the FE model agreed with the tests in that the load of the structure was transferred to the haunches by means of axial compressive hoop strains which increase in the direction of the front support (webs A and B). According to the more detailed data provided by the FE model, the hoop stresses spread in an area which was narrower at the extrados than at the intrados. In both faces however the strains showed a pattern that was clearly concentrated around the ribs, rather than the curved edges.

In the direction parallel to the symmetry vertex, the FE model predicted successfully the quite low strains that develop at the intrados (AB1H and DB1H and Fig. 5.19d). On the other hand, the nave arch was expected to rotate due to its low (compared with the wall) out-of-plane stiffness and this explains the unsymmetrical pattern of the deformation, which, however, affects mainly the transverse barrel vault. Regarding the hoop strains in these webs, both portions of the web tend to function independently, as the support along their ends (wall, nave arch) was more important and they were less influenced by the ribs. This was further illustrated by the sharp change of curvature around the keystone at the more rigidly supported back portion D (cf. Fig. 5.18). The location of the strain gauge DT1V permitted to capture only a part of the high strain concentration that occurred (Fig. 5.19e), as the built-in support on the wall left the rest of the back transverse web D practically unstressed. This change of curvature was much less sharp in the front portion A, but it was more constant in a wider area.

Any variation of the material or geometric parameters so far (like the stiffness of the materials, geometric properties etc.) affected mainly the magnitude of the measured quantities and less their pattern. In the test, the strains were recorded on the units and not the corresponding portion of the masonry, but the actual low values of stress made the discrepancies observed during the test on the wallettes (§4.4) less evident. Most important, however, can be the way the mortar joints and the interface between them and the units can influence the distribution of stress. The effect of this aspect will be examined in more detail in §5.4.4 with the analysis of a FE micromodel of the vault.

5.3.4 Analysis of the stiffened structure (Test DL4)

5.3.4.1 The actual FE model

In test DL4, the groin was strengthened by filling the area between the joining webs with mortar and repointing the joint between the web and the rib from the intrados and subsequently the vault was loaded with the same amount as in the previous test (§5.2.5). An immediate simulation of this intervention can be to concentrate the benefit only to the rib and consider an increased depth of its section by a reasonable value of 25%. This causes the moment of inertia about the horizontal axis to double and the parametric study in §5.3.3.2 showed what influence similar changes can have on the deflection.

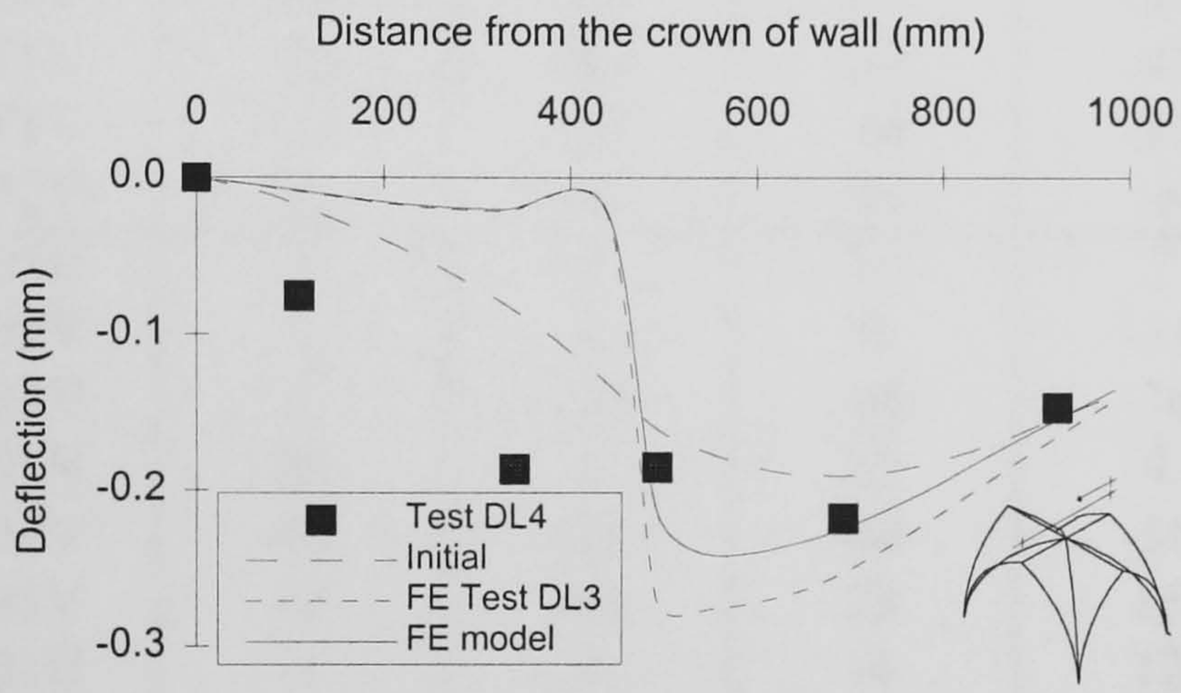

FIGURE 5.20 Deflection of the symmetry vertex assuming stiffer ribs

Applying this modification to the FE model with spring elements at the groins (§5.3.3.5) resulted in a small reduction of the deflections, as the symmetry vertex can illustrate (Fig. 5.20). In test DL4 however, the improved co-action between the webs allowed the deformations to spread more uniformly around the keystone and the longitudinal vertex. The difference from the prediction of the FE model can be attributed therefore not to the elastic modulus of the ribs but to the presence of the (weak) joints that have been modelled as springs and a closer agreement with the pattern can be observed at the initial approach, which was based on a continuous model (Fig. 5.20).

Similarly to the deflections, this configuration yielded only a uniform reduction of the stresses, without any significant redistribution, as the strains can illustrate (Table 5.11). The agreement improved for most of the gauges located close to the vertices, and a symmetric

pattern could still develop around the longitudinal vertex. Another new element of this test however was the scale of the reduction of the hoop strain at the haunches, especially at the front transverse web, A. Despite the differences with the test, this FE configuration showed a tendency of the hoop strains to concentrate in an area closer to the ribs (Fig. 5.19c, f). More detailed examination of the geometry of the ribs in the next section can verify the role and the importance of this member in the distribution of the loads.

TABLE 5.11 The effect of the stiffness of the ribs on the strains in test DL4 (in 10^{-6})

Gauge	Experiment	FEA		
	Data	Initial	DL3	Springs & stiffer ribs
AT1V	-29	-24	-38	-51
AT2V	7	-35	-36	-56
BT1V	-30	-54	-51	-40
CT1V	-34	-26	-57	-46
DT1V	-11	-29	-19	-26
DT2V	2	-9	-16	-6
AB1H	1	13	11	7
AB2V	1	1	0	-11
AB3V	1	-24	-66	-76
BB1V	20	6	23	9
BB2V	-18	-26	-66	-50
CB1V	-9	-40	28	15
DB1H	-1	4	-6	12
DB1V	3	-6	4	-6

5.3.4.2 Further on the stiffness of the joint between the webs and the rib

As an intermediate solution to the problem, the linear springs were gradually substituted by beam elements, with similar material properties and a cross section equivalent to the part of the groin that was replaced. The study started with the springs connecting the area immediately around the keystone, continued with the top third of the groin and concluded with the top two thirds of this area. From the deflection of the symmetry vertex (Fig. 5.21) it can be seen that stiffening the keystone caused a sharp change in the pattern and as the intervention propagated further in the haunches, only its magnitude reduced moderately. Similarly in the experiment, the strengthened area of the keystone enhanced the co-action between the webs and although this was not achieved to

the degree indicated by the experiment, clearly the back transverse web contributes effectively in the reduction of the deformation of the vault.

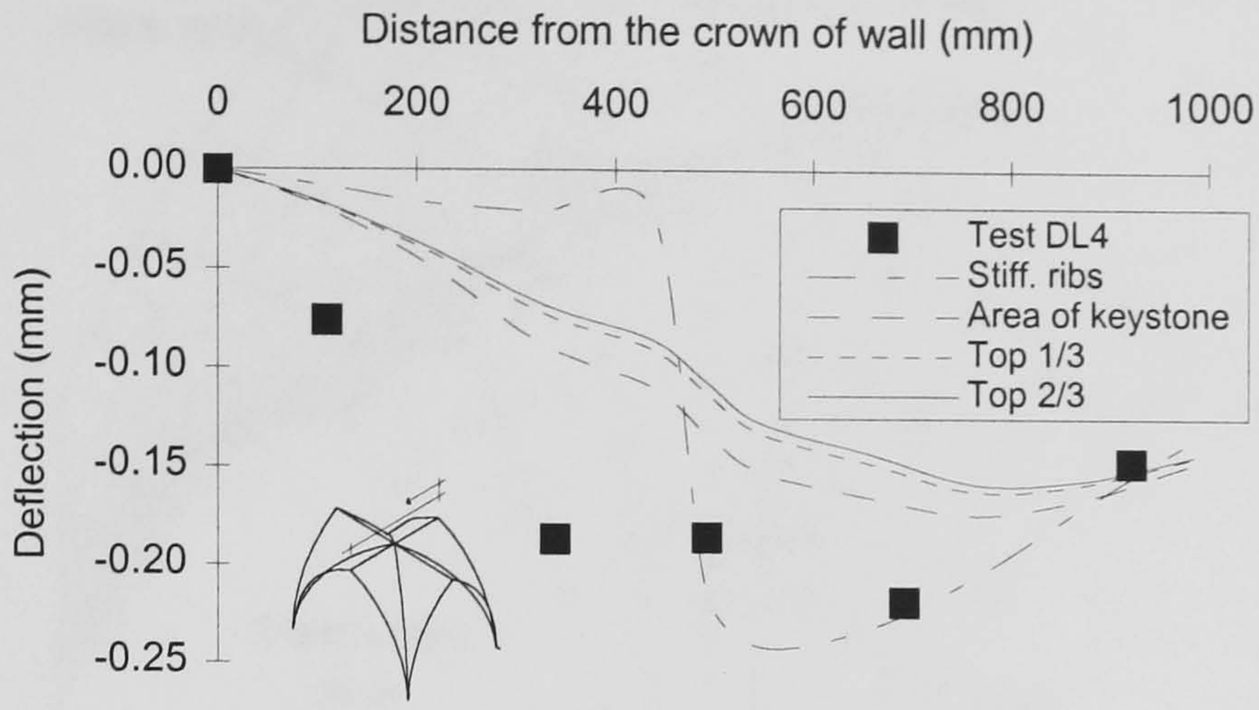

FIGURE 5.21 Deflection of the symmetry vertex for various configurations of the joint between the webs and the ribs

This FE modelling served mainly the purpose of underlining the importance of the quality of execution of the area of the groins, as a comparison with the continuous FE model showed a better agreement both in terms of deflections (Fig. 5.20) and strains (Table 5.4). The substitution of the spring elements with beam elements clearly restored the structural continuity indicated by test DL4 and, vice-versa, the stiffened groins strengthened quite effectively the structure. As a result, FE models where continuity is assumed between the two joining webs (as in §5.3.2) appear as more suitable for representing the behaviour of the vault in this test.

5.3.4.3 Modelling of the groins with shell elements

As was seen in §5.3.3.2, the elastic modulus of the rib affected mainly the magnitude of the deflections of the symmetry vertex and similar observations can be made even in the case of the continuous FE models. The role of this element is to guarantee a good level of execution of the intersection between the two joining barrels and it is mostly the joint between the web and the rib that affects the distribution of the loads in the vault. An alternative way to restore the co-action of the webs, while maintaining their partially independent response, can be to model the groin with shell elements of the same width. The Fortran pre-processor was modified to allow for the generation of elements of a width either constant or a fraction of the length of the neighbouring shell elements. This detail can be

considered to behave similarly to the bed joint in the web masonry, so the mechanical properties of the masonry in the hoop direction were assigned to these elements.

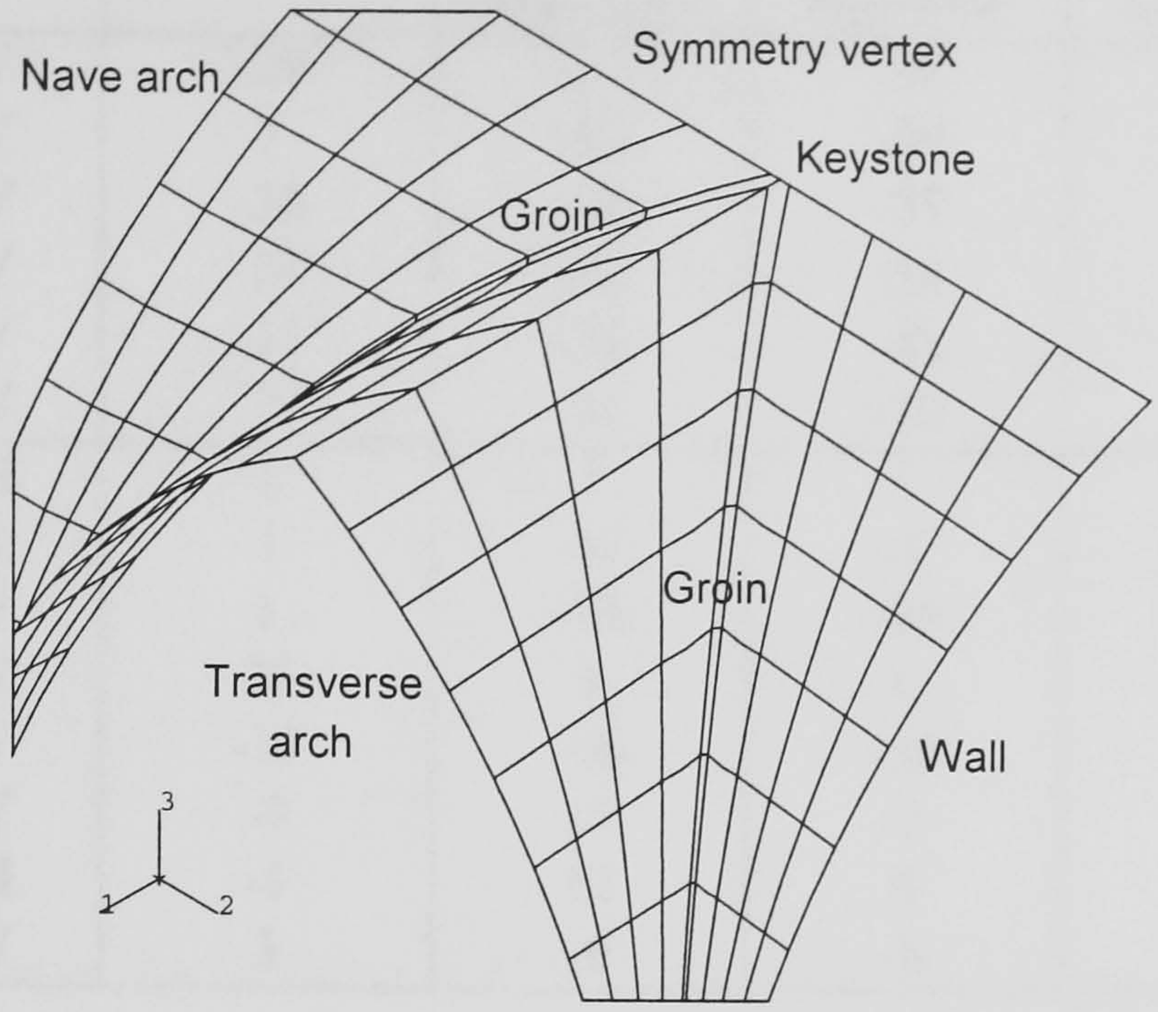

FIGURE 5.22 Groin modelled with shell elements

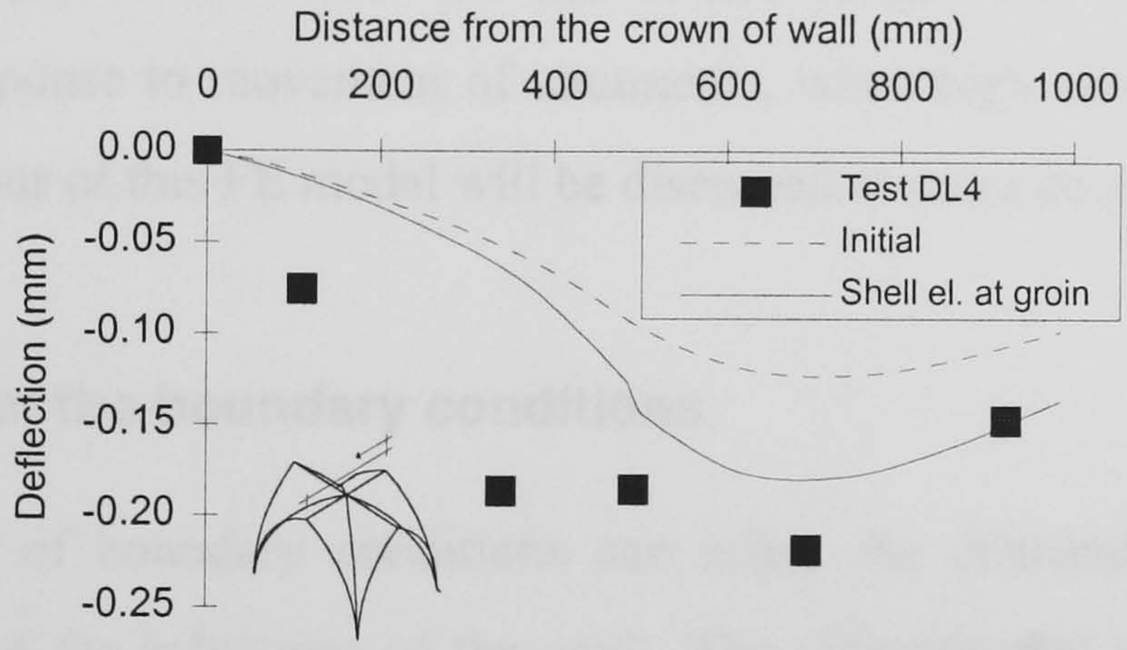

FIGURE 5.23 Groin modelled with shell elements - deflection of the symmetry vertex

The resulting deflection of the symmetry vertex (Fig. 5.23) was an improvement on the previous model. The study of the development of strain illustrates the transition from the independent behaviour of the longitudinal webs to a greater co-action in bearing the loads (Table 5.12). The symmetrical pattern at the longitudinal webs that was recorded in the modelling with spring elements was disturbed and resembled the pattern recorded in the continuous FE model (Table 5.8).

TABLE 5.12 The effect of the geometry of the groin - strains in test DL4 (in 10^{-6})

Gauge	Experiment	Finite Element		
	Data	Springs & stiffer ribs	Strength. keystone	Shell elem. at groins
AT1V	-29	-51	-38	-56
AT2V	7	-56	-69	-59
BT1V	-30	-40	-35	-54
CT1V	-34	-46	-28	-8
DT1V	-11	-26	-48	-26
DT2V	2	-6	-10	-7
AB1H	1	7	7	5
AB2V	1	-11	-7	-4
AB3V	1	-76	-90	-74
BB1V	20	9	6	37
BB2V	-18	-50	-50	-56
CB1V	-9	15	-3	-40
DB1H	-1	12	6	8
DB1V	3	-6	-8	-8

Further benefits from this modelling were that failure can be introduced along the groin as in the masonry of the webs. The use of this feature will become more evident during the of the response to movement of abutments, when high stresses are expected to develop. The behaviour of this FE model will be discussed in more detail in §5.3.4.5.

5.3.4.4 The effect of the boundary conditions

The definition of boundary conditions can affect the distribution of loads to the supports and therefore the behaviour of the vault. The ultimate goal of this research is to establish the extent to which externally imposed changes in the geometry (in this case when the abutments are forced to move) are able to cause the failure of the structure. It was also seen in the introductory chapters how it is generally accepted that small changes of this kind can have an immediate effect. In order to track the movement of the abutments in the next phase as exactly as possible, dial gauges in the transverse axis were placed at the middle of the height of the *tas-de-charge*, in order to avoid interference with the mechanism (§4.4).

The readings during Test DL4 showed very low values, in the order of 0.06 mm, which were similar to the horizontal displacements recorded by the FE model in the same area. In this case, a lower limit can be established by releasing the degree of freedom (DOF)

at the base of the FE model in the transverse direction (2 in the notation of Abaqus). The action of the dead load caused the base to move unconstrained outwards by 0.8 mm and the keystone to deflect by 0.25 mm (Fig. 5.24). The deflection pattern showed higher values spreading closer to the keystone, although this scheme overpredicted the experimental data.

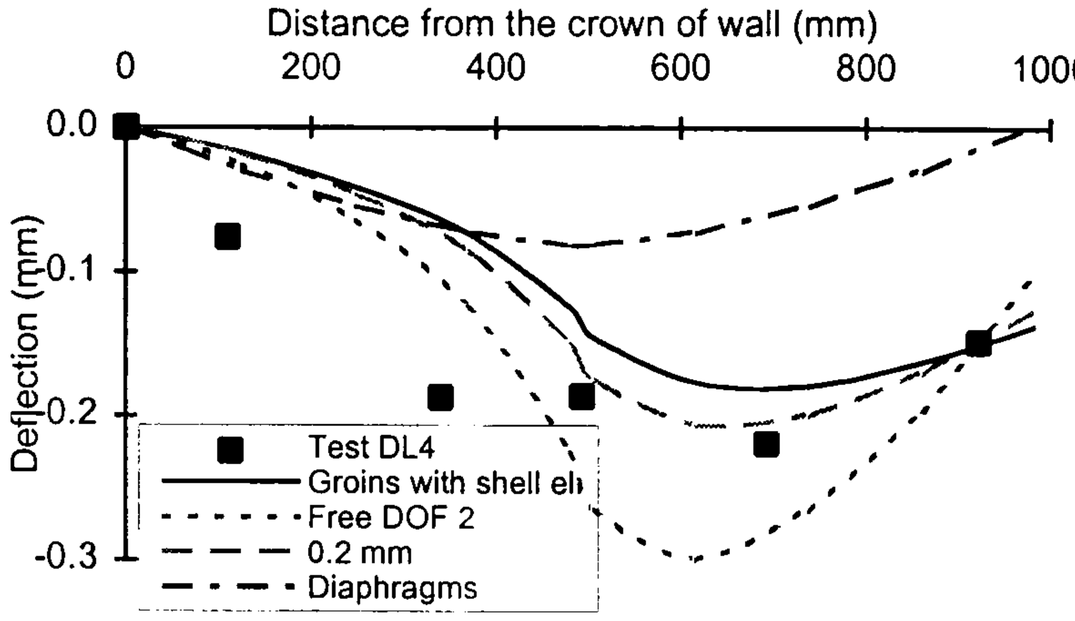

FIGURE 5.24 Deflection of the symmetry vertex for various support conditions

TABLE 5.13 The effect of the support conditions upon the strains for test DL4 (in 10^{-6})

Gauge	Experiment	Finite Element		
	Data	Shell elem. at groins	Free DOF 2	Movement 0.2 mm
AT1V	-29	-56	-62	-58
AT2V	7	-59	-77	-63
BT1V	-30	-54	-131	-73
CT1V	-34	-8	30	2
DT1V	-11	-26	-26	-26
DT2V	2	-7	-8	-7
AB1H	1	5	-2	4
AB2V	1	-4	2	-2
AB3V	1	-74	-94	-62
BB1V	20	37	146	63
BB2V	-18	-56	18	-38
CB1V	-9	-40	-101	-55
DB1H	-1	8	9	8
DB1V	3	-8	-10	-8

The higher deflections around the longitudinal vertex were accompanied by a substantial increase of curvature in either side. Their pattern, however, deviated from the almost symmetric pattern that was achieved previously sections, although there was agreement in the sign at the front side of the vertex (Table 5.13). An interesting feature was

the reduction of the hoop strain at the haunches of the longitudinal web (BB2V) which is accompanied by an increase of the hoop strain at the front haunches (AB3V, AT2V), most probably the result of the eliminated thrust in the transverse direction.

In order to examine any possible influence of uncertainties in the support conditions of the front base, small displacements were imposed on these bases. For a displacement of 0.2 mm, the hoop strain at BB2V was reduced close to the experimental magnitude and the increased values of the strain around the longitudinal vertex were within the limits of difference expected by the fact that the strain gauges are mounted on the units (§4.2). In addition, this action resulted in a very good agreement of the deflections at the front portion of the vault.

So far as the discrepancy at the back portion was regarded (Fig. 5.24), the examination of the strains at the back web D showed that this part remained almost unaffected by the changes in the stress regime of the rest of the FE model. It is quite possible therefore that, despite all the attention during the strengthening of the structure, a local fault may have occurred that increased the deformation of this part of the vault. As the values of the deflections were relatively small, this fault can have a disproportionally high effect. These observations are examined again during the study of the behaviour of the vault due to movement of the abutments (§6.3), where the area of the groins is expected to have a crucial role.

5.3.4.5 The behaviour of the structure in Test DL4

The effect on the deflections of the most important steps of the analytical modifications for the Test DL4 are summarised in Table 5.14. From the discussion in the previous sections, the best agreement with the experimental data emerged from the FE modelling of the groins area with shell elements, as it gave a more balanced prediction of the deformation and strain distribution than the previous model with the spring web-rib joints (Fig. 5.25). This was more evident on the behaviour of the front half of the vault, as it can be judged by the deflections. Despite an overestimation at the front transverse web A (TWF1, TWF2) and underestimation at the back (LWB1), the FE models developed made clear that changes in the stiffness of the joint between the webs over the groin can be critical in improving the strength of the structure.

TABLE 5.14 Analytical predictions of the deflections for Test DL4 (in mm)

Dial	Test DL4	Finite Element		
	Data	Initial	Stiffened ribs	Shell elem. at groins
LWB1	0.157	0.045	0.106	0.039
LV1	0.103	0.079	0.137	0.085
LWF1	0.068	0.104	0.096	0.117
LV2	0.157	0.101	0.187	0.116
TWF1	0.110	0.124	0.148	0.149
TWF2	0.078	0.099	0.085	0.103
SV1	0.074	0.017	0.009	0.017
SV2	0.184	0.067	0.021	0.073
SV3	0.183	0.109	0.214	0.135
SV4	0.215	0.141	0.219	0.180
SV5	0.145	0.122	0.153	0.149

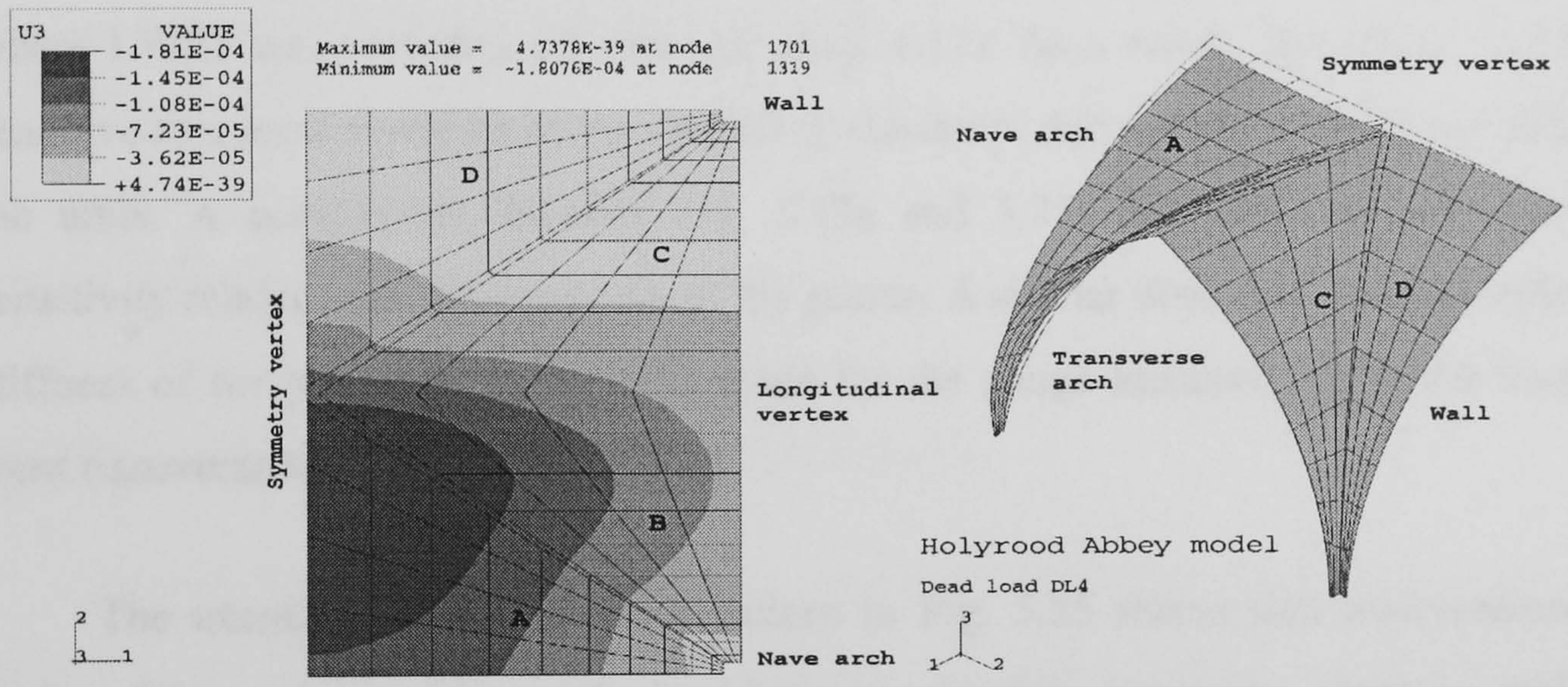

(a) Deflections (m)

(b) Deformation of the model

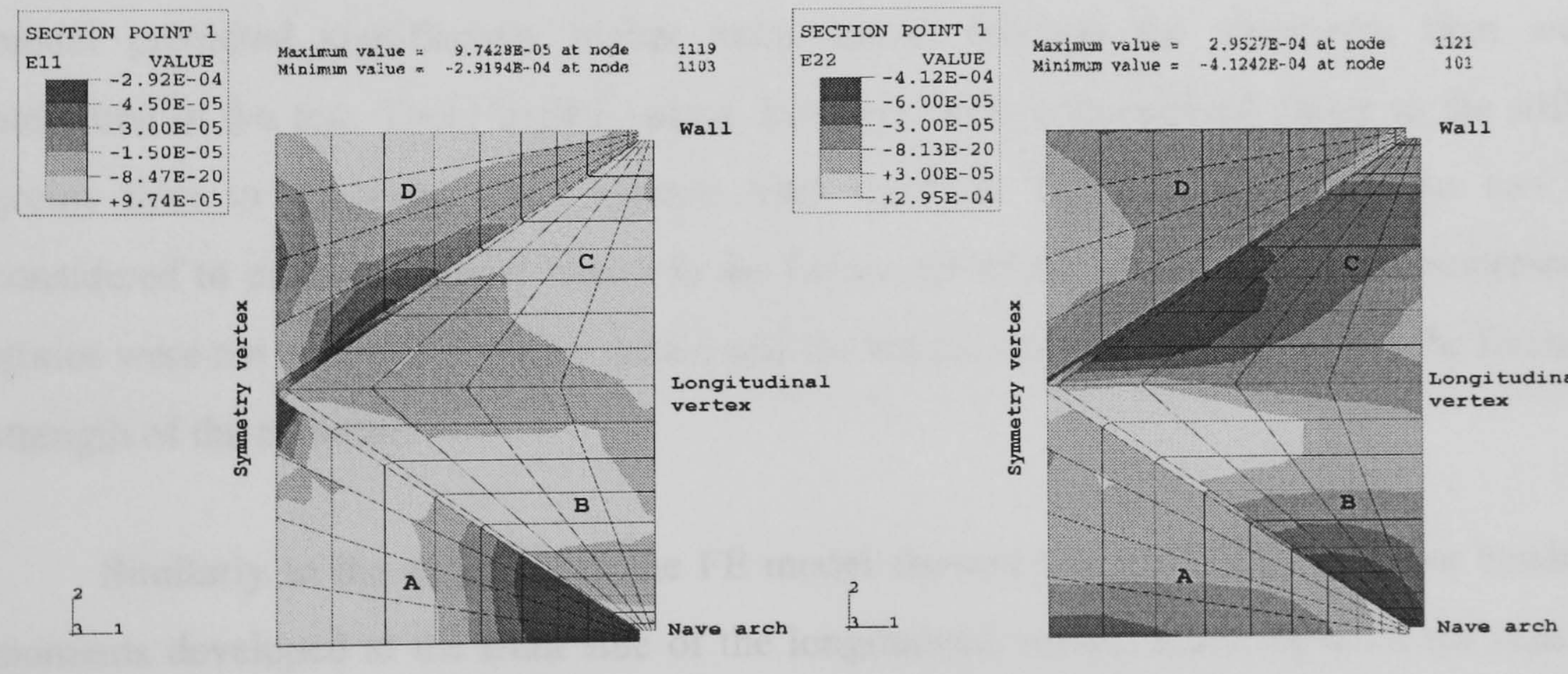

(c) Strain in global X direction - intrados

(d) Strain in global Y direction - intrados

FIGURE 5.25 Deformation pattern and distribution of strain in the FE model for test DL4

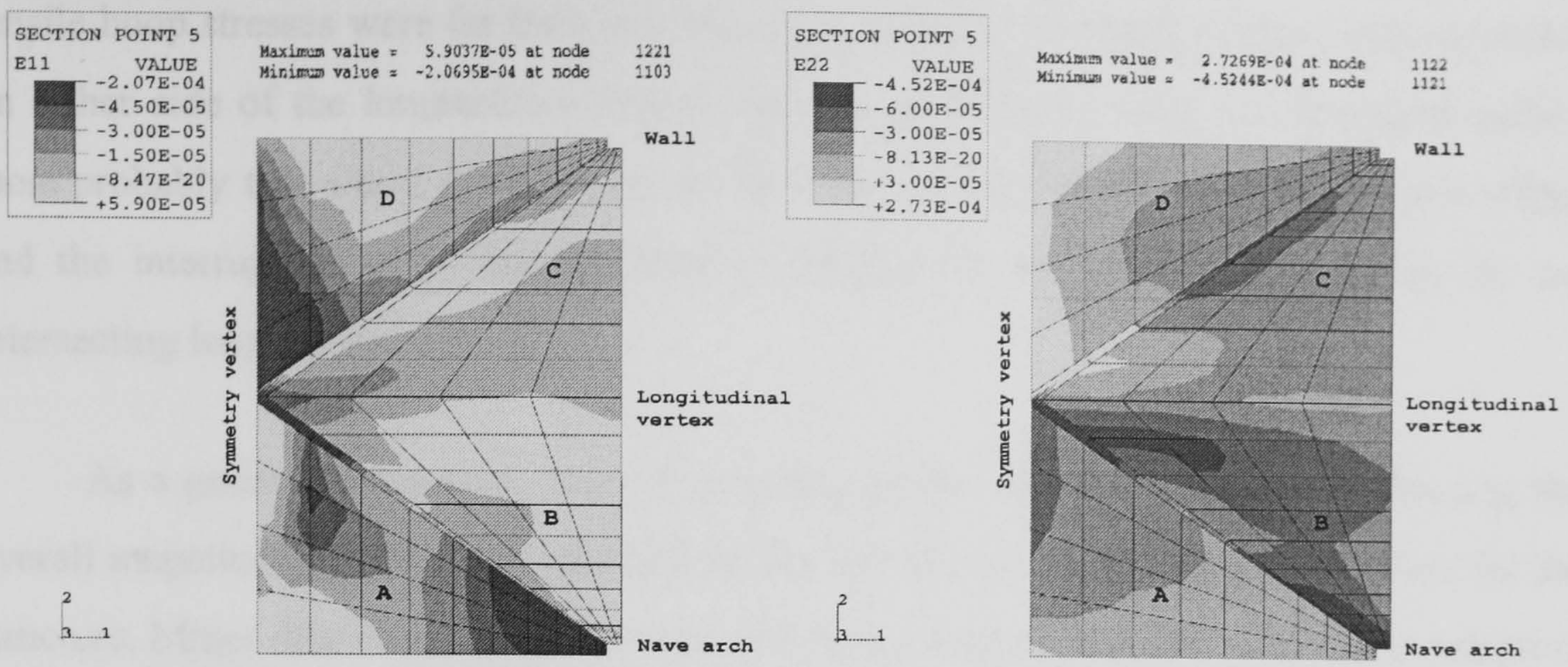

(e) Strain in global X direction - extrados (f) Strain in global Y direction - extrados

FIGURE 5.25 Deformation pattern and distribution of strain in the FE model for test DL4

On the other hand, the deflections dropped quite rapidly at the front haunch, the area where LWF1 was recorded for example (Fig. 4.12). As a result, the region can be quite sensitive to a local variation of the moduli of elasticity, due to the relatively variable size of the units. A comparison between Fig. 5.19a and 5.25a can show a further source of sensitivity related with the condition of the groins. A similar observation on the effect of the stiffness of the haunches can also be made for the gauge locations along the hoop of the front transverse web, TWF1 and TWF2.

The examination of the strain pattern in Fig. 5.25 shows that interventions to the groins of the vault can enhance the load-bearing role of the transverse direction, making less necessary the use of transverse arches. A further result of this scheme was that the shell FE model predicted significantly higher hoop strains towards the abutments than were measured in the test. These higher values, however, were concentrated closer to the stiffer groins than in the case when springs were inserted. The present simulation can be considered to provide a lower bound to the behaviour of the structure, as the compressive strains were not expected to cause failure and the tensile strains were well below the flexural strength of the material.

Similarly to the experiment, the FE model showed that significant positive bending moments developed at the front side of the longitudinal vertex, initiating from the area of the keystone (Figs. 5.25d and f). The strain gauges at the intrados were located in the same area where cracks were expected, according to structural surveys and they showed that the

tensile hoop stresses were far from exceeding the strength. The high concentration of strain on either side of the longitudinal vertex was also made more clear. As discussed earlier, most probably this was a combination of the effect of the sharp fold at the pointed ridges and the interruption at the regular flow of load in the transverse barrel caused by the intersecting longitudinal barrel.

As a general conclusion, the strengthening of the ribs was effective in reducing the overall magnitude of the strains and deflections and the ribs functioned as stiffeners for the structure. Minor displacements of the supports during the test may account for the reduction of hoop strain at the haunches. Further reduction can result if higher elastic moduli were considered in the properties of the haunches, as it can be expected due to the smaller size of the units. High bending stresses were predicted from the FE model at the critical areas around the longitudinal vertex, but probably the geometry of the model vault allowed the loads to distribute more uniformly around that area, as it was also confirmed by the spread of deflections behind the keystone. Another crucial area affected by the actual geometry of the rib joint was the back transverse web D, whose potential function as a rigid body became evident from the analytical study within the two limits of the geometry.

5.3.5 The effect of the spandrel fill (Test DL5)

Test DL5 (§5.2.6) was an attempt to understand better the role of the spandrel fill on the behaviour of the vault. Both heights of the fill applied (0.5H and 0.7H) gave quite similar results, for both deflections (Table 5.5) and strains (Table 5.6), so during the analytical study in this section only one set of data is used, Test DL5b. Initially, two FE simulations were used to investigate the degree in which the presence of the fill may stiffen the haunches of the vault, as it is assumed in some cases of cross vaults due to a combined action with the buttressing system (§1.2.2). The changes in the geometry and the adjustment of the weight in each case were carried out with the help of the Fortran pre-processor. Typical deflection development can be illustrated again by the symmetry vertex (Fig. 5.26).

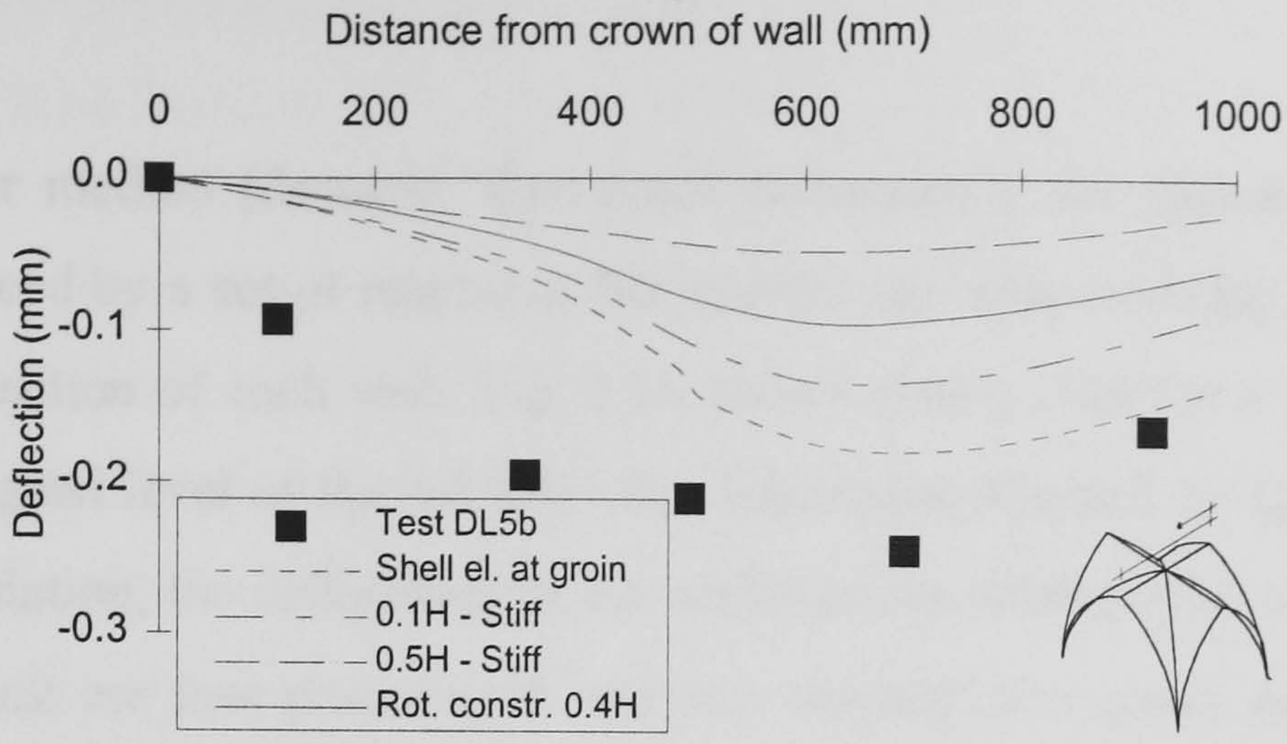

FIGURE 5.26 Deflection of symmetry vertex for various heights of the spandrel fill

The first method (denoted as "Stiff spandrel"), was applied to FE models by Barthel (1994). The weight of the fill was assumed to exert a lateral pressure on the haunches that can cancel the thrust of the vault. This effect can stabilise the haunches and the vault above that level can be considered as simply supported upon the level of the fill. Considering a "stiffened spandrel" height of 0.1H caused a reduction of the deflection of the vault, which affected mainly the front portion of the model, while no significant change was observed in the pattern (Fig. 5.26). When the fill was considered to affect the vault until mid-height (0.5H), the deflections dropped uniformly to almost the third of the initial prediction. Similar changes occurred to the strain distribution and their pattern was almost unaltered.

TABLE 5.15 Strains for test DL5 (in 10^{-6})

Gauge	Experiment	FEA		
	Test DL5b	Shell elem. at groins	Rot. constr. at 0.4H	Load at 0.7H
AT1V	-47	-56	-49	-59
AT2V	7	-59	-56	-87
BT1V	-19	-54	-34	-49
CT1V	-42	-8	-18	6
DT1V	-20	-26	-24	-21
DT2V	5	-7	-7	-4
AB1H	-1	5	2	3
AB2V	-2	-4	-26	15
AB3V	-4	-74	-50	-106
BB1V	15	37	6	39
BB2V	-22	-56	-43	-78
CB1V	-7	-40	-17	-56
DB1H	0	8	9	6
DB1V	4	-8	-5	-6

In the other method (denoted "Rotational constraint"), the spandrel fill at various heights was replaced by a set of reactions that restrain the rotational degree of freedom in the horizontal direction of each web. Fig. 5.26 shows clearly that for a set of constraints applied at the original level of the fill 0.4H the deflections dropped by almost 60%. As in the previous simulation, the differences in the deformation between the front and the back portion of the vault are less pronounced and this resulted in a strain pattern which was balanced around the longitudinal web in a manner similar to the experiment (Table 5.15).

This support condition did not affect the back transverse web D while in the rest of the structure the strains reduced almost uniformly, especially around the longitudinal vertex. The consequence of the effect of both the analytical schemes examined in this section was the increase of lateral thrust, which makes critical the stiffness and good condition of the front spandrels and the wall.

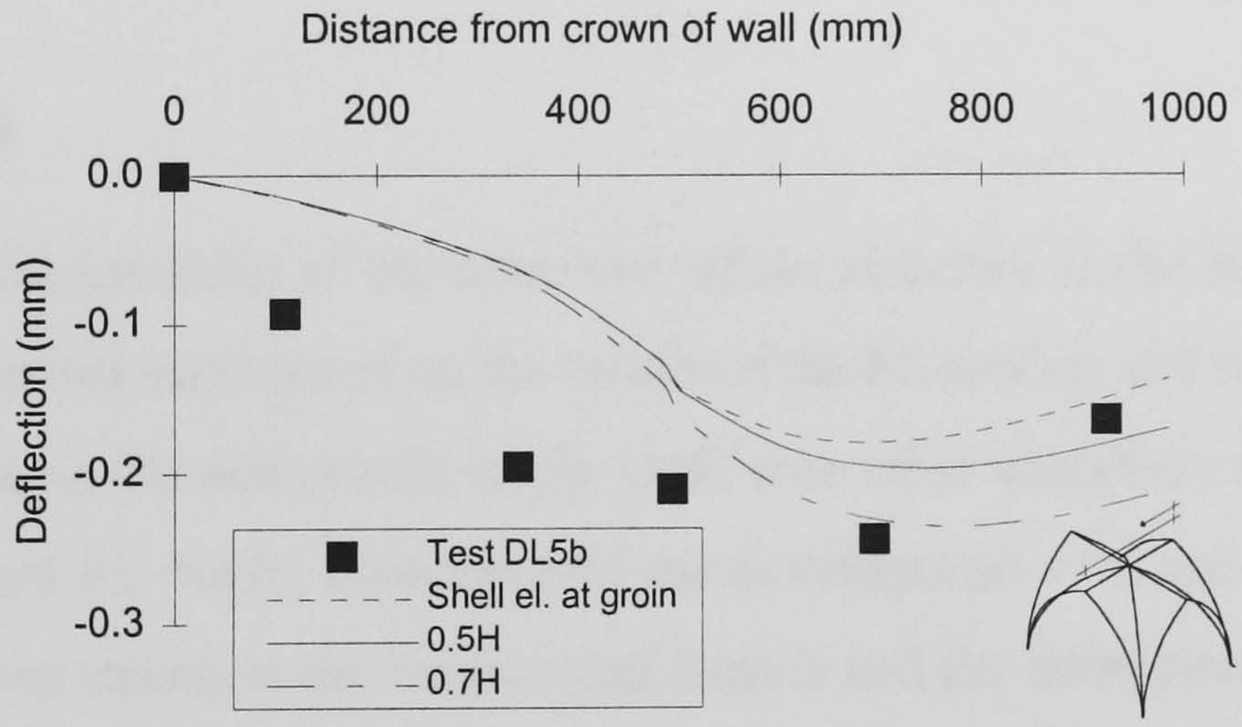

FIGURE 5.27 Effect on the deflection of the symmetry vertex due to the weight of the spandrel fill

The previous simulations indicated that the fill in the present configuration did not function as a constraint of the area of the haunches, but rather as a plain source of load over the corresponding area. Therefore, for the case of a spandrel fill up to 0.5H, an amount of 350N was applied directly to each haunch. The resulting deflection of the symmetry vertex (Fig. 5.27) showed that this new load affected mainly the front portion of the vault, to a degree similar to what occurred during this test. Due to the steep slope of the vault until the mid-height, the load was carried to the front support with higher compressive hoop strains,

while the back haunches remained almost unaffected as a result of their fixed supports. The strains around the longitudinal vertex remained almost at the same level.

Similar observations were made for the case of 0.7H spandrel height. A substantial increase of the deflections occurred (Fig. 5.27), but the higher hoop strains of the front portion of the model (Table 5.15) did not agree with the experimental pattern. The rest of the strains and deflections around the vertices did not change significantly.

The results from the simulations with spandrel constrains and dead load application can be considered as an upper and a lower bound of the FE solution, respectively. Their joint examination indicated the fill does not act purely as dead load but it can also exert a lateral pressure upon the haunches area, similar to the effect of earth pressure. In the course of the later stages of the analysis to failure due to movement of the abutments (Chapter 6), it will be seen that appropriate containment of the thrusts is fundamental for the ability of the structure to resist large changes of geometry and failure due to spreading of the supports can be a direct consequence of this.

5.3.6 Discussion

An overall interpretation of the behaviour of the structure in the main tests DL3 and DL4 can be made in this stage based on the results of the FE models and some points will be discussed again during the assessment of the vault with other analytical models in the next sections. The refined FE model demonstrated the development of a one-way behaviour at the vault, as the hoop strains at the longitudinal barrels and the deflections were distributed uniformly along the transverse axis (Figs. 5.19d, f and Figs. 5.25d, f). The vault developed tensile stresses mainly at the intrados of the front of the longitudinal vertex due to the difference in stiffness between the wall and the nave arch. Similarly, the maximum deflections were detected at the front portion of the vault.

The back of the transverse barrel showed a behaviour similar to a rigid region. Its outer edge was fixed along the wall, while yield lines could potentially develop along the joints at the groins (on which the co-action between the webs depends), as the FE model indicated the presence of tensile stresses (Fig. 5.25f). Since the wall and the nave arch acted to a degree as diaphragms, bending in the transverse webs (A and D) was restrained and

membrane forces prevailed in the hoop direction. At the front web A, however, the loads were directed to the abutments, resulting in higher compression at the haunches (Figs. 5.19c, e and 5.25c, e).

It was also seen that uncertainties in the support conditions can have a significant effect on the deformation of the vault (§5.3.4.4). Most probably, the stiffening of the groins, which enhanced the co-action between the webs, reduced this effect on the model vault. As a result, the high compressive strains in the direction of the abutments tended to concentrate closer to the ribs.

5.4 OTHER ASPECTS OF THE PERFORMANCE OF THE VAULT

Further aspects of the behaviour of the vault under dead load can be examined at the FE model where the groins area was simulated with shell elements (§5.3.4). The analytical solution of a shell structure is determined by the boundary conditions assumed at its curved ends and longitudinal edges, which correspond to the end arches and the ribs of each of the two joining barrel vaults at the cross vault. The role of each set of these conditions is assessed in §5.4.1 and §5.4.2 respectively. Regarding the sensitivity of the behaviour of the vault to the properties of masonry, a parametric study was carried out, treating masonry as an orthotropic (§5.4.3) or composite material (§5.4.4). Knowledge of the thrust exerted by the vault is very important for the design of interventions and it is determined in §5.4.5.

5.4.1 Boundary conditions at the end arches

Design practice and most of the shell theories (Gibson & Cooper 1958, Flügge 1973) consider that barrel vaults have to be supported on diaphragms (plane stiffening members, capable of accepting from the shell only forces lying in their plane) at its curved ends. Various other conditions apply for the longitudinal edges, but most commonly the shear forces developing there are received by a beam. In this model vault, this set of conditions was partially fulfilled in the transverse webs, where the supports at the nave arch and the wall functioned as diaphragms and their edges at the groins were stiffened by the ribs.

TABLE 5.16 FE analysis considering the model is supported upon diaphragms at the edges - Strains (in 10^{-6})

Gauge	Experiment	Finite Element	
	Test DL4	Test DL4	Diaphragms
AT1V	-29	-56	-64
AT2V	7	-59	-6
BT1V	-30	-54	-30
CT1V	-34	-8	-30
DT1V	-11	-26	-46
DT2V	2	-7	-15
AB1H	1	5	-2
AB2V	1	-4	-22
AB3V	1	-74	-5
BB1V	20	37	4
BB2V	-18	-56	-20
CB1V	-9	-40	4
DB1H	-1	8	10
DB1V	3	-8	-1

In order to investigate the extent in which the arches at the edges of the vault act as diaphragms, all the degrees of freedom in the plane of the curved ends at the FE model were constrained. This resulted in a symmetrical deflection of the whole vault around the keystone, where the maximum value recorded (0.089 mm) was smaller than in the previous model (0.135 mm) and the experiment (0.186 mm). The strains were distributed symmetrically around the longitudinal vertex (Table 5.16), similarly to the FE model with the spring joints at the groin. A more interesting feature, however, was the reduction of the hoop strains at the haunches, concentrating in a narrow zone around the rib (BB2V).

This study showed that the arch behaved already partially as a diaphragm, due to its in-plane stiffness, and this can account for the low strains at the haunches. The deformation of the FE model was restrained mainly due to the assumption of diaphragms along the transverse edges and the role of these edges in the response of the vault will be further examined in the course of the movement of the abutments.

5.4.2 Further on the role of the ribs

The function of ribs in cross vaults is similar to the edge beams required today in shell design practice, which is to reduce the high tensile longitudinal forces N_x. These edge

beams are usually quite deep, as they are designed to carry almost the whole of the tension of the shell roof, working in the same manner as the reinforcement at the bottom fibres of a concrete beam. Such a scheme is also justifiable by intuition. However, the medieval master mason, who used much of his intuition in the design, could not employ ribs of large dimensions as they would hamper the visual effect of the aisles and nave. Even earlier examples of Romanesque vaults show that initial attempts in this direction were soon abandoned for lighter and moulded ribs.

In modern vault design, a distinction is made between edge conditions for inner and outer shells, which applies to a series of barrel roofs. In the case of inner vaults, the lateral thrusts are mutually cancelled and no lateral movement takes place. In this context, each of the intersecting pointed webs was studied separately here. A straight beam with the section properties of the ribs was considered to stiffen the edges in both cases and the corresponding arches at the curved ends were maintained, while the same amount of dead load as in the tests was applied. Regarding the edge conditions for inner shells, the longitudinal edge was considered as symmetrically restrained, while for outer-shell type, the edge was free.

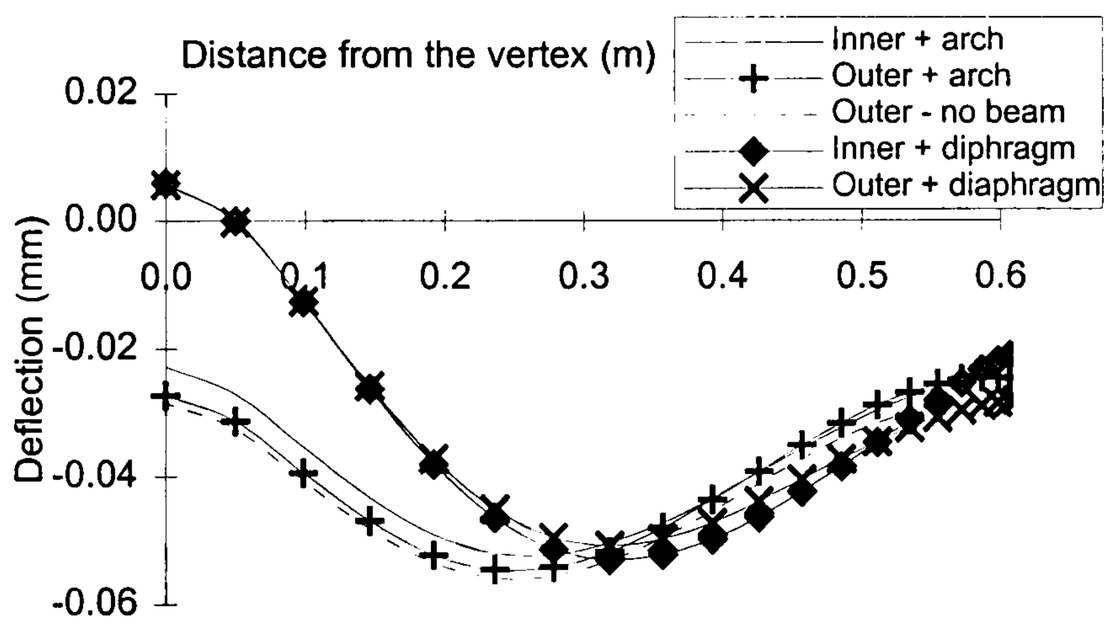

FIGURE 5.28 Deflections along the middle section of the isolated transverse web

If the transverse web is assessed, the higher values of deflections have shifted from the vertex to almost mid-height (Fig. 5.28), but the edge boundary conditions (outer+arch / inner+arch) have had only a moderate effect. If diaphragms are assumed at the ends instead of arches (as it is usual for the shell theory), although the deflections at the edges did not change, the pattern around the vertex was significantly different, as it appeared to be lifted by the load (Fig. 5.28). The lateral constraint with edge beams made only a small difference and this was probably due to the short span and stiff end arches.

In the case of the longitudinal web, which had narrower arches of a smaller cross-section (the transverse arches) at the ends but a longer longitudinal span, the pattern was quite different. The application of inner-type edge supports resulted in lower deflections at the vertex than in the outer-type, while they were almost constant along the hoop, and they were overall lower than those of the longitudinal web.

The moderate effect of the edge beam was a result of the deep profile of the vault and the dimensions of the cross section of the ribs, which supports further the observations in §5.3.3.2. As was mentioned earlier, the role of the ribs is mainly to enhance the construction quality of the intersection along the groins and to ensure the continuity between the two portions of the vault.

5.4.3 Orthogonal ratio of elasticity

The effect of the orthogonal ratio of elasticity was examined by keeping the value for the hoop direction E_φ (E_2 - the lower of the two) constant to 670 N/mm^2 and varying the longitudinal modulus E_x (4260 N/mm^2) within the range of the values recorded, 1530 and 6180 N/mm^2. In this manner, the actual ratio of 6.36 varied between 2.28 and 9.22 and the study of the distribution of hoop strain at the intrados parallel to the longitudinal vertex may indicate how this could affect the way the load is shed between the two directions.

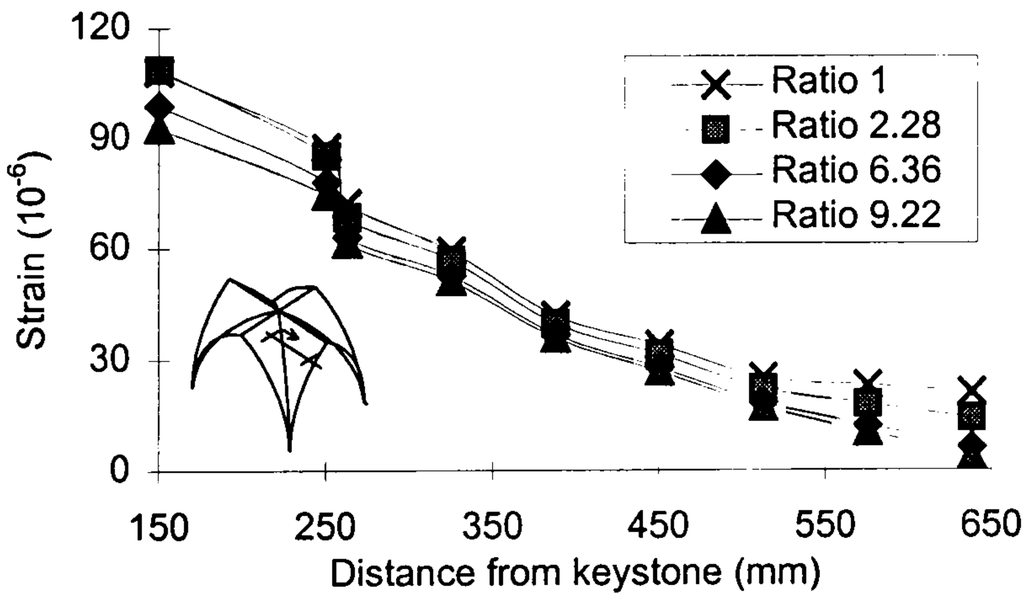

FIGURE 5.29 Distribution of hoop strain close to the longitudinal vertex, at the intrados, as a result of the variation of the orthogonal ratio of elasticity

Fig. 5.29 shows clearly that variations of the longitudinal stiffness had a quite limited influence on the distribution of the hoop strain, especially at the critical areas around the longitudinal vertex. The reduction of strain with the increase of the ratio was rather uniform.

Relatively higher tensile strains recorded when the material was considered as isotropic (orthogonal ratio 1), and the overall variation for this range was at the order of 10%.

5.4.4 Analysis of the masonry vault using a "micromodel"

During the study of the masonry properties in §4.2, a micromodel was used to simulate the behaviour of the wallettes by modelling separately the units and the mortar joints. This kind of analysis is suitable for the study of structural elements where a heterogeneous state of stress and strain is expected (Lourenço 1998). In this case, the difference between the properties of the units and the joints caused high strains to concentrate in the weaker joints, especially for higher loads and closer to failure. Although the level of stress in each material direction is low, a similar type of analysis of the vault can be useful to assess any local influence the properties of the constituent materials might have.

A new and denser mesh was generated, with a number of divisions in the hoop equal to the number of courses, approximately 40 in each half web. This density had to be doubled to provide for the mortar joints between the units, so the shell elements S9R5 could not be used any more as this caused numerical problems from the start. Instead, S4R5 were employed and the mesh density would guarantee their rate of convergence (§5.3.1.2). Next, the properties of the constituent materials, discussed in §4.2.3, had to be adjusted to conform with the mechanical properties of masonry used so far. The modulus of elasticity for the units was assessed as 27000 N/mm^2 in the longitudinal direction and 3200 N/mm^2 in the transverse. So far as the mortar was concerned, from the range established in Chapter 4, the best and numerically stable approximation was found by assuming a very low modulus of 100 N/mm^2. The rest of the geometry in the FE model were kept the same.

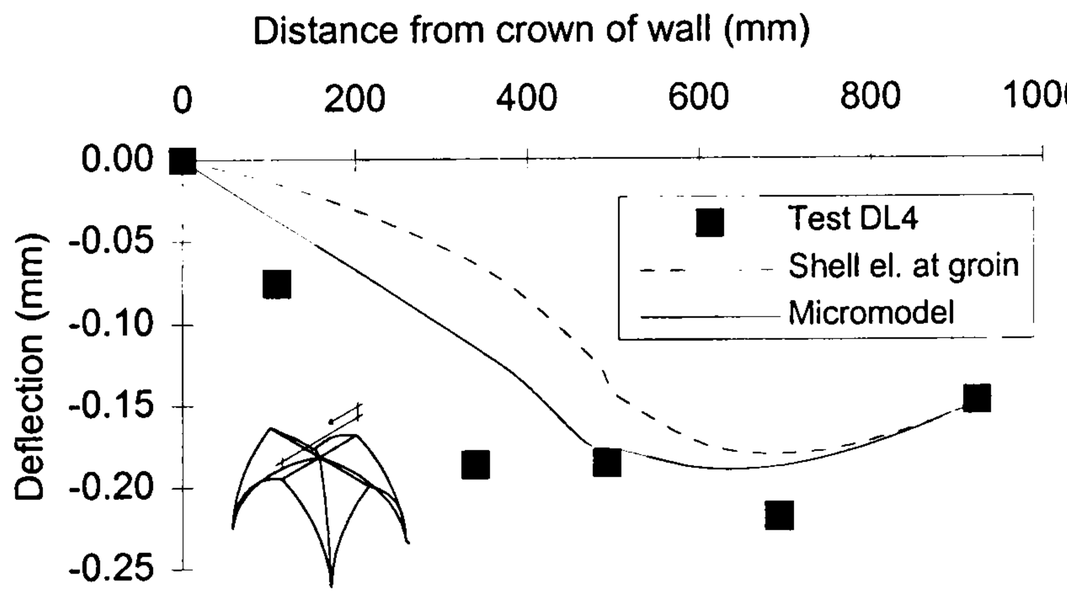

FIGURE 5.30 Deflection of the symmetry vertex after a micromodelling analysis

TABLE 5.17 FE micromodel analysis - strains recorded at the units (in 10^{-6})

Gauge	Experiment	Finite Element	
	Test DL4	Test DL4	Micromodel
AT1V	-29	-56	-14
AT2V	7	-59	4
BT1V	-30	-54	-37
CT1V	-34	-8	-3
DT1V	-11	-26	-21
DT2V	2	-7	5
AB1H	1	5	16
AB2V	1	-4	1
AB3V	1	-74	-14
BB1V	20	37	44
BB2V	-18	-56	-3
CB1V	-9	-40	-9
DB1H	-1	8	2
DB1V	3	-8	-4

A small and uniform increase of the deflection of the symmetry vertex was observed (Fig. 5.30), which was in quite good agreement with the experiment. The deformation spreaded more evenly along the vertex due to the effect of the less rigid mortar joints. More interestingly, however, the strains recorded at the units (Table 5.17) showed a significant part of the strain at the haunches was actually originating from the mortar joints. In the rest of the structure, the pattern resulting from the homogeneous model was maintained in almost all the gauges.

Although micromodelling appeared as a more realistic approach for this material, the model does not make the best use of the Finite Element method as the high difference between the deformations of the closely located nodes of the units and joints compromises the fundamental assumption of a continuous medium. This may cause numerical instabilities for higher loadings and the limits of such a modelling will become more apparent when the failure of the structure by movement of the abutments is dealt with in the next chapter.

5.4.5 Development of thrust

The remarks made in §5.3.5 on the role of the spandrel fill and the haunches in general can be concluded with a study on the development of thrust in the FE models in the transverse direction. The distribution of the reactions normal to the wall evaluated for both

tests DL3 and DL4 is plotted in Fig. 5.31. In most of the height, the common pattern of the tests shows that thrust was acting outwards and that only around the crown was the vault pulling inwards. This illustrates clearly the tendency of the vault to detach from the wall even at this stage of low stresses and it serves as an indication of the possible areas where cracks may develop in later stages of increased loads. Higher values were recorded when the groins were considered as strengthened (DL4), as most of the thrust of the longitudinal webs was effectively transmitted to the wall through the transverse webs, due to the enhanced co-action between these webs.

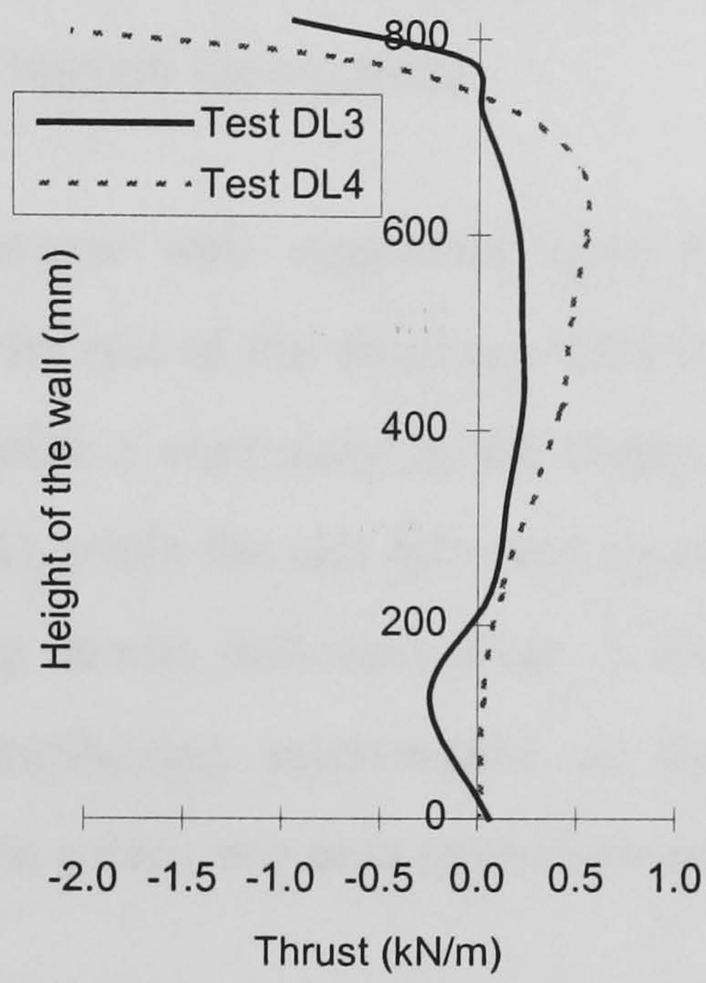

FIGURE 5.31 Distribution of thrusts along the wall

This co-action affected also the level of the thrust that had to be balanced along the groin. The nave arch was quite effective in keeping the lateral displacements and the thrust of the transverse web in the longitudinal axis of the vault (global X direction) low. As a consequence, the longitudinal web exerted only its own thrust in that axis and, as its transverse arches burst only moderately outwards, their cross section was sufficient to constraint the web in that direction. On the contrary, the lateral displacements (and thrusts) of this web in the transverse axis of the vault (global Y direction) were quite higher, especially at the deeper sections close to the ends. The reasons for this were the small cross-section of transverse arch (compared with the nave arch) and the longer span of the longitudinal web. This amount of thrust is capable of bringing the nave arch out of plumb at the abutment, if it is not stiff enough. This last feature can enhance the effect of the

movement of the abutments, as it can be seen in the next chapter, since this action can disturb almost immediately the equilibrium achieved under dead load.

5.4.6 Structural behaviour of the vault under dead load

Following the study of these parameters and the examination of the contribution of various components discussed during the test arrangements (§5.3), the behaviour of the FE model as a simulation of the experimental structure showed a prevalence of the transverse direction in carrying the loads. Higher hoop strains were recorded at the longitudinal webs and the difference in stiffness between the wall and the nave arch caused the vault to deform mostly towards the front part, beyond the keystone.

The part of the transverse web supported upon the wall showed signs of an independent behaviour from the rest of the structure, although the bond between the webs along the groin could still enable a continuity in the displacements. The wall carried also most of the dead weight (65%), while the rest followed a path towards the front abutments, as the high compressive hoop strains indicated (Figs. 5.19c, e). Modifications in the FE model reproducing the strengthening intervention at the groins caused a moderate concentration of these strains in a narrower area around the groins (Figs. 5.25c, e).

The role of the ribs in this scheme was to permit a good execution of the difficult to construct geometry of the groins and to reinforce the irregularities that usually occur there. It certainly reduced the maximum deflections (those observed around the symmetry vertex), but its influence was confined in that part only. The role of edge beams / ribs was much less necessary at the transverse webs due to their geometry, while the longitudinal web was closer to the behaviour of an asymmetrically supported pointed barrel vault.

The model cross vault, under the present support conditions, can be considered as an assembly of four pointed barrel vaults which meet along their common boundary along the groins (Fig. 5.32). Each barrel vault is supported mainly at the end arches, while the compatibility between them is enforced by the ribs along the groins. The supports in each of the intersecting vaults vary from fully fixed (at the edge of the back transverse web on the wall) to very flexible (at the end arches of the longitudinal webs). The system groin-ribs is fundamental for this scheme as its strength regulates the degree of co-action between the

parts. If this system is weak, as in Test DL3, the cantilever-type behaviour of each web is more pronounced, as that test showed that the deflections recorded in all the webs were increasing towards the keystone.

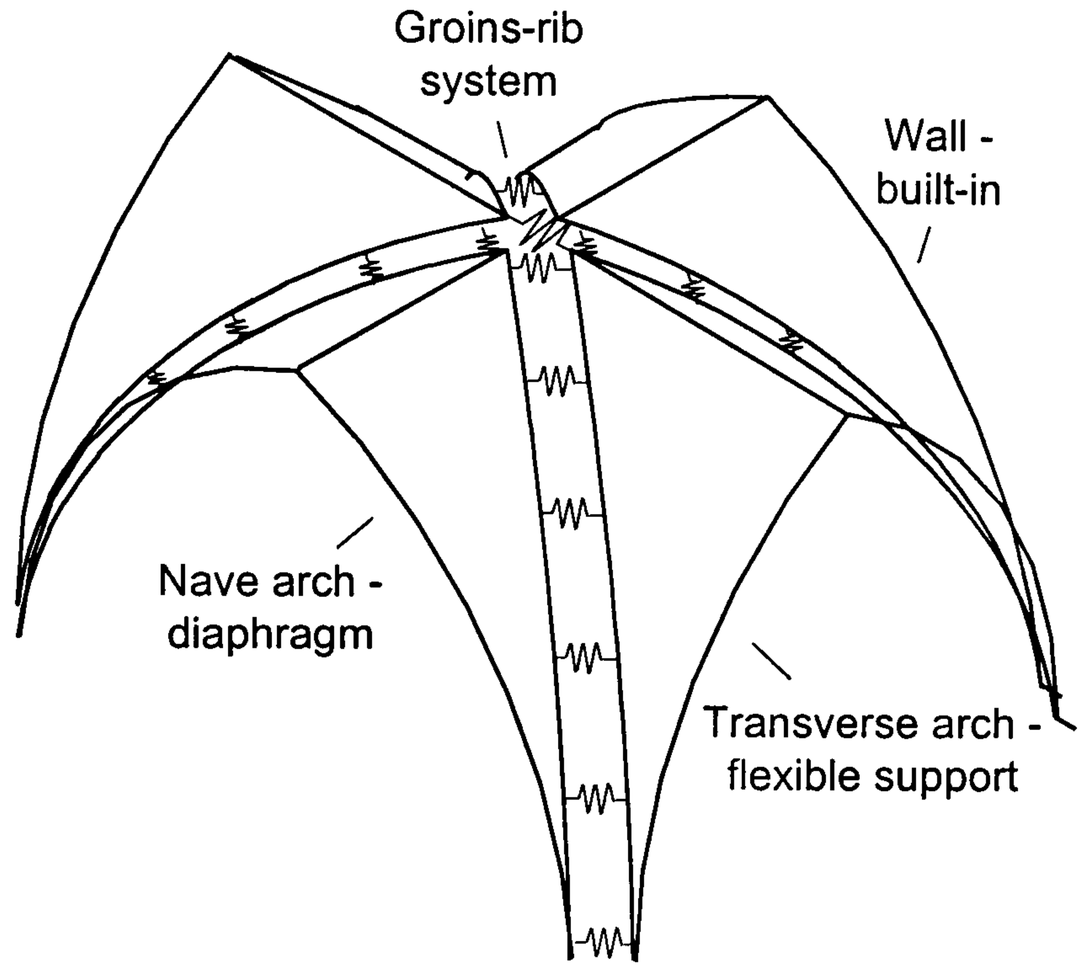

FIGURE 5.32 Scheme of the behaviour of the vault under service loads

The thrust of the longitudinal web prevailed over that of the transverse around the haunches, but they could effectively brace each other closer to the keystone. Moreover, the scheme of the intersecting (pointed) barrel vaults actually cuts away an important part at the middle of each of the barrels which in vaults with a similarly deep profile is usually in high tensile longitudinal forces N_X.

5.5 SUMMARY AND CONCLUSIONS

The following conclusions can be drawn from the study of the behaviour of the vault under dead load:

(1) The deformation of the model vault is asymmetrical, with maximum deflections recorded in the area between the longitudinal vertex and the nave arch.

(2) The area of the front haunches is in a state of pure membrane compression.

(3) The co-action between the four webs is highly dependent on the strength of the groins.

(4) For this magnitude of load, the stresses are well below the strength of the material.

(5) Areas of tensile stress develop at the intrados, at the front part of the longitudinal vertex, and normal to edge over the wall, indicating possible zones of cracks initiation.

(6) Spandrels filled up to 70% of the total height have no significant effect on the vault.

The effect of the geometry of the groin was initially simulated with a FE model that represented the low strength of the area with spring elements inserted between the webs. When the joint was adequately stiffened later, the FE model was further refined and the system of groins-ribs was best simulated with shell elements.

A parametric study on the FE model showed that the material properties and the geometry of the structure affected mainly the magnitude of the deformation of the vault under dead load. Most important was the role of the support conditions. The stiffness of the nave arch affected the degree in which the vault behaved symmetrically about the longitudinal vertex, while uncertainties in the support conditions of the abutments can be responsible for changes in the stress pattern locally.

Chapter 6

INVESTIGATION OF THE BEHAVIOUR OF THE VAULT DUE TO THE MOVEMENT OF ABUTMENTS

6.1 INTRODUCTION

The behaviour of the vault under service load was characterised by a relatively low level of stress which confirmed the reserves in strength expected for these structures. As discussed in §1.4, imposed deformations from the failure of the upper structure are more likely to result in the damages observed in Gothic churches.

At the model cross vault under examination, these imposed deformations were simulated experimentally by the movement of front abutments, at the initial rate of 1 mm (§4.4.2), until failure was recorded, at a total displacement of 30 mm. The effect of this action on the deflection of the vault and the strains distribution is presented and discussed in §6.2.

The FE model developed during the assessment of the response to dead load was in good agreement with the experimental results, after some necessary modifications were applied (§6.3). Further interpretations of the behaviour of the vault were based on this FE model, while aspects like the thrust, minimum required thickness or the acceptable range of abutments movement were examined by performing an ultimate limit state analysis of the structure.

Further, a parametric investigation was done to study the effect of the geometry, the material properties and the service load on the behaviour of the vault.

6.2 EXPERIMENTAL RESULTS

6.2.1 Experimental set-up

In the previous stages of the experiment, the model vault was tested under dead load and FE models were generated to simulate the response of the vault. In this phase the front abutments of the vault were displaced in order to reproduce the collapse of the prototype structure in Holyrood due to imposed deformations. As was explained in §4.4.2, the same amount of dead load was used as previously and the spandrels were filled until the original height of 40% of the total height of the vault (Test DL4). The movement was applied to the abutments by means of a turnbuckle (Fig. 4.10) and was controlled with dial gauges. The development of deflections and strains was monitored in the locations indicated in Fig. 4.12.

In the elastic range, the induced displacement of abutments was increased at a regular interval of 1 mm until the appearance of the first cracks at 10 mm. After that stage, the development of the crack pattern was also recorded. The displacement was progressively increased until a sufficient number of fracture lines developed to transform the vault into a mechanism at a displacement of 30 mm.

6.2.2 Deflections

Deflections were monitored at various locations and stages on the vertices and the webs, as indicated in Fig. 4.12. The overall deformation of the vault can be illustrated by the symmetry vertex, in Fig. 6.1a for the first 5 mm of abutments movement and in Fig. 6.1b for the rest of the test. Detailed data for all the dial gauges are reported in Fig. 6.2.

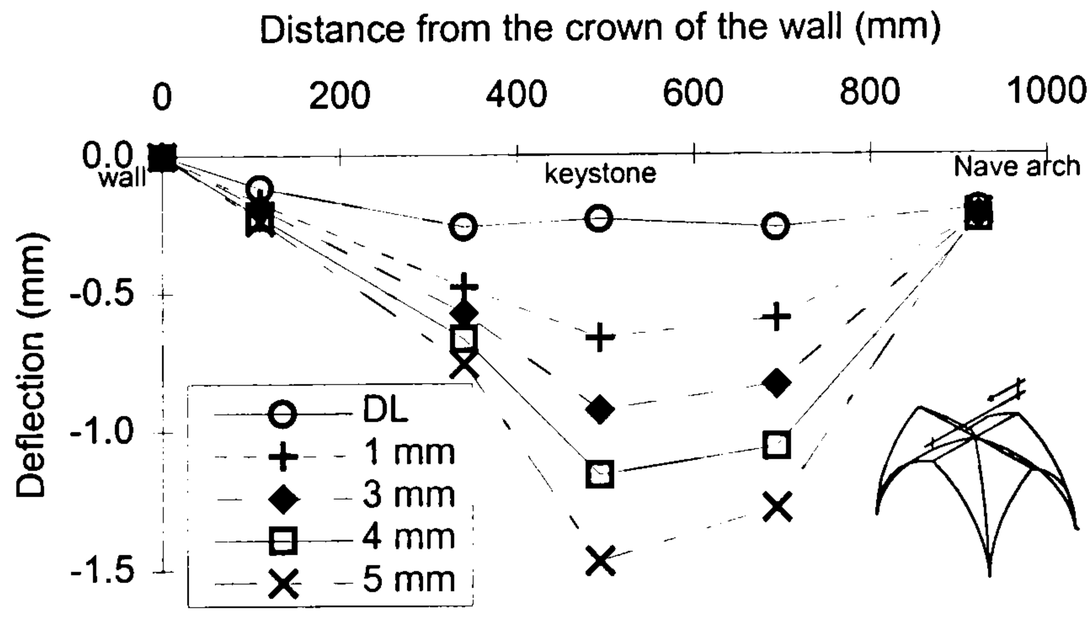

(a) Movement of 5 mm

FIGURE 6.1 Deflection of the symmetry vertex due to movement of abutments

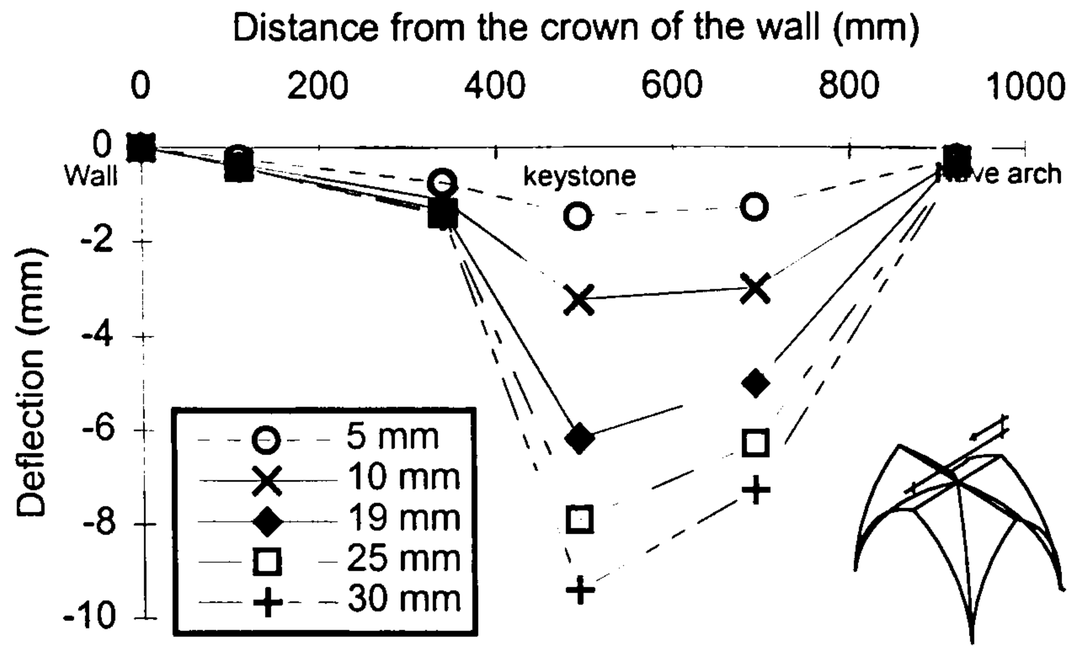

(b) Movement of 30 mm

FIGURE 6.1 Deflection of the symmetry vertex due to movement of abutments

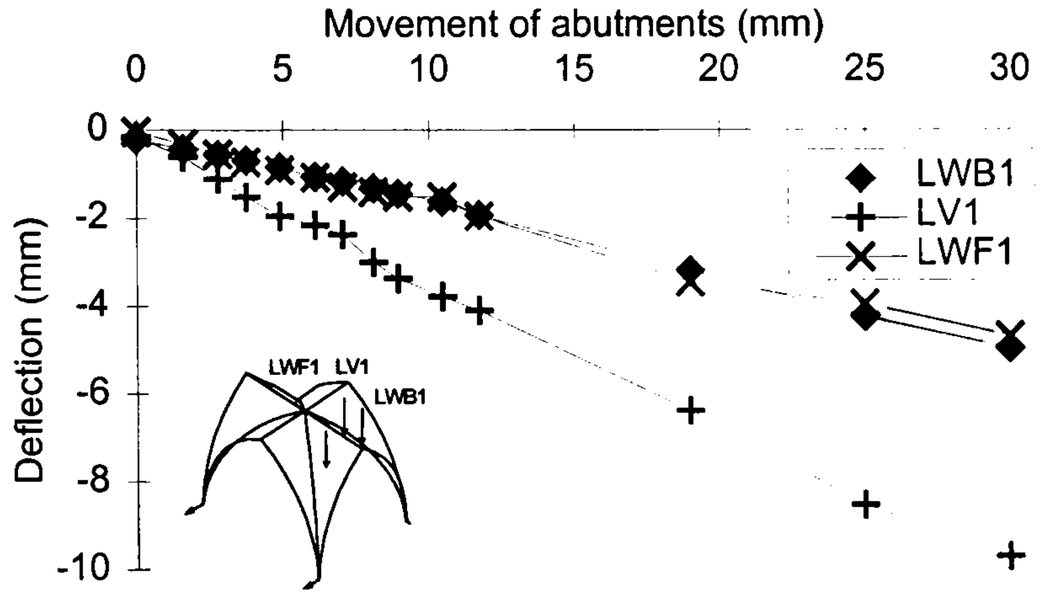

(a) Longitudinal web

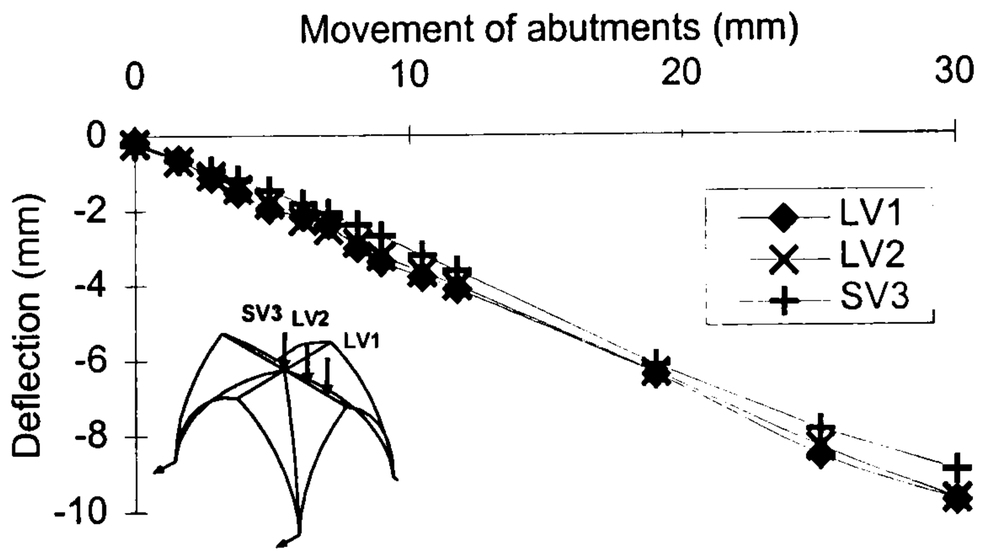

(b) Longitudinal vertex

FIGURE 6.2 Deflections during the movement of abutments (location of gauges on vault in Fig. 4.12)

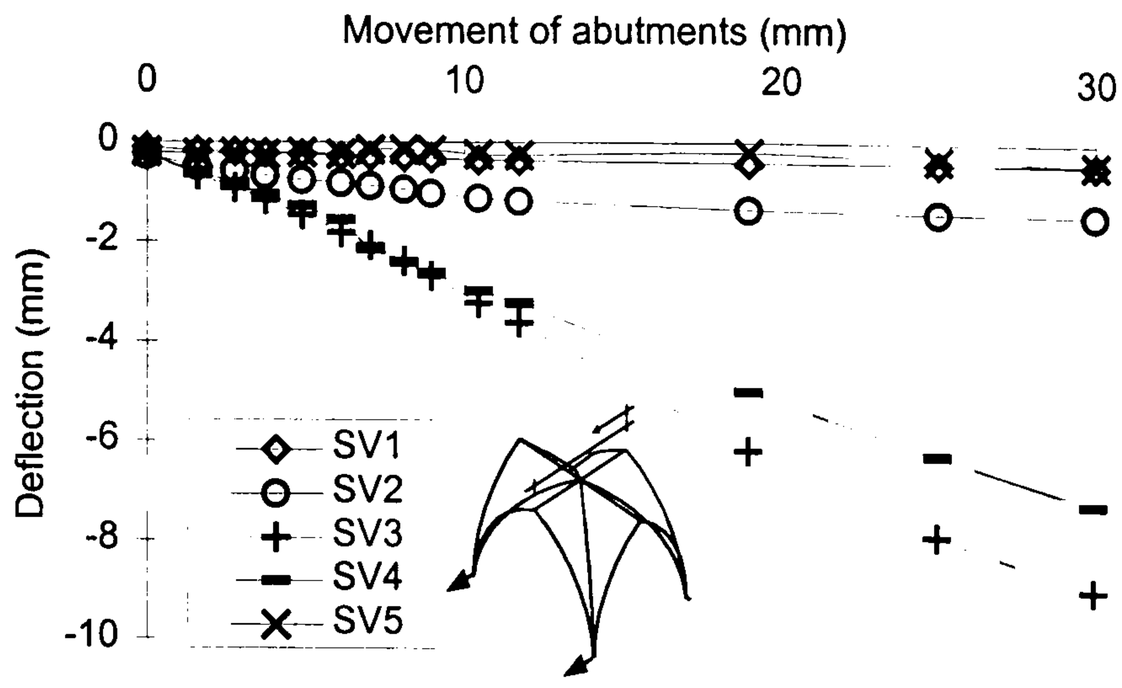

(c) Symmetry vertex

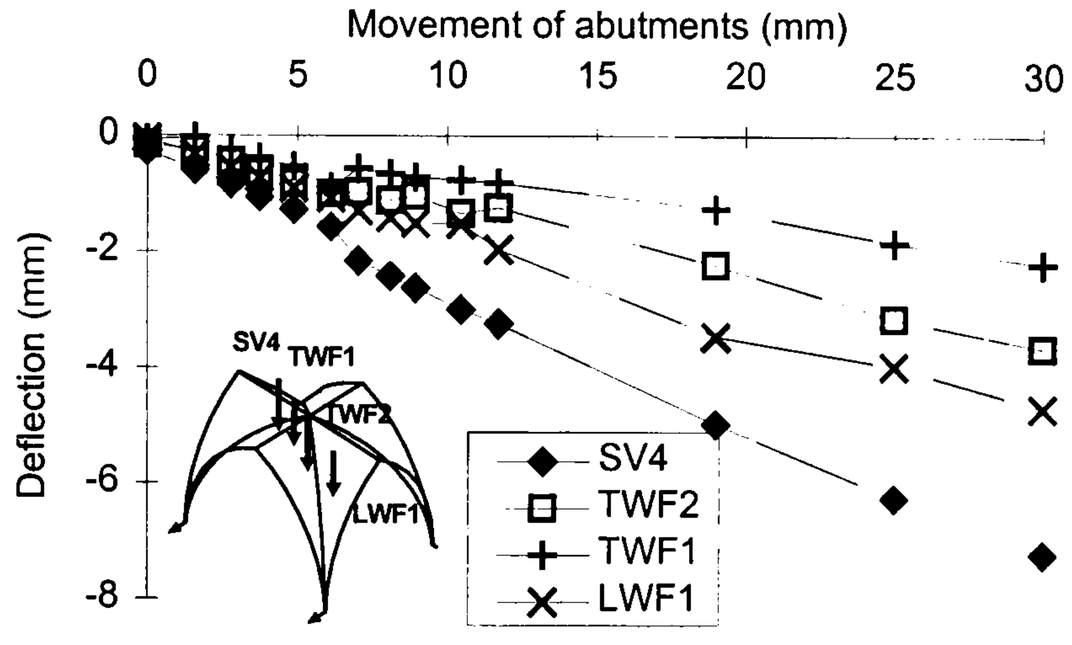

(d) Front transverse web A

FIGURE 6.2 Deflections during the movement of abutments (location of gauges on vault in Fig. 4.12)

The study of the symmetry vertex (Fig. 6.1) showed that the movement of abutments affected uniformly the deflection in the area around the keystone as observed during the dead load tests. The discontinuity between the deformation of the back transverse web and the rest of the structure became evident already at a movement of 5 mm. No significant increase in the deflection of this area occurred thereafter (see also gauges SV1 and SV2 in Fig. 6.2c), so this part of the structure can be considered to behave as a rigid region. Deflections at the other end of the vault were also constrained due to the stiffness of the nave arch (gauge SV5 in Fig. 6.2c). The maximum values were clearly concentrating at the keystone, which was the weakest point of all the four webs forming the vault, due to the degradation of the co-action between the two parts of the structure (cf. §5.4.6).

Regarding the response of the vault in the longitudinal direction, the difference between the values at the dial gauges over the longitudinal vertex was insignificant (Fig.

6.2b), as the whole of the ridge deflected uniformly. This pattern did not spread further within the webs as the deflections recorded did not reduce uniformly parallel to the longitudinal vertex, but they decreased closer to the groins, probably as a result of the stiffening action of the ribs (Fig. 6.2d). So far as the longitudinal web is concerned, the progressive detachment of this part of the vault from the back transverse web was expected to result in an increasingly independent behaviour of this web as a pointed barrel vault. The similar values recorded on either side of the longitudinal vertex (Fig. 6.2a) confirm this pattern, indicating an almost symmetric response was developing around this vertex.

6.2.3 Strains and crack pattern

The behaviour of the model vault during the abutments movement is summarised in Table 6.1. The recorded strain at some critical positions (indicated in Fig. 4.12b) is shown in Fig. 6.3 and it will be examined together with the crack pattern, which is displayed in its final form in Fig. 6.4. Further information is provided in Fig. 6.4 on the direction in which the cracks appeared to propagate during the test.

TABLE 6.1 The behaviour of the model vault during the movement of abutments

Movement of abutments (mm)	Effect on the model vault
0	Action of dead weight only
3	Initiation of cracks at intrados at front of longitudinal vertex and dislocation of ribs (Figs. 6.5 and 6.6)
5	Hinge at the springing voussoir of nave arch and cracks at crown of wall (Figs. 6.7 and 6.10)
8	Crack at back of keystone, propagating along back groins (Fig. 6.9); bifurcation of *tas-de-charge* crack to the joint between the nave arch and the web (Fig. 6.8)
15	Full extent of cracks at back groin and penetration within the back transverse web C (Fig. 6.9)
30	Failure of model vault (Fig. 6.4)

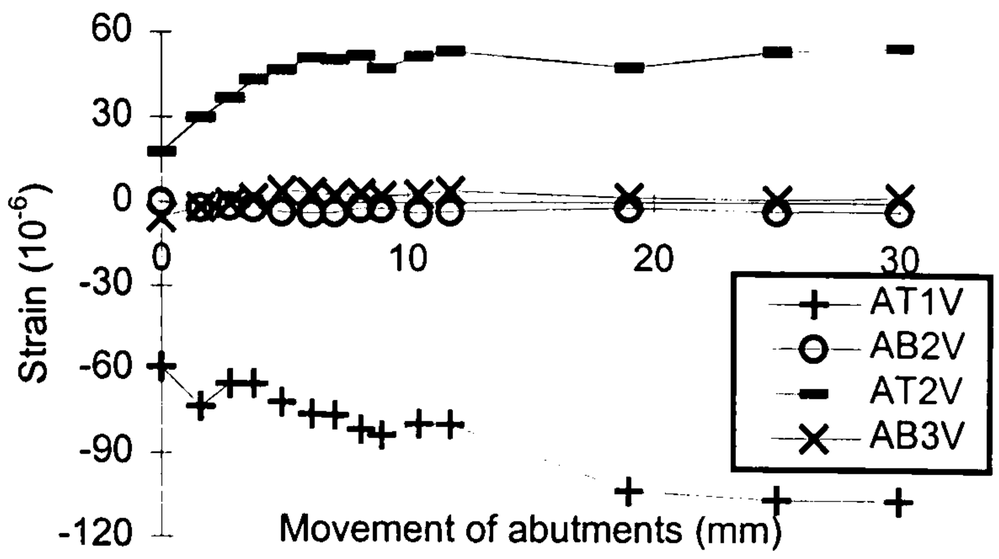

(a) Hoop strain at the front transverse web (A)

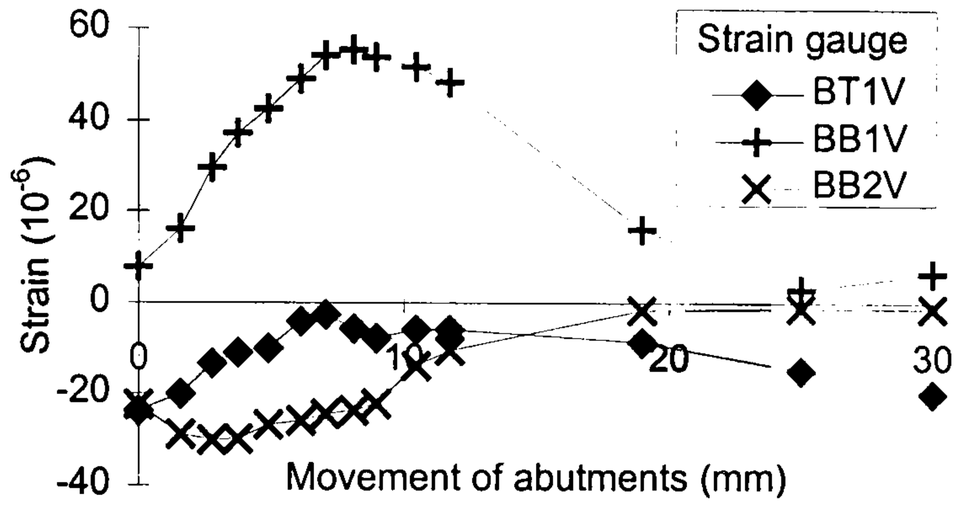

(b) Hoop strain at the front longitudinal web (B)

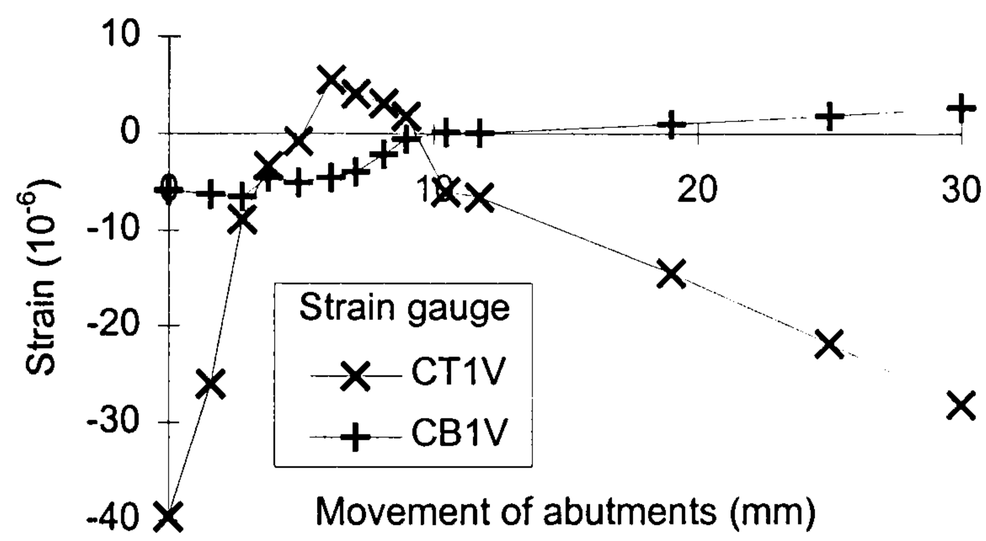

(c) Hoop strain at the back longitudinal web (C)

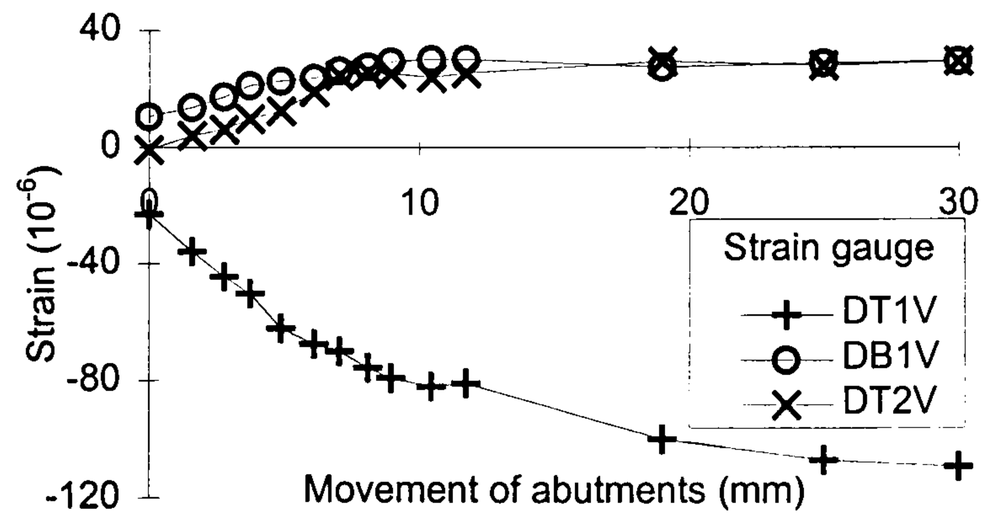

(d) Hoop strain at the back transverse web (D)

FIGURE 6.3 Strain recorded during the movement of front abutments (refer to Fig. 4.12b for locations of the gauges on the vault)

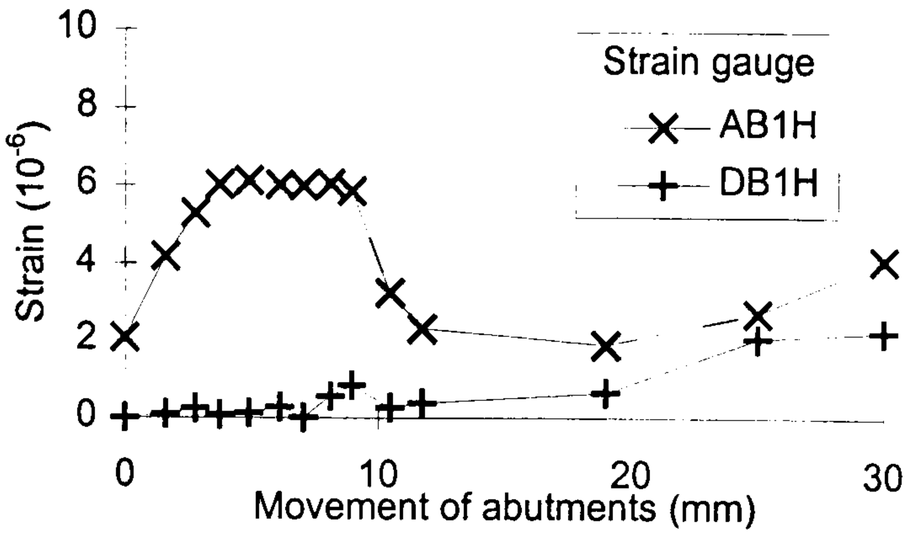

(e) Horizontal strain at the symmetry vertex

FIGURE 6.3 Strain recorded during the movement of front abutments (refer to Fig. 4.12b for locations of the gauges on the vault)

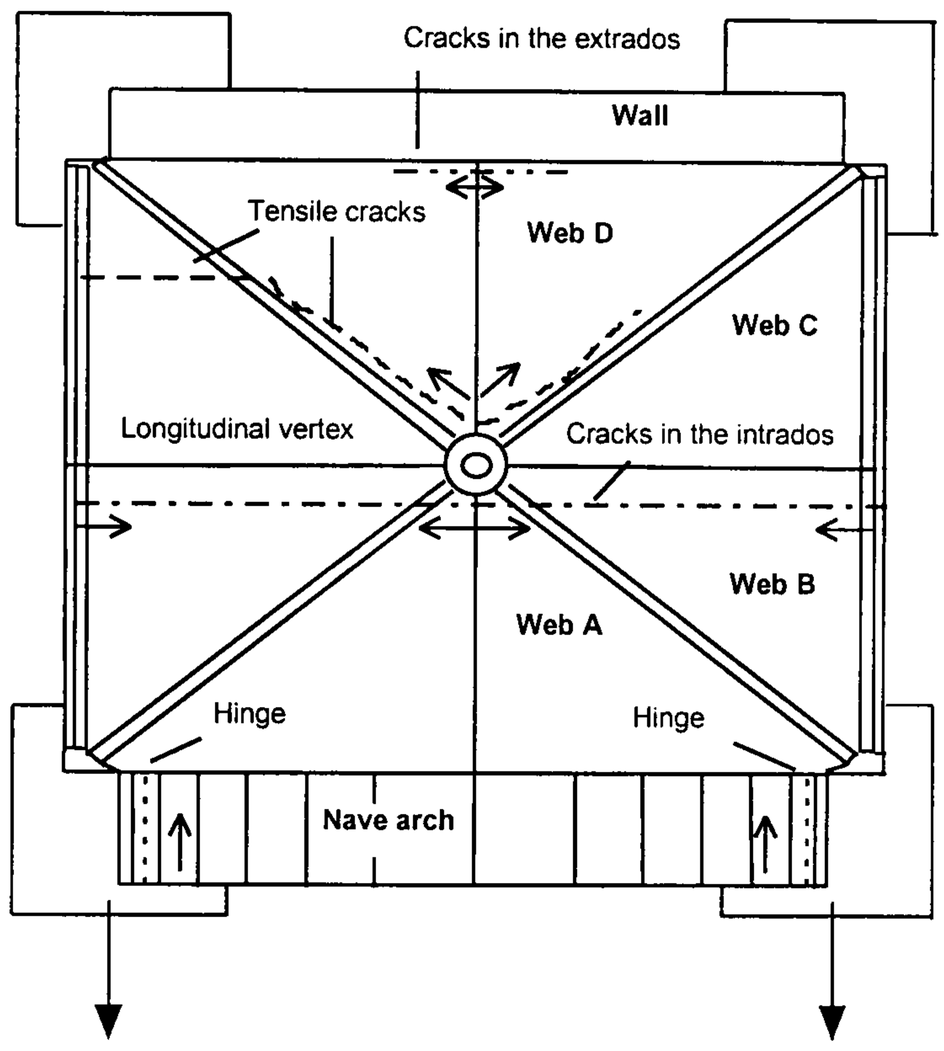

FIGURE 6.4 Crack pattern after 30 mm of abutments movement

6.2.3.1 The first cracks at the longitudinal vertex and the abutments

No cracks were observed until an abutment movement of 3 mm. At that stage, cracks initiated close to the keystone at the intrados, at the front side of the longitudinal vertex (Figs. 6.4 and 6.5). In later stages, cracks also developed at the other end of the vertex, at the crown of the transverse arches (Fig. 6.6). These cracks propagated slowly within the vault and finally formed a single fracture line. An examination of the strain close to the longitudinal vertex can offer some further insight to the redistribution of the loads that occurred (Fig. 6.3b). Tensile strains started increasing at the intrados (BB1V), while the

compression at the extrados was decreasing (BT1V), indicating the development of higher axial tensile forces. At 5 mm the hinge forming had further propagated within the longitudinal web after the ribs were fractured at the joint of their last voussoir with the keystone (Fig. 6.5).

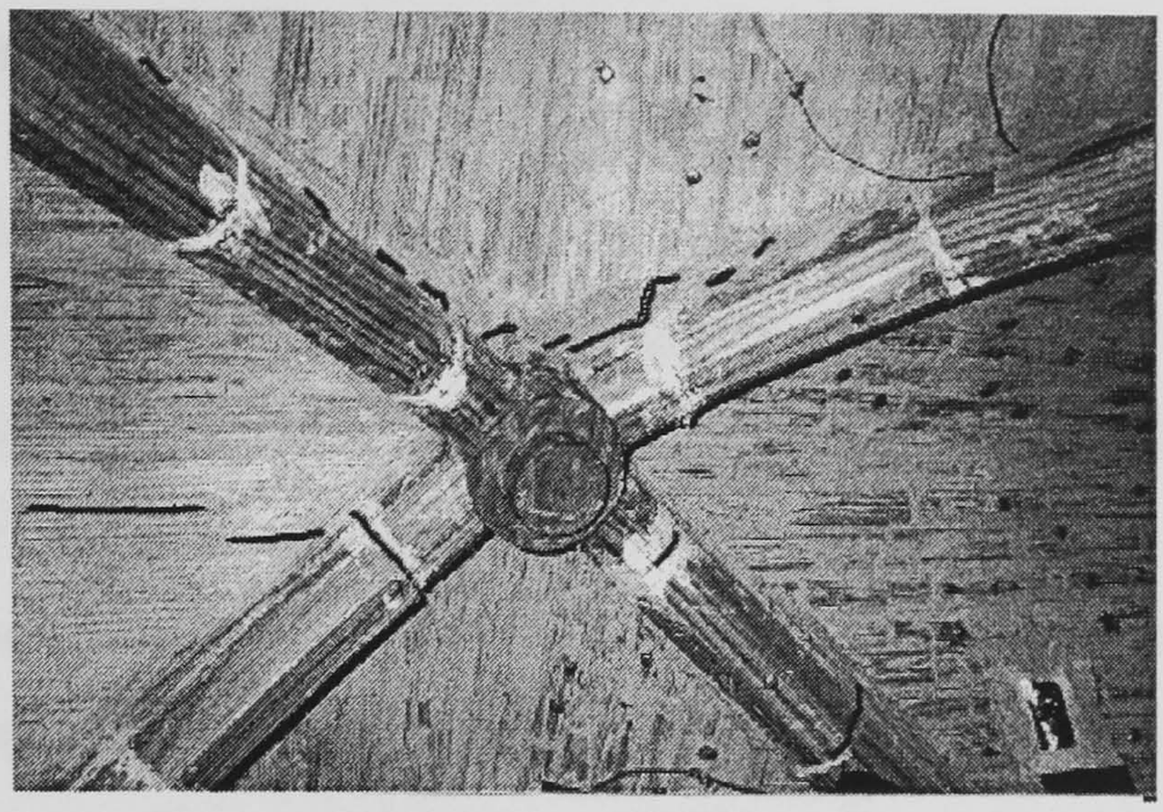

FIGURE 6.5 Initial crack formation at the intrados at the front side of the keystone

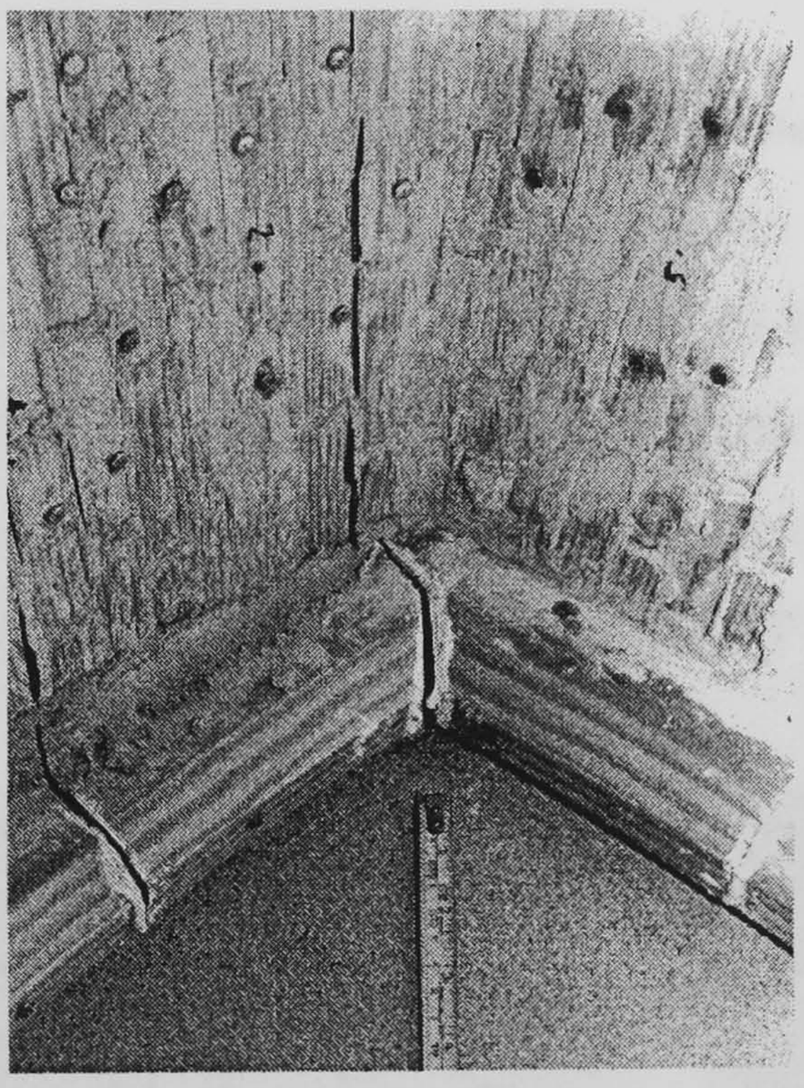

FIGURE 6.6 Crack at the crown of the transverse arch

It was possible to detect the associated transfer of load from the back to the front portion of the vault in the decreasing compressive hoop strains at the back side of the longitudinal vertex on web C, on both the extrados (CT1V) and the intrados (CB1V) surfaces (Fig. 6.3c). This redistribution occurred at a slower rate at the front transverse web

A, as the relatively moderate increase of the hoop strains can show (Fig. 6.3a). The nave arch functioned like a diaphragm-type support for the vault, yielding low deflections (Fig. 6.1a) and offering no resistance to forces or actions normal to its plane. A significant amount of load was already carried by this web, as was seen during the dead-load tests, and the changes in this amount were affected by the degree to which the nave arch reacted to the movement of abutments.

The upper half of the vault appeared to be sufficiently constrained by the arch and the small change of the deformation that was recorded indicated the area was acting as a rigid region. A more rapid change of the hoop strain was recorded at the area of the haunches which was directly affected by the movement of the supports (AT2V in Fig. 6.3a). Moreover, a change of curvature was observed compared with the response of the vault under dead load (especially test DL3 - Table 5.6). A similar development was recorded at the haunch of the longitudinal web B (gauge BB2V in Fig. 6.3b). The compressive strain increased at the initial stages, due to the propagation of the cracks and the associated redistribution of the load.

Regarding the response of the back transverse web D the rapid, compared to web A, increase in the compressive hoop strain at the extrados of the vertex (DT1V) and the low hoop strain at the haunches (Fig. 6.3d) can be considered as a consequence of the development of the independent behaviour of this web from the rest of the vault (Fig. 6.1a). The built-in support of this web upon the wall caused a reduction of the deflections in the area, with the development of higher strains at the upper part of the web.

FIGURE 6.7 Hinge at the base of the nave arch

Indications on the development of this fracture line at the front of the longitudinal vertex were already evident from the dead-load tests, where an area of high tensile strain was already detected. After the release of energy at this area, fracture needed to occur in other areas where high moments were expected to develop. As a result, another hinge started to form after a movement of 5 mm at the springing voussoir of the nave arch, spreading quite rapidly to the *tas-de-charge*, the base of the ribs (Fig. 6.7). Once the latter block was reached, the crack bifurcated to the joint between web A and the nave arch at the intrados (Fig. 6.8), while no fault was visible from the extrados.

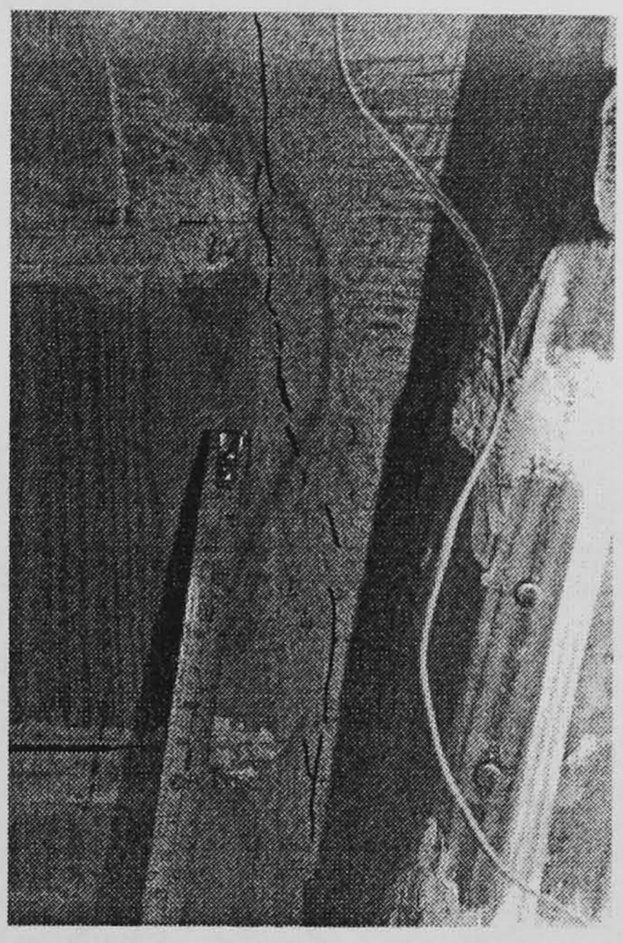

FIGURE 6.8 Crack at the joint between the nave arch and front transverse web A

6.2.3.2 Separation of the webs along the groins

After further increment of the movement of abutments, a third fracture line started developing at 8 mm at the back of the keystone, at the intrados (Fig. 6.4). This crack would then propagate along the groins towards the haunches and after 15 mm the whole depth of the joint between the rib and the back transverse web D was fractured, resulting in a net separation of the web from the ribs (Fig. 6.9). After this stage, the development of this crack was quite rapid and on the left portion of the vault, at the area of the haunch of the back longitudinal web C, the fault deviated within the shell. This crack penetrated into the whole section of the web and propagated until the transverse edge of the web (Fig. 6.4). The reason why a similar crack did not develop also at the right portion of the vault may be the result of local conditions at the groin, such as a weak mortar joint between the ribs and web C closer to the haunch that "channelled" the fault in that direction.

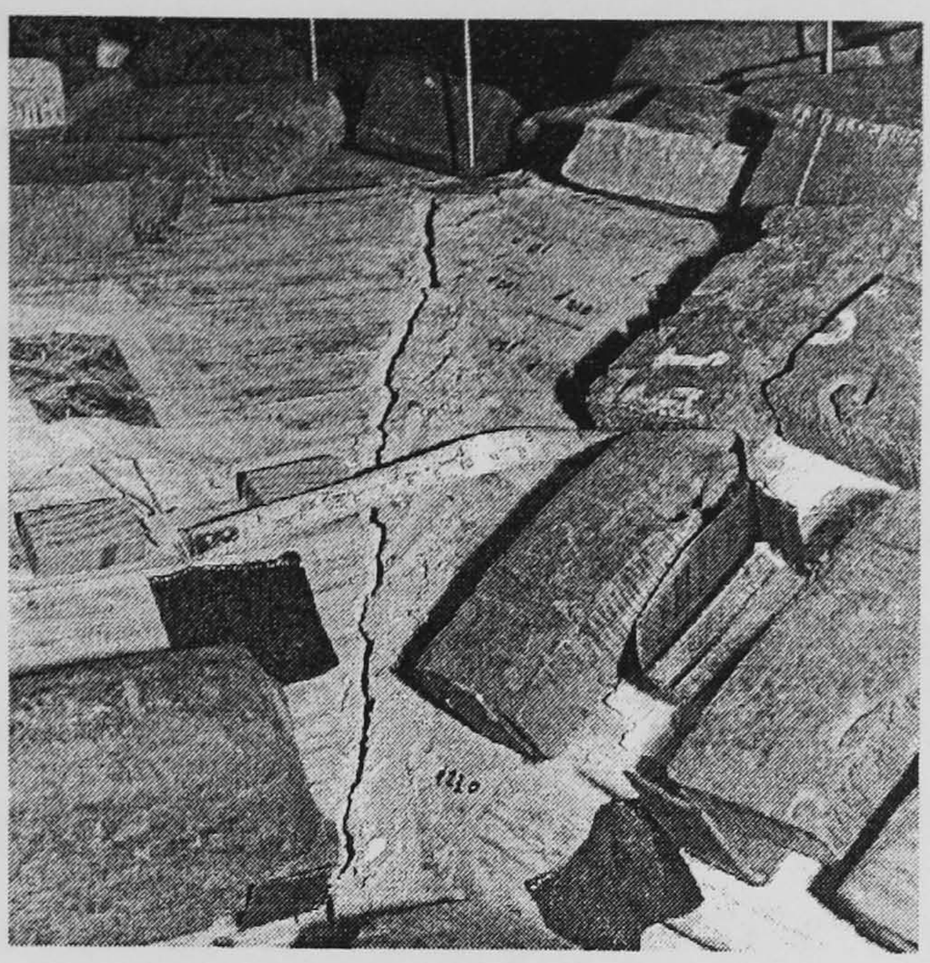

(a) Global view of the fault line

(b) The fault at the lower courses

FIGURE 6.9 The separation of the back transverse web D from the back groin, extrados

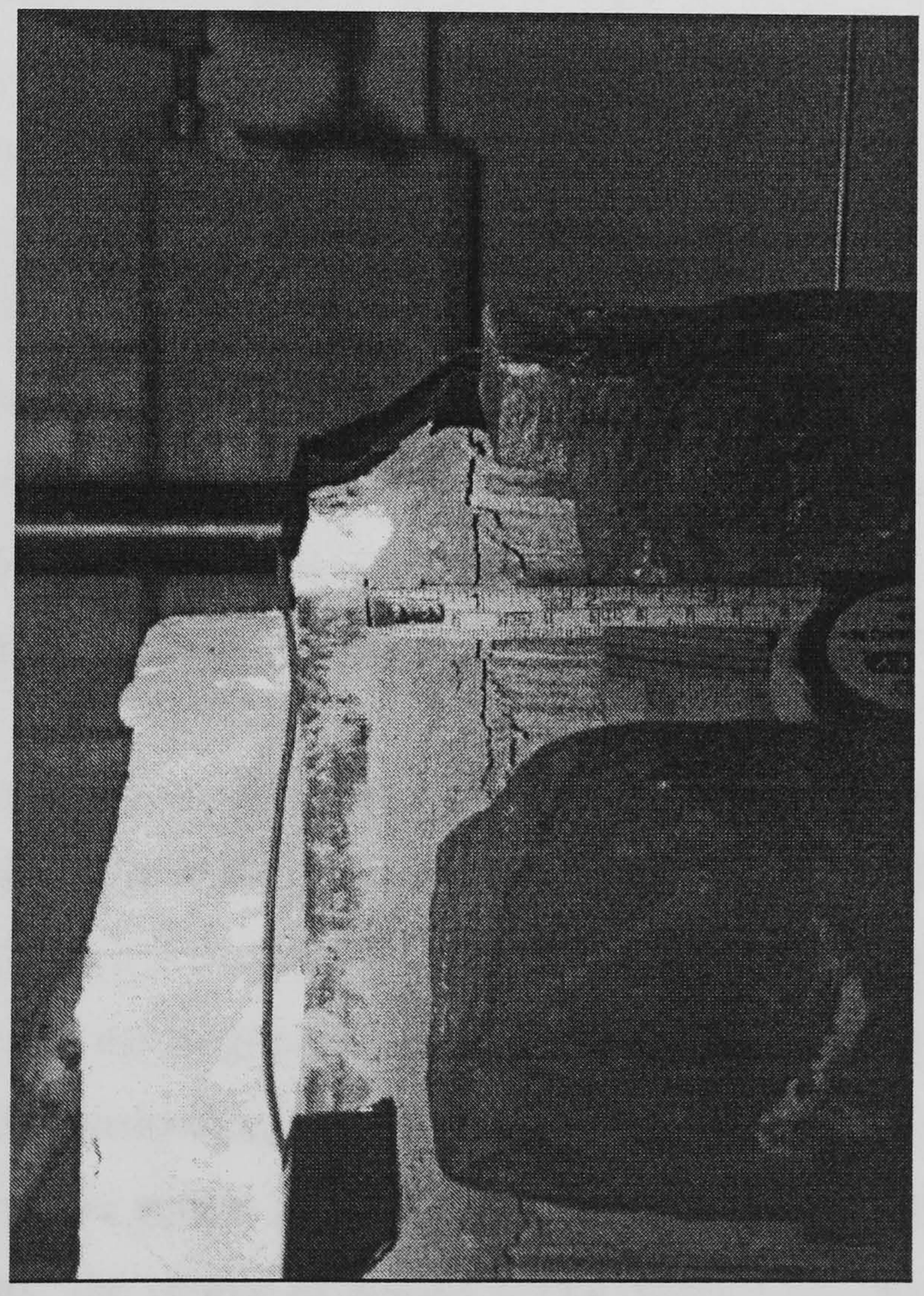

FIGURE 6.10 Cracks at the crown of the wall

According to the widespread accepted crack pattern of Fig. 1.16, this third fracture line was expected to occur not at the groins but at the joint of the vault over the wall, where

the higher strains and moments were developing. Indeed, hairline cracks formed at the extrados of this joint initiating around the crown after a movement of 5 mm (Fig. 6.4). Although they reached almost a third of the length of this joint, these cracks did not spread any further after energy was released at the area of the groins (Fig. 6.10).

It was possible to continue the abutments movement until 30mm (1/32 of span) without causing complete collapse in the structure. An essential characteristic in this vault was that the co-action between the webs and the ribs was achieved by the rebate on top of the rib and the construction of the vault around them (Figs. 1.9 and 1.12). Despite the width of the cracks, the webs could still rest upon the ribs underneath while the latter were sliding due to the movement of abutments, until the width of the voussoir was exceeded (cf. Fig. 3.18) and the webs could drop (Fig. 6.9).

It has to be noted that all cracks were concentrated at the joints and no failure of the blocks was observed. Overall, the formation of these three major cracks (base of nave arch, longitudinal vertex and back groin - Fig. 6.4) simply enhanced the deflections pattern observed in the early phase of this test. After a 10 mm movement, the deformation of the back transverse web D did not progress any more due to its separation from the rest of the vault (Fig. 6.1b). This was in sharp contrast with the rest of the symmetry vertex and the vault, where the deflections increased significantly as a result of the changing geometry and the redistribution of the load. The trend for the deflection of the rest of the vault was similar to the initial phase, increasing linearly with the abutments movement (Fig. 6.2).

So far as the effect of the crack pattern on the strains is concerned, the strain gauges at the front of the longitudinal crack for example (Fig. 6.3b) had already shown a maximum tensile hoop strain of $60x10^{-6}$ developing close to the crack, at the intrados in BB1V, at 8 mm. Consequently and as the longitudinal crack had spread to the whole length of the vertex and the ribs were visibly dislocating (Fig. 6.11), the tensile strain recorded started dropping to 0, while the compressive strains increased again at the extrados in BT1V. At the back of the longitudinal vertex, the couple of gauges CT1V and CB1V showed that the tension developing at the extrados had already dropped after 8 mm when the groin cracks were formed (Fig. 6.3c), representing the bifurcation of cracks within the left portion of web C.

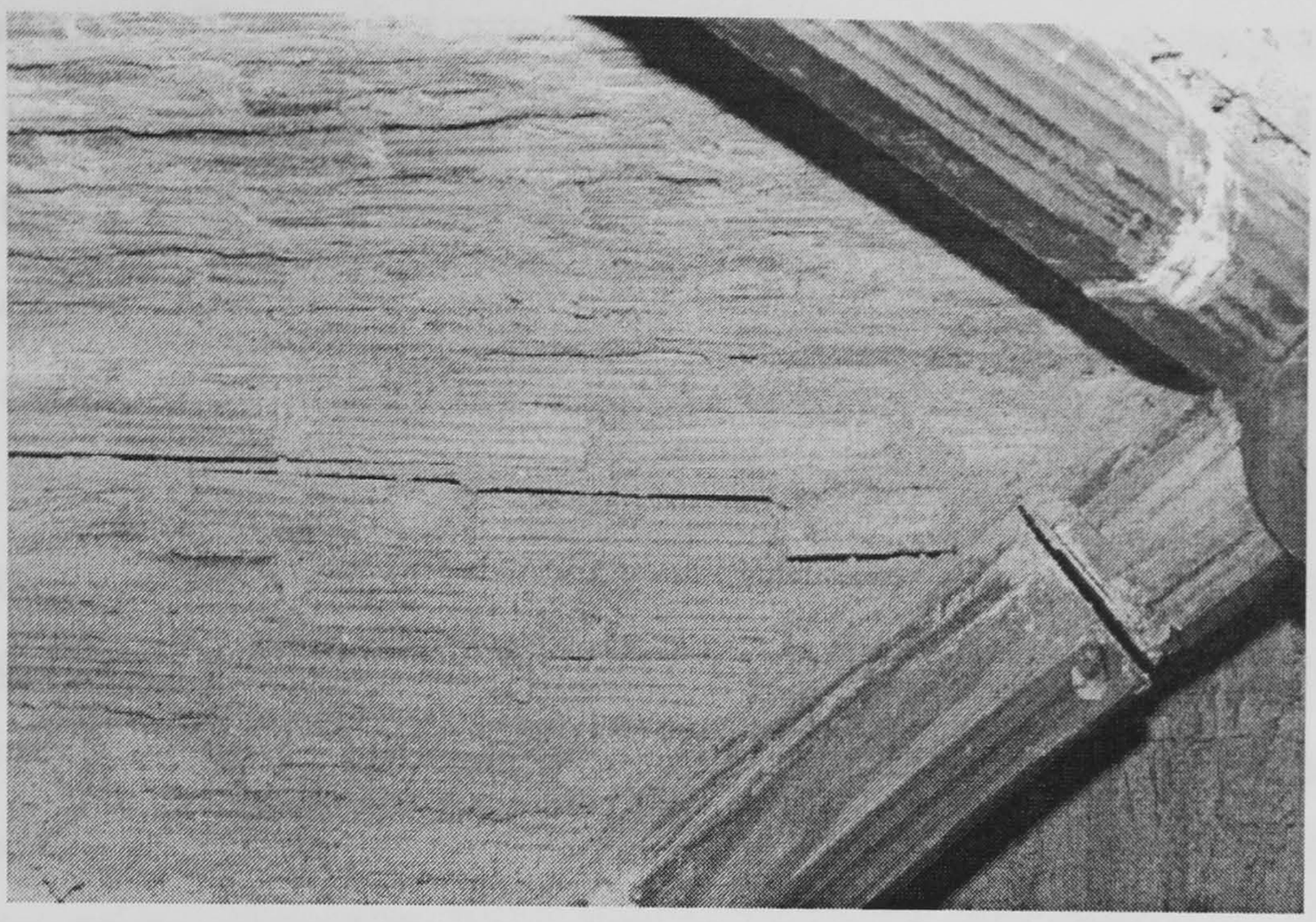

FIGURE 6.11 Dislocation of the ribs and propagation of the crack parallel to the longitudinal vertex

Contrary to the hoop strains, quite low values of horizontal strain were recorded at the intrados of the symmetry vertex (Fig. 6.3e). The strain gauges were located along the stiffer direction of the material and the assessment of the material properties earlier (§4.2) had shown a significant difference between the two orthogonal directions. Although the low magnitude of the recorded strain does not permit a safe interpretation of the behaviour of the vault in the area, the effect of the release of energy after the initiation of cracks at the back groin was more evident at the front symmetry vertex (AB1H).

6.2.4 Discussion

The crack pattern attained at 30 mm (Fig. 6.4) was sufficient to transform the structure into a mechanism. With reference to the widespread accepted crack pattern of Fig. 1.16, the fracture line at the front of the longitudinal vertex was formed first, at the area where the maximum bending stress was suggested by the deflection pattern for lower loads. As the longitudinal web was less stiff in the transverse direction of the vault than the transverse web, it could deform more and exert a relatively higher thrust to the front transverse web A. The latter web was constrained between the nave arch and the ribs and the function of this arch as a diaphragm allowed the web to work as a rigid body, so the hinge was formed starting from the weaker point of the arch, at its springings.

The pattern of Fig. 1.16 shows that such cracks can also propagate to the joint between the vault and the nave arch. Indeed, this could have occurred after the crack bifurcated to the joint, as the hinge at the base of the nave arch was progressing towards the support of the ribs. Most probably, the vault might have failed earlier, before this crack reached the crown of the transverse web A. Moreover, since the pattern of Fig. 1.16 describes the behaviour of a vault in its proper structural context, these early comparisons with the suggested behaviour from the prototype structures must take into consideration the corresponding boundary conditions. As a consequence, the hinge at the springing of the nave arch would not have opened to this extent, as the weight of the above-standing lateral wall would have been able to stabilise this plane (Figs. 1.5 and 7). Since this hinge opened relatively early, cracks might form eventually but it will be the effect of creep and further progressive distortion of the geometry that would make this area vulnerable.

A similar development was detected as expected in another area, the joint of the vault over the wall. Here the crack started at the crown of the wall but did not expand further once the vault was fractured in another weaker area, the joint along the groins.

The very low deflection of the nave arch (Fig. 6.1b) indicates the vault was supported almost symmetrically between this arch and the wall, but the maximum values were still recorded on the side of the vertex close to this arch, due to the hinge at its base. Although the longitudinal vertex deformed rather uniformly (Fig. 6.2b), the stiffer area of the haunches constrained the maximum deflections from spreading at the same rate over the whole of the transverse barrel (Fig. 6.12d).

The combination of the high deflections at the keystone, the weakness of the joint along the groin and the function of the back transverse web as a rigid region favoured the cracks expected at the wall to open actually at the back groins. For similar reasons, the cracks at the longitudinal vertex spreaded and joined at the front side of the keystone. The discontinuity at the back groin was quite visible and soon after the shell would be outside the width of the ribs upon which was supported, the collapse of the vault should occur.

6.3 FE ANALYSIS

6.3.1 Discussion of the FE model

6.3.1.1 Deflection pattern and geometric changes

The FE method was used to predict the deformed geometry of the structure and its crack pattern. The experiment had demonstrated the critical influence of the geometry of the groin, which can be examined between the two bounds established during the study of behaviour under dead load: joints between the webs and the ribs replaced with spring elements and a continuous, but smooth junction, modelled with shell elements. A nonlinear material and geometric analysis (NLMGA) was performed, using the failure envelope in biaxial bending (Sinha 1997) as introduced into Abaqus with the subroutine USDFLD in §4.3.3. This routine was suitably modified to account for the change in the material direction between the two intersecting webs. The supports were displaced in the global direction 2 (Y) by fixed increments of 1 mm until numerical failure at 33 mm.

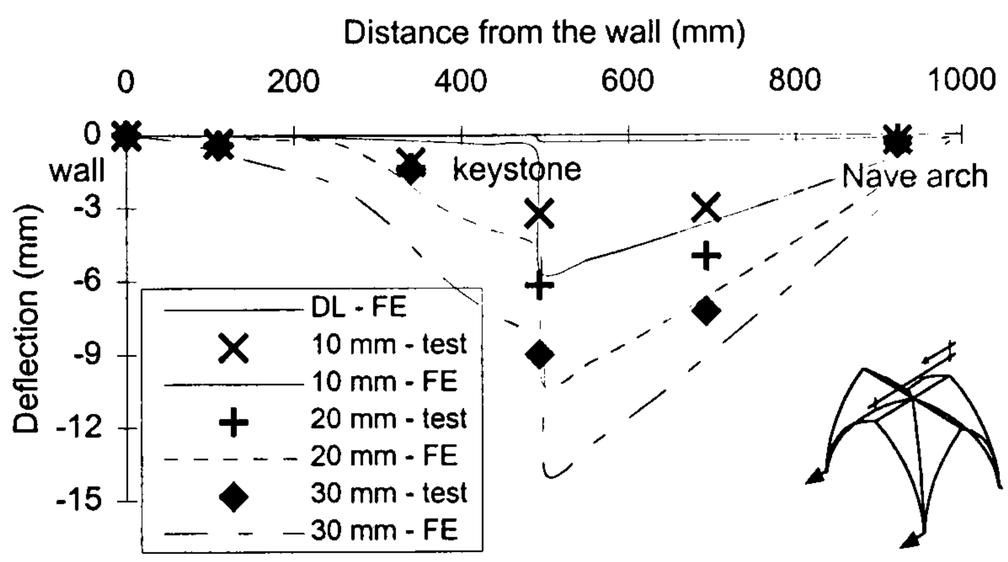

FIGURE 6.12 Modelling of the groin area with spring elements. Deflection of the symmetry vertex during the movement of abutments

The introduction of line spring elements between the webs and the ribs, acting in the direction linking the two nodes, precludes the development of part-through cracks along the groin. In this sense, this modelling may be treated as an upper bound solution to the problem similarly to the evaluation under service conditions. The FE model developed in §5.3.2.4 was suitably modified with the aid of the Fortran pre-processor to include the degradation of the stiffness matrix and the effects of the smeared crack approach on the webs. The deflection of the symmetry vertex (Fig. 6.12) during the movement of the abutments

confirmed the crucial role of the area of the groins. Due to the unconstrained degrees of freedom in the directions not normal to the ribs, the back transverse web developed almost immediately an independent behaviour from the rest of the vault, quite close to the detachment observed during the test.

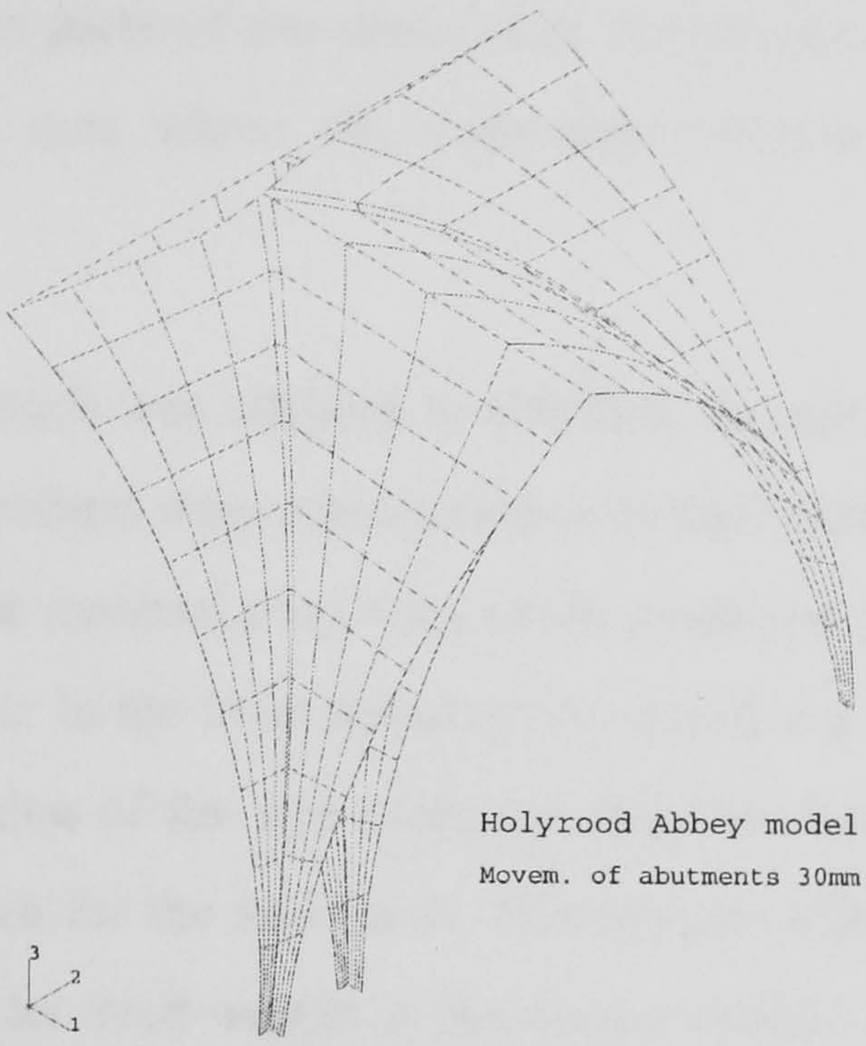

(a) Deformation of the vault at 30 mm

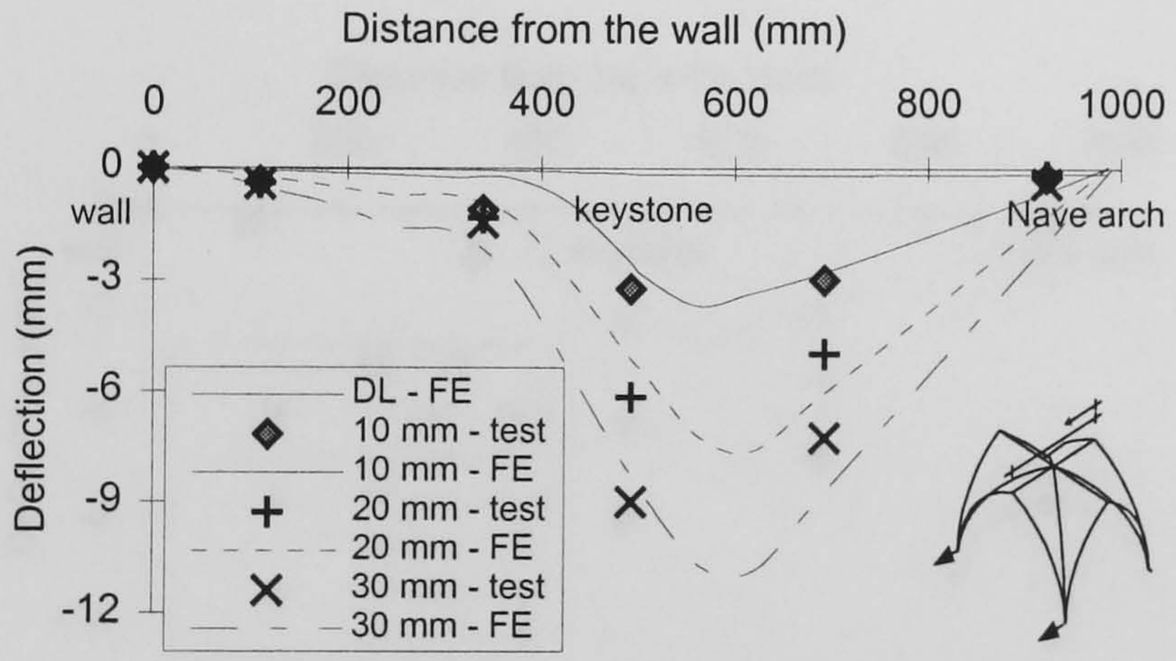

(b) Deflection of the symmetry vertex for the movement of abutments

FIGURE 6.13 Simulation of the groins with shell elements

The FE simulation of the ribs with shell elements of the same geometric and material properties during the modelling for dead load (§5.3.4.3) resulted in a geometry with a less sharp change of curvature between the webs. Using this model, the boundary conditions were not altered and failure was allowed initially to occur at the shell only. The deformed vault after a movement of 30 mm (Fig. 6.13a) showed a hinge forming at the front of the longitudinal vertex and the back transverse web D detaching from the rest of the model at

the back of the back groin, starting from the keystone. This response was a satisfactory approximation to the behaviour of the vault in the test and the locations of cracks observed. The release of web D from the rest of the vault transformed it gradually into a rigid region, as this can be confirmed by the low deformation of the most of the back portion of the symmetry vertex (Fig. 6.13b). Due to the smeared crack approach, there was no net separation between the two parts of the cross vault due to compatibility of deformations, even at the stage of 30 mm where the experiment showed web D became almost independent from the rest.

A more global approach was adopted to simulate the failure observed at the groins and the nave arch. Both members were represented with shell elements and their dimensions were chosen to yield similar material properties as the prototype (cf. Table 4.3). In addition, failure was allowed to occur in the hoop direction by specifying material properties similar to the corresponding direction of the web masonry: from the longitudinal web for the ribs and from the transverse web for the nave arch. This did not affect significantly the elastic behaviour of the model under dead weight as the elastic moduli in the hoop direction were quite similar.

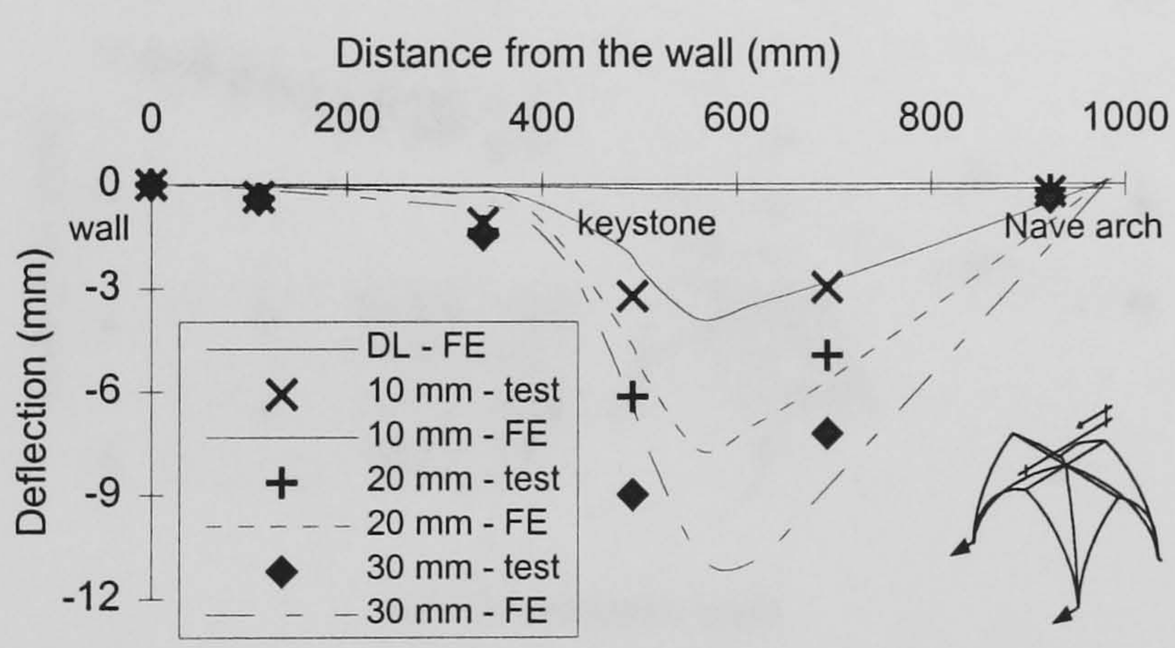

FIGURE 6.14 Simulation of the groins and the nave arch with shell elements: deflection of the symmetry vertex

The resulting deflection of the symmetry vertex for movement of 10, 20 and 30 mm. (Fig. 6.14) showed an improvement in the simulation of the deformation of the vault. An overall good agreement with the experiment was observed. The lower deformation of the back portion of the vault occurred to the same degree as in the structure, confirming the behaviour of the area as a rigid region.

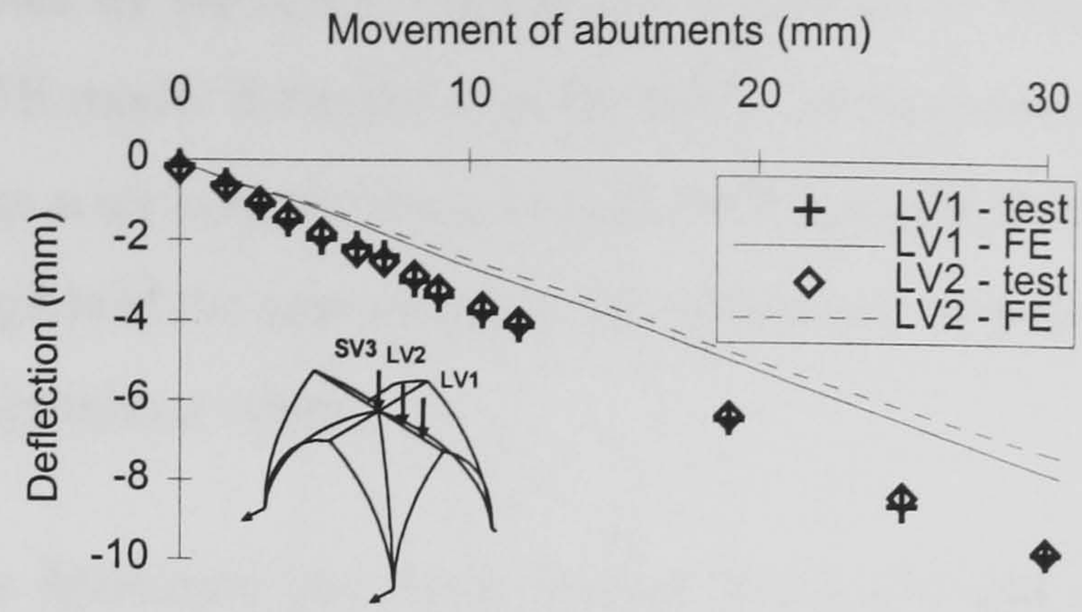

(a) Longitudinal vertex

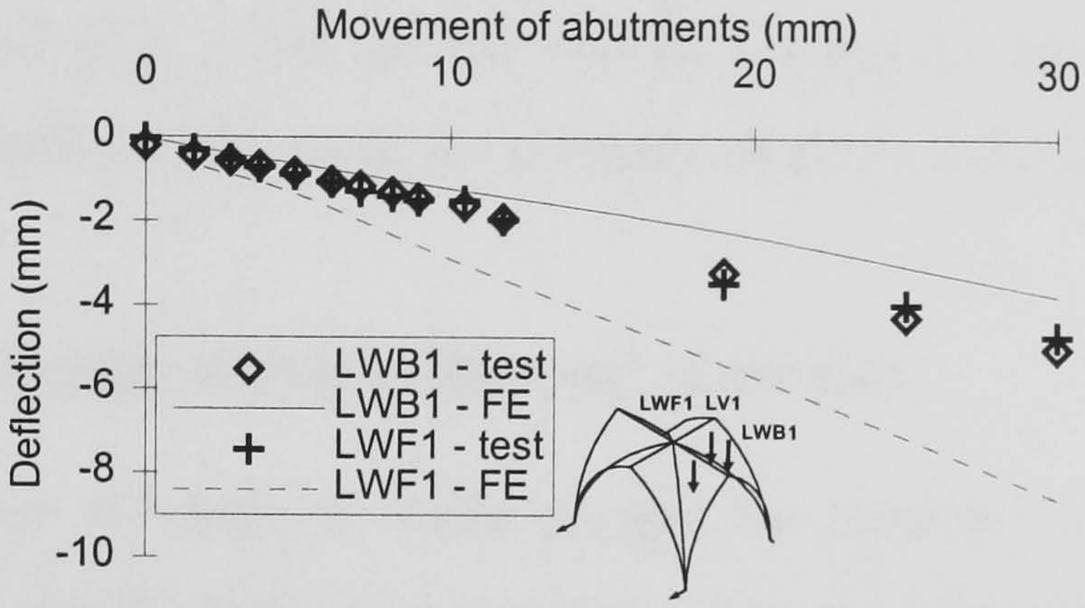

(b) Longitudinal web

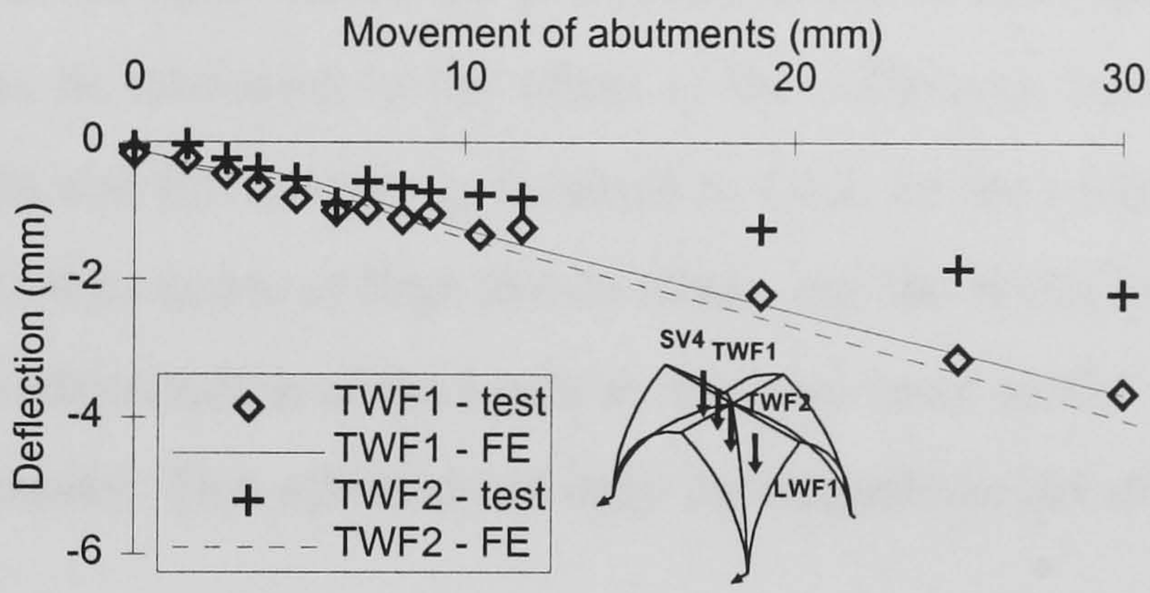

(c) Transverse web

FIGURE 6.15 Deflections of the longitudinal vertex and transverse and longitudinal webs during the movement of abutments. Comparison between the experiment and the FE model (refer to Fig. 4.12a for locations of the dial gauges on the vault)

The development of the deflections at the keystone and other critical locations on the vertices is displayed in Fig. 6.15. The successful prediction of the behaviour of the front portion of the vault by the FE model can be further verified at the longitudinal vertex (Fig. 6.15a) and the middle of the front longitudinal web (gauge LWF1 in Fig. 6.15b). The agreement at a section in the middle of the front transverse web (gauge TWF2 in Fig. 6.15c)

may be however affected by the rapid reduction of deflection in the proximity of the nave arch (Fig. 6.14). The FE model deflected more towards the front portion, while at the cross vault higher deflections were concentrating around the longitudinal vertex. The differences, however, can be negligible if the area of maximum deflections is considered within a wider context around the longitudinal vertex.

The trend of the deflection was linear for the first 5 mm and after a short nonlinear stage, they increased again linearly. During the movement of the abutments, the vault behaved increasingly as a one-way slab, spanning in the global direction 2 (Y), between the nave arch and the wall (Fig. 6.14), as this can be verified by the low variation in the deflection of the top portion of the vault in the longitudinal (X) direction (Fig. 6.15a).

6.3.1.2 Strain distribution and development of cracks

The development of strain in some gauges, as predicted by the FE model, is illustrated in Fig. 6.16 for the hoop direction and in Fig. 6.17 for the horizontal direction, together with the trend resulting when only geometric non-linearity (NLGA) was considered (§6.4.1.3). Contrary to the deflections, the prediction of the strain pattern by the FE model was poor and this can be attributed to the effect of the difference between the mechanical properties of the units and the mortar, as detected in §4.2. In the smeared crack approach, the cracks are simulated as zones of high tensile strain, but the brittle nature of the masonry would not allow the redistribution of the loads at the cross vault model to occur to the same degree as in the FE model. This affected not only the magnitude but also the pattern of the analytical strain.

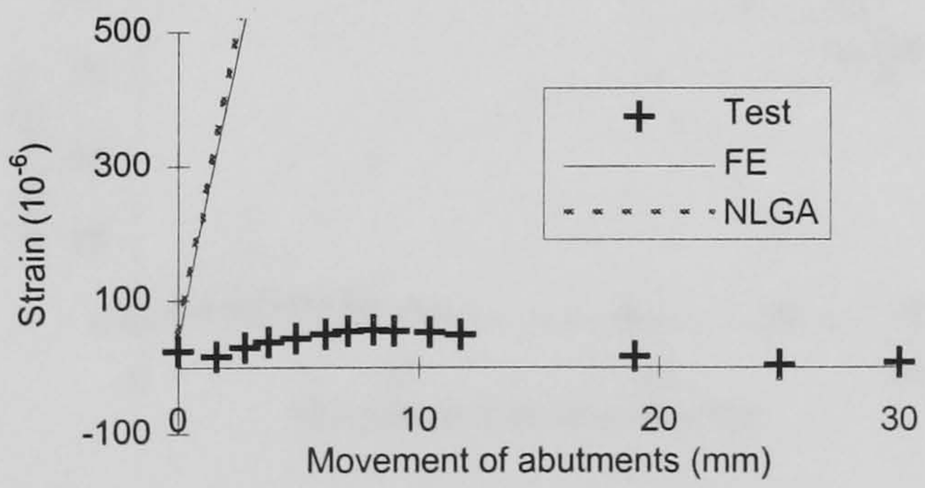

(a) Front of longitudinal vertex, intrados (BB1V)

FIGURE 6.16 Simulation of the groins and nave arch with shell elements. Development of hoop strain

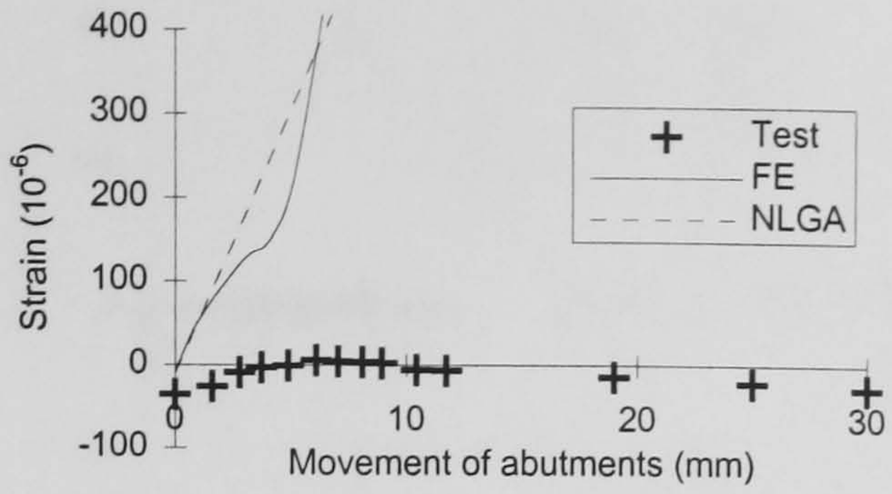

(b) Back of longitudinal vertex, extrados (CT1V)

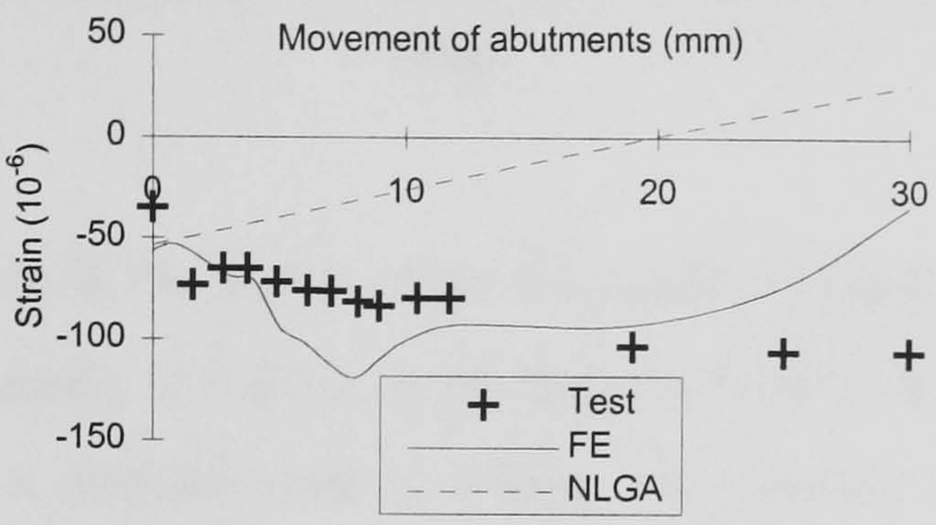

(c) Front symmetry vertex, extrados (AT1V)

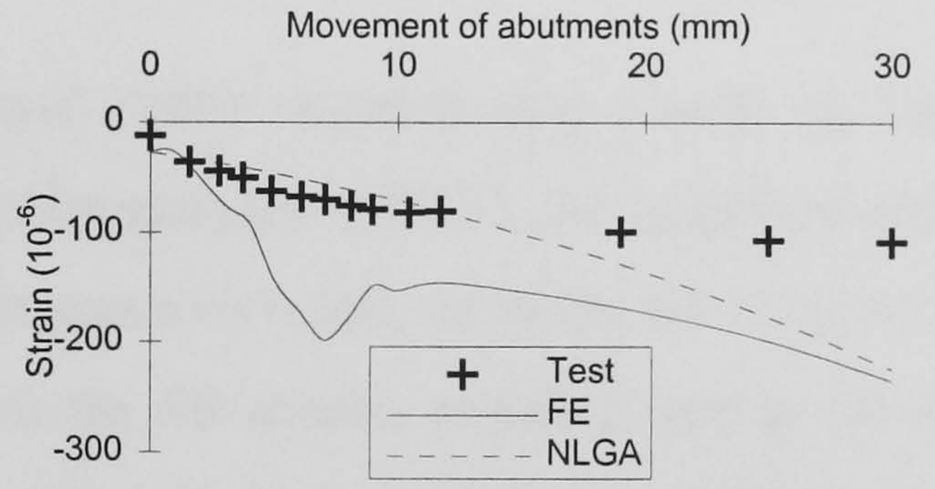

(d) Back symmetry vertex, extrados (DT1V)

FIGURE 6.16 Simulation of the groins and nave arch with shell elements. Development of hoop strain

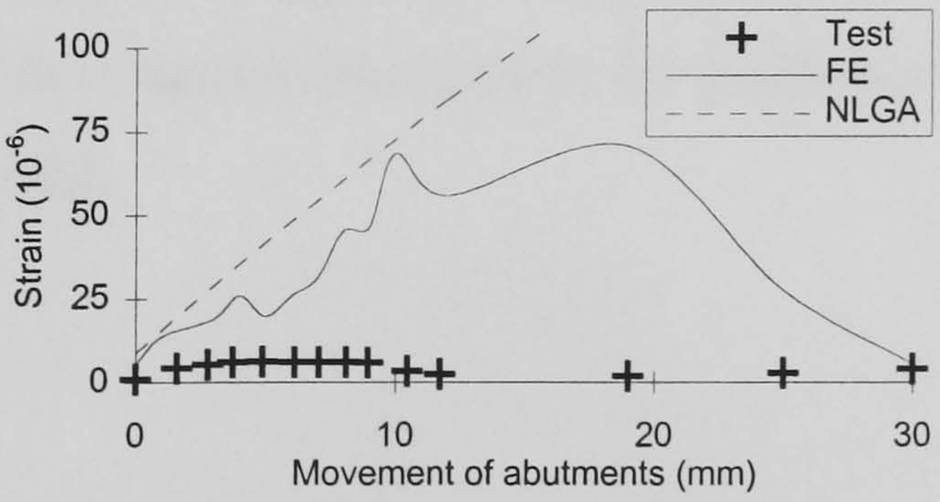

(a) Vertex of front transverse web A, intrados (AB1H)

FIGURE 6.17 Simulation of the groins and nave arch with shell elements. Development of horizontal strain.

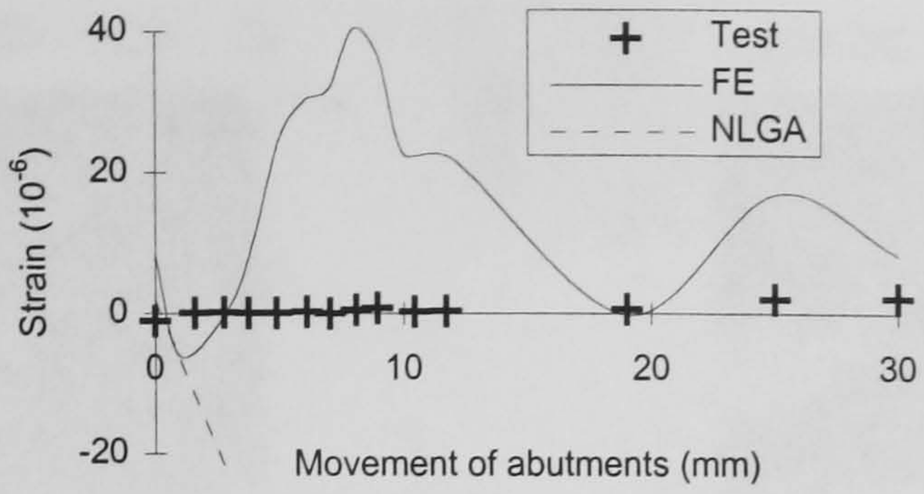

(b) Vertex of back transverse web D, intrados (DB1H)

FIGURE 6.17 Simulation of the groins and nave arch with shell elements. Development of horizontal strain.

A limited assessment of the ability of the FE model to represent the formation of the longitudinal crack can be made. Similarly to the test, the hoop tensile strain at the FE model in BB1V increased until a displacement of 5 mm, when failure of the section was quite advanced at the vault (Fig. 6.16a). The resulting loss of strength at the section was simulated by the FE model with a rapid inversion of the sign of strain after 5 mm.

This pattern developed almost symmetrically around the longitudinal vertex. On the other side of the vertex, at the extrados (CT1V), the analytical compressive strains became tensile following the abutments movement, as in the test (Fig. 6.16b). At about 5 mm, the strain increased sharply in the FE model, probably due to the development of smeared cracks, close to the stage when loss of strength was observed in the test at 8 mm when cracks started forming at the back groins.

The small variation in the hoop strain predicted by the FE model at the vertices of the transverse webs represented the progressive detachment and increasingly independent behaviour of these parts, as it can be illustrated in the location of the gauges AT1V (Fig. 6.16a) and DT1V (Fig. 6.16b).

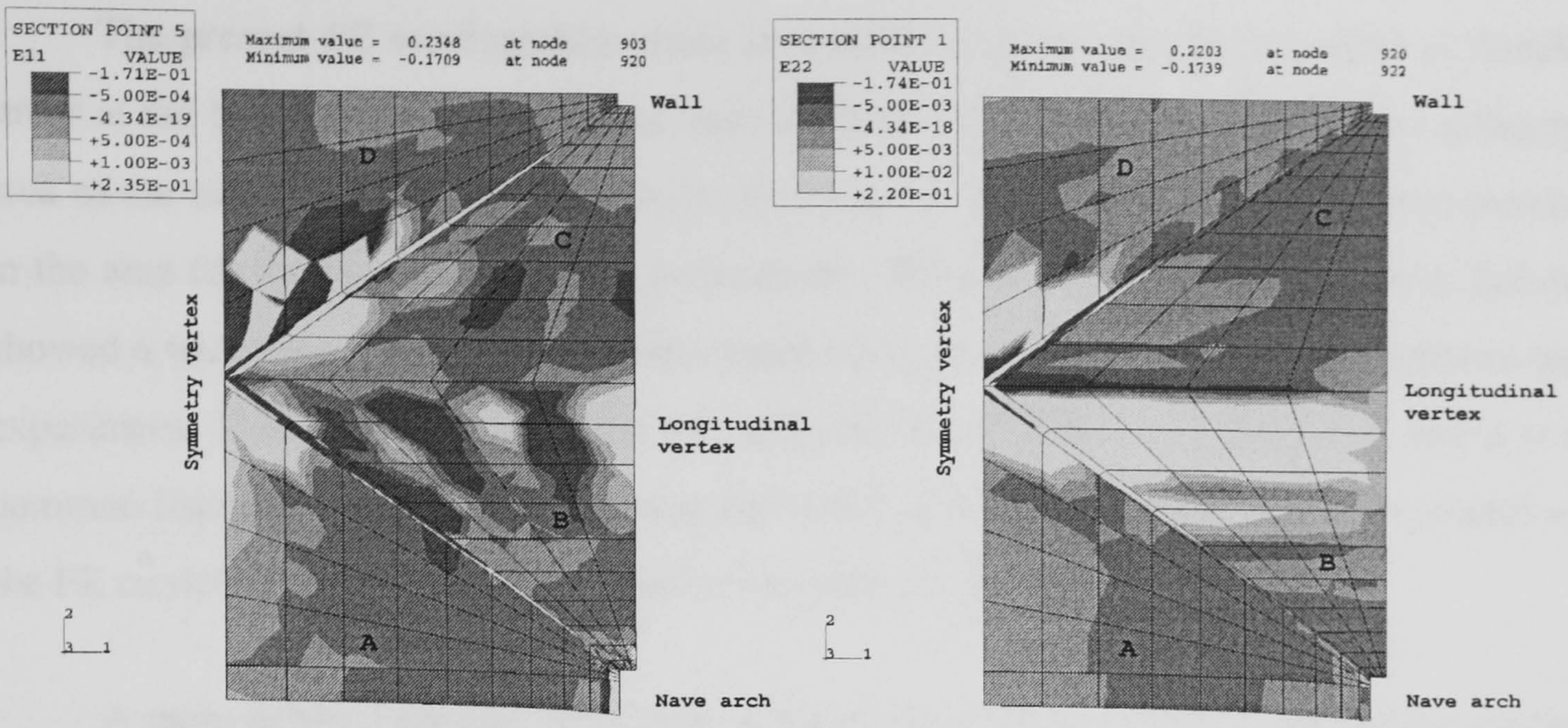

(a) Strain in direction 1 (E11) at extrados (b) Strain in direction 2 (E22) at intrados

FIGURE 6.18 Simulation of the groins and nave arch with shell elements. Strain at the FE model after an abutments movement of 30 mm (plan)

On the other hand, the areas where the FE model indicated smeared cracks would occur were in good agreement with most of the observed crack pattern (Fig. 6.4). Cracks from axial tensile forces were predicted normal to the keystone at the back transverse web D and they slowly propagated towards the back haunches (see back groin in Fig. 6.18). These cracks could eventually bifurcate and link with those at the back side of the longitudinal vertex, forming a fracture line crossing the entire vault (web C in Fig. 6.18b), symmetrical to the hinge at the front side although developing at a slower rate. In the model vault, these cracks were formed at a lower location, since the stem over the voussoirs could have acted as a barrier (Fig. 3.18) and this feature could not be simulated in these FE models. Cracks normal to the wall (Fig. 6.18b) had propagated much slower and were restrained into a quite narrow area.

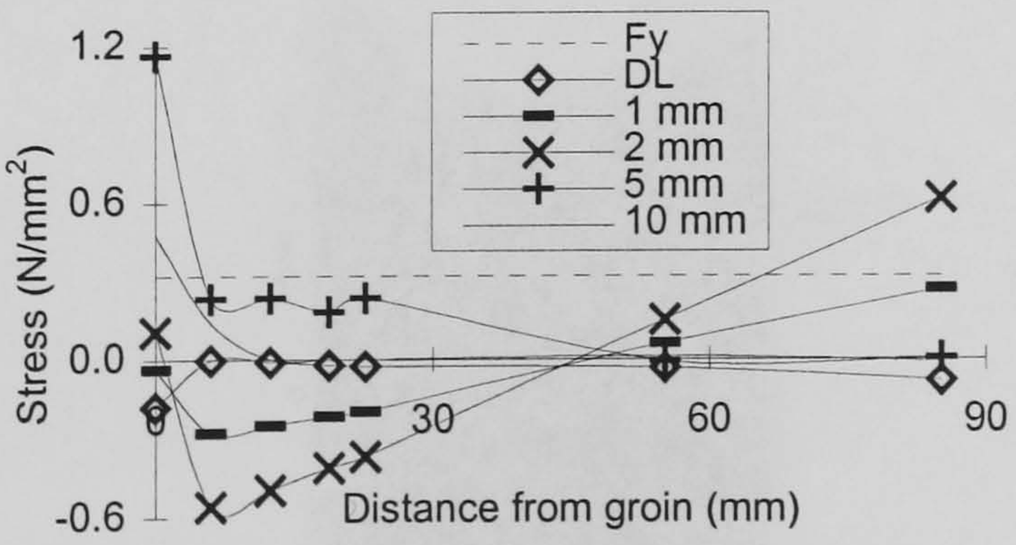

FIGURE 6.19 Simulation of the groins and nave arch with shell elements - failure at the abutment. Development of hoop stress at the base - extrados (cf. E11 in Fig. 6.18a)

The present FE configuration made it possible to detect the development of tensile stress at the base of the nave arch and trace the slow propagation of cracks to the adjacent area of the transverse web A. This can be illustrated in Fig. 6.19 by the hoop stress pattern in the area for the displacement of the abutments. The distribution of hoop strain at failure showed a wide area of tensile strain corresponding to the same area that was detected in the experiment. This hinge was an immediate effect of the movement of abutments and it is a common feature to cross vaults, as it was also detected by Jagfeld (2000) at the abutments of the FE model of an unribbed, cylindrical cross vault (Fig. 2.11).

A more detailed account on the rate in which the critical sections failed and the cracks propagated will be given in §6.3.4 where the behaviour of the vault is discussed.

6.3.1.3 Linear elastic range

During the discussion of the response of the vault, the vault showed clearly an almost linear trend up to an abutments displacement of about 5 mm. In order to assess the range of the elastic response of the vault, material nonlinearity (NLMGA) was deactivated in the FE model, leaving only the effect of geometric changes (NLGA). The linear elastic development of strain for some of the gauges positions was plotted together with the FE results for NLMGA in Fig. 6.16 and 6.17. A common trend with the NLMGA was observed up to a movement of 5 mm, which marked the overall elastic limit of the behaviour of the FE model, although in some cases deviations from the NLGA started almost immediately.

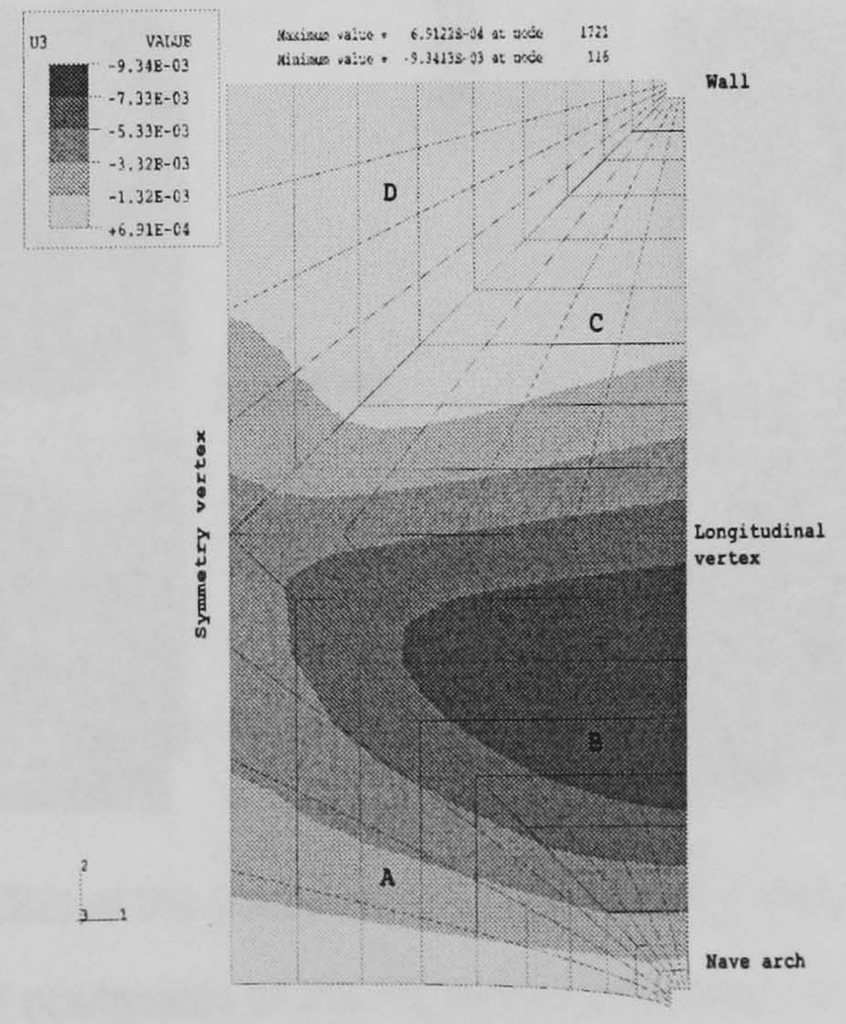

FIGURE 6.20 Non-linear geometric analysis (NLGA). Vertical displacement of the vault at 30 mm.

At the displacement of 30mm, which was considered to mark the ultimate limit state of the vault, the deflection of the FE model (Fig. 6.20) was almost half the experimental or the values from the FE model in NLMGA (Fig. 6.14). The pattern of deformation of the vault, without considering the effect of material non-linearities, concentrated rather around the outer side of the front portion of the longitudinal web B, closer to the transverse arch.

6.3.2 Boundary conditions

During the analysis under dead load (§5.3), the application of lateral constraints to the transverse edges of the FE model had almost no effect on the behaviour of the structure. Similarly, any activation of lateral constraints in the course of the movement of the abutments did not alter the distribution of loads, due to the pronounced one-way response of the vault. Moreover, the effect from a fixed support at the wall edge of the FE model during the dead load case was confined at the back transverse web D (§5.3.4.4) and a similar observation was made also in this phase of loading.

Concerning the application of the displacement of the abutments, in order to detect the extent of the area directly affected, an upper bound was established by considering the movement acting upon the whole of the first voussoir of the nave arch and the base of the ribs (the *tas-de-charge*). This unit corresponded to the first row of elements at the front base of the model and the movement was applied to all the nodes in the same manner as before.

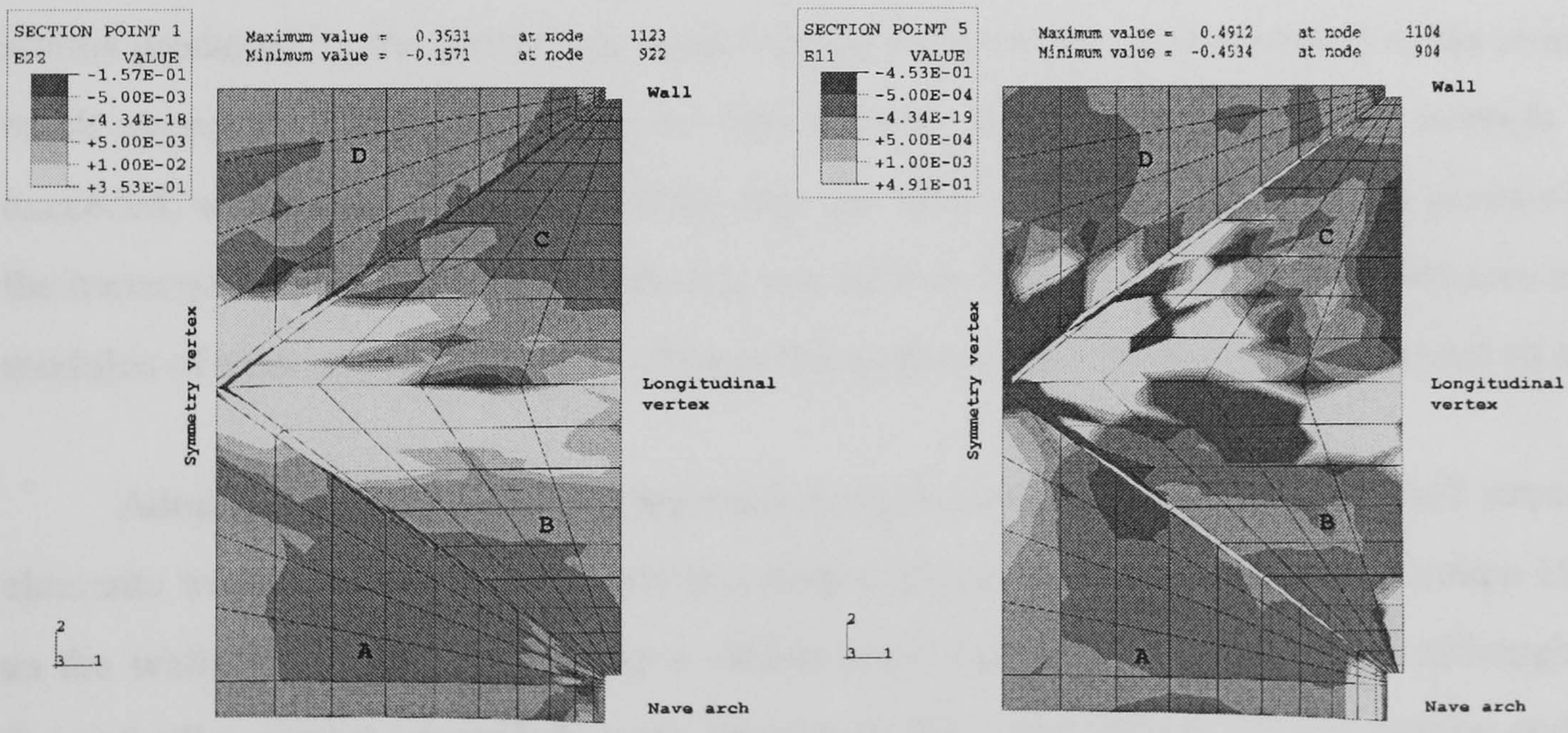

(a) Strain in direction 2 (E22) at the intrados (b) Strain in direction 1 (E11) at the extrados

FIGURE 6.21 Movement of abutments of the FE model involving the whole *tas-de-charge* (28 mm)

Numerical failure of the FE model occurred at an earlier stage, at 28 mm. Overall, as the action affected a larger area of the model, failure propagated more rapidly than in the previous models (Fig. 6.21). The area of higher deformations spread into a wider area around the longitudinal vertex (Fig. 6.21a), although in general terms the deflection pattern of the structure was not altered. The wider extent of this zone, however, resulted in a slower rate in the detachment of the back web D and the earlier development of an independent behaviour at the front web A. This was further assisted by the rapid formation of the hinge, immediately above the *tas-de-charge* (Fig. 6.21b) and not at the base (Fig. 6.18a).

Overall, the study showed it is reasonable to expect a monolithic action of the *tas-de-charge* during the imposed movement. This behaviour of the base became more evident during the test at the extreme stages, as a result of the hinge that formed at the joint between the first two voussoirs. The earlier formation of the hinge at the abutment in this simulation caused the hoop component of the stresses along the back groin to prevail during the detachment of the back transverse web D from the rest of the model (Fig. 6.21b). The significance of this observation is further discussed during the assessment of the response of the vault in §6.5.

6.3.3 Micromodelling approach

The high difference in the magnitude of strain at the longitudinal web that was observed between the vault and the FE model was the result of the averaged stresses and strains produced by the continuous model (§4.2). Furthermore, in the context of the smeared crack approach, failure could not be concentrated at the joints and, after strength was exceeded, wider areas entered gradually into the fully plastic domain that was assumed for the material. The homogenisation process was further compromised by the differences in the modulus of elasticity and strength between the units and the mortar, as was assessed in §4.2.

Adopting a micromodelling approach is more suitable for the case of small structural elements where a strongly heterogeneous state of stress and strain occurs (Lourenço 1998), as the wallettes in §4.2. Following a similar procedure for the entire vault, although not theoretically correct, provided some insight to the development of the cracks and the redistribution of stress in the immediate area. The FE model and the material properties were already adjusted to the problem in §5.4.4 during the analysis for dead load, increasing

the mesh density and using the 4-noded S4R5 elements instead of the 9-noded S9R5, and the results were satisfactory (Fig. 5.30). As in the case of the wallettes (§4.2.4), failure was concentrated at the joints and was simulated with a smeared crack approach (Sinha 1997). The brittle elastic mortar was modelled as an isotropic, linear elastic - perfectly plastic material and the maximum stress failure theory was used (Fig. 4.6), implemented in Abaqus with the USDFLD subroutine (§4.3).

Since it was not possible to apply the displacement of the abutments at constant increments like before, the modified Riks method, as provided by Abaqus, was used. The algorithm uses the proportion of the loading to be applied as an additional unknown and the increments taken along the load-displacement response curve are defined accordingly. This lead to very small internal increments, causing a very slow rate of convergence of the numerical solution. Eventually, it was not possible to displace the abutments for more than 5 mm, as the highly warped elements of the joints caused incompatibility of deformations with the adjacent units and the FE solution failed to converge.

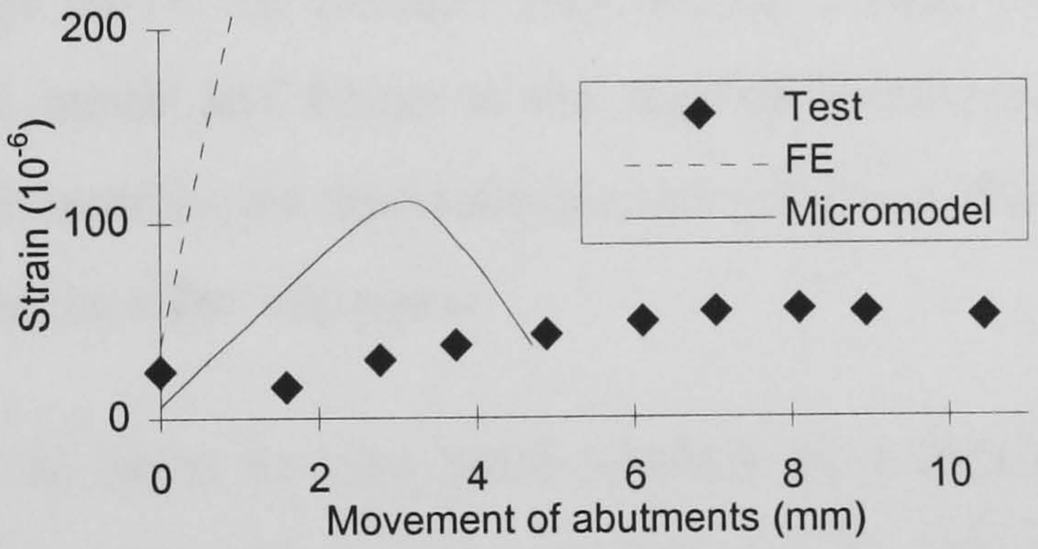

(a) Front side of longitudinal vertex, intrados (BB1V)

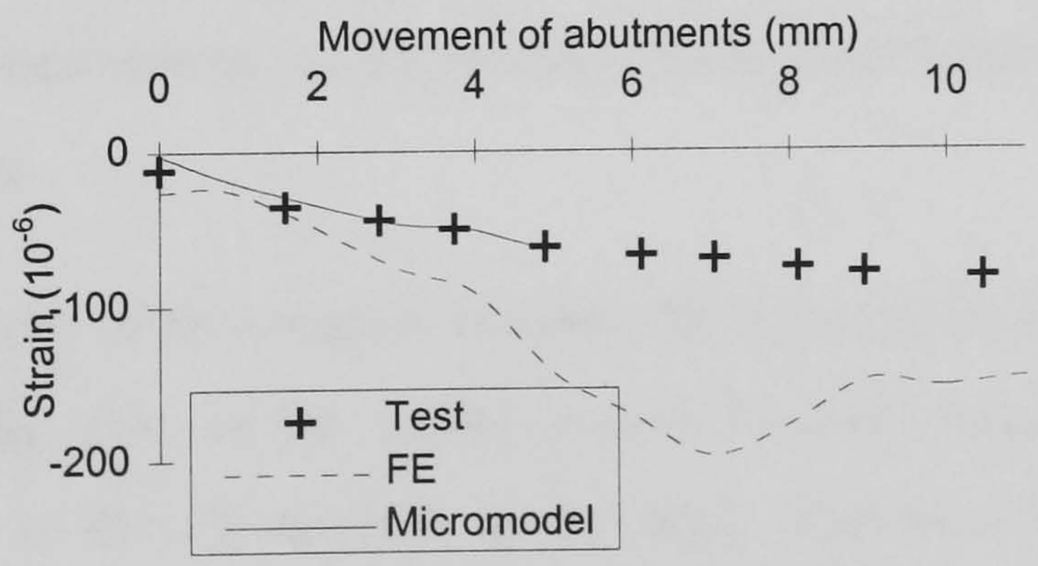

(b) Back transverse vertex, extrados (DT1V)

FIGURE 6.22 Development of hoop strain at the FE micromodel during the movement of the abutments

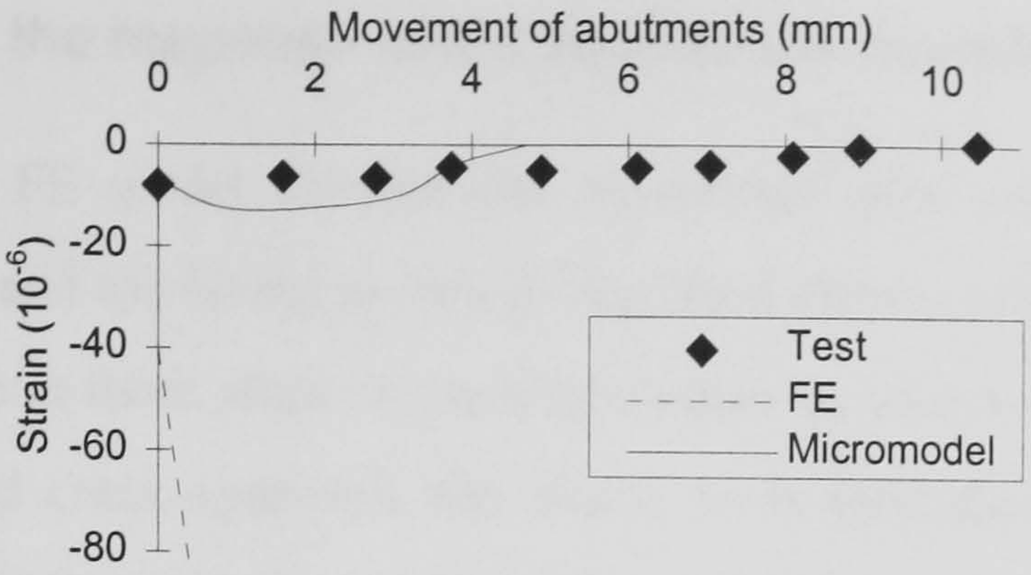

(c) Back side of longitudinal vertex, intrados (CB1V)

FIGURE 6.22 Development of hoop strain at the FE micromodel during the movement of abutments

This movement of the abutments coincided with the final stages of the elastic domain as was observed during the experiment (Fig. 6.3). The deformation of the model was in good agreement with both the experiment and the previous FE model, as the deflection of the keystone can show (1.38 mm evaluated against 1.469 mm of the test). Most importantly however, the strain recorded at the units had a magnitude similar to the experimental values, while the pattern of response was maintained and failure propagated rapidly in similar areas. In the case of the gauge BB1V for example (Fig. 6.22a), a rapid increase of tensile stress was recorded at the FE model and failure at the adjacent mortar joints occurred at only 3 mm of movement. Subsequently, the strain dropped as in the test, due to the release of stress and the load shedding to the other direction.

The agreement was better in other areas where a more homogeneous state of stress was observed, as in the case of the back transverse web D. The FE model captured the progressive detachment of the web from the rest of the vault (increasing compressive hoop strain at gauge DT1V in Fig. 6.22b). As there were no significant changes from the pattern established in the previous continuous FE model, similar observations can be made for most of the rest of the gauges.

The incompatibility of deformation between the adjacent areas of the units and joints due to the high bending stress at the central area of the vault could not conform with the principal assumptions of the FE method, as the early numerical failure indicated. Other issues, like the high density of the mesh and the high computational load required, limited further the practical significance of this modelling. Further research is therefore required in the proper modelling of the structure using interface elements at the joints or a more sophisticated numerical implementation of the failure criterion (Lourenço 1997).

6.3.4 Discussion of the response of the vault to the movement of abutments

The continuous FE model showed the importance of a correct simulation of the geometry of the groin and the lateral arches. Using shell elements for the purpose, allowed the failure to propagate in these areas in a similar manner as observed during the test. In the context of the smeared crack approach, the cracks were identified as areas of excessive tensile strain and this model correctly predicted the appearance of a fracture line at the front side of the longitudinal vertex (intrados), of a membrane crack at the back groin and a hinge at the front haunches (cf. Fig. 6.4). Good agreement was observed in the deflections of the vault, which confirmed the asymmetric development of maximum values at the front of the longitudinal vertex (Fig. 6.14). Another feature that was successfully predicted was the progressive detachment of the back transverse web D from the rest of the vault along the groin at about the same stage as in the test.

The effect of the difference between the mechanical properties of the constituent materials, as detected and discussed in §4.2, constrained the prediction of the strain development, although in many cases a good agreement in terms of trend was observed. On the other hand, due to the smeared crack approach, failure spread rapidly to the adjacent areas, with possible implications for the response of the structure. These are, however, implicit drawbacks of this analytical approach, which can be interpreted by studying the evolution of the pattern rather than the ultimate state at collapse. Other side effects of the method can be observed at the propagation of cracks within the back longitudinal web C after initiating along the back groin. On the right-hand half of the structure, this occurred at a lower location, since probably a local defect of the rib stem joint compromised the role of this feature as a barrier, while it appeared to be so on the other half (Fig. 6.4).

6.3.4.1 Redistribution of the loads

Incorporating reasonable assumptions, the FE model verified the one-way behaviour of the vault, in the transverse direction. Further aspects of the response of the structure to the imposed geometric changes can be examined through the discussion of the modified FE model. This will be assisted by further studies on the sensitivity of the FE solution to some significant factors, like the material properties and the geometry of the structure (§6.5), similarly to the assessment carried out for service loads in §5.4.

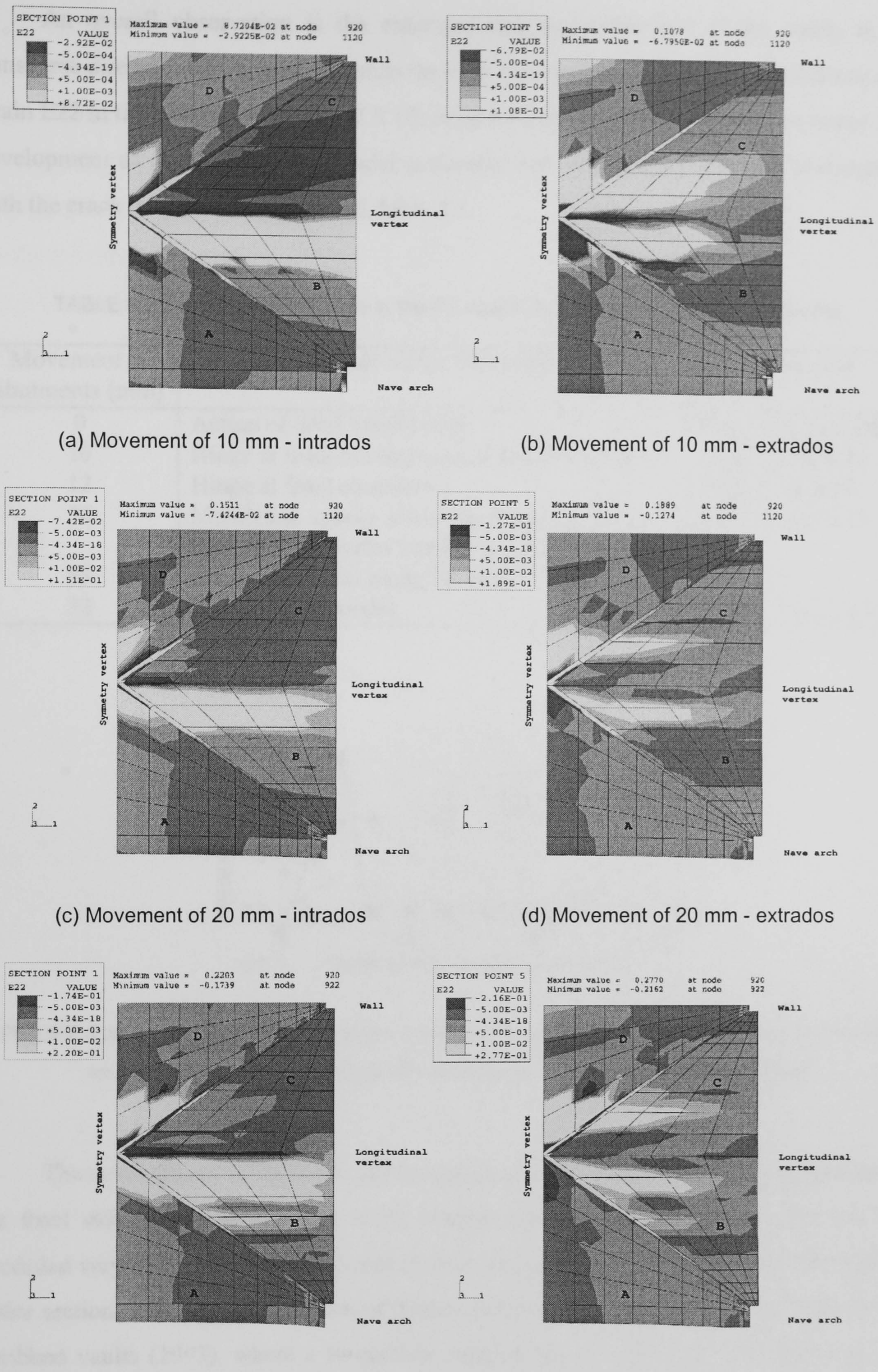

(a) Movement of 10 mm - intrados

(b) Movement of 10 mm - extrados

(c) Movement of 20 mm - intrados

(d) Movement of 20 mm - extrados

(e) Movement of 30 mm - intrados

(f) Movement of 30 mm - extrados

FIGURE 6.23 Strain E22 in the global 2 (Y) direction developing at the FE model during the movement of abutments

An overall observation is the enhanced one-way behaviour of the vault, in the transverse direction which spans between the nave arch and the wall. Fig. 6.23 illustrates the strain E22 in this direction (the global Y (2) axis) for both the intrados and the extrados. The development of failure in the FE model is summarised in Table 6.2 and can be compared with the crack pattern in Fig. 6.14 and Table 6.1.

TABLE 6.2 Development of failure in the FE model during the movement of abutments

Movement of abutments (mm)	Effect on the FE model	Reference
0	Action of dead weight only	Fig. 5.25, Test DL4
10	Hinge at front of longitudinal vertex (intrados)	Figs. 6.23a, 6.24
12	Hinge at front abutment	Figs. 6.18, 6.19
20	Membrane cracks along back groin; cracks at back of long. vertex already extensive at 10 mm	Figs. 6.23d, 6.25
33	Extensive cracks along the wall	Fig. 6.35
33	Failure of FE model	Figs. 6.23e, f; 6.37

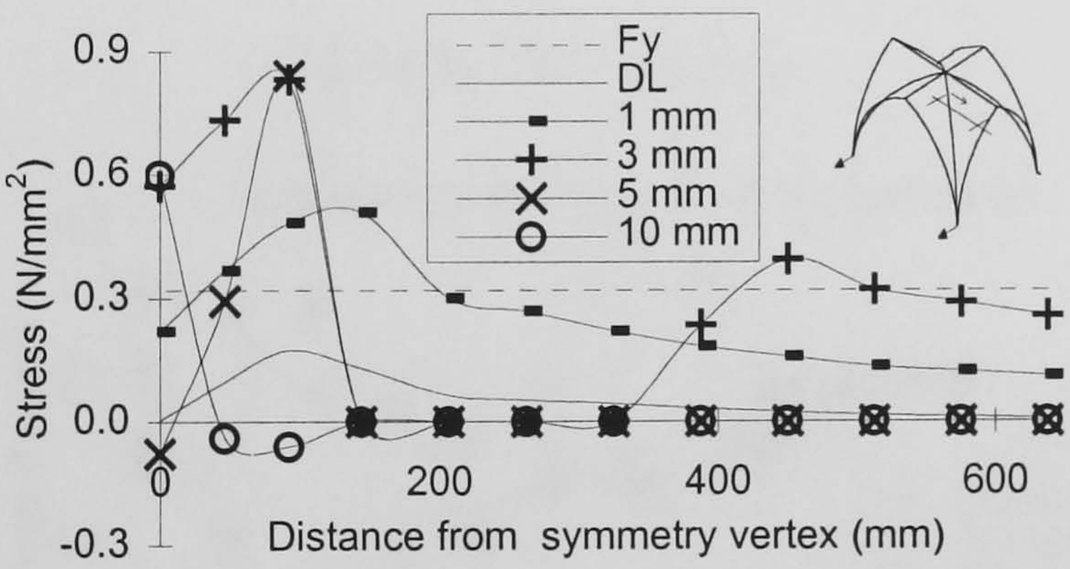

FIGURE 6.24 Development of stress in the hoop direction, intrados, in a section at the front of the longitudinal vertex due to movement of abutments (cf. strain E22 in Fig. 6.23a)

The development of failure as can be assessed by the distribution of the hoop stress at the front side of this vertex (Fig. 6.24) showed that the strength in that direction was exceeded very early and after only 5 mm of movement no stress was transmitted through the entire section. This rapid progression of failure confirmed earlier observations by Barthel on unribbed vaults (1993), where a no-tension material was assumed (§2.3.5). However, the higher amount of abutments displacement that was required in this model was a result of an improved modelling of the reserves in strength of the masonry (see failure criterion in Fig. 4.6) and demonstrates the beneficial role of the ribs.

The rapid progression of failure at the section was probably due to the smeared crack approach, as it is not reasonable to expect an extent of the crack pattern to such a degree after this moderate support displacement. The discrepancies with the FE model recorded on either side of the longitudinal vertex can be further attributed to this feature, as the model managed to capture the experimental trend at the earlier stages. The absence of masonry crushing during the test showed the compressive strength of the vault was never exceeded. No provision was made in the analysis for failure at the compressive domain and the good agreement with the test verified the low influence of these forces to the safety of the vault.

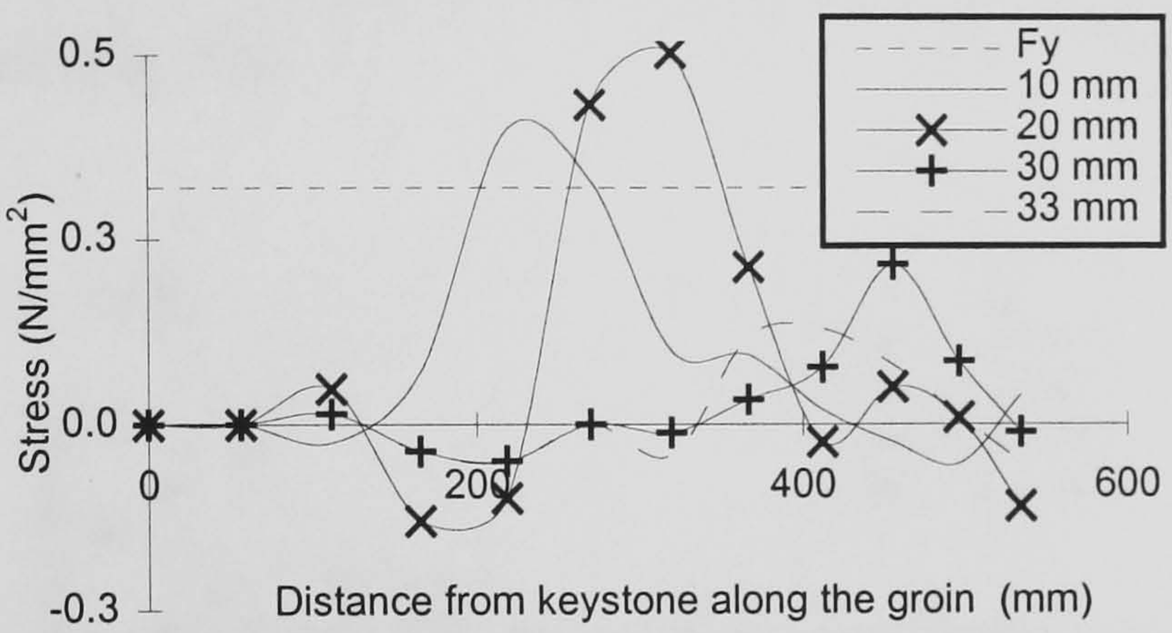

(a) Stress S22 - extrados

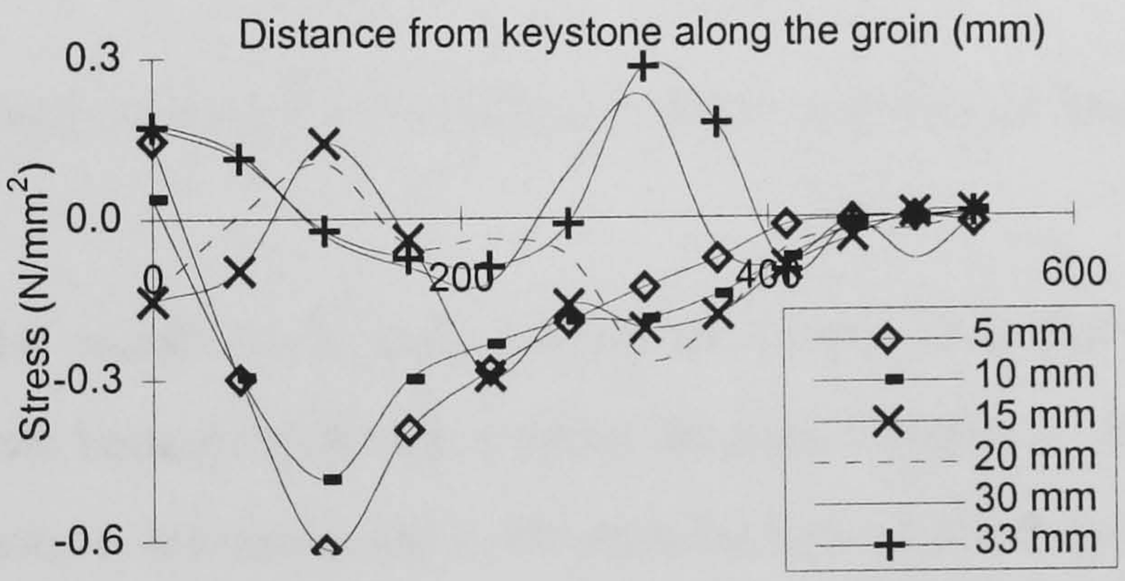

(b) Shear stress at the intrados

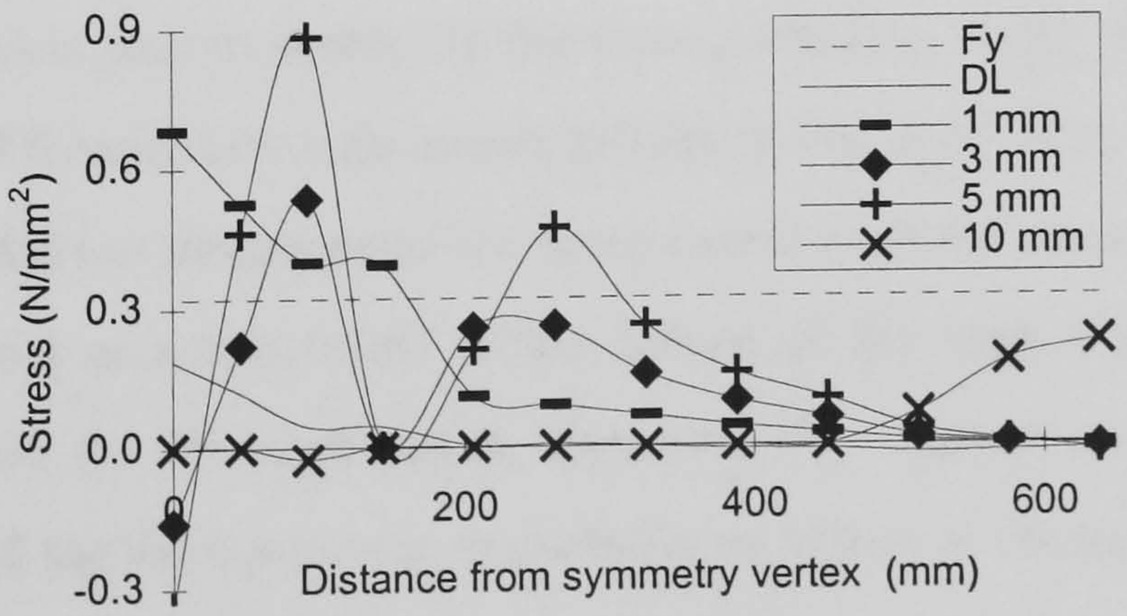

(c) Stress S22 at the back of the longitudinal vertex (web C)- extrados

FIGURE 6.25 Development of stress at the back groin

The rest of the cracks at the groin and the base of the nave arch progressed at a slower rate. The development of stress normal to the groin at the extrados of the back transverse web D (Fig. 6.25a) showed the section had cracked extensively already at a displacement of 10 mm, while relatively low compressive stress was recorded at the intrados. This demonstrated that tensile membrane forces prevailed in the separation of web D from the rest of the vault. The loss of a co-action between the rib and the web can also be detected by the deterioration of shear occurring at a similar rate, although no failure criterion had been established for the behaviour of the structure in shear (Fig. 6.25b). The critical significance of this development was also observed earlier by Croci (1995) at the FE model of a vault from Vitoria Cathedral (Fig. 2.5).

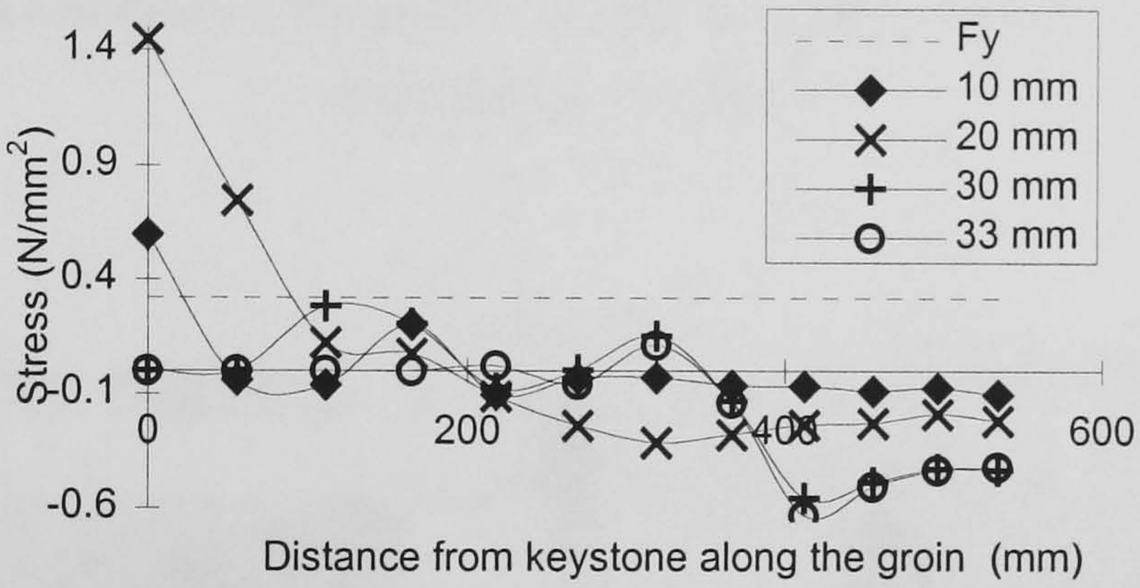

FIGURE 6.26 Development of failure at the front groin - Stress in the global direction 2 (S22), intrados

The origin of the cracks at the back side of the longitudinal webs as a product of the failure of the back groin became more clear when their development was compared, in Figs. 6.25b and c. The structure demonstrated both possibilities, as the cracks propagated within the back longitudinal web C in an area where most probably a local fault at the joint between the stems deviated the crack from the groin (Fig. 6.4). On the other hand, a closer examination of the stress pattern normal to the front groin (Fig. 6.26) showed that the cracks that appeared in the FE model as high tensile strains in Fig. 6.23 have developed at a much slower rate. As they did not propagate to the same extent as at the corresponding back groin, they can be considered as a side effect of the failure of the front side of the longitudinal vertex, resulting from the smeared crack approach. The separation of this failure area between the front and the back portions is probably an effect of the pointed vertex, since in the case of cylindrical cross vaults (Fig. 2.11) this hinge forms closer to the area of the (smooth) vertex (Jagfeld 2000).

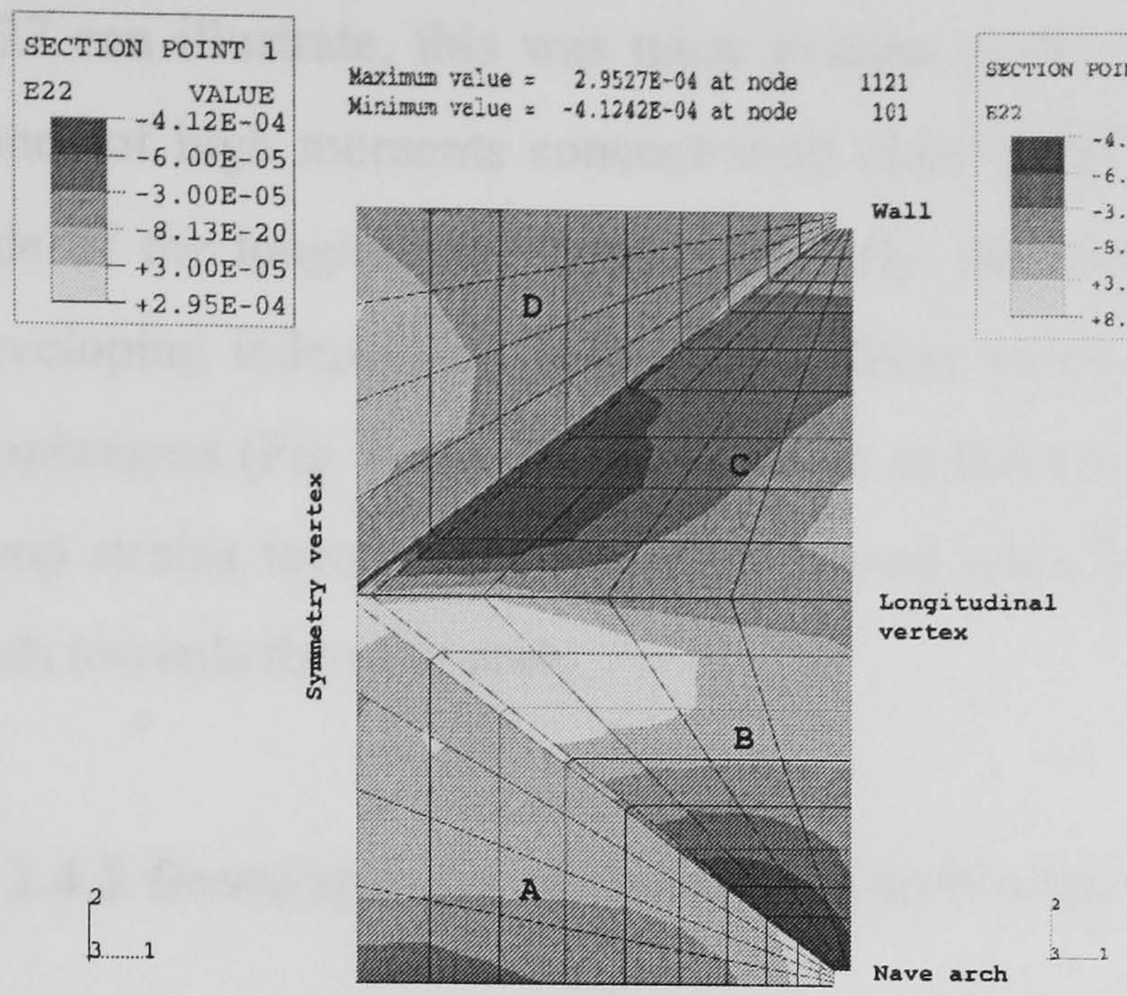

(a) Dead load (b) Movement of 1 mm

FIGURE 6.27 Distribution of strain in the global Y (2) direction (E22), intrados, at the first stages of the movement of abutments

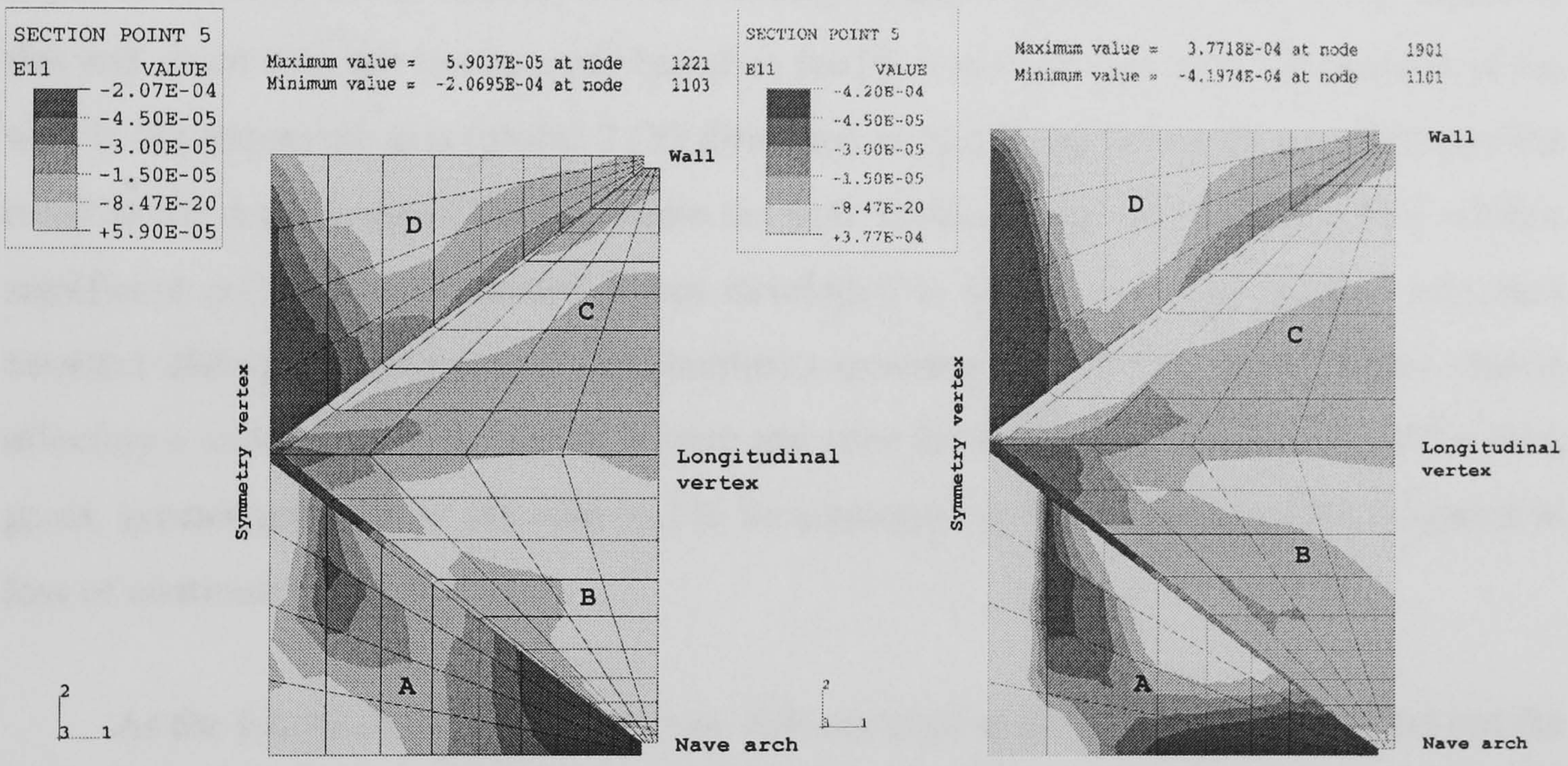

(a) Dead load (b) Movement of 1 mm

FIGURE 6.28 Distribution of strain in the global X (1) direction (E11), extrados, at the first stages of the movement of abutments

A study on the redistribution in the loads of the vault that occurred after only 1 mm of movement can illustrate in more detail the response of the vault to the movement of abutments. The comparison with the response under service (dead load) conditions (see for example Figs. 6.24 and 25) showed that most of the pattern discussed so far was already present and subsequently enhanced by the abutments movement. As the hoop strain in Fig.

6.27 can illustrate, this was more evident in the case of the longitudinal web, where the zones of high moments concentrating close to the groins spread quite rapidly along each side of the longitudinal vertex. Similarly, the transverse webs reflected quite rapidly the developing independent behaviour of these webs as pointed barrel vaults supported upon diaphragms (Fig. 6.28). The top portion of these webs remained largely unaffected, but the hoop strains towards the haunches moved away from the groins, following an alternative path towards the nave arch.

6.3.4.2 Development of thrust and behaviour of the transverse web

The development of thrust is another important aspect of the behaviour of the vault that has to be assessed. As was seen in the literature survey (§2.4), most of the theories formed to resolve problems associated with the design of these structures in their original context focused on the value of thrust, as this was necessary to dimension the buttresses required to maintain the stability of the building. Thrust was not recorded in the course of this test, so an estimate can be made based on the FE model. In Fig. 6.29, the reaction of the wall in the transverse axis (global 2 (Y) direction) is plotted and the negative values are the result of the detachment of the vault from the wall. Quite rapidly, the thrust doubled, while a significant component of inward forces developed at the crown. This scheme remained constant afterwards for most of the abutments movement. However, when failure started affecting a wider area of the wall at 20 mm and after the almost complete failure of the back groin, greater amounts of the load had to be contained by the wall due to the progressive loss of continuity at the web.

As the failure of the back transverse web occurred at the edge of the groin and not the wall, the outward thrust concentrated at the upper portion on the wall. An appraisal of the thrust exerted upon the wall at those stages can be made by evaluating the total outward force in Fig. 6.29 below the point where inward forces exert, indicating failure of the section. The total value varied around 0.1 kN during the most of the abutments movement. Thrust development is also discussed in §6.4.2.2, following approximate evaluation with an ultimate limit state analysis.

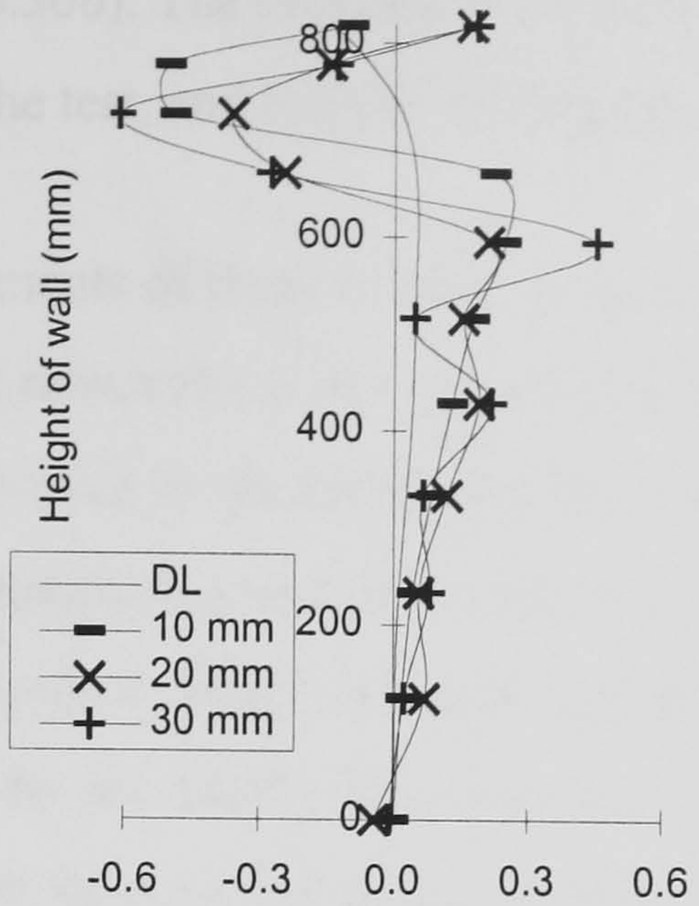

FIGURE 6.29 Development of lateral thrust upon the wall for the main stages of the abutments movement

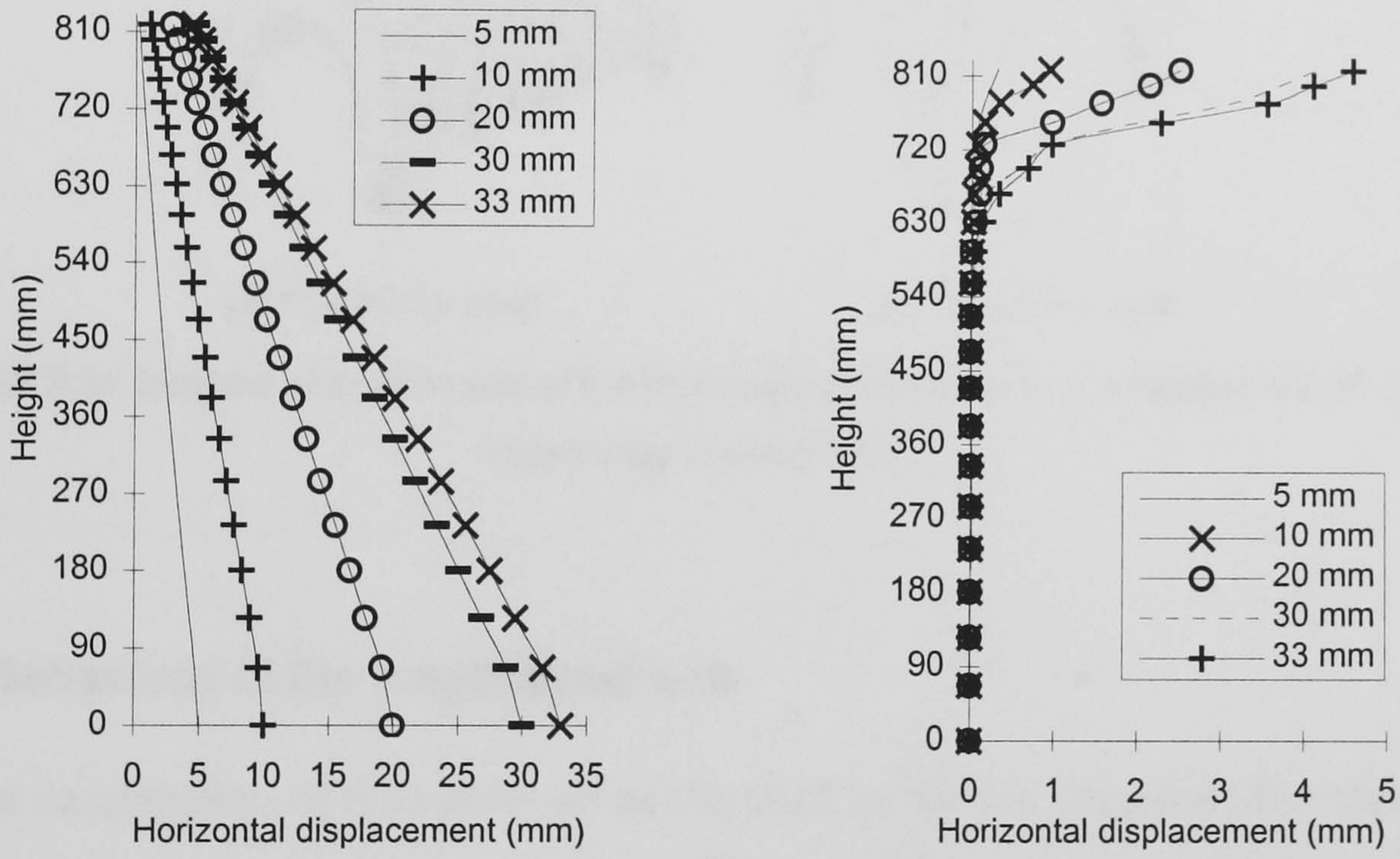

(a) Nave arch

(b) Back groin

FIGURE 6.30 Horizontal displacements during the movement of the abutments

The FE model can also improve the understanding of the extent the abutments movement directly affected the vault. The horizontal displacement of the nave arch during the loading (Fig. 6.30a) showed an almost linear reduction of the applied action at the support of the arch towards the crown. A similar pattern resulted in the front groin, with small deviations at about mid-height. The back groin however did not follow the movement

of the rest of the model (Fig. 6.30b). The progressive detachment of the back transverse web started from the crown, as in the test, and became visibly detected after a 10mm movement.

The horizontal displacements of these critical sections indicated a reduced elongation of the top portion of the vault relatively to the spreading of the lower portion. If this cross vault is represented as a barrel vault in the transverse direction, it can be postulated that the top portion of the vault developed compressive longitudinal forces, with tensile at the lower one (Fig. 6.31). Under the modern design recommendations for shell structures (Flügge 1955), a beam would have to be provided in the latter area, a role partially fulfilled by the ribs. with respect to this pattern however the design of these vaults seems to be optimised as the tensile bottom section was removed and the boundary of the cut-off was strengthened transversally by the longitudinal web (Acland 1972).

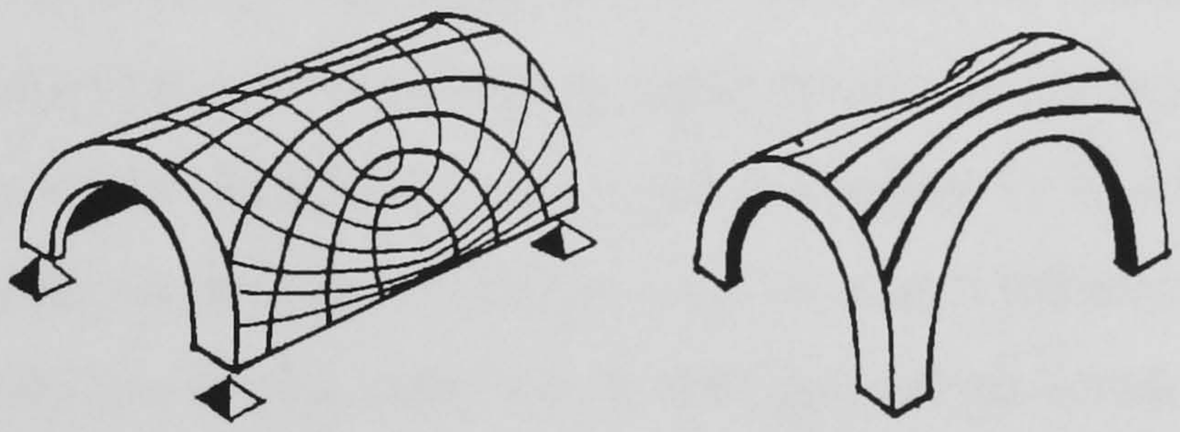

(a) Full barrel vault (b) Tension cut-off

FIGURE 6.31 Scheme of the function of the intersecting barrel vault as a tension cut-off - stress trajectories (Acland 1972)

6.3.4.3 Behaviour of the longitudinal web

The examination of the behaviour of the vault so far has supported the observations made during the discussion of the response of this type of vaults to service loads (§5.4). The compatibility of the deformations between the transverse and the longitudinal webs, and therefore the degree of independence of these systems, depended highly on the integrity and geometry of the groin. The slow degradation of these conditions, which occurred more rapidly in the FE model, enhanced the independent behaviour of each web. As a result, the web in the transverse direction was transformed into a barrel vault supported upon diaphragms (§6.3.4.2), while in the longitudinal direction, the ribs provided the continuity with the rest of the vault. In addition, the webs abutted each other along the groin by means of the thrusts they exerted.

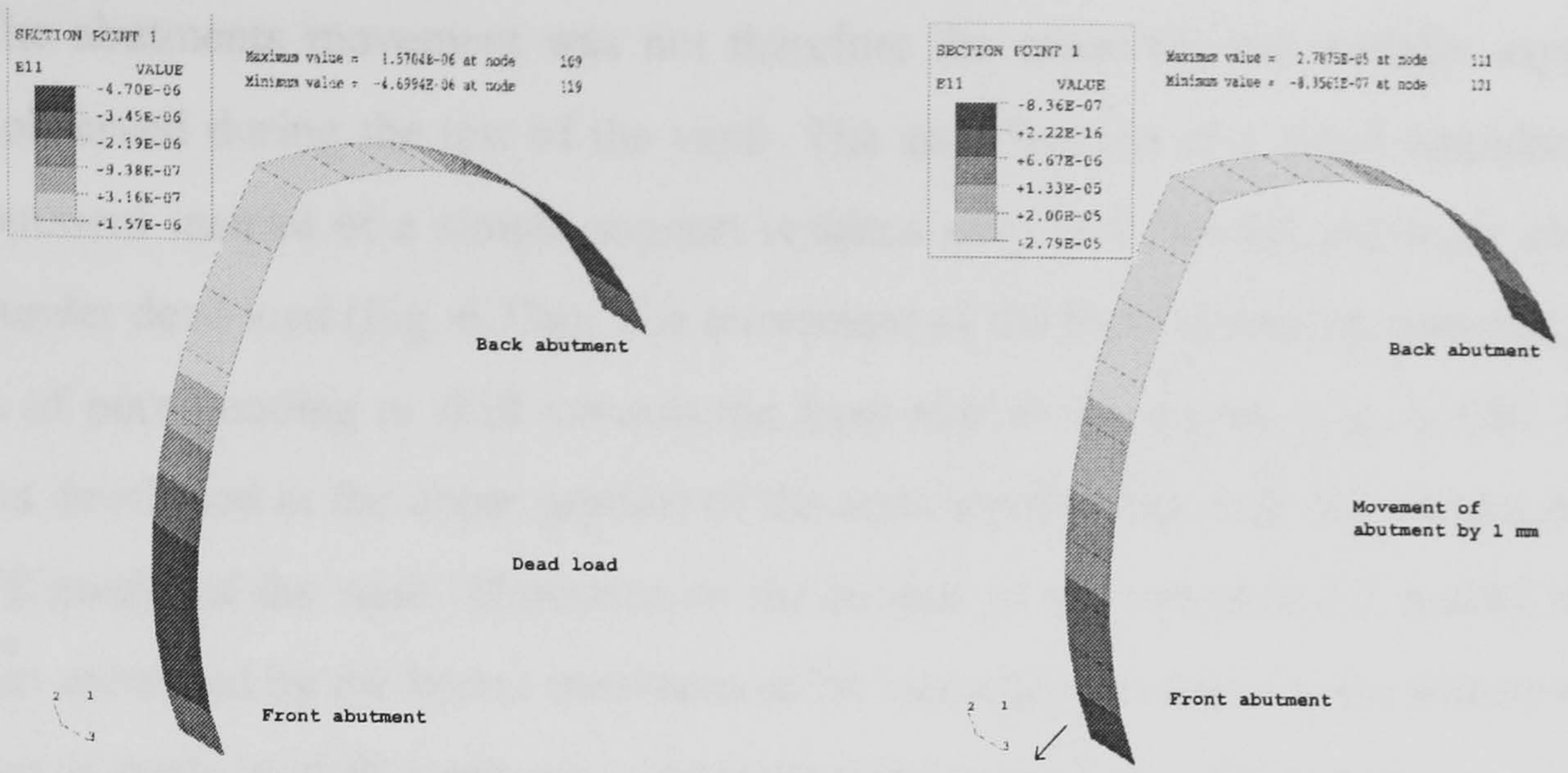

(a) Dead load (b) Movement of front abutment by 1 mm

FIGURE 6.32 Strip analysis of the longitudinal web. Simply supported abutments. Hoop strain, intrados

Regarding the failure of the longitudinal web, the variation of the stress regime along its axis can be considered as negligible, so the web can be simulated as a series of independent pointed arches, whose springing angle reduces as the keystone of the vault is approached. A strip of the longitudinal barrel corresponding to its outermost section was analysed as a uniformly-loaded, free-standing arch, considered initially as simply supported. Under dead load, very low tensile hoop strains developed at the intrados close to the crown (Fig. 6.32a). The displacement of only the front abutment caused a sharp increase in the magnitude of strain recorded (Fig. 6.32b), but quite interestingly, the pattern remained symmetrically arranged around the crown. The failure of the upper portion rapidly propagated towards the abutments, although cracks developed subsequently at the extrados of the abutments, until early failure of the arch after 3 mm of supports movement.

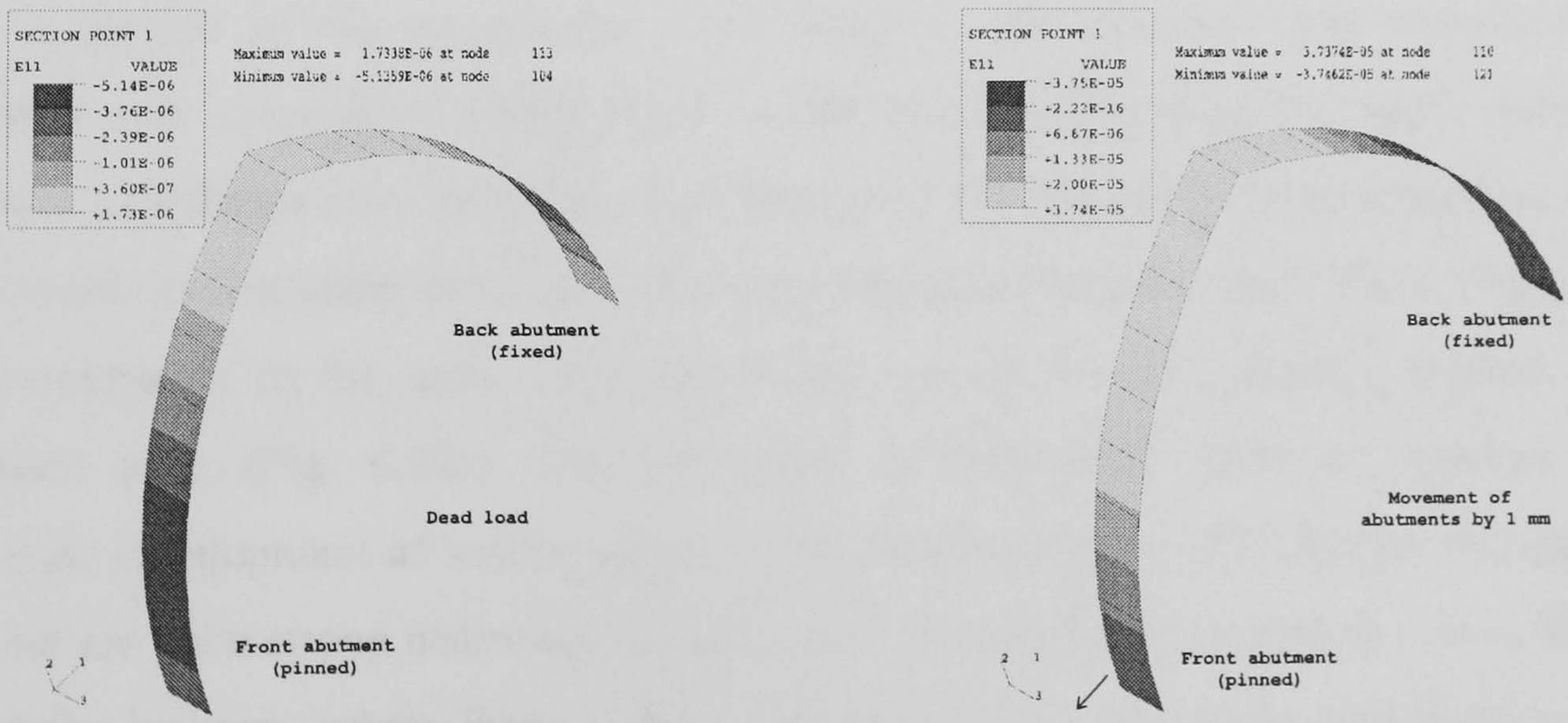

(a) Dead load (b) Movement of front abutment by 1 mm

FIGURE 6.33 Strip analysis of the longitudinal web. Front abutment is simply supported and back is fixed. Hoop strains, intrados

The abutments movement was not therefore the cause for the initially asymmetric pattern observed during the test of the vault. The specification of a fixed boundary at the back abutment instead of a simple support resulted only in a limited and local change of pattern under dead load (Fig. 6.33a). The movement of the front abutment, however, caused the area of pure bending to shift towards the front side of the crown (Fig. 6.33b). Positive moments developed at the upper portion of the arch, conforming with the pattern observed at the FE model of the vault. Moreover, in the context of the complete FE model, they can be further enhanced by the lateral constraint at the haunches provided by the transverse web, since part of the load of this web was carried directly by the longitudinal web.

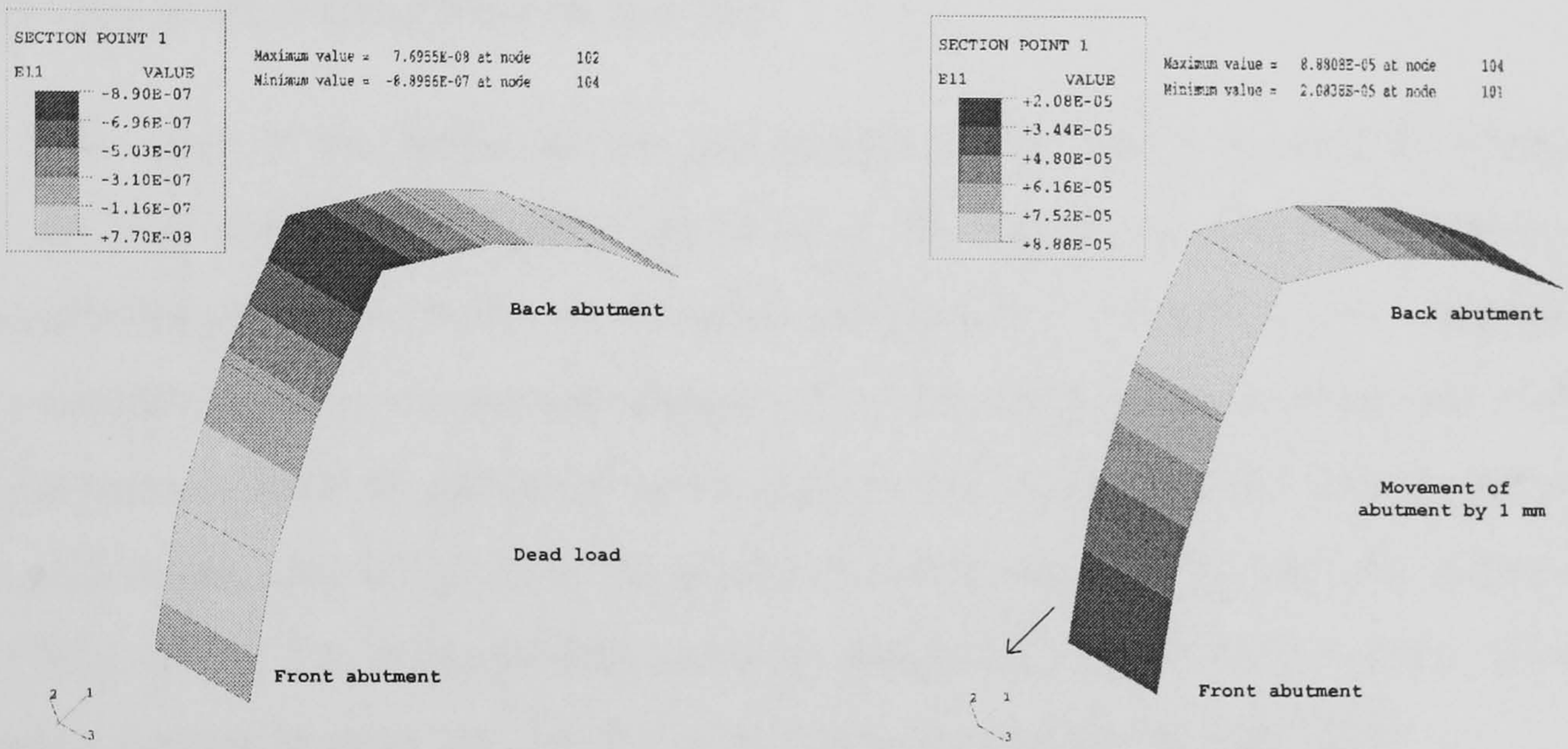

(a) Dead load (b) Movement of front abutment by 1 mm

FIGURE 6.34 Strip analysis of the longitudinal web. Arch cut-off at mid-height. Simply supported abutments. Hoop strains, intrados

A section of the longitudinal web closer to the keystone was examined next, generated over a springing height equal to half the total height of the vault. Symmetric boundary conditions were specified once again and the loadings were arranged as before. Hoop tensile strains under dead load were concentrated at the haunches (Fig. 6.34a), an area that corresponds to the same relatively height where this area became evident at the outermost edge (Fig. 6.32a). The movement of abutments, however, resulted in an immediate development of tensile strains at the intrados (Fig. 6.34b). Rather flat arches of this kind are quite strong under service loads and the high deflections observed in the vault around the keystone where these profiles appear are the result of the deformation of the supporting ribs. Their high sensitivity to geometric changes, like those due to the abutments movement, can explain the rapid propagation of failure around the longitudinal vertex.

6.3.5 Collapse mode

The collapse of the vault is expected to occur after the formation of a sufficient number of fracture lines which are capable of transforming the structure into a mechanism. The study of the response of the vault model to the movement of the abutments had identified three major areas of failure until the movement of 30 mm (Fig. 6.4):

1) the front area of the longitudinal vertex

2) the front haunch, starting from the nave arch

3) the back groin, starting from the keystone

The result of the third zone was the gradual detachment of the back transverse web from the rest of the vault. Further movement of the supports could most probably have enhanced this pattern and led to the complete detachment of this web and its transformation into a cantilever built-in on the wall. Already from that stage, however, high tensile stresses had developed normal to the crown of the wall, so the cracks that had already appeared at the initial stages could have been expected to re-open rapidly following the failure of the groin (Fig. 6.35). The final outcome could be comprised of four fracture lines, which is a sufficient number to cause the collapse of arched structures (Kooharian 1958).

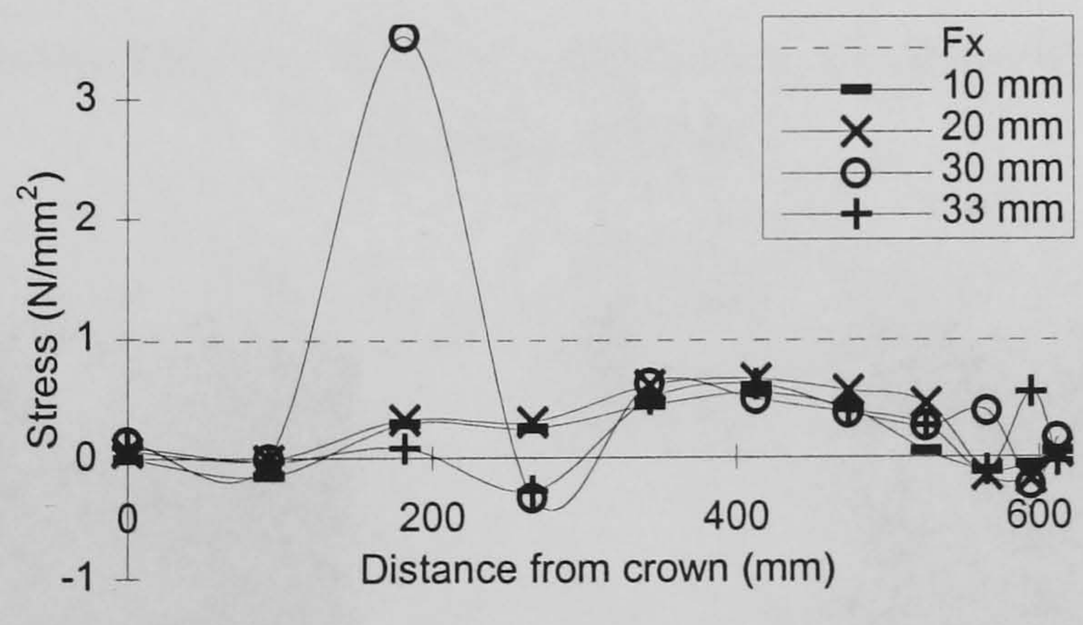

FIGURE 6.35 Development of failure along the wall. Stress S22 in the global direction 2 (Y), intrados

The present configuration of the FE model reached a numerical failure at a movement of 33 mm. This margin fell within the available space at the extrados of the ribs, upon which the webs were still supported at 30 mm. The boundary conditions corresponding to the area were quite complex. They required the definition of a joint in the direction normal to the

surface containing the groin, while at the same time the extrados of the rib would support vertically the web. It was attempted to solve this problem by specifying a material that allowed failure to occur similarly to the webs. Moreover, the adopted smeared crack approach contributed partially to the maintenance of continuity between the web and the rib.

Similarly to the study of the response of the vault under service loads, the behaviour of the vault due to the movement of abutments can be considered within the two bounds established by the FE model simulating the bond between webs and ribs with springs and the actual model, representing the groins and the nave arch with shell elements (Fig. 6.36). The experiment made evident the critical role of the groin in the failure process and the improvement in the behaviour of the back transverse web was significant. The front part of the vault appeared to be less sensitive to these changes, at least so far as the final failure pattern is regarded. The early formation of the longitudinal crack was a common characteristic for all the models and was dominant in the behaviour of this part of the vault.

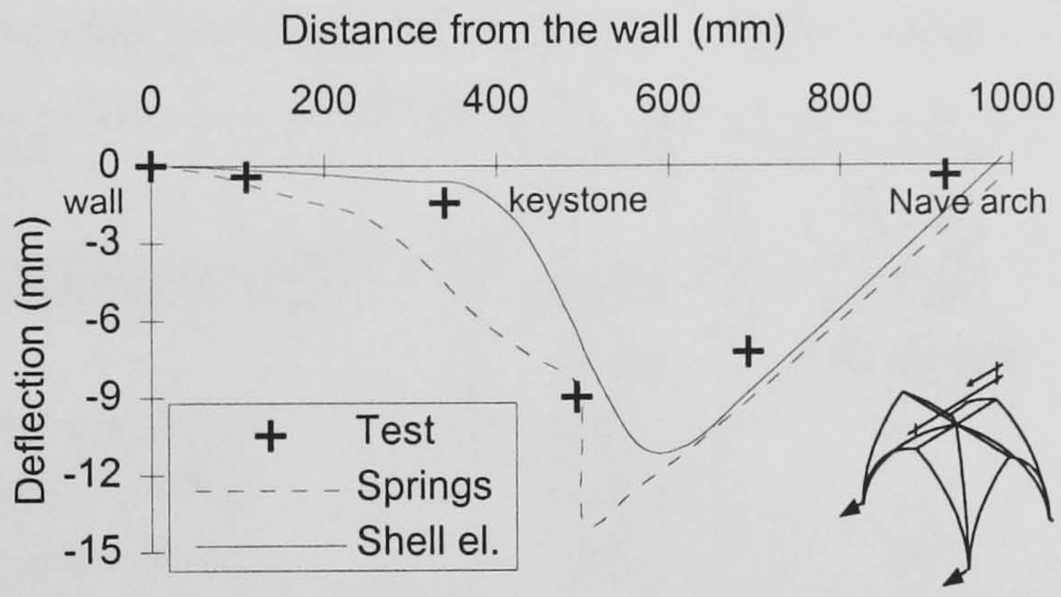

FIGURE 6.36 Evaluation of the main FE models. Deflection of the symmetry vertex after abutment movement of 30 mm

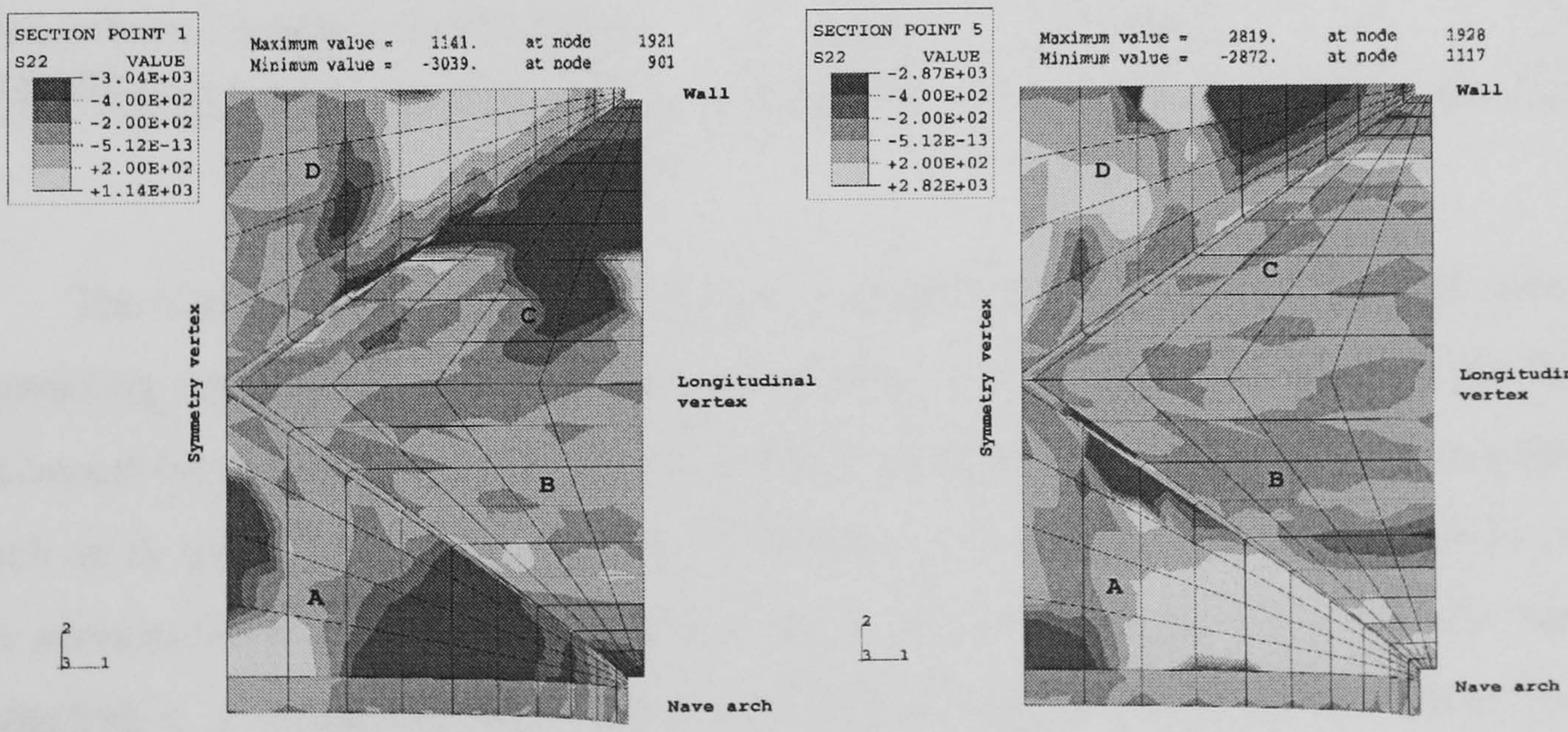

(a) Intrados

(b) Extrados

FIGURE 6.37 Stress S22 in the global direction 2 (Y) after abutment movement of 33 mm

The extent of the cracks in the cross vault can be summarised by the stress pattern in the transverse direction at the FE model at the stage of 33 mm (Fig. 6.37). The areas of failure are represented as zones of zero stress.

6.4 APPROXIMATE METHODS OF ASSESSMENT OF THE SAFETY OF THE MODEL VAULT

6.4.1 Range of the abutments movement

The range of horizontal displacements that is expected to develop at the front abutments of the vault can be assessed from available survey data on the deformation of the lateral walls of some cathedrals. Values from these surveys are summarised in Table 6.3 and most of the cases are discussed below.

TABLE 6.3 Movement of abutments observed in historic masonry cross vaults

Case	Position	Movement, *u* (mm)	Span, *s* (m)	u / s
Vitoria Cathedral (Sabbadini 1993)	central	174 (max)	9.24	1/53
id	aisle	120 (max)	5.5	1/46
Amiens Cathedral (Bilson 1906)	aisle	50	7.52	1/150
Beverley Minster (Bilson 1906)	aisle	-		1/19
Holyrood Abbey (Mylne 1766)	aisle	75	3.77	1/50
S. Angelo dei Lombardi (Ortolani 1988)	nave	260	7.74	1/28
León cathedral (Martínez 2000)	nave	150	7.5	1/50
FE model (Jagfeld 2000)	nave	404	10	1/25
St. Martin, Landshut (Jagfeld 2000)	nave	116 (total)	11.6	1/100
Bronnbach, cloister (Jagfeld 2000)	aisle	140 (total)	3.6	1/26
Maulbronn, cloister (Jagfeld 2000)	aisle	320 (total)	4.2	1/13

The Cathedral of Vitoria, Spain, is an example where the distortion of the nave was threatening the stability of the building and drastic interventions were required (§1.4). The horizontal displacement of various bays in Fig. 6.38 (Sabbadini 1993) shows values that can reach up to 1/50 of the transverse span of the aisle, a ratio that can be considered to exceed the serviceability limit of the structure. In buildings of larger scale, as the Amiens Cathedral, it is normal to find the abutments of the aisle vaults spreading at about 50 mm, corresponding to 1/150 of the transverse span (Bilson 1906). Although at the nave vaults of Amiens, despite some earlier interventions, cracks close to the walls are still visible today

(Fig. 1.15a), the safety of this building is not compromised and displacements of this kind can be considered as the expected range under service conditions.

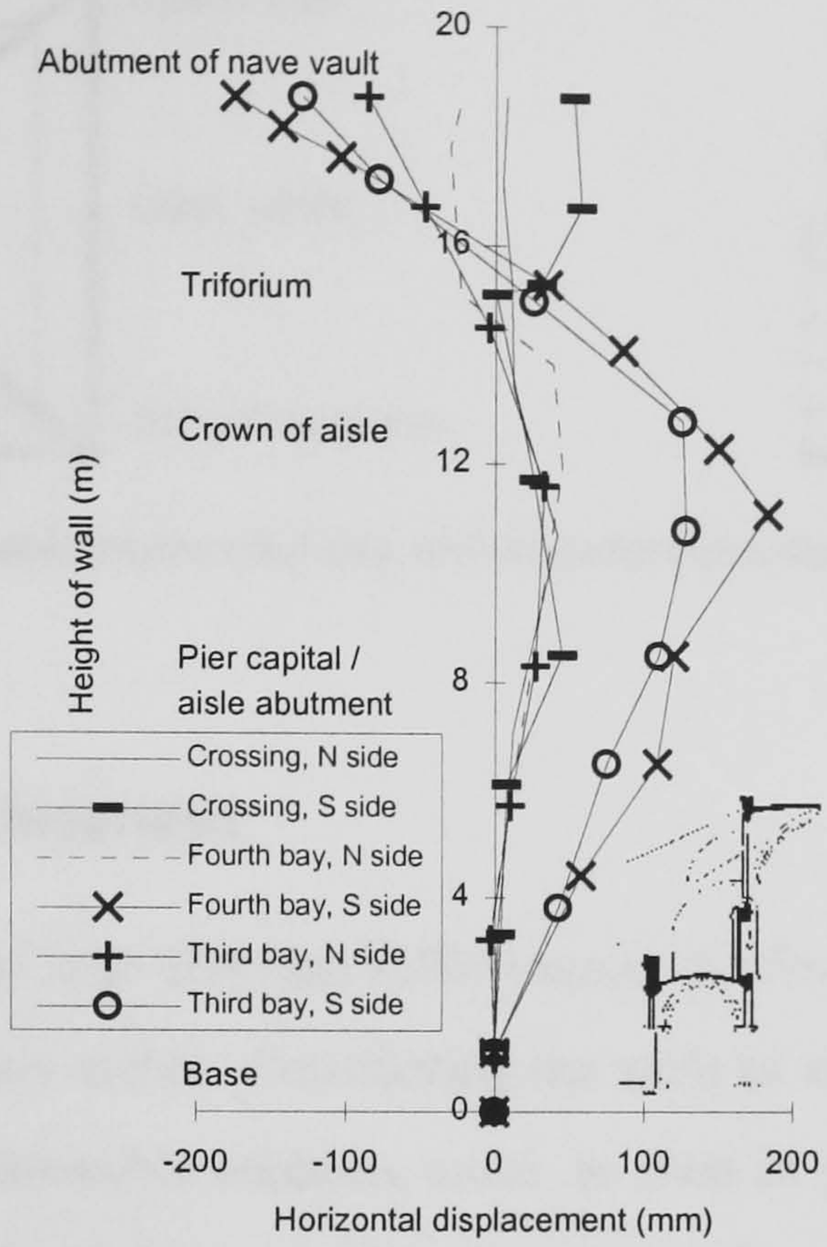

FIGURE 6.38 Deformation of the lateral wall in Vitoria Cathedral (Sabbadini 1993)

Regarding the case of the prototype vault in Holyrood, Mylne in his survey preceding the collapse (§3.2.3.3) had detected a movement of the vaults abutments by 3 in. (75 mm), corresponding to 0.075 / 3.77 = 1/50 of the transverse span, a value which is quite close to the observations in Vitoria. On the other hand, the tests on a brick cross vault discussed in §2.2.2 (Ortolani 1988), indicated a collapse at a displacement of 260 mm or 1/28 of the span (Fig. 2.4). From the above values, the ratio of 1/50 can be considered as the service limit for the cross vault model, which results in a permissible movement of the abutments by 0.925 m / 50 = 19 mm.

6.4.2 Ultimate limit state of the model vault

The vault can be considered to reach an ultimate limit state when it collapses due to the failure of a sufficient number of critical sections, which transform the structure into a mechanism. The strip method, which is a form of ultimate limit state analysis usually applied for slabs, was used to determine the thrust, the minimum required thickness of the vault and the location of hinges at that stage. The vault was considered as completely

segmented along the principal axes into a series of arches (Fig. 6.39), so no beneficial effect was taken from the spatial continuity of the shell.

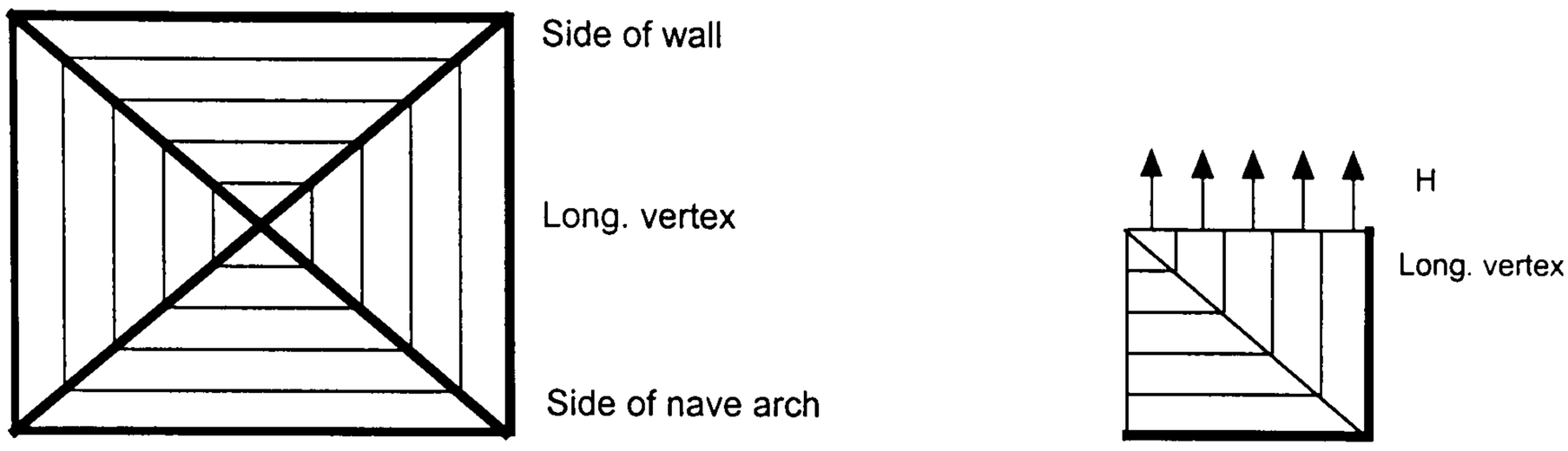

FIGURE 6.39 The cross vault segmented into arches perpendicularly to the global axes (plan)

6.4.2.1 Assessment of thickness

Kooharian (1953) and later Heyman (1966) made the first applications of the plastic design philosophy to voussoir arches. Considering the vault as sliced into a series of parallel rings is a safe, statically admissible solution, since, as seen in §1.4, cracks are expected to develop parallel to the wall and the nave arch (Fig. 1.16). Once that portion of the vault is detached, the rotational degree of freedom (DOF) parallel to the crack is released. The remaining web is weakened due to this hinge as the resulting moment redistribution causes rupture of further sections to progress more rapidly. Similarly to the strip method, the load in this solution is carried by bending in either the global 1 (X) or 2 (Y) direction, disregarding the continuity in the longitudinal axis. The fracture (discontinuity) lines are considered to form along the intersection of the webs, the groins, and the individual strips are supported on the ribs.

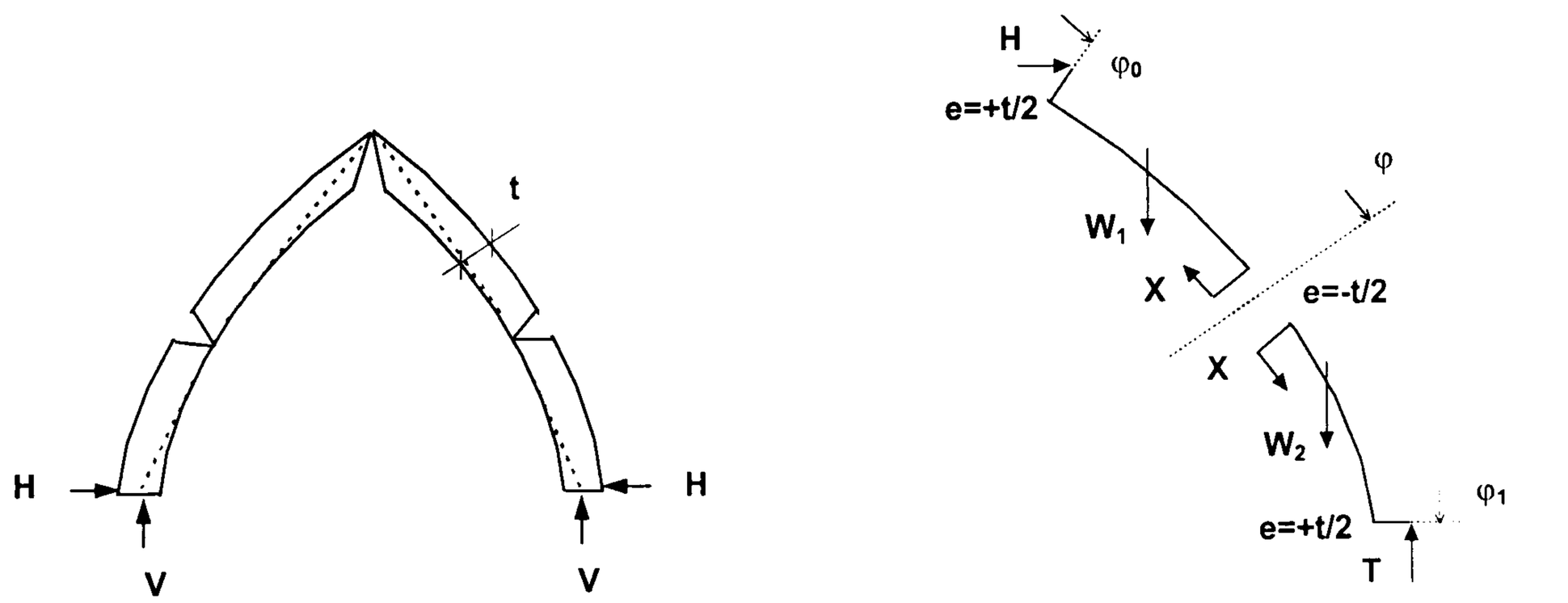

(a) Location of thrust line and cracks (b) Free body diagram and definition of geometry

FIGURE 6.40 Evaluation of thrust exerted by a pointed arch and minimum required thickness

To study the ultimate limit state of the cross vault model, each strip was examined separately and a crack pattern was considered, representing the lower limit of each arch. Cracks were assumed to form at the crown (intrados) and the haunches (extrados), where the thrust line was tangent to the surface of the arch (Fig. 6.40a). The generic case of a pointed arch defined by a crown angle φ_0 and a springing angle φ_1 was studied. The minimum required thickness of the shell that is sufficient to contain the line of thrust was evaluated by assuming the hinge at the haunches forms at an angle φ from the vertical (Fig. 6.40b). At that point, the thrust is offset by half the thickness, t. In Fig. 6.41 the minimum required thickness of each web can be assessed at each slice defined by the springing angle φ_1.

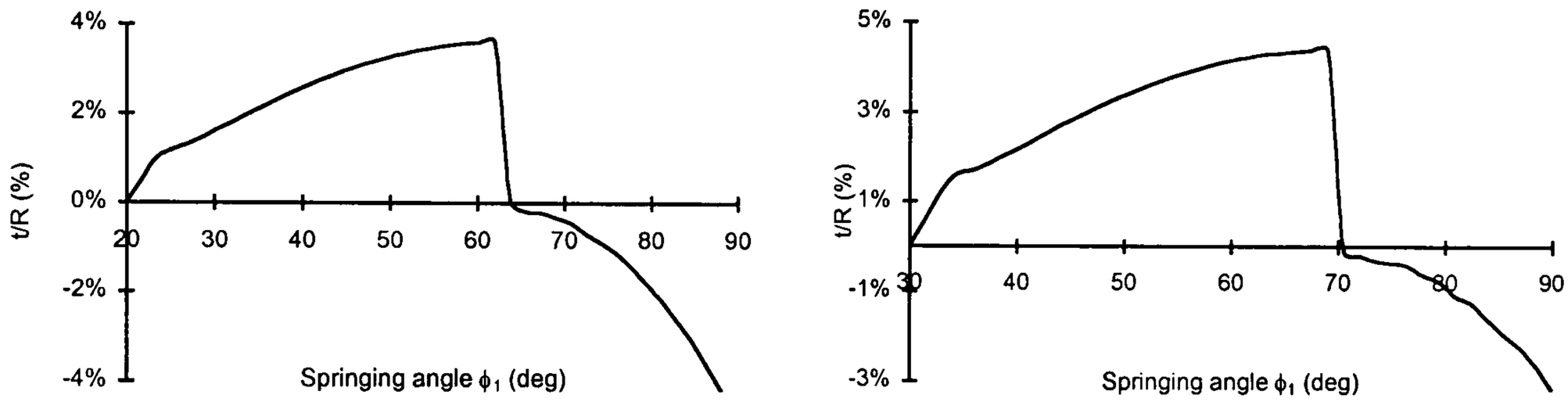

(a) Transverse web – $\varphi_0 = 20°$ and $\varphi_1 = 85°$ (b) Longitudinal web – $\varphi_0 = 30°$ and $\varphi_1 = 90°$

FIGURE 6.41 Minimum required thickness of the sliced webs of the vault

The transverse web (Fig. 6.41a) is safe as the thickness of the shell (35 mm) is always above the minimum thickness required, which reaches a maximum value of 3.6% of the radius, or 34 mm. The sharp change of sign after $\varphi_1 = 62°$ indicates a change in the face of crack. For $\varphi_1 = 90°$ the minimum thickness required exceeds the actual geometry, but actually $\varphi_1 = 85°$ so the arch is overall safe. The study of the longitudinal web, however (Fig. 6.41b), showed that the stripes defined between $\varphi_1 = 60°$ and 70° required a thickness of 42 mm (4.4% of R), after which point the face of the crack was inverted. In that area, cracks are expected to form at an angle $\varphi = 42°$ or 12° from the crown ($\varphi_0 = 30°$). The continuity of the web in the longitudinal direction and the boundary conditions along the groin have reduced significantly the deformations during the response of the vault to dead load. Disturbance of these conditions due to movement of the abutments are therefore critical for the safety of the web.

6.4.2.2 Evaluation of thrust

From the static equilibrium of each ring, as defined in Fig. 6.40, the thrust H exerted was determined in terms of the unit weight of the structure expressed as a surface load w = 1930 N/m^2 and wR^2 = 1.724 kN (§5.2.1). The diagrams elaborated by Heyman (1966, 1995), were reworked for each of the two webs of the cross vault according to values for the crown angle φ_0 not available in (Heyman 1966), while φ_1 was considered as a variable (Fig. 6.42). The total thrust exerted by the cross vault to the wall and the nave arch (transverse direction), was evaluated as the sum of thrusts per unit width of all the strips in which the longitudinal web was divided (Fig. 6.39) and it is given in Table 6.4.

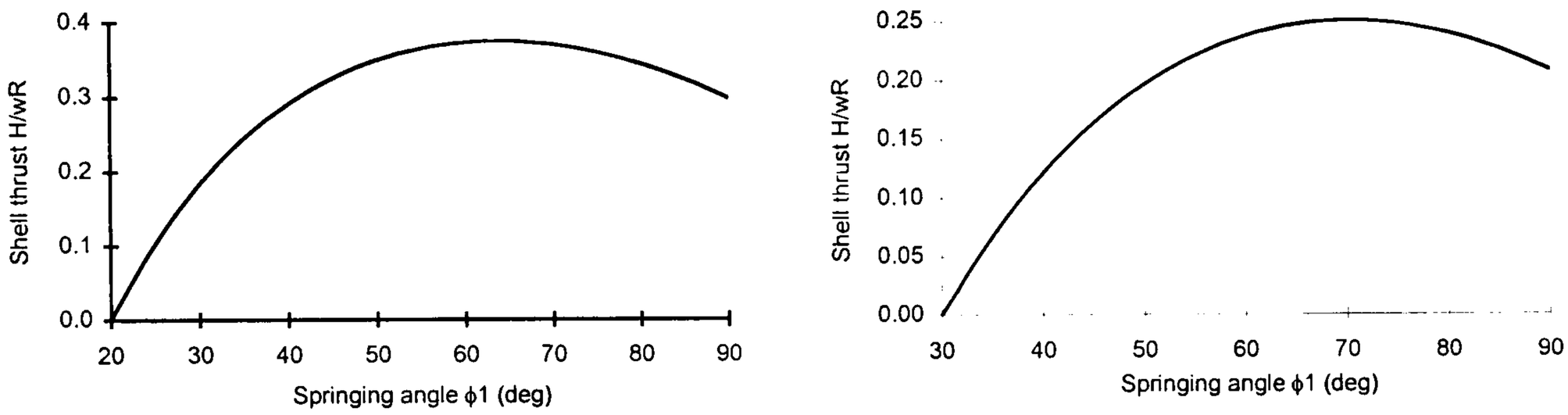

(a) Transverse web – φ_0 = 20° and φ_1 = 85° (b) Longitudinal web – φ_0 = 30° and φ_1 = 90°

FIGURE 6.42 Shell thrusts per unit width for the sliced webs of the vault

Alternatively, Heyman (1966) evaluated an upper limit for the value of the thrust as the horizontal component of the hoop stress resultants along the edge (Fig. 6.12b). The transverse barrel, however, was regarded as complete and not cut-off by the increasing springing angle φ_1 at the sections closer to the keystone of the cross vault (Fig. 6.39).

A further evaluation of thrust was made using the Table 2.1 (Ungewitter and Mohrmann 1890). The actual height / span ratio is 818 / 945 = 0.866 (range of 5:6 to 1:1) and, as an approximation, a "1/2 lightweight brick" was assumed. The total surface is 1.225·0.945 = 1.158 m^2 and from Table 2.1 the total weight results in 3.9 kN, compared with the applied amount of 3.3 kN in Tests DL3 and DL4 (§4.4.1).

TABLE 6.4 Summary of methods used to evaluate the thrust exerted by the half vault to the wall

Source	Method	H (wR^2)	H (kN)
Heyman (1966)	single arches	0.144	0.248
Heyman (1966)	stress resultant	0.486	0.838
Barthel (1993)	hinge lines	0.155	0.267
Ungewitter (1890)	line of thrust	0.269	0.463
Pieper (1983)	hinge lines	0.156	0.269
present work	FE model (§6.3.4.2)	0.058	0.1

6.4.2.3 Location of cracks

In order to evaluate the possible location of hinges in the cross vault, a procedure similar to the case of the individual arches (§6.4.2.1) was followed, as suggested by Barthel (1993) for a semicircular cross vault spanning over a square compartment. These hinges were assumed to form in the simply supported vault at the crown and haunches (defined by an angle α in Fig. 6.43a). At the latter point, as in the arches (Fig. 6.40a), the line of thrust was considered to be tangent to the intrados.

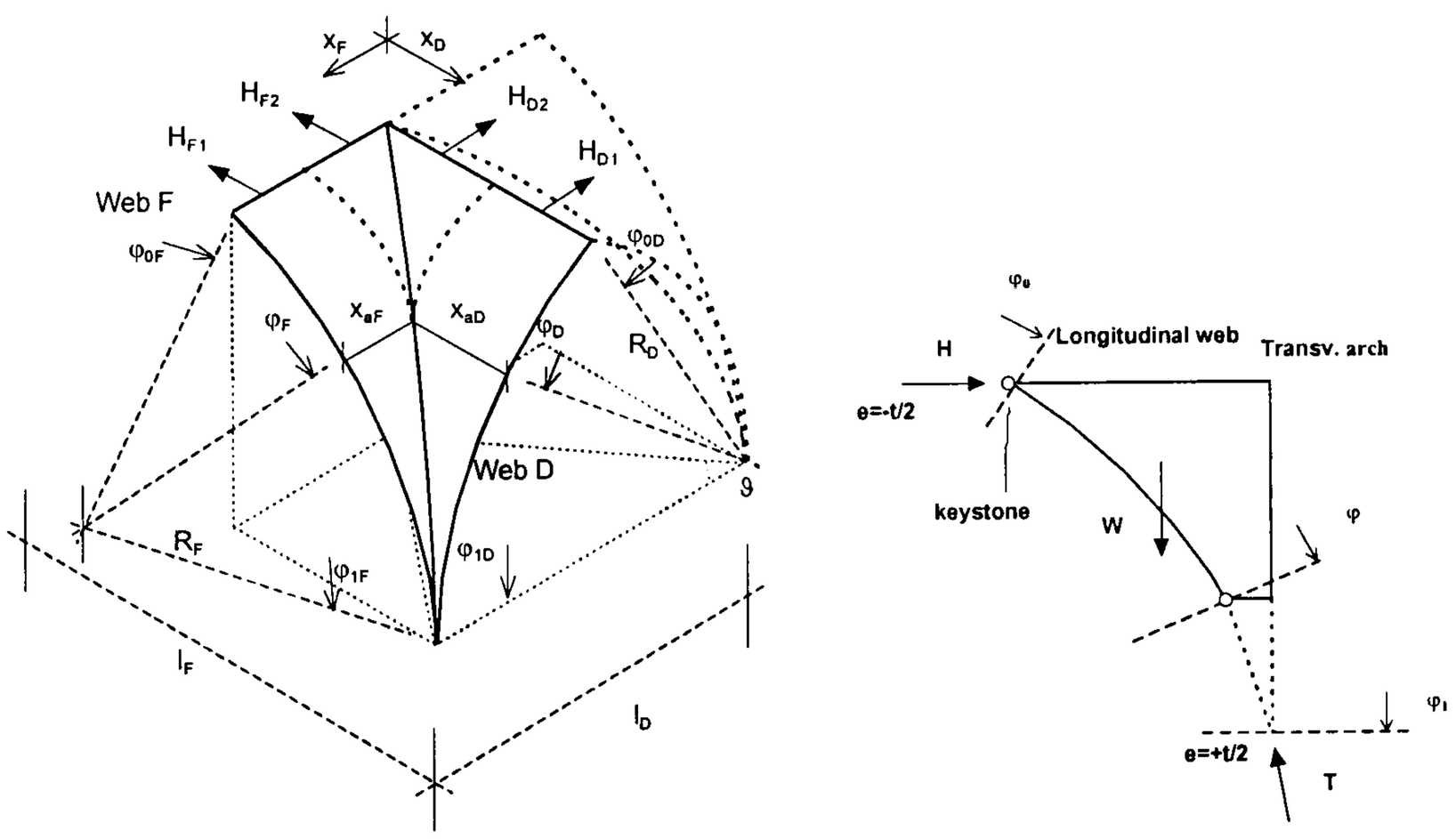

(a) Geometry

(b) Free-body diagram

FIGURE 6.43 Ultimate limit state analysis for the location of cracks at the cross vault

From moment equilibrium around the hinge at the horizontal projection of the vault (Fig. 6.43b), the angle of the hinge α can be evaluated. The formation of the final equation, combining the component from each of the four portions of the vault in Fig. 6.43a, was arranged and solved by means of a Fortran program. Cracks (hinges) are expected to form at

an angle of 62.5° or a height of 0.52·h=0.52·818 mm =425 mm. The resulting thrust H for the half vault (Table 6.4) is quite similar to the value obtained earlier by the strip method. This value compared well with the empirical expression proposed by Pieper (after Barthel 1993), where the hinge line in a cylindrical cross vault was assumed to form at 0.6 of the height. The resulting thrust becomes $H = 0.156 \cdot w \cdot R^2 = 0.269$ kN.

So far as the location of cracks is concerned, the longitudinal cracks at the FE model were formed at the intrados at an angle $\alpha = 40°$ or a height of 0.88·h= 726 mm (Fig. 6.23c). Moreover, the FE model produced a set of cracks along the groin, while no hinges developed at the longitudinal vertex proper. Due to the spatial continuity of the model, each web transmitted its load to the other proportionally to their geometry, resulting in a non-uniform distribution of the dead load and the change in the response of the sections as pure arches. As a consequence, the two hinges from the limit state analysis, at the haunches and the vertex, appeared to have been joined into one at the FE model.

6.5 PARAMETRIC STUDY

6.5.1 General

In this section, a parametric study is carried out to investigate the effect of the material properties, geometric variations and boundary and loading conditions on the FE model. The aim of this study was not only to define the expected range of uncertainty in the analytical prediction of the response of the structure, but also to identify some further crucial factors for the distribution of the loads. In the case of the effect of the material properties (modulus of elasticity and strength), it was useful to consider as a datum the behaviour of the FE model with isotropic strength and stiffness properties. The properties of the web masonry in the weakest direction were specified and the elastic modulus was equal to E_2=670 N/mm^2 and strength equal to F_2=320 N/mm^2.

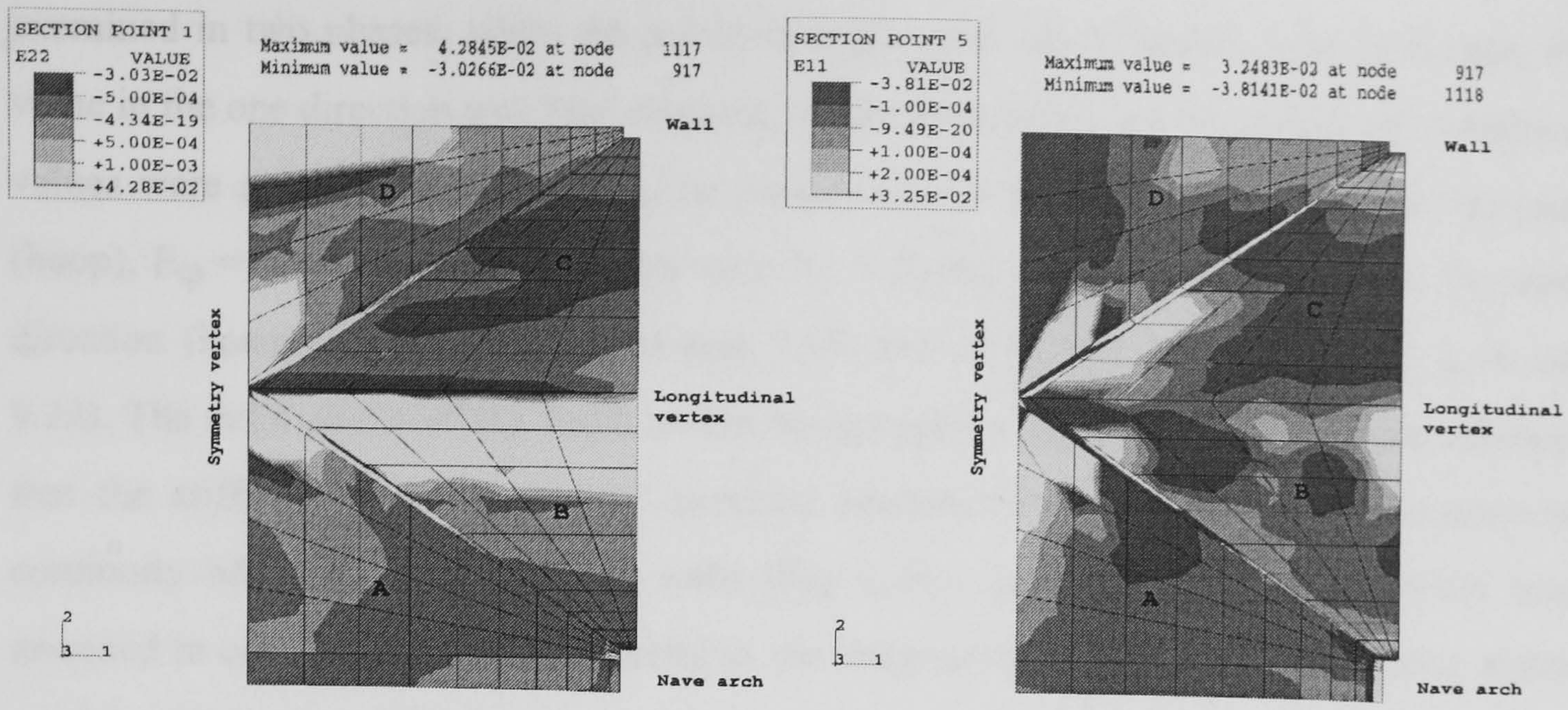

(a) Strain in global direction 2 (E22) at intrados (b) Strain in global direction 1 (E11) at extrados

FIGURE 6.44 Isotropic material properties - strain due to movement of the abutments (10 mm)

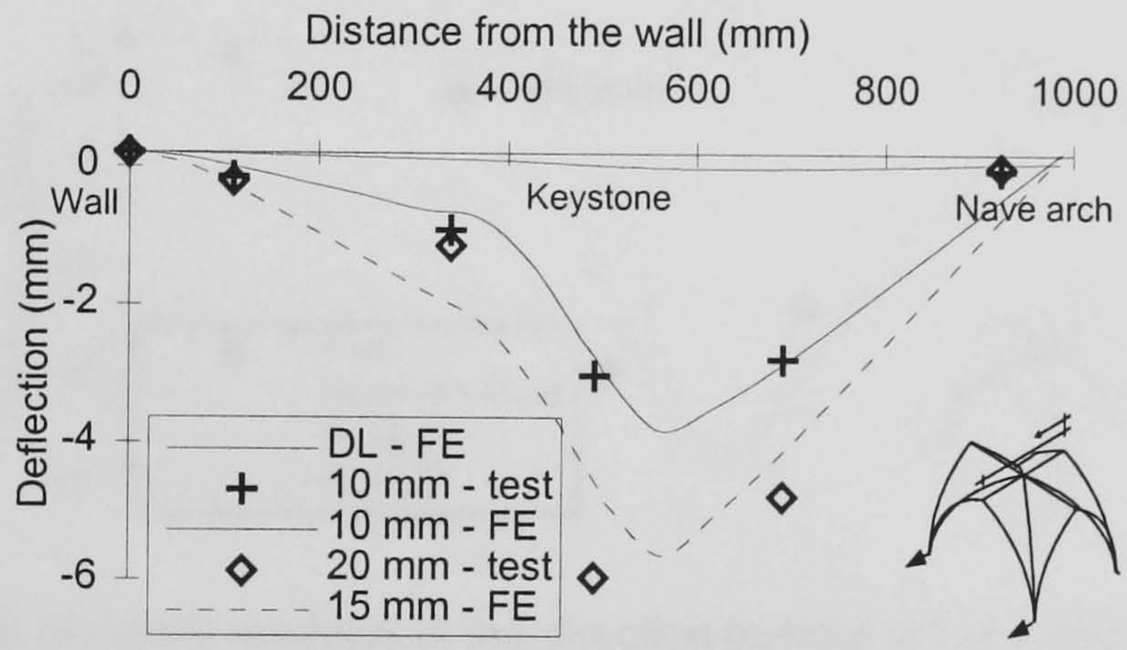

FIGURE 6.45 Isotropic material properties - deflection of the symmetry vertex

The combination of these properties resulted in an earlier failure of the FE model, at a 15 mm movement of abutments. Substantial cracks formed at the wall edge and not along the back groin, although high tensile membrane strains had already propagated along the top portion of this groin at 10 mm (Fig. 6.44a - cf. Fig. 6.23a). The stiffness in the direction parallel to bed joints is however less significant for the longitudinal webs B and C, as the pattern of strain E11 (Fig. 6.44b) remained largely unaltered. The shift of failure away from the groin as the material became more uniform caused a higher deformation of the entire vault, as it can be illustrated by the symmetry vertex in Fig. 6.45.

6.5.2 Effect of stiffness orthotropy

The effect of the variation of the stiffness ratio in the two major directions was

examined in two phases, while the initial strength ratio was maintained. In each case, the value in the one direction was kept constant, while in the other, the maximum and minimum values were specified. Starting with the modulus in the direction normal to the bed joint (hoop), E_φ = 670 N/mm^2 (orthogonal ratio $R_1 = E_x/E_\varphi$ = 6.36), the modulus in the other direction (horizontal) was varied between 1530 and 6180 N/mm^2 (R_1 between 2.28 and 9.22). The deformation of the vault, as can be represented by the symmetry vertex, showed that the stiffness in the horizontal direction contributed mainly to the maintenance of continuity between the two joining webs (Fig. 6.46). As the area of the groin had been assumed to consist of the same material as the longitudinal web (§6.3.1), the higher elastic modulus strengthened the bond between the webs and distributed more uniformly the loads, although it was not expected to yield higher deflections.

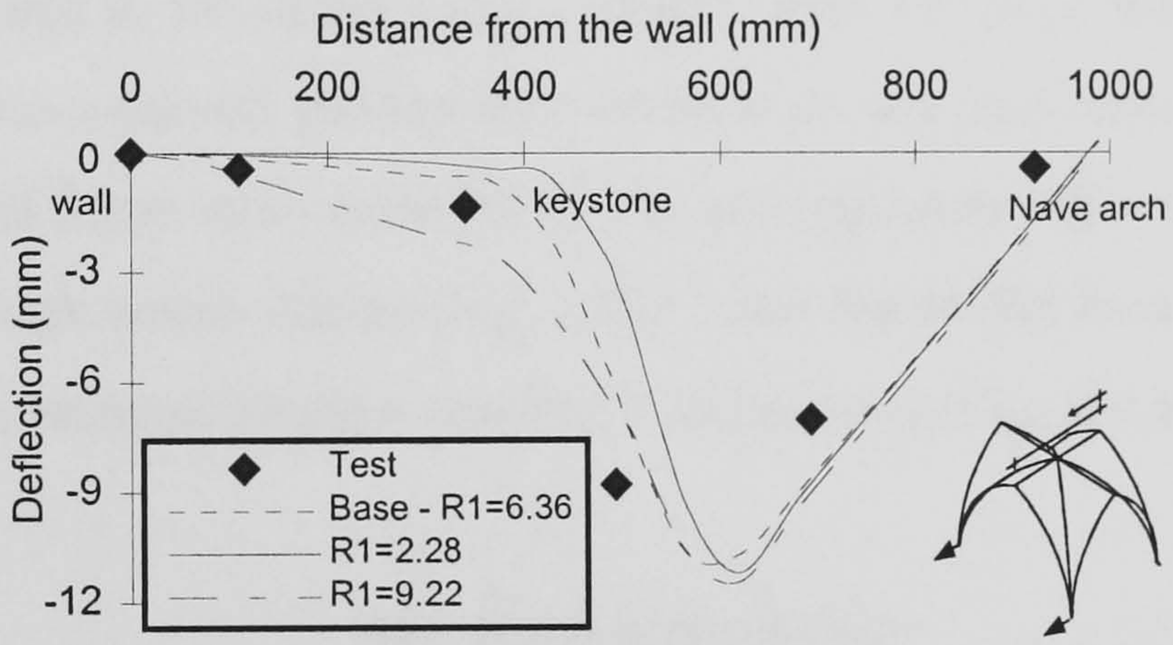

FIGURE 6.46 Variation of elastic modulus in the direction parallel to the bed joints, E_x. Deflection of symmetry vertex for a 30 mm movement of abutments

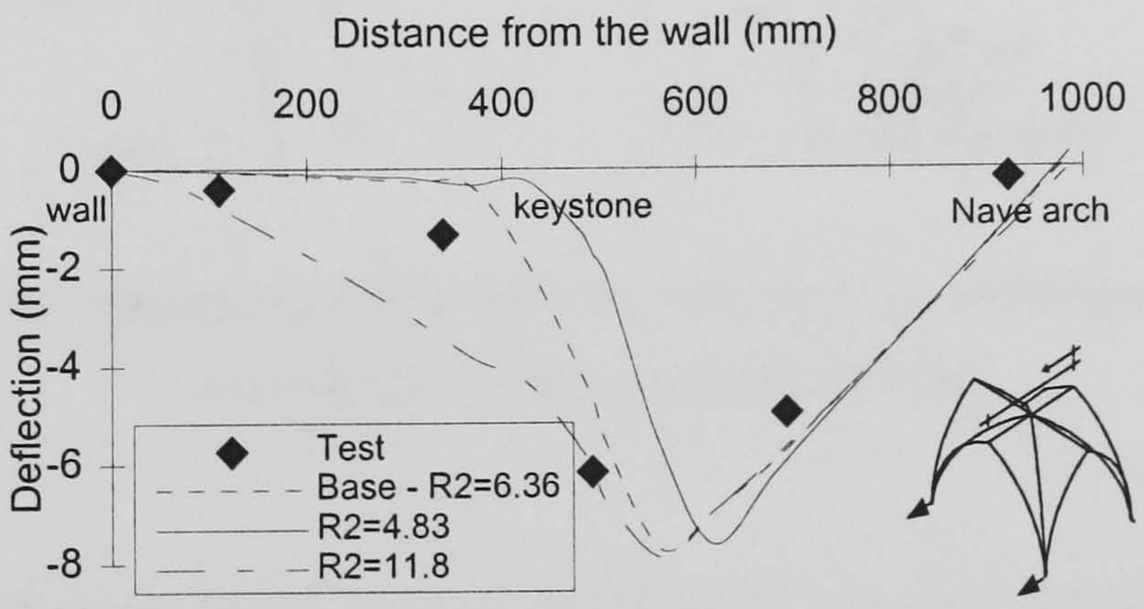

FIGURE 6.47 Variation of elastic modulus in the direction normal to the bed joints, E_φ (hoop). Deflection of symmetry vertex for a 20 mm movement of abutments

It was more difficult to assess the role of the modulus in the hoop direction E_φ, as for lower orthogonal ratios the model failed earlier. While E_x was kept constant to 4250

N/mm^2, the values for E_φ were varied between 360 ($R_2 = E_x / E_\varphi = 11.8$) and 880 N/mm^2 ($R_2 = 4.83$). From the profile of the symmetry vertex for 20 mm (Fig. 6.47), observations similar to the previous case can be made. The localised effect of the orthotropic material was also observed in the 3D FE models of a cylindrical cross vault developed by Jagfeld (2000), in which no detailed modelling had been carried out for the area of the unribbed groin (§2.3.5). In that case, the location and formation rate of the hinge above the abutment was not significantly affected and failure occurred at an earlier abutments movement of 404 mm, compared with the stage at the isotropic model of 550 mm.

6.5.3 Variation of flexural strength

A similar effect had variations in the strength of the materials, while the orthogonal stiffness ratio was kept to its initial value. Starting with the hoop direction, a very low tensile strength F_φ was assumed. Failure at some sections occurred quite rapidly, before the previously set limit of 5 mm movement (§6.3.1.3), and the loads were redistributed without the development of high tensile strains (Fig. 6.48), while the model failed at a movement of 13 mm. Doubling the material strength resulted in failure occurring at a much later stage.

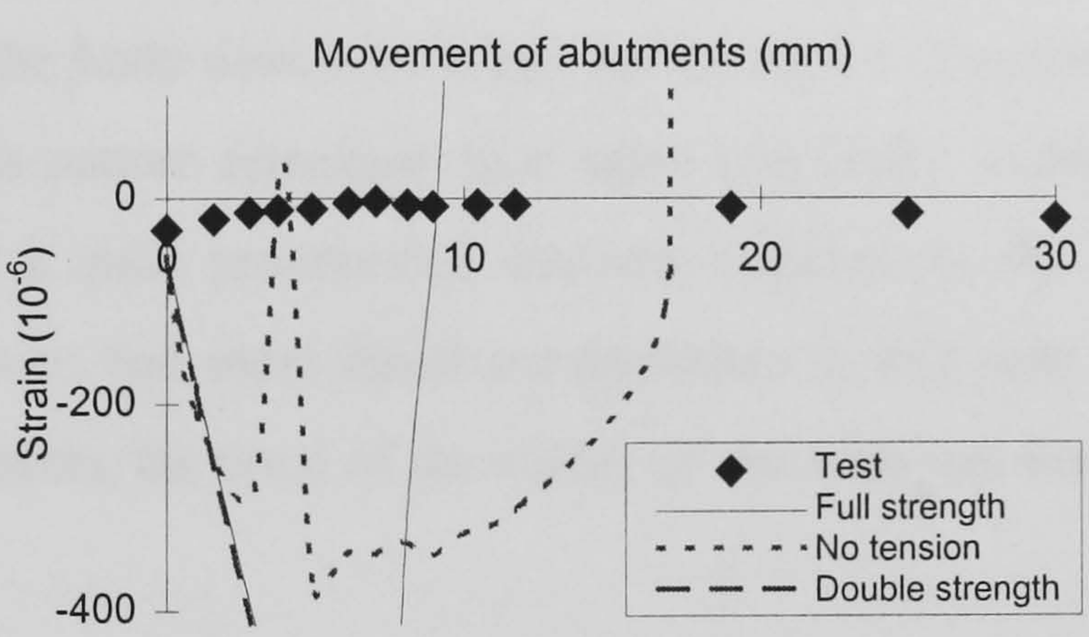

FIGURE 6.48 Effect of the flexural strength in the hoop direction, F_φ, on the hoop strain at the front of the longitudinal vertex - extrados (BT1V)

A more detailed variation of the hoop strength F_φ can give further insight on the rate of formation of the cracks at the back groin. The profile of the symmetry vertex at 10 mm (Fig. 6.49) showed that high deflection of the front portion can be the result of low hoop strength that caused the early separation of the back transverse web. As it was also discussed earlier, a fully cracked back groin can lead to the immediate collapse of the back portion of the vault, as it can occur for $F_\varphi = 0$. It was also seen in many occasions that the

movement of abutments caused a very rapid increase in the stresses to such an extent that failure was much less influenced by the actual values of strength in one direction. As a consequence, as the material became more isotropic in terms of strength (F_φ approaching $F_X = 0.98$ N/mm^2), the deformation pattern stabilised to that already established for $F_\varphi = 0.32$ N/mm^2.

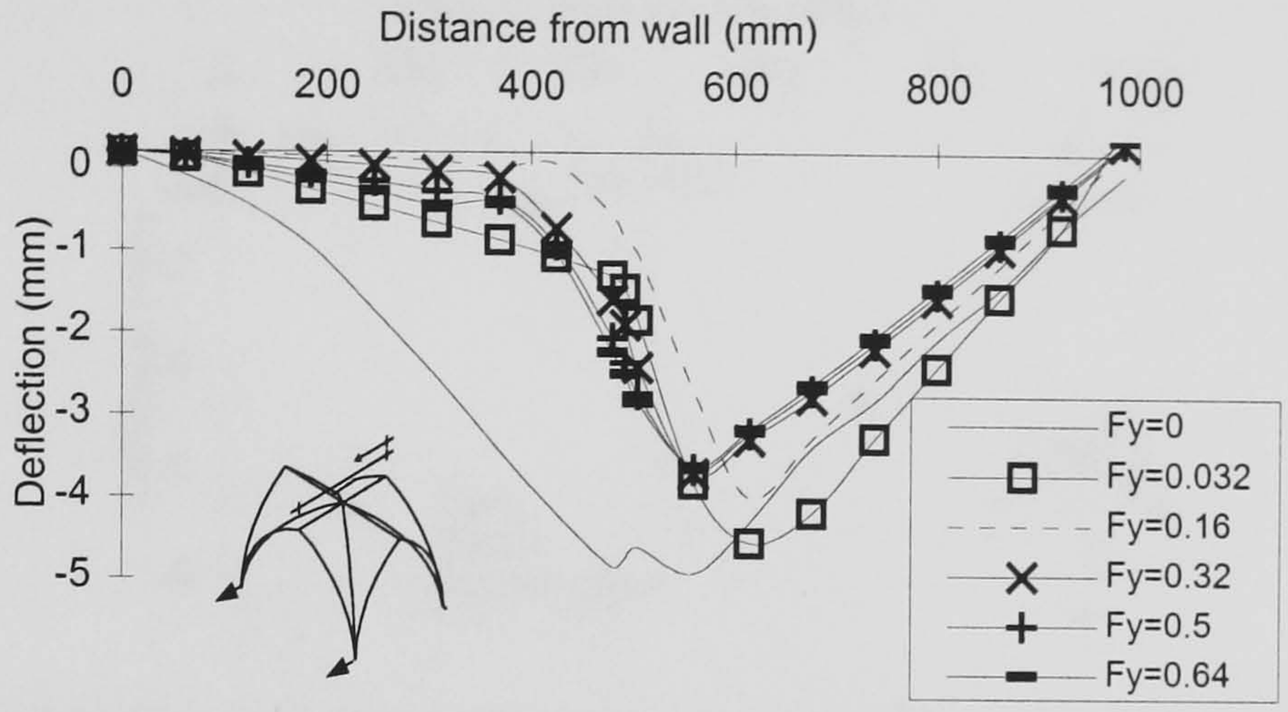

FIGURE 6.49 Effect of the flexural strength in the hoop direction, F_φ - deflection of the symmetry vertex at 10 mm movement of the abutments

Overall, no significant change in the load distribution pattern was observed for higher values of strength in the hoop direction. When the strength in the horizontal direction was varied (F_X) , the stress pattern remained once again practically unaltered, as the structure had already exhibited a quite pronounced one-way response in the transverse axis. Low tensile strength, however, had more direct consequences in this case, as after only a short displacement of abutments, the bond of the model on the wall was severed and the collapse was immediate.

6.5.4 Variations in the geometry

Discrepancies from the predictions of the FE model due to variations in the geometry of the vault were examined in the dead load analysis (§5.3.3.3) by simulating effects due to the quality of the masonry as random imperfections added to the nodal coordinates during the mesh generation. It was not possible, however, to apply imperfections greater than ±1mm as some elements became highly warped, giving rise to geometric discontinuities incompatible with the activated geometric nonlinearity. The response did not change significantly even when random imperfections of 5mm were applied mainly at the top

portion of the FE model (Fig. 6.50). The early failure of the model at a 21 mm movement of abutments was probably associated with the previously mentioned incompatibility problems rather than with structural reasons.

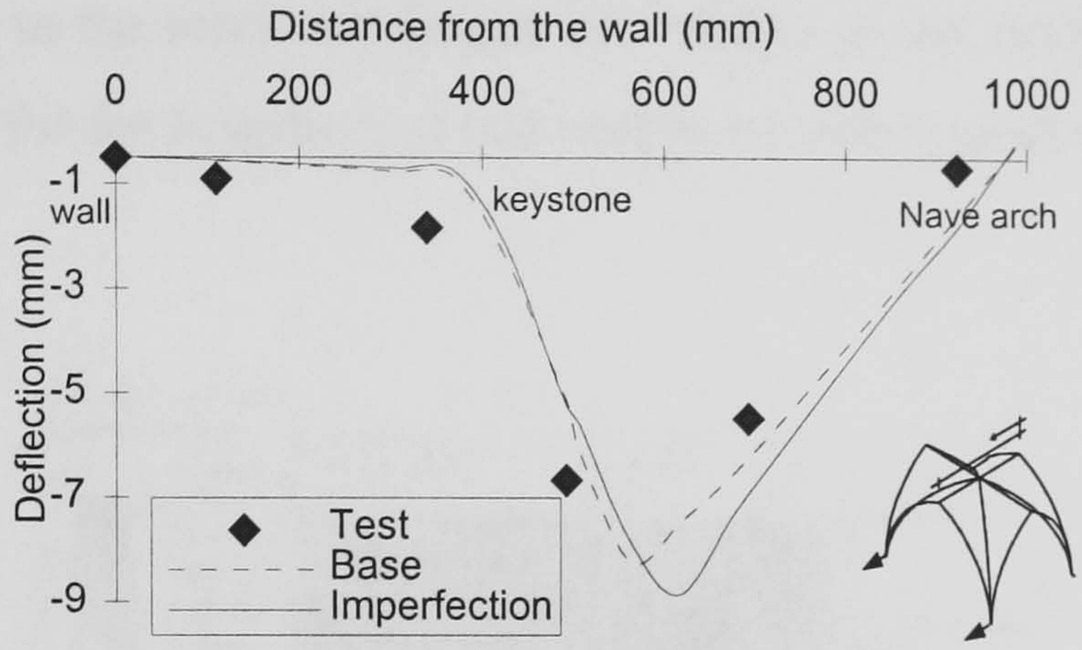

FIGURE 6.50 FE model with random geometric imperfections of 5 mm applied at the top portion of the vault for 20 mm movement of abutments

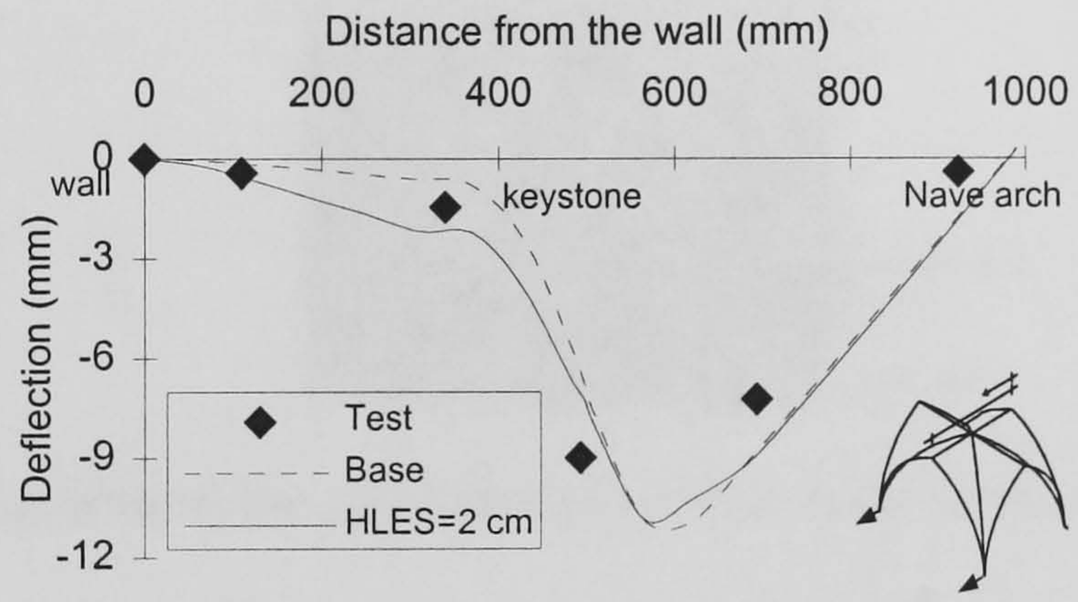

FIGURE 6.51 FE model with smoother vertices (lower uniform height by 2 cm) for a 30 mm movement of abutments

A more adequate approach to the problem of deviations from the original geometry would be to apply a uniform reduction in the height of the vertex and the immediately surrounding nodes of the FE model with the use of the Fortran pre-processor. A reasonable value of 2 cm was assumed (§5.3.3.3). The effect of smoother vertices was the development of higher bending moments at the top portions of the vault and the formation of cracks in wider areas around the groin, apart from the longitudinal cracks. As a result, the detachment of the back transverse web occurred later (Fig. 6.51) although the vault failed at 31 mm.

Further examination of the geometry of the abutments can improve the understanding of the support conditions. In Test DL5 it was seen that moderate increases in the weight and height of the spandrel fill did not have a significant effect on the response of the model vault to service conditions (§5.3.5). During the movement of abutments, however, the resistance from the pressure of the fill can produce a bending moment over the haunches that opposes to the rotation of the area caused by the spreading of the vault. This action can be simulated as a set of constraints to the rotational degree of freedom in the horizontal axis of each of the haunches (4 and 5 for the longitudinal and transverse web respectively in the notation of Abaqus).

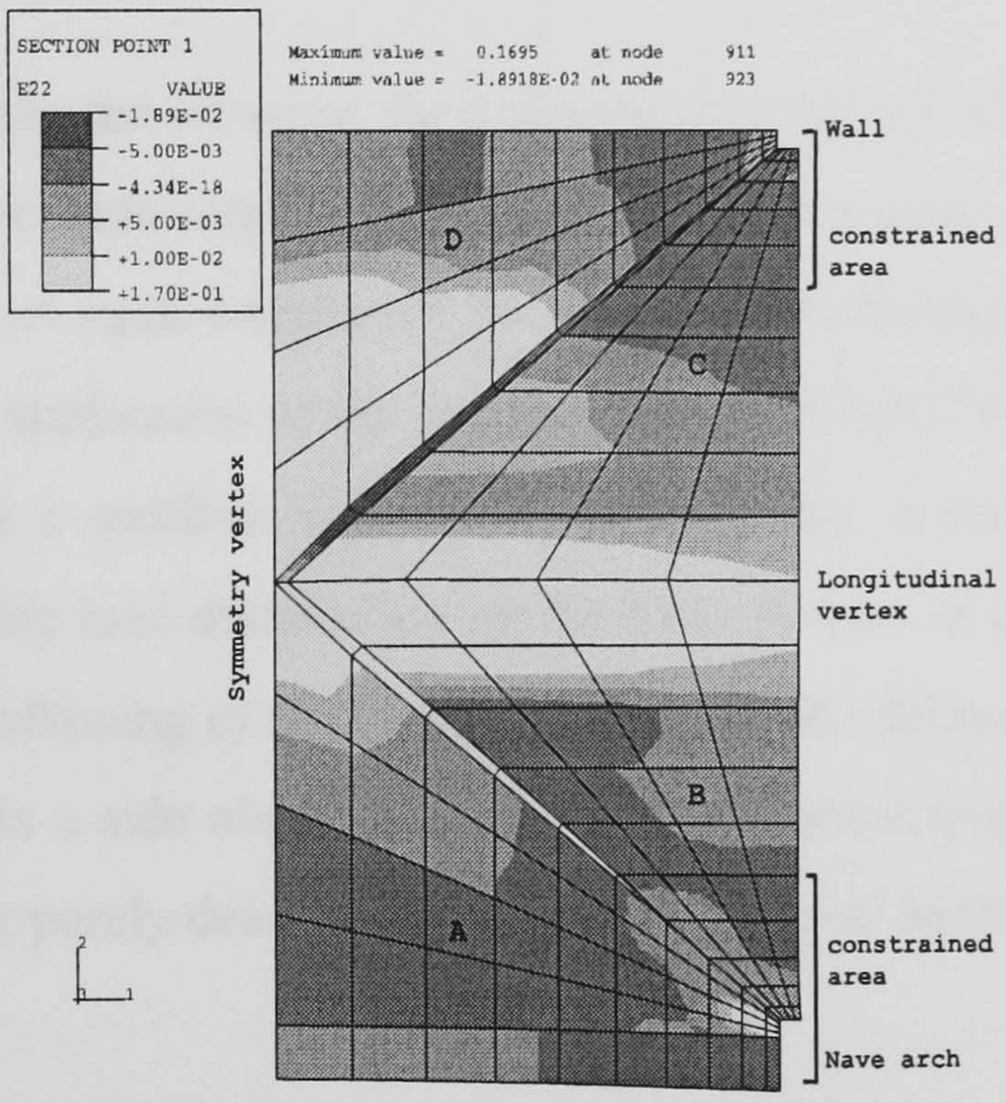

(a) Strain in the global direction 2 (E22) at the intrados

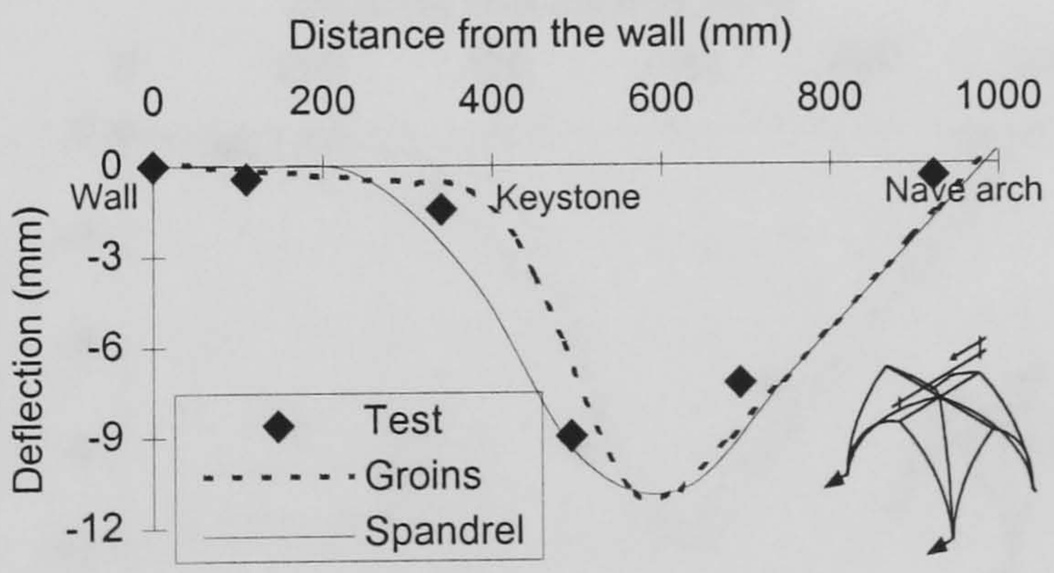

(b) Deflection of symmetry vertex

FIGURE 6.52 FE simulation of the spandrel fill at 40% of the total height with a set of rotational constraints. Response to 30 mm movement of the abutments

The major change in the response of the FE model was a higher deformation of the back portion of the vault (Fig. 6.52). The deformation pattern became more symmetrically arranged about the longitudinal vertex and the predicted smeared cracks at the front of the vertex shifted from the original area. This type of constraint increased the importance of the area of the groins as it showed that the high tensile strains propagated earlier within that area. Overall, these discrepancies were small and became more significant only when the restrained area was increased. As a result, the actual geometry of the spandrel fill did not seem to have a major effect on the response of the model vault.

6.5.5 The service load

As discussed during the set-up of the experiment in §4.4, it was not practical to apply the entire amount of the dead load that corresponded to the scale selected. Since only an amount of w=1930 N/m^2 (unit weight γ = 55 kN/m^3) was distributed on the surface, the effect of a hypothetical application of the desired load of w=2800 N/m^2 (γ = 80 kN/m^3) was examined. This caused a uniform increase by 45% in the initial stress regime, which, however, did not alter the load distribution on the front portion of the vault (Fig. 6.53), but resulted in an earlier weakening of the support at the wall and delayed the detachment of the back transverse web. As a side observation, it would be interesting to investigate whether the failure pattern under purely dead load is expected to extend to the area of the groins.

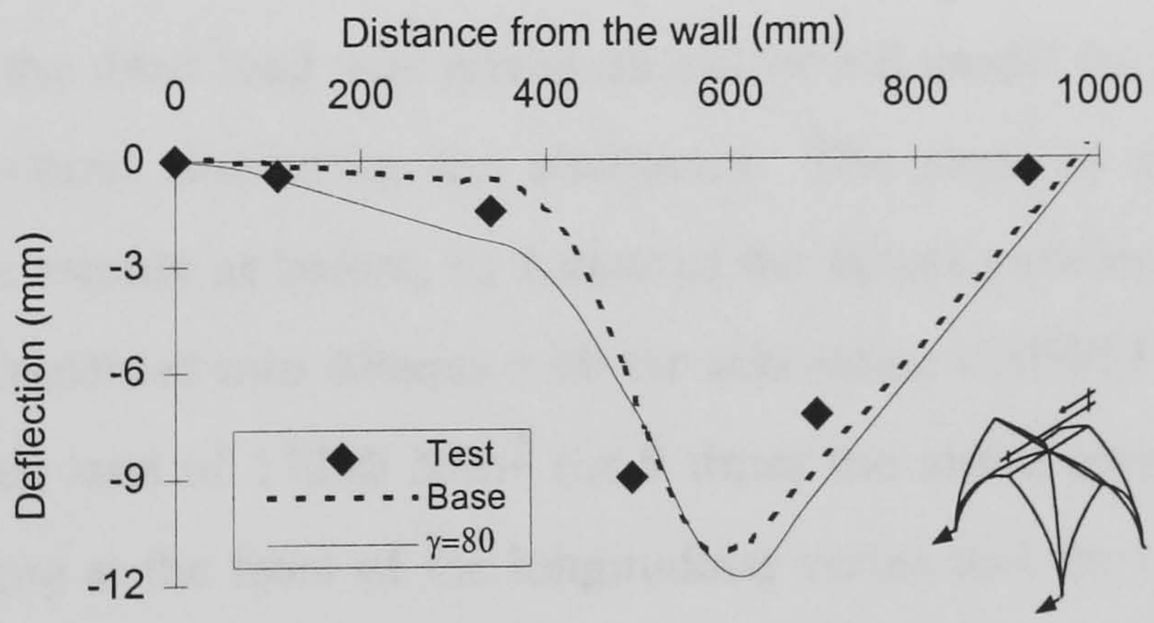

FIGURE 6.53 Effect of the amount of service load on the deflection of the symmetry vertex at a 30 mm abutment movement

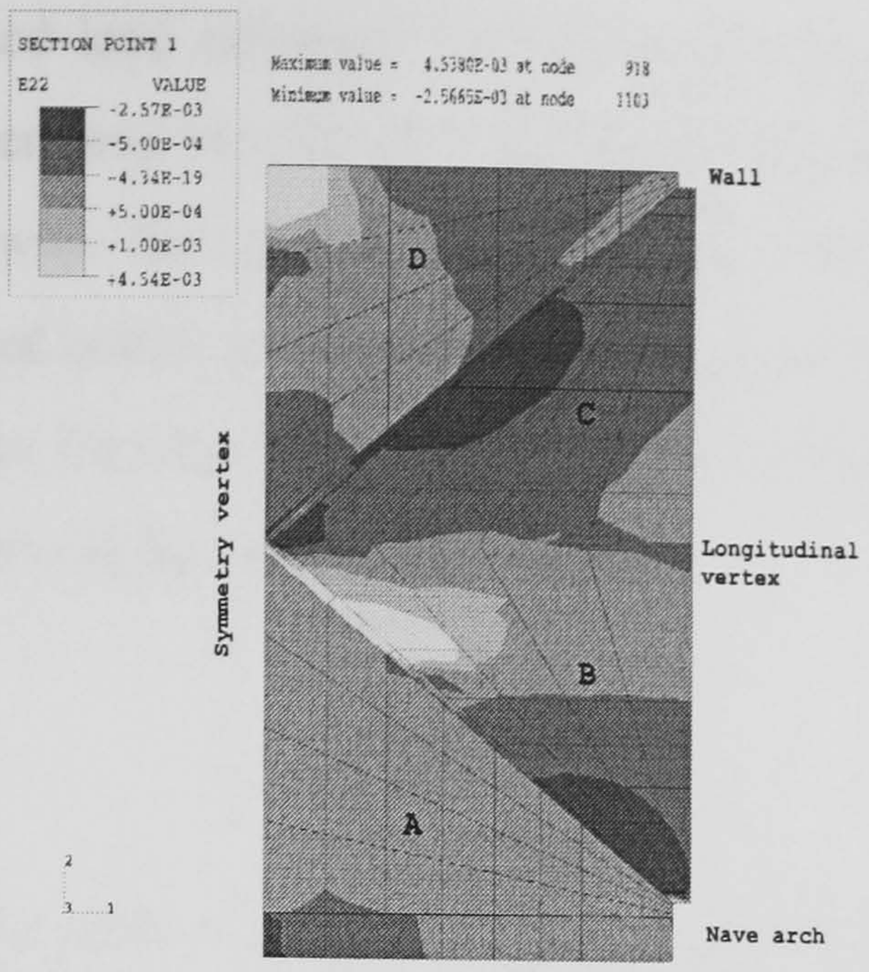

(a) Strain in the global direction 2 (E22) at w=17280 N/m^2 - intrados

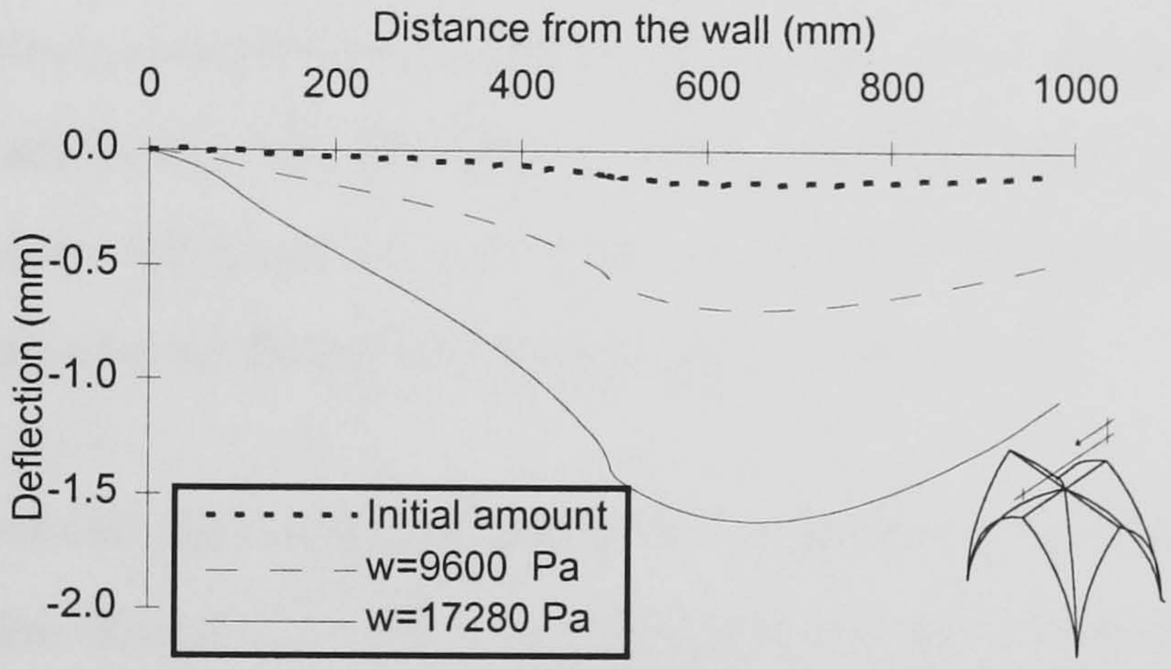

(b) Deflection of the symmetry vertex - load w distributed uniformly over the surface (in N/m^2)

FIGURE 6.54 Failure of the FE model due to dead load

Subsequently the dead load was increased on the FE model by constant increments until failure, but without displacing the abutments. The smeared crack approach was followed in the same manner as before, by means of the failure envelope in biaxial bending (Sinha 1997) as implemented into Abaqus with the subroutine USDFLD (§4.3). Failure was recorded for a surface load of 17280 N/m^2 (or 9 times the initial amount of 1920 N/m^2), with cracks developing at the front of the longitudinal vertex and the wall (Fig. 6.54a). As no failure occurred at the groin, the back transverse web did not detach from the rest of the vault and the deformation pattern was smoother around the keystone (Fig. 6.54b). Moreover, the variation of stress in the longitudinal direction was significant and the one-way behaviour was quite restrained.

Overall, the increased load enhanced the pattern observed at the FE model in the study of the response under dead weight (§5.3.4). The deformation of the vault was quite moderate in comparison with the sharp changes recorded during the movement of the abutments. The formation of cracks along the back groin appeared to be a typical feature of the response of the vault to imposed deformations, as it resulted from their absence here, although the same geometric configuration was adopted.

6.5.6 Discussion

The parametric study showed that uncertainties in the material properties or the geometry of the structure can affect mainly the location of failure at the back transverse web. The hinges at the front of the longitudinal web and the abutment (Fig. 6.4) appeared as an inherent characteristic of the geometry of the vault and their rather early development has been a common feature among all the modified FE models. Once the geometry of the groin was suitably simulated (within the limitations of the available analytical tools), the factors that drive the process of failure at the back edge of the vault and the location of the faults (wall edge or back groin) were better understood (Figs. 6.46, 47, 48).

As a final comment, the cross vault model was examined under the conditions of limit state considered in the design of modern structures. So far as reinforced concrete slabs are regarded, the deflection control in the design of a slab with similar plan dimensions as the cross vault under examination (1260 x 950 mm) requires that the final (maximum) deflection (including effects of creep and shrinkage) should not exceed (for a two-way slab) the (shorter) span / 250 ratio (BS 8110). Here, this expression yielded 4 mm and this value was recorded in the vault during the tests at an abutments movement of 10 mm, or approximately 1/100 of the transverse span. At that stage, the hinges at the front portion of the vault (abutment, longitudinal vertex) were already quite visible and the membrane crack at the back groin had started to open, although visibly appreciable only from the extrados (§6.3.2.1). As a consequence, a 10 mm movement can be considered as the serviceability limit strength of the structure, when examined under the boundary conditions specified in this test.

Regarding the minimum required thickness, the basic span / effective depth ratio for a simply supported slab, spanning less than 10 m in the shorter side, has to be less than 20,

resulting in a thickness of 47 mm, compared with the available of 35 mm. Apparently, the vault has a higher margin of safety due to the membrane action of shell structures, further enhanced by the pointed profile that adopts efficiently to the developing line of thrust and minimises the eccentricity of forces.

6.6 SUMMARY AND CONCLUSIONS

The movement of the front abutments of the structure caused a redistribution of the loads mainly closer to the edges and a sharp increase in their magnitude, even for a short imposed displacement. This led to an early development of cracks and failure according to a four-hinge pattern (Fig. 6.4), which developed in this order (cf. the widespread accepted pattern of Fig. 1.16):

1) Hinge at the front of the longitudinal vertex, intrados.

2) Hinge at the front abutment.

3) Membrane crack at the back groin.

4) Detachment from the wall.

At 30 mm movement of the abutments (Figs. 6.1 and 2) the maximum deflections occurred at the keystone, while a strong one-way behaviour developed in the transverse direction (spanning between the wall and the nave arch). Moreover, the failure of the vault appeared to be highly influenced by the stress regime of the groin.

Using a FE model that represented properly the effect of the geometry of the groin, resulted in a good level of prediction of the experimental pattern. This made possible to investigate other aspects of the response of the vault to this loading. Similarly to the discussion during service load (§5.4), the role of the groin appeared to be fundamental in the improvement of the co-action between the intersecting pointed barrel vaults. The progressive failure of the groin during the loading allowed the webs to develop an increasingly independent behaviour: as a barrel vault supported on diaphragms at the end arches for the transverse web and as a skew, wide arch for the longitudinal web.

Chapter 7

SUMMARY AND CONCLUSIONS

7.1 SUMMARY OF THE PRESENT RESEARCH

The conservation of the architectural heritage requires accurate and cost-effective interventions, which depend on the understanding of the structural scheme of the buildings. A great number of structures like cathedrals and abbeys are roofed with stone cross vaults and their structural scheme is highly determined by the containment of their lateral thrusts.

Cross vaults are very sensitive to geometric alterations, which produce a failure pattern of longitudinal cracks at the intrados of the longitudinal vertex and the extrados of the edges. Dead load and movement of the abutments are the most important actions upon these vaults and until recently the response to these loadings has been mainly established through experience.

Only few experimental projects have been carried out so far to examine the safety of cross vaults, which was correctly linked to failure due to the movement of abutments. Some quite particular case studies were investigated, however, and the data produced were not sufficient. Most of the research actually concentrates on the development of analytical models, which are mainly based on the Finite Element (FE) method or the principles of the limit state analysis.

An experimental programme was presented in this work, in which the response of a cross vault to service loading conditions and its failure mode due to movement of abutments was studied. The tests were designed to establish a failure pattern and provide a sufficient amount of data which would improve the calibration of FE models and other analytical methods. On the basis of these tests, the behaviour of the vault under service loads can be summarised as follows:

1) The deformation of the model vault is asymmetrical, with maximum deflections recorded in the front portion of the vault.

2) The area of the front haunches is in a state of pure membrane compression.

3) The co-action between the four webs is highly dependent on the strength of the groins.

4) In service loading conditions, the stresses are below the strength of the material.

5) Areas of tensile stress develop at the intrados, at the front part of the longitudinal vertex, and normal to edge over the wall, indicating possible zones of cracks initiation.

6) Spandrels filled up to 70% of the total height have no significant effect on the behaviour of the vault.

FE models were developed to analyse and further interpret the behaviour of the vault. The preliminary FE model had to be refined by introducing spring elements between the webs joining at the groin and the ribs, in order to simulate the effect of the geometry of the groins. After this area was strengthened during the tests, a FE model that represented the groins with shell elements gave the best agreement with the experiment.

The failure of the vault occurred due to the formation of four hinges during the movement of abutments. The hinges formed in the following order:

1) Hinge at the front of the longitudinal vertex, intrados.

2) Hinge at the front abutment.

3) Membrane crack at the back groin.

4) Detachment from the wall.

This pattern confirmed that aisle vaults at the church of Holyrood Abbey, which is the case study examined here, may have collapsed due to an excessive movement of their abutments, caused by an unsuitable intervention which overloaded the central vault.

This action caused a redistribution of the loads at the abutments and the wall and a sharp increase in the deformation. A strong one-way behaviour developed in the transverse direction. The deformation of the vault was more symmetrical, as the nave arch acted as a

diaphragm similarly to the wall, and maximum deflections were recorded at the keystone. A parametric study and an examination of some features of the model vault with the FE model showed that the above mentioned failure pattern depended less on the material properties or the exact geometric configuration and the vault had a quite high strength against dead load.

The role of the groin appeared to be important and its progressive failure during the loading allowed the webs to develop an increasingly independent behaviour: the transverse web acted as a barrel vault, supported on diaphragms at the end arches, and the longitudinal web acted as a skew wide arch.

7.2 SUGGESTIONS FOR FURTHER RESEARCH

During the discussion on the behaviour of the vault it became apparent that certain aspects would need to be addressed in more depth as part of further research on the safety evaluation of cross vaults.

A model vault of a bigger scale would permit the use of demec gauges or LVDT's to determine the distribution of the loads within the shell. In that case, a higher amount of dead load could also be applied more safely. In addition, some details like the groins could be treated suitably and geometric or material variations would have a smaller effect. The effect of the spandrel fill needs to be more exhaustively investigated by even considering a complete coverage of the vault.

So far as other aspects of the loading are concerned, failure can be studied as a result of differential horizontal movement of the abutments or settlement of the supports. Another loading condition regards the effect of the upper structure of the churches, which can be simulated as a dead load upon the front portion of the model vault.

Some analytical aspects of the problem could be better resolved with a suitable representation of the crack development. Simulations like micromodels can be useful for an initial assessment of the cracks initiation. Furthermore, the possibilities of other sophisticated models for the masonry can be investigated. In all these modellings, a balance has to be achieved between the rate of numerical convergence and the correct representation of certain geometric features.

REFERENCES

Abraham, P. (1934). *Viollet-le-Duc et le rationalisme médiéval*. Vincent, Paris, France (after Heyman 1995).

Acland, J. H. (1972). *Medieval structure: the gothic vault*. Univ. of Toronto Press, Toronto, Canada.

Adam, J. P. (1999). Roman building; materials and techniques. Routledge, London.

(Les) Allemands destructeurs de cathédrales et de trésors du passé: mémoire relatif aux bombardements de Reims--Arras--Senlis--Louvain--Soissons, etc. (1919). Hachette et cie., Paris, France (in French).

Angotti, F., Chiostrini, S., and Vignoli, A. (1991). "An experimental research on the behaviour of stone masonry structures." *Proc., 9th Int. Brick/Block Masonry Conf.*, W. Jäger, ed., Berlin, Germany.

Arnot, H. (1788). *The history of Edinburgh from the earliest accounts to the present time*. Robinson & Co., Edinburgh.

Ashwell, D. G. and Gallagher, R. H., Editors, (1976). *Finite elements for thin shells and curved members*, John Wiley and Sons, London.

BAA (British Archaeological Association) (1986). *Medieval art and architecture at Lincoln Cathedral*. Conference transactions v. VIII (1982).

Bailey, R. M. (1996). *Scottish Architects' papers - a source book*. Rutland Press, Edinburgh.

Baldwin Brown, G. (1909). "Preservation of Holyrood Chapel." *J. Royal Inst. British Architects*, 3rd series, vol. XVI, 20 March.

Baronio, G., and Binda, L. (1991). "Experimental approach to a procedure for the investigation of historic mortars." *Proc., 9th Int. Brick/Block Masonry Conf.*, W. Jäger, ed., Berlin, Germany.

Barthel, R. (1989). "Computer simulation of the structural behaviour of masonry cross vaults." *Proc. Struct. Conservation Historic Masonry*, ICCROM, Athens, Hellas.

Barthel, R. (1993). "Crack formation in masonry cross vaults." *Proc., Symp. Struct. Preservation of the Architectural Heritage*, IABSE, Zurich, Switzerland.

Barthel, R. (1994). "Tragverhalten und Berechnung gemauerter Kreuzgewölbe." *Erhalten historisch bedeutsamer Bauwerke, Jahrbuch 1992, SFB 315, Universität Karlsruhe*, Ernst & Sohn, Berlin, Germany (in German).

Beckmann, P. (1994). *Structural aspects of building conservation*. McGraw-Hill, Berkshire.

Benedetto, C., Del Bufalo, A. (1991). *MTM T3 - Volte, archi e cupole: aspetti costruttivi*. University of L'Aquila, Faculty of Engineering, L'Aquila, Italy (in Italian).

Benvenuto, E. (1990). An introduction to the history of structural mechanics. v. 2 Vaulted structures and elastic systems. Springer-Verlag, New York, USA.

Bilson, J. (1906). "Amiens Cathedral and Mr. Goodyear's "refinements" - a criticism." *J. Royal Inst. British Architects*, 3rd series, vol. XIII, No. 15.

Biodata (1991). *Microlink Hardware user's manual*. Biodata Ltd.

Blasi, C. and Foraboschi, P. (1995). "Analytical approach to collapse mechanisms of circular masonry arch", *J. Struct. Engrg.*, ASCE, 120(8).

Bork, R., Mark, R., and Murray, S. (1997). "The openwork flying buttresses of Amiens Cathedral." *J. Soc. Architectural Historians*, 56(4).

Boyd, T. D. (1978). "The arch and the vault in Greek architecture." *Am. J. of Archaeology*, v. 82.

BSI (British Standard Institution) (1992). "Code of practice for structural use of masonry:" *BS5628; Unreinforced masonry: part 1*, London.

Bunyan, I. T., Fairhurst, J. A., Mackie, A., and Macmillan, A. A. (1987). *Building stones of Edinburgh.* Edinburgh Geological Society, Edinburgh.

Cassinello Plaza, M. J. (1997). "Bóvedas góticas españolas. Influencia de la configuración constructiva actual en su estabilidad." *Proc., 1st Nat. Cong. on History of Construction.* Instituto Juan de Herrera, Madrid, Spain (in Spanish).

Cauvin, A. and Stagnitto, G. (1995). "Criteria of design and methods of structural analysis of gothic ribbed vaults using traditional and computer methods." *Proc., Spatial structures: past, present and future*. IASS, Milan, Italy.

Ceradini, V. (1996). "Modelli sperimentali di volte." *Proc., La meccanica delle murature tra teoria e progetto*, Univ. of Messina, Pitagora Editrice, Bologna, Italy (in Italian).

Chen, W. F. and Saleeb, A. F. (1982). *Constitutive equations for engineering materials, Vol.1, Elasticity and modeling.* Chichester-Wiley, New York, USA.

Choisy, A. (1873). *L'art de bâtir chez les Romains*. Paris, France (in French).

Cigni, G. (1983). *Il consolidamento murario.* Edizioni Kappa, Rome (in Italian).

Clifton-Taylor, A. (1986). *The Cathedrals of England*. Thames and Hudson Ltd., London.

Coles, F. R. (1896). "Notes on Saint Anthony's Chapel; with views and plans", *Proc. Soc. Antiquarians of Scotland*, vol. XXX.

Coste, A. (1995). "Le calcul par la méthode des éléments finis appliqué à la restauration. Une expérience: la cathédrale de Beauvais." *Proc., Entre mécanique et architecture*. E. Benvenuto and P. Radelet-de-Grave, eds., Birkhäuser Verlag, Basel, Switzerland (in French).

Coste, A. (1998). "The relationship between the Gothic model and the conception of bridges." *Proc., 2nd Int. Arch Bridge Conf.*, A. A. Balkema, Rotterdam, Holland.

Croci, G., Viskovic, A., and Sabbadini, F. (1995). "Some aspects of the structural behaviour of gothic cathedrals." *Proc., Spatial structures: past, present and future*, IASS, Milan, Italy.

Croci, G. (1998a). "The basilica of St. Francis of Assisi after the September 1997 earthquake.", *Structural Engrg Int.*, IABSE, 8(1).

Croci, G. (1998b). "The collapses occurred in the Basilica of St. Francis of Assisi and in the Cathedral of Noto." *Proc. Structural analysis of historical constructions II*, P. Roca, J. L. González, E. Oñate and P. B. Lourenço, eds., CIMNE, Barcelona, Spain.

Cross, M. (1994). *Bibliography of monuments in the care of the Secretary of State for Scotland*. University of Glasgow, Department of Archaeology, Glasgow.

Dally, J. W., and Riley, W. F. (1965). *Experimental stress analysis*. McGraw-Hill, New York, USA.

EAA (Edinburgh Architectural Association) (1910). "The proposed restoration of the Chapel Royal, Edinburgh.", *Trans. Edinburgh Archit. Ass.*, vol. 5.

Eeles, F. C. (1915). "Mediaeval stained glass recently recovered from the ruins of Holyrood Abbey Church", *Proc. Soc. Antiquarians of Scotland*, vol. XLIX.

Fawcett, R. (1995). *Scottish Abbeys and Priories*. HMSO, London.

Fawcett, R. (1998). *Scottish Cathedrals*. B. T. Batsford Ltd, London.

Fitchen, J. (1961). The construction of Gothic cathedrals: a study of medieval vault erection. Clarendon Press, Oxford.

Fletcher, B. F. , Cruickshank, D., Saint, A., Blundell-Jones, P., and Frampton, K. (1996). *Sir Banister Fletcher's history of architecture*. Architectural Press, London.

Flügge, W. (1973). Stresses in shells. Springer-Verlag, New York, USA.

Gibson, J. E., and Cooper, D. W. (1954). *The design of cylindrical shell roofs*. E & FN Spon, London.

Gifford, J., McWilliam, C., and Walker, D. (1984). *The buildings of Scotland: Edinburgh*. Penguin, Harmondsworth, London.

Gilman, R. (1920). "The theory of gothic architecture and the effect of shellfire at Rheims and Soissons." *Am. J. of Archaeology*, 2nd series, vol. 24, no. 1.

Giovannoni, G. (1972). *La tecnica di costruire presso i Romani*. Bardi Editore, Rome, Italy (in Italian).

Giuffré, A. (1988). "Restauro e sicurezza in zona sismica; la Cattedrale di Sant'Angelo dei Lombardi." *Palladio, Rivista di Storia dell'Architettura e Restauro*, Istituto Poligrafico e Zecca dello Stato, Rome, Italy, n. s., anno I, No. 2. (in Italian).

Giuffré, A. (1991). *Lettura sulla meccanica delle murature storiche*. Edizioni Kappa, Rome, Italy (in Italian).

Giuffredi, A., Iemmi, F., and Cigarini, C. (1991). *Il cantiere di restauro*. Alinea editrice s.r.l., Florence, Italy (in Italian).

Giuliani, C. F. (1990). *L'edilizia nell'antichitá*. Studi superiori NIS, La Nuova Italia Scientifica, Rome, Italy (in Italian).

Goodyear, W. H. (1905). *Illustrated catalogue of photographs & surveys of architectural refinements in medieval buildings: lent by the Brooklyn Museum of Arts and Sciences*. Morrison and Gibb, Edinburgh.

Goodyear, W. H. (1909). "Amiens cathedral and Mr. Bilson's rejoinder." *J. Royal Inst. British Architects*, vol. XVI, third series, 25 September.

Grodecki, L. (1986). *Gothic architecture*. Faber, London.

Harrison, J. (1919). *The history of the Monastery of the Holy-rood and of the Palace of Holyroodhouse*. W. Blackwood and Sons, Edinburgh and London.

Harvey, W. J. (1988). "Application of the mechanism analysis to masonry arches." *The Structural Engineer*, Inst. of Struct. Engineers 66(5).

Hendry, A. W. (1976). "Test on walls of Craigleith stone masonry." *Proc. Bearing walls, meeting of CIB working commission W23A*. Edinburgh.

Hendry, A. W., Sinha, B. P. and Davies, S R. (1997). *Design of masonry structures*. E & FN Spon, London.

Hetenyi, M. (1950). *Handbook of experimental stress analysis*. Wiley, New York, USA.

Heyman, J. (1966). "The stone skeleton." *Int. J. Solids Structures*, vol. 2, pp. 249-279.

Heyman, J. (1977). *Equilibrium of shell structures*. Clarendon Press, Oxford.

Heyman, J. (1995). *The stone skeleton. Structural engineering of masonry architecture*. Cambridge University Press, Cambridge.

HKS (Hibbit, Karlsson & Sorensen Inc.) (1998). *ABAQUS/Standard User's Manual, Version 5.8*. HKS Inc., Pawtucket, RI, USA.

"Holyroodhouse Abbey falls down." (1768). The Scots Magazine, 3 December.

Huang, H. C. (1989). *Static and dynamic analyses of plates and shells*. Springer-Verlag, London.

Illston, J. M., Dinwoodie, J. M., Smith, A. A. (1979). *Concrete, timber and metals; the nature and behaviour of structural materials*. Van Nostrand Reinhold, New York, USA.

Jäger, W., Bergander, H. (1997). "Non-linear analysis of ancient structures." *Proc., Int. Conf. on Studies in Ancient Structures*, Yildiz Technical University, Istanbul, Turkey.

Jagfeld, M. (2000). *Tragverhalten und statische Berechnung gemauerter Gewölbe: Untersuchungen mit der Finite-Elemente-Methode*. Shaker, Aachen, Germany (in German).

James, J. (1979). *The contractors of Chartres*. Mandorla, Dooralong, Australia.

James, J. (1991). "The rib vaults of Durham Cathedral."

Kooharian, A. (1953). "Limit analysis of voussoir (segmental) and concrete arches", *J. Am. Concrete Inst.*, ACI, 89(1).

Laing, D. (1852). "On the state of the Abbey Church of Holyrood subsequently to the devastations committed by the English Forces in the years 1544 and 1547." *Proc. Soc. Antiquarians of Scotland*, vol. I.

Lenza, P. (1991). "Elastic models for a seismic analysis of masonry vaults." *Proc., 9th Int. Brick/Block Masonry Conf.*, W. Jäger, ed., Berlin, Germany.

Lilley, D. M. (1993). "An appraisal of the topology and loading of a section of the vaulted roof of Durham Cathedral." *Proc., Engineering a Cathedral, Durham*, M. Jackson, ed., Thomas Telford, London.

Lilley, D. M. (1995). "The structural performance of the vaulted masonry roof of Durham Cathedral." *Proc, 4th Int. Masonry Conf., Proc. of the British Masonry Soc. (7)*, London.

Lourenço, P. B. (1998). "Continuum model for masonry: parameter estimation and validation." *J. Struct. Engrg.*, ASCE 124(6).

Lourenço, P. B. (1999). "Two examples of analysis of historical structures." *36th Meeting of the Committee W023 - Wall Structures from CIB*, Porto, Portugal.

MacDonald, W. L., Pinto, J. A. (1995). *Hadrian's Villa and its legacy*. Yale University Press, New Haven, USA.

MacGibbon, D., Ross, T. (1897). The ecclesiastical architecture of Scotland from the earliest Christian times to the seventeenth century. D. Douglas, Edinburgh.

Mainstone, R. J. (1968). "Structural theory and design before 1742." *The Architectural Review*, April 1968.

Mainstone, R. J. (1998). *Developments in structural form*. Architectural Press, London.

Maitland, W. (1757). *The history and antiquities of Scotland, from the earliest account of time*.... A. Millar, London.

Mark, R., Abel, J. F. and O'Neill, K. (1973). "Photoelastic and Finite-element Analysis of a Quadripartite Vault." *Experimental Mechanics*, Vol. 13, August.

Mark, R. (1982). *Experiments in gothic structures*. MIT Press, Cambridge, Mass., USA.

Mark, R. (1990). Light, wind and structure: the mystery of the master builders. MIT Press, Cambridge, Mass., USA.

Martínez, J. L., Martín-Caro, J. A., Torrico, J. and León, J. (2000). "The "Silla de la Reina" tower in the Cathedral of León." *Proc. 12th Int. Brick/Block Masonry Conf.*, Madrid, Spain

Masson, H. (1935). "Le rationalisme dans l'Architecture du Moyen Age." *Bulletin monumental*, XCIV (in French).

Maunder, E. W. A. (1995). "Some structural studies of Exeter Cathedral." *The Structural Engineer*, Inst. of Struct. Engineers 73(4).

Méry, E. (1840). "Memoire sur l'équilibre des voûtes en berçeau." *Annales des Ponts et Chaussées* (in French; after Benvenuto 1990).

Molins, C. and Roca, P. (1998). "Capacity of masonry arches and spatial frames." *J. Struct. Engrg.*, ASCE 124(6).

Murray, S. (1989). *Beauvais Cathedral: architecture of transcendence*. Princeton University Press, Princeton, N.J., USA.

Murray, S. (1996). Notre-Dame Cathedral of Amiens; the power of change in Gothic. Cambridge University Press, Cambridge.

Mylne, R. S. (1893). *The Master Masons to the Crown of Scotland and their works*. Scott & Ferguson and Burness & Co., Edinburgh.

Ng, C. L. (1996). *Experimental and theoretical investigation of the behaviour of brickwork cladding panel subjected to lateral loading*. PhD Dissertation. Dept. of Civil Engrg. University of Edinburgh.

Oldrieve, W. T. (1911). "Recent excavations and researches at Holyrood." *The Book of the Old Edinburgh Club*, vol. IV, Edinburgh.

Oldrieve, W. T. (1912). "Notes on recent excavations and researches." *Trans. Scottish Ecclesiological Soc.*, v. 3.

Ortolani, F. (1988). "Effetti del terremoto sulle strutture laterizie voltate." *Palladio, Rivista di Storia dell'Architettura e Restauro*, Rome, Italy, n. s., anno I, No. 2. (in Italian).

Owen, D. R. J. and Hinton, E. (1980). *Finite elements in plasticity: theory and practice*. Pineridge Press Ltd., Swansea.

Paton, H. M., Imrie, J., and Dunbar, J. G. (1982). *Accounts of the masters of Works for building and repairing Royal Palaces and Castles*. HMSO, Edinburgh.

Pieper, K. (1983). *Zur Sicherung historischer Bauten*. Ernst & Sohn, Berlin, Germany (in German).

Poleni, G. (1748). *Memorie istoriche della Gran Cupola del Tempio Vaticano*. Stamperia del Seminario, Padova, Italy (in Italian).

Porter, A. K. (1911). *The construction of Lombard and Gothic vaults*. Yale University Press, New Haven, USA.

Press, W. H. et al. (1992). *Numerical recipes in FORTRAN : the art of scientific computing*. Cambridge University Press, Cambridge.

Quintas Ripoll, V. and De La Torre, J. F. (1993). "On gothic structural behaviour." *Proc., Symp. Public assembly structures from antiquity to the present*. IASS, Constantinople (Istanbul), Turkey.

Quintas Ripoll, V. (1995). "A study of the structural behaviour of Beauvais Cathedral" *Structural studies of historic buildings IV*, C. A. Brebbia and B. Leftheris, eds., Computational Mechanics Publications, Southampton.

RCAHMS (1951). *Inventory of Monuments in Edinburgh*. Royal Comission of Ancient and Historic Monuments of Scotland, HMSO, Edinburgh.

Rebasa Diaz, E. (1997). "Técnicas góticas y renacentistas en el trazado y la talla de las bóvedas de crucería españolas del siglo XVI." *Proc., 1st Nat. Congress of History of Construction,* Instituto Juan de Herrera, Madrid, Spain (in Spanish).

Rivoira, G. T. (1925). *Roman architecture and its principles of construction under the Empire: with an appendix on the evolution of the dome up to the XVIIth century*. The Clarendon Press, Oxford.

Robertson, W. W. (1892). "Holyrood Abbey and Palace." *Trans. Edinburgh Architectural Ass.*, vol. 2.

Roca, P., Pellegrini, L., Oñate, E., and Hanganu, A. (1998). "Analysis of the structure of Gothic cathedrals; Application to Barcelona Cathedral." *Proc., Structural Analysis of Historical Constructions II*, P. Roca, J. L. González, E. Oñate and P. B. Lourenço, eds., CIMNE, Barcelona, Spain.

Ronca, P. (2000). "Numerical testing on the structural seismic performance of the Gothic vaults: the case of the Basilica Superiore in Assisi." *Proc., 12th Int. Brick/Block Masonry Conf.*, Madrid, Spain.

Rondelet, J. (1848). *Traité théorique et pratique de l'art de bâtir*. Paris, France (in French: after Benvenuto 1990).

Rosenberg, G. (1936). "The functional aspect of the Gothic style." *J. Royal Inst. British Architects*, v. XLIII.

Rovira y Rabassa, A. (1899). *Estereotomía de la piedra.* Librería y estampería artística. Barcelona, Spain (in Spanish).

Sabbadini, F. (1993). *Analisi del comportamento strutturale di una cattedrale gotica.* Engineer's Thesis, Dept. Struct. and Geotechnical Engrg., University of Rome "La Sapienza", Rome, Italy (in Italian).

Sanabria, S. L. (1982). "The mechaniazation of design in the 16th century: the structural formulae of Rodrigo Gil de Hontañón.", *J. Soc. Architectural Historians*, XLI(4).

Scherer, G. W. (1999). "Crystallization in pores." *Cement Concr. Res.*, 29, 1347-1358.

Scordelis, A. and Lo, K. S. (1964). "Computer analysis of concrete shells." *J. Am. Concrete Inst.*, ACI, 61.

Sinha, B. P. (1978). "A simplified ultimate load analysis of laterally loaded model orthotropic brickwork panels of low tensile strength." *The Structural Engineer*, Inst. of Struct. Engineers, 56b(4).

Sinha, B. P. (1980). "An ultimate load analysis of laterally loaded brickwork panels." *Int. J. Masonry Construction*, 1(2).

Sinha, B. P., Ng, C. L., and Pedreschi, R. F. (1997). "Failure criterion and behaviour of brickwork in biaxial bending." *J. Materials in Civil Engrg.*, ASCE, 9(2).

Sinopoli, A. (1997). "Modern formulation for pre-elastic theories for masonry arches." *J. Eng. Mechanics*, ASCE 123(3).

Stalley, R. (1999). *Early medieval architecture*. Oxford History of Art, Oxford University Press, Oxford.

Taupin, J. L. (1993). "Cathédrale de Beauvais: de l'incertitude à la decision." *Proc., Symp. Struct. Preservation of the Architectural Heritage*, IABSE, Zurich, Switzerland (in French).

Theodossopoulos, D. (1995). *Analisi strutturale della Cattedrale di Burgos*. Specialization Thesis, Sc. Spec.ne Restauro Monumenti, Univ. of Rome "La Sapienza", Italy (in Italian).

Ungewitter, G. G. and Mohrmann, K. (1890). *Lehrbuch der gotischen Konstruktionen*. Tauchnitz, Leipzig, Germany (after Barthel 1994 and Heyman 1995).

Viollet-le-Duc, E. E. (1868). *Dictionnaire raisonnée de l'Architecture Française du XI au XVI Siècle*. B. Bance, Paris (1858-68).

Zevi, B (1957). *Architecture as space: how to look at architecture*. Horizon Press, New York, USA.

ARCHIVE SOURCES

National Archives of Scotland (NAS)

Exchequer Records (Inventory of records of the King's Remembrancer's Office (Treasury Department), 1708-1837, vols. E301-350)

- E305 Treasury Minutes Book. Vol. 7: 30/11/1763-23/2/1770
- E306 Register of Orders (Orders relating to Treasury and Revenue business). Vol. 2: 16/2/1738-22/2/1754. Vol. 3: 23/2/1754-1/10/1771
- E310/1/2 King's Remembrancer Letter Book 1748-1783
- E342 Buildings and Works. Vol. 9: 1773-1833

National Library of Scotland (NLS)

MS 5371 Stewart Stevenson

DRAWINGS AND GRAPHIC MATERIAL

Edinburgh City Library (ECL)

pYDA 2065(753) - 1961 "The Abby Church of Holyrood-House", drawn by Fourdrinier. 1753.

pYDA 2065(753) - 599 "Inside of Holy Rood Chapel; viewd from the East", drawn by Sparron, 1788.

National Monuments Record, Scotland (NMR)

A46263 "Aerial view from NW (prior to collapse)". original from an album of examples collected by J. Brown, ca. 1830

EDD/3/7 "Abbey Church of Holyrood. Details of one bay on south side", 1909.

EDD/3/8 "Holyrood Abbey Church. Details of nave, elevations and sections", 1909

EDD/3/143/P "Interior from W (prior to collapse as it was in the reign of James VII". Restored by N. Tennant, achitect, engraved by J. Weir, 1849.

EDD/3/151/P "Perspective elevation". Signed James Gillespie Graham 1836. Drawing and design by A W N Pugin.

EDD/3/153/P "Interior perspective". Signed James Gillespie Graham 1836. Drawing and design A W N Pugin.

EDD/3/197/P "South wall. Interior as existing". James Gillespie Graham or office (dated 1832)

EDD/3/232 "Compartment. Elevation & section". James Gillespie Graham, drawn by. A. W. N. Pugin. 1837.

EDD/4/105/P. Plans for Holyroodhouse Palace by John Mylne, 1663. (Original in the Bodleian Library, Oxford)

EDD/4/82/P. View from N (prior to collapse). Copy from a panelled overdoor at Dyrham Park, Glos., 1700.

APPENDIX

PUBLISHED PAPERS

Theodossopoulos, D., Sinha, B. P., Usmani. A. S., and Macdonald, A. J. (2000). "Structural behaviour of historic masonry cross vaults." *Proc., 12th Int. Brick/Block Masonry Conf.*, Madrid, Spain, 1791-1800.

Theodossopoulos, D. , Sinha, B. P., Usmani. A. S., and Macdonald, A. J. (2000). "Assessment of the behaviour of masonry cross vaults." *Proc. Meeting on Structural Monitoring,* BSSM, Inst. of Civil Engineers, Inst. of Structural Engineers, Glasgow.

Lemaitre J., Chaboche J.L. (1985) "Mécanique des matériaux solides", Dunod-Bordas, Paris.

Mazars J., Berthaud Y., Ramtani S. (1990) "The unilateral behaviour of damaged concrete", Engng. Fracture Mech., vol. 35, pp. 629-635.

Mirabella Roberti G., Anzani A. and Binda L. (1998) "The behaviour of ancient masonry towers under long term and cyclic actions" in 'Computer Methods in Structural Masonry – 4', ed. by G. N. Pande, J. Middleton & B. Kralj (E & FN Spon, London and New York) pp. 236-243.

Papa E., Taliercio A. (1996) "Anisotropic damage model for the multiaxial static and fatigue behaviour of plain concrete", Engng Frac. Mech., vol. 55, p. 163-179,

Papa E., Taliercio A. (1998) "Anisotropic damage model for the triaxial creep behaviour of plain concrete", in 'Damage Mechanics in Engineering Materials', ed. by G.Z. Voyiadjis, J.-W.W. Ju, J.-L. Chaboche, Elsevier Science, pp. 337-350.

12TH INTERNATIONAL
BRICK/BLOCK
Masonry
CONFERENCE

12th IBMaC
MADRID-SPAIN
25-28 June 2000

The

STRUCTURAL BEHAVIOUR OF HISTORIC MASONRY CROSS VAULTS

D. Theodossopoulos[1], B. P. Sinha[1], A. S. Usmani[1], A. J. Macdonald[2]
[1]School of Civil and Environmental Engineering, University of Edinburgh,
King's Buildings, EDINBURGH EH9 3JN, UK
[2]Departament of Architecture, University of Edinburgh,
20 Chambers Street, EDINBURGH EH1 1 JZ, UK

ABSTRACT

Masonry cross vaults are one of the main structural features of medieval Gothic Cathedrals. In order to preserve their functional integrity, their safety must be assessed under a variety of loading conditions up to failure. A 1/4 scale model was built, representing an aisle vault from the Church of the Holyrood Abbey in Edinburgh, that has partially collapsed. The model was loaded with dead weight and deformations and strains were recorded. Theoretical analysis with FEM is in good agreement with the experimental stress and deflections pattern, showing an area of development of tensile stress around the transverse vertex and the wall.

Key words: *Cross-vaults, masonry, monument, Holyrood, conservation, Gothic*

INTRODUCTION

Cross vaults were used in medieval structures when large spans had to be covered in an inexpensive and safe manner. As a result of the intersection of two barrel vaults, their arch profile allowed the loads to be carried mainly in compression, while the stiffness of the groin, enhanced with a rib, reduced significantly the longitudinal stresses. They could carry great amount of load allowing for large windows to be opened and creating well-lit public assembly spaces, when the arch thrusts were properly contained.

Due to this, cross vaults were employed extensively in the building of churches in Medieval Europe, being strongly linked with Gothic Architecture, and together they reached a formal and structural perfection by the end of the 13th c. At a typical bay, a quadripartite nave vault can be supported at the four corners upon the pier extension, while the lateral thrusts are stabilised with flying buttresses. As a result, the weight of the nave is brought down to the columns mainly with vertical forces, reducing drastically the horizontal component of the thrusts of the lateral vaults over the capitals.

The most common reason for their collapse is the sudden increase of thrust caused either by the failure of the buttressing system or the severe change of the vaults' geometry (usually due to unexpected loadings or degradation of the fabric). The lateral walls then move out-of-plumb and the weight produces a moment at the base of the aisle vault which the weak cross-section cannot resist. This base is transformed to a hinge and the aisles start deforming rapidly as well, until fracture lines are formed along the transverse vertex and the wall joint, leading eventually to failure.

Vaults are the key elements of this scheme, so a better understanding of their behaviour and pathology is essential for the preservation of many important medieval churches, limiting necessary conservation to the minimum with compatible and low cost interventions. The important areas of knowledge are the determination of a typology according to their technical features and structural role within the building, the definition of loadings and partial safety factors, the assessment of material properties, the behaviour under various types of stress (axial forces, bending moment, shear, torsion) and the determination of serviceability limit states of deflection and cracking.

It should be recognised, however, that this task becomes very difficult due to the great diversity of forms and pathologies of cross vaults. It is essential then that programmes of study should be established towards the collection of empirical and historical observations and the evaluation of safety in existing structures. The project presented here was concerned with the study of the behaviour of a typical quadripartite lateral rib vault under service loads, namely dead weight. At a later stage, the collapse under a change of geometry due to the failure of the nave vault will be assessed, simulated as a horizontal movement of the abutments.

This study focuses on the elastic behaviour of the Church of the Holyrood Abbey in Edinburgh. A test model was built, using appropriate construction techniques. Dead weight was applied and the response of the vault was monitored. A simulation with FE was also performed and the results are in good agreement with the experimental data.

THE LATERAL VAULTS OF THE CHURCH OF HOLYROOD ABBEY

One of the remaining vaults of the Church of Holyrood Abbey in Edinburgh has been chosen as a case study. The vault belongs to the middle of the S aisle, it is quadripartite and almost square in plan (4.9 x 3.78 m). The ribs are generated from the same radius, equal to the shorter side of the plan, and they have long, plain voussoirs, except from the roll-and-hollow moulded nave arch. The shell is considered 140 mm thick, made of long and roughly-shaped slabs laid in irregular courses (Fig 1), while the vertices are horizontal without ridge-ribs The vault is supported at the front on compound piers while the back side rests on piers engaged at the external wall.

In plan the church is a nave flanked with aisles and the walls were composed by a triforium and clerestory windows. It was completed by the middle of the 14th c.[6] and flying buttresses were added to the nave between 1460-83. In 1570, the ruined choir and transepts were demolished, and the remaining nave was repaired. During the refurbishment of the central roof in 1758, however, the wooden trusses were replaced by stone diaphragms, the void of the pitch filled with rubble and then topped with heavy stone slabs, adding weight that the aged and insufficiently-pinned lateral walls could not contain. These walls moved gradually out of plumb, leading eventually in 1768 to the collapse of the nave and the N aisle[5].

Figure 1. The cross-vault at the S aisle of the Holrood Abbey Church.

EXPERIMENTAL APPROACH

The construction of the test structure

The behaviour of the vault was studied by building a test structure in quarter scale. With the help of a measured survey, the size of the constitutive elements was determined and the important geometric proportions were defined. The construction of the model has given valuable information on factors which have a crucial influence on the structural behaviour and provided an opportunity to review

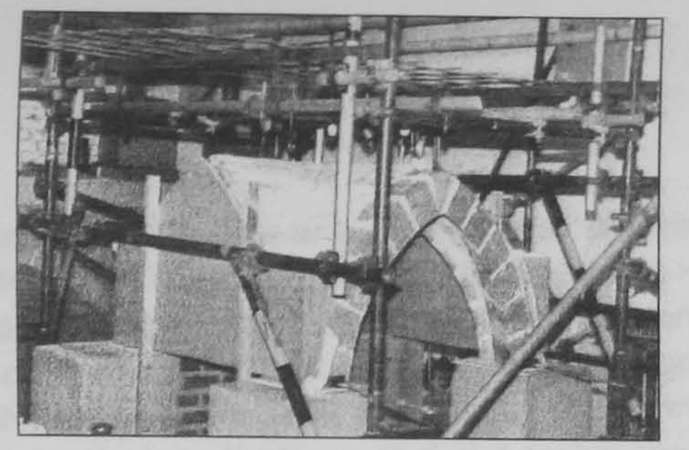

Figure 2. Completed test structure.

many of the standard textbooks which describe the phenomena mainly in a theoretical manner[3].

In the construction sequence, the shell is laid upon already built ribs. A projecting stem along the back of the ribs allows the webs to fit in the shelves created. The common radius of curvature for the ribs and webs permitted the use of templates and the standardisation of many of the elements. The diagonal and the transverse arches have the same cross-section, while the nave arch, running under the full thickness of the lateral walls in the Abbey, was simulated with a trapezoid form (Fig 2).

The voussoirs of the arches and the keystone had to be defined and built before the rest of the vault. Subsequently, the webs had to be filled, but the rubble masonry was difficult to reproduce accurately. Therefore, an effort was made to dress most of the blocks into standard proportions of 1:4 between the width and the length. A further difficulty occurred along the joint of the webs with the diagonal arches. In order to fit the blocks at best within the shelf over the rib, their ends had to be wedged according to a constantly changing bi-hedral angle. This verified the beneficial role of the rib in covering a difficult geometrical intersection and demonstrated the possible weakness of the joint, the effect of which is considered later in the analysis.

The courses were bound with a lime based mortar that had to simulate the low strength of the real binder. Special scaffolding was used for the shells and the building proceeded by carefully laying the blocks at few courses each time. The vertices required wedge shaped blocks similar to the ribs joint, slanted at the long faces, in a thick bed of mortar. Once the vault was complete, the scaffolding was removed, but no plastering was considered, since the aim is to study the structure in its pure form.

Material properties of masonry

The necessary material properties of the masonry for the theoretical analysis are the moduli of elasticity and the flexural strengths. Wallettes were subjected to four line loads (Fig 3) and from the measurement of the deflection at the centre, the modulus of elasticity was evaluated, while the stress at the failure of the specimen represented its flexural strength. The vault exhibits stiffness and strength

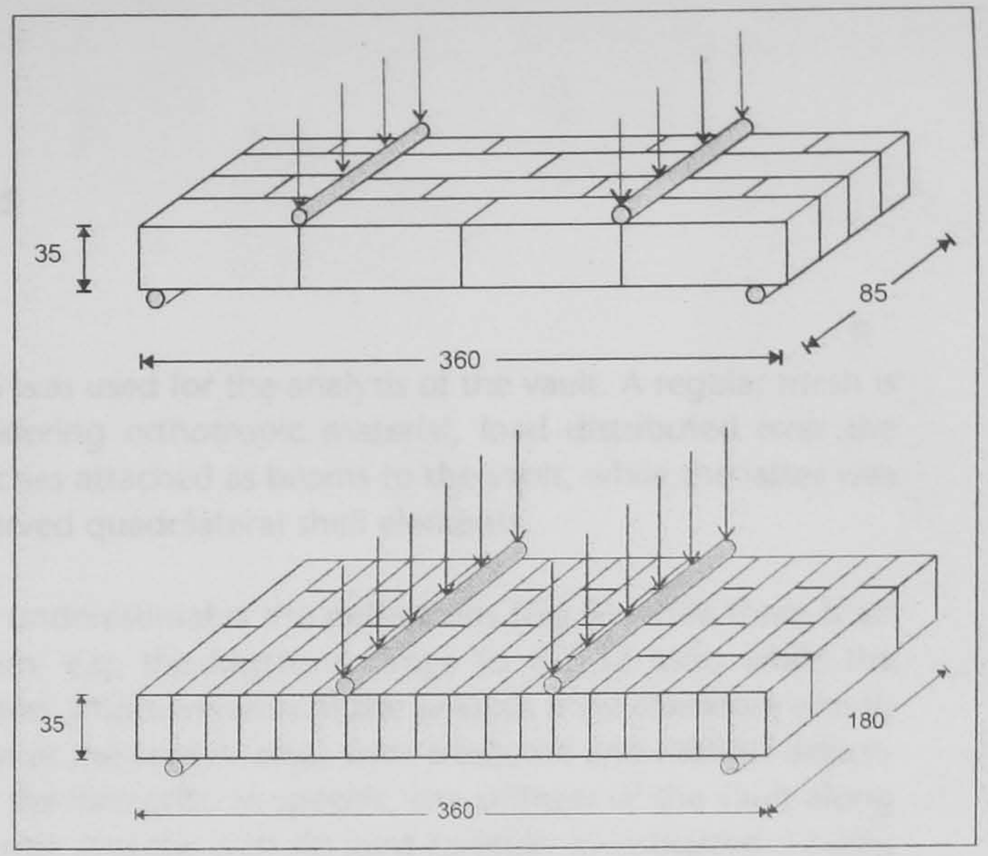

Figure 3. Set-up of the wallette test.
1. Direction parallel to bed joints.
2. Direction normal to bed joints.

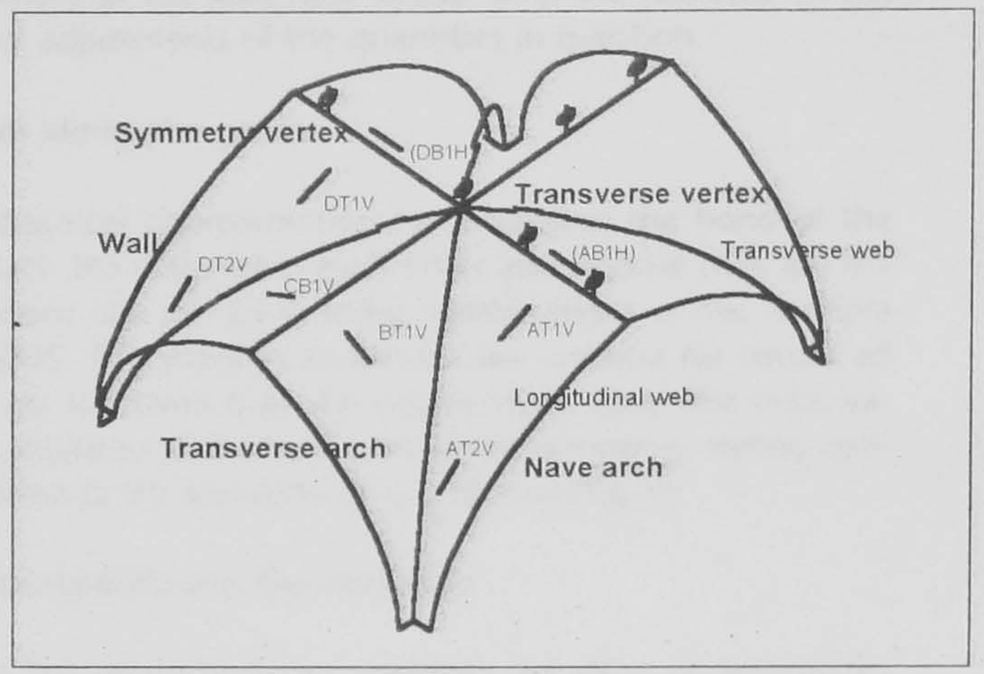

Figure 4. Placement of the instrumentation.

orthotropy in the local longitudinal (parallel to bed joint - 1) and hoop (normal to bed joint - 2) direction. Therefore, wallettes representing the two directions were built, keeping the shear span to depth ratios constant.

The evaluated moduli of elasticity were E_1 = 1500 N/mm² and E_2 = 360 N/mm². The material demonstrated a brittle behaviour in both directions, with flexural strengths F_1 = 0.62 N/mm² and F_2 = 0.24 N/mm², respectively. The modulus of elasticity of the arches was found to be 500 N/mm².

Set-up of the experiment

The dead load was distributed over the model by means of lead weights. It became evident, however, that below mid-height the slope of the surface was such

Table 1. Comparison betwen the strains recorded in the experiment and those evaluated in the FE analysis.

Strain gauges			Strain (in 10-6)	
Location of strain gauge	Shell face and strain direction	Gauge code	Experiment	FEA: Pin joints & top load
Transverse vertex - front side	Extrados - hoop Intrados - hoop	BT1V BB1V	-65 -3	-111 34
Transverse vertex - back side	Extrados - hoop Intrados - hoop	CT1V CB1V	-71 -6	-47 -82
Symmetry vertex - side to wall	Extrados - hoop Intrados -hoop	DT1V DB1V	-29 0	-42 -12
Symmetry vertex - side to nave arch	Intrados - long.	AB1H	2	31
Front spandrel	Extrados - hoop Intrados - hoop	AT2V AB3V	-37 -28	-76 -43

part of the vertex, with -0.212 mm at the keystone where the experiment gives the maximum of -0.252 mm, and the best agreement is at the crown of the nave arch.

So far as strain pattern is concerned (Table 1), it is mainly the hoop strains at the extrados which are closer to the experimental level of compression. The zone of tension appearing at the front intrados of the transverse vertex spreads also to the web of the nave arch, corresponding to an area where cracks may appear, according to experience[1]. The low values recorded there may serve as a first indication and the development of strain should be critical during the monitoring of the failure process.

The magnitude of the strain recorded is in general lower than that of the analytical model and reasons can be that the gauges were installed on the web blocks, which are stiffer than the masonry and, inevitably, local variations of elasticity may have been more influential than expected.

THE RESPONSE OF THE STRUCTURE

The overall behaviour of the cross-vault (Fig 6), shows the loads are carried mainly along the direction of the symmetry vertex. This can be a consequence of the facts that the vault spans between the two major supports (wall and nave arch) and the corresponding direction of elasticity in the longitudinal webs is almost four times stiffer. As a result, the role of the transverse supports becomes almost insignificant and this remains so even when, in the model, the transverse arch is removed or the original continuity with the neighbouring vaults is restored by means of a plane of symmetry.

The different deflections between the nave arch and the wall give rise to an eccentricity of the hoop axial force N_θ along the joint of the shell on this arch, allowing membrane tensile forces to develop normal to the wall, mostly at its crown.

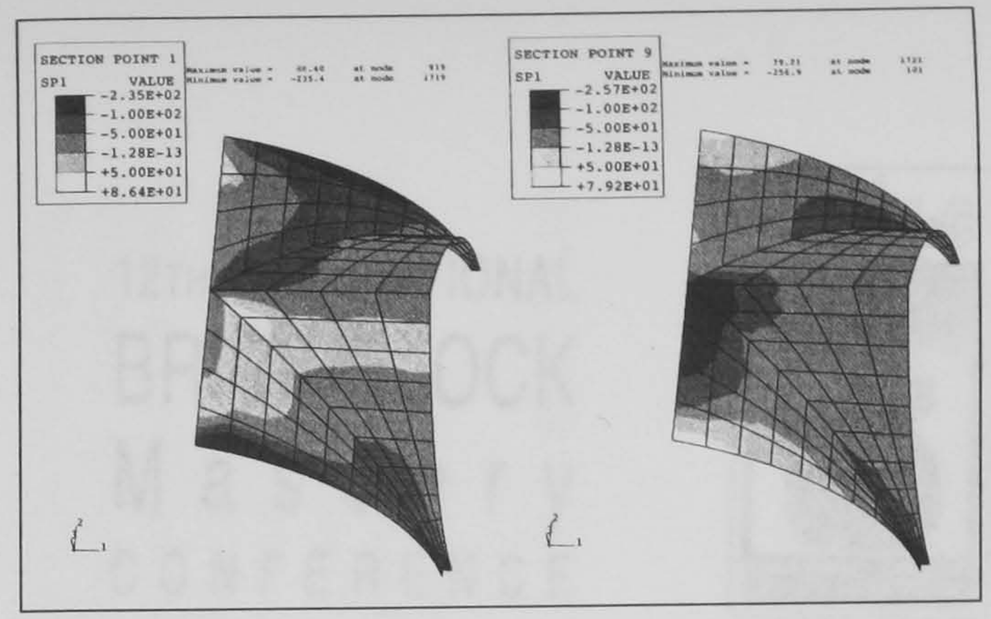

Figure 6. Min principal stresses - intrados and extrados.

Table 2. Distribution of strain along a pointed simply-supported arch, between the crown (0) and the springing.

Arch at the end of transverse web			Arch at the middle of transverse web		
Angle (10^{-6})	Intrados strain (10^{-6})	Extrados strain (10^{-6})	Angle (10^{-6})	Intrados strain (10^{-6})	Extrados strain (10^{-6})
0	315	-511	0	-94	-145
12	214	-416	6	-101	-140
24	-47	-175	12	-118	-127
36	-339	88	18	-140	-113
48	-464	176	24	-151	-111
60	-164	-164	30	-134	-137

Since these two ends of the vault act in some degree as diaphragms, this prevents the (short) longitudinal webs from a full shell behaviour, so actually only membrane forces develop in their hoop direction. The symmetry vertex is mainly compressed around the area of the central keystone, while higher compressive forces appear at the front spandrels.

Since these webs have relatively no substantial support along their end arches, their behaviour is similar to that of a pointed barrel vault, pinned along the edge, in which case the hoop stresses derive from the analysis of arches with the same profile as the cross-section of the vault. Table 2 lists strains developing along a simply supported pointed arch with the same proportions as the transverse web(evaluated using equations of equilibrium and compatibility of deformations). Positive curvature close to the crown is produced by eccentricity of the normal forces, but less deep arches (smaller springings angle) are completely under compressive membrane forces.

As the deformation of the whole cross-vault is biased towards the nave arch, this curvature along the transverse vertex have shifted to the front part of this web, which is now being almost everywhere in compression at the extrados. Moving closer to the keystone, the hoop strains are largely reduced, allowing for the tensile strains that develop at the front longitudinal web to shed into this area. This

does not happen at the back side of the cross-vault, because the corresponding web is solidly supported on the wall.

Some final remarks about the thrust on the wall, since this is crucial for the performance of the various buttressing systems. When the test load of 1.3 kN/m² is applied, the analysis gives an outward thrust of 161 N, against 393 N according to Heyman method[4] and 186 N according to Barthel method[1]. Both used analytical procedures for the evaluation of thrust and considered that the vaults are usually cracked already and partialised. The first method[4] is based on the Membrane Theory and the other[1] developed from the procedure that evaluates the thickness an arch must have in order to contain its own line of thrust. The method proposed by Heyman overestimates the thrust. Barthel method of obtaining the thrust appears to correlate well with the FE analysis.

CONCLUSIONS

1. The study of the behaviour of a cross-vault through the construction of a scale model can clarify the performance of crucial elements like the ribs.

2. The deformation of the vault is strongly shifted towards the nave and deflections depend on the stiffness of the nave arch and the ribs.

3. No cracks are expected for service loads and the strains all over are low. Both the experiment and the FE analysis predict the effect of the bending stresses around the vertices and the keystone.

REFERENCES

1. Barthel, R. (1993). "Crack formation in masonry cross-vaults." *Conf. Proc., Structural preservation of the architectural heritage.* IABSE, Rome.

2. Croci, G., Viskovic, A. and Sabbadini, F. (1995). "Some aspects of the structural behaviour of gothic cathedrals." *Conf. Proc., Spatial structures: past, present and future.* IASS, Milan.

3. Fitchen, J. (1961). *The construction of Gothic cathedrals: a study of medieval vault erection.* Clarendon Press, Oxford.

4. Heyman, J. (1995). *The stone skeleton.* Cambridge University Press.

5. National Archives of Scotland (1768). *Exchequer. Treasury Minutes Book 30/11/1763 - 23/2/1770.*

6. RCAHMS (1951). *Inventory of Monuments in Edinburgh.* "Royal Commission of Ancient and Historic Monuments, Scotland", HMSO, UK.

12TH INTERNATIONAL BRICK/BLOCK Masonry CONFERENCE

12th IBMaC MADRID-SPAIN 25-28 June 2000

Tim

SEISMIC RESPONSE OF RC CONCRETE FRAMES INFILLED WITH BED JOINT REINFORCED MASONRY PANELS

G.M. Calvi1, D. Bolognini[1], P. Timpermann[2]

[1]Dipartimento di Meccanica Strutturale, Università di Pavia, Via Ferrata 1, 27100 Pavia, Italy

[2]Bekaert S.A., Zwevegem, Belgium

ABSTRACT

The research work presented in paper is related to the seismic response of RC frames infilled with weak masonry panels. More specifically, the benefits derived from the insertion of murfor® bed joint reinforcement, in the mortar layers or welded wire mesh (distanet®) in the external plaster, are studied in some detail. Experimental tests have been performed on different types of infilled frames to investigate the in-plane response at different earthquake intensity level and the out-of-plane strength as a function of the in-plane damage. A series of parametric simulations have then been performed to evaluate the effects of the different panel characteristics on the response of whole buildings, with different infill patterns. Both in-plane and the out-of-plane response have been considered. The results are described in terms of peak ground acceleration required to induce given limit states of serviceability or damage relatively far from the collapse of the structure, which is governed by the RC frame design more than by the infill panel properties.

Keywords: *infilled frame, infill panel, mortar layer reinforcement, external mesh, out-of-plane collapse, damage limit state.*

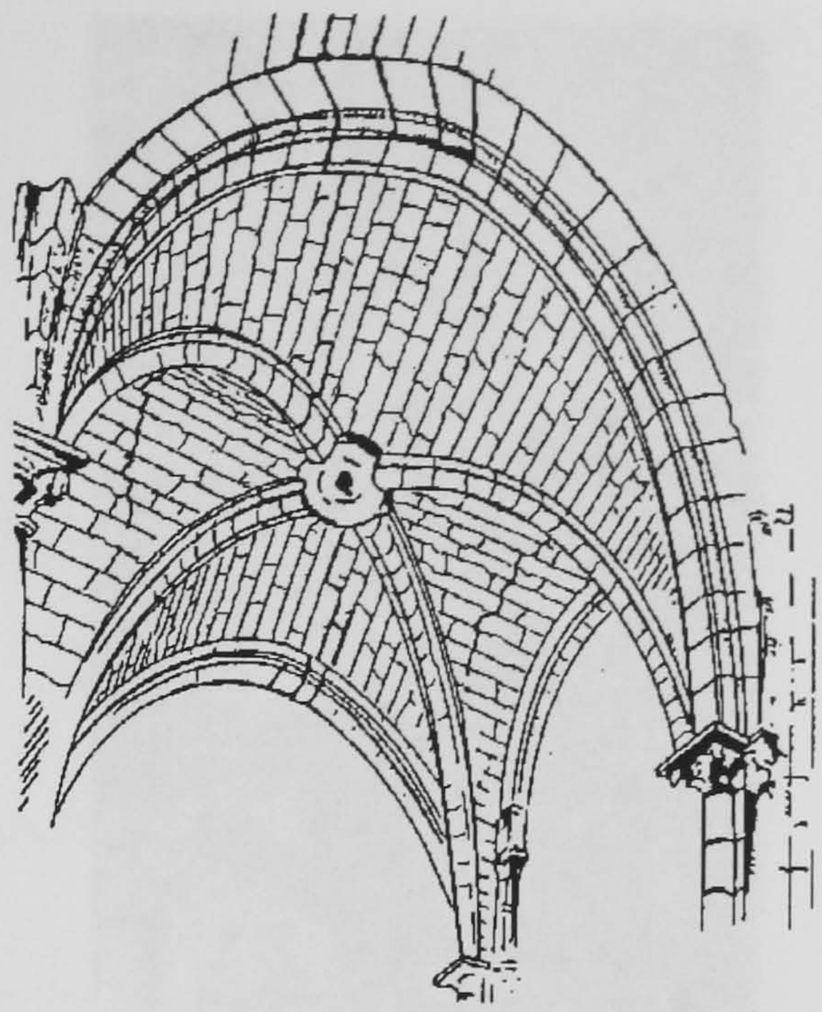

FIGURE 1. Typical crack pattern in a lateral cross vault (from [2])

It is very difficult however to quantify the effect of all the incidents which affect the structural behaviour during the lifetime of a monument. The construction of experimental structures on the other hand allows the effects of various expected loadings to be studied separately and then superimposed to produce the complete range of responses. An earlier attempt was made by Ceradini [4] to define the extent of imposed deformations a full-scale brick cross vault can resist but with limited experimental results. The structure, reproducing the nave of a partially collapsed church in S. Italy, spans 7.36 m, has no ribs and the bricks are laid in a manner that permits a good bond between the two intersecting vaults. The failure of the supporting system was simulated by a horizontal outward movement of all the four supports until 180 mm (1/40 of the span), when the fracture pattern was formed. Subsequently, the vault was repaired and the abutments were further displaced until a total of 260 mm (1/28 of span). No detail is given however about the order of deflections attained or the redistribution of the loads within the shell.

The experimental project presented here studies the collapse of an existing monument, the church of the Holyrood Abbey in Edinburgh. A lateral vault is considered in this occasion. Firstly it is loaded with dead weight to assess its response to service loads. Secondly, by moving gradually only the two front supports, the progressive change in the geometry and the distribution of loads is monitored until the sufficient number of cracks is formed and the structure reaches instability. Some results from the on-going simulation with Finite Element (FE) models are presented here in order to

THE MODEL OF AN AISLE VAULT FROM THE CHURCH OF THE ABBEY OF HOLYROOD

The church of the Abbey of Holyrood in Edinburgh was completed in the 13th century following in many aspects the Cathedral of Lincoln. The vaults of the nave were sexpartite and those of the aisles plain quadripartite ones (Fig 2). After a history of alterations and negligence, an unsuccessful intervention to the roof in 1758 caused the slow movement out of the vertical of the lateral walls and the collapse of the nave and the N aisle in 1768. The architect W. Mylne, who was called in 1766 to survey the condition of the fabric, reported: many of the walls and pillars incline to the N 2 to 3 in. (50 to 75 mm) out of perpendicular at some height, *"so that I imagine the walls & pillars will incline seven or eight inches from the perpendicular that is at the greatest height"* [5]. Moreover, several coins (voussoirs) of the vaults had fallen or were in course to.

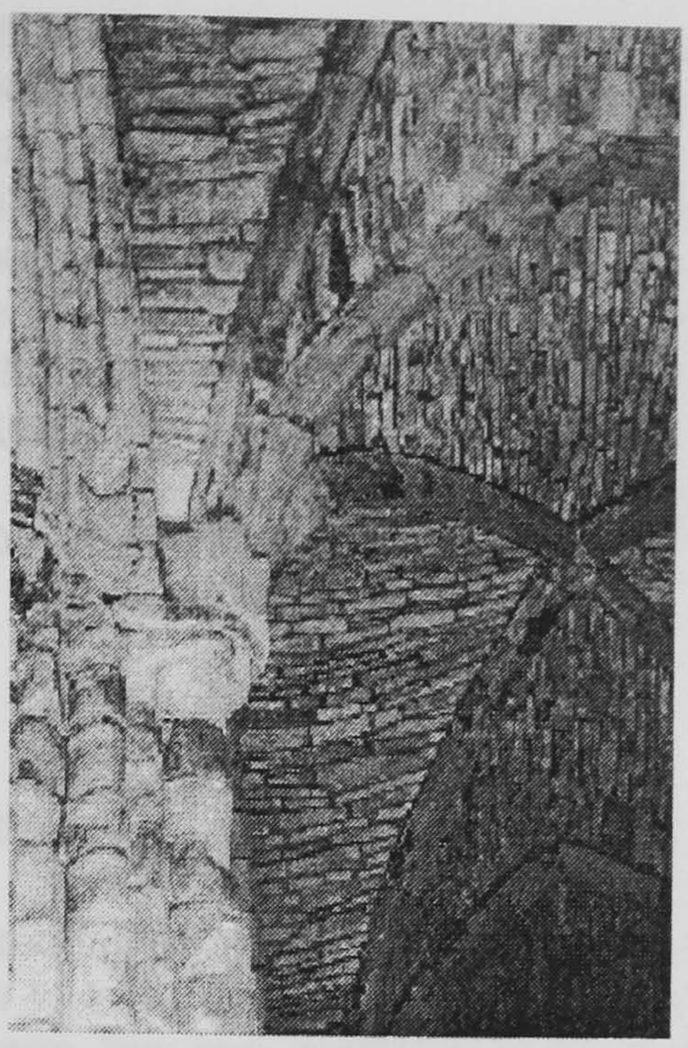

FIGURE 2. An aisle cross vault from the church of the Holyrood Abbey

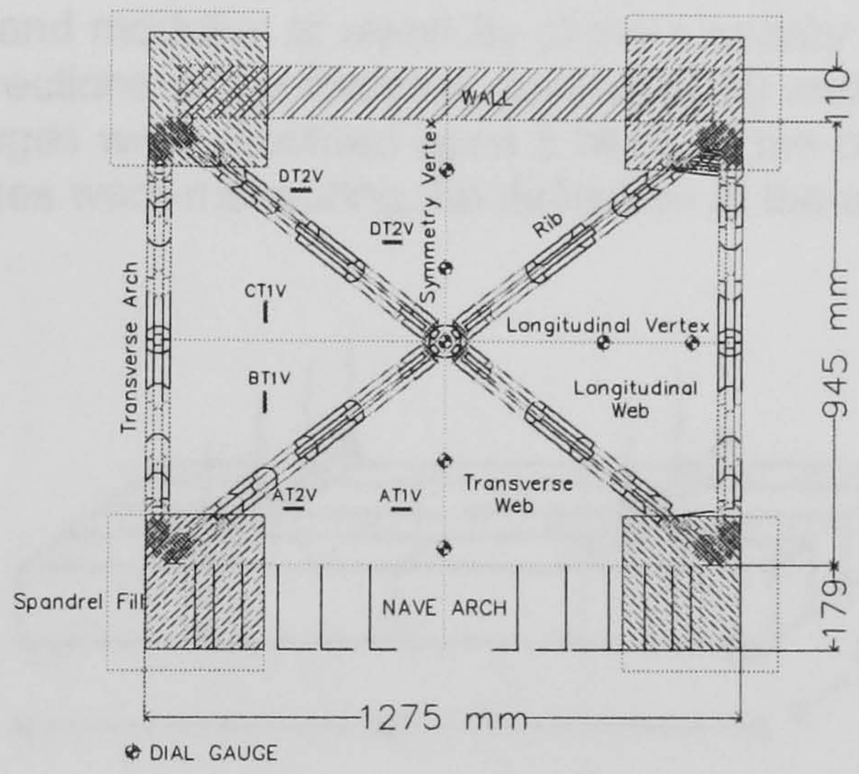

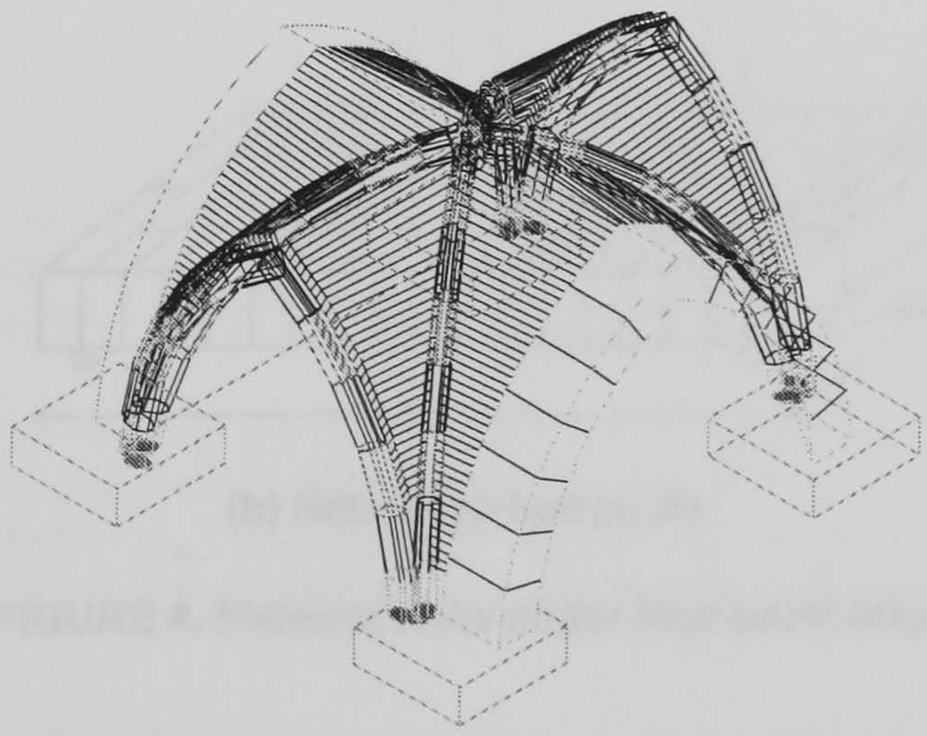

FIGURE 3. Layout and dimensions of the test structure and experimental set-up

From this report it becomes clear that the collapse occurred after an excessive deformation of the spandrels of the aisles due to the incapacity of the lateral walls to contain the thrust of the nave vault. One of the remaining aisle vaults (Fig 2) was constructed in a quarter scale in the laboratory and the collapse was reproduced with the movement of the two front abutments. The

prototype is a ribbed quadripartite vault with severies made of rubble masonry composed of irregularly placed sandstone blocks and bound together with thick mortar joints that were repointed in 1911. Wood (Southern yellow pine) and lime mortar were used in the test structure for the blocks and the joints respectively and this permitted a quite faithful reproduction of the ribs and the overall geometry [6]. In the case of the webs, the irregular pattern of the original was simulated with oblong blocks of a length four times the width, giving shell thickness of 35 mm. The blocks were varnished to minimise any side effect from the water of the mortar and to prime the surface for the application of strain gauges later. Fig. 3 illustrates the dimensions of the structure and the role of the ribs as a skeleton to the vault. A particular feature is the use of rib voussoirs rebated at their extrados, which enabled the segmented erection of the severies and a better bond between the rib and the shell.

EXPERIMENTAL SET-UP

Assessment of material properties

The use of wood and mortar allowed for a faster construction and a more effective experimentation with form in order to simulate the original geometry. Moreover, the difference in the elasticity and the strength between the two materials was a quite good approximation of the situation expected at the prototype vault between the (decayed) lime mortar and the sandstone, as, for example, the elasticity moduli of these materials are in the order of 800 N/mm^2 and 5000 N/mm^2 respectively.

Flexural tests under four-point load were performed in two types of wallettes in order to assess the flexural strength and modulus of elasticity of the masonry (Fig 4). Each type represents one of the two orthotropic directions of the material, parallel (1-X) and normal (2-Y) to the bed joint. Electric resistance strain gauges were mounted upon a block at the centre on both the top and the bottom surface and dial gauges were measuring the deflection at the supports and the centre.

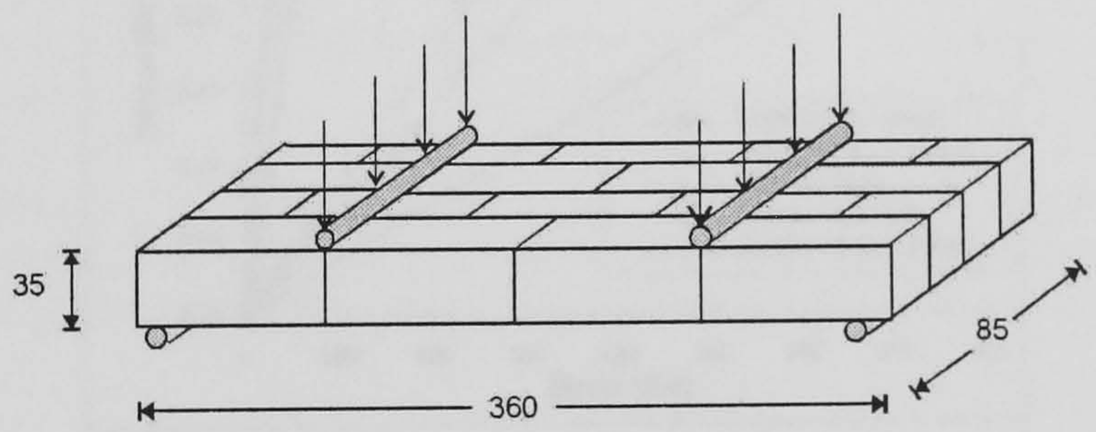

(a) Parallel to bed joints

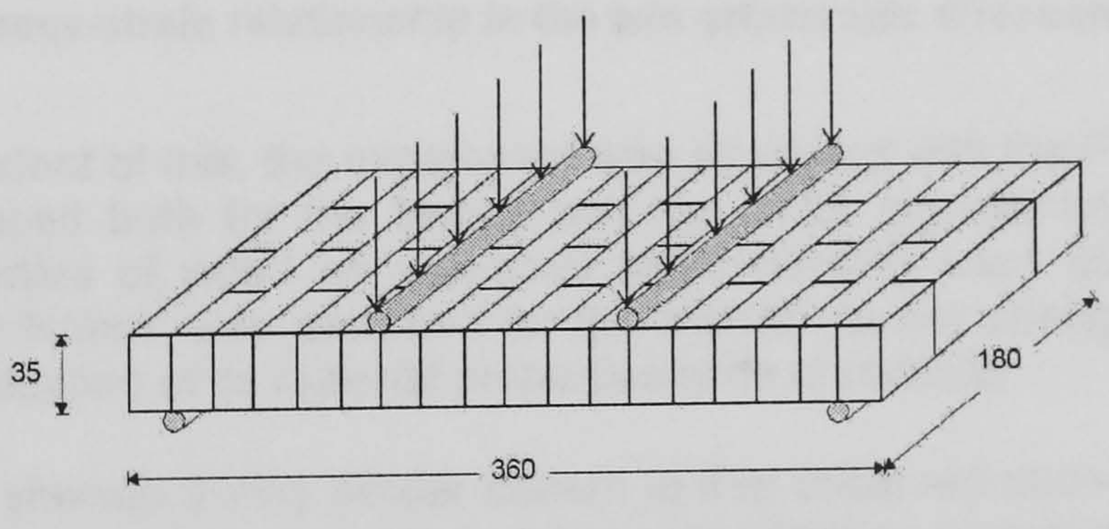

(b) Normal to bed joints

FIGURE 4. Flexural tests under four-point load

For each orthotropic direction of the masonry three specimens were tested and the results for both measurement methods are summarised in Table 1 and Figure 5. An examination of the elasticity properties shows a difference between the methods and the reason is probably that the strain measured represents the response of the block and not the masonry as a whole. The material properties of the wood in each of the orthotropic directions (parallel and normal to the grain) were also assessed with flexural tests, but the specimens were not tested to failure as fracture is expected only at the mortar joints (Table 1).

TABLE 1. Material properties from flexural tests

	Masonry		Wood	
	Parallel to bed joint (X)	Normal to bed joint (Y)	Parallel to grain (X)	Normal to grain (Y)
Elasticity from strains (N/mm^2)	27100	8900	23600	1900
Elasticity from deflections (N/mm^2)	4200	670	21600	1730
Flexural strength (N/mm^2)	0.980	0.319	-	-

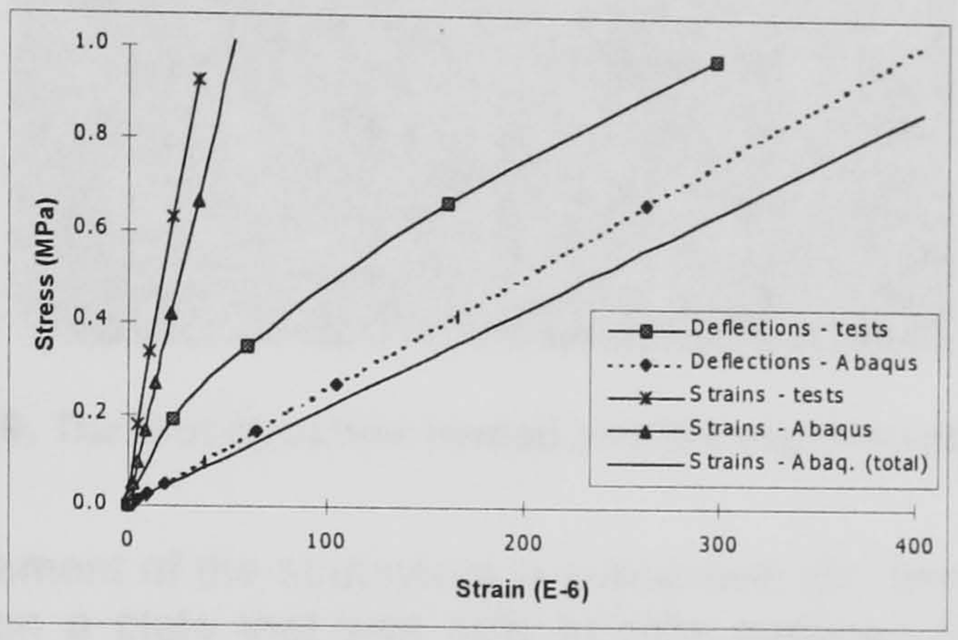

(a) Parallel to bed joints - X

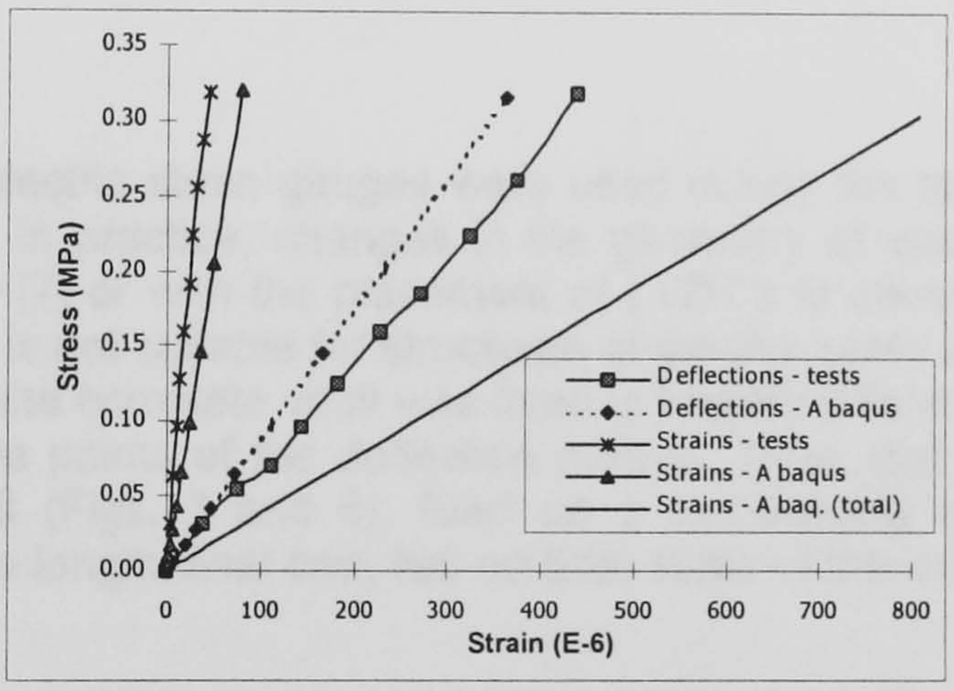

(b) Normal to bed joints - Y

FIGURE 5. Stress-strain relationship in the two orthotropic directions of masonry

To verify the extent of this, the experiment was simulated with the FE package Abaqus. 3D brick elements were used both for the blocks and the joints representing the geometry of the specimens. The properties of wood as assessed experimentally were used (Tab 1) and a low elastic modulus of 100 N/mm^2 was assumed for the mortar (its low strength would have made a direct experimental evaluation of its material properties quite unreliable).

The FE model showed a very similar pattern to that observed during the tests (Fig 5), both for deflections and strains as measured. High stress concentration is recorded at the joints and the stress-strain relationship resembles once again to that obtained only from deflections when strains from nodes on the blocks and the joints very close to each other are averaged.

Loading procedure

Dead weight and imposed deformation of the supports are the two loadings considered in this project. Stone masonry has a typical specific weight of about 20 kN/m^3 and, as the vault is built in quarter scale, the load applied to simulate the self weight should be $4 \cdot 20 = 80$ kN/m^3 (distributed uniformly as a surface load of $80 \cdot 0.035 = 2.8$ kN/m^2) to produce stresses compatible with the scale. Airbags could be used to apply uniformly this load, but the geometry of the vault makes it quite complicated. Lead weights were used instead, placed very close to each other and only until the

height of the spandrel fill since the high shell curvature below that point does not prevent the weights from sliding (Fig 6). The final value of 52 kN/m^3 (1.8 kN/m^2) was attained by gradually increasing the load and the elastic response of the structure was evaluated.

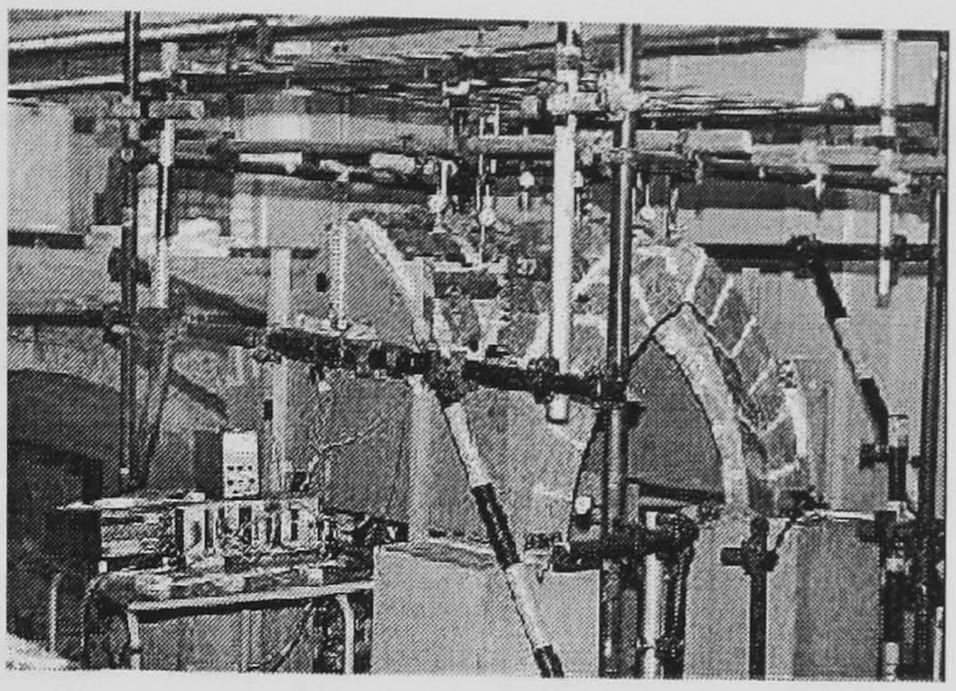

FIGURE 6. The test structure loaded and the experimental set-up

So far as the movement of the abutments is concerned, the two front blocks of the *tas-de-charge* were mounted upon a plate that was able to slide between two rails when pulled by a turnbuckle. Since the elastic limit may reach within the first few millimetres of the lateral movement, dial gauges were used for an accurate monitoring of this movement.

Instrumentation

Dial gauges and electric strain gauges were used during the test of the vault to study the response of the structure. In practice, changes in the geometry of vaults can be monitored by a system of geodetic survey [7] or with the placement of LVDT's in several important areas [8], but the range of both methods is not suitable for structures of smaller scale as that of the vault in exam. A preliminary FE model of the complete vault was used to identify critical zones for the development of strain and representative points of the deflection pattern. Thus, dial gauges were placed upon several points of the vault (Figs. 3 and 6), fixed on a self-bearing steel frame: five along the symmetry vertex, two at the longitudinal one, two on both sides of the longitudinal barrel and two on the transverse barrel.

Regarding the measurement of strain, a demountable 'demec' gauge of 100 mm span and resolution of 11· 10^{-6} strain was employed initially. However, this span can not represent the behaviour of a single point in the actual scale of the structure and further inaccuracies may arise in areas of high strain concentration. Moreover, the resolution of the instrument would not allow to record some of the lower values expected, so the more accurate electric strain gauges were preferred. Again, the same precautions as in the case of wallette tests were taken during monitoring and the gauges were mounted on both the surfaces (Fig 3): at the extrados, in the hoop direction (normal to bed joint) close to the vertex and the bases and at the intrados, again in the hoop direction, close to all the vertices and the back and front spandrel area, and in the longitudinal direction, (parallel to bed joint) at the vertices of the front and the back of transverse barrels.

TEST UNDER DEAD WEIGHT

Experimental data

a) Test under dead weight – Test DW1

This series of tests served to monitor the response of the structure under service load and to calibrate the FE models in the elastic range. A surface load of 1.8 kN/m^2 was applied uniformly. The behaviour of the structure at this stage and the theoretical analysis of the results are discussed more extensively in [6] and here they can be summarised as follows. Since the vault spans between two strong supports (wall and nave arch) and because at the area of the symmetry vertex the material is much stiffer in the direction parallel to this axis, the loads can be considered to be

carried mainly along this axis. Membrane forces act mainly close to the spandrels (Table 2) and bending stresses develop at the upper parts, with the area of higher values shifted away from the keystone towards the front, as it can also be assessed from the deflection of the symmetry vertex (Fig 7).

TABLE 2. Dead weight. Strains at various locations

Strain gauges			Strain (in 10^{-6})	
Location of strain gauge	Shell face and strain direction	Gauge code	DW1	DW2
Longitudinal vertex - front side	Extrados - hoop Intrados - hoop	BT1V BB1V	-65 -3	-31 24
Longitudinal vertex - back side	Extrados - hoop Intrados - hoop	CT1V CB1V	-71 -6	-36 -8
Symmetry vertex - side to wall	Extrados - hoop Intrados -hoop	DT1V DB1V	-29 0	-12 4
Symmetry vertex - side to nave arch	Intrados - long.	AB1H	2	2
Front haunch	Extrados - hoop Intrados - hoop	AT2V AB3V	-37 -28	10 -2

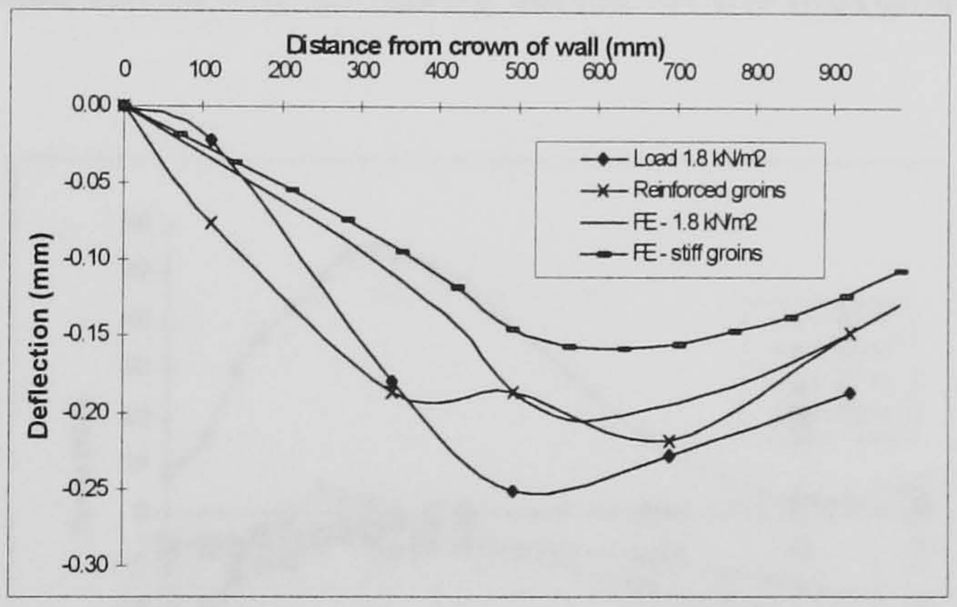

FIGURE 7. Deflection of the vertex under dead weight

b) Stiffening of the ribs – Test DW2

It was considered that the joints between the severies and the ribs were not covered sufficiently to withstand the higher stresses expected in the following stages due to imposed deformations as they would have in real situation. Subsequently to this series of tests, the area of the groins was reinforced at the extrados with mortar and further tested under the same loading condition. The strain recorded in Table 2 shows at the vertices an overall shift of the neutral surface of the shell towards the intrados and an extended presence of bending closer to the spandrels, since probably the stiffer groins have enforced a co-action between wider areas of the vault into carrying the loads, reducing the strain of the vertex area. Similarly, the deflection of the symmetry vertex (Fig 7) shows a lower but more uniform spread of the maximum values around the keystone.

Theoretical assessment

A different FE approach from that used earlier [6] was developed to study more carefully and separately the response of the blocks and the mortar joints, still considering the material as orthotropic. Shell elements were used once more, but the vault was discretised between areas of blocks and mortar, employing the corresponding material properties. The research focuses at present on the solution of numerical problems that have arisen from this scale of modelling, but the results at this stage show a similar deflection pattern for the symmetry vertex (Fig 7). The level of strains obtained is lower but with a good agreement in the overall pattern, except at the area of the front spandrels, which the FE model shows they are mainly in axial compression.

COLLAPSE DUE TO IMPOSED DEFORMATIONS

Experimental results

Following the test under dead weight, the structure was tested to failure by the movement of the two front abutments until a sufficient number of fracture lines is formed to transform the vault into a mechanism. Typical deflection pattern can be illustrated by the symmetry vertex (Fig 8) as the dial gauges located along the longitudinal vertex give similar readings to those of the keystone. Figure 9 shows the strain behaviour at the front and back side of the longitudinal vertex, in the hoop direction and for both the intrados and extrados surfaces.

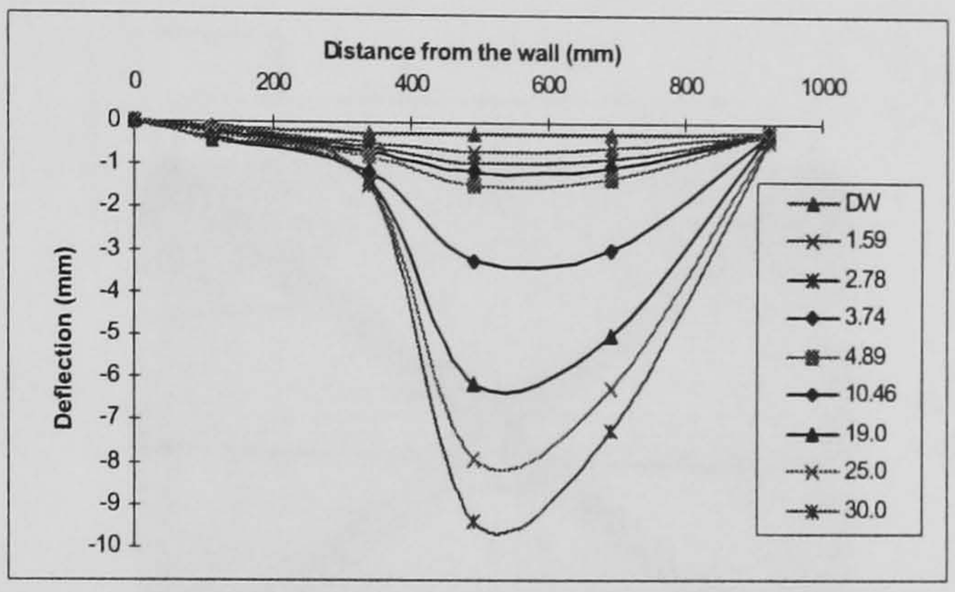

FIGURE 8. Deflection of the symmetry vertex for the movement of supports

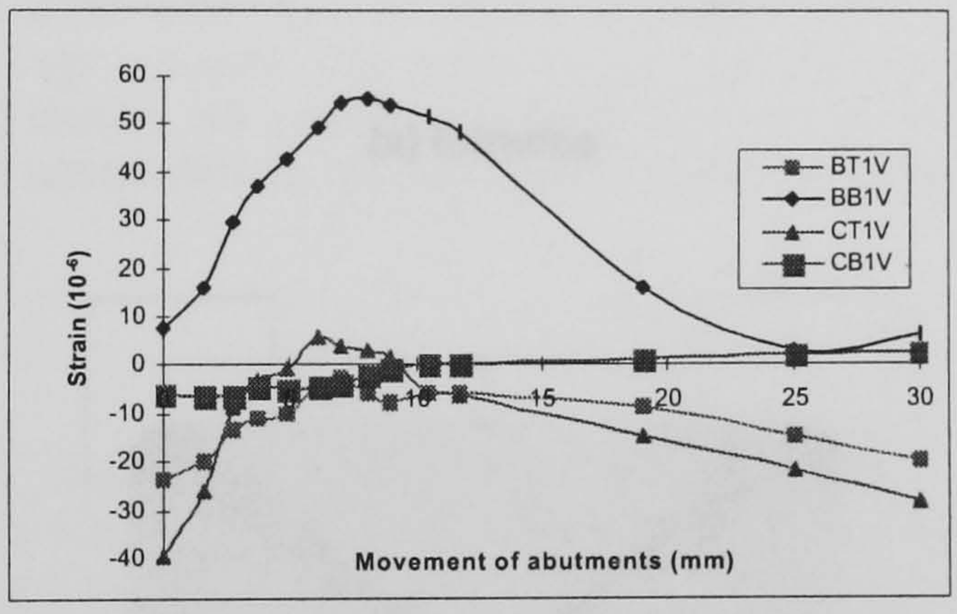

FIGURE 9. Strains at the front and back side of the longitudinal vertex

At a movement of 3 mm, the cracks initiated at the intrados of the front side of the longitudinal vertex, close to the transverse arch and the keystone, and in the following stages they slowly propagated parallel to the vertex until they united, while the ribs were visibly dislocating from the keystone. At 5 mm a hinge formed at the springing voussoir of the nave arch and the crack then bifurcated to the base of the ribs and the joint between the transverse web and the nave arch.

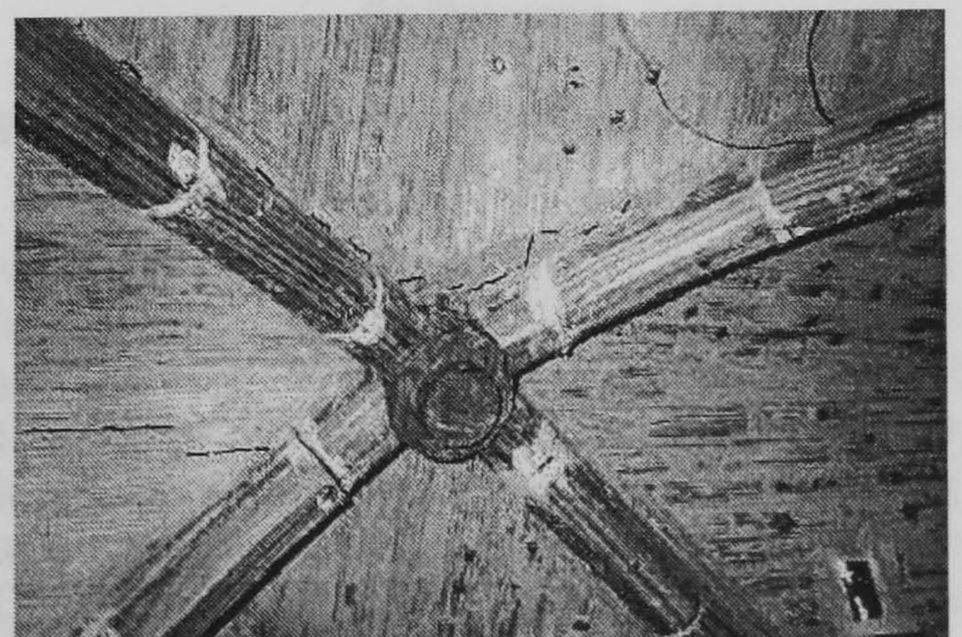

FIGURE 10. Crack formation at the intrados

The third fracture line was finally created at 8 mm, at the intrados on the back of the keystone and in the next stages it propagated along the ribs, penetrating the whole of the groin until there was a net separation of the severies from the ribs (Fig 10). On the left half of the vault, at the area of the back spandrel, the fault deviated within the shell but this could have been an effect of a local condition at the joints. Minor cracks formed at the joint of the vault with the wall, but they did not develop any more after the groin cracks. It was possible to continue displacing the supports until 30mm (1/32 of span) without the structure reaching complete collapse, but this is due to the geometry of the groin upon which the severies could still rest. It has to be noted that all the faults were concentrated in the joints and no failure at the blocks was observed. The final crack pattern is shown in Figure 11, for both the intrados (a) and extrados (b) surfaces.

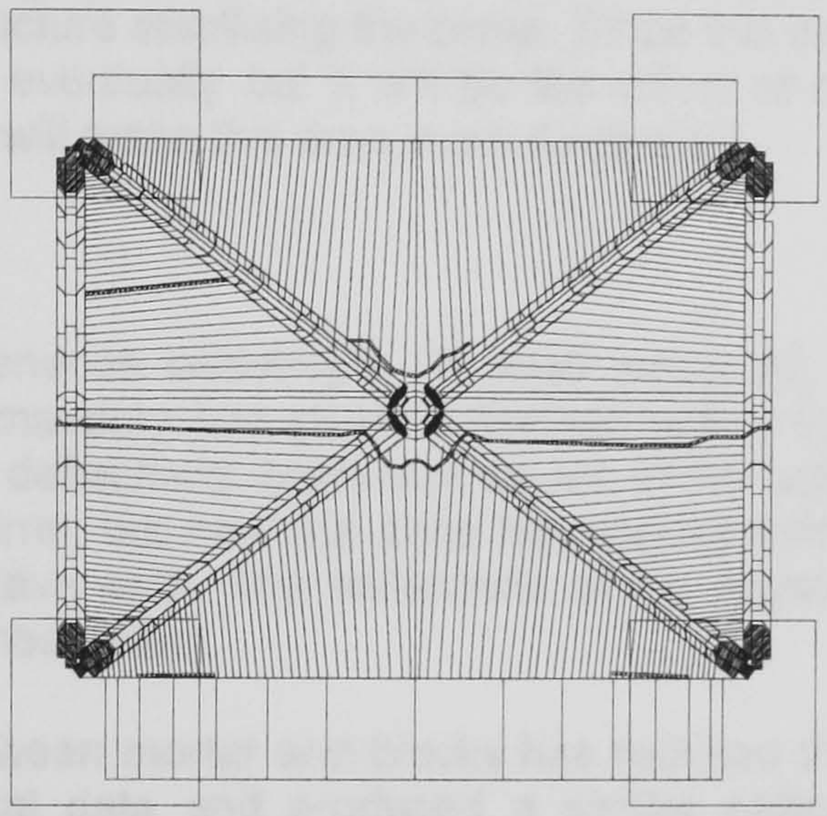

(a) Intrados

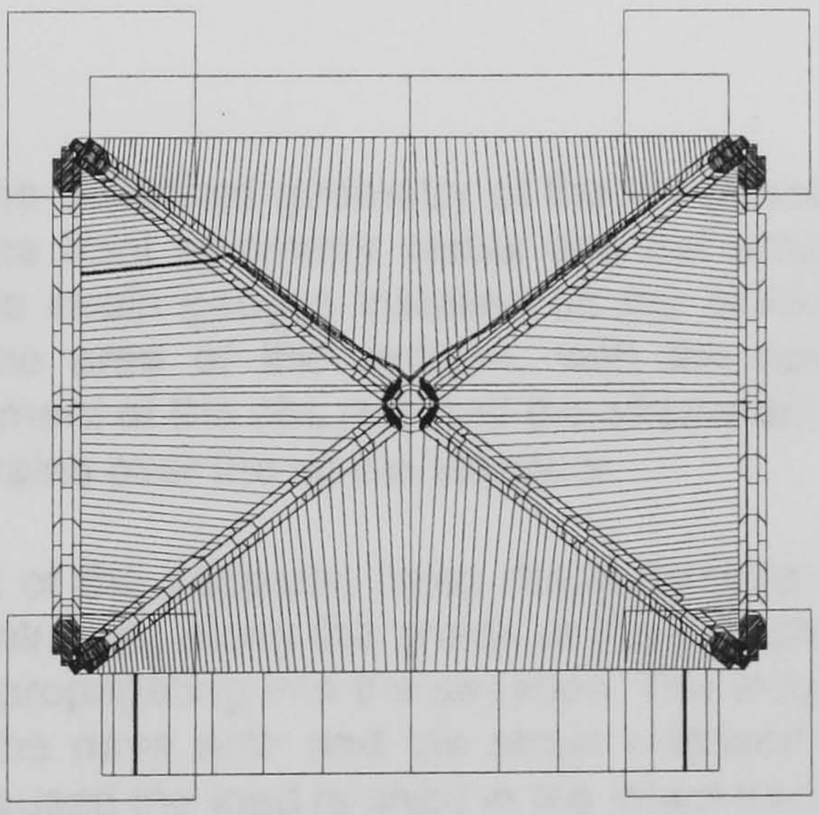

(b) Extrados

FIGURE 11. Crack pattern after 30 mm of supports movement

The movement at which the third fracture line formed coincides quite well with the sudden decrease of strain or change of sign in some gauges (Fig 9). Close to the longitudinal crack for example (gauges BT1V and BB1V), a maximum tensile strain of $60 \cdot 10^{-6}$ was attained at the intrados and then it started dropping to 0, while the compressive strains increased at the extrados. At the back of the longitudinal web, where the deflections start reducing (Fig 8), the pair of gauges CT1V and CB1V shows that the tension developing at the extrados drops also after 8 mm when the groin cracks are formed. Compression is recorded afterwards, as a result of the cracks opening further.

Contrary to the hoop strains, quite low values of horizontal strain were recorded parallel to the symmetry vertex, at the intrados. This is a result not only of this direction being the stronger one of the material, but also of the progressive detachment of the back of the transverse barrel from the groin and the subsequent release of stress normal to ribs and keystone. Moreover, the load sheds slowly to the front part of this barrel as it can be verified by the increasing hoop compression at the top areas. As this part is constrained between the nave arch and the ribs, receiving the increasing thrust from the spreading longitudinal barrel, the hinge at the base of the nave arch is formed when the supports are shifted and the severy moves as a rigid body.

With reference to the widely accepted crack pattern of Figure 1 [2], the crack expected close to the wall has formed here along the groins and this can be attributed to the fact that the joint between the shell and the groin is weaker compared with that of the wall. Moreover, at the prototype structure the hinge at the springing of the nave arch would not open to this extent, as there would act the weight of the upper structure stabilising the plane. Since this hinge opens in a relatively early stage, minor cracks will form eventually but it will be the effect of creep and further progressive distortion of the geometry that will make this area more evident [2].

Theoretical assessment

The use of a homogeneous orthotropic FE shell model [6] with a failure criterion and a smear crack analysis for the masonry has given unrealistic high values for the strain, despite the very good agreement with the deflections. Maximum values of the latter are always recorded at the front part of the transverse barrel, but now this zone has spread further to a wider area within the severies and parallel to the nave arch. The deflections of the keystone and the nave arch have developed following a rather linear trend.

The discretisation between mortar and blocks has reduced the strain close to the order of magnitude of the experimental data and produced a similar pattern for many of the gauges. Numerical problems however caused the solution to diverge at an earlier stage than the homogeneous model used before, so strains can be studied only until the initial stages of failure. The analysis is at present concentrating on the rate of failure and the sensitivity of the model to some material parameters.

CONCLUSIONS

Under dead weight, the deformed geometry of the cross vault shows maximum deflection concentrated at the area of the front symmetry vertex and not around the keystone. The strains, recorded by electric resistance strain gauges installed on the blocks of the vault, show initially a higher level of bending at the area of the vertices, with the spandrels being mainly in axial compression. A later reinforcement of the ribs reduced the strains and the deflections and caused a more uniform distribution of strains over the whole structure.

During the movement of the supports, three major fracture lines were observed: close to the longitudinal vertex at the intrados; along the groins at the extrados; and a hinge opening at the base of the nave arch, slowly propagating into the severies. The maximum deflections have spread into a wider area parallel to the nave arch and the strain released after the cracks were formed along the longitudinal vertex caused the load to shed in the intact transverse severy.

REFERENCES

Fitchen, J. (1961) The construction of Gothic cathedrals - a study of medieval vault erection. Clarendon Press, Oxford.

Heyman, J. (1995) *The stone skeleton.* Cambridge University Press.

Croci, G., Viskovic, A. and Sabbadini, F. (1995) Some aspects of the structural behaviour of gothic cathedrals. *Proc. IASS Conf. Spatial structures: past, present and future*, Milan, 1207-1214.

Ceradini, V. (1996) Modelli sperimentali di volte. *Proc. Nat. Conf. La meccanica delle murature tra teoria e progetto*, Messina, 157-166.

National Archives of Scotland (1768) Exchequer. Treasury Minutes Book 30/11/1763 - 23/2/1770.

Theodossopoulos, D, Sinha, B. P., Usmani, A. S. and Macdonald, A. J (2000) Structural behaviour of historic masonry cross vaults. *Proc. 12th Int. Brick/Block Masonry Conf.*, Madrid, 1791-1800.

Taupin, J. L. (1993) Cathédrale de Beauvais: de l'incertitude à la décision. *Proc. IABSE Symp. Structural Preservation of the Architectural Heritage*, Rome, 645-652.

Martínez, J. L., Martín-Caro, J. A., Torrico, J. and León, J. (2000) The "Silla de la Reina" tower in the Cathedral of León. Structural monitoring combined with numerical analysis. *Proc. 12th Int. Brick/Block Masonry Conf*, Madrid, 1197-1206.